

# **Supercritical Fluid Extraction**

## **Principles and Practice**

**2ND EDITION**

---

**Mark A. McHugh**

Department of Chemical Engineering  
Johns Hopkins University

**Val J. Krukonis**

Phasex Corporation

**BUTTERWORTH–HEINEMANN**

Boston London Oxford Singapore Sydney Toronto Wellington

Copyright © 1994 by Butterworth-Heinemann  
A member of the Reed Elsevier group  
All rights reserved.

No part of this publication may be reproduced, stored in a retrieval system, or transmitted, in any form or by any means, electronic, mechanical, photocopying, recording, or otherwise, without the prior written permission of the publisher.

∞ Recognizing the importance of preserving what has been written, it is the policy of Butterworth-Heinemann to have the books it publishes printed on acid-free paper, and we exert our best efforts to that end.

#### **Library of Congress Cataloging-in-Publication Data**

McHugh, Mark A.

Supercritical fluid extraction : principles and practice / Mark A.

McHugh, Val J. Krukonis. — 2nd ed.

p. cm. — (Butterworth-Heinemann series in chemical engineering)

Includes index.

ISBN 0-7506-9244-8

1. Supercritical fluid extraction. I. Krukonis, Val J.

II. Title. III. Series.

TP156.E8M39 1993

660'.284248—dc20

93-31797

CIP

#### **British Library Cataloguing in Publication Data**

A catalogue record for this book is available from the British Library

Butterworth-Heinemann  
313 Washington Street  
Newton, MA 02158-1626

10 9 8 7 6 5 4 3 2

Printed in the United States of America

# BUTTERWORTH-HEINEMANN SERIES IN CHEMICAL ENGINEERING

---

## SERIES EDITOR

HOWARD BRENNER

Massachusetts Institute of Technology

## ADVISORY EDITORS

ANDREAS ACRIVOS

The City College of CUNY

JAMES BAILEY

California Institute of Technology

MANFRED MORARI

California Institute of Technology

E. BRUCE NAUMAN

Rensselaer Polytechnic Institute

J.R.A. PEARSON

Schlumberger Cambridge Research

ROBERT K. PRUD'HOMME

Princeton University

## SERIES TITLES

Bubble Wake Dynamics in Liquids and Liquid-Solid Suspensions *Liang-Shih Fan and Katsumi Tsuchiya*

Chemical Process Equipment: Selection and Design *Stanley M. Walas*

Chemical Process Structures and Information Flows *Richard S.H. Mah*

Computational Methods for Process Simulations *W. Fred Ramirez*

Constitutive Equations for Polymer Melts and Solutions *Ronald G. Larson*

Fluidization Engineering, 2nd ed. *Daizo Kunii and Octave Levenspiel*

Fundamental Process Control *David M. Pretz and Carlos E. Garcia*

Gas-Liquid-Solid Fluidization Engineering *Liang-Shih Fan*

Gas-Separation by Adsorption Processes *Ralph T. Yang*

Granular Filtration of Aerosols and Hydrosols *Chi Tien*

Handbook of Industrial Crystallization *Allan S. Myerson*

Heterogeneous Reactor Design *Hong H. Lee*

Interfacial Transport Processes and Rheology *David A. Edwards, Howard Brenner, and Darsh T. Wasan*

Introductory Systems Analysis for Process Engineers *E. Bruce Nauman*

Laminar Flow and Convective Transport Processes *L. Gary Leal*

Microhydrodynamics: Principles and Selected Applications *Sangtae Kim and Seppo J. Karrila*

Modeling With Differential Equations in Chemical Engineering *Stanley M. Walas*

Molecular Thermodynamics of Nonideal Fluids *Lloyd L. Lee*

Phase Equilibria in Chemical Engineering *Stanley M. Walas*

Physicochemical Hydrodynamics: An Introduction *Ronald F. Probstein*

Porous Media: Geometry and Transports *Pierre M. Adler*

Slurry Flow: Principles and Practice *Clifton A. Shook and Michael C. Roco*

Transport Processes in Chemically Reacting Flow Systems *Daniel E. Rosner*

Viscous Flows: The Practical Use of Theory *Stuart W. Churchill*

## REPRINT TITLES

Advanced Process Control *W. Harmon Ray*

Applied Statistical Mechanics *Thomas M. Reed and Keith E. Gubbins*

Elementary Chemical Reactor Analysis *Rutherford Aris*

Kinetics of Chemical Processes *Michel Boudart*

Reaction Kinetics for Chemical Engineers *Stanley M. Walas*

---

# Contents

---

1. Introduction	1
2. Historical Perspective	17
3. Phase Diagrams for Supercritical Fluid–Solute Mixtures	27
Phase Diagrams for Binary Mixtures	31
Solid–Supercritical Fluid Phase Diagrams	45
Polymer–Supercritical Fluid Phase Diagrams	61
Phase Diagrams for Ternary Mixtures	71
4. Experimental Techniques in High-Pressure Studies	85
Dynamic Methods for Measuring Solubilities in Supercritical Fluids	85
Static Methods for Measuring Solubilities in Supercritical Fluids	91
Methods for Determining Phase Border Curves	94
5. Thermodynamic Modeling of Supercritical Fluid–Solute Phase Behavior	99
Intermolecular Forces	99
Solubility Parameters	105
Vapor–Liquid Calculations	110
Liquid–Liquid–Vapor Calculations	114
Polymer–Supercritical Fluid Calculations	120
Solid–Supercritical Fluid Calculations	127
6. Process Operations	135
7. Early Industrial Applications	145
Propane Deasphalting	145
Solexol Process	150
ROSE Process	153
8. Supercritical Fluid Process Development Studies	157
Activated Carbon Regeneration	158
Separation of Organic–Water Solutions	170
Breaking an Azeotrope	182
9. Polymers and Monomers Processing	189
High-Pressure Polyethylene Polymerization	189
Polymer Fractionation Processes	192
Polyethylene Fractionation	198



Fractionation of Ethylene-Based Copolymers	205
Polysiloxane and Polysiloxane/PMMA Copolymer Fractionation	217
Fractionation of Polymer Binders for Solid Propellants	250
Oligomer Extraction from Polymers	257
Supercritical Fluid Chromatography Analysis of Polystyrene	258
Polymer Fiber Spinning	260
Fractionation of Various Polymers	262
Polymer–Organic Solvent Phase Separation	280
Monomer Purification	285
10. Processing Pharmaceuticals, Natural Products, Specialty Chemicals, and Waste Streams	293
Coffee Decaffeination	294
Edible Oils Extraction	299
Extraction of Chemotherapeutic Agents	304
Isomer Separations	307
Treatment of Waste Streams	309
11. Chemical Reactions in Supercritical Fluids	311
Enzyme Reactions	311
High-Temperature Reactions	321
Heterogeneous Catalysis	322
Viscosity Effects	325
Reaction/Separation Schemes	326
Enhanced Reaction Rates and Selectivities	328
12. Special Applications	333
Supercritical Fluid Nucleation	333
GAS Antisolvent Recrystallization	342
Swelling of Polymers	357
Formation of Porous Polymers	360
13. Epilogue	367
References	373
Appendix A. Patent Reviews	395
1. The Zosel Patent	397
2. Petroleum and other Fossil Fuels Separations	399
3. Coffee Decaffeination	417
4. Extraction of other Vegetable and Animal Materials	427
5. Polymers Processing	441
6. Separation of Organic-Water Solutions	444
7. Materials Processing	449
8. Miscellaneous	453
Appendix B. Calculating Binary, Vapor-Liquid Equilibria using the Peng- Robinson Equation of State	463

Calculating Ternary, Vapor-Liquid Equilibria using the Peng- Robinson Equation of State	470
Calculating Ternary, Vapor-Liquid-Liquid Equilibria using the Peng-Robinson Equation of State	478
Calculating Binary, Solid-SCF or Solid-Liquid-Gas Equilibria using the Peng-Robinson Equation of State	487
Calculating Binary, Vapor-Liquid Equilibria using the Sanchez- Lacombe Equation of State	492
Calculating Polymer-Solvent-Solvent, Vapor-Liquid Equilibria using the Sanchez-Lacombe Equation of State	497
Calculating Polymer-Solvent-Solvent, Vapor-Liquid-Liquid Equilibria using the Sanchez-Lacombe Equation of State	500

Index	503
-------	-----

---

# Introduction

---

In the first edition we were both moderately quiet about the hype and hoopla, and the myth, magic, and mystery of supercritical fluids (SCFs) that was epidemic during the late 1970s and early 1980s, especially in articles in such widely subscribed technical and business journals as *Chemical & Engineering News*, *Business Week*, *Chemical Week*, and *Chemical Engineering* (table 1.1). Based upon SCF information provided to journalists by companies in the field, the article titles summarize the events of that time.

The trade literature touted SCF technology as a panacea for the chemicals, petroleum, and foods industries; it was going to solve all sorts of problems in energy reduction, waste treatment, chemicals separation, and biotechnology. Quotes from some of these articles attest to the unbridled and, in our opinion, unwarranted enthusiasm for this new technology.

Ideal solvents . . .

It's an exciting technology, and it is just about to take off.

They [SCFs] have a tremendous capacity to dissolve.

This technology will become a significant alternative to distillation.

Critical-fluid extraction is a process . . . that has been studied before only in the laboratory.

We're on the threshold of a new technology.

SCF extraction is nothing less than a new unit operation.

The technology for scaling up is not that well known.

The mystique of the term supercritical alone commands attention.

. . . they are putting this magic gas-liquid to work . . .

The magic of supercritical fluids . . . .

Unfortunately, the term "magic" was pervasive throughout the articles. Most of the large-scale processes that were promised in the articles did not come to fruition during the 1978–1984 period, and supercritical fluids lost favor. Perhaps it is no wonder that an article appeared in *Chemical Engineering* (February, 1985) with a title that could have been an ominous portent: "Supercritical Fluids: Still Seeking Acceptance." During this time Europe was very quietly building supercritical fluid extraction plants capable of processing

**Table 1.1** Articles on SCF Technology Appearing in the Trade Literature

<i>Title</i>	<i>Magazine</i>
Supercritical Fluids Try for CPI Applications	<i>Chemical Engineering</i> , 1979
Critical Fluids Aim for a Broad Industrial Role	<i>Chemical Week</i> , 1980
Gas Solvents: About to Blast Off	<i>Business Week</i> , 1981
Supercritical Fluids Offer Improved Separations	<i>Chemical &amp; Engineering News</i> , 1981
The Promise for Supercritical Fluids	<i>Chemical Week</i> , 1983
Separation Technology: Keep an Eye on Supercritical Extraction	<i>Chemical Process</i> , 1985

scores of millions of lb/yr material. A plant for decaffeinating coffee beans was built in Bremen, Germany, and several plants for extracting hops and spices were built in Germany, France, and the United Kingdom. It is apparent that some of the statements above were grossly overstated, particularly those that related to the “fact” that supercritical fluid extraction had been studied only in the laboratory due to lack of scale-up information.

We didn’t include information from trade literature from the 1978–1984 period in the first edition. So why have we chosen to discuss it in the second edition? By mid-1985 when we had completed the penultimate draft of the first edition the media was rather quiet. Some large-scale developments in the United States were becoming known (but now with no hoopla) within the supercritical fluids community. Supercritical fluids were, therefore, no longer a laboratory curiosity; no more “promises” and no more “blast-offs” were seen in the trade literature from 1985 to early 1986. So we thought the supercritical fluids community had matured.

Unfortunately, in about 1987 the hype of supercritical fluids was renewed, this time in concert with another subject that was being discussed with impassioned fervor: cholesterol. Low cholesterol or no cholesterol became a prominent marketing slogan in 1988. Cholesterol-free corn oil and margarine, to name just two, appeared on the supermarket shelves. The irony is that these vegetable oils never had any cholesterol to begin with, but “cholesterol-free” was a powerful consumer attractant. Table 1.2 bears witness to the merging of supercritical fluids and cholesterol issues in another swirl of activity reminiscent of the early 1980s, when SCF technology was touted for energy reduction and other applications.

The SCF–cholesterol articles listed in table 1.2 also have broad claims.

You can have a tasty, juicy steak without fat and cholesterol—just as soon as scientists perfect a process they call supercritical fluid extraction.

... basing their hope on a process called supercritical fluid extraction.

**Table 1.2** Articles on SCF Technology Applied to Cholesterol Applications Appearing in the Trade Literature

<i>Title</i>	<i>Magazine</i>
Process for Removing Cholesterol from Milk Seen as Commercially Viable	<i>Chemical Reporter</i> , 1989
High Tech Lowers Dairy Cholesterol	<i>Food Development</i> , 1989
Scientists Are Working to Remove Fat and Cholesterol from Meat	<i>Illinois Agricultural News</i> , 1989
Dairies Skim Cholesterol from Milk	<i>Wall Street Journal</i> , October, 1988
In Search of a Cholesterol Solution	<i>Farm Forum</i> , 1990

... supercritical fluid extraction could have a world-wide impact on the dairy industry.

... the [SCF] process may have other benefits ... it can help reduce the unhealthy saturated fats in butter that are still present after cholesterol has been removed.

... egg yolks are fed down a column, CO<sub>2</sub> removes 75–85% cholesterol while retaining flavor ...

Some of these statements and the attendant hopes are lamentable. It might be advantageous to extract the cholesterol from a juicy steak without altering any of its other properties, such as taste, for example, but it won't happen because carbon dioxide cannot penetrate the dense protein–lipoprotein structure to extract the inextricably entwined cholesterol; it's not because the scientists won't "perfect" the process they call supercritical fluid extraction. On the other hand, some food scientists have finally recognized that fact and are using carbon dioxide to extract cholesterol and fat from meat products that have first been freeze dried. This process makes the fat and cholesterol amenable to extraction, but even here selective extraction of cholesterol is not possible. The processing of liquid egg yolks with SCF solvents to remove the cholesterol is also another difficult proposition based on scientific facts. Merely passing egg yolks downward in a column with supercritical carbon dioxide is inadequate. The solvent will not selectively extract a significant amount of cholesterol without drying the egg yolk or without also removing a significant part of the lipids. This is because a large solvent-to-feed ratio is required. Even presaturating the carbon dioxide with water does not remove the difficulty of selectively extracting cholesterol from liquid egg yolks. If the egg yolk is dried by spray or freeze drying, it is possible to remove cholesterol and lipids from the egg. And concerning the statement above about "extracting saturated fats from butter after removing the cholesterol" since butter contains over 50% saturated fatty acids, we wonder what will be the result if the "unhealthy saturated fats in butter" are removed along with the cholesterol.

Because of all the ill-advised and ill-fated developments of the early 1980s, and because of the sometimes desperate attempts of various research groups to garner publicity on their applications of supercritical fluids to develop low cholesterol milk, meat, and liquid eggs, supercritical fluids are still today frequently met with skepticism whenever they are suggested as a solution to a real problem even in spite of general knowledge of the large-scale industrial successes in coffee, tea, hops, spices, and hops. We have chosen to discuss these less than lustrous periods in the progression of supercritical fluid technology to highlight the exaggerated claims that were later found to be merely that, exaggerations. Supercritical fluids may have been misapplied in the past, but that is no reason to dismiss them in the future. We reiterate throughout the book that each application must be evaluated on a case-by-case basis to determine the potential viability of supercritical fluids. In later chapters, we discuss some of the technical developments mentioned in the above articles, and we point out why some of the developments were ill-fated.

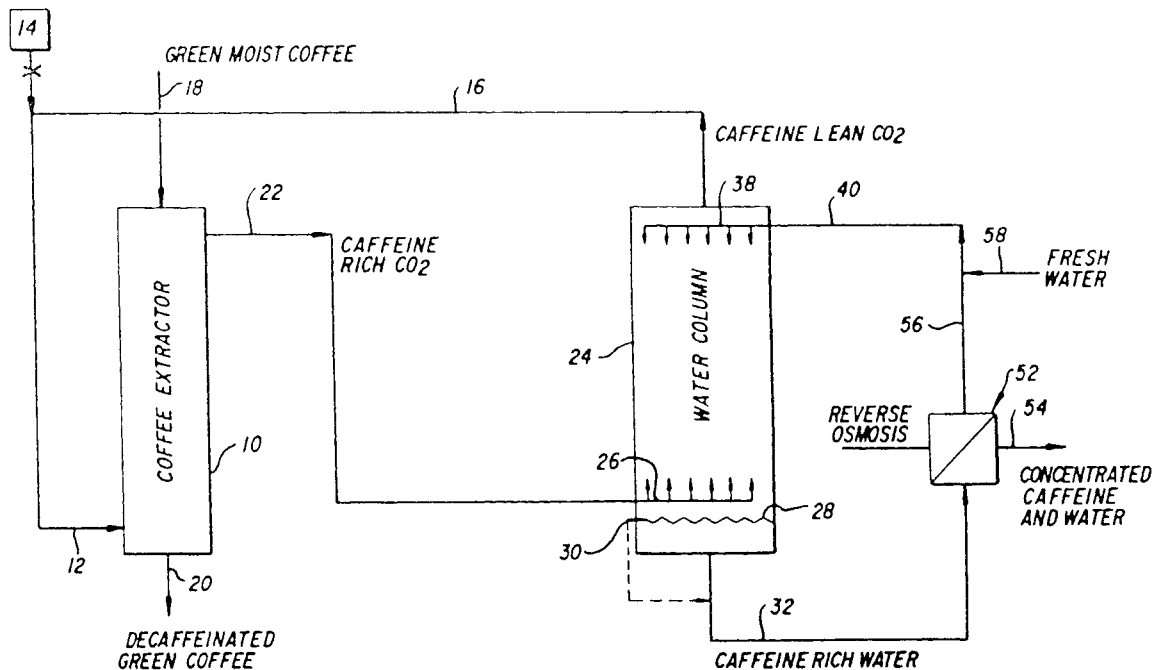
Several large-scale plants are in operation throughout the United States and Europe. Events in Europe were very different from events in the United States. Plants in Germany, France, and the United Kingdom were commissioned for coffee, tea, hops, spices, and flavor extraction, while in the United States the difficulties of scaleup and the magic properties of SCF were being discussed. However, in mid-1985 Pfizer began operation of a hops extraction plant in Sydney, Nebraska, stated to be the largest carbon dioxide extraction plant in the world (Cookson, 1987); Kraft General Foods (Maxwell House Coffee Division) started construction on a coffee decaffeination plant in Houston, Texas, and we use information about that plant to corroborate that supercritical fluid extraction is no longer a laboratory curiosity.

Figure 1.1 shows part of the coffee decaffeination plant at a very early stage of construction. A vessel 7 ft diameter  $\times$  70 ft fall (roughly scaled from other parts of the photograph, namely the personnel at the top of the yet unfinished structural steel), is being brought into position by a crane; the crane, quite interestingly, is the world's largest. Figure 1.2 is a diagram of the Maxwell House coffee decaffeination process described in a Kraft General Foods coffee patent (US 4,996,317, Katz et al., 1990). We consider the process an engineering marvel that combines technical, economic, and environmental aspects of an advanced technology that is applied to a commodity material (a quite inexpensive commodity, we point out, with wholesale coffee beans selling at about \$1 per pound).

In the process depicted in figure 1.2, coffee beans charged to the extractor, 10, via line (18) are decaffeinated with supercritical carbon dioxide. The caffeine-laden  $\text{CO}_2$  stream leaving the extractor is passed into the bottom of a water-wash column where the caffeine is removed from the  $\text{CO}_2$ . (Chapter 8 describes the thermodynamic equilibrium situation for the water-wash column.) The caffeine-free  $\text{CO}_2$  is recycled to the coffee bean column, and decaffeinated coffee beans leave the extractor via line 20. Let's now follow the water stream leaving the bottom of the  $\text{CO}_2$  scrubbing tower. The caffeine-



**Figure 1.1** Extraction vessels used in the Maxwell House Coffee Company super-critical  $\text{CO}_2$  decaffeination plant in Houston, Texas.



**Figure 1.2** The first semicontinuous solid-supercritical fluid decaffeination process to be developed and commercialized.



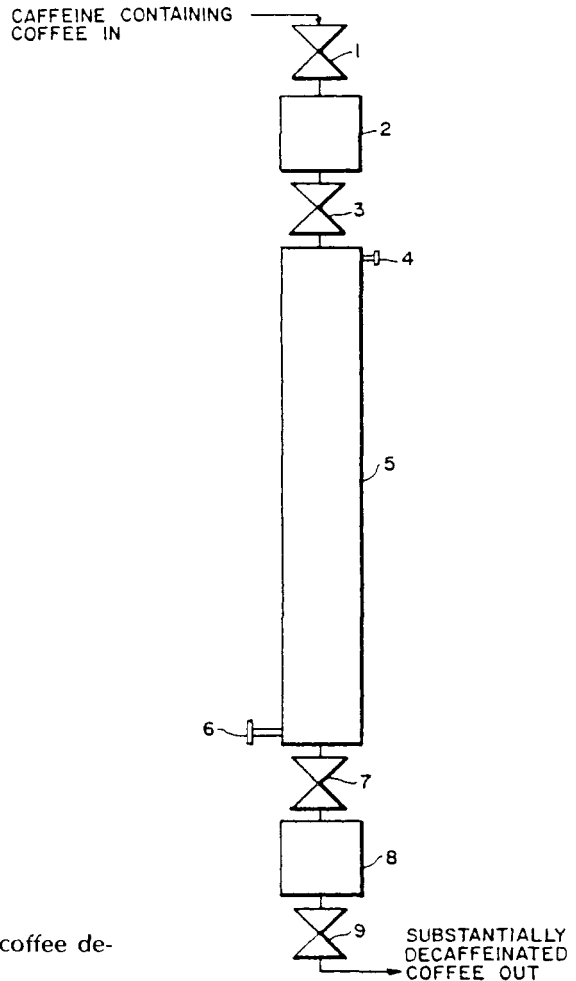


**Figure 1.3** The Maxwell House coffee decaffeination process.

laden water stream leaving the bottom of the  $\text{CO}_2$  scrubbing tower is sent to a reverse osmosis (RO) separator, the caffeine is concentrated, and the “purified” water stream (56) is returned to the water-wash column. The high concentration caffeine-water stream leaving the RO separator is recrystallized to recover caffeine. The net products are decaffeinated (green) coffee beans, which are sent to roasting towers, and caffeine, which is sold to pharmaceuticals and/or cola companies. Although Kraft General Foods has never announced the throughput of the plant, the “intelligence” in the supercritical fluid community places the production volume at about 50 million lb/yr.

Let us describe some of the engineering details of the operation of the decaffeination column given in another patent (US 4,820,537, Katz, 1989). In later chapters we describe two types of processing. One is batch-continuous

processing, where a batch of solid material is charged to a vessel and then is contacted with a continuous stream of gas. The other is continuous countercurrent processing, where continuous liquid–fluid streams flowing in opposite directions are contacted. The decaffeination process whose schematic diagram is shown in figure 1.2 is the first semicontinuous solid–supercritical fluid process that has been developed and commercialized. Semicontinuous signifies that coffee beans are intermittently charged to and removed from the decaffeination vessel under pressure without shutting down the process. In figure 1.3 the extractor is fitted with lock hopper vessels above and below the extractor (2 and 8, respectively). While operating under pressure, the inlet and outlet valves (3 and 7) are energized. While the supercritical carbon dioxide is flowing through the decaffeination vessel, some of the vessel volume is discharged to the bottom hopper and coffee beans are simultaneously fed to the extractor from the top hopper. The valves are then closed and the respective lock hoppers filled and emptied simultaneously, ready for the next charge to the extractor.

The Katz patent states that about 15% of the coffee beans in the extractor are discharged and admitted during a semicontinuous pulse. To provide an estimate of the scale of the process we here calculate the amount of coffee beans moved during a pulse. The vessel is 70 ft tall  $\times$  7 ft diameter; this equates to an internal volume of about 2500 ft<sup>3</sup>. Coffee beans have a density of about 40 lb/ft<sup>3</sup>, so the extraction vessel holds about 100,000 lb of coffee beans. A 15% replenishment is a rate of 15,000 lb per pulse, and the pulse happens about every 30 to 60 min—this is not laboratory scale operation. There are still many other hops extraction, coffee decaffeination, and spice extraction plants throughout the United States and Europe; several of them operate at 30 to 60 million lb/yr throughput, further exemplifying that SCF extraction is not just a laboratory curiosity.

Another pictorial example that SCF extraction is being operated on a large scale, figure 1.4 is a photograph of the tea decaffeination plant built and operated by SKW/Trosstberg in Meunschmeunster, Germany. Lipton's decaffeinated tea is processed at this plant, and the intelligence in the community places the production volume at about 15,000,000 lb/yr. The photograph shows only the tops of the three extraction vessels, but the size of the vessels can be scaled from a plant technician who is visible in the doorway at the left of the photograph. The bottom of each vessel extends down two stories, and each vessel is charged with about 2,000 lb of tea leaves for the extraction cycle. The tea decaffeination process, like the General Foods process described previously, operates at constant pressure; the caffeine-containing CO<sub>2</sub> stream leaving the extractor passes through an activated carbon adsorber which removes the caffeine, and the CO<sub>2</sub> is recycled.

It is worthwhile at this point to review briefly some of the interesting properties and characteristics of supercritical fluids. With a supercritical fluid (SCF) solvent it is possible to separate a multicomponent mixture by capitalizing on both the differences in component volatilities (i.e., the salient



**Figure 1.4** A tea decaffeination plant.

feature of distillation) and the differences in the specific interactions between the mixture components and the SCF solvent (i.e., the salient feature of liquid extraction). As the critical point of a substance is approached, its isothermal compressibility tends to infinity, thus its molar volume or density changes dramatically. In the critical region a substance that is a gas at normal conditions exhibits a liquid-like density and a much increased solvent capacity that is pressure-dependent. The variable solvent capacity of a supercritical fluid is the basis on which separations processes can be devised. Table 1.3 lists the critical temperatures and pressures for a variety of candidate SCF solvents, and figure 1.5, a schematic pressure-temperature diagram, shows the region where the largest changes in solvent properties occur. A cursory inspection of the entries in this table shows that many hydrocarbons have a critical pressure close to 45 bar and the critical temperature of SCF solvents increases as the molecular weight of the solvent increases or as the polarity or intramolecular hydrogen bonding of the solvent increases. This means that the solvent's vapor pressure curve extends to very high temperatures (see figure 1.5). So even though water is a low molecular weight compound, it has an extremely high critical temperature. It takes a large amount of thermal energy to break the hydrogen bonds between water molecules to allow them to vaporize into the gas phase. As table 1.3 shows, the critical temperatures of gases and liquids can differ by hundreds of degrees; this difference suggests the use of specific supercritical fluids in specific applications. For example, because the critical temperatures of carbon dioxide, ethane, and ethylene are near ambient, they are attractive solvents for processing heat-sensitive flavors, pharmaceuticals,

**Table 1.3** Critical Conditions for Various Solvents

<i>Solvents</i>	<i>Critical Temperature (°C)</i>	<i>Critical Pressure (bar)</i>
Carbon dioxide	31.1	73.8
Ethane	32.2	48.8
Ethylene	9.3	50.4
Propane	96.7	42.5
Propylene	91.9	46.2
Cyclohexane	280.3	40.7
Isopropanol	235.2	47.6
Benzene	289.0	48.9
Toluene	318.6	41.1
<i>p</i> -Xylene	343.1	35.2
Chlorotrifluoromethane	28.9	39.2
Trichlorofluoromethane	198.1	44.1
Ammonia	132.5	112.8
Water	374.2	220.5

labile lipids, and reactive monomers. Substances that are less temperature-sensitive, such as most industrial chemicals and polymers, are readily treated with the C<sub>3</sub> and C<sub>4</sub> hydrocarbons with critical temperatures in the range 100–150°C; the C<sub>3</sub> and C<sub>4</sub> hydrocarbons are generally better solvents for polymers than the C<sub>2</sub> hydrocarbons. Still higher molecular weight hydrocarbons, such as cyclohexane and benzene, with high critical temperatures of 250–300°C, are used to process nonvolatile substances such as coal and high molecular weight petroleum fractions. Supercritical water, at the high end of the temperature spectrum of common solvents, has a critical temperature of 374.2°C; it is being tested for hazardous-waste detoxification and hydrocarbon reforming.

Scientists and engineers have been aware of the enhanced solvent characteristics of SCF solvents for more than one hundred years, but it is only in the past two decades that SCF solvents have been the focus of active research and development programs and much media hype. Not all of the hype from the media was without merit, as the technical community devoted a great deal of time and money to the study of supercritical fluids and their properties. There was a large increase in the number of symposia, review papers, and short courses or tutorials between 1940 and 1972 (Booth and Bidwell, 1949; Rowlinson and Richardson, 1958; Valteris, 1966; Paul and Wise, 1971; Ellis, 1971) and 1977 to the mid-1980s (Irani and Funk, 1977; Gangoli and Thodos, 1977; Schneider, Stahl, and Wilke, 1980; Williams, 1981; Brunner and Peter, 1981; Randall, 1982; Paulaitis et al., 1983; Johnston, 1984; McHugh and Krukonis, 1984; Mansoori et al., 1985; McHugh, Krukonis, and Davidson, 1985; McHugh, 1986).

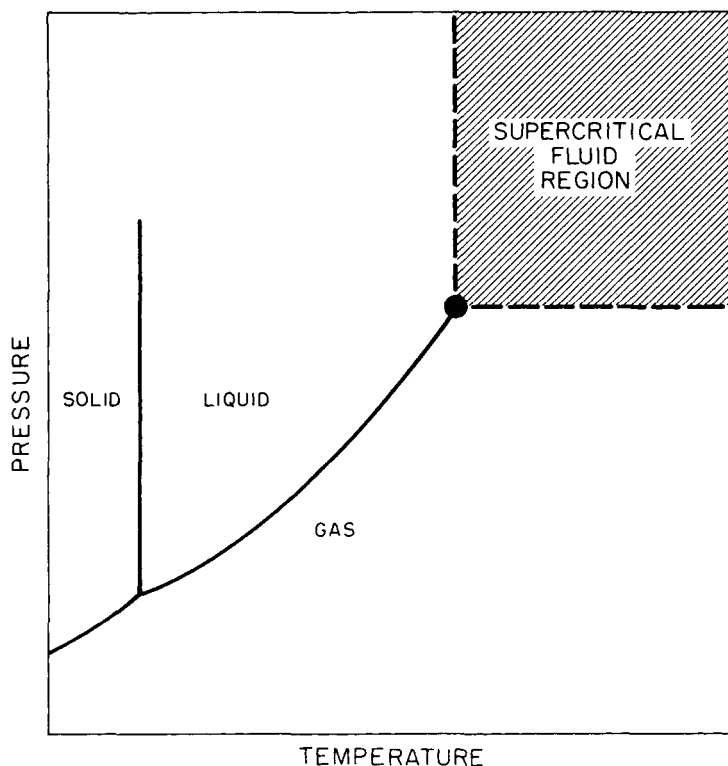


**Figure 1.5** Pressure-temperature diagram for a pure component.

Supercritical fluids begin to exhibit significant solvent strength when they are compressed to liquid-like densities (see chapter 5). This makes physical sense intuitively since we all know that gases are not considered as solvents. Figure 1.6 shows how the density of a pure solvent changes in the region of its critical point. For a reduced temperature ( $T_R = T/T_c$ ) in the range 0.9–1.2 the reduced solvent density ( $\rho_R = \rho/\rho_c$ ) can increase from gas-like values of 0.1 to liquid-like values of 2.5 as the reduced pressure ( $P_R = P/P_c$ ) is increased to values greater than  $\sim 1.0$ . But as  $T_R$  is increased to 1.55, the supercritical fluid becomes more expanded and reduced pressures greater than ten are needed to obtain liquid-like densities. By operating in the critical region, the pressure and temperature can be used to regulate density, which regulates the solvent power of a supercritical fluid.

Let us briefly describe one example of the ability to fine-tune the solvent power of an SCF solvent by considering the solubility behavior of solid naphthalene ( $T_m = 80.2^\circ\text{C}$ ) in supercritical ethylene ( $T_c = 9.3^\circ\text{C}$ ,  $P_c = 50.5$  bar) near the critical point of pure ethylene (Diepen and Scheffer, 1953; Tsekhanskaya, Iomtev, and Mushkina, 1964). Figure 1.7 shows how

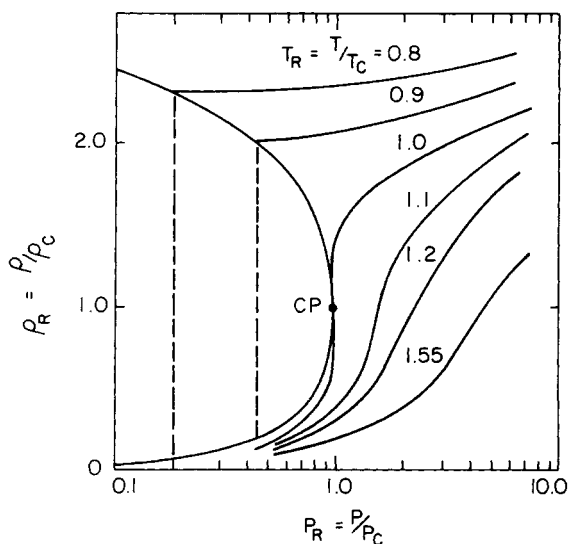


**Figure 1.6** Variation of the reduced density ( $\rho_R$ ) of a pure component in the vicinity of its critical point.

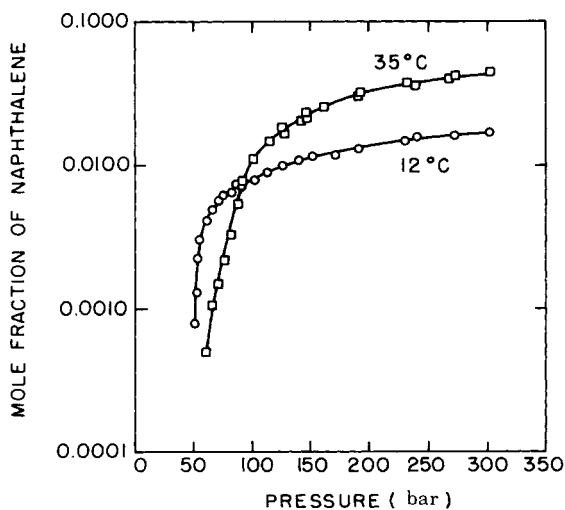


**Figure 1.7** Solubility behavior of solid naphthalene in supercritical ethylene (data of Tsekhanskaya, Iomtev, and Mushkina, 1962; and Diepen and Scheffer, 1948b).

naphthalene solubility changes with temperature and pressure. Along the 12°C ( $T_R = 1.01$ ) isotherm, the solubility of solid naphthalene in supercritical ethylene increases quite dramatically as the pressure is increased to 50 bar, essentially the critical pressure of ethylene. At pressures below 50 bar, naphthalene solubility is extremely low, as we would expect for the solubility of a solid in an expanded gas. At pressures much greater than about 90 bar, the solubility of naphthalene in ethylene reaches a limiting value of about 1.5 mol%. The solubility behavior along this isotherm is closely related to the

variation in the reduced density of ethylene depicted in the reduced isotherm at 1.0 in figure 1.6. Note that the 12°C isotherm has the same characteristic shape as the reduced density isotherm at 1.0. Although this example suggests that, to a first approximation, SCF solvent strength is related to solvent density, it is the interactions between solvent and solute molecules that determine how much solute dissolves in the SCF solvent. By compressing the solvent to liquid-like densities we have only increased the probability that solvent and solute molecules will interact. The types of interactions (e.g., dispersion, polar, hydrogen bonding) depend on the physical characteristics of each of the species in the mixture.

Let us do a simple calculation to obtain an appreciation of the enhancement in solvent power obtained by compressing a gas into its critical region. An estimate of the solubility of a solid in an SCF solvent can be made using the following expression, explained in detail in chapter 5.

$$y_2 = \left( \frac{P_2^{\text{sub}}}{\phi_2 P} \right) \exp \left( \int_{P_2^{\text{sub}}}^P \frac{v_2^s}{RT} dP \right), \quad (1.1)$$

where the subscript 2 refers to the solid component,  $P_2^{\text{sub}}$  is the sublimation pressure of the solid,  $v_2^s$  is the molar volume of the solid, and  $\phi_2$  is the fugacity coefficient, a factor that accounts for specific repulsive and attractive interactions that occur between solvent and solid component molecules (Prausnitz, 1969). Now let us compare the experimentally observed solubility of naphthalene ( $y_2$ ) at 100 bar and 12°C with the solubility calculated if the supercritical fluid phase is assumed to behave like an ideal gas—that is, when  $\phi_2$  is equal to one. At 12°C and 100 bar the sublimation pressure of naphthalene is 0.000 0303 bar (Diepen and Scheffer, 1953), and for pressures up to about 1,000 bar,  $v_2^s$  is a constant equal to 111.9 cc/mol (Vaidya and Kennedy, 1971). Hence, at 100 bar and 12°C, we find that:

$$\frac{y_2^{\text{observed}}}{y_2^{\text{calculated}}} = 16,156. \quad (1.2)$$

This large increase in the solvent power of ethylene on compression to 100 bar cannot be attributed to a hydrostatic pressure effect on the vapor pressure of naphthalene, since the pressure effect is explicitly accounted for in the exponential term in equation 1.1. Instead, the large difference in experimental and calculated naphthalene solubility at high pressures is associated with the nonideal behavior of ethylene as it is compressed to liquid-like densities in its critical region. It is the strength of the interactions between solvent and solute molecules that fixes the solubility depending of course on whether the solvent molecules are in close enough proximity to interact. Chapters 3 and 5 delve more deeply into intermolecular interactions and solubility behavior.

Solid naphthalene–SCF behavior is used throughout this book as a model system whose principles can be applied to many practical SCF separation

problems, such as the extraction of (almost solid) oleoresins, the color and taste ingredients from spices and red peppers (Stahl et al., 1980); the separation of solid aromatic isomers (Krukonis and Kurnik, 1985); and the removal of lower molecular weight constituents from coal at elevated temperatures using an SCF with a high critical temperature, such as toluene (Williams, 1981). Of course, there are many other examples of industrial separations in which the components to be separated are liquids not solids. The SCF solvent can be appreciably soluble in the liquid mixture, whereas it was previously assumed that the SCF solvent did not dissolve in the crystalline solid. Another distinct subset of solid-SCF behavior occurs with amorphous solid polymers that can sorb large amounts of SCF solvent (Liau and McHugh, 1985). The mutual solubility of SCFs and liquids complicates the phase behavior somewhat, but the descriptions of SCF-liquid phase diagrams are no more complicated than the ones used to describe conventional liquid-liquid extraction processes (McCabe and Smith, 1976).

In addition to its unique solubility characteristics, a supercritical fluid possesses certain other physicochemical properties that add to its attractiveness. For example, even though it possesses a liquid-like density over much of the range of industrial interest, it exhibits gas-like transport properties of diffusivity and viscosity (Schneider, 1978). Additionally, the very low surface tension of supercritical fluids allows facile penetration into microporous materials to occur.

Figure 1.8 shows the self-diffusivity of carbon dioxide over a wide pressure-temperature range and, for comparative purposes, the range of diffusivities for solutes in organic liquids (averaging, as is well known, about  $10^{-5}$  cm<sup>2</sup>/sec) is also provided (Paulaitis et al., 1983a). The self-diffusion coefficient for carbon dioxide (which is approximately the same as the diffusion coefficient of a similarly sized molecule diffusing through carbon dioxide) is about one or two orders of magnitude higher than the diffusivity of solutes in liquids.

The viscosity behavior of carbon dioxide is shown in figure 1.9. Although the viscosity changes rapidly in the critical region (similar to diffusivity in figure 1.8), even at the high pressure levels of 300–400 bar it is only about 0.09 centipoise (cps), an order of magnitude below typical viscosities of liquid organic solvents (de Filippi et al., 1980). The properties of gas-like diffusivity and viscosity, zero surface tension, and liquid-like density combined with the pressure-dependent solvent power of a supercritical fluid have provided the impetus for applying SCF technology to a gamut of separations problems experienced in many segments of industry. Although the combination of properties of an SCF solvent does indeed make it a potentially attractive solvent, sometimes these properties offer no advantage relative to the properties of conventional solvents. SCF technology needs to be evaluated case by case, as illustrated by the numerous examples covered in this book.

Perhaps the most often misinterpreted properties of supercritical fluids are their mass transfer properties. It is often claimed that SCF extraction processes



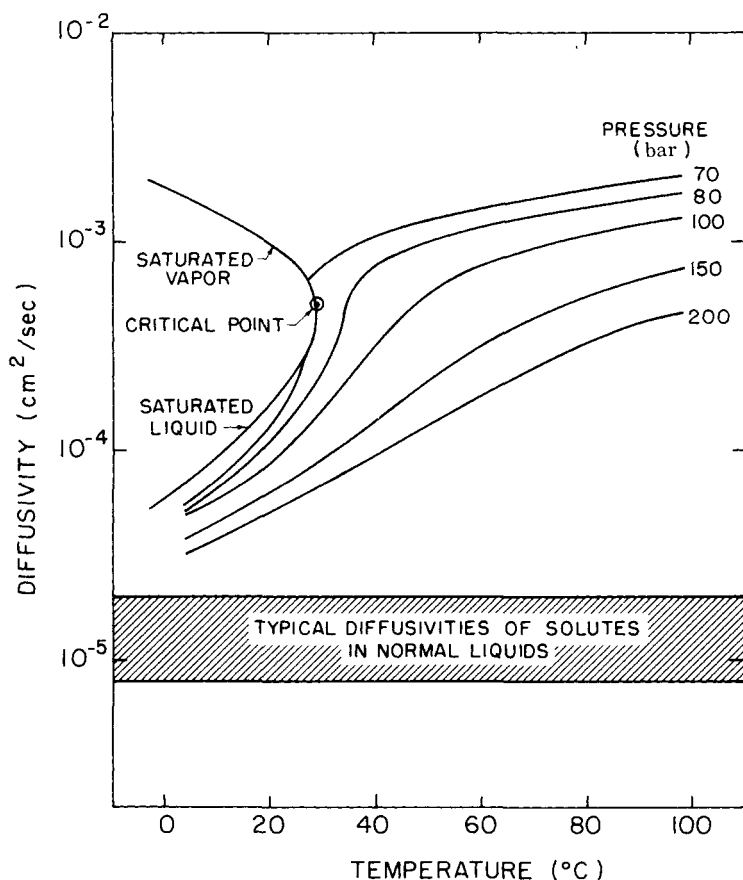
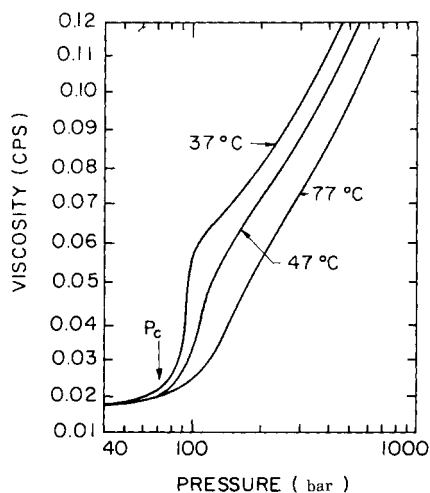


Figure 1.8 Diffusivity behavior of carbon dioxide.

do not experience the mass transfer limitations of a liquid extraction process. This statement is quite often incorrect. If the rate-limiting step (or the largest mass transfer resistance) of a separations process is the actual transfer of a material from the surface of a solid to the extract phase, then a gas-like diffusivity will certainly enhance diffusion in an extraction carried out with a supercritical fluid relative to the extraction carried out with a liquid solvent. If, on the other hand, the extraction is from a liquid phase into a supercritical fluid phase, probably more typical in an industrial situation, then the resistance to diffusion in the liquid phase will probably be the rate-determining step. In this situation, the gas-like diffusion characteristics of the SCF solvent will not have an enhancing effect on the overall mass transfer rate. Similarly, if the extraction is occurring from within a nonporous particle, such as a polymer, where internal solid phase diffusion will probably govern the overall rate of mass transfer, the external phase diffusion (of a gas, a liquid, or an SCF) will



**Figure 1.9** Viscosity behavior of carbon dioxide.

have little or no effect on the rate of mass transfer. But if the SCF phase alters the internal characteristics of the polymer, it will affect the rate of mass transfer. This can occur with certain SCF-polymer systems and is discussed in chapters 9 and 12.

The practical as well as fundamental principles governing SCF processing are considered in detail in later chapters. These principles have fascinated chemists and chemical engineers for more than a century. The history of these unique solvents is detailed in chapter 2. The reader will, in fact, find that a substantial amount of information was known about supercritical fluids as far back as the early 1800s.

---

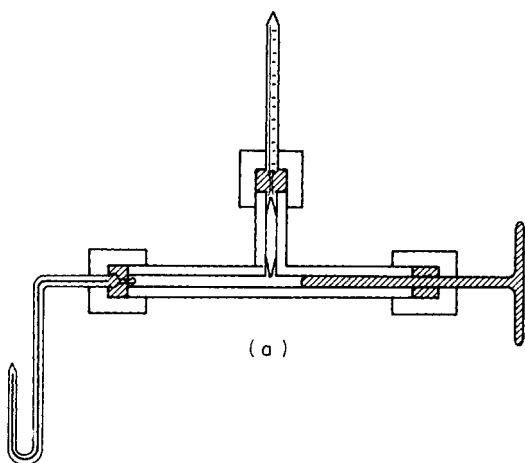
## Historical Perspective

---

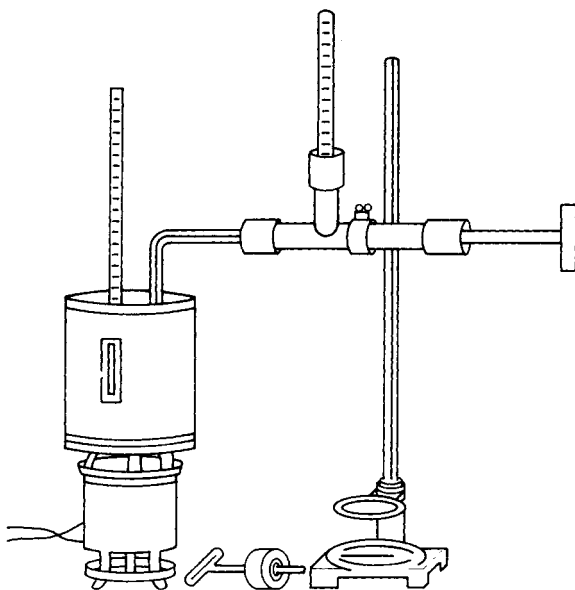
The ability of a supercritical fluid to dissolve low-vapor-pressure solid materials was first reported by Hannay and Hogarth at a meeting of the Royal Society of London in 1879 (Hannay and Hogarth, 1879, 1880). Hannay and Hogarth described their experiments, carried out in small-diameter glass tubes, in which they observed that changes in pressure caused several inorganic salts (e.g., cobalt chloride, potassium iodide, and potassium bromide) to dissolve in or precipitate from ethanol at a temperature above the critical temperature of ethanol ( $T_c = 234^\circ\text{C}$ ). They found that increasing the pressure on the system caused the solutes to dissolve and that decreasing the pressure caused the dissolved materials to nucleate and precipitate “as a snow.”

A brief description of the apparatus used by late nineteenth century scientists measuring critical phenomena and SCF solubility highlights their experimental techniques, their care, and their precision. Figure 2.1a is a schematic diagram of the glass view cell, pressure generator, and pressure measurement device used by Hannay and Hogarth. The liquid or solid phase is first placed inside a small-bore glass tube, which is then bent and inserted into the pressure generator system. The tee bar seen at the right in figure 2.1a is a screw-feed plunger that is fitted and sealed against leakage inside a small-bore glass tube filled with mercury. The vertical tube seen in the figure is an air manometer used for pressure measurement. As the plunger is advanced, it compresses both the air in the manometer and the contents in the glass tube. From the observed volume decrease of air and the accepted volumetric properties of air, the pressure in the system is calculated. The temperature of the material in the bent tube is adjusted by the bath shown in figure 2.1b.

Other types of early experimental designs described in the literature attest to the creativity of Hannay and Hogarth's predecessors and contemporaries working with high pressures. For example, Baron Cagniard de la Tour discovered the critical point of a substance in 1822. In fact, for many years the critical point was referred to as the Cagniard de la Tour point. In his earliest experiments Cagniard de la Tour (1822) used a piece of rifled cannon for his high-pressure investigations. He sealed a liquid and a flint ball in the cannon barrel, heated the barrel, and rocked it while listening for changes in the sound of the rolling ball or for changes in the sound made when the barrel was



(a)



(b)

**Figure 2.1** Schematic diagram of the experimental apparatus used by Hannay and Hogarth to obtain solid solubilities in supercritical fluids. The glass tubing (a) is first connected to an air manometer and is then immersed in the constant temperature bath (b).

tapped. Discontinuities in the sound (noted while the baron held his ear to the sealed end of the cannon) led him to describe the point we today know as the critical point. He later carried out experiments in glass tubes so that he could visually observe critical phenomena.

Supercritical carbon dioxide attracted much attention in the latter half of the nineteenth century. Dr Thomas Andrews, vice-president of Queen's

College, Belfast, carried out an extensive investigation in the mid-1800s on the phase behavior of carbon dioxide. In his now quite famous Bakerian Lecture delivered to the Royal Society in 1869 he described his experimental apparatus (which was modified slightly by Hannay and Hogarth) and his observations of the critical properties of carbon dioxide (Andrews, 1875–76). In his lecture he related that

On partially liquefying carbonic acid by pressure alone, and gradually raising at the same time the temperature to 88°Fahr., the surface of demarcation between the liquid and gas became fainter, lost its curvature, and at last disappeared. The space was then occupied by a homogeneous fluid, which exhibited, when the pressure was suddenly diminished or the temperature slightly lowered, a peculiar appearance or flickering striae throughout its entire mass. At temperatures above 88°F no apparent liquefaction of carbonic acid, or separation into two distinct forms of matter, could be effected, even when a pressure of 300 or 400 atmospheres was applied.

The values that Dr Andrews reported for the critical point of carbon dioxide, 30.92°C and 74.0 bar, are in close agreement to presently accepted values, 31.1°C and 73.8 bar.

In 1879 Amagat described a method for compressing gases to ~400 bar using mercury columns extending to the bottom of a mine shaft (Amagat, 1879). And in 1891, two years after the construction of the Eiffel Tower, Cailletet generated high pressures with a mercury column reaching to the top of the tower (Cailletet, 1891). These high-pressure experiments were not without their problems, however, as many reports of ruptured steel tubes (of 0.64 cm inside and 5.08 cm outside diameter) are recorded in the literature during this period.

There was substantial controversy about the initial finding of the pressure dependence of solubility in a supercritical fluid after it was first reported at the October 1879 Royal Society meeting. One month after hearing the paper of Hannay and Hogarth, Professor William Ramsay of the chemistry department, University College, Bristol, reported to the Royal Society that he had carried out the experiments described by Hannay and Hogarth and concluded from these reproductions that “the gentlemen have observed nothing unusual, but merely the ordinary phenomenon of solubility of a solid in a hot liquid” (Ramsay, 1880).

In later presentations to the Royal Society, Hannay responded to Ramsay’s charge, asking “permission to point out some errors into which Prof. Ramsay had fallen.” In addition to pointing out those errors, Hannay discussed still other experiments that later substantiated the pressure-dependent dissolving power of a supercritical fluid as a new phenomenon (Hannay, 1880).

This older literature provides very interesting reading. Professor Ramsay, who questioned the results of Hannay and Hogarth, went on to write scores of papers on critical-point phenomena, thermodynamics, and vapor–liquid equilibria, but he was wrong about his “hot liquid” conclusion. It must be

remembered that the exchanges at the Royal Society meetings occurred when critical point phenomena were still incompletely understood or accepted. During this period such luminaries as van der Waals were explaining the volumetric behavior of real gases, and Amagat, Joule, Thomson, Cailletet, Clausius, and Dewar were engaged in other experimental and theoretical investigations of critical phenomena.

Although Hannay and Hogarth first studied the solubility of inorganic salts in supercritical ethanol, the pressure-dependent dissolving power of an SCF is not limited to inorganic salt solutes. It is a general phenomenon exhibited by all supercritical solvent-solute pairs (as long as the solute is not infinitely miscible with the solvent). After the first report by Hannay and Hogarth, a number of other authors reported solubility phenomena with a variety of SCF solvents and organic solid and liquid solutes. SCF solvents included carbon dioxide, nitrous oxide, and the light hydrocarbons; and solutes covered the gamut of organic compounds, namely, aliphatics, aromatics, halogenated hydrocarbons, heteromolecules, triglycerides, and the like.

Although emphasis in this book is given to solubility phenomena at supercritical conditions, a number of early studies reported in the literature focused on the phase behavior and solvent characteristics of near-critical, liquid carbon dioxide. The earliest published work on liquid CO<sub>2</sub> as a solvent is that of Gore (1861). Gore found naphthalene and camphor to be soluble in liquid CO<sub>2</sub>, but he concludes that liquid CO<sub>2</sub> is "a very feeble solvent of substances in general." He made this general conclusion after having tested only a small number of organic compounds, some of which just happened to exhibit very low solubility. In fact, liquid carbon dioxide is a very good solvent for many classes of compounds.

In 1896 Villard published a review of supercritical fluid solubility phenomena (Villard, 1896). He described the ability of methane, ethylene, carbon dioxide, and nitrous oxide to dissolve a number of liquids and solid hydrocarbons such as carbon disulfide, camphor, stearic acid, and paraffin wax. He reported on a (then) strange phenomenon. As solid camphor is subjected to ethylene at increasing pressure, it liquefies then "vaporizes" (i.e., it dissolves in the ethylene at higher pressures). This is, perhaps, the first reported observation of the interaction of a high-pressure gas with a solid hydrocarbon that results in the lowering of the normal melting point of the pure solid. The melting point depression and the topic of solid solubilities in supercritical fluids are discussed at length in chapter 3, where the work of Diepen, Scheffer, and coworkers is described. Villard published other papers on high-pressure phenomena and he is perhaps better known for his experimental work on gas hydrates (Villard, 1888).

Several years after Villard's paper, E. H. Büchner reviewed the literature and also made significant additions to the experimental data base of high-pressure SCF-solute mixtures (Büchner, 1906). He carried out his studies over a wide temperature range, and he used observations of cloud points, freezing points, and the number of phases present for his solubility determinations.

Although his work was primarily of a qualitative nature, the concept of a cloud point and a freezing (or melting) point depression of a solid can be extended to yield quantitative solubility information. The present day experimental techniques used to determine the melting point depression of a solid are covered in chapter 4.

Within the past ten years a large number of authors have cited the solubility behavior of the naphthalene–ethylene system as the impetus for their own SCF studies. We trace the origins of naphthalene–SCF phase behavior studies because this system has, in fact, been very extensively studied and the features of the phase behavior are evident in many other solute–SCF systems. Büchner was the first to investigate the solubility behavior of naphthalene in carbon dioxide. A few years later, Prins explored the solubility of naphthalene in both supercritical ethane and carbon dioxide (Prins, 1915). Prins determined three-phase border curves and critical end points for naphthalene in both gases. Researchers of the late 1800s and early 1900s met and overcame many obstacles in carrying out their studies. Today if one desires to measure the solubility of naphthalene in ethane, for example, the acquisition of materials would be quite easy. Calling the appropriate manufacturers and suppliers of chemicals and gases and placing the orders is all that is required, but it is of historical value to relate how Prins “acquired” his ethane. As he stated in his paper

The ethane was prepared by electrolyzing sodium acetate. The anode gas was purified by bromine water and a strong solution of potassium hydroxide dried over soda lime and condensed in a receiver with liquid air. Subsequently it was again dried over phosphorous pentoxide and separated from the more volatile part by fractionating by the use of liquid air. The disappearance of the discharge in a Geisler tube attached to the apparatus served as criterion on purity.

All this just to get the ethane for his supercritical fluid solubility studies.

Investigations of naphthalene solubility in supercritical fluids slowed until the late 1940s when Professor Scheffer and coworkers of the Technical University of Delft began to publish extensively on ethylene–naphthalene phase behavior. In 1948, a study of the solubility and phase behavior of naphthalene dissolved in supercritical ethylene was reported (Diepen and Scheffer, 1948b). This now classic paper was followed by several others on high-pressure phase behavior by the two authors and their coworkers (van Gunst, Scheffer, and Diepen, 1953a, 1953b; van Welie and Diepen, 1961a–e, 1963; van Hest and Diepen, 1963; Swelheim, de Swaan Arons, and Diepen, 1965; Koningsveld, Diepen, and Chermin, 1966; Koningsveld, Kleintjens, and Diepen, 1984; Koningsveld and Diepen, 1983; de Swaan Arons and Diepen, 1963; de Loss, Poot, and Diepen, 1983). These publications provided the impetus for other groups to examine the characteristics of naphthalene solubility in a variety of supercritical fluid solvents.

In the early 1960s, the solubility of naphthalene in a variety of other gases

was studied. Tsekhanskaya, Iomtev, and Mushkina (1962, 1964) from the Soviet Union measured naphthalene solubilities in ethylene and in carbon dioxide. Other naphthalene-SCF investigators included the following: King and Robertson (1962), who studied the solubility of naphthalene in supercritical hydrogen, helium, and argon; Najour and King (1966), who studied the solubility of naphthalene in supercritical methane, ethylene, and carbon dioxide; McHugh and Paulaitis (1980), who studied the solubility of naphthalene in supercritical carbon dioxide; Kurnik, Holla, and Reid (1981), who also studied the solubility of naphthalene in supercritical carbon dioxide; Schmitt and Reid (1984), who studied the solubility of naphthalene in supercritical ethane, trifluoromethane, and chlorotrifluoromethane; and, Krukonis, McHugh, and Seckner (1984) and McHugh et al. (1988), who studied the solubility and phase behavior of naphthalene using supercritical xenon as the solvent. Naphthalene solubility has been tested quite thoroughly and a large amount of data exists on its behavior over a wide range of pressures, temperatures, and compositions.

Scores of other researchers have investigated solubility phenomena with supercritical fluid solvents, and many works are cited in subsequent chapters. But in its breadth the work of A. W. Francis far surpasses his contemporaries'. In a single 1954 paper, he presented an extensive, quantitative study on the solvent properties of liquid CO<sub>2</sub> with hundreds of compounds (Francis, 1954). Primarily interested in the phase behavior of ternary systems containing liquid CO<sub>2</sub>, he collected data for 464 ternary phase diagrams and determined the solubilities of 261 compounds in near-critical, liquid CO<sub>2</sub>. He included many classes of organic compounds, e.g., aliphatics, aromatics, heterocyclics, and compounds with a large variety of functional groups. From his tables of data it is possible to formulate general rules on the solubility behavior of compounds in carbon dioxide. As an example of the breadth of his solubility studies, table 2.1 lists about fifty compounds and their solubilities in CO<sub>2</sub> studied by Francis.

Although Francis studied solubility behavior in liquid carbon dioxide (at approximately 25°C, 66 bar (950 psia)), his results are very general. For example, a compound that is soluble in liquid carbon dioxide will also be soluble in supercritical carbon dioxide. The level of solubility, which can be more or, in fact, less than that found in liquid CO<sub>2</sub>, will depend on the operating region in *P-T-x* space. Thus, the data of Francis can be used to assess the potential of supercritical fluid extraction for many separations before any experimental work is carried out. The importance of Francis's contribution cannot be overemphasized.

Since naphthalene-SCF mixtures have been so widely studied, it is instructive to consider the solubility behavior of just one of these systems, the naphthalene-CO<sub>2</sub> system, to highlight the solvent properties of a supercritical fluid solvent. In chapter 1 the effects of pressure and temperature on the solubility of naphthalene in ethylene were described. The solubility behavior is quite similar in carbon dioxide, in trifluoromethane, or even in xenon, although each system achieves its own absolute solubility level of naphthalene.



**Table 2.1** Solubilities of Selected Compounds in Liquid Carbon Dioxide at 25°C

	Weight Percent		Weight Percent
<i>Esters</i>		<i>Amines and Heterocyclics</i>	
Benzyl benzoate	10	Aniline	3
Butyl oxalate	M <sup>a</sup>	<i>o</i> -Chloroaniline	5
Butyl phthalate	8	<i>m</i> -Chloroaniline	1
Butyl stearate	3	<i>N,N</i> -Diethylaniline	17
Ethyl acetate	M	<i>N,N</i> -Dimethylaniline	M
Ethyl acetoacetate	M	Diphenylamine	1
Ethyl benzoate	M	<i>N</i> -Ethylaniline	13
Ethyl chloroformate	M	<i>N</i> -Methylaniline	20
Ethyl maleate	M	$\alpha$ -Naphthylamine	1
Ethyl oxalate	M	2,5-Dimethylpyrrole	5
Ethyl phthalate	10	Pyridine	M
Methyl salicylate	M	<i>o</i> -Toluidine	7
Phenyl phthalate	1	<i>m</i> -Toluidine	15
Phenyl salicylate	9	<i>p</i> -Toluidine	7
<i>Alcohols</i>		<i>Phenols</i>	
<i>t</i> -Amyl alcohol	M	<i>o</i> -Chlorophenol	M
Benzyl alcohol	8	<i>p</i> -Chlorophenol	8
Cinnamyl alcohol	5	<i>o</i> -Cresol	2
Cyclohexanol	4	<i>m</i> -Cresol	4
1-Decyl alcohol	1	<i>p</i> -Cresol	2
Methyl alcohol	M	2,4-Dichlorophenol	14
Ethyl alcohol	M	<i>p</i> -Ethylphenol	1
2-Ethylhexanol	17	<i>o</i> -Nitrophenol	M
Furfuryl alcohol	4	Phenol (MP 41°C)	3
Heptyl alcohol	6	$\beta$ -Methoxyethanol	M
Hexyl alcohol	11	Phenylethanol	3
<i>Carboxylic Acids</i>		<i>Nitriles and Amides</i>	
Acetic acid	M	Acetonitrile	M
Caproic acid	M	Acrylonitrile	M
Caprylic acid	M	Phenylacetonitrile	13
Formic acid	M	Succinonitrile	2
Isocaproic acid	M	Tolunitriles (mixed)	M
Lactic acid	0.5	Acetamide	1
Lauric acid	1	<i>N,N</i> -Diethylacetamide	M
Oleic acid	2	<i>N,N</i> -Dimethylacetamide	M
		Formamide	0.5

<sup>a</sup>M = miscible.

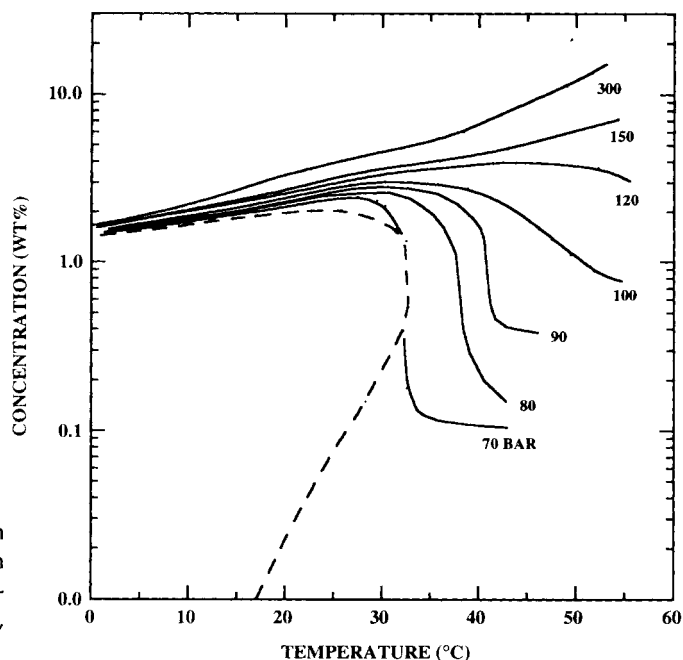


**Figure 2.2** Solubility of solid naphthalene in supercritical carbon dioxide (data assembled by Modell et al., 1979).

Figure 2.2 assembles data on the solubility of naphthalene in supercritical carbon dioxide from the large number of previously mentioned naphthalene studies. The data in this figure are plotted in a slightly different format, i.e., as solubility isobars. This method of displaying data removes the crossing of the curves seen in figure 1.7. Depending upon the pressure level, the temperature is seen to affect naphthalene solubility quite differently. For example, at 300 bar an increase in the temperature increases the solubility of naphthalene in carbon dioxide, whereas at a low pressure of 80 or 90 bar an increase in temperature decreases naphthalene's solubility.

The silica–water system shown in figure 2.3 is an example of another system that exhibits the general solubility behavior shown in figure 2.2. The critical properties of water are quite different from those of carbon dioxide and the solubility levels on the respective graphs are one or two orders of magnitude apart. But comparison of the two figures shows that the characteristic shapes of the solubility curves are similar. At a high pressure level, 1,750 bar in this case, increasing temperature causes the solubility of silica to increase; at the low pressure of 400 bar the solubility falls with increasing temperature.

The solubility of silica in supercritical water was first studied in the laboratory in 1879. It has some far-reaching influences in industry. During the production of high-pressure steam, silica that is present in the water is dissolved. The silica enters the (almost) closed-loop steam side partly through

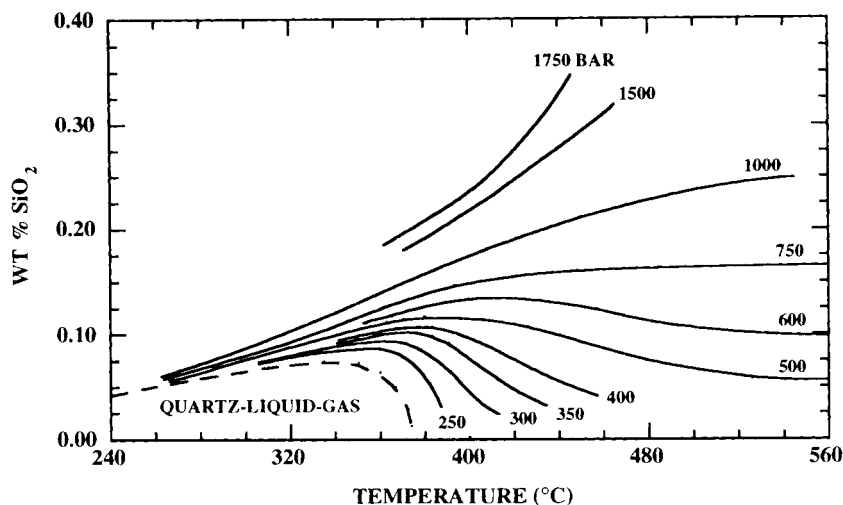


**Figure 2.3** Solubility behavior of solid silica in supercritical water (Kennedy, 1950).

makeup-water and mostly from condenser water leakage (silica is ubiquitous in groundwater). The silica dissolved in the supercritical steam is transported as dissolved species to the turbines. During the pressure decrease as the steam travels through the turbine, the silica deposits on the turbine blades. Eventually the turbine is shut down for cleaning. The presence of the silica in the turbines was not fully understood until the solubility and phase equilibria of the silica–water system were studied.

Besides silica–water, many other solid systems, such as phenanthrene, benzoic acid, phenol, and biphenyl, exhibit the same characteristic behavior as shown in figure 2.3 (Van Leer and Paulaitis, 1980; McHugh and Paulaitis, 1980; Kurnik, Holla, and Reid, 1981; Johnston, Ziger, and Eckert, 1982; Johnston and Eckert, 1981).

It is by now quite clear to the reader that the phenomenon of enhanced solubility in supercritical fluids has been known for more than a century. So why are there not scores of supercritical fluid extraction processes in operation today?

It is important to remember that during the first three quarters of the twentieth century energy was cheap. There was no motivation to develop energy-efficient processes. In contrast, chapter 8 shows that the preoccupation with energy conservation and efficiency virtually became a national obsession in the mid- to late 1970s. This drive for energy efficiency was a major impetus for many research and development programs. Chapters 7 and 9 mention a few high-pressure processes developed in the late 1930s and early 1940s, not because they were necessarily more energy-efficient than competing processes,

but because there was no other way to produce the desired product (e.g., low-density polyethylene).

It is also important to realize that the development of a high-pressure process depends on an understanding of the phase behavior of the system and that phase behavior at high pressures can be quite perplexing. A cursory review of the thermodynamic textbooks used in the 1940s through the 1960s shows that very little attention is paid to the phase behavior of mixtures at high pressures. Information on the high-pressure phase behavior of mixtures has developed quite rapidly within the past two decades or so.

In the following chapters we shall progress to a discussion of high-pressure phase behavior and to an examination of applications research that has been described in the literature. The phase behavior of SCF-solute systems exhibits enough peculiarities that the timetable of a research and development program stands the chance of being lengthened because of seemingly inexplicable data. The engineer must be aware of the phase behavior that is exhibited by SCF-solute mixtures so that he can take advantage of this behavior in novel ways in the development of supercritical fluid processes. The high-pressure phase behavior of SCF-solute systems is considered in some detail in chapter 3.

---

## Phase Diagrams for Supercritical Fluid–Solute Mixtures

---

Oftentimes the question is asked “Why bother with the phase diagram for a particular solute–supercritical fluid solvent mixture when the key issue really is, ‘does the solute dissolve’ in the supercritical fluid?” The answer is simple. Don’t bother if you can reliably calculate solubility. But there is a difficulty. Our current level of understanding of the intermolecular interactions in dense fluids precludes the possibility of reliably calculating solubility levels in many cases. More is said about calculations in chapter 5. So what, then, are our options for screening potential applications of supercritical fluid solvents? Although the familiar heuristics on solubility found in chemistry textbooks can be employed to assess whether a solute will be soluble in a candidate supercritical fluid, these heuristics do not quantify the pressures and temperatures needed for a given solubility level. Experimentally determined solubilities are ultimately needed to make an informed decision whether a potential SCF application merits further financial investment. A knowledge of the possible types of phase diagrams applicable for the mixtures of interest can help minimize the amount of experimental work needed to determine solubility levels over wide ranges of temperature and pressure.

Fortunately the wide variety of phase behavior that can occur when operating at high pressures can be cataloged with a small number of schematic phase diagrams (Scott, 1972; Scott and van Konynenburg, 1970; Hicks and Young, 1975). Interpreting as well as extrapolating high-pressure phase behavior data need not be a formidable task even if the mixture is composed of components that differ in molecular size, shape, structure, and attractive potential. Many of the features of the phase diagrams for multicomponent mixtures are identical to those found with the phase diagrams of binary mixtures. Therefore, let us first describe the limiting case of a phase diagram of a binary mixture consisting of a single SCF solvent and a single solute (Streett, 1983). An understanding of the phase behavior of this limiting case provides a basis for generalizing the phase equilibrium principles that are operative during the SCF solvent extraction of mixtures.

Before describing the features of the phase diagrams, it is instructive to

consider the geometrical constraints on the topology of phase diagrams for mixtures imposed by the phase rule (Streett, 1983) given by the relation:

$$\text{Degrees of freedom} = \text{number of components} + 2 - \text{number of phases.} \quad (3.1)$$

This simple equation gives the number of independent, intensive variables (i.e., the degrees of freedom) that must be set to fix all of the intensive properties of the equilibrium system. For example, unique values of the compositions of the equilibrium phases for a two-phase binary mixture can be obtained either by experiment or calculation if the temperature and pressure are fixed. For a two-phase ternary mixture one more variable must be fixed, such as overall mixture composition, in addition to temperature and pressure. The phase rule not only provides the number of independent variables that must be fixed to define multiphase, multicomponent mixtures, it also specifies the topology of the phase diagrams used to represent that behavior. Table 3.1 lists the geometrical features that are imposed by the phase rule. Knowing these geometrical constraints helps clarify the interpretation of the number of phases in the various regions of the phase diagram.

When operating an SCF process, it is prudent to avoid regions of multiple phases in pressure–temperature–composition ( $P$ – $T$ – $x$ ) space such as three-phase liquid–liquid–vapor (LLV), solid–liquid–vapor (SLV), or solid–solid–vapor (SSV) equilibria. When these regions of multiple phases are projected onto a two-dimensional  $P$ – $T$  diagram, their geometrical representations are simplified because pressure and temperature are field variables (Streett, 1983)—they are the same in each of the equilibrium phases. Pressure, temperature, and chemical potential are field variables, whereas molar volume is not. Two surfaces representing equilibrium between two phases in  $P$ – $T$ – $x$  space project as a single surface in  $P$ – $T$  space because the pressure and temperature are the same in both phases. Three lines representing three equilibrium phases in  $P$ – $T$ – $x$  space project as a single line in  $P$ – $T$  space because the pressure and temperature are the same in all three phases. Four points representing four equilibrium phases in  $P$ – $T$ – $x$  space project as a single point in  $P$ – $T$  space. Therefore, complex phase behavior can be more readily interpreted when a  $P$ – $T$  diagram (i.e., a field variable diagram) is used. Of course, the limitation of a  $P$ – $T$  diagram is that the composition and density of the equilibrium phases are not readily apparent. But many features of high-pressure phase behavior consistently appear in limited ranges of mixture compositions. By reviewing and cataloging many examples of the phase behavior of particular classes of mixtures, it is possible to make reasonable estimates of the mixture composition, depending on the operating temperature, pressure, and vicinity to a pure component critical point.

Although nature provides us with countless numbers of possible binary phase diagrams, Scott and van Konynenburg show that virtually all of the experimentally observed phase behavior can be represented with five schematic  $P$ – $T$  diagrams (Scott, 1972; Scott and van Konynenburg, 1970). Streett (1983)

**Table 3.1** Summary of the Geometrical Features of Phase Diagrams for One- and Two-component Systems

Number of Equilibrium Phases		Degrees of Freedom	Geometrical Features
One-component System	Two-component System		
3	4	0	Points
2	3	1	Lines
1	2	2	Surfaces
*	1	3	Volumes

Source: Streett (1983).

describes a sixth classification not predicted by the van der Waals equation but it is much less common and we do not describe it. The phase diagram classification scheme is simplified by using a two-dimensional projection of critical mixture curves and three-phase lines from three-dimensional  $P$ - $T$ - $x$  diagrams. The five classes of possible phase diagrams described in this chapter are shown in figure 3.1. We do not discuss the formation of multiple solid

**Figure 3.1** Five classes of possible binary phase diagrams as determined from the van der Waals equation of state. Points  $C_1$  and  $C_2$  are the critical points of components 1 and 2, respectively. The dashed curve in each figure is the critical mixture curve for the binary mixture. The open triangles are critical end points.

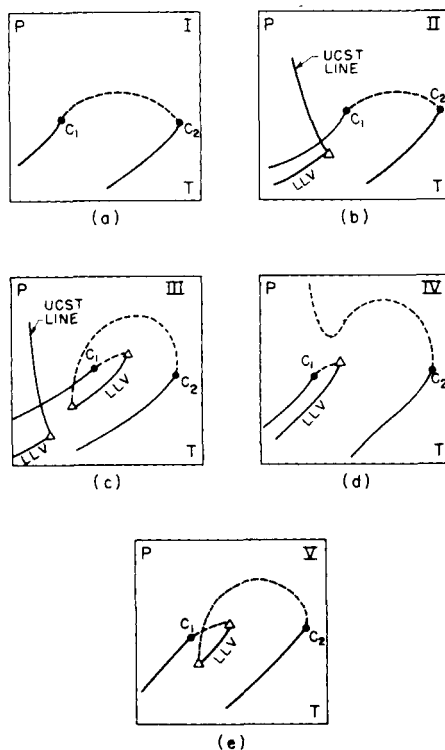


**Table 3.2** Definitions of Phase Transitions Occurring at High Pressures

<i>Abbreviation</i>	<i>Transition</i>	<i>Description</i>
LCST	Lower critical solution temperature	(a) Temperature at which two liquids critically merge to form a single liquid phase as the system temperature is isobarically lowered. (b) Temperature at which the transition described in (a) occurs in the presence of a gas phase.
UCST	Upper critical solution temperature	Temperature at which two liquids critically merge to form a single liquid phase as the system temperature is raised; the UCST is at a lower temperature than the LCST.
UCEP	Upper critical end point	(a) For solid–supercritical fluid systems the UCEP is the point at which the higher-temperature branch of the solid–liquid–gas line intersects the critical mixture curve; at the UCEP a liquid and gas phase critically merge to form a single fluid phase in the presence of a noncritical solid phase. (b) For liquid–supercritical fluid systems the UCEP occurs at the intersection of the UCST curve and a three-phase liquid–liquid–vapor curve where two liquid phases critically merge to form a single fluid phase in the presence of a noncritical gas phase as the temperature is increased; the UCEP is also the intersection of the LLV line with the lower temperature branch of the critical mixture curve, where a liquid and gas phase critically merge to form a single fluid phase in the presence of a noncritical liquid phase.
LCEP	Lower critical end point	For solid–supercritical fluid systems the LCEP occurs at the intersection of the low-temperature branch of the solid–liquid–gas line and the critical mixture curve; at the LCEP a liquid and gas phase critically merge to form a single fluid phase in the presence of a noncritical solid phase.

phases and multiple liquid phases at cryogenic temperatures. For a detailed treatment see, for example, Luks and Kohn (1984) and Rowlinson and Swinton (1982).

Before describing the five classes of possible phase diagrams exhibited by SCF–solute systems, we first define some abbreviations that appear in the discussion of these diagrams. These definitions, shown in table 3.2, are used to



describe points in  $P$ - $T$ - $x$  space where two phases merge or coalesce into a single phase (Rowlinson and Swinton, 1982). Sometimes this merging takes place in the presence of a third phase, which acts as an “uninterested observer” of the phase transition. For instance the designation “lower critical solution temperature” (LCST) is oftentimes used to define the temperature at which two liquid phases become critically identical in the presence of a noncritical gas phase. Unfortunately, the designation LCST is also used for a liquid + liquid  $\rightarrow$  liquid transition when a gas phase is not present. These definitions are a matter of bookkeeping; table 3.2 should prove useful when deciphering the abbreviations found in this chapter.

Quite frequently three-dimensional  $P$ - $T$ - $x$  diagrams can be overwhelming at first glance, especially for some of the more complex systems. The approach taken in this chapter is to construct  $P$ - $T$ - $x$  diagrams by compiling a number of isothermal  $P$ - $x$  diagrams since it is a relatively straightforward task to describe the experimental determination of the  $P$ - $x$  diagram. Constructing the  $P$ - $T$ - $x$  diagram in this manner should remove the confusion associated with the two-dimensional  $P$ - $T$  projection of the  $P$ - $T$ - $x$  diagram.

## PHASE DIAGRAMS FOR BINARY MIXTURES

### Type I

Figure 3.1a shows the phase diagram for a type-I system, the simplest possible phase behavior for a binary mixture. The distinguishing traits of type-I phase behavior are that only a single liquid phase exists throughout the phase diagram and that the critical mixture curve runs continuously from the critical point of the more volatile component to the critical point of the less volatile component. A continuous critical mixture curve usually occurs when the mixture components are of similar molecular diameter or size and similar interaction strengths, or have critical properties of comparable magnitude (Rowlinson and Swinton, 1982).

Constituents from a particular homologous series, such as the normal paraffins, usually deviate from type-I phase behavior only when the size difference between them exceeds a certain value. This is because the constituents are so close in molecular structure that they cannot distinguish whether they are surrounded by like or unlike species. It is important to remember that the critical curve depicted in figure 3.1a is only one possible representation of a continuous curve. It is also possible to have continuous critical mixture curves that exhibit pressure minimums rather than maximums with increasing temperature, that are essentially linear between the critical points of the components (Schneider, 1970), and that exhibit an azeotrope at some point along the curve.

Now let us progress to the construction of the general three-dimensional  $P$ - $T$ - $x$  diagram for type-I binary mixtures, shown in figure 3.2. The  $P$ - $T$ - $x$

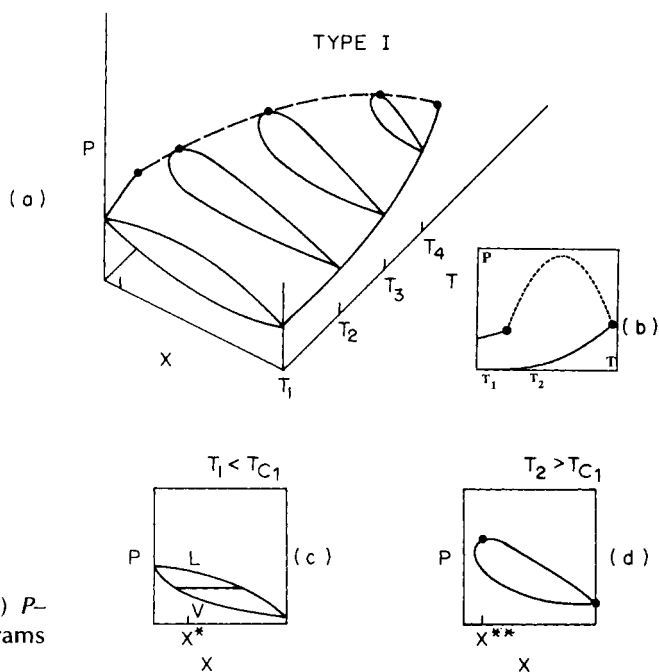


**Figure 3.2** (a)  $P$ - $T$ - $x$ , (b)  $P$ - $T$ , and (c, d)  $P$ - $x$  diagrams for a type-I mixture.

diagram can be constructed by compiling a number of isothermal  $P$ - $x$  plots, as shown in figure 3.2c, d. Throughout this chapter  $x$  denotes the composition of the heavy component. Let us make the first  $P$ - $x$  diagram at  $T_1$ , a temperature below the critical temperature of the two components. The process of holding temperature constant while changing pressure and composition can be represented as a vertical line in the  $P$ - $T$  diagram of figure 3.2b, that crosses both of the vapor pressure curves for the pure components at two different pressures. Hence, we can immediately identify two points on the  $P$ - $x$  diagram in figure 3.2c: the vapor pressure of pure component 1 [ $P_1^{\text{vap}}(T_1)$ ] located at the far left end of the composition axis and the vapor pressure of pure component 2 [ $P_2^{\text{vap}}(T_1)$ ] located at the far right end of the composition axis.

Figure 3.2c shows the familiar cigar-shaped vapor–liquid envelope found in many elementary textbooks on phase equilibria. At a fixed overall composition (denoted by  $x^*$  in this figure) there exists a single vapor phase at very low pressures. As the pressure is isothermally increased, the two-phase vapor–liquid envelope is intersected and a dew or liquid phase now appears. The locus of points that separates the two-phase vapor–liquid region from the one-phase vapor region is called the dew point curve. The concentration of the equilibrium vapor and liquid phases within the two-phase boundary of the vapor–liquid envelope is determined by a horizontal tie line similar to the one depicted in this figure.

As the pressure is further increased at this fixed overall composition, the amount of the liquid phase increases while the amount of the vapor phase shrinks until only a small bubble of vapor remains. If the pressure is still further increased, the bubble of vapor finally disappears, then a single liquid phase exists. The locus of points that separates the two-phase vapor-liquid region from the one-phase liquid region is called the bubble point curve. This vapor-liquid envelope can now be inserted into the three-dimensional  $P$ - $T$ - $x$  diagram in figure 3.2a.

Let us now construct a  $P$ - $x$  diagram at  $T_2$ , a temperature above the critical temperature of the light component, but, still below the critical temperature of the heavy component. A vertical line at this temperature in the  $P$ - $T$  diagram of figure 3.2b now misses the vapor pressure curve for the light component but it does cross the vapor pressure curve for the heavy component. Hence, we can now only immediately identify one point on the  $P$ - $x$  diagram in figure 3.2d—the vapor pressure of pure component 2 [ $P_2^{\text{vap}}(T_2)$ ] located at the far right end of the composition axis. The vapor-liquid envelope at  $T_2$  and at high concentrations of component 2 looks very similar to the envelope in figure 3.2c. But the left-hand side of the vapor-liquid envelope in figure 3.2d does not touch the pressure axis at pure component 1 because the vapor-liquid equilibrium line for component 1 is never crossed at this temperature.

If an experiment is performed at an overall composition equal to  $x^{**}$  in figure 3.2d, the vapor-liquid envelope is first intersected along the dew point curve at low pressures. The vapor-liquid envelope is again intersected at its highest pressure, which corresponds to the mixture critical point at  $T_2$  and  $x^{**}$ . This mixture critical point is identified with the intersection of the dashed curve in figure 3.2b and the vertical isotherm at  $T_2$ . At the critical mixture point, the dew point and bubble point curves coincide and all the properties of each of the phases become identical. Rowlinson and Swinton (1982) show that  $P$ - $x$  loops must have rounded tops at the mixture critical point, i.e.,  $(\partial P/\partial x)_T = 0$ . This means that if the dew point curve is being experimentally determined, a rapid increase in the solubility of the heavy component will be observed at pressures close to the mixture critical point. The maximum pressure of the  $P$ - $x$  loop will depend on the difference in the molecular sizes and interaction energies of the two components.

Another distinguishing characteristic of the mixture critical point is that the solution will appear a characteristic bluish white color if light is reflected through the solution or it will appear a characteristic reddish orange color if light is transmitted through the solution (Travers and Usher, 1906). This phenomenon is known as critical opalescence. It is a consequence of the long-range concentration fluctuations that occur in the solution when a sufficient number of molecules group together for a long enough time to form a correlated structure with dimensions large enough to scatter visible light. Since the vapor-liquid envelope has pulled away from the left-hand axis of the  $P$ - $x$  diagram, dew points will be observed if the overall mixture composition is slightly to the left of  $x^{**}$  and bubble points are observed if the overall

composition of the mixture is to the right of  $x^{**}$ . This vapor-liquid envelope at  $T_2$  can now be inserted into the  $P$ - $T$ - $x$  diagram in figure 3.2a.

For type-I systems, the vapor-liquid envelopes obtained at temperatures higher than  $T_2$  will look similar to the envelope in figure 3.2d, but they will pull further away from the left-hand pressure axis and they will be shifted to slightly higher pressures as the vapor pressure of component 2 continually increases with increasing temperature. A representative number of  $P$ - $x$  diagrams are assembled in figure 3.2a to form the three-dimensional  $P$ - $T$ - $x$  representation of type-I phase behavior. The genesis of the critical mixture curve shown in figure 3.2b should now be evident. It is obtained by drawing a dashed line through the locus of critical mixture points that are the maximums of the various  $P$ - $x$  curves. It should now also be clear that the critical mixture curve shown in the two-dimensional  $P$ - $T$  diagram in figure 3.2b represents the critical points for mixtures of differing composition. For a binary mixture, two equilibrium phases are found in the  $P$ - $T$  region of the phase diagram bounded by the critical mixture curve and the two pure component vapor pressure curves. At  $P$ - $T$  conditions above the critical mixture curve, one more variable in addition to  $P$  and  $T$  must be specified before the system is uniquely defined, since a single phase exists (see table 3.1).

Type-I phase behavior is probably the type of behavior most familiar to chemical engineers, since the description of this phase behavior can be found in many undergraduate thermodynamic textbooks. Rowlinson and Swinton (1982) present compilations of type-I mixtures as well as other types of mixtures. Hicks and Young (1975) also present an extensive compilation of  $P$ - $T$ - $x$  information on a wide variety of solvent-solute pairs from which the specific type of each system can easily be determined. Two examples of type-I  $P$ - $x$  diagrams are shown in figure 3.3 (Li, Dillard, and Robinson, 1981; Ng and Robinson, 1978). For these two examples, the  $P$ - $T$  trace of the critical mixture curve exhibits a maximum in pressure.

## Type II

Type-II phase behavior is shown in figure 3.1b. The type-II phase diagram is similar to the type-I phase diagram. In this case the critical mixture curve is again a continuous curve between the critical points of the two pure components. But now there are specific pressures and temperatures where the liquid phase splits into two liquid phases; this results in a liquid-liquid-vapor (LLV) line in the  $P$ - $T$  diagram. As shown in table 3.1, the LLV surface is represented as an LLV line on a  $P$ - $T$  diagram. A three-dimensional  $P$ - $T$ - $x$  representation of the three-phase liquid-liquid-vapor (LLV) surface is shown in figure 3.4. Notice that the two liquids become critically identical in the presence of a gas phase at the upper critical end point (Streett, 1983). Critical opalescence will be evident at this liquid-liquid critical point. Only liquid-liquid equilibria exist at pressures above the ruled surface representing

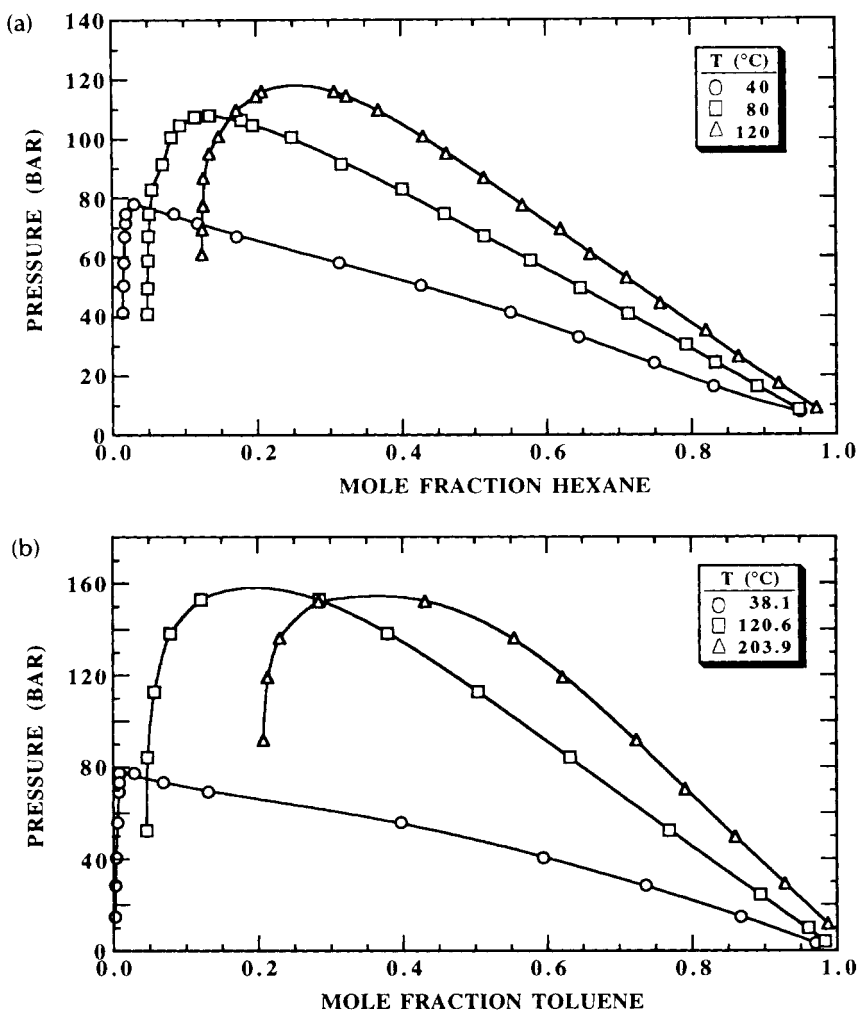


**Figure 3.3** Pressure–composition behavior of (a) the carbon dioxide-*n*-hexane system (Li, Dillard, and Robinson, 1981) and (b) the carbon dioxide-toluene system (Ng and Robinson, 1978). Both systems exhibit type-I phase behavior.

equilibrium of the three phases. The  $P$ - $T$  locus of liquid–liquid critical points is termed a UCST line. The UCST line is very steep on the  $P$ - $T$  diagram; this indicates that the location of the critical points is relatively insensitive to pressure. This is not surprising, since liquid–liquid UCST points are usually governed by enthalpic interactions between the mixture components in a system of essentially constant density (Prausnitz, 1969). The carbon dioxide-*n*-octane system is an example of a binary mixture exhibiting this type of phase behavior.

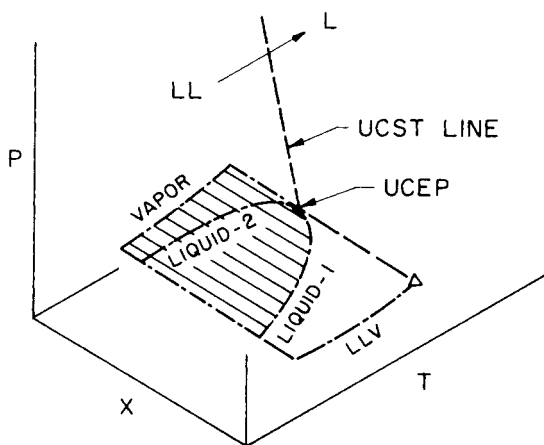


**Figure 3.4**  $P$ - $T$ - $x$  diagram for the three-phase liquid-liquid-vapor region of a binary mixture.

### Type III

Type-III phase behavior is shown in figure 3.1c. The distinguishing trait of type-III phase behavior is the occurrence of an LLV region located very close to the critical point of the more volatile component. The branch of the critical mixture curve starting at the critical point of the component with the higher critical temperature intersects the LLV line at the low-temperature end called a lower critical solution temperature (LCST). The other branch of the critical mixture curve, which starts at the critical point of the other component, intersects the LLV line at the high-temperature end sometimes called a UCEP or a type-k point. At temperatures below the LCST, a region of LLV behavior again appears similar to that found with type-II phase behavior.

When the critical properties of the two mixture components differ substantially, type-III phase behavior is usually observed. The critical properties of a given substance are a function of the molecular weight, structure, and intermolecular forces between the molecules. For binary mixtures comprised of normal hydrocarbons, type-III behavior occurs when the size difference between the components reaches a certain value. The occurrence of three phases in this instance is an entropically driven phenomenon since the enthalpic interactions between two different normal hydrocarbons should be indistinguishable from the interactions between two of the same hydrocarbons.

LLV behavior near the critical point of methane ( $T_c = -82.5^\circ\text{C}$ ,  $P_c = 46.4$  bar) occurs when the ratio of carbon atoms between methane and the second component exceeds 5.0. For binary ethane-hydrocarbon mixtures, LLV behavior occurs near the critical point of ethane ( $T_c = 32.3^\circ\text{C}$ ,  $P_c = 48.8$  bar) when the ratio of carbon atoms between ethane and the second component exceeds 9.5. And for binary propane-hydrocarbon mixtures LLV behavior occurs near the critical point of propane ( $T_c = 96.7^\circ\text{C}$ ,  $P_c = 42.5$  bar)

when the ratio of carbon atoms between propane and the second component exceeds 13.5 (Rowlinson and Swinton, 1982). The general characteristics of type-III phase behavior are identical when they occur for the methane-hydrocarbon, ethane-hydrocarbon, and propane-hydrocarbon systems even though the temperatures for the occurrence of three phases in these systems differ by as much as  $\sim 170^\circ\text{C}$ , since the three-phase region typically occurs near the critical point of the solvent. Therefore, three phases are not normally observed for many methane-hydrocarbon mixtures as long as the temperature of operation is at room temperature or above which is well above the critical temperature of methane.

LLV behavior can also occur if the species in the mixture differ considerably in the strength of their intermolecular potential. In this instance, the occurrence of LLV behavior is an enthalpically driven phenomenon. Perhaps the most straightforward examples of enthalpically driven LLV behavior are alcohol-SCF mixtures where alcohol-alcohol hydrogen bonding interactions overwhelm alcohol-SCF interactions. Kuenen and Robson (1899) presented an interesting study of ethane-alcohol mixtures which highlights the trends observed in alcohol-SCF mixtures. They showed that the temperature span of the LLV line is  $\sim 9^\circ\text{C}$  for the ethane-ethanol system,  $\sim 3^\circ\text{C}$  for the ethane-propanol system,  $\sim 2^\circ\text{C}$  for the ethane-butanol system, and it is not found for the ethane-isopentyl alcohol system. The behavior exhibited by the mixtures studied by Kuenen is an example of the well-known heuristic that the solubility of an alcohol in a hydrocarbon solvent increases as the hydrocarbon nature of the alcohol increases, or conversely, as the amount of alcohol-alcohol hydrogen bonding decreases.

The  $P$ - $T$ - $x$  diagram for type-III phase behavior is shown in figure 3.5. The lower-temperature portion of this diagram is omitted since, for all practical purposes, the  $P$ - $T$  region of interest for SCF technology is located between the critical points of the pure components. Now let us progress to the construction of the general three-dimensional  $P$ - $T$ - $x$  diagram for type-III binary mixtures, shown in figure 3.5a. If the first  $P$ - $x$  diagram is constructed at  $T_1$ , a temperature below the LCST, we obtain a diagram that is similar to figure 3.2c described for a type-I system. An isotherm at  $T_1$  drawn in figure 3.5b misses the LLV line and only crosses the two pure component vapor pressure curves. The  $P$ - $x$  diagram at  $T_1$  is already inserted into the  $P$ - $T$ - $x$  diagram of figure 3.5a.

If the temperature is raised to  $T_2$ , now only slightly below the LCST, an isotherm drawn in figure 3.5b barely misses the LLV line and we get the  $P$ - $x$  diagram shown in figure 3.5c that has the characteristic shape of a system on the verge of liquid immiscibility (i.e., the single liquid phase of the vapor-liquid envelope is on the verge of splitting into two liquids to form a three-phase, LLV mixture). A tie line is shown in figure 3.5c precisely at the horizontal inflection in the bubble point curve of the vapor-liquid envelope.

At a slightly higher operating temperature, the LLV line in figure 3.5b will be intersected indicating that two liquids appear in the presence of a vapor

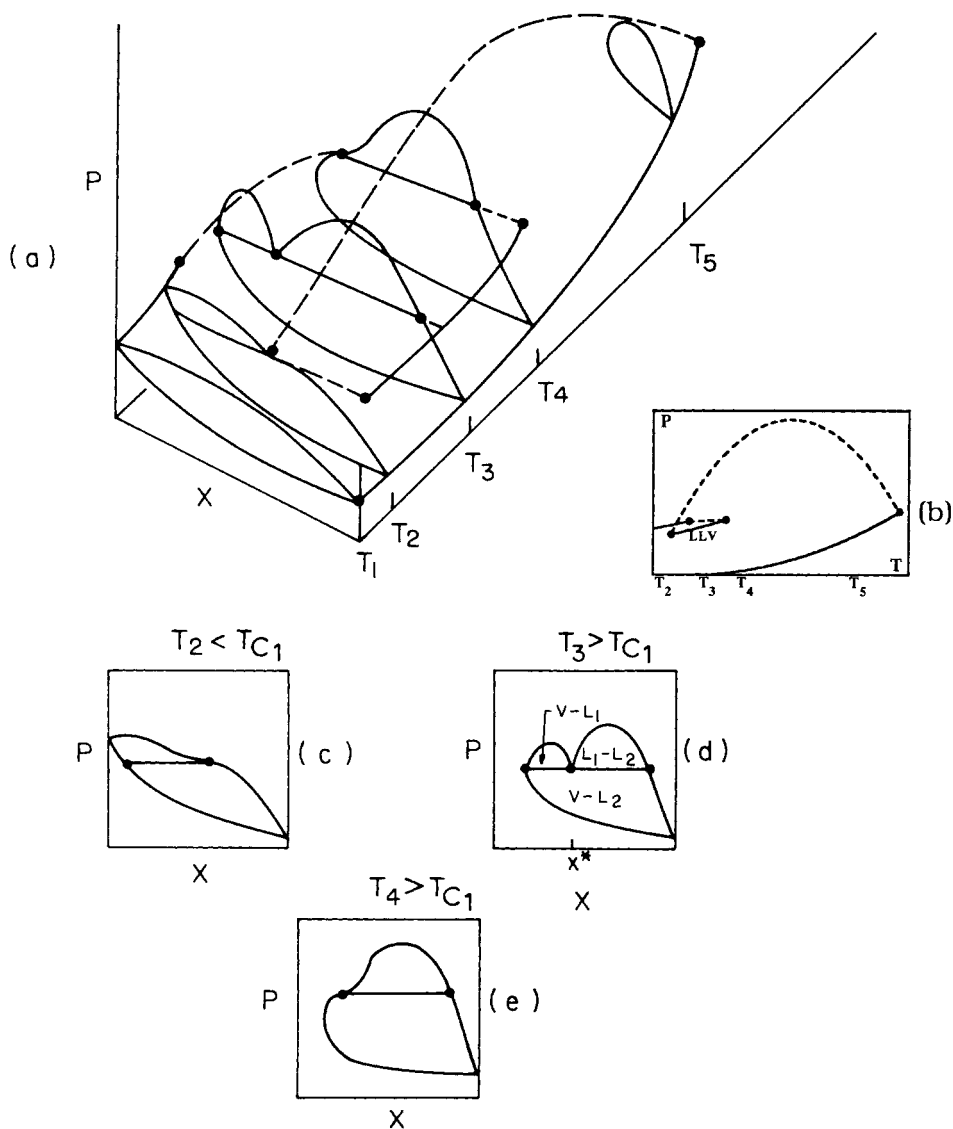


**Figure 3.5** (a)  $P$ - $T$ - $x$ , (b)  $P$ - $T$ , and (c, d, e)  $P$ - $x$  diagrams for a type-III binary mixture. The low-temperature portion of the diagram is omitted.  $T_{C1}$  is the critical temperature of the more volatile component.



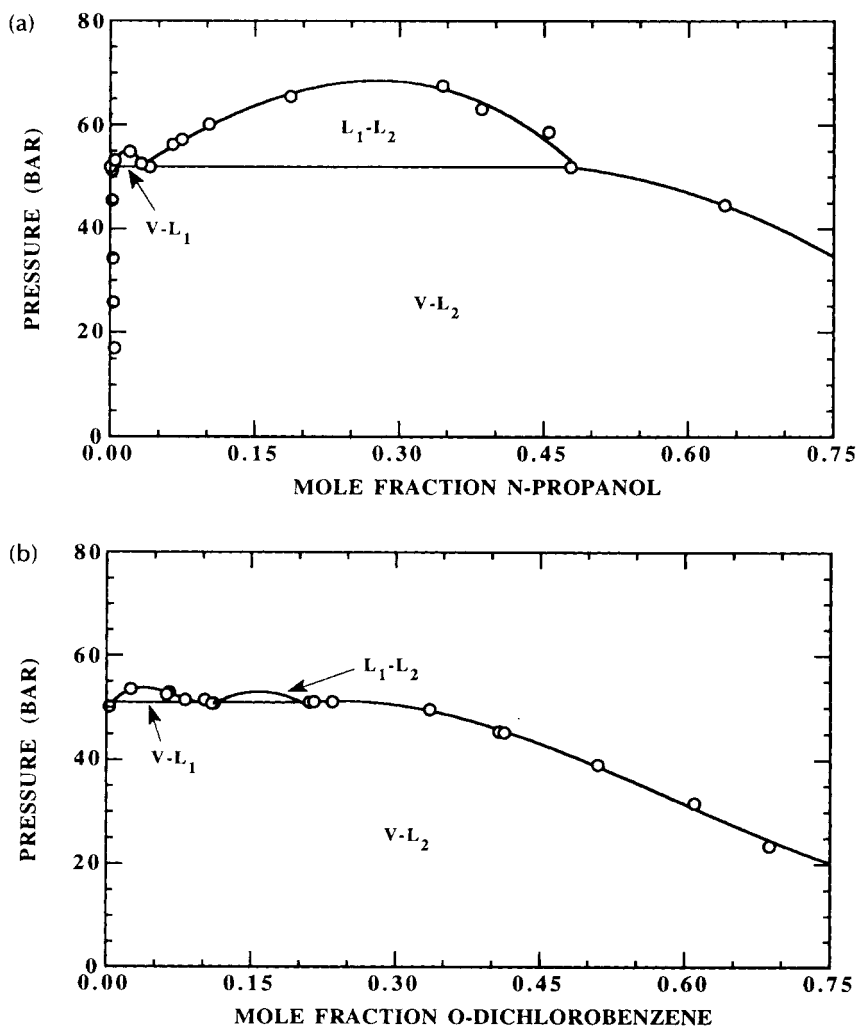
phase. Hence, the horizontal inflection in the bubble point curve represents the point where the two liquid phases have just coalesced into a single phase in the presence of a vapor phase (i.e., the LCST). The branch of the critical mixture curve that starts at the critical point of the less volatile component intersects the LLV line precisely at the LCST, as shown in figure 3.5a.

Figure 3.5d shows the construction of a  $P$ - $x$  diagram at temperature  $T_3$ , an isotherm that intersects the vapor pressure curve of the less volatile component, the LLV line, and both branches of the critical mixture curve (see figure 3.5b). At low pressures, a single vapor phase exists until the dew point curve of the vapor-liquid envelope is intersected and a liquid phase is formed. Vapor-liquid equilibrium is observed as the pressure is increased further until the three-phase LLV line is intersected, indicated by the horizontal tie line shown in figure 3.5d. There now exists a single vapor phase and two liquid phases.

If the pressure is increased further and if the overall mixture composition is less than  $x^*$ , a vapor-liquid envelope is obtained that is very similar to those shown in figure 3.2. As with the type-I system, a vapor-liquid critical point is observed at a pressure and composition corresponding to the very top of the envelope. If the overall mixture composition is greater than  $x^*$ , a liquid-liquid envelope is observed that is very similar to the vapor-liquid envelope observed for concentrations less than  $x^*$ . A liquid-liquid critical point is observed at a pressure and composition corresponding to the very top of the liquid-liquid envelope.

At  $T_3$ , two critical points are observed, depending on the overall composition of the mixture. In fact, the vapor-liquid and the liquid-liquid critical points both exhibit virtually the same physical characteristics, such as critical opalescence. The  $P$ - $x$  diagram of figure 3.5d is also shown in the  $P$ - $T$ - $x$  diagram of figure 3.5a. Todd and Elgin (1955) found several examples of type-III mixtures in their phase behavior studies with supercritical ethylene-organic solvent mixtures. Figure 3.6 shows type-III,  $P$ - $x$  diagrams for the ethylene-*n*-propanol and the ethylene-*o*-dichlorobenzene systems determined by Todd and Elgin.

The  $P$ - $x$  diagram shown in figure 3.5e is obtained if the temperature is raised to the UCEP temperature,  $T_4$ . With increasing pressure the isotherm intersects the vapor pressure curve for the less volatile component, the high-temperature end of the LLV line (i.e., the UCEP), and eventually the critical mixture curve. As with the previous isotherm, a single vapor phase exists until the dew point curve is intersected. As the pressure is isothermally increased the UCEP is eventually intersected where the gas phase and the middle liquid phase merge to form a single phase. A tie line is shown in figure 3.5e precisely at the horizontal inflection in the dew point portion of the vapor-liquid envelope. At  $T_4$ , then, only two phases exist over the entire pressure range. Notice that when this  $P$ - $x$  diagram is added to the  $P$ - $T$ - $x$  diagram in figure 3.5a, the branch of the critical mixture curve that starts at the critical point of the more volatile component terminates at the inflection point.



**Figure 3.6** Two examples of type-III mixtures found by Todd and Elgin (1953): (a) the ethylene-*n*-propanol system is obtained at 14.5°C and (b) the ethylene-*o*-dichlorobenzene system is obtained at 11.5°C.

At temperatures above  $T_4$  the isotherms only intersect the vapor pressure curve of the less volatile component and the critical mixture curve. The three-phase LLV line is no longer intersected, therefore the simple  $P$ - $x$  loops described for type-I systems are now observed. One such simple  $P$ - $x$  loop is shown in figure 3.5a at temperature  $T_5$ .

The two branches of the critical mixture curve are now clearly evident in figure 3.5. The tie lines representing the compositions of the three equilibrium phases in the LLV region project as a single line on the temperature face of the

$P$ - $T$ - $x$  diagram. A two-dimensional  $P$ - $T$  projection of the  $P$ - $T$ - $x$  is shown in figure 3.5b.

## Type IV

Type-IV phase behavior is shown in the  $P$ - $T$  diagram of figure 3.1d. Originally, Scott and van Konynenburg (1968) listed this behavior as type-III. But it is easier to explain the genesis of the behavior shown in figure 3.1d (i.e., type-IV in this book) by following the order presented here. It is reasonable to assume that the  $P$ - $T$  trace of the UCST curve in figure 3.1c for type-III behavior will shift to higher temperatures and the branch of the critical mixture curve that intersects the LLV line at the LCST will shift to lower temperatures if the differences in size, structure, or strength of the intermolecular forces between the mixture constituents is very large. In other words, the two two-phase regions of the diagram, the liquid-liquid and vapor-liquid regions, will extend over wider ranges of temperature and pressure as the properties of the mixture constituents become more dissimilar.

Eventually the UCST curve will superpose onto the critical mixture curve to give rise to the critical mixture curve that is shown schematically in figure 3.1d. Once again there are two branches of the critical mixture curve. But the branch of the critical mixture curve that starts at the critical point of the less volatile component no longer intersects a region of LLV behavior, as it did for type-III phase behavior. The first  $P$ - $x$  diagram is constructed at  $T_1$ , a temperature less than the critical temperature of the more volatile component. An isotherm at  $T_1$  intersects the vapor pressure curve of the less volatile component, the three-phase LLV line, and the vapor pressure curve of the more volatile component shown in figure 3.7b.

Figure 3.7c shows that at low pressures, a single vapor phase exists. At a higher pressure the dew point curve is intersected and a liquid and vapor phase now exists. As the pressure is increased further, the three-phase LLV line is intersected. If the pressure is increased still further, and if the overall mixture composition is less than  $x^*$ , we observe a vapor-liquid envelope, which intersects the pressure axis at  $P_1^{\text{vap}}$ , corresponding to the intersection of the vapor pressure curve of the more volatile component at  $T_1$  in figure 3.7b. But, for type-IV phase behavior, the liquid-liquid envelope at overall mixture concentrations greater than  $x^*$  no longer exhibits a closed dome with a mixture critical point. Both branches of the liquid-liquid envelope rise steeply with increasing pressure; in fact, they can diverge at very high pressures. This type of liquid-liquid phase behavior is representative of mixtures in which the components have a strong "dislike" for each other, as for instance with hydrocarbon-water mixtures at modest temperatures (Culberson and McKetta, 1951).

If the next  $P$ - $x$  diagram is constructed at a slightly higher temperature,  $T_2$ , the LLV line is intersected but the vapor pressure curve of the more volatile

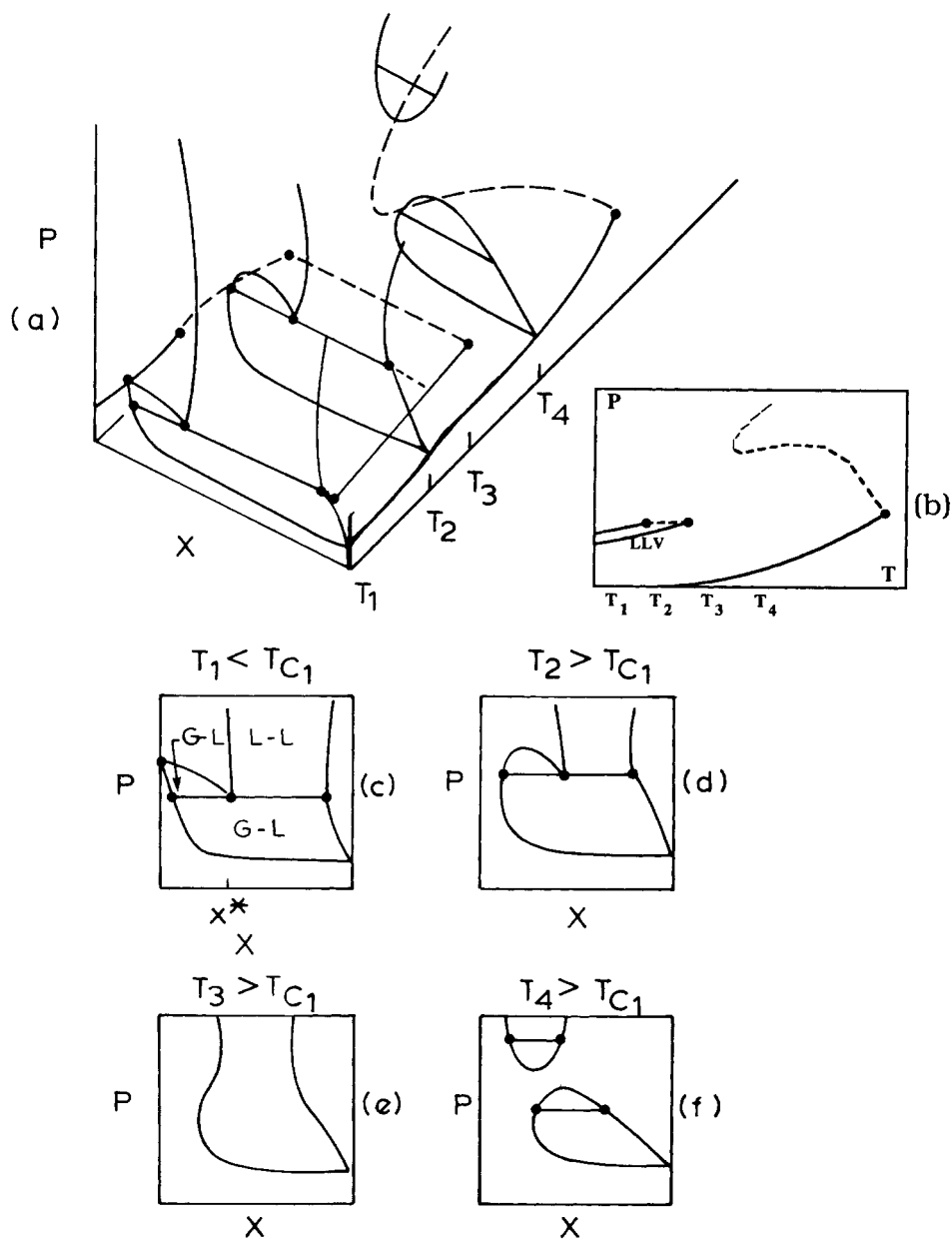


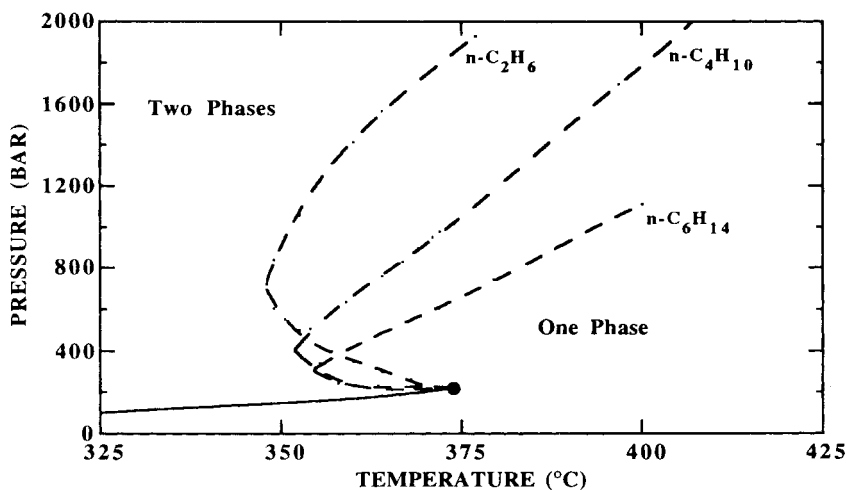
**Figure 3.7** (a)  $P$ - $T$ - $x$ , (b)  $P$ - $T$ , and (c, d, e, f)  $P$ - $x$  diagrams for a type-IV binary mixture. In these diagrams G, which denotes gas, is used interchangeably with V, which denotes vapor.  $T_{C1}$  is the critical temperature of the more volatile component.

component is not intersected (see figure 3.7b). At pressures higher than the three-phase LLV pressure, the left-hand side of the vapor–liquid envelope exhibits a closed dome with a maximum in pressure equal to the pressure of the isothermal intersection of the branch of the critical mixture curve closest to the critical point of the pure solvent. But, again, the liquid–liquid envelope at high concentrations does not exhibit a closed dome with a mixture critical point (see figure 3.7d).

If the temperature is raised to  $T_3$ , the phase behavior shown in figure 3.7e occurs. This temperature is greater than the UCEP temperature, therefore two phases exist as the pressure is increased as long as the critical mixture curve is not intersected. The two branches of the vapor–liquid phase envelope approach each other in composition at an intermediate pressure and it appears that a mixture critical point may occur. But as the pressure is further increased, a mixture critical point is not observed and the two curves begin to diverge. To avoid confusion, the phase behavior shown in figure 3.7e is not included in the  $P$ – $T$ – $x$  diagram.

An interesting type of phase behavior occurs if the temperature of the system is increased to  $T_4$  (see figure 3.7f). In this instance, the vapor–liquid envelope does exhibit a closed dome with a mixture critical point at a moderate pressure equal to the intersection of the mixture critical curve at this temperature. A single fluid phase now exists at this temperature for pressures greater than the mixture critical pressure. But if the pressure is increased much beyond the mixture critical pressure, the single fluid phase splits into two phases. Two representative tie lines are shown in the two-phase regions of this diagram. Figure 3.7f shows two mixture critical points occur at this temperature, depending on the overall composition of the mixture. One critical point occurs at the maximum of the vapor–liquid envelope as the pressure is isothermally raised from a low to a moderate value. The other mixture critical point occurs at the minimum of the fluid–liquid envelope, which exists at higher pressures. The phase behavior at  $T_4$  is shown in figure 3.7a.

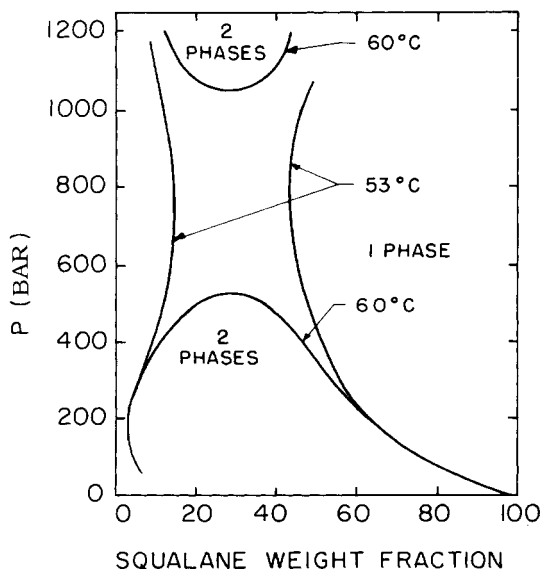
When the locus of mixture critical points is connected, the  $P$ – $T$  diagram shown in figure 3.7b is generated. The reader is cautioned that the critical mixture curve shown in figure 3.1d is only a schematic representation of type-IV behavior as the curve does not necessarily have to exhibit a minimum in pressure. In fact, for many binary water–solute mixtures the critical mixture curve starts at the critical point of water and initially shows a negative slope rising to higher pressures as the temperature is decreased but eventually reverses direction and shows a positive slope at higher pressures (see figure 3.8) (Yiling, Michelberger, and Franck, 1991). Therefore, many supercritical water–solute systems exhibit two-phase behavior at temperatures less than the critical temperature of water. Thus, operation in a single-phase region for a supercritical water reaction process requires  $P$ – $T$  conditions greater than, not less than, the critical conditions of water. Numerous other examples of type-IV phase behavior are reported in the literature. An example with carbon dioxide is shown in figure 3.9 for the carbon dioxide–squalane



**Figure 3.8** Critical mixture curves for water–normal hydrocarbon mixtures near the critical point of water (Yiling, Michelberger, and Franck, 1991). The solid line is the vapor pressure curve for pure water.

(2,6,10,15,19,23-hexamethyltetracosane) system (Liphard and Schneider, 1975). Finally we note that the branch of the mixture critical curve that starts at the critical point of the less volatile component can have many shapes, as shown in figure 3.10 for carbon dioxide–solute systems.

**Figure 3.9**  $P$ - $x$  behavior for the carbon dioxide–squalane system (Liphard and Schneider, 1975). At 53°C the two phases do not merge into a single fluid phase regardless of the pressure level, whereas at 60°C the two phases first merge into a single fluid phase at approximately 500 bar then split into two phases as the pressure is further increased above ~1,100 bar. These two isotherms are similar to isotherms  $T_3$  and  $T_4$  in figure 3.7e, f.



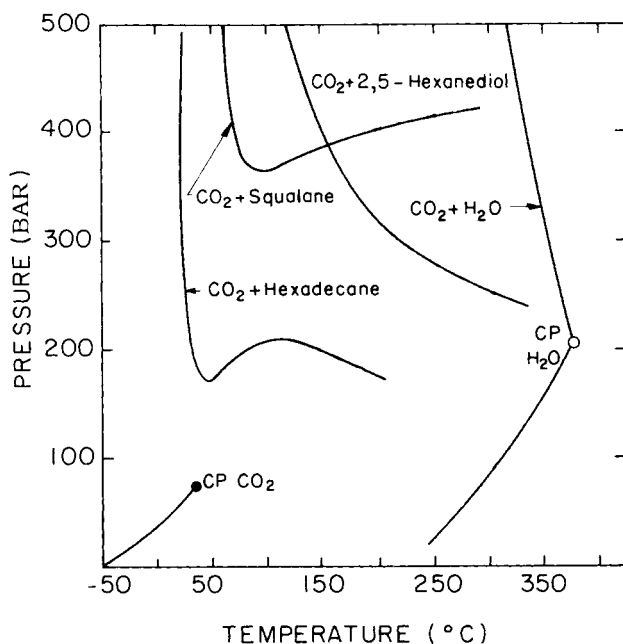


**Figure 3.10** Examples of the various types of critical mixture curves that can occur for a type-IV system (Schneider, 1970). For clarity the vapor pressure curves for squalane, hexadecane, and the 2,5-hexanediol are not shown.

## Type V

As shown in figure 3.1e, this phase behavior is very similar to the previously described type-III system. But in type-V phase behavior, there is no region of liquid immiscibility at temperatures below the LCST.

## SOLID-SUPERCRITICAL FLUID PHASE DIAGRAMS

Solid-SCF mixtures constitute a very large and important subset of binary mixtures. For these types of mixtures, the normal melting temperature of the solid is greater than the critical temperature of the SCF. In this section we describe the two schematic solid-SCF phase diagrams that depict solid-SCF equilibria to very high pressures (Diepen and Scheffer, 1948a; Streett, 1976; McHugh, 1981).

In the following descriptions of solid-supercritical fluid phase diagrams the designations vapor (V) and gas (G) are used interchangeably. Shown in figure 3.11 is the simplest  $P$ - $T$  diagram of a solid-SCF system. Curves CD and MH are the pure component vapor pressure curves of the light (SCF) and heavy (solid) component, respectively. Curve MN is the pure heavy component melting curve, and curve EM the pure heavy component sublimation curve. Points D and H represent pure component critical points. The distinguishing trait for this type system is that the critical mixture curve runs continuously

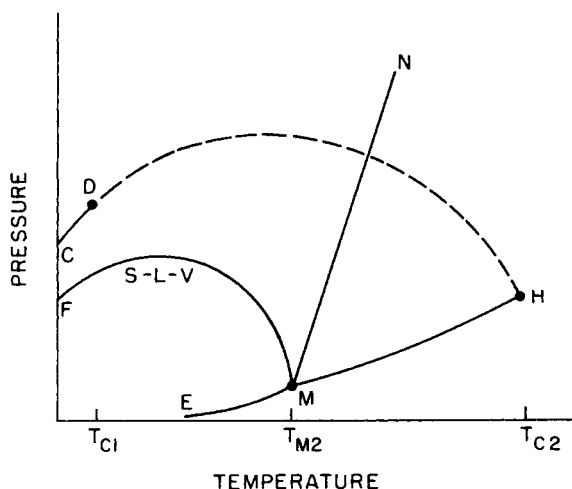


**Figure 3.11**  $P$ - $T$  diagram for a heavy solid-supercritical fluid system. In this instance the SLV curve is continuous.

between the critical point of the heavier component to the critical point of the lighter component. Also, a continuous three-phase solid-liquid-vapor (SLV) line is observed. This SLV line begins at the normal melting point of the heavy component, bends back toward lower temperatures as the pressure is increased, and finally ends at a temperature usually well below the critical temperature of the lighter component.

Normally, increasing hydrostatic pressure increases the melting point of the pure solid. But when the solid is compressed in the presence of an SCF, the melting point of the solid decreases with increasing pressure. The reason for this melting point (or freezing point) depression is analogous to the reason water freezes below its normal freezing point when salt is added to the water. As the pressure increases, more and more gas dissolves in the heavy liquid phase, which is now a mixture, therefore the temperature needed to freeze the heavy solid decreases substantially (de Swaan Arons and Diepen, 1963). This depression of the solid melting point is manifest as an SLV line as shown in figure 3.11.

Shown in figure 3.12a is the  $P$ - $T$ - $x$  diagram for the type of solid-SCF system described in the previous paragraph. The phase behavior depicted in figure 3.12c is observed if a  $P$ - $x$  diagram is experimentally determined at  $T_1$ , a temperature below the critical temperature of the lighter component  $T_{C1}$ . At low pressure solid-vapor equilibria are observed until the three-phase SLV line is intersected. Three equilibrium phases exist at this pressure: a pure solid, a liquid, and a gas.

If the overall mixture composition is less than that of the liquid phase, then a vapor-liquid envelope is observed as the pressure is further increased. The vapor-liquid envelope eventually intersects the pressure axis at the vapor pressure of pure component 1, since  $T_1$  is less than the critical temperature of



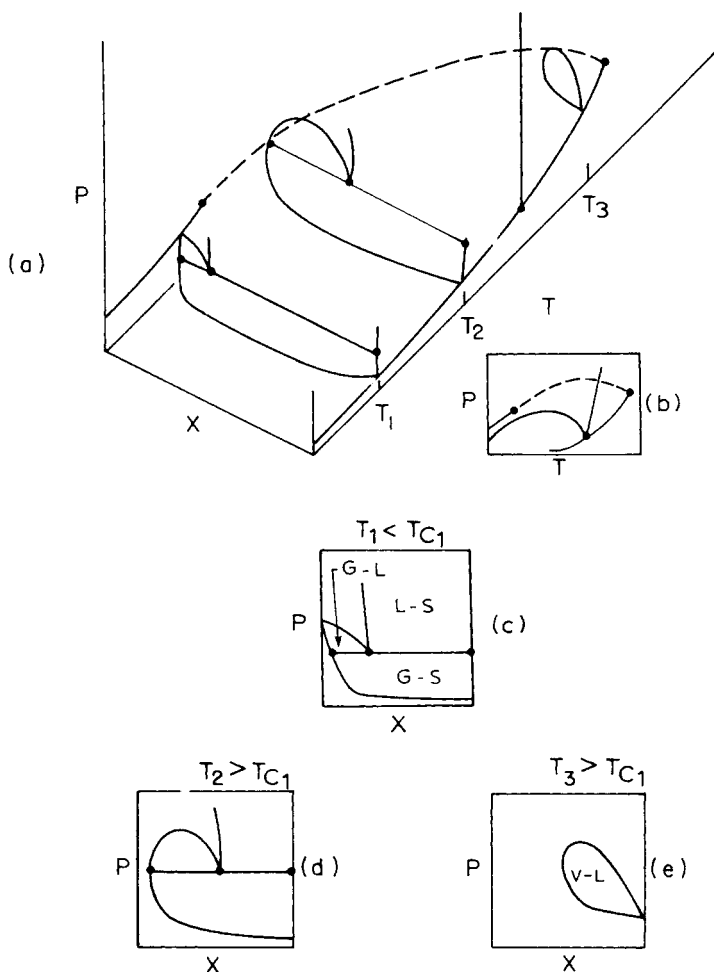


**Figure 3.12** (a)  $P$ - $T$ - $x$ , (b)  $P$ - $T$ , and (c, d, e)  $P$ - $x$  diagrams for heavy solid-supercritical fluid system depicted in figure 3.11.  $T_{C1}$  is the critical temperature of the more volatile component.

component 1. If the overall mixture composition is greater than that of the liquid phase, then liquid-solid equilibria exist as the pressure is increased above the three-phase pressure. The isothermal  $P$ - $x$  phase behavior at  $T_1$  is also shown in figure 3.12a.

Figure 3.12d shows the phase behavior if the temperature is increased to  $T_2$ , a temperature greater than the critical temperature of component 1. In this instance, the left-hand side of the vapor-liquid envelope no longer contacts the pressure axis and a vapor-liquid mixture critical point occurs at the highest pressure of the vapor-liquid envelope. The vapor-liquid envelope is much larger at  $T_2$  than at  $T_1$  because  $T_2$  is higher than  $T_1$ . Again, there are

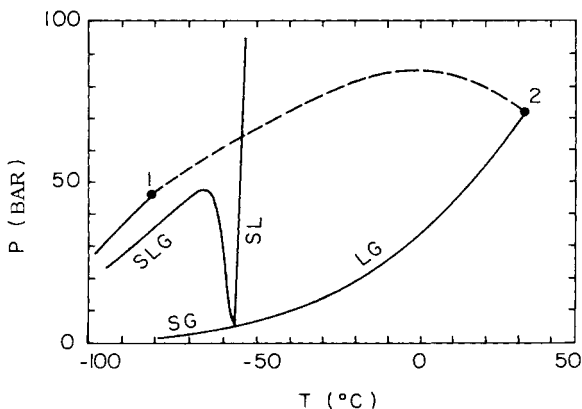
liquid-solid phase equilibria at pressures above the SLV line pressure for mixtures rich in the heavy component. Notice, also, that the concentration of heavy component in the liquid phase has increased substantially as a result of the higher operating temperature. This  $P$ - $x$  phase behavior is also included in the three-dimensional diagram of figure 3.12a (Rowlinson and Richardson, 1958).

If an operating temperature is chosen that is much greater than the normal melting point of the heavy component then the much simpler phase behavior depicted in figure 3.12e occurs. There is a straightforward vapor-liquid envelope with a mixture critical point at the highest pressure of the envelope. Figure 3.12b is obtained if the constant pressure tie lines representing three-phase SLV equilibrium in figure 3.12a are projected onto the temperature face of the  $P$ - $T$ - $x$  diagram along with the projections of the critical mixture curve and the pure component equilibrium curves.

Numerous examples of this type of solid-SCF phase behavior are reported in the literature. Normally this type of phase behavior occurs for mixtures whose components are chemically similar. Figure 3.13 shows one example of such a solid-SCF system (Donnelly and Katz, 1954).

The previously described solid-SCF phase behavior represents the simpler of two possible types. In the more complex type, figure 3.14, the SLV line is no longer a continuous curve and the critical mixture curve is also no longer continuous. It usually occurs when the solid and the SCF differ considerably in molecular size, structure, or intermolecular strength. In descriptive terms, this type of solid-SCF phase behavior occurs for systems in which the two components of the system do not "like" each other nearly as much as in the previously described solid-SCF system. In the more complex behavior, the light gas is not very soluble in the heavy liquid, even at high pressures. Therefore, the melting point depression of the heavy solid is not extremely large. The branch of the three-phase SLV line starting at the normal melting point of the heavy solid does not bend toward lower temperatures with

**Figure 3.13**  $P$ - $T$  diagrams for the methane-carbon dioxide system (Donnelly and Katz, 1954). Component 1 is methane and component 2 is carbon dioxide.



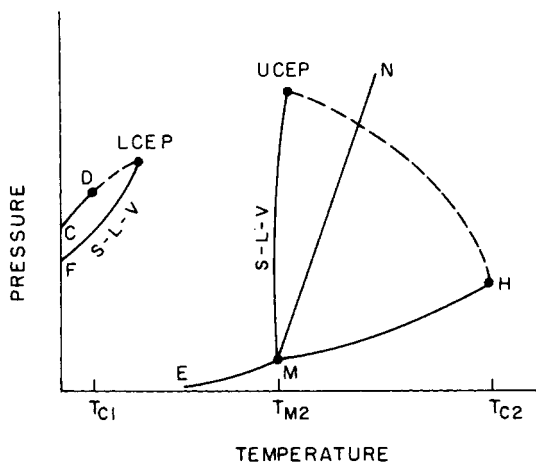


**Figure 3.14**  $P$ - $T$  diagram for a mixture consisting of a heavy nonvolatile solid and a light supercritical fluid whose critical temperature is less than the melting point of the solid. The SLV curve is no longer continuous.

increasing pressure. Instead it rises steeply with increasing pressure and intersects the critical mixture curve at a UCEP. The lower-temperature branch of the SLV line intersects the critical mixture curve at the LCEP. Only solid-gas equilibria exist between these two branches of the SLV line (Diepen and Scheffer, 1948a).

The  $P$ - $T$ - $x$  phase behavior for this second type of solid-SCF system is shown in figure 3.15. A  $P$ - $x$  diagram at temperature  $T_1$ , similar to figure 3.12c, has already been inserted into the  $P$ - $T$ - $x$  diagram. The phase behavior shown in figure 3.15c occurs if the operating temperature is increased to temperature  $T_2$ , slightly greater than the critical temperature of the lighter component  $T_{C1}$  (McHugh, 1981). At  $T_2$ , the SLV line is intersected at a higher pressure. Notice, also, that the vapor-liquid envelope has shrunk considerably and that the pressure of the vapor-liquid mixture critical point is only slightly greater than the three-phase pressure. This  $P$ - $x$  diagram is incorporated in the  $P$ - $T$ - $x$  diagram of figure 3.15a.

If the operating temperature is now increased to  $T_3$ , the phase behavior shown in figure 3.15d occurs. At  $T_3$  the mixture critical point pressure of the vapor-liquid envelope occurs precisely at the same pressure at which the three-phase SLV line is intersected. Hence, a vapor-liquid mixture critical point is observed in the presence of excess solid. This vapor-liquid mixture critical point in the presence of excess solid is the lower critical end point (LCEP) (Diepen and Scheffer, 1948a). If the temperature is increased slightly above the LCEP temperature, only solid-SCF phase behavior is observed at all pressures, since the three-phase (SLV) line ends at the LCEP.

A schematic representation of solid-SCF phase behavior is shown in figure 3.15e. The curve shown in this figure represents the solubility of the heavy solid in the SCF phase. By operating at a temperature close to the LCEP temperature, the solid solubility curve shows an inflection (i.e., a solubility

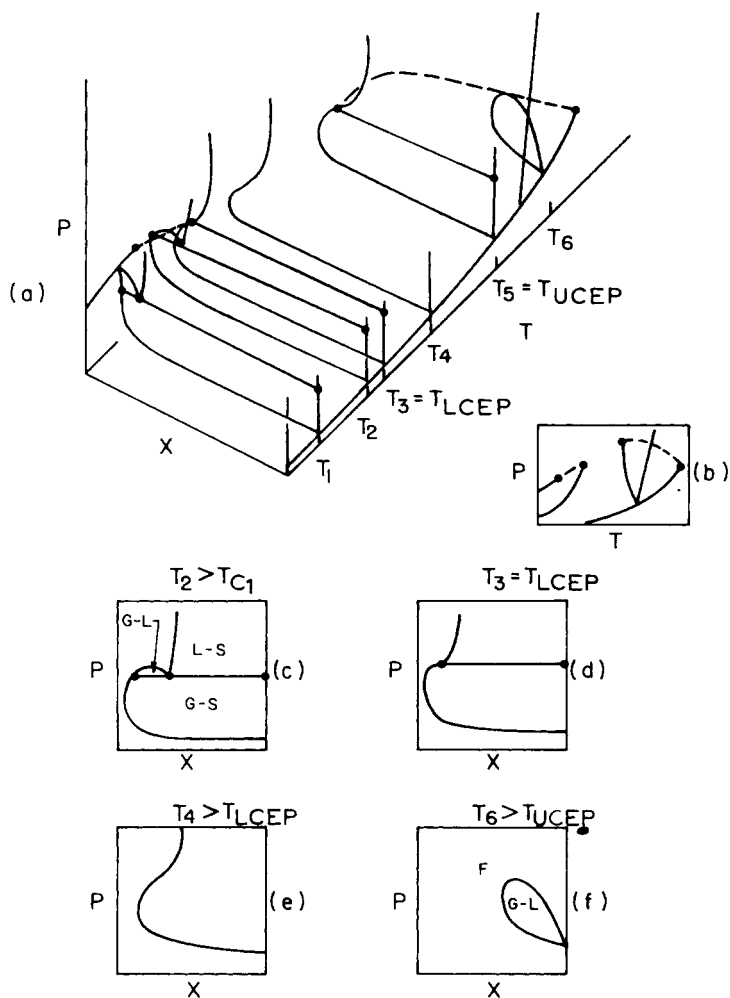


**Figure 3.15** (a)  $P$ - $T$ - $x$ , (b)  $P$ - $T$ , and (c, d, e, f)  $P$ - $x$  diagrams for binary solid-supercritical fluid system depicted in figure 3.14.  $T_{C1}$  is the critical temperature of the more volatile component.

enhancement) at pressures close to the LCEP pressure. At any vapor–liquid critical point, the vapor (or dew point) curve must exhibit a zero slope on a  $P$ - $x$  diagram, i.e.,  $(\partial P/\partial x)_T = 0$  (Rowlinson and Swinton, 1982). Therefore, at the LCEP, the solubility of the heavy component in the vapor (or gas) phase increases very rapidly. If the temperature is increased slightly above  $T_{LCEP}$  a vapor–liquid envelope no longer exists, as shown in figure 3.15e. The solid solubility isotherm is still influenced by the vapor–liquid critical behavior at the LCEP and the isotherm also tries to exhibit a zero slope, or equivalently a large solubility enhancement in  $P$ - $x$  space.

**Table 3.3** Experimentally Observed LCEPs and UCEPs for Binary Gas-Solid Mixtures

System (Component 1 + Component 2)	Component 1		LCEP		UCEP		UCEP (mol%)
	$T_c$ (°C)	$P_c$ (bar)	$T$ (°C)	$P$ (bar)	$T$ (°C)	$P$ (bar)	
Ethylene + naphthalene <sup>a,c</sup>	9.2	50.4	10.7	-51.9	52.1	176.5	16.8
Ethylene + biphenyl <sup>a,f</sup>			11.2	51.7	41.6	228.5	<sup>g</sup>
Ethylene + anthracene <sup>c</sup>			9.4	51.2	<sup>g</sup>	<sup>g</sup>	<sup>g</sup>
Ethylene + octacosane <sup>a,f</sup>			9.5	50.6	43.0	209.1	
Ethylene + hexaethylbenzene <sup>c</sup>			11.6	52.9	<sup>g</sup>	<sup>g</sup>	<sup>g</sup>
Ethylene + hexamethylbenzene <sup>c</sup>			9.8	51.1	<sup>g</sup>	<sup>g</sup>	<sup>g</sup>
Ethylene + stilbene <sup>c</sup>			9.5	50.9	<sup>g</sup>	<sup>g</sup>	<sup>g</sup>
Ethylene + dinitrobenzene <sup>c</sup>			9.3	50.7	<sup>g</sup>	<sup>g</sup>	<sup>g</sup>
Ethylene + hexachloroethane <sup>c</sup>			12.4	53.4	<sup>g</sup>	<sup>g</sup>	<sup>g</sup>
Ethylene + 1,3,5-trichlorobenzene <sup>f</sup>			13.1	53.4	<sup>g</sup>	<sup>g</sup>	<sup>g</sup>
Ethylene + <i>p</i> -chlorobromobenzene <sup>f</sup>			13.4	53.8	<sup>g</sup>	<sup>g</sup>	<sup>g</sup>
Ethylene + <i>p</i> -chloriodobenzene <sup>f</sup>			12.0	52.6	<sup>g</sup>	<sup>g</sup>	<sup>g</sup>
Ethylene + <i>p</i> -dibromobenzene <sup>f</sup>			10.6	51.4	<sup>g</sup>	<sup>g</sup>	<sup>g</sup>
Ethylene + hexatriacontane <sup>f</sup>			9.6	50.6	<sup>g</sup>	<sup>g</sup>	<sup>g</sup>
Ethylene + benzophenone <sup>f</sup>			9.9	50.9	<sup>g</sup>	<sup>g</sup>	<sup>g</sup>
Methane + naphthalene <sup>c</sup>	-82.6	46.0	<sup>g</sup>	<sup>g</sup>	87.3	1320.3	18.5
Ethane + naphthalene <sup>a,d</sup>	32.2	48.8	36.8	52.2	56.5	124.1	19.8
Ethane + biphenyl <sup>a</sup>			<sup>g</sup>	<sup>g</sup>	48.7	199.1	
Ethane + octacosane <sup>a</sup>			<sup>g</sup>	<sup>g</sup>	38.9	87.5	
CO <sub>2</sub> + naphthalene	31.0	73.8	<sup>g</sup>	<sup>g</sup>	60.1	256.0	~16.0
CO <sub>2</sub> + biphenyl <sup>a</sup>			<sup>g</sup>	<sup>g</sup>	55.1	475.2	~17.0
CO <sub>2</sub> + octacosane <sup>a,b</sup>			32.2	73.6	<sup>g</sup>	<sup>g</sup>	<sup>g</sup>

<sup>a</sup>McHugh and Yogan (1984).<sup>b</sup>McHugh, Seckner, and Krukoni (1984).<sup>c</sup>van Hest and Diepen (1963).<sup>d</sup>van Welie and Diepen (1963).<sup>e</sup>van Gunst, Scheffer, and Diepen (1953a).<sup>f</sup>Diepen and Scheffer (1948a).<sup>g</sup>No data available.

We can now explain the sudden increase in the solubility of naphthalene in supercritical ethylene reported at ~50 bar and 12°C. This solubility increase is a result of being very close to the LCEP for this system, which is 51.9 bar and 10.7°C (Diepen and Scheffer, 1948a). As shown in table 3.3, the LCEP usually occurs very close to the critical point of the pure SCF for most of the solid-SCF systems reported in the literature; even though there is a large solubility enhancement, the amount of solid in the SCF phase at the LCEP is quite low.

The solubility of a heavy solid will increase if the temperature is increased but it is not possible to indefinitely raise the system temperature to increase the

solubility of the solid in the SCF phase. This is because the higher-temperature branch of the SLV line will eventually be intersected and the solid will melt. The higher-temperature branch of the SLV line begins at the normal melting temperature of the heavy solid and ends at the intersection of the critical mixture curve with the SLV line at the upper critical end point (UCEP). At the UCEP, a vapor–liquid mixture critical point occurs in the presence of excess solid, similar to the phase behavior observed at the LCEP.

At temperatures slightly below the UCEP temperature, a large solid solubility enhancement is observed in the vicinity of the UCEP pressure as a result of the vapor–liquid mixture critical point behavior. As shown in table 3.3, the solubility of a heavy solid in the SCF phase can be very large near the UCEP (van Welie and Diepen, 1961c; van Hest and Diepen, 1963; McHugh and Paulaitis, 1980). A  $P$ - $x$  isotherm precisely at  $T_{UCEP}$  is shown in figure 3.15a. This isotherm looks similar to the isotherm in figure 3.15d except that the inflection in the solubility isotherm at the UCEP temperature is much greater.

At temperatures greater than the melting temperature of the heavy solid, the now familiar vapor–liquid envelope is observed, as shown in figure 3.15f at  $T_6$ . Figure 3.15b is obtained if the constant pressure tie lines representing three-phase SLV equilibrium in figure 3.15a are projected onto the temperature face of the  $P$ - $T$ - $x$  diagram along with the projections of the critical mixture curves and the pure component equilibrium curves.

As noted by McHugh and Paulaitis, very different high-pressure phase behavior can occur for solid–SCF mixtures that are superficially quite similar (McHugh, 1981; McHugh, Seckner, and Krukoni, 1984; McHugh, 1986; Paulaitis, McHugh, and Chai, 1983). For instance, let us compare the solid solubility behavior for the naphthalene–ethylene system (Diepen and Scheffer, 1953) with that of the biphenyl–carbon dioxide system (McHugh, 1981; McHugh and Yogan, 1984).

Naphthalene and biphenyl are heavy, nonvolatile solids with similar structures and with melting temperatures well above room temperature, 80.2 and 69.5°C, respectively. Ethylene and carbon dioxide are light gases at ambient conditions with relatively mild critical conditions, 9.3°C and 50.4 bar and 31.1°C and 73.8 bar, respectively. Our expectation is that the characteristic shapes of the solid solubility isotherms for these two systems should be quite similar.

Figure 3.16a shows three solubility isotherms for the naphthalene–ethylene system. The 50°C isotherm exhibits a large solubility enhancement sensitive to small changes in pressure around 175 bar. Notice also that for an isobar of ~200 bar the increase in the solubility of naphthalene in ethylene from 45 to 50°C is substantially greater than that from 25 to 45°C. The sensitivity of the solubility to small changes in pressure as well as temperature near 175 bar and 50°C is a consequence of being extremely close to the naphthalene–ethylene UCEP, 177 bar and 52.1°C (Diepen and Scheffer, 1948a, 1948b, 1953). Also, the loading of naphthalene in supercritical ethylene can be quite substantial

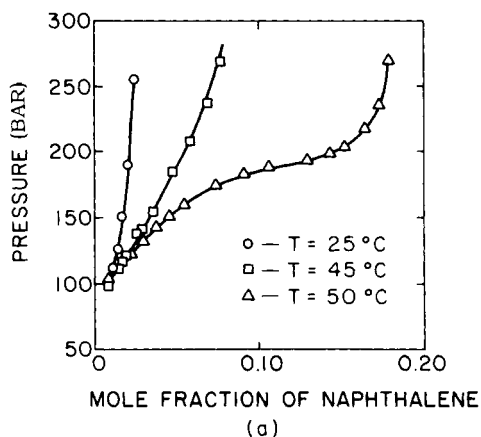
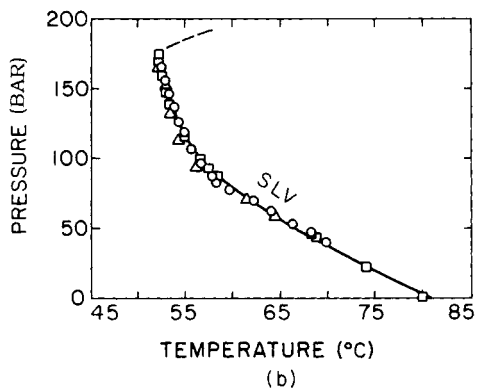


**Figure 3.16** Phase behavior of the naphthalene–ethylene system: (a) the solubility of naphthalene in supercritical ethylene at 25°C, 45°C, and 50°C (Diepen and Scheffer, 1948a, 1948b); (b) the  $P$ - $T$  projection of the naphthalene–ethylene three-phase SLV line ending at the mixture UCEP (van Gunst, Scheffer, and Diepen, 1953a, 1953b).



near the UCEP (i.e., 15 mol% naphthalene corresponds to approximately 45 wt% naphthalene in supercritical ethylene).

Now compare the solubility behavior of the previously described naphthalene–ethylene system with that exhibited by the biphenyl–carbon dioxide system shown in figure 3.17a. The 55°C isotherm has certain characteristics that are similar to the 50°C isotherm of the naphthalene–ethylene system shown in figure 3.16a. The 55°C isotherm exhibits a large solubility enhancement sensitive to small changes in pressure near 465 bar. The isobaric solubility behavior of the biphenyl–carbon dioxide system near 450 bar is similar to that of the naphthalene–ethylene system near 175 bar. At ~465 bar the increase in the solubility of biphenyl in supercritical carbon dioxide from 50 to 55°C is substantially greater than the increase from 36 to 50°C. The sensitivity of the solubility to small changes in pressure as well as temperature near 465 bar and 55°C is a consequence of being extremely close to the biphenyl–carbon dioxide UCEP, 475.1 bar and 55.1°C (McHugh, 1981; McHugh and Yogan, 1984; McHugh and Paulaitis, 1980). As with the naphthalene–ethylene system, the

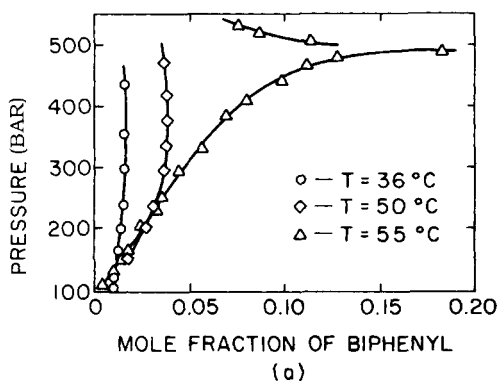
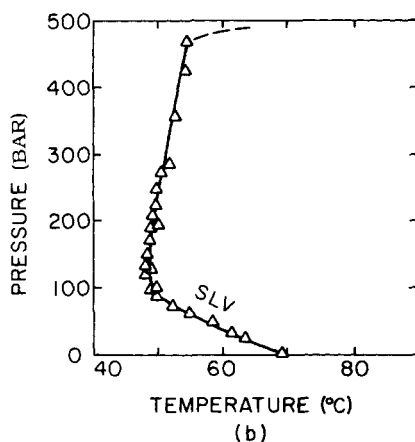


**Figure 3.17** Phase behavior of the biphenyl–carbon dioxide system: (a) the solubility of biphenyl in supercritical carbon dioxide at 36°C, 50°C, and 55°C (McHugh, 1981); (b) the  $P$ – $T$  projection of the biphenyl–carbon dioxide three-phase SLV line ending at the mixture UCEP (McHugh and Yogan, 1984).



loading of biphenyl in supercritical carbon dioxide is very high near the mixture UCEP (i.e., 15 mol% biphenyl is equivalent to approximately 33 wt% biphenyl in supercritical carbon dioxide).

The similarity in  $P$ – $x$  behavior near the UCEP for naphthalene–ethylene and biphenyl–carbon dioxide suggests that the location of the UCEP can be estimated solely from solubility data. Hence, it is possible to assume (incorrectly) that the solubility data of both the naphthalene–ethylene and the biphenyl–carbon dioxide systems represent solid solubilities in a supercritical fluid solvent. Notice, however, that the  $P$ – $x$  behavior for these systems is very different at pressures greater than their respective UCEP pressures. At 55°C and at pressures greater than 465 bar, the solubility of biphenyl in supercritical carbon dioxide decreases dramatically for a small increase in pressure; at 50°C and at pressures greater than 175 bar, the solubility of naphthalene in supercritical ethylene increases for a small increase in pressure until at higher pressures the solubility eventually reaches a limiting value. Obviously these two systems are not as similar as we initially conjectured. How can we explain these experimental observations?



The differences in the solubility behavior of the naphthalene–ethylene and biphenyl–carbon dioxide systems near their mixture UCEPs can be readily explained by considering the  $P$ – $T$  trace of the three-phase SLV line for each system. Shown in figure 3.16b is the  $P$ – $T$  trace of the SLV line along with the  $P$ – $x$  isotherms for the naphthalene–ethylene system. Similar diagrams for the biphenyl–carbon dioxide system are shown in figure 3.17b. The biphenyl–carbon dioxide SLV line exhibits a temperature minimum with increasing pressure, whereas the naphthalene–ethylene SLV line exhibits no such minimum. The different shapes of the SLV lines are a consequence of the amount of “like” or “dislike” the components have for each other. The reason for the differences in the solubility behavior for these two systems near their UCEPs is directly related to the mutual solubility of the mixture components. Let us examine the phase behavior characteristics of these two solid–SCF systems in more detail.

Consider first the schematic  $P$ – $T$  and  $P$ – $x$  diagrams for the naphthalene–ethylene system. Figure 3.18b depicts the solubility behavior of naphthalene in supercritical ethylene at a temperature greater than the UCEP temperature. Solid–gas equilibria exist at low pressures until the three-phase SLV line is intersected. The equilibrium vapor, liquid, and solid phases are depicted as points on the horizontal tie line at pressure  $P_d$ . As the pressure is further increased a vapor–liquid envelope is observed for overall mixture concentrations less than  $x_L$ . A mixture critical point is observed for this vapor–liquid envelope, as described earlier. If the overall mixture composition is greater than  $x_L$ , then solid–gas equilibria are observed as the pressure is increased above  $P_d$ .

Shown in figure 3.18c is a solubility isotherm at a temperature,  $T_b$ , that is less than the previous temperature,  $T_d$ , but still higher than the UCEP temperature. The solubility behavior at  $T_b$  is similar to the behavior in figure 3.18b. But at  $T_b$ , the three-phase SLV line is intersected at a higher pressure, closer to the UCEP pressure. Hence, the vapor–liquid envelope has diminished in size and the solid–gas equilibrium curve is shifted toward higher solvent concentrations. As a result, the solid–gas curve is now much closer to the vapor branch of the vapor–liquid envelope.

Now consider a solubility isotherm at  $T_a$ , slightly less than the UCEP temperature (figure 3.18d). At this temperature, solid–gas equilibria exist at all pressures, since the SLV line is never intersected. As the UCEP pressure is approached the gas phase becomes highly compressible, due to the influence of the vapor–liquid critical point, and the solubility of the solid in the gas phase begins to increase. As the pressure is increased in the immediate vicinity of the UCEP pressure, the  $T_a$  isotherm exhibits a large solubility enhancement. At pressures much higher than the UCEP pressure, the gas is less compressible, therefore the solubility of the solid quickly reaches a limiting value. This solid solubility behavior is similar to the 50°C naphthalene–ethylene isotherm.

Less dramatic solubility enhancements are observed for isotherms at lower temperatures that are further removed from the UCEP temperature. Solid

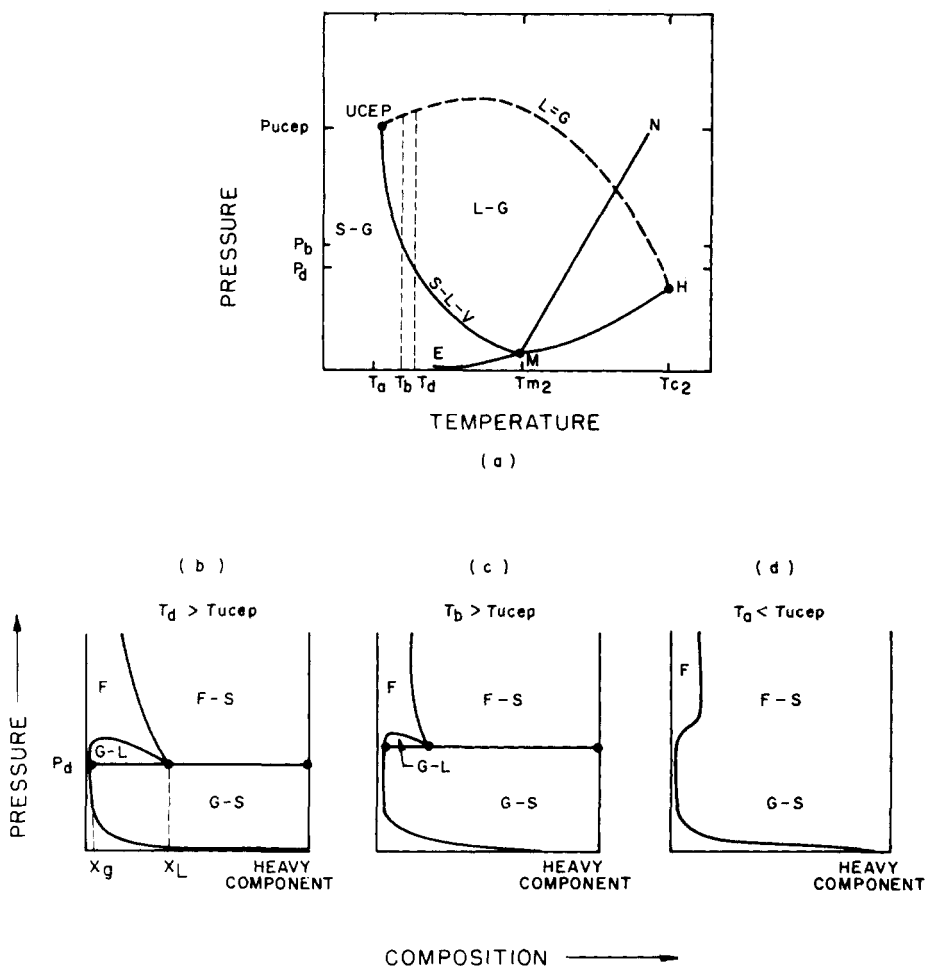


**Figure 3.18** (a) Schematic  $P$ - $T$  and (b, c, d)  $P$ - $x$  diagrams for the naphthalene-ethylene system (McHugh, 1981).

solubility isotherms at these lower temperatures are observed to have the same characteristics as the 25 and 45°C naphthalene-ethylene isotherms (see figure 3.16a). As the operating conditions are further removed in temperature and pressure from the UCEP, the solid solubility isotherm becomes less sensitive to changes in pressure or temperature.

Now let us use  $P$ - $T$  and  $P$ - $x$  diagrams to examine the behavior of the biphenyl-carbon dioxide system. The solubility behavior near the UCEP of the biphenyl-carbon dioxide system differs from the solubility behavior of the naphthalene-ethylene system because the biphenyl-carbon dioxide SLV line has a temperature minimum, shown schematically in figure 3.19. We first

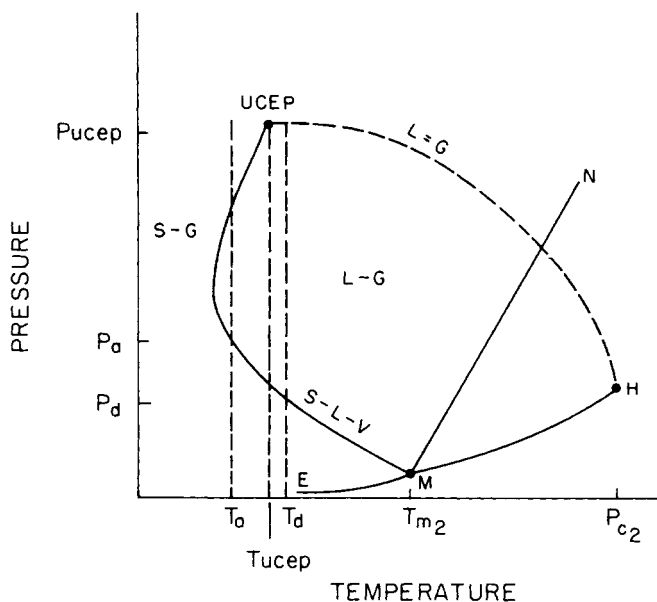


**Figure 3.19** Schematic  $P$ - $T$  diagram for the biphenyl-carbon dioxide system (McHugh, 1981).

consider a solubility isotherm at a temperature less than the UCEP temperature then proceed to higher-temperature isotherms. The solubility isotherms at temperatures below the minimum in the SLV line are of little interest in this case because solid-gas equilibria exist at all pressures.

Shown in figure 3.20a is a  $P$ - $x$  isotherm at a temperature greater than the temperature minimum of the SLV line but still less than the UCEP temperature. A variety of phase behaviors is exhibited at this temperature, indicated by the two intersections of the SLV line. At low pressures, solid-gas equilibrium is maintained until the system reaches pressure  $P_a$  where the three phases are found, depicted by a horizontal tie line in this diagram. Depending on the concentration of the overall mixture, either liquid-gas, solid-liquid, or a single liquid phase exists as the pressure is increased. With increasing pressure, the solid-liquid equilibrium curve bends back toward compositions richer in the light component. Eventually it merges with the liquid branch of the liquid-gas loop, where the three-phase line is again intersected at a higher pressure. At this point the liquid and gas phases are closer in composition than they were at the point represented by the intersection of the three-phase line at the lower pressure. As the pressure is increased above the three-phase pressure, solid-fluid equilibrium is maintained. The fluid phase at these high pressures is now less compressible and quickly attains a limiting solubility value.

The solid line shown in figure 3.20b is the portion of the solubility isotherm that is experimentally obtained if the SCF is allowed to flow through columns packed with the heavy component. The limitation of this experimental technique is that it is not possible to ascertain the physical state of the heavy

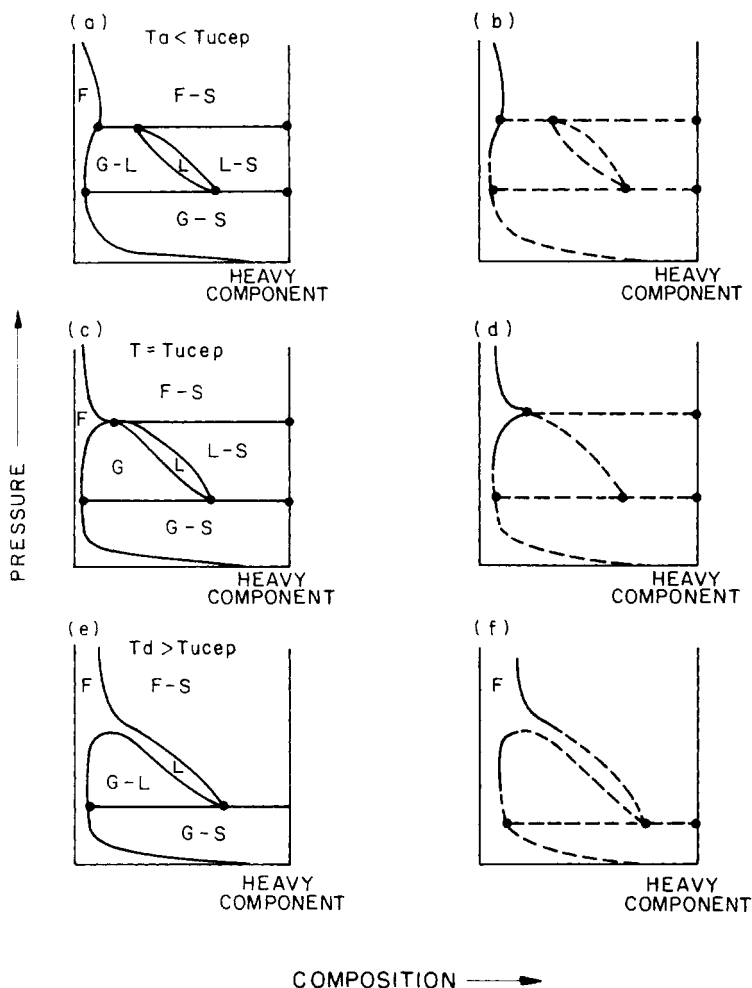


**Figure 3.20** Schematic  $P$ - $x$  diagram for the biphenyl-carbon dioxide system (McHugh, 1981).

component from the shape of the solubility isotherm. Techniques for visually determining high-pressure phase behavior are described in chapter 4. The solid line starting at pressures greater than the critical pressure of the light component represents the solubility of the heavy component in the SCF phase at a temperature greater than the temperature minimum of the three-phase line but still less than the UCEP temperature. The dashed lines show all possible phase behaviors, described in figure 3.20a. It is apparent from this figure that a vast majority of phase behavior information is missed when only the solubility of the heavy component in the SCF phase is determined. Also the solubility of the heavy component in the SCF phase represents liquid solubilities at low to

moderate pressures and solid solubilities at elevated pressures. Referring back to figure 3.17, it should also now be obvious that the 50°C biphenyl–carbon dioxide isotherm represents the solubility of liquid biphenyl in carbon dioxide for pressures up to ~300 bar and the solubility of solid biphenyl for pressures greater than 300 bar.

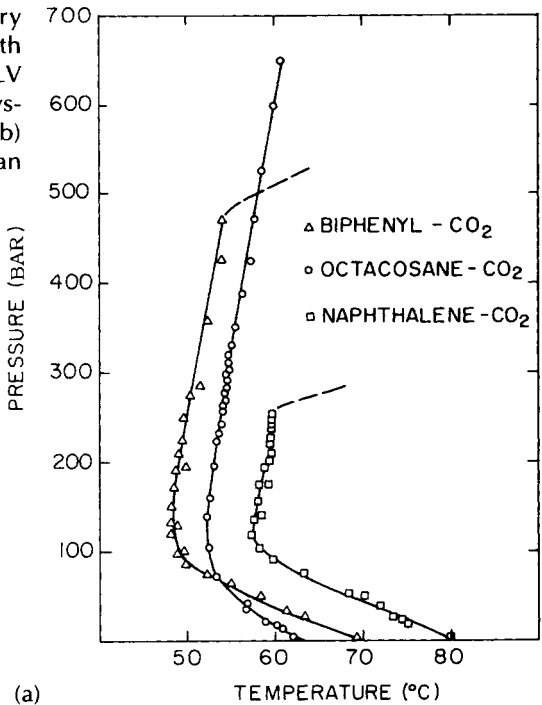
Now consider the case depicted in figure 3.20c, an isotherm at the UCEP temperature (see figure 3.19). At the UCEP pressure there is a vapor–liquid critical point in the presence of solid. This requires the solid–liquid equilibrium curve to intersect the liquid–gas envelope precisely at the binary liquid–gas critical point and, hence, exhibit a negative horizontal inflection, i.e.,  $(\partial P/\partial x)_T = 0$ . Notice that the vapor–liquid envelope has not shrunk to a point, as it did at the naphthalene–ethylene UCEP. The solid curve shown in figure 3.20d is the solubility isotherm obtained if a flow-through apparatus is used and only the solubility in the SCF phase is determined. This solid curve has the characteristics of the 55°C biphenyl–carbon dioxide isotherm shown in figure 3.17. So the 55°C isotherm represents *liquid* biphenyl solubilities at pressures below ~475 bar and *solid* biphenyl solubilities at pressures above 475 bar.

For the naphthalene–ethylene and biphenyl–carbon dioxide systems, the effect of the binary liquid–gas critical point is rapidly diminished as the pressure is increased above the UCEP pressure. For the naphthalene–ethylene system, where the UCEP is at a modest pressure, the solid–fluid equilibrium curve quickly attains a limiting solubility at pressures greater than the UCEP pressure. For the biphenyl–carbon dioxide system, where the UCEP pressure is more than twice that of the naphthalene–ethylene system, the solid–fluid equilibrium curve decreases sharply to lower concentrations of heavy component as the pressure is increased above the UCEP pressure. This solubility behavior is a consequence of a free volume effect that results from the large disparity in size between biphenyl and carbon dioxide (Rance and Cussler, 1974; von Tapavicza and Prausnitz, 1976). At very high pressures, increasing the pressure further reduces the free volume between carbon dioxide molecules available to the biphenyl molecules and reduces the solubility of biphenyl. Carbon dioxide essentially “squeezes out” the biphenyl at these high pressures.

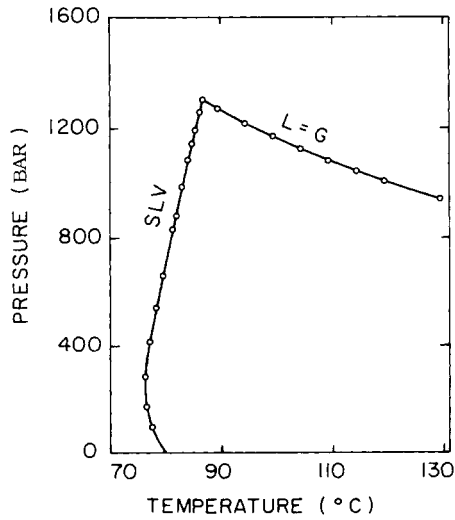
Figure 3.20e shows the solubility behavior at a temperature well above the UCEP temperature (see figure 3.19). This diagram shows that a variety of phase behaviors can exist at high pressures. The liquid–solid equilibrium curve now does not reintersect the liquid–gas envelope at high pressures, since the SLV line is not reintersected at high pressures.

A number of solid–SCF systems have been reported in which a temperature minimum exists in the three-phase SLV line (van Hest and Diepen, 1963; McHugh and Yogan, 1984). Some examples are shown in figure 3.21. The UCEP for the methane–naphthalene system is at very high pressures compared to the carbon dioxide–naphthalene system. The large difference in UCEP conditions for these two systems is a direct manifestation of the much reduced solvent power of methane compared to carbon dioxide. Simply put, methane is behaving more like an ideal gas, since its reduced temperature,  $T_R =$

**Figure 3.21** Examples of binary solid–supercritical fluid systems with a temperature minimum in the SLV line: (a) carbon dioxide–solid systems (McHugh and Yogan, 1984); (b) methane–naphthalene system (van Hest and Diepen, 1963).



(a)



(b)

$(T/T_c) \approx 2.0$ , is very high compared to that of carbon dioxide,  $T_R \approx 1.1$ . To overcome ideal gas behavior, it is necessary to compress methane to very high pressures to obtain reasonable methane densities and, hence, solvent power.

It is very important to be aware that a solid can melt at temperatures well below its normal melting point when in contact with a supercritical fluid at high pressures. For instance, King and coworkers describe a spectroscopic technique for obtaining solid-solubility data at high pressures; the solubility data were subsequently used to calculate the second cross-virial coefficient for the solid-SCF mixture (King and Robertson, 1962; Najour and King, 1966). But in some cases, their thermodynamic analysis of the data is wrong, since they did not recognize that the heavy solid had, in fact, melted at certain experimental temperatures and pressures. It is virtually impossible to determine whether the solid melts on the basis of the shape of the solubility isotherm if only SCF solubility data are obtained. As previously described, it is not possible to determine whether the 50°C biphenyl–carbon dioxide isotherm in figure 3.16, by itself, represents solid–SCF or liquid–SCF equilibria. Chapter 4 describes experimental techniques that can be used to determine the  $P$ – $T$  location of the SLV line so that blind solid solubility measurements can be made reliably.

Another pitfall awaits the experimentalist who is unaware of the melting behavior of a heavy solid under the influence of an SCF. It is possible that at certain  $P$ – $T$  conditions the SCF-rich phase can become more dense than the liquid phase that is formed when the solid melts. If this density inversion occurs, also called a barotropic phenomenon, the heavy liquid phase is pushed out of the extractor by the SCF-rich phase in a flow-type experiment. Such a density inversion is observed by McHugh and coworkers for the carbon dioxide–octacosane system (McHugh and Yogan, 1984). At 52°C and at pressures above about 260 bar, the carbon dioxide-rich “gas” phase becomes more dense than the octacosane-rich liquid phase. The  $P$ – $T$  and  $P$ – $x$  diagrams for this system are shown in figure 3.22. A density inversion has also been observed for the xenon–naphthalene system (McHugh, Seckner, and Krukoni, 1984; McHugh et al., 1988). The  $P$ – $T$  and  $P$ – $x$  diagrams for the supercritical xenon–naphthalene system are shown in figure 3.23.

## POLYMER–SUPERCRITICAL FLUID PHASE DIAGRAMS

An important subset of high-pressure phase diagrams is that of polymer–SCF mixtures. This area has not been as extensively studied since it wasn’t until about the late 1920s that polymers were accepted as substances having well-defined molecular identities (Munk, 1989). Although it was known for almost 100 years that alcohol–SCF mixtures can exhibit LLV behavior near the critical point of the SCF solvent (Kuenen and Robson, 1899), it wasn’t until the early 1960s that similar phenomena were discovered for nonpolar polymer–solvent mixtures (Freeman and Rowlinson, 1960). The scientific interest in the high-pressure phase behavior of polymer solutions was initially driven by the

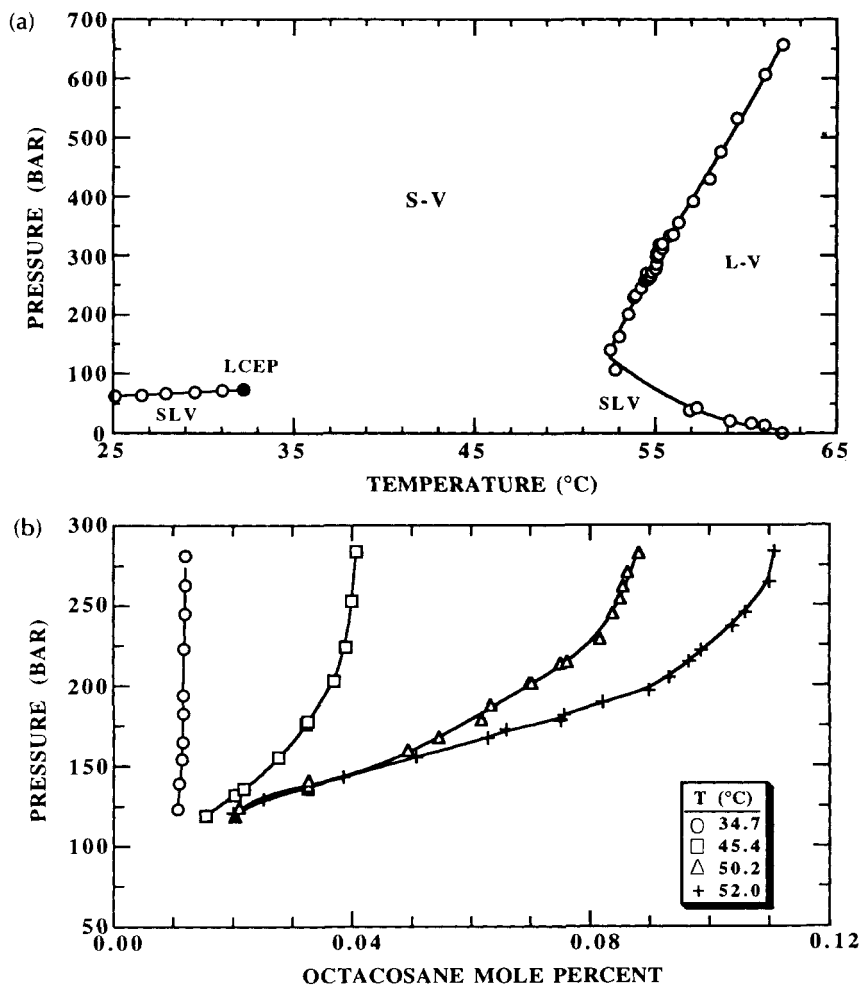


**Figure 3.22** Phase behavior of the carbon dioxide-octacosane system (McHugh, Seckner, and Yogan, 1984): (a)  $P$ - $T$  trace of the SLV lines; (b)  $P$ - $x$  diagram. The pressure limitation of the equipment was reached before the UCEP was obtained.

technological need to make polyethylene. A large percentage of the polyethylene market is supplied by free-radical production at pressures in the vicinity of 2,000 bar and temperatures of 150–250°C. Introduction of the Unipol® process by the Union Carbide Corporation in the late 1970s threatened to make obsolete the high-pressure polymerization process. But the free-radical process for producing polyethylene homopolymer and ethylene-based copolymers has survived and, because of its robust chemistry, has even flourished (Baron, 1990). Hence, there has been renewed interest in understanding the high-pressure behavior of a variety of polymer-solvent mixtures.



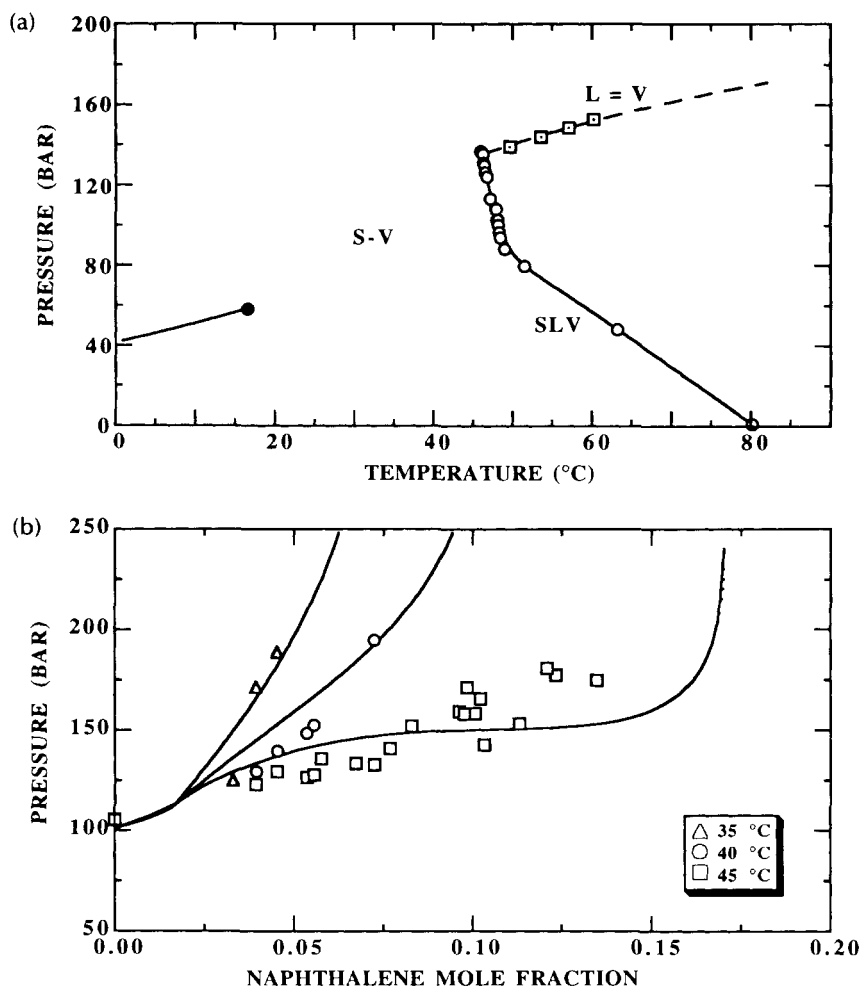


**Figure 3.23** Phase behavior of the xenon-naphthalene system (Krukoniš, Seckner, and McHugh, 1984; Watkins et al., 1988): (a)  $P$ - $T$  trace of the SLV lines; (b)  $P$ - $x$  diagram.

Ehrlich and coworkers are credited with the earliest fundamental high-pressure phase behavior studies of polyethylene-solvent mixtures published in the mid-1960s (Ehrlich, 1965; Ehrlich and Graham, 1960; Ehrlich and Kurpen, 1963). In the late 1960s and early 1970s Patterson and coworkers developed a large number of polymer-solvent phase diagrams (Zeman et al., 1972; Zeman and Patterson, 1972; Siow, Delmas, and Patterson, 1972). Within the past ten years, the polymer-SCF data base has increased considerably (Irani and Cozewith, 1986; Rätzsch, Findeisen, and Sernow, 1980; Rätzsch et al., 1982, 1983; Wohlfarth et al., 1982; Condo, 1989; Chen and Radosz, 1991; Kiran,

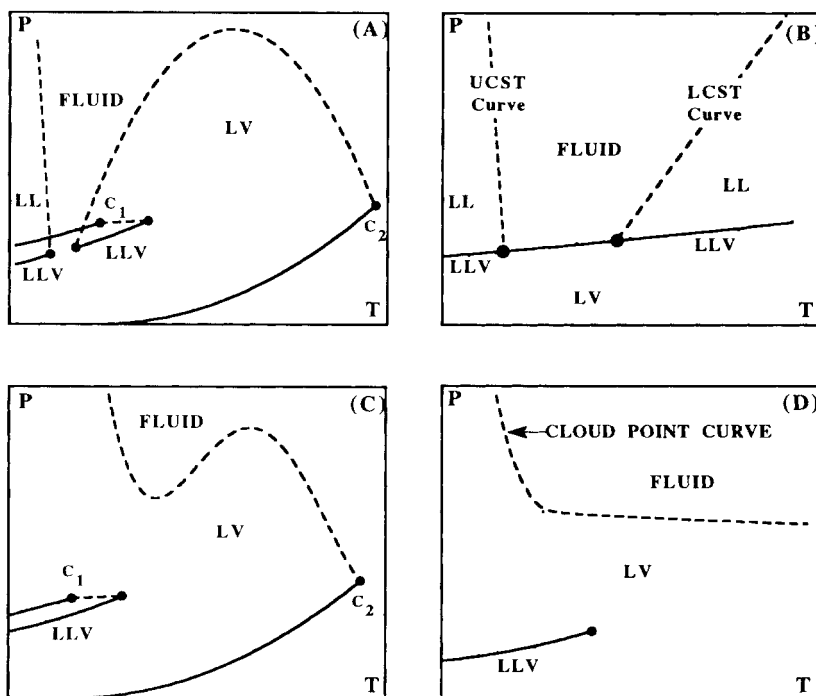


**Figure 3.24** Comparison of the schematic  $P$ - $T$  diagrams for small molecule systems with those for polymer-solvent systems: (A), type-III system for a small molecule system where the vapor-liquid equilibrium curves for two pure components end in their respective critical points,  $C_1$  and  $C_2$ ; (B), polymer-solvent type-III system; (C), type-IV system for a small molecule system; and (D), polymer-solvent type-IV system.

Saraf, and Sen, 1990; Kiran, Zhuang, and Sen, 1991; Saraf and Kiran, 1988a, 1988b; Hasch et al., 1992, 1993; McHugh, Hasch, and Lee, 1991; Meilchen, Hasch, and McHugh, 1991; Meilchen et al., 1991; Watkins et al., 1991). Fortunately, it is possible to treat a polymer as a pseudosingle component and, thus, to describe phase behavior using the same diagrams as given in the previous pages. Following the format of this chapter, we first describe the phase behavior of mixtures consisting of amorphous polymers that do not crystallize. We then describe the behavior for those mixtures that have crystallizable polymers.

The phase behavior for the polymer-solvent systems can be described using two classes of binary  $P$ - $T$  diagrams, which originate from  $P$ - $T$  diagrams for small molecule systems. Figure 3.24A shows the schematic  $P$ - $T$  diagram for a type-III system where the vapor-liquid equilibrium curves for two pure components end in their respective critical points,  $C_1$  and  $C_2$ . The steep dashed line in figure 3.24A at the lower temperatures is the  $P$ - $T$  trace of the UCST

curve described earlier. The UCST type of critical mixture curve represents liquid + liquid  $\rightarrow$  fluid transitions, which are usually governed by enthalpic interactions between the mixture components. Enthalpic interactions are less sensitive to pressure; this leads to a curve with a very steep slope. The other critical mixture curve shown in figure 3.24A starts at the critical point of the less volatile component, exhibits a pressure maximum, and eventually intersects an LLV region at conditions typically close to the critical point of the more volatile component. The labeling in figure 3.24A implies that liquid + vapor  $\rightarrow$  fluid transitions occur along this critical mixture curve. But the transitions experimentally observed along this curve at conditions near the critical point of the more volatile component are more characteristic of liquid + liquid  $\rightarrow$  fluid transitions. So this portion of the curve is termed an LCST curve, as the two phases coalesce into a single phase when the temperature is lowered isobarically.

Figure 3.24B shows the schematic  $P$ - $T$  diagram for a pseudobinary polymer-solvent mixture that is the analog of the diagram given in figure 3.24A (Freeman and Rowlinson, 1960; Allen and Baker, 1965; Baker, Clemson, and Allen, 1966; Zeman et al., 1972; Zeman and Patterson, 1972; Siow, Delmas, and Patterson, 1972; McHugh and Guckes, 1985; McClellan, Bauman, and McHugh, 1985; McClellan and McHugh, 1985). It is the large difference in size between the mixture components that suppresses many of the features of the phase diagram shown in figure 3.24A. A pure polymer does not have a critical point or a vapor pressure curve, so the high-temperature portion of the critical mixture curve does not exist. It is therefore eliminated from figure 3.24B.

Experimentally the high-temperature and low-temperature LLV lines for a polymer-solvent mixture superpose onto the vapor pressure curve of the pure solvent. The LLV line at high temperatures is bounded at one end by a liquid + vapor  $\rightarrow$  fluid transition in the presence of a second liquid phase and, at the other end, by the intersection of the higher-temperature branch of the critical mixture curve where a liquid + liquid  $\rightarrow$  fluid transition occurs in the presence of a vapor phase.

Both the UCST and LCST branches of the critical mixture curve are often referred to as cloud point curves. For polymer-solvent systems, the pressure or temperature interval for a clear to totally opaque fluid  $\rightarrow$  liquid + liquid transition along the UCST or LCST curves can be one hundred times greater than the interval for small molecule systems, if the polymer has a weight-average to number-average molecular weight ratio greater than  $\sim 1.5$ . The phase transition is not very distinct, it just progressively gets cloudier and cloudier; hence the name cloud point.

It is common to report the cloud point as the condition where a 90% decrease in light transmitted through the solution is observed. Although theoretically the concentration of the mixture at each  $P$ - $T$  point along the cloud point curve should be different the variation in concentration is usually between 5 and 15 wt% (Zeman et al., 1972; Irani and Cozewith, 1986). This is equivalent to saying that the rounded tops of the pressure-composition

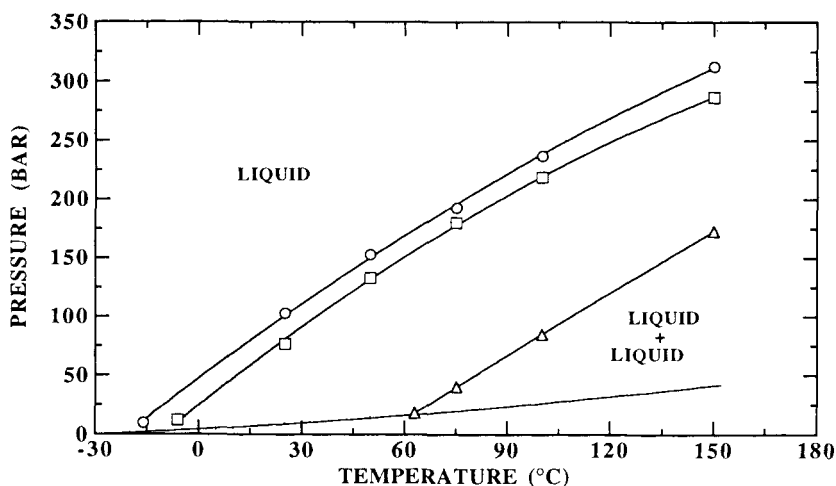
isotherms are essentially flat over a modest composition range. A good approximation to an LCST or UCST curve can thus be obtained by determining the  $P$ – $T$  trace of a constant composition cloud point curve with a polymer concentration of  $\sim 5$  wt%.

The genesis of the UCST curve for polymer–solvent systems is usually ascribed to enthalpic interactions between the mixture components, which are relatively insensitive to pressure for these constant density systems. The UCST curve can be modeled well with a liquid solution model that adequately accounts for specific interactions between the segments of polymer and the solvent. Examples of interactions are hydrogen bonding and polar interactions. The model also needs to account for the combinatorial entropy of mixing solvent molecules with the many segments that make up a single polymer chain (Prausnitz, 1969).

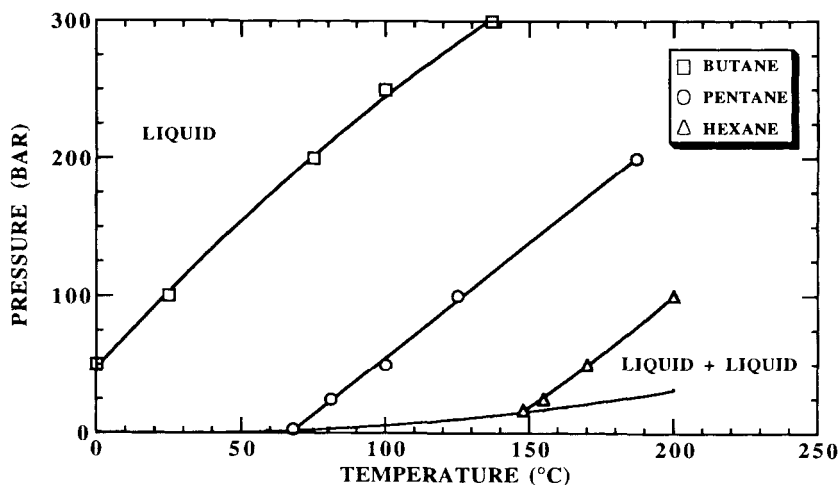
On the other hand, the genesis of the LCST curve is usually ascribed to the large differences in the thermal expansion or free volume of the polymer and solvent (Patterson, 1968). As the polymer solution is heated, the solvent expands at a much faster rate than the polymer so that the dissolution of the polymer in the solvent is associated with a large decrease in the change of entropy of mixing. This entropy decrease occurs as solvent molecules are forced to condense around the polymer to dissolve it. Eventually the loss in entropy in forming a single phase is so great that the free energy of mixing becomes positive and the solution splits into two phases. It is necessary to use a model that allows for density changes in the solution to predict an LCST curve. Although the entropic effect can be quite large at an LCST, enthalpic effects cannot be summarily dismissed when explaining the occurrence of the cloud point. It is therefore reasonable to expect the  $P$ – $T$  location of the LCST curve to be a function of the chemical nature of the polymer and solvent as well as the molecular weight of the polymer and the critical temperature of the solvent.

Figure 3.25 shows typical cloud point behavior for a nonpolar polymer, polyisobutylene (PIB), in a nonpolar hydrocarbon solvent, butane (Zeman et al., 1972). The UCST curves are not shown in this figure. As the molecular weight of the polymer increases, the cloud point curve is shifted to lower temperatures so that the single-phase region of polymer–solvent miscibility is reduced. The magnitude of the temperature shift of the cloud point curve diminishes as the molecular weight of PIB becomes very large. Figure 3.26 demonstrates the effect of solvent quality on the  $P$ – $T$  location of the cloud point curve (Zeman et al., 1972). In this instance the molecular weight of the PIB is fixed at  $1.66 \times 10^6$  and the solvents are butane, pentane, and hexane. The cloud point curve is shifted to higher temperatures—the region of miscibility is increased—as the difference between the free volume of the solvent and the PIB decreases with progressively higher molecular weight solvents.

Figure 3.24C shows a type-IV  $P$ – $T$  diagram that can occur with small molecule mixtures if the disparity in the size and/or the intermolecular



**Figure 3.25** Effect of molecular weight on the phase behavior of the nonpolar polyisobutylene (PIB) in nonpolar butane (Zeman et al., 1972). PIB  $M_w$ :  $\circ$   $-1.7 \times 10^6$ ;  $\square$   $-0.7 \times 10^6$ ;  $\triangle$   $-6.0 \times 10^3$ .



**Figure 3.26** Effect of solvent quality on the location of the cloud point curve for polyisobutylene in butane, pentane, and hexane (Zeman et al., 1972). The molecular weight of the polyisobutylene is  $1.66 \times 10^6$ .

potentials of the mixture components becomes very large. The occurrence of the phase behavior shown in figure 3.24C can be traced back to figure 3.24A. As the disparity in the properties of the two components increases, the temperature range between the UCST and the critical mixture curves shown in figure 3.24A becomes smaller and smaller. Eventually the difference in properties of

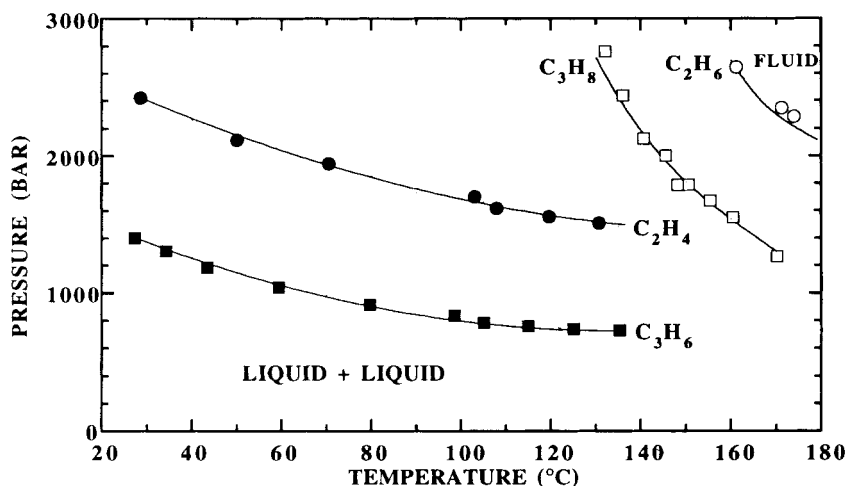


**Figure 3.27** Cloud point behavior of the poly(ethylene-*co*-methyl acrylate) (69 mol% ethylene and 31 mol% methyl acrylate) in ethane, propane, ethylene, and propylene. The copolymer concentration is fixed at 5 wt% and the weight-average molecular weight of the copolymer is 99,000 with a molecular weight polydispersity of 3.0. (Hasch et al., 1993.)

the mixture components becomes so large that the UCST and critical mixture curves merge into a single critical mixture curve exhibiting a pressure minimum at low temperatures. It is important to remember that the critical mixture curve in figure 3.24C is only one possible schematic representation of type-IV behavior. For example, certain water–hydrocarbon mixtures have critical mixture curves that have a positive slope going to higher temperatures and pressures starting at the critical point of water.

Figure 3.24D shows how figure 3.24C is transformed for polymer–solvent systems. The cloud point curve in figure 3.24D can be roughly interpreted as a combination of LCST-type transitions at high temperatures and UCST-type transitions at lower temperatures. An example of the phase behavior shown in figure 3.24D is given in figure 3.27 for a number of poly(ethylene-*co*-methyl acrylate)–hydrocarbon solvent mixtures. The cloud point curves in figure 3.27 demonstrate dramatically the role of polar interactions and free volume effects in governing copolymer solubility characteristics for a polar copolymer (64 mol% ethylene and 36 mol% methyl acrylate) with four very simple hydrocarbon solvents: ethane, ethylene, propane, and propylene.

Despite its higher polarizability and critical temperature, propane is a much poorer solvent than ethylene for this copolymer (see table 3.4). It is the polar interactions between ethylene, which has a quadrupole moment, and the methyl acrylate groups in the backbone of the copolymer, which have dipole moments, that dominate free volume effects. There is no significant difference between the molar densities of propane and ethylene at the temperatures and

**Table 3.4** Properties of the Solvents Used in a Poly(Ethylene-*co*-Methyl Acrylate)–Hydrocarbon Study. The symbols for polarizability, dipole moment, and quadrupole moment are  $\alpha$ ,  $\mu$ , and  $Q$ , respectively

<i>Solvent</i>	$T_c$ (°C)	$P_c$ (bar)	$\rho_c$ (g/cm <sup>3</sup> )	$\alpha \cdot 10^{25}$ (cm <sup>3</sup> )	$\mu$ (debye)	$Q \cdot 10^{26}$ (erg <sup>1/2</sup> cm <sup>5/2</sup> )
C <sub>2</sub> H <sub>4</sub>	9.2	50.4	0.217	42.3	0.0	+1.5
C <sub>2</sub> H <sub>6</sub>	32.3	48.8	0.203	45.0	0.0	−0.65
C <sub>3</sub> H <sub>8</sub>	96.7	42.5	0.217	62.9	0.0	?
C <sub>3</sub> H <sub>6</sub>	91.9	46.2	0.236	62.6	0.4	?

pressures shown in figure 3.27. When using nonpolar propane, operating temperatures need to be high enough to reduce the polar segment–segment interactions within the polymer. This is to make the polymer accessible to the solvent. At high temperatures, elevated pressures are needed to increase the density of propane. This reduces the free volume difference between the polymer and solvent and makes the polymer soluble in propane.

The impact of the quadrupole moment contribution of the solvent on the cloud point behavior is further seen by comparing the cloud point curves for solvents of the same size and polarizability but of different polarity. Ethane and ethylene have very similar critical properties, densities, and polarizabilities, as do propane and propylene. The cloud point curve for propylene is shifted to lower temperatures by more than 125°C relative to the curve with propane, and it is also shifted by ~800 bar to lower pressures. Hence, with propylene, a much expanded single-phase region is obtained. A shift of similar magnitude and a similar expanded single-phase region are also observed with ethylene compared to ethane. Propylene can be considered as a pseudomixed solvent system for this copolymer; it has a quadrupole moment comparable to that of ethylene that should interact with the polar methyl acrylate segments of the copolymer, and it has a higher polarizability than ethylene to interact with the nonpolar ethylene segments of the copolymer. In addition, propylene has a small dipole (~0.36 debye) which interacts favorably with the polar methyl acrylate groups.

If the polymer exhibits any significant degree of crystallinity, it is possible for the crystallization boundary to intrude on the fluid phase portion of the phase diagram and obscure the low-temperature branch of the cloud point curve (Ehrlich and Kurpen, 1963; Meilchen, Hasch, and McHugh, 1991). At conditions near the crystallization temperature of the polymer, fluid → liquid + vapor transitions become fluid → fluid + solid transitions. The phase behavior of solid polymer–SCF mixtures is schematically similar to that of the ethylene–naphthalene system described previously. Because of its large size and molecular weight distribution, the polymer does not melt and solidify at precisely the same temperature as it does for a small molecular weight

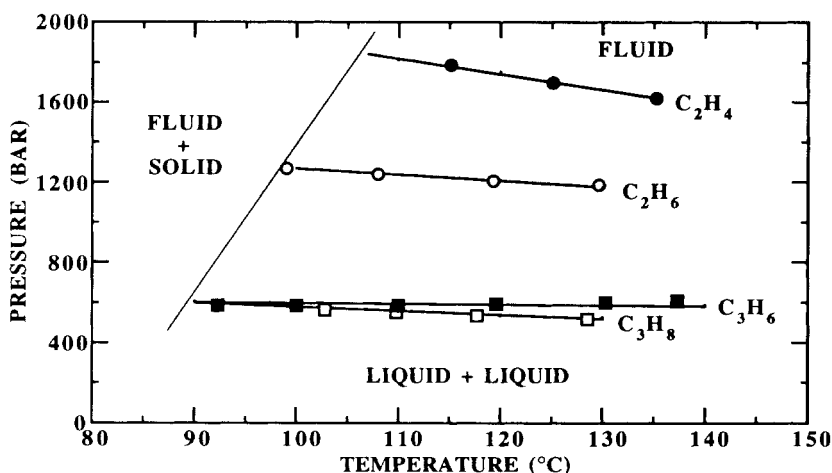


**Figure 3.28** Cloud point curves for polyethylene in ethylene, ethane, propane, and propylene. The polymer concentration is ~5 wt%. The weight-average molecular weight of the polyethylene is 108,000 with a molecular weight polydispersity of 5.4. The polyethylene is 37% crystalline with a  $T_{\text{melt}}$  of 113°C. (Hasch et al., 1993.)

crystalline solid. Also, the melting point depression of the polymer is much less than that exhibited by other low molecular weight solids, since the solubility of the solvent in the polymer-rich liquid phase is usually quite modest.

Figure 3.28 shows the  $P$ - $T$  diagram for four polyethylene–low molecular weight hydrocarbon mixtures. The cloud point pressures decrease substantially with increasing carbon number, or conversely polarizability, as a result of increased dispersion interactions between polyethylene and the solvent. Free volume differences between polyethylene and the hydrocarbons also decrease as the carbon number is increased. Even though ethane and ethylene have virtually identical polarizabilities, the cloud point curve with ethane is at a much lower pressure than that with ethylene, since the quadrupole moment of ethylene enhances ethylene–ethylene interactions relative to ethylene–polyethylene interactions because polyethylene is a nonpolar polymer. The two cloud point curves for polyethylene with propane and propylene are virtually identical. Evidently, the quadrupole moment for propylene is weak enough that propylene–propylene polar interactions do not substantially influence the strong dispersion interactions between polyethylene and each of these two solvents of virtually identical polarizabilities.

The molecular weight distribution of the polymer does have another effect on the phase diagram. Figure 3.24B shows that at pressures below the LLV line, vapor and liquid exist in equilibrium. But if the molecular weight distribution of the polymer is large, the LLV line becomes an area. This is because the system is now truly a multicomponent system. The LLV line



shown schematically in figure 3.24B actually represents the highest pressure at which three phases exist for a highly polydisperse polymer.

## PHASE DIAGRAMS FOR TERNARY MIXTURES

In the 1950s Francis measured what is undoubtedly the single largest collection of ternary phase diagrams for mixtures with carbon dioxide at 25°C and its saturation pressure (Francis, 1954). Although Francis did not extend his phase behavior studies into the critical region of carbon dioxide, his work does provide a basis for obtaining a qualitative estimate of the ability of supercritical carbon dioxide to separate a wide variety of binary mixtures. Recently, Dandge, Heller, and Wilson (1985) reformulated Francis's work in a manner that describes the effect of functional groups on the solubility behavior of carbon dioxide-solute systems. More will be said about the factors affecting the phase behavior of SCF-solute mixtures in chapter 5.

Unfortunately, the number of ternary phase diagrams reported in the literature for mixtures in which one of the components is a supercritical fluid is much more scarce than are low-pressure, liquid phase ternary diagrams. However, a compilation of supercritical ethylene-water-organic solvent phase diagrams can be found in the work of Elgin and coworkers (Elgin and Weinstock, 1959; Weinstock, 1952). They also report on the phase behavior of a large number of binary SCF-organic solvent mixtures with the objective of extrapolating binary phase behavior to ternary systems at conditions very near the critical point of the SCF (Chappelear, 1960; Close, 1951; Todd, 1952). The objective of the Elgin studies was to determine whether an organic-water mixture would be homogenized or split into two phases of different compositions if a low molecular weight supercritical fluid is forced into the liquid mixture.

It is instructive to consider the phase behavior classification scheme used by Elgin and coworkers for ternary systems consisting of a supercritical fluid with two other components that are liquids at room conditions. The ternary phase diagrams are grouped into three different classes based on the appearance of LLV regions in the diagrams. There are three binary pairs of components that make up the limiting behavior of a ternary mixture. Each of the three axes of a triangular diagram, at a given pressure and temperature, represents a single tie line from the appropriate  $P$ - $x$  diagram for that binary pair.

We will build the ternary diagrams by first considering the limiting behavior of the three binary pairs, that is the behavior along the three axes of the diagram, and then considering the behavior possible at all mixture compositions. Since we are now dealing with a three-component mixture, it is necessary to fix three degrees of freedom, such as  $P$ ,  $T$ , and overall mixture composition, to uniquely fix the compositions of the equilibrium phases if two phases exist. In the following section we fix temperature and vary pressure.

The isothermal ternary diagrams will get stacked one on top the other to build a prism that shows the effect of pressure on the phase behavior. The three sides of the prism are, in fact, the  $P$ - $x$  diagrams for each binary pair at the system temperature. The ternary diagrams in this chapter always put the SCF in the lower right-hand corner of the triangle. A, the component least soluble in the SCF, is always placed in the lower left-hand corner; B, the third component, is placed at the top of the triangle. We will assume that components A and B have vapor pressures that are less than 5 bar at modest temperatures, typical of organic solvents.

## Type I

A schematic representation of type-I ternary phase behavior is shown in figure 3.29. The three diagrams in this figure represent mixtures at a fixed temperature slightly higher than the critical temperature of the SCF but at three different pressures. The distinguishing feature of type-I ternary phase behavior is the absence of LLV immiscibility regions within the ternary

**Figure 3.29** Schematic phase diagrams for a type-I ternary mixture (Weinstock, 1952).

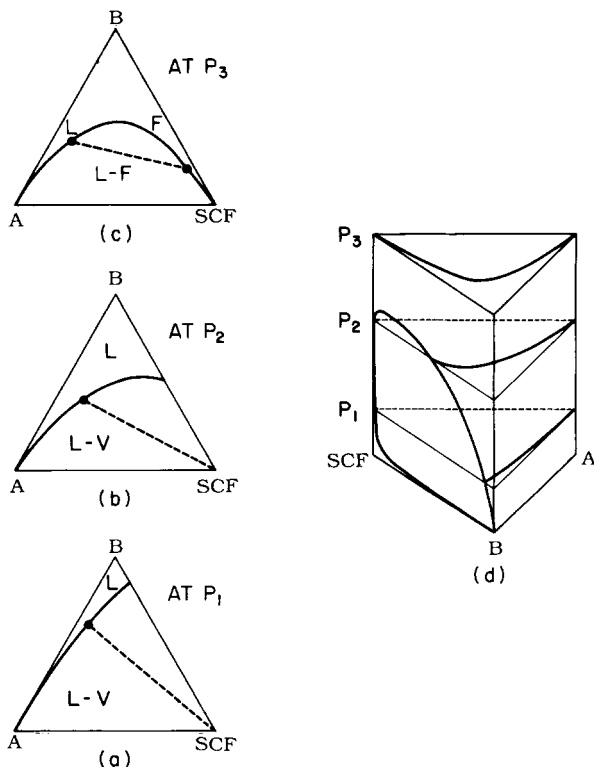


diagram. The phase behavior for this system at atmospheric pressure,  $P_1$ , is shown in figure 3.29a. At this pressure component A is miscible in all proportions with component B, while the SCF is virtually insoluble in A and only slightly soluble in B. The solid curve in the diagram is the binodal curve that separates the one-phase liquid region from the two-phase vapor-liquid region. Each axis of the ternary diagram can be obtained from the tie lines at  $P_1$  of the  $P$ - $x$  diagrams for the SCF-A system, SCF-B system, and the A-B system. In this example, components A and B are infinitely miscible at the temperatures and pressures considered in figure 3.29 so there are no tie lines on any of the A-B axes of the ternary diagrams. The tie line shown in figure 3.29a indicates that the gas phase is virtually pure ethylene at this temperature and very low pressure.

In figure 3.29b the pressure of the system has been increased to a point slightly below the critical pressure of the SCF. At this pressure the SCF still remains virtually insoluble in component A but its solubility in B has increased markedly, i.e., the tie line for the SCF-B mixture has gotten smaller to reflect the increased solubility of component B in the SCF-rich phase and of the SCF in the B-rich phase. The binodal curve in the ternary diagram now bends further toward the SCF apex. The vapor phase composition remains essentially pure SCF since, at this temperature, we are assuming that the vapor pressures of components A and B are extremely low.

In figure 3.29c the pressure has now been increased to a value greater than the critical pressure for the SCF-B mixture. The SCF is now miscible in all proportions with B, and the binodal curve no longer intersects the SCF-B binary axis of the ternary diagram. Even at this elevated pressure, the SCF still remains virtually insoluble in A, as would be the case if the supercritical fluid were a low molecular weight hydrocarbon and component A were water (Culberson and McKetta, 1951). As shown in figure 3.29c, the binodal curve intersects the SCF-A binary axis in two locations. The tie lines for the ternary system now indicate that a liquid phase, mostly a mixture of A and B, is in equilibrium with a fluid phase, mainly the SCF with component B.

The slope of the tie line indicates that component B, which is miscible with A at low pressures, is now selectively extracted from the A-B mixture with SCF. An example of this type of SCF extraction process is suggested by the phase behavior shown in figure 3.30 for the ethanol-water-supercritical ethane system (McHugh, Mallett, and Kohn, 1983). There exist, at most, only two phases in the diagram at 50°C. This type of phase behavior is also observed for the ethanol-water-carbon dioxide system (Paulaitis, Gilbert, and Nash, 1981), the ethanol-water-ethylene system (Paulaitis, Gilbert, and Nash, 1981), and the isopropanol-water-carbon dioxide system (Kuk and Montagna, 1983) at modest temperatures. Elgin and Weinstock (1959) also present a number of organic solvent-water-ethylene systems that exhibit type-I ternary phase behavior.

An isothermal pressure-composition phase diagram is shown in figure 3.29d (Elgin and Weinstock, 1959; Treybal, 1968). As mentioned previously,

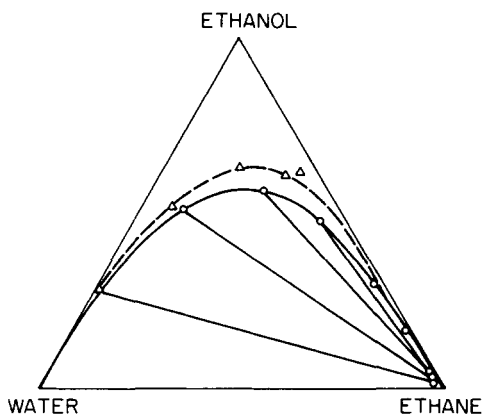


**Figure 3.30** Phase behavior of the ternary ethanol–water–supercritical ethane system at 50°C and 50.7 bar (triangles) and 81.1 bar (circles) (McHugh, Mallett, and Kohn, 1983).

the three faces of the prism represent the isothermal pressure–composition behavior for the three binary mixtures that comprise the ternary mixture.

## Type II

Type-II phase behavior is depicted in the isothermal ternary phase diagrams shown in figure 3.31. The distinguishing feature of type-II ternary phase behavior is that an LLV region appears within the pressure–composition prism but does not extend to the SCF–B face of the prism. The phase behavior at atmospheric pressure, shown in figure 3.31a, is identical to that previously described for type-I ternary phase behavior shown in figure 3.29a. If the pressure is increased to  $P_2$ , a pressure below the critical pressure of the SCF, a miscibility gap appears for varying SCF–A–B compositions. This creates liquid–liquid (LL) and liquid–liquid–vapor (LLV) regions in the phase diagram (see figure 3.31b). As the pressure is increased further (see figure 3.31c), the LL and LLV regions expand considerably.

The tie lines in the LL region in figure 3.31c are nearly parallel to the A–B axis of the diagram. When the tie lines are parallel to the A–B binary axis, the selectivity, defined as  $(y_A/x_A)/(y_B/x_B)$ , can approach values much greater than 1.0; this indicates that a very good separation of A from B is realized at this condition.

In the LLV region of the phase diagram the compositions of the three equilibrium phases are invariant, although the amount of each phase depends on the overall mixture composition. The composition of each of the three phases is defined by the location of the three corners of the LLV region within the ternary diagram.

If the pressure is further increased above the critical pressure for the SCF–B binary mixture, shown in figure 3.31d, the LLV miscibility gap disappears and the phase behavior becomes identical to that described for a

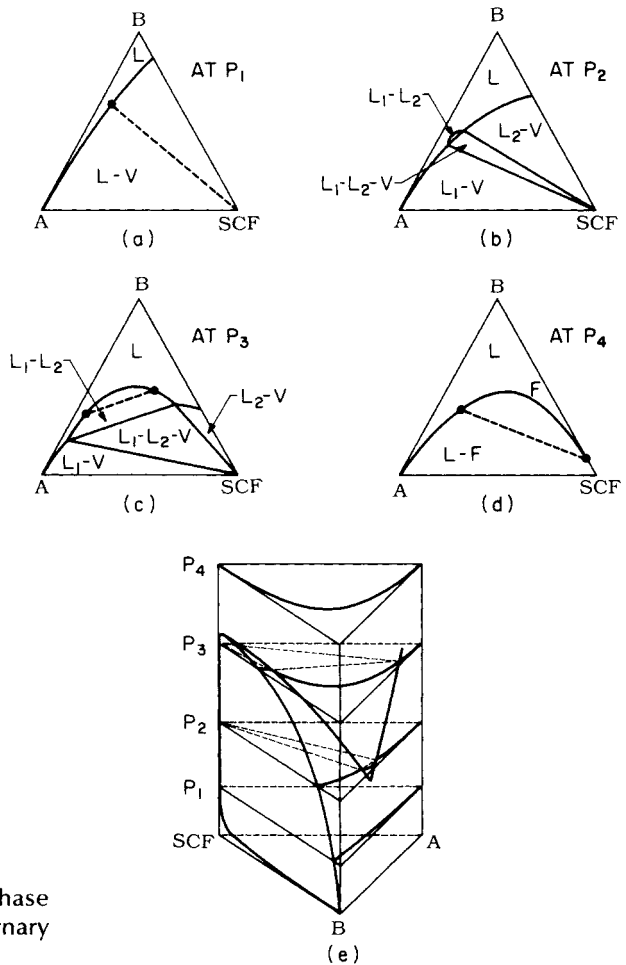


**Figure 3.31** Schematic phase diagrams for a type-II ternary mixture (Weinstock, 1952).

type-I ternary system at the same pressure. At this pressure, there exist at most two phases. An example of type-II ternary phase behavior is shown in figure 3.32 for the *n*-propanol–water–ethylene system (Weinstock, 1952). Numerous other type-II ternary systems are reported in the literature (Elgin and Weinstock, 1959; Paulaitis, Gilbert, and Nash, 1981; Kuk and Montagna, 1983; Paulaitis, Kander, and Diandreth, 1984).

### Type III

The distinguishing feature of type-III ternary phase behavior is that the binary A–B mixture already shows liquid–liquid immiscibility at very low pressures (see figure 3.33a). As SCF is added to the A–B mixture, a very large LLV

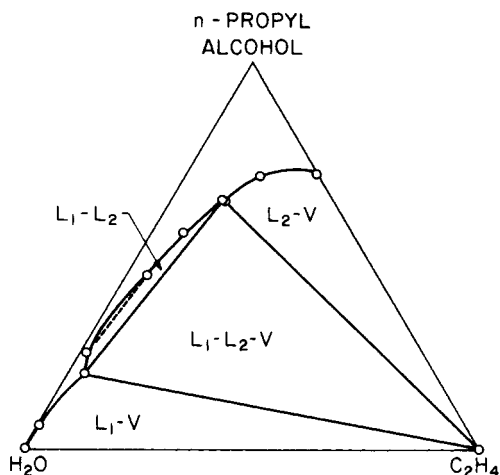


**Figure 3.32** Phase behavior of a ternary *n*-propanol–water–ethylene system at 15°C and 51.7 bar (Weinstock, 1952).

region appears in this diagram. As the pressure is increased (see figure 3.33b), the liquid–liquid region close to the A–B axis expands. As the pressure is increased to a value greater than the critical pressure for the SCF–B binary mixture, a single liquid–fluid solubility curve exists. In figure 3.33c the liquid–fluid solubility curve intersects the A–B axis at the ends of the binary A–B tie line. This indicates that, even at an elevated pressure, a miscibility region still exists in the A–B binary system.

For type-III ternary systems the liquid–liquid region increases with increasing SCF content (see figure 3.33b). Although B is only slightly miscible with A at low pressures and in the absence of SCF, it is now possible to use the SCF to separate even more A from B.

The methyl ethyl ketone (MEK)–water–ethylene system exhibits type-III ternary phase behavior, as shown in figure 3.34. Elgin and Weinstock (1959) use this phase behavior as a basis for a proposed single-stage process for dehydrating MEK–water mixtures using supercritical ethylene.

Although the classification of ternary phase behavior is described here at a fixed temperature, it is important to remember that a single ternary system can exhibit all three types of phase behaviors as the temperature of the system changes. Based on our classification of binary phase behavior, type-I ternary phase behavior above the critical temperature of the SCF solvent may revert to type-II or type-III ternary phase behavior if the operating temperature and pressure are adjusted to values near the critical point of the SCF solvent.

Kohn, Luks, and coworkers have compiled an extensive body of information on the binary and ternary phase behavior for mixtures consisting of normal hydrocarbons ranging from  $C_1$  through  $C_{36}$  with  $CO_2$ ,  $N_2$ , and various alcohols (Kim et al., 1967; Kohn, 1967; Rodrigues and Kohn, 1967; Rodrigues, McCaffrey, and Kohn, 1968; Wagner, McCaffrey, and Kohn, 1968; Huie, Luks, and Kohn, 1973; Zarah, Luks, and Kohn, 1974; Yang, Luks, and Kohn,

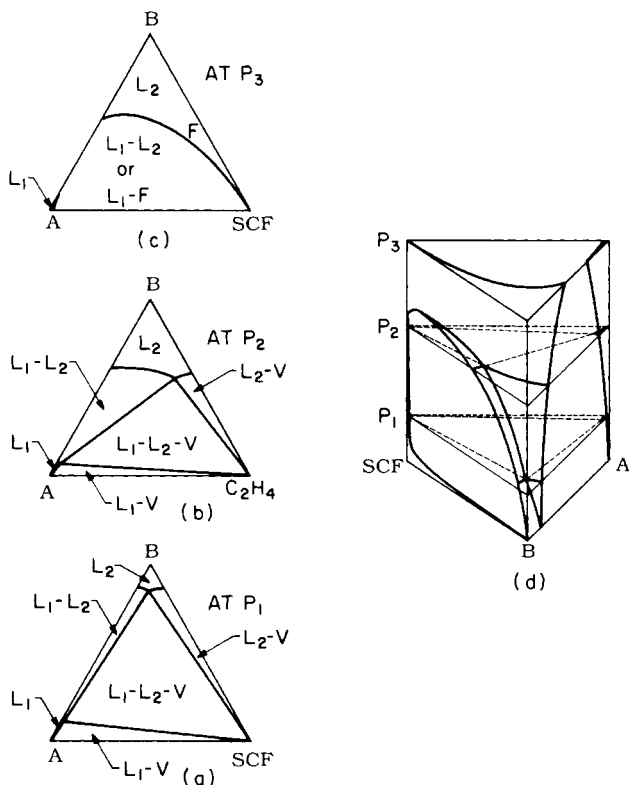


**Figure 3.33** Schematic phase diagrams for a type-III ternary mixture (Weinstock, 1952).

1976; Tiffin et al., 1978a, 1978b; Kohn et al., 1980; Hottovy, Kohn, and Luks, 1981, 1982; Kohn, Merrill, and Luks, 1983; Merrill, 1983; Merrill, Luks, and Kohn, 1983; Fall and Luks, 1984; Fall, Fall, and Luks, 1985). More recently Peters, de Swaan Arons, and coworkers have added  $C_2$  and  $C_2$ -hydrocarbon mixtures to this data base (Peters, Lichtenthaler, and de Swaan Arons, 1986; Peters, de Roo, and Lichtenthaler, 1987; Peters, van der Kooi, and de Swaan Arons, 1987; Peters, de Roo, and de Swaan Arons, 1987; Peters, Spiegelhaar, and de Swaan Arons, 1988; Coorens, Peters, and de Swaan Arons, 1988; de Goede et al., 1989). Much of this work is performed at cryogenic temperatures so it has application in the liquefied natural gas industry. Nonetheless, the phase behavior observed for these systems is entirely analogous to the phase behavior of the previously described systems.

Kohn and coworkers also report on the phase behavior of ternary systems consisting of ethane ( $C_2$ ) with  $n$ -hexadecane ( $C_{16}$ ) +  $n$ -eicosane ( $C_{20}$ ) (Wagner, McCaffrey, and Kohn, 1968) and  $n$ -nonadecane ( $C_{19}$ ) +  $n$ -eicosane ( $C_{20}$ ) (Kim et al., 1967). Both ternary mixtures exhibit LLV behavior in the vicinity of the critical point of ethane. For these systems it is possible to use supercritical ethane to separate  $C_{16}$  from  $C_{20}$  and to a lesser degree to separate  $C_{19}$  from  $C_{20}$

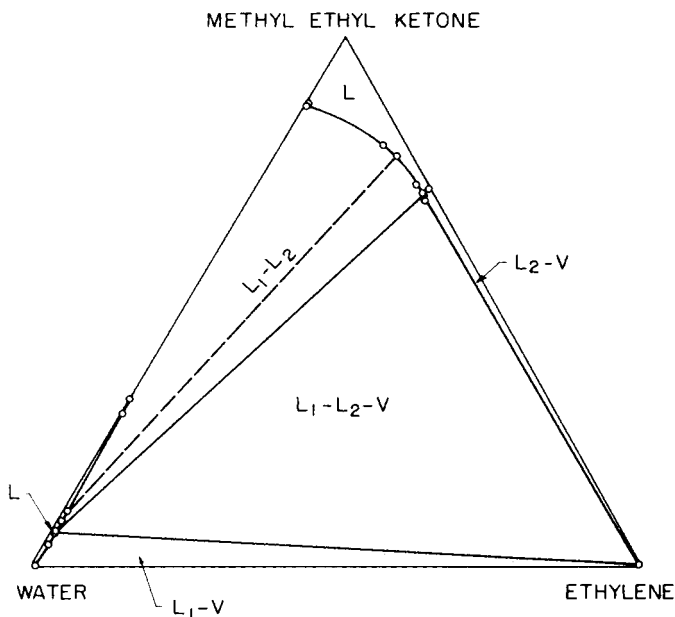


**Figure 3.34** Phase behavior of the methyl ethyl ketone–water–ethylene system at 15°C and 51.78 bar.

along the LLV curve. On an ethane-free basis, the selectivity is  $\sim 1.3$  for the  $C_2-C_{16}-C_{20}$  system compared to  $\sim 1.1$  for the  $C_2-C_{19}-C_{20}$  system.

The amount of experimental information available for ternary mixtures consisting of a single supercritical solvent and two nonvolatile solids is very limited. The  $P$ - $T$  diagram for such a system was described in detail in 1953 (van Gunst, Scheffer, and Diepen, 1953b), in a work that was an extension of research done by Smits in the early 1900s (Smits, 1903). An example of the  $P$ - $T$  behavior for solid<sub>1</sub>-solid<sub>2</sub>-SCF systems is shown in figure 3.35. The solubility data for the ethylene-naphthalene-hexachloroethane system was reported by van Gunst in his PhD dissertation (van Gunst, 1950). For solid<sub>1</sub>-solid<sub>2</sub>-SCF systems, a liquid-gas criticality may occur in the presence of both solids at a double critical end point. The solubility of both solids in the SCF-rich phase increases substantially due to the liquid-gas critical point, as explained previously for solid-SCF mixtures.

Kurnik and Reid described the solubility behavior for a number of binary solid mixtures consisting of combinations of phenanthrene, naphthalene, benzoic acid, and 2,3- and 2,6-dimethylnaphthalene extracted with supercritical carbon dioxide and ethylene. They found that for a binary solid mixture, the presence of one of the solid components solubilized in the SCF-rich phase enhances the solubility of the other solid component in the SCF-rich phase. They suggest that the first solid component acts as an entrainer, or so-called cosolvent, to enhance the solvent power of the pure SCF. For example, they



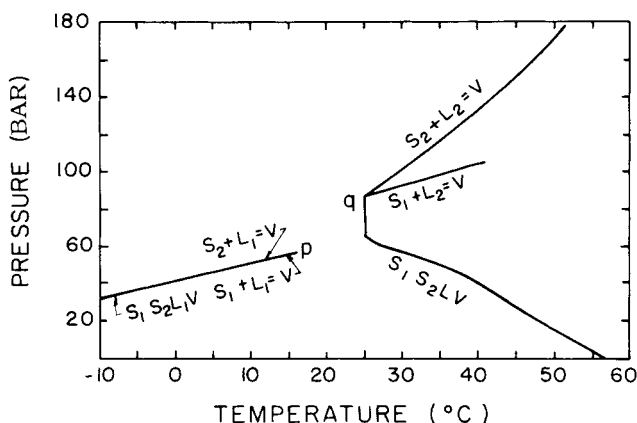


**Figure 3.35**  $P$ - $T$  behavior of a ternary mixture consisting of naphthalene, hexachloroethane, and supercritical ethylene (van Gunst, Scheffer, and Diepen, 1953b). The  $S_1S_2LV$ ,  $S_2 + L = V$ , and  $S_1 + L_1 = V$  lines superpose on one another. The  $S_2 + L_2 = V$  and  $S_1 + L_2 = V$  lines are critical mixture curves that occur when a solid phase is present.

show that the presence of naphthalene can enhance the solubility of phenanthrene by 200–300%. Although the solubility enhancements reported by Kurnik and Reid are very high, the absolute amount of the second component solubilized in the SCF-rich phase is still quite low. This might be anticipated because the solubility of the entrainer solid is quite high (e.g., about 10 wt%) and it substantially changes the solvent power of the solvent mixture relative to the pure SCF solvent. Conversely, the solubility of the entrainer solid is not materially enhanced by the small amount of the second component in the SCF-rich phase.

Schmitt (1984) verified the entrainer behavior reported by Kurnik and Reid. Schmitt and Reid (1984) show that very small amounts of an entrainer in the SCF-rich phase have very little effect on the solubility of a second component in that phase. This observation is consistent with the work of Kohn and Luks for ternary mixtures at cryogenic temperatures. The data of Kurnik and Reid have been corroborated for the naphthalene–phenanthrene–carbon dioxide system (Gopal et al., 1983). Lemert and Johnston (1989, 1990) also studied the solubility behavior of solids in pure and mixed solvents at conditions close to the upper critical end points. Johnston finds that adding a cosolvent can reduce the temperature and pressure of the UCEP while simultaneously increasing the selectivity of the solid in the SCF-rich phase. In these studies Johnston found the largest effects with a cosolvent capable of hydrogen bonding to the solute.

Some thirty years after their classic work on the phase behavior of

solid<sub>1</sub>-solid<sub>2</sub>-SCF systems, Koningsveld and Diepen described in detail the phase diagrams for systems consisting of two nonvolatile solids and a single SCF solvent (Koningsveld and Diepen, 1983; Koningsveld, Kleintjens, and Diepen, 1984). The ternary diagrams describe the solubility behavior that can be expected in various regions in  $P$ - $T$  space. Because of the complex phase behavior for this type of ternary system, no general guidelines are given for determining the selectivity of the SCF solvent for a given solid in a binary solid mixture. Lira and coworkers do a good job explaining the phase diagrams for solid<sub>1</sub>-solid<sub>2</sub>-SCF systems, reviewing the literature in this area, and determining the phase behavior for ternary systems with CO<sub>2</sub> as the SCF (White and Lira, 1991a, 1991b).

Another class of ternary mixtures are those of copolymer-solvent-cosolvent mixtures. While the effect of cosolvents on copolymers has been studied using light scattering and viscometry, very little attention has been paid to the contribution of a cosolvent to the global phase behavior of copolymer-solvent mixtures. One exception is the poly(ethylene-*co*-vinyl acetate) (EVAc)-ethylene-vinyl acetate system, which has been thoroughly investigated by Rätzsch and coworkers (Rätzsch, Findeisen, and Sernov, 1980; Rätzsch et al., 1982; Wohlfarth et al., 1982, 1984; Wohlfarth and Rätzsch, 1983). They first determined cloud point curves for binary mixtures of EVAc of varying acetate content in ethylene (Rätzsch et al., 1982).

The cloud point curves shift to lower pressures by as much as 250 bar as the vinyl acetate content in the backbone of the copolymer is increased from 3 to 20 mol%. This behavior is consistent with the results of Hasch and coworkers (Hasch et al., 1992) who found that the pressure of poly(ethylene-*co*-methyl acrylate)-ethylene cloud point curves decreased when the acrylate content was increased from 0 to 18 mol%. The decrease in the cloud point pressures can be rationalized as a consequence of the favorable increased polar interactions between ethylene, which has a quadrupole moment, and vinyl acetate or methyl acrylate, both of which have dipole moments. Rätzsch and coworkers (Rätzsch, Findeisen, and Sernov, 1980) followed up their EVAc-ethylene binary study with cosolvent studies using vinyl acetate as the cosolvent at concentrations equal to the vinyl acetate concentration in the backbone of the copolymer. The cosolvent studies showed that vinyl acetate as a cosolvent can lower the pressure of the cloud point curve by as much as 450 bar. This is not surprising; the copolymer is comprised of nonpolar ethylene and polar vinyl acetate repeat units, which should make it readily soluble in solvent mixtures of polar and slightly polar components. Another effect of adding a liquid cosolvent to a supercritical fluid solvent is to increase the density of the solvent mixture and, therefore, to decrease the free volume difference between the copolymer and the solvent. This density enhancement alone cannot explain the large changes in the cloud point pressures that are observed.

McHugh and coworkers have presented an extensive investigation of the effect of polar and hydrogen bonding cosolvents on the phase behavior of

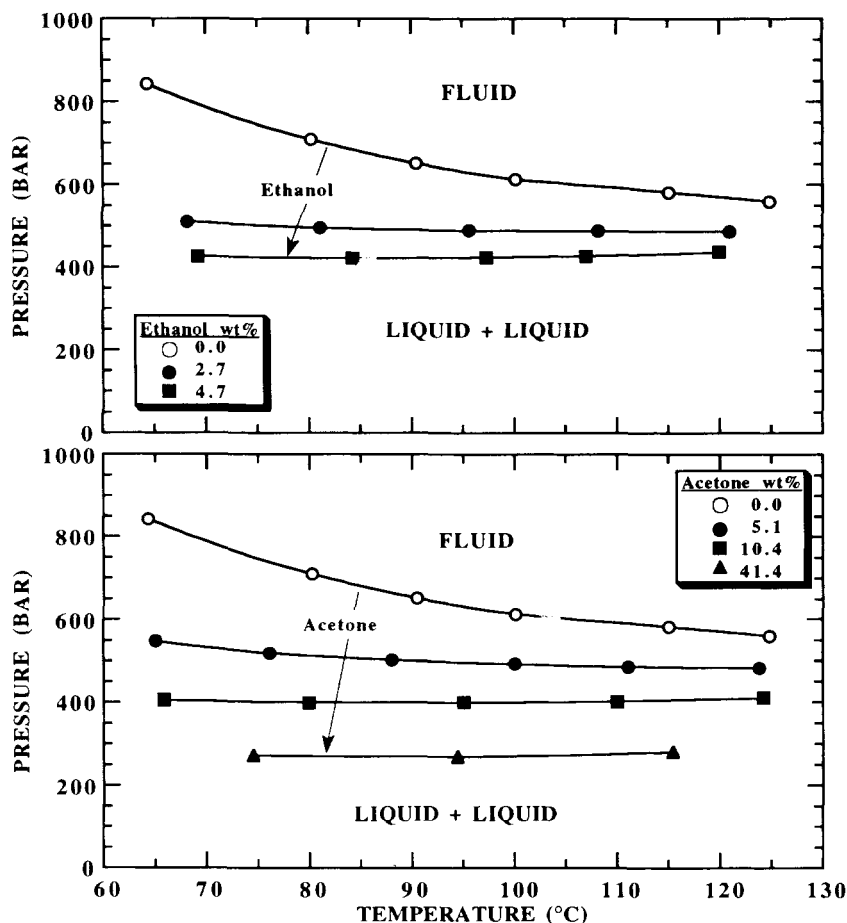


**Figure 3.36** The effect of ethanol and acetone cosolvents on the cloud point pressure of the poly(ethylene-co-methyl acrylate) (90 mol% ethylene and 10 mol% methyl acrylate)-propane system. The copolymer concentration is fixed at 5 wt% and the weight-average molecular weight of the copolymer is 34,000 with a molecular weight polydispersity of 2.0. This copolymer is ~15% crystalline. (Hasch et al., 1993.)

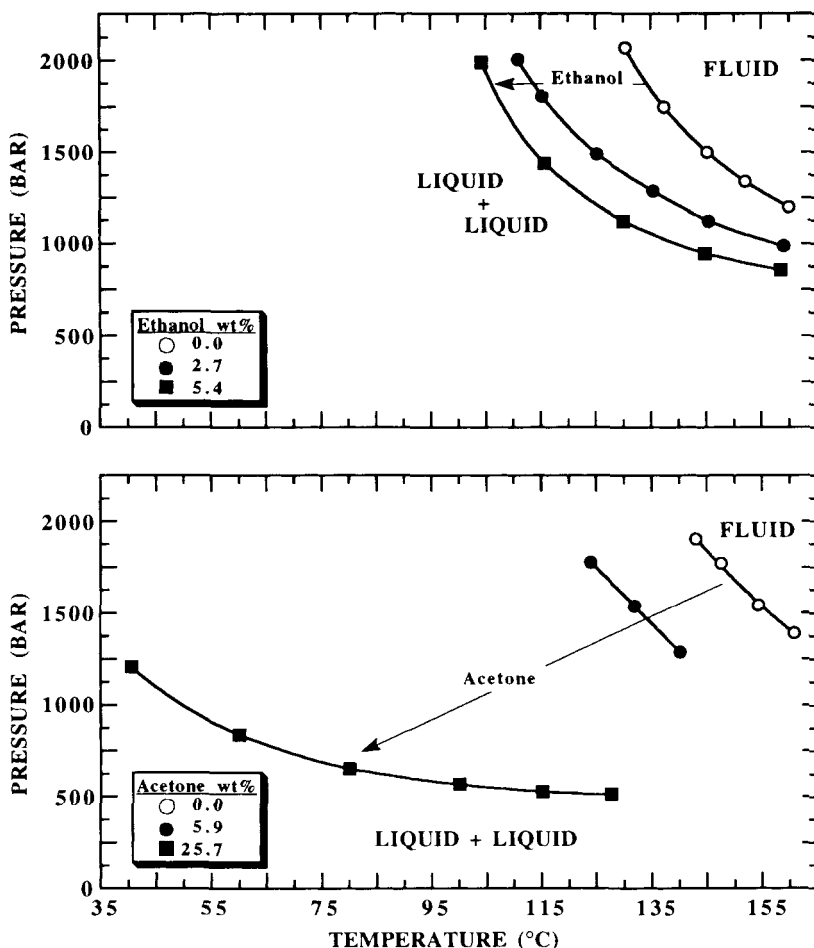
poly(ethylene-co-methyl acrylate) copolymers of varying acrylate content in propane and chlorodifluoromethane (Freon 22) (Meilchen, 1991; Meilchen et al., 1991; Hasch et al., 1993). All of their data were presented as cloud point curves; we highlight some of their results to show the effect of various intermolecular forces on the phase behavior. For this discussion the copolymers will be designated  $\text{EMA}_{A/B}$  where E represents ethylene, MA represents methyl acrylate, and the subscripts  $A/B$  represent the mole fraction of ethylene and methyl acrylate, respectively, in the backbone of the copolymer.

Figure 3.36 shows that ethanol and acetone both lower the cloud point

pressure of the EMA<sub>90/10</sub>–propane system. But at low concentrations, the decrease in cloud point pressures caused by ethanol is greater than the decrease caused by an equivalent amount of acetone. For example, at 100°C, 2.7 wt% ethanol reduces the cloud point pressure by ~100 bar, 4.7 wt% reduces the cloud point pressure another ~60 bar, but 7.0 wt% causes the polymer to fall out of solution. At low concentrations nearly twice as much acetone is needed to achieve the same reduction in pressure. The reason that ethanol is a better cosolvent at low concentrations is that ethanol can hydrogen bond to the methyl acrylate. However, once all the acrylate sites are occupied, the excess ethanol will hydrogen bond to itself and dramatically change the character of the mixed solvent. The occurrence of long-chain ethanol “associated complexes” causes the dielectric constant of the solvent to increase nonlinearly, which substantially increases the polarity of the mixed solvent. Since EMA<sub>90/10</sub> is predominantly nonpolar polyethylene, it cannot tolerate a highly polar solvent environment and it subsequently falls out of solution as the solvent polarity increases. Although acetone is a polar cosolvent that will eventually drive the EMA<sub>90/10</sub> out of solution, greater concentrations of acetone can be tolerated because acetone does not self-associate.

Figure 3.37 shows the experimental results for the EMA<sub>64/36</sub>–propane–cosolvent systems. Now the copolymer has increased amounts of methyl acrylate. The effect of ethanol on the phase behavior of the EMA<sub>64/36</sub>–propane is shown in the upper graph of figure 3.37. Ethanol at 2.5 wt% shifts the cloud point curve by ~30°C at an arbitrarily chosen pressure of 1,800 bar. But increasing the ethanol concentration to 5.4 wt% results only in an additional ~5°C increase in the miscibility region. Again, increasing the ethanol concentration to ~7 wt% causes the polymer to precipitate out of solution. Adding 6 wt% acetone to the EMA<sub>64/36</sub>–propane system reduces the cloud point temperature by about 25°C, while 2.5 wt% ethanol causes a 30°C shift. Hydrogen bonding makes ethanol the stronger cosolvent at low cosolvent concentrations. But figure 3.37 shows that significantly more acetone can be added to the system before the copolymer falls out of solution mainly because acetone does not self-associate. Notice that 26 wt% acetone increases the region of miscibility by over 100°C and also reduces the cloud point pressure by ~800 bar compared to the case of no acetone. This large shift in the cloud point curve is much greater than that observed for the EMA<sub>90/10</sub>. It is apparent that the addition of polar acrylate groups in the backbone of the polymer has a large impact on the location of the cloud point curve.

Finally, let us consider the effect of adding acetone or ethanol to the PMA–chlorodifluoromethane (Freon 22) system. Now the homopolymer and the solvent are polar. In addition, Freon 22 can hydrogen bond to base molecules but it does not self-associate. Figure 3.38 shows that now the cloud point curves have positive slopes typical of many polymer–liquid solvent mixtures. The data in figure 3.38 also show that only modest pressures are needed to obtain a single phase at temperatures greater than 70°C. The single phase region is expanded considerably with both cosolvents, although the effect of ethanol is slightly greater than the effect of acetone. It is not



**Figure 3.37** The effect of ethanol and acetone cosolvents on the cloud point pressure of the poly(ethylene-co-methyl acrylate) (69 mol% ethylene and 31 mol% methyl acrylate)-propane-system. The copolymer concentration is fixed at 5 wt% and the weight-average molecular weight of the copolymer is 58,900 with a molecular weight polydispersity of 1.9. (Hasch et al., 1993.)

surprising that both cosolvents have similar effects in Freon 22 since Freon 22 hydrogen bonds to methyl acrylate, to acetone, and to ethanol. The Freon 22 is in excess compared to the cosolvent concentration, so it hydrogen bonds to PMA and reduces the impact of ethanol. Any “free” ethanol will hydrogen bond to Freon 22, which reduces the possibility of ethanol self-association and also reduces the possibility of ethanol exhibiting “antisolvent” characteristics.

We have described the phase behavior of polymer-solvent-cosolvent mixtures where the cosolvent generally increases the solubility of the polymer

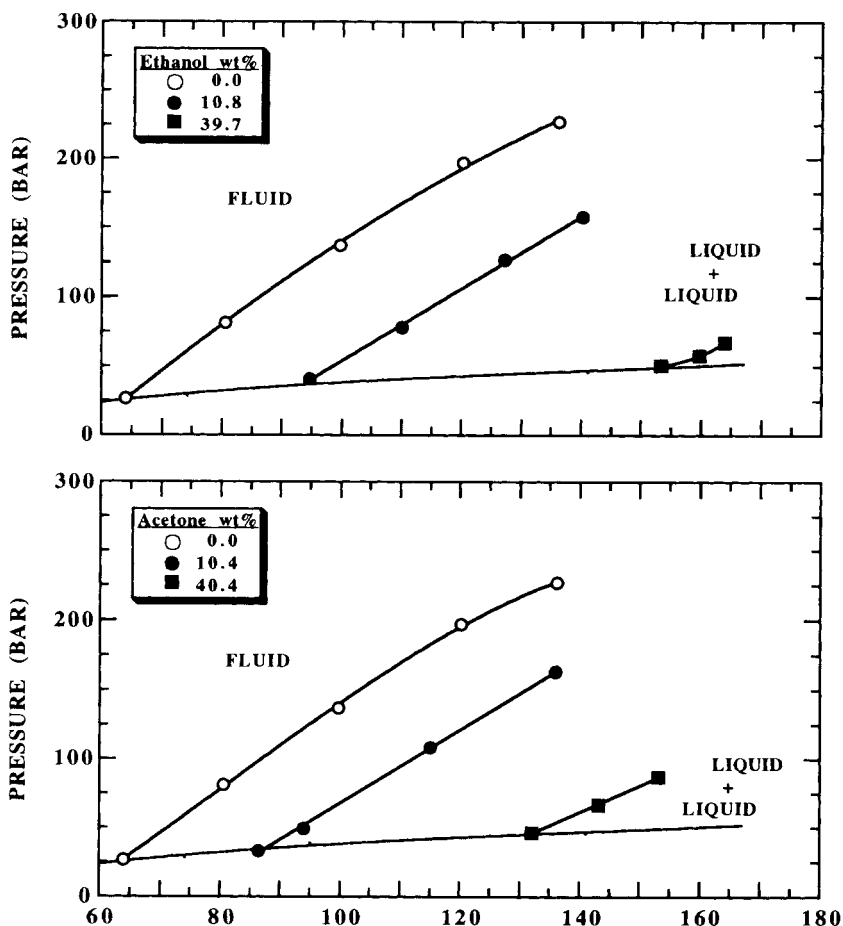


**Figure 3.38** The effect of ethanol and acetone cosolvents on the cloud point pressure of the poly(methyl acrylate)–chlorodifluoromethane system. The polymer concentration is fixed at 5 wt% and the weight-average molecular weight of the polymer is 30,700 with a molecular weight polydispersity of 2.9. (Hasch et al., 1993.)

in the supercritical fluid. There is another class of ternary polymer solution behavior in which a supercritical fluid is added to a polymer–solvent mixture to force the polymer out of solution. This type of phase behavior is considered in some detail by McHugh and coworkers (McHugh and Guckes, 1985; McClellan, Bauman, and McHugh, 1985; McClellan and McHugh, 1985) and by a number of workers at Exxon Chemical Company (Irani and Cozewith, 1986; Radosz et al., 1991). The principles underlying such a polymer–solvent–“SCF antisolvent” phase split are similar to those used in the propane deasphalting of petroleum mixtures. We return to these phase diagrams in chapter 9 when we discuss polymer–solvent phase splitting.

---

## Experimental Techniques in High-Pressure Studies

---

As described in the previous chapter, a wide variety of phase behavior can occur for mixtures at high pressures. It should now be obvious that it is extremely important to pinpoint the  $P$ - $T$  location of phase border curves, such as LLV and SLV curves, before doing solubility studies so that solubility behavior can be interpreted and cataloged correctly. Experimental techniques are described in this chapter for measuring the solubility of a heavy liquid or a heavy solid in a supercritical fluid. These techniques are either dynamic, where the solute is continually swept with the supercritical fluid, or static, where the solute and solvent are loaded into some type of high-pressure cell. Static techniques are used to determine the location of phase border curves in  $P$ - $T$  space and the solubility of a heavy solute in a supercritical fluid. Dynamic or flow techniques are typically used for determining solute solubilities in a supercritical fluid and also for stripping and fractionating studies. The advantages and limitations of each of these techniques are presented in this chapter. Poor experimental techniques can impede the progress of a supercritical fluid project, so it is worth spending time to design an experimental system that maximizes the amount of information obtained from the minimum amount of time and effort.

### **DYNAMIC METHODS FOR MEASURING SOLUBILITIES IN SUPERCRITICAL FLUIDS**

A flow apparatus representative of the type used to determine the solubility of a heavy liquid or solid in a supercritical fluid is shown in figure 4.1. The description of the apparatus and procedures for this system is taken from Van Leer and Paulaitis (1980). Although other flow methods are described in the literature, Van Leer's simplified technique embodies all the main features of a typical flow apparatus for obtaining solubility information (Prausnitz and Benson, 1959; Simnick et al., 1977; Kurnik, Holla, and Reid, 1981; Johnston

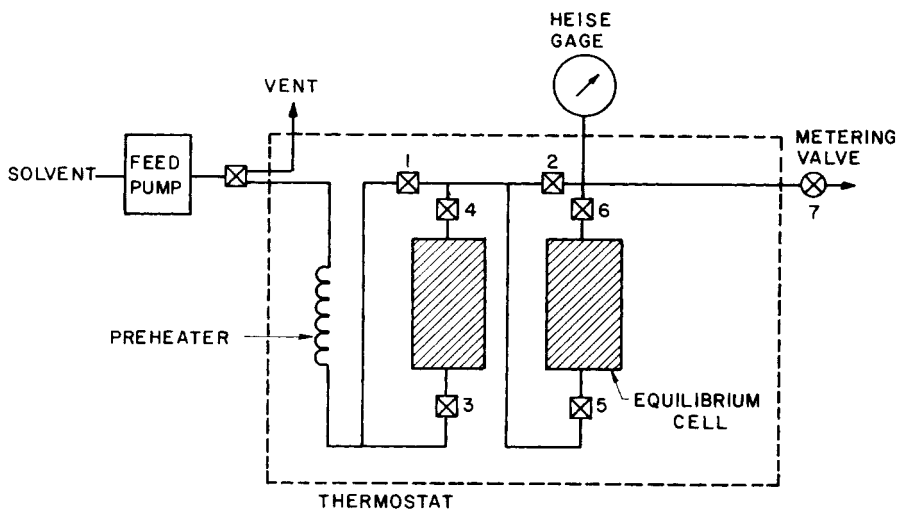


**Figure 4.1** Schematic diagram of a dynamic flows apparatus used to obtain liquid or solid solubilities in a supercritical fluid (Van Leer and Paulaitis, 1980).

and Eckert, 1981; Krukoniš and Kurnik, 1985). Figure 4.1 shows that the supercritical fluid of interest is charged to the system with a high-pressure pump and compressed to the desired operating pressure. The pump used in this step can be a high-pressure liquid chromatographic pump or perhaps a small diaphragm compressor. In many cases it is necessary to cool both the inlet stream to the compressor and the compressor head; this insures that the check valves on the outlet line of the compressor operate efficiently. Typical equilibrium-type flow rates are  $\sim 1.0$  l/min determined at 1.0 bar and  $0^\circ\text{C}$ . Of course, if the objective is to fractionate or strip material from the heavy solute, flow rates as high as 15 to 30 l/min are more standard.

After exiting the pump, the supercritical fluid flows through a section of tubing or a preheat column within the constant temperature bath; this insures that it reaches the bath temperature before it contacts the heavy solute. The supercritical fluid is then fed to the high-pressure columns carefully packed with the heavy solute to insure proper contacting, to maintain the solute in the columns even if it liquefies at operating conditions, and to allow for sufficient room for the heavy liquid to expand as the supercritical fluid dissolves in it. Typically the column is packed first with a small amount of glass wool in the bottom, then with a  $\sim 10$  mm layer of glass beads, then with solute, and finally with glass wool. Entrainment of the heavy solute in the SCF-rich phase is prevented by glass wool plugs inserted at the exit of each packed column.

After the saturated SCF-rich phase exits the second column, it is expanded to atmospheric pressure across a heated metering valve; the heavy component falls out of solution and is collected in a cold trap. The temperature of the cold



trap is dictated by the vapor (or sublimation) pressure of the heavy solute. To avoid clogging, the metering valve is maintained at a temperature greater than the bath temperature to offset any Joule–Thomson cooling during the expansion of the gas. Since the pressure of the system is determined by the pumping rate of the SCF and the regulation of the metering valve, it is important to minimize the clogging of the valve to maintain a constant flow rate and pressure. The amount of heavy solute collected in the cold trap is determined gravimetrically and the corresponding volume of SCF is typically measured with a dry-test meter. The instantaneous flow rate of the expanded supercritical fluid is measured with a simple rotameter or bubble-flow meter. The equilibrium pressure of the system is measured at the exit of the second column with a Bourdon tube Heise pressure gauge.

It is a straightforward matter to dampen pressure fluctuations caused by the high-pressure pump or diaphragm compressor by placing a surge tank before the preheater. If a surge tank is used, Meilchen et al. (1991) recommend that a pressure regulator (Tescom Inc.) be placed between the preheat column and the tank and that the tank be maintained at  $\sim 200$  bar higher pressure than the column pressure. With this configuration it is possible to dampen fluctuations to less than  $\sim 2$  bar by throttling the SCF to the desired operating pressure using the regulator. The temperature of the system, measured using any of several suitable devices, can usually be maintained easily within  $1^\circ\text{C}$  or better, depending on the flow rate. This type of flow system has several positive characteristics:

- off-the-shelf equipment is used;
- reasonably large amounts of solubility data can usually be obtained rapidly and reproducibly;
- equilibrium, stripping, or fractionation data can be obtained; and
- a straightforward sampling procedure is used.

But it does have several limitations:

- at high pressures the density of the supercritical fluid-rich phase can become greater than the density of the solute-rich liquid phase, which causes the liquid phase to be pushed out of the columns thus leading to erroneous solubility information;
- undetected phase changes can occur in the columns, e.g., transitions such as solid  $\rightarrow$  liquid and liquid<sub>1</sub>  $\rightarrow$  liquid<sub>1</sub> + liquid<sub>2</sub>;
- only the lighter phase is sampled so that there is no way of knowing the solubility of the supercritical fluid in the liquid phase;
- equilibrium experiments with multicomponent mixtures must be carefully designed to avoid completely depleting one or more of the components during the experiment;
- with a liquid solute, entrainment of the liquid in the supercritical fluid-rich phase is possible at high flow rates; and

- a heavy solid or liquid can clog the metering valve and cause solute holdup, which leads to errors in measuring solubilities.

The flow method is the technique of choice in many instances. It is possible to overcome many of its limitations with straightforward modifications to the apparatus. The simplest modification of this flow apparatus is to add a chromatographic switching valve to the system to obtain a sample of the supercritical fluid-rich phase before it flows through the heated metering valve. In this manner, holdup problems are avoided and it is possible to determine the molar volume of the supercritical fluid-rich phase. This sampling technique is shown in figure 4.2a and is described below (McHugh and Paulaitis, 1980).

The contents of the sample loop are analyzed in the following manner (see figure 4.2b). When the loop is switched out of the system, the sample expands into the transfer lines between valves A and B (the total volume of the sample loop and transfer lines is approximately 0.5 ml). As a result of this expansion, some of the heavy component precipitates in the lines. The amount of supercritical fluid in the sample loop can be ascertained by slowly opening valve B to vent the fluid into a calibrated graduated tube (e.g., a 100 ml class A burette with the bottom removed) filled with water presaturated with the gas of interest. As the supercritical fluid expands to atmospheric pressure, its solvent power drops significantly, and the solid or liquid solute drops out of solution. Care must be exercised to avoid entrainment of the heavy solute in the gas phase during venting. The volume of gas vented from the sample loop is determined by the volume of the water displaced corrected for the vapor pressure of water and the volume of gas remaining in the sample loop. The heavy component that has precipitated in the sample loop and transfer lines can be removed by replacing the graduated tube in figure 4.2b with a volumetric flask and flushing a large amount of a suitable liquid organic solvent through the system at valve A. The amount of heavy component in the solvent solution is determined by gas or liquid chromatography.

It is important to deal with the possibility that a phase transition can occur in the columns without the experimenter's knowledge. Chang and Morrell (1985) recommend installing a high-pressure glass gauge packed with the heavy solute in parallel with their packed columns. By this expedient, it is possible to observe phase transitions that occur during an experiment. Alternatively, solute-SCF phase border curves can be determined before performing blind dynamic solubility studies. A method for determining the  $P$ - $T$  trace of phase border curves is described later in this chapter.

It is worth mentioning briefly a variation of the flow technique that minimizes the residence time of a solute when operating at very high temperatures. This technique is also useful when determining tie lines for ternary mixtures where samples of both equilibrium phases are needed. Figure 4.3 shows a simplified schematic diagram of the continuous flow apparatus that is capable of operating to 400°C and ~350 bar (Wilson and Owens, 1970; Simnick et al., 1977; Paulaitis, Gilbert, and Nash, 1981; Hutchenson, Roebers, and Thies,

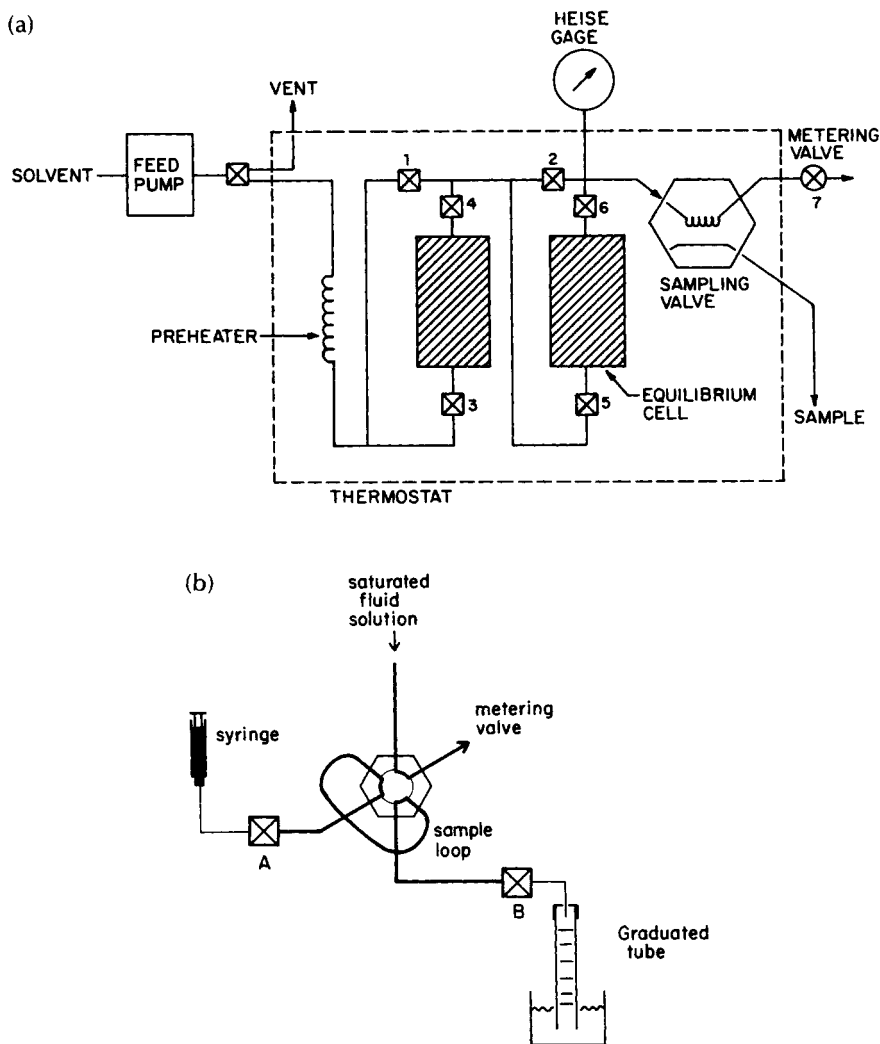


**Figure 4.2** Sampling technique used to obtain solubility information (McHugh, 1981). In (a) the location of the sampling valve is shown; in (b) the setup for removing the sample is depicted.

1990; Bolaños, Hochgeschurtz, and Thies, 1991). Either a pure component or a solution mixture can be delivered to the system using dual inlet pumps shown in the diagram.

When determining the phase behavior of a ternary mixture, one of the pumps delivers the supercritical fluid of interest and the other delivers a binary mixture of fixed concentration. The overall loading of the solution delivered to the system is fixed by the flow rates of the pumps. The streams from each

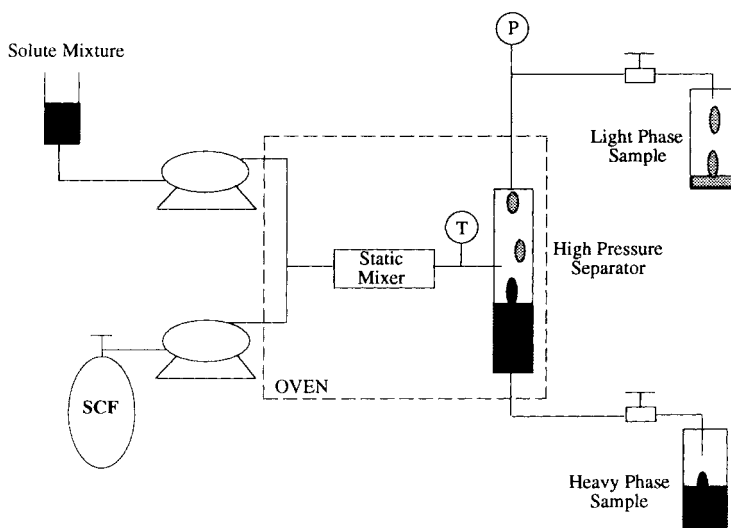


**Figure 4.3** Schematic diagram of a continuous flow apparatus capable of operating to 400°C and ~350 bar with multicomponent mixtures that are thermally labile (adapted from Bolaños, Hochgeschurtz, and Thies, 1991).

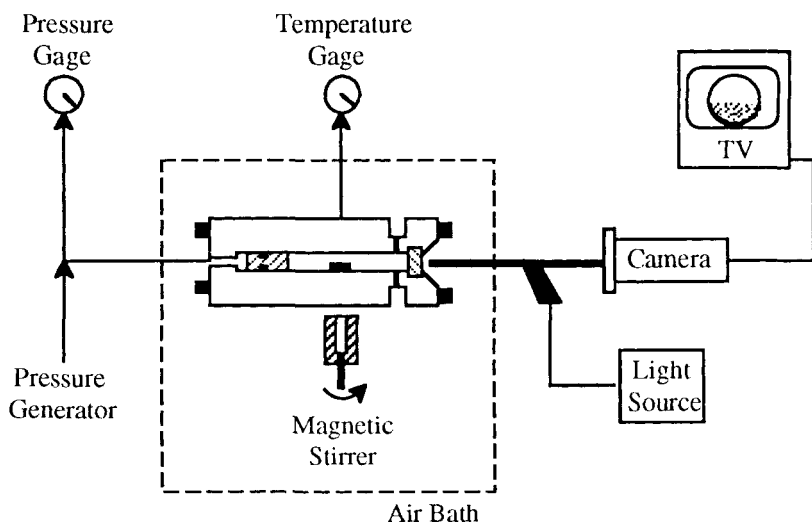
pump merge at a tee and mix as they flow through a section of line that acts as a preheater. Thies recommends using a static mixer when viscous solutes are studied to insure that the solution reaches equilibrium before entering the high-pressure separator (Bolaños, Hochgeschurtz, and Thies, 1991). Downstream from the static mixer is a high-pressure windowed vessel where the stream splits into a light phase, removed as overheads, and a heavy phase, removed as bottoms. Typically, a Jerguson liquid-level gage (Jerguson Gage and Valve Co.) is used as the high-pressure separator.

To accommodate high-temperature operation, three modifications of the separator are suggested by Thies and coworkers (Hutchenson, Roebbers, and Thies, 1990; Bolaños, Hochgeschurtz, and Thies, 1991). The glass in the separator should be replaced with an aluminosilicate glass (MacBeth®, Corning Glass Works); the gaskets which normally are Teflon should be made from graphite (Grafoil®, Union Carbide); and the washers that help hold the level gage together should be Bellville spring washers (Associated Springs Inc.) since they maintain a viable seal by compensating for expansion of the metal bolts at high temperatures. The level of the interface in the separator is maintained by adjusting the micrometering valve on the bottoms stream and the system pressure is fixed by adjusting the micrometering valve on the overheads stream. Tie lines on a ternary diagram at a single  $P$  and  $T$  are obtained by varying the flow rate of one of the pumps, which varies the overall mixture composition, while adjusting the micrometering valves to maintain the same system pressure.

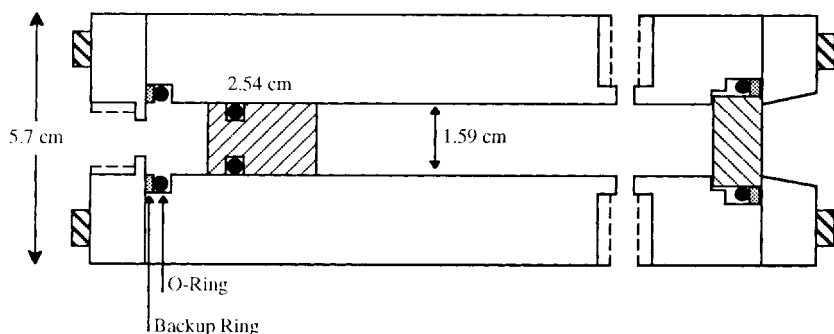
## STATIC METHODS FOR MEASURING SOLUBILITIES IN SUPERCRITICAL FLUIDS

Figure 4.4 shows a schematic diagram of a typical static view cell apparatus used for obtaining solubility information (McHugh, Seckner, and Yogan, 1984; Seckner, McClellan, McHugh, 1988; McHugh and Guckes, 1985). The main component of this system is a high-pressure, variable-volume view cell similar to the one described by Li, Dillard, and Robinson (1981), Jacoby and Rzasca (1952), and more recently, by Franck and coworkers (Diguët, Deul, and Franck, 1987). This cell allows for visual determination of the phases present at equilibrium. Figure 4.5 shows a schematic diagram of a cell constructed of a high nickel content steel (Nitronic 50®, Armco Corp.) (5.7 cm OD  $\times$  1.59 cm ID,  $\sim 25$  cm<sup>3</sup> working volume, fitted with a 1.9 cm OD  $\times$  1.3 cm thick sapphire window) (Diguët, Deul, and Franck, 1987).

The cell is initially loaded with a measured amount of liquid or solid and purged five times or more at room temperature with the gas of interest at  $\sim 4$  bar to remove any entrapped air. Gas is then transferred into the cell gravimetrically using a high-pressure bomb. The solution can be compressed to the desired operating pressure by displacing a movable piston fitted within the cell using water or any other suitable fluid pressurized with a high-pressure generator. The pressure of the solution is determined by measuring the pressure of the water with a Heise gage. A small correction of  $\sim 1$  bar is added for the pressure needed to move the piston. The temperature of the cell



**Figure 4.4** Schematic diagram of a typical static view cell system.



**Figure 4.5** Schematic diagram of view cell of high nickel content steel used for pressures greater than 1,000 bar.

is measured with a platinum-resistance device connected to a digital multimeter. The contents of the cell are mixed by a stir bar activated by a magnet located below the cell.

A data point is obtained in the following manner. At a fixed temperature the mixture in the cell is compressed to a single phase at high pressures. The pressure is then slowly decreased until a second phase appears. Typically the image of the mixture in the cell is projected onto a video monitor using a borescope (Olympus Corp.) placed against the sapphire window and connected to a video camera. The reported solubility data point is in the pressure interval between the two-phase state and the single fluid-phase state. The heavy solute can be alternately solubilized and precipitated a number of times in an effort to decrease the pressure interval from two phases to one phase. The solubility in this pressure interval is known from the amounts of gas and solute loaded into the view cell.

If a liquid solute is being studied, the vapor-liquid phase transition is determined in a similar manner (Occhiogrosso, 1985). The piston is slowly adjusted to lower the system pressure into the two-phase region. This decompression step is performed very slowly. If the pressure of the system is within  $\sim 2$  bar of the phase-split pressure, the rate of decompression is usually maintained at  $\sim 0.03$  bar/sec. The actual phase transition for the liquid solute is in the pressure interval between this two-phase state and the previous single, fluid-phase state. The entire procedure is then performed several times to decrease the pressure interval from two phases to one phase, so it falls within an acceptable range. The system temperature is now raised and the entire procedure is repeated to obtain more VLE information without having to reload the cell. In this manner, without sampling, an isopleth (constant composition at various temperatures and pressures) is obtained.

When working with a liquid solute, a bubble point, dew point, or mixture critical point can be visually detected. A bubble point is defined as the

condition at which a small vapor bubble appears in the cell as the pressure is lowered. The liquid concentration is determined from the amount of material loaded in the cell, exclusive of the negligible amount of material contained in the vapor bubble. A dew point is defined as the condition at which a small amount of dew, or fog, forms in the cell as the pressure is lowered. When determining the concentration of the vapor phase at the dew point, the negligible amount of material in the dew is ignored.

The mixture critical point is defined to be the pressure and temperature at which critical opalescence is observed for a slight change in either pressure or temperature. At the mixture critical point, a slight change in temperature or pressure causes a dramatic change in the amount of fluid phase or liquid phase present in the view cell. As an example of the dramatic change that occurs, the phases present in the cell change from a single supercritical fluid phase to about 50 vol% liquid phase and 50 vol% vapor phase when the pressure is adjusted by only 0.34 bar or the temperature is adjusted by 0.1°C. The advantages of a variable-volume view cell apparatus are:

- the phase transitions are determined visually, and phase inversions are easily detected;
- the solubilities of solids and liquids in binary mixtures are obtained without sampling;
- heavy solids, liquids, or polymers can be studied;
- minimum amounts of heavy components or supercritical fluids are used in an experiment;
- the pressure of the mixture can be continuously adjusted at a fixed composition and temperature; and
- with multicomponent mixtures, the equilibrium phases can be sampled.

The disadvantages are:

- “supercritical fluid stripping or fractionation” data are not as easily obtained; and
- typically only one macrosized sample can be obtained per cell loading.

Kiran and coworkers describe how solution viscosity can also be measured using a static view cell apparatus (Sen and Kiran, 1990; 1991). A high-pressure tube is attached to one of the ports of the cell so that the tube is positioned vertically. The solution in the cell is pressurized into the one-phase region, removed through the bottom port of the cell, and circulated in a closed loop through the vertical tube and back to the cell. After circulating for a few minutes, the flow is shut off and the viscosity is measured by determining the time it takes for a cylindrical “sinker” to fall through the solution in the vertical tube. The fall time of the sinker is determined using three linear displacement devices placed around the tube. By calibrating the fall time of the sinker with liquids of known viscosity it is possible to determine the solution

viscosity. Kiran also uses a linear displacement device to determine the location of the piston in the cell to determine the density of the solution. Therefore, in a single experiment, it is possible to obtain the phase transition, density, and viscosity of the solution in the cell.

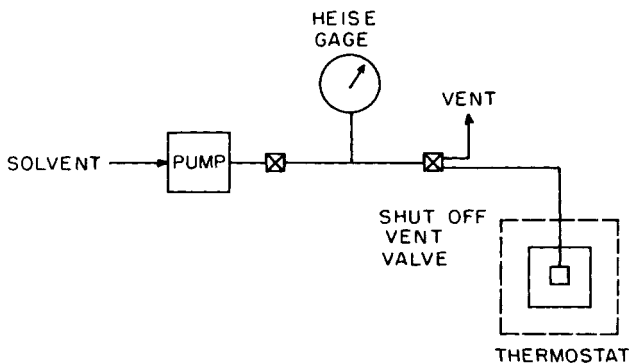
## METHODS FOR DETERMINING PHASE BORDER CURVES

Chapter 5 shows that it is possible to predict qualitatively, and in some cases quantitatively, solid solubility data by first measuring the system's  $P$ - $T$  trace of the three-phase SLV line. This is a relatively straightforward experiment since there is no sampling involved. In this instance, a constant-volume view cell (i.e., a Jerguson gage) is used as the high-pressure view cell. The description of this apparatus (see figure 4.6) and procedures is taken from McHugh and Yogan (1984).

The supercritical fluid of interest is charged at ambient temperature to a suitable gas/liquid compressor, where it is compressed and delivered to a high-pressure equilibrium view cell. The constant-volume high-pressure view cell is immersed in a water bath, which can easily be controlled to within  $\pm 0.1^\circ\text{C}$ . The pressure of the system is measured with an appropriate Bourdon tube Heise gage. The cell contents are mixed when the cell is rocked approximately  $180^\circ$ , causing a small stirring bar previously inserted into the cell to move through the cell contents.

The  $P$ - $T$  trace of the three-phase solid-liquid-gas line is determined by the following procedure. The view cell, loaded with a heavy solid, is pressurized to approximately 4 bar with the gas of interest then purged five times or more to remove any residual air from the system. An amount of gas is then transferred into the cell to obtain a desired operating pressure. After waiting approximately 30 min, to ensure thermal equilibrium, the experiment is started. Starting with a solid-fluid condition in the cell, the temperature is then raised until the solid begins to melt. This temperature is maintained with periodic stirring for  $\sim 10$ – $20$  min to determine if complete melting occurs. The

**Figure 4.6** Schematic diagram of an experimental apparatus used to obtain the  $P$ - $T$  trace of the three-phase line.





procedure is repeated until complete melting occurs and a liquid–fluid condition exists in the cell. At this point, the three-phase temperature is in the interval between the liquid–fluid state and the previous solid–fluid state. The solid is alternately solidified and melted a number of times to decrease the temperature interval between solid–fluid and liquid–fluid phases so it is less than 0.1°C.

One branch of the SLV line ends at the LCEP, the other ends at the UCEP (chapter 3). Both critical end points are defined as the pressure and temperature at which critical opalescence is observed in the presence of excess solid for a very slight change in either pressure or temperature. At the UCEP a small change in temperature or pressure causes a dramatic change in the amount of fluid phase, liquid phase, or solid phase present in the view cell. In certain instances, adjusting the temperature approximately 0.1°C can change the phases present in the cell in only a few seconds from a single fluid phase to about 50 vol% liquid and 50 vol% fluid. The same critical phenomena in the presence of excess solid are observed at the LCEP.

The advantages of this type of static system are:

- off-the-shelf equipment is used;
- the experimental design and procedures are straightforward; and
- solubility isotherms for a given supercritical fluid–solid system can be semiquantitatively estimated by fitting the SLV data to an equation of state (see chapter 5).

The disadvantages are:

- the compositions of the equilibrium phase along the SLV line are not determined;
- the pressure of the system is controlled by the amount of supercritical fluid introduced to the cell, which changes the overall concentration in the cell.

A more exacting experimental technique (van Welie and Diepen, 1961a) can be employed if a very accurate determination of the UCEP is desired, or if the concentrations of the gas and liquid phases along the SLG line are desired. In this instance a variable-volume view cell is used since we need the option of varying the system pressure without changing the overall composition. After a known amount of solid and SCF are loaded in the view cell, the mixture is compressed to the desired pressure and it is heated until there exists either two phases, liquid + vapor, or a single liquid, vapor, or fluid phase in the cell. The type of single phase can only be determined by crossing a phase boundary. The high-pressure view cell is isobarically cooled very slowly and the type of phase transition is noted. Four different types of transitions can be observed depending on the overall mixture composition.

If a liquid and a vapor are initially present and if, upon isobaric cooling, a solid falls out of solution, an SLG point is obtained. But if all the liquid in the

cell disappears before solid is formed, the transition is a dew point, as shown in figure 4.7A. If all of the vapor disappears before solid is formed, the transition is a bubble point as shown in figure 4.7B. A critical point does not occur for the constant-composition  $P$ - $T$  loop shown in figure 4.7A. This is because the loop is intersected by a solid phase region. But a critical point does occur on the  $P$ - $T$  loop for the mixture shown in figure 4.7B.

Finally, if only a single vapor or liquid phase is initially present in the cell and if, upon isobaric cooling, solid precipitates from the solution without the formation of a third phase, the temperature of the solid-fluid transition can be either less than (figure 4.7A) or greater than (figure 4.7B) the SLG temperature. Using the technique described in the previous paragraphs, the solubility of naphthalene in supercritical xenon at the UCEP is obtained by repeating the SLG determination with differing overall mixture compositions.

The critical mixture curve is measured in the following manner (Occhio-grosso et al., 1986). At a temperature slightly higher than the UCEP temperature, a vapor-liquid mixture at a fixed overall concentration is compressed to a single phase. The pressure is then isothermally decreased very slowly until the system becomes turbid and a second phase just begins to precipitate. A critical mixture point is obtained if critical opalescence is observed during the transition process and if two phases of equal volume are present when the mixture phase-separates.

Two other types of high-pressure experimental techniques are high-pressure spectroscopy and partial molar property measurements. Many researchers have begun using spectroscopic techniques to explore the strength of interactions and the local ordering, if any, in supercritical fluid mixtures (Johnston, Kim, and Combs, 1989; Yonker et al., 1986; Yonker and Smith, 1988; Brennecke and Eckert, 1990; Knutson et al., 1992). Although a spectroscopic method is most applicable for infinitely dilute mixtures, it does provide information on intermolecular interactions in solution. High-pressure spectroscopy is typically performed using conventional spectrophotometers interfaced with specialized high-pressure, windowed cells similar to those described earlier in this chapter. The crucial design consideration with these cells is choosing an appropriate window (Suppes and McHugh, 1989a). The ultimate choice of window is dictated by two competing considerations: the range of transmittance, fixed by the window material, and the amount of transmittance, fixed by the window thickness.

A number of researchers have developed techniques to determine partial molar volume. Eckert and coworkers (Eckert et al., 1986) provide a very good description of the method for obtaining partial molar volumes. They facilitated this difficult measurement by using a vibrating-tube densitometer (Mettler-Paar DMA 512). The major uncertainties with this technique are associated with the temperature control, which becomes crucial if experiments are performed at infinite dilution near the solvent's critical point. Shim and Johnston (1991) also note that it is possible to determine partial molar volume information using supercritical fluid chromatography if the mobile and stationary phases can be thermodynamically characterized.

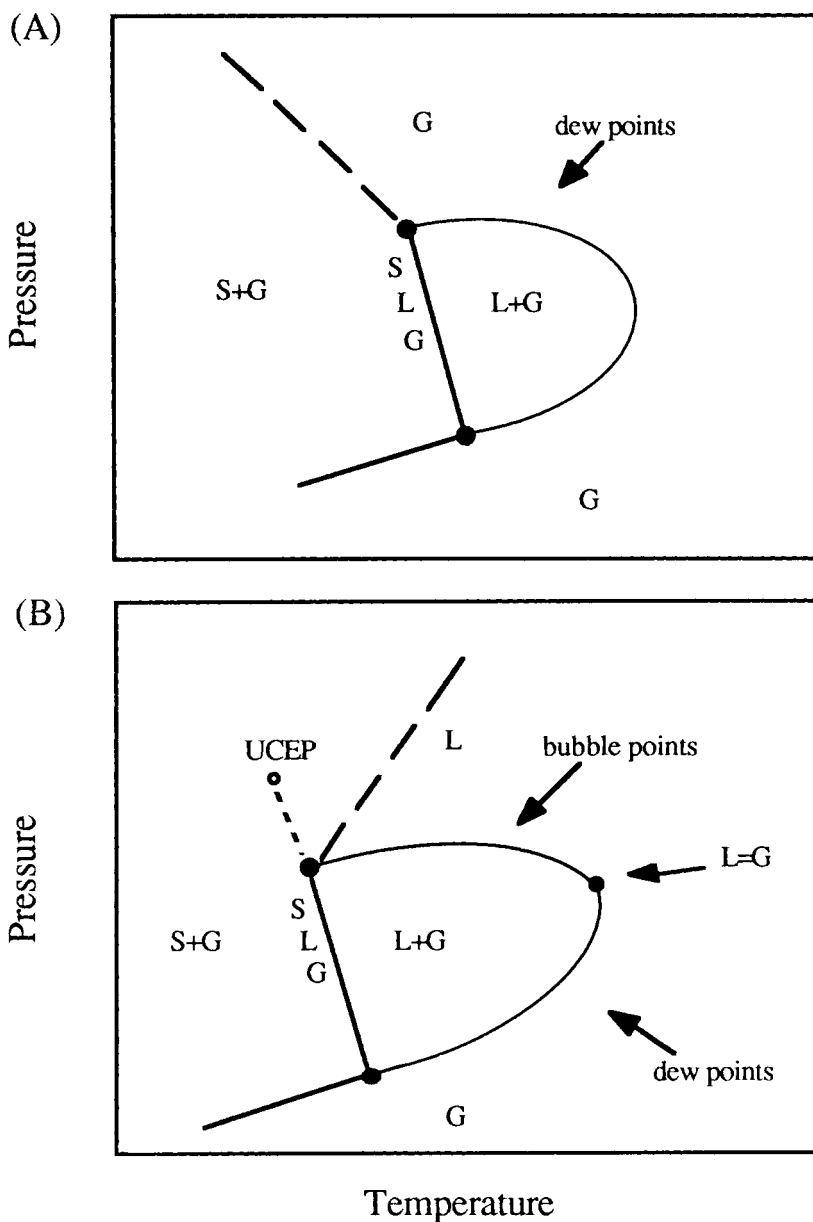


**Figure 4.7** Schematic  $P$ - $T$  diagram showing the effect of composition on the types of phase transitions that can occur near the UCEP. (A) A constant-composition loop at a heavy component concentration less than the concentration at the UCEP. (B) A constant-composition loop at a heavy component concentration greater than the concentration at the UCEP. The dotted portion of the SLG line in (B) is not observable since the overall concentration is too high.

Christensen and Izatt (Christensen et al., 1981; Christensen and Izatt, 1984) give information on heat effects on mixing in the critical mixture region. They designed and built a high-temperature, high-pressure flow calorimeter capable of operating to  $\sim 425^{\circ}\text{C}$  and 405 bar. With calorimetric information it is possible to determine the type and strength of intermolecular interactions in solution, e.g., hydrogen bonding (Izatt et al., 1983). Schneider and coworkers describe a slightly different technique for obtaining heat of mixing information at high pressures (Schneider et al., 1987).

Regardless of the experimental techniques that are used to measure high-pressure fluid-solute phase behavior and solution properties, it is important that the experiments are performed with a great deal of care, since a wide variety of phase behavior can occur at high pressures. It is possible to reduce the amount of experimental work by modeling the resultant phase behavior and extending the phase behavior information with calculated phase diagrams. The equations and methods used to model high-pressure phase behavior are developed in chapter 5.

---

# Thermodynamic Modeling of Supercritical Fluid–Solute Phase Behavior

---

In this chapter we describe the methods used to calculate solubility isotherms as well as the entire phase diagram for binary and ternary solute–SCF mixtures. The objective of the first part of the chapter is to discuss the relevant physical properties of the solute and solvent pair that are needed to describe the intermolecular forces in operation between molecules in a mixture that ultimately fix solubility levels. A brief description is provided on the application of solubility parameters to supercritical fluids.

## INTERMOLECULAR FORCES

The determination of whether a given solute will dissolve in a particular supercritical fluid solvent depends on the free volume differences between the solute and the solvent, and the intermolecular forces in operation between solvent–solvent, solvent–solute, and solute–solute pairs in solution. We first address the issue of how intermolecular interactions affect solubility. To gain a better understanding of why certain solutes readily dissolve in certain SCF solvents, we use simplified expressions to interpret qualitatively the properties of the components that fix the strength of their intermolecular forces (Prausnitz, 1969).

Every molecule has a momentary dipole due to electron oscillations that induces a dipole in neighboring molecules resulting in a net attractive interaction that determines the solubility level of a nonpolar solute in a nonpolar solvent. For nonpolar molecules these momentary dipoles average to zero over time due to their rapidly changing direction and magnitude. A simplified expression can be used to describe the induced dipole–induced dipole potential energy, known more commonly as dispersion energy.

$$\Gamma_{ij} \approx -C_1 \frac{\alpha_i \alpha_j}{r^6}, \quad (5.1)$$

where  $\Gamma_{ij}$  is the potential energy between an  $i$  and a  $j$  molecule,  $\alpha$  is the polarizability,  $r$  is the distance between the two molecules, and  $C_1$  is a constant. Since force is the derivative of potential energy with respect to intermolecular distance, equation 5.1 shows that the attractive force due to dispersion is independent of temperature and is very short-range. The polarizability is the key molecular property of the molecule that provides an indication of the strength of the solvent. Generally, within a given class of molecules, the polarizability increases with the size of the molecule since the more electrons a molecule has, the less tightly they are held (Castellan, 1971). For example, the polarizabilities of the noble gases increase from  $2.0 \times 10^{-25} \text{ cm}^3$  for helium, a very small molecule, to  $40.1 \times 10^{-25} \text{ cm}^3$  for xenon, a quite large molecule. Interestingly, xenon has a polarizability comparable to that of ethane or ethylene. This helps to explain why xenon is such a good supercritical fluid solvent.

In addition to dispersion forces between molecules, there can be an additional force of attraction between the molecules if they have permanent dipoles whose strength and direction are fixed as a result of their molecular structure. The simplified expression that accounts for permanent dipole–dipole potential energy is

$$\Gamma_{ij} \approx -C_2 \frac{\mu_i^2 \mu_j^2}{r^6 kT}, \quad (5.2)$$

where  $\mu$  is the strength of the dipole moment in debye,  $T$  is the absolute temperature,  $k$  is Boltzmann's constant, and  $C_2$  is a constant. In this case, the force of attraction varies as the inverse seventh power of the intermolecular distance but it also varies inversely with temperature. Dipole–dipole interactions increase in strength with decreasing temperature since the effect of  $kT$  thermal energy decreases sufficiently to allow the permanent dipoles of the two molecules to align. Here the key molecular parameter is the dipole moment, which has a large effect on the properties of the molecule if the magnitude of the dipole is larger than  $\sim 1.0$  debye. Substances that are very polar at room conditions, such as acetone, typically have high critical temperatures ( $T_c = 234.9^\circ\text{C}$ ) since large amounts of thermal energy are needed to overcome attractive dipolar energy when vaporizing the substance. Although a polar SCF solvent, such as acetone, always has a dipole moment due to its molecular structure, regardless of its physical state or the temperature, it will exhibit interactions more like those of a nonpolar SCF solvent at the very high temperatures needed to make it supercritical. In fact, it is this temperature dilemma that precludes the possibility of finding a polar SCF solvent that is also a polar liquid solvent. A molecule's physical size and structural complexity fixes the strength of the effective dipole moment. Larger, more complex molecules have diminished dipole interactions as the dipole operates over a very large volume (Castellan, 1971).

Molecules can also have higher-order polar moments, such as a quadru-

pole moment. Carbon dioxide, perhaps the most commonly used supercritical fluid, has a rather large quadrupole moment (Prausnitz, 1969). In this instance the simplified formula for the intermolecular potential energy becomes

$$\Gamma_{ij} \approx -C_3 \frac{Q_i^2 Q_j^2}{r^{10} kT}, \quad (5.3)$$

where  $Q$ , the quadrupole moment, is now the important parameter. Like dipolar forces of attraction, quadrupolar forces of attraction are inversely proportional to temperature but they fall off with intermolecular distance much faster than polar forces. This is because the potential energy is inversely proportional to the tenth power in  $r$ . Therefore, the effect of a quadrupole moment on thermodynamic properties is expected to be much less significant than a dipole moment. Quadrupoles and dipoles can also interact according to the simplified expression

$$\Gamma_{ij} \approx -C_4 \frac{\mu_i^2 Q_j^2}{r^8 kT} - C_5 \frac{\mu_j^2 Q_i^2}{r^8 kT}. \quad (5.4)$$

Molecules that have permanent dipole or quadrupole moments generate an electric field that induces an attractive response in nonpolar molecules by polarizing the nonpolar molecule so that it exhibits a temporary dipole. In fact, polar molecules can also have induced dipoles due to the electric field effect of another polar molecule in close proximity. The simplified expression for these induced intermolecular potential energies is

$$\Gamma_{ij} \approx -C_6 \frac{\mu_j^2 \alpha_i + \mu_i^2 \alpha_j}{r^6} - C_7 \frac{Q_j^2 \alpha_i + Q_i^2 \alpha_j}{r^8}. \quad (5.5)$$

Typically, induced intermolecular potentials are weaker than the potentials caused by permanent moments.

To determine whether a solute will dissolve in a given solvent, it is necessary to consider the balance of the intermolecular forces of attraction between solvent-solvent, solute-solute, and solvent-solute pairs of molecules in solution. This balance of forces is given as the interchange energy  $E$  of mixing  $i$ - $j$  pairs of molecules

$$E = z[\Gamma_{ij} - \frac{1}{2}(\Gamma_{ii} + \Gamma_{jj})], \quad (5.6)$$

where  $z$  is the number of dissimilar solvent-segment pairs in solution. From this formula, and from the simplified expression given in equations 5.1 through 5.5, we can now qualitatively address the question of whether a particular solute will dissolve in a given SCF solvent. If the strength of like-like interactions,  $\Gamma_{ii}$  and/or  $\Gamma_{jj}$ , are much greater than unlike interactions  $\Gamma_{ij}$ , then it is not likely that the solute will dissolve in an SCF solvent. The simplified expressions for the intermolecular attractive potentials that are given here fail at very high pressures or, more appropriately, at very high densities, since repulsive forces become large and they tend to dominate attractive forces

(Lira, 1988). As mentioned in chapter 3, that is why solid solubilities decrease with increasing pressure at very high pressures. The solution density is high enough that repulsive forces dominate attractive forces and “squeeze” the heavy solute out of solution.

In addition to physical forces of attraction that are enumerated in equations 5.1 through 5.5, molecules can exhibit chemical forces of attraction (Prausnitz, 1969). Chemical forces include hydrogen bonding and electron acceptor–donor complexing. There are two major differences between chemical and physical forces. Chemical forces become saturated while physical forces do not. Chemical forces typically decrease with increasing temperature, since they depend on the alignment of the molecules in solution, while many physical forces are much less dependent on temperature. For example, in every molecule there is a fixed number of possible sites for hydrogen bonding and once those sites are occupied, no other hydrogen bonds will form. But if the system temperature is increased, the molecular motion of the molecules increases and decreases the number of hydrogen bonds because the molecules cannot align properly to make a bond. Unfortunately, chemical forces are much harder to quantify than physical forces. To illustrate the impact of chemical forces on solubility, let us consider the cosolvent studies of Van Alsten, Hansen, and Eckert (1984) and Schmitt and Reid (1986) that clearly show how the solvent power of a supercritical fluid increases when the cosolvent can chemically interact with the solute. Walsh, Ikonmou, and Donohue (1987) do an excellent job explaining the differences in these two studies.

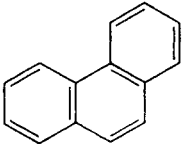
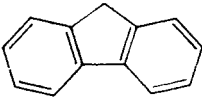
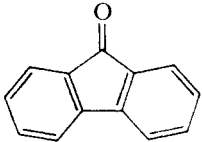
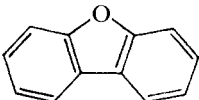
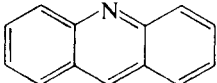
The study by Van Alsten and coworkers compared the solubility of the five solids shown in table 5.1 in pure CO<sub>2</sub> and in a solvent mixture of 95 wt% CO<sub>2</sub> and 5 wt% methanol. Only acridine showed any enhancement when methanol is added to CO<sub>2</sub>. Schmitt and Reid determined the solubility of two different solids, phenanthrene and benzoic acid, in two supercritical solvents, CO<sub>2</sub> and ethane, with benzene, cyclohexane, acetone, and methylene chloride as cosolvents. In this case, the solubility of benzoic acid was greatly enhanced in supercritical ethane when acetone was the cosolvent. But no cosolvent effect was observed for all other combinations of solids, supercritical solvents, and cosolvents. Walsh and coworkers argue that the two systems that showed a large increase in solubility can be explained by assuming either the cosolvent hydrogen bonded to the solute or the cosolvent and the solute formed an acid–base complex.

To support their argument, Walsh performed liquid phase spectroscopic studies of the solutes and cosolvents in liquid acetone, as an analog to supercritical carbon dioxide, and in liquid hexane, as an analog to supercritical ethane. The spectra from the phenanthrene, fluorene, fluorenone, and dibenzofuran solutes dissolved in acetone with 1 mol% methanol clearly show no complex formation. But the spectra also clearly show that acridine forms a complex with methanol. To interpret the Schmitt and Reid study, Walsh and coworkers used hexane as the liquid analog to supercritical ethane. They found



**Table 5.1** Chemical Structures of the Five Solids Investigated by van Alsten, Hansen, and Eckert (1986)

---

Phenanthrene	
Fluorene	
Fluorenone	
Dibenzofuran	
Acridine	

---

that the spectra from the benzoic acid–hexane–benzene, –cyclohexane, and –methylene chloride systems did not reveal a complex. But the benzoic acid–hexane–acetone system clearly showed a complex, in agreement with the increased solubility of benzoic acid in supercritical ethane with added acetone.

Walsh, Ikonomou, and Donohue (1986) also make the cogent point that the role of the supercritical solvent cannot be ignored when interpreting the differences in solute solubility. When  $\text{CO}_2$  was used as the solvent, Schmitt and Reid did not find a cosolvent effect. But  $\text{CO}_2$  itself will compete with the solute for the cosolvent, since  $\text{CO}_2$  has two carbonyl oxygens that will accept hydrogen bonds (Hyatt, 1984). Ethane does not compete for hydrogen bonds. It is important to remember that the supercritical solvent is in excess in the solution so that if the solvent can compete for hydrogen bonds, as  $\text{CO}_2$  does, it will hydrogen bond to the cosolvent before the cosolvent can affect solute solubility levels.

In addition to intermolecular forces, yet another consideration determines whether a given solute dissolves in a particular SCF solvent—the free volume difference between the mixture components. By free volume we essentially mean the expansivity of a substance, or inversely, its compressibility. The key question is whether the molecules in solution are within close enough proximity to interact. Statistical thermodynamics provides us with the equations that

reveal the effect of density on interaction level. For example, consider the equation for the internal energy of attraction,  $U_{\text{total}}$ , for a homogeneous isotropic fluid

$$\frac{U_{\text{total}}}{kT} \approx A_0 + A_1 \rho \int u(r) g(r) r^2 dr, \quad (5.7)$$

where  $u(r)$  is the pair potential energy of  $ii$ ,  $jj$ , and  $ij$  interactions,  $g(r)$  is the radial distribution function,  $A_0$  and  $A_1$  are constants that depend on the properties of the components in solution, and  $\rho$  is the density (Lee, 1989). Equation 5.7 provides an explanation for the heuristic that, to a first approximation, the solubility of a solute in an SCF solvent is proportional to density. It shows how the strength of an SCF solvent can be fine-tuned by varying the solvent density. It also shows why this heuristic is only true to a first approximation. A great deal of physics is buried in the  $u(r)$  and  $g(r)$  terms.

What then are our options for modeling or calculating phase behavior and solubility isotherms? Johnston does a good job describing the pros and cons of some supercritical mixture models (Wong, Pearlman, and Johnston, 1985; Johnston, Peck, and Kim, 1989). He explains that certain issues still need to be resolved before a single model will be applicable for all situations. In this chapter we use two types of mean-field equations for calculating phase behavior: a cubic equation of state and a lattice–gas equation of state. Cubic equation of state models have successfully been used to describe high-pressure phase behavior in a quantitative manner even though most cubic equations typically account for only dispersion-type interactions. Equation 5.2 shows that polar interactions should decrease with increasing temperature, so it should be possible to mimic the effect of polar or hydrogen bonding interactions by making mixture interaction parameters temperature-dependent (Sanchez and Balazs, 1989), although this semiempirical construct should be used with caution. The other difficulty that must be addressed when calculating phase behavior with an equation of state is that mixing rules are strictly empirical. Typically, mixing rules are employed that assume the molecules are randomly distributed in the mixture; this is a poor assumption for components that hydrogen bond. Many researchers are addressing the issue of the appropriate mixing rules for mixtures that exhibit nonrandom mixtures (Walsh and Donohue, 1989; Walsh, Jin, and Donohue, 1991; Saini et al., 1991; Melhem and Saini, 1991; Dahl, Fredenslund, and Rasmussen, 1991). Nevertheless, Scott and van Konynenburg (1970) have shown that the van der Waals equation with random mixing rules can generate the five classes of phase diagrams that describe virtually all of the known variations for binary mixtures. Recognizing these limitations, we develop in detail a straightforward equation of state approach, since it can potentially reduce the amount of experimental work needed to interpret and extrapolate experimental data. A coherent calculational approach is an extremely useful tool for guiding experimentation when searching for regions of three-phase LLV or SLV behavior, if for nothing more than to avoid such regions when designing an SCF extraction process.

Throughout this chapter we purposely avoid the issue of clustering of solvent molecules around solute molecules in mixtures at infinite dilution very close to the critical point of the pure solvent (Johnston, Peck, and Kim, 1989; Cochran and Lee, 1989; Wu, Lee, and Cochran, 1990; Knutson et al., 1992; Debenedetti, 1987; Debenedetti, Petsche, and Mohamed, 1989; Kim and Johnston, 1987a, 1987b; McGuigan and Monson, 1990; Economou and Donohue, 1990; Petsche and Debenedetti, 1991). To explain solubility behavior various research groups have invoked the concept of local structure for infinitely dilute mixtures based on spectroscopic studies (Johnston, Kim, and Combs, 1989; Yonker et al., 1986; Yonker and Smith, 1988; Brennecke and Eckert, 1990; Knutson et al., 1992) and partial molar volume studies (Eckert et al., 1983, 1986; Shim and Johnston, 1991). However, the notion of a static stable aggregate of solvent molecules clustered around a solute molecule is no longer the accepted view of what occurs with an infinitely dilute solute molecule near the solvent's critical point (McGuigan and Monson, 1990; Economou and Donohue, 1990; Shaw et al., 1991). The enhanced local properties around an infinitely dilute solute molecule are now viewed as a consequence of a dynamic interchange of an excess of solvent molecules entering and leaving the region in the immediate proximity of the solute molecule, due to attractive solvent-solute interactions (Shaw et al., 1991). It is our good fortune that mean-field equations work well even at conditions very close to infinite dilution at the pure solvent's critical point, since these equations are numerically very tractable (Economou and Donohue, 1990). Our intent in this chapter is to demonstrate how solubilities can be predicted and modeled over wide ranges of temperatures, pressures, and compositions. We are willing to sacrifice a small loss in quantitative results at infinite dilution conditions near pure component critical points if we can secure good results with solutions richer in solute and at conditions removed from the solvent's critical point. The underlying motivation for our approach is that the majority of practical situations which employ SCF solvents, such as in coffee decaffeination and polymer fractionation, are at temperatures and pressures typically far removed from those at the solvent's critical point and they rarely deal with mixtures at infinite dilution.

We now discuss how predictions of solubility and phase behavior can be carried out. Before proceeding with the equation of state approach, we present a brief discussion of the solubility parameter concept because solubility parameters continue to be presented in the literature as one means of correlating SCF-solute behavior.

## SOLUBILITY PARAMETERS

For liquids, the solubility parameter can be calculated from the expression

$$\delta = (\Delta U/V)^{1/2}, \quad (5.8)$$

where  $\delta$  is the solubility parameter,  $\Delta U$  is the internal energy change during

vaporization in cal/mol, and  $V$  is the liquid molar volume in cc/mol. The units of solubility parameters are  $(\text{cal/cc})^{1/2}$  and have recently been termed hildebrands, i.e.,  $1 (\text{cal/cc})^{1/2} = 1$  hildebrand. Solubility parameters were first introduced as a means of categorizing solute–solvent behavior in “regular” solutions; it is informative to review some of the basic tenets of regular solution theory proposed by Hildebrand and Scott (1949).

Recalling, first, ideal solution theory, the solubility of a solid in a liquid is related to the heat of fusion of the solid and the temperature of the solution, ignoring  $\Delta C_p$  and  $\Delta V$  terms.

$$\ln x_2 = \frac{\Delta H_f}{R} \left( \frac{1}{T_f} - \frac{1}{T} \right), \quad (5.9)$$

where  $x_2$  is the mole fraction of the dissolved solute,  $\Delta H_f$  is the heat of fusion,  $T_f$  is the melting point of the solute, and  $T$  is the temperature of the solution. Many references and texts have described the requirements for equation 5.9 to hold. The primary requirement for ideal solution theory to be descriptive of the situation is that there be only a dispersion force interaction between solute and solvent. Hildebrand defines an ideal solution as one in which the activity equals the mole fraction over the entire composition range and over a nonzero range of temperature and pressure.

These are usually heat effects during dissolution of solids (and liquids) in solvents, and the ideal solution relation is modified by an energy term that takes into account heats of mixing. The term modifies the ideal solution equation to give the regular solution theory prediction of solubility

$$\ln x_2 = \frac{\Delta H_f}{R} \left( \frac{1}{T_f} - \frac{1}{T} \right) - \frac{V_2 \Phi_1^2 (\delta_2 - \delta_1)^2}{RT}, \quad (5.10)$$

where  $\Phi_1$  is the volume fraction of component 1.

From purely mathematical grounds, an examination of equation 5.10 shows that the solubility of a solute in a solvent is maximized when the respective solubility parameters are the same (or when the difference is small). Hildebrand enunciated the conditions that apply for equation 5.10 to describe the solute–solvent behavior: the two compounds must exhibit primarily dispersion force attractions (or at most, only weak chemical interactions) and the energy of interaction between the two unlike molecules is given by the geometric mean of the interaction energies of the two like molecules. Hildebrand’s books and papers give many examples of the utility of solubility parameters in correlating and predicting solubility behavior. The rule of thumb, that miscibility will occur if  $\delta_1 - \delta_2$  is about 1, derives from the many examples Hildebrand gives. Solid–liquid and liquid–liquid behavior can be predicted reasonably well from the rule of thumb, but it is not generally applicable to supercritical fluids as we bring out subsequently.

Many articles on calculations of solubility parameters of supercritical fluids

have appeared in the literature, e.g., Prausnitz (1958); Cernia and Mancinis (1965); Giddings et al. (1968); King (1983); Allada (1986). We do not review all the methods of calculation. Instead we present some exceptions and allow readers to draw their own conclusions as to the general utility of solubility parameters in predicting supercritical fluid, liquid, or solid solute behavior.

Prausnitz (1958) showed that the solubility parameter relations for liquids could not be applied to supercritical fluids, and he showed that regular solution theory could not be applied to gas-liquid solutions because of certain considerations that caused gas-liquid mixing to be outside the bounds of liquid-liquid or liquid-solid mixing; the most notable consideration is that the mixing of gas and liquid is not a constant volume process. To overcome this limitation Prausnitz separated the mixing process into three steps. He derived the free energy changes for each step and calculated the solubility parameter of the gas from the step of mixing at constant pressure, temperature, and volume. He showed the calculations based upon his assumptions to be in good agreement with the experimental work of Todd and Elgin (1955).

To derive the solubility parameter of a gas Cernia and Mancini (1965) used the relation suggested by Hildebrand (1951) that a gas solubility parameter is equal to the square root of the ratio of the internal compression energy and the molar volume. Using the van der Waals equation of state, Cernia and Mancini obtained solubility parameters for ethylene, but they related that calculations carried out along the classical lines of interpolating Mollier chart data were time-consuming.

The works of Giddings and coworkers in the late 1960s (1968, 1969) are, perhaps, the most well-known and most referenced papers on the extension of Hildebrand solubility parameters to supercritical fluids. We excerpt from Giddings et al. and we italicize parts of their statements and phrases to accent their feelings and intentions. We concentrate on the applicability of their methods for calculating solubility parameters of dense gases; their telling statements are often not heeded.

Giddings sought a way "for making sense out of an immense variety of possible experimental conditions and solute-solvent pairs" (Giddings et al., 1968). Because, they said, "the theoretical description of gases at high densities entails considerable complexity" and because they "could not rely on clear, rigorous guidelines for the choice of gas solvents, temperatures, and pressures," they "sought instead to uncover the gross elements of gaseous solubility and to find a common mathematical framework to correlate gases with one another and with the liquid solvents." They suggested that the solvent power of a compressed gas depends in part on its state relative to its critical condition and in part on its chemical effect. Giddings stated that the chemical effect is dependent upon polarity, acid-base properties, hydrogen bonding tendencies, etc., and the state effect is dependent upon compression and temperature. Pay close attention to their words. Giddings "felt *intuitively* that reduced density is the principal variable of the state effect, i.e., reduced density reflects mean distances and interactions between molecules." Thus, if a gas is compressed to

a liquid-like density, Giddings expected a liquid-like solvent effect, and they quoted statements from some of Hannay's first reports (Hannay, 1880)

The liquid condition of fluids has very little to do with their solvent power, but only indicates molecular closeness. Should this closeness be attained by external pressure instead of internal attraction, the result is that the same or even greater solvent power is obtained.

Giddings et al. go on to relate that the “chemical effect” of the mobile phase in chromatography is manifested in the eluotropic series, which orders the elution strength of various liquids. They compared the elution power of a number of liquids with their solubility parameters, and they found a striking parallel between the two, i.e., Snyder's  $\epsilon^0$  values correlated very well with Hildebrand's  $\delta$ . Therefore, Giddings et al. suggested that the elution power of compressed gases may be related to the solubility parameter. But they stated explicitly

*Hildebrand and Scott warned that it is dangerous to employ solubility parameters for esters, ketones, alcohols, and other polar liquids.*

It is unfortunate that many researchers and authors often forget or ignore this warning when discussing solubility parameters.

In the now classic series of papers, Giddings goes on to say

We wish to see what can be deduced by assuming that (i) the solubility parameter is relevant to the “state effect” as well as the “chemical effect” . . . and (ii) the gas obeys the van der Waals Equation of State . . .

With some manipulation, by correlation with liquid data, and assuming the equivalence of gases and liquids at a common density, they derived the expression

$$\delta = 1.25P_c^{1/2}(\rho_r/\rho_{r,l}), \quad (5.11)$$

where  $\delta$  is the solubility parameter,  $P_c$  is the critical pressure of the gas or liquid,  $\rho_r$  is the reduced density of the gas or liquid, and  $\rho_{r,l}$  is the reduced density of the gas or liquid at its normal boiling point, a value of about 2.66. The state effect is identified with  $\rho_r/\rho_{r,l}$ , and the term  $1.25 P_c^{1/2}$  is associated with the chemical effect; with  $P_c$  in atmospheres the numerical value calculated from equation 5.11 is the solubility parameter with units of  $(\text{cal/cc})^{1/2}$ .

Throughout his articles Giddings made other qualifying statements which subsequent researchers apparently fail to recall. He related such provisos as

*We have stretched the concept of the solubility parameters to the limit . . . the latter will be in doubt when . . . specific solvent effects exist . . . hydrogen bonding . . . polar molecules are excluded from the considerations of Hildebrand.*

**Table 5.2** Solubility Parameters of Selected Liquids

<i>Liquid</i>	<i>Solubility Parameter <math>\delta</math> at 25°C</i>
Hexane	7.3
Methanol	14.5
Dimethyl formamide (DMF)	12.1
<i>N</i> -Methyl pyrrolidone (NMP)	13.8
Dimethyl sulfoxide (DMSO)	13.0

Solubility parameters of several gases calculated from equation 5.11 are shown in table 5.2 (King, 1984). Choosing a pressure level of 400 atm, the solubility parameter of carbon dioxide is about 7.3 (at 40°C) and about 6.0 (at 37°C) for ethane. We shall refer to these values subsequently when we present some interesting experimental facts on the behavior of certain liquids with these two gases. If we assume that the rule of thumb,  $\delta_2 - \delta_1 \cong \pm 1$ , can be used to predict the miscibility behavior of pairs of liquids, then we conclude that hexane is not miscible with methanol, DMF, NMP, or DMSO. In fact, hexane is not miscible with these liquids, so we might initially be pleased with the prediction. But just because the rule of thumb seems to apply to the hexane-liquid cases given here, we should not conclude that its use is justified for predicting miscibility behavior. Remember Hildebrand and Giddings cautioned against employing solubility parameters for esters, ketones, alcohols, and other polar liquids; DMF, NMP, DMSO, and methanol are certainly very polar liquids.

Now let's examine the miscibility situation of supercritical CO<sub>2</sub> with the same liquids; at 400 bar and 40°C the solubility parameter of CO<sub>2</sub> is about 7.3. Carbon dioxide at 400 bar is miscible with hexane, so again we might be pleased with the fact that  $\delta_2 - \delta_1 = \pm 1$  predicts miscibility behavior. But CO<sub>2</sub> is also miscible with methanol, DMF, NMP, and DMSO, and the solubility parameters for the respective four liquids are clearly different by more than 1 H. How do we explain that CO<sub>2</sub> is miscible with the liquids? Although CO<sub>2</sub> is strictly a nondipolar molecule, i.e., its dipole moment is zero, it has strong bond dipoles or, equivalently, a large quadrupole, which can interact with other polar molecules.

Let's progress now to the situation with supercritical ethane. There are dangers to blindly employing solubility parameters with any gas-liquid pair. We can illustrate them by investigating supercritical ethane at 400 bar and 37°C. What does it do with the five liquids listed in table 5.2? The solubility parameter of ethane is about ~6.0 H. Ethane is miscible with hexane; we previously related that fact in chapter 3, and we would predict that ethane and hexane would be miscible based upon solubility parameter considerations. Hildebrand solubility parameters can in fact be employed here because only dispersive intermolecular forces are in play and ethane has a liquid-like

density. Contrary to the prediction of the solubility parameter approach, ethane is miscible with methanol (Brunner, 1985). Ethane at 37°C, 400 bar is not miscible with DMF, NMP, and DMSO, so we might conclude that Hildebrand solubility parameters appear to have predicted that behavior. We state again, however, that Hildebrand solubility parameters shouldn't even have been applied to these three polar liquids nor to methanol. Finally, even though the Hildebrand solubility parameters for both gases calculated from equation 5.10 are very similar, CO<sub>2</sub> and ethane are very different in their behavior with the four polar liquids (and perhaps with many other liquids, too). This fact should not give us any concern because CO<sub>2</sub> has a huge bond dipole (2.4 debye), and ethane does not.

## VAPOR–LIQUID CALCULATIONS

Various modeling procedures have been proposed in the literature to predict the phase behavior of vapor–liquid systems at high pressures. (The designation vapor will be used synonymously with supercritical fluid in this chapter.) Regardless of the modeling procedure, the following thermodynamic relationships, or their equivalent relationships in terms of chemical potentials, must be satisfied for two phases to be in equilibrium.

$$f_i^V(T, P, y_i) = f_i^L(T, P, x_i), \quad i = 1, 2, 3 \dots m, \quad (5.12)$$

where  $f_i^L$  is the fugacity of component  $i$  in the liquid phase,  $f_i^V$  is the fugacity of component  $i$  in the vapor phase,  $x_i$  is the mole fraction of component  $i$  in the liquid phase, and  $y_i$  is the mole fraction of component  $i$  in the vapor or SCF phase. The number of equations implied in equation 5.12 is equal to the number of components that appear in both the vapor and liquid phases. The most computationally straightforward and thermodynamically consistent method for calculating high-pressure phase behavior is to choose an equation of state to model both the liquid and the vapor or SCF phases. With this approach the fugacity in each phase can now be written as

$$f_i^L(T, P, x_i) = x_i \phi_i^L P, \quad (5.13)$$

$$f_i^V(T, P, y_i) = y_i \phi_i^V P, \quad (5.14)$$

where  $\phi_i^L$  is the fugacity coefficient of component  $i$  in the liquid phase,  $P$  is the system pressure,  $T$  is the system temperature, and  $\phi_i^V$  is the fugacity coefficient of component  $i$  in the vapor phase. Fugacity coefficients for the vapor and liquid phases are calculated from the exact thermodynamic relationships (Prausnitz, 1969)

$$\ln \phi_i^V = \frac{1}{RT} \int_{v^V}^{\infty} \left[ \left( \frac{\partial P}{\partial n_i} \right)_{T, V, n_{i+j}} - \frac{RT}{V} \right] dv - \ln \left( \frac{Pv^V}{RT} \right), \quad (5.15a)$$



$$\ln \phi_i^L = \frac{1}{RT} \int_{v^L}^{\infty} \left[ \left( \frac{\partial P}{\partial n_i} \right)_{T, V, n_{i+j}} - \frac{RT}{V} \right] dv - \ln \left( \frac{Pv^L}{RT} \right), \quad (5.15b)$$

where  $R$  is the gas constant,  $v^V$  is the molar volume of the vapor phase,  $v^L$  is the molar volume of the liquid phase, and  $n_i$  and  $n_j$  are the moles of components  $i$  and  $j$ , respectively. A single equation of state can now be used to determine the analytical form of  $(\partial P / \partial n_i)_{T, V, n_{i+j}}$  for calculating both fugacity coefficients. It is a straightforward matter to show that the fugacity coefficient is equal to 1.0 if the ideal gas law is used in equation 5.15. While it is tempting to use the fundamentally rigorous virial equation to calculate fugacity coefficients, in practice this is not done since we do not have reliable values for third- and higher-order virial coefficients needed to obtain an adequate representation of the PVT properties of a substance at high pressures. Fortunately, in many cases, high-pressure phase behavior can be reasonably represented with a cubic equation of state (EOS) if the components in the mixture do not differ too substantially in intermolecular strengths or in size, structure, or shape.

The most commonly used cubic EOSs are the Peng–Robinson (Peng and Robinson, 1976) and the Soave–Redlich–Kwong (Soave, 1972) equations. They produce essentially equivalent results since both equations are cubic in volume. We will use the Peng–Robinson (PR) EOS since we have the most experience with this equation. The PR equation is

$$P = \frac{RT}{v-b} - \frac{a(T)}{v(v+b) + b(v-b)} \quad (5.16)$$

where  $v$  is the molar volume,  $a$  accounts for intermolecular interactions between the species in the mixture, and  $b$  accounts for size differences between the species of the mixture. Peng and Robinson give the following prescriptions for  $a$  and  $b$ .

$$b = 0.07780 \left( \frac{RT_c}{P_c} \right), \quad (5.17)$$

$$a(T) = a(T_c) \alpha(T_R, w), \quad (5.18)$$

$$a(T_c) = 0.45724 \frac{R^2 T_c^2}{P_c}, \quad (5.19)$$

$$\alpha = \sqrt{1 + m(1 - T_R^{1/2})}, \quad (5.20)$$

$$m = 0.37464 + 1.54226\omega - 0.26992\omega^2, \quad (5.21)$$

$$w = 1.000 - \log_{10} \left( \frac{P^{\text{sat}}}{P_c} \right)_{T_R=0.7}, \quad (5.22)$$

where  $T_c$  is the critical temperature,  $P_c$  is the critical pressure,  $T_R$  is the

reduced temperature ( $T_R = T/T_c$ ), and  $w$  is the acentric factor for component  $i$ . Each of these pure component properties, including the acentric factor, can usually be found in the literature for most of the common low-to-moderate molecular weight hydrocarbons (Reid, Prausnitz, and Polling, 1987).

When dealing with gas and liquid mixtures, it is necessary to define combining rules for  $a_{\text{mix}}$  and  $b_{\text{mix}}$  to use the equation of state to calculate mixture properties. In this development we will use the so-called van der Waals-1 mixing rules that assume random mixing of the components. These equations are used once for the gas phase mixture and once for the liquid phase mixture.

$$a_{\text{mix}} = \sum_i \sum_j x_i x_j a_{ij}, \quad (5.23)$$

$$a_{ij} = (a_{ii} a_{jj})^{0.5} (1 - k_{ij}), \quad (5.24)$$

$$b_{\text{mix}} = \sum_i \sum_j x_i x_j b_{ij}, \quad (5.25)$$

$$b_{ij} = \frac{(b_{ii} + b_{jj})}{2} (1 - \eta_{ij}), \quad (5.26)$$

where  $k_{ij}$  and  $\eta_{ij}$  are mixture parameters, usually determined by fitting pressure–composition data, and  $x$  denotes either liquid or gas phase mole fraction. With these mixing rules the analytical expression obtained for the vapor phase fugacity coefficient of component  $i$  is

$$\ln \phi_i^V = \frac{b_i^*}{b_{\text{mix}}} \left( \frac{Pv^V}{RT} - 1 \right) - \ln \left( \frac{Pv^V}{RT} - B \right) - \frac{A}{2.828B} \left( \frac{2 \sum_j x_j a_{ij}}{a_{\text{mix}}} - \frac{b_i^*}{b_{\text{mix}}} \right) \ln \left( \frac{\frac{Pv^V}{RT} + 2.414B}{\frac{Pv^V}{RT} - 0.414B} \right), \quad (5.27)$$

where  $a_{\text{mix}}$  and  $b_{\text{mix}}$  are determined using equations 5.23 through 5.26 with the gas phase mole fractions, and  $A$  and  $B$  are

$$A = \frac{a_{\text{mix}} R^2 T^2}{P},$$

$$B = \frac{b_{\text{mix}} RT}{P}.$$

The term  $b_i^*$  is defined as

$$b_i^* = \left[ \frac{\partial(b_{\text{mix}} N)}{\partial N_i} \right]_{T, V, n_{j \neq i}} = 2 \sum_k x_k b_{ik} - b_{\text{mix}}, \quad (5.28)$$

where  $N$  is the total number of moles in the mixture and  $x$  denotes either liquid or gas phase mole fractions. The analytical expression obtained for the liquid phase fugacity coefficient of component  $i$  is similar to equation 5.27.

$$\ln \phi_i^L = \frac{b_i^*}{b_{\text{mix}}} \left( \frac{P_{v^L}}{RT} - 1 \right) - \ln \left( \frac{P_{v^L}}{RT} - B \right) - \frac{A}{2.828B} \left( \frac{2 \sum_j x_j a_{ij}}{a_{\text{mix}}} - \frac{b_i^*}{b_{\text{mix}}} \right) \ln \left( \frac{\frac{P_{v^L}}{RT} + 2.414B}{\frac{P_{v^L}}{RT} - 0.414B} \right). \quad (5.29)$$

Neither  $k_{ij}$  nor  $\eta_{ij}$  are expected to be functions of temperature, pressure, or composition. Normally, both are expected to have absolute values much less than 1.0. The parameter  $k_{ij}$  is a binary mixture parameter associated with the intermolecular interactions between a pair of unlike species. The value of this parameter usually never gets larger than about 0.150. It can also be negative, although a negative value usually indicates the presence of specific chemical interactions, such as hydrogen bonding. It is questionable whether an EOS approach should be used when calculating the properties of a mixture that has components that hydrogen bond, because a cubic EOS accounts only for dispersion forces between the mixture components and not for chemical forces. Also, a different set of mixing rules is needed for  $a_{\text{mix}}$  and  $b_{\text{mix}}$  since the mixture components are not expected to distribute randomly in solution if they can hydrogen bond.

The binary mixture parameter  $\eta_{ij}$ , typically a small negative number, is associated with the packing of unlike components. Many times it is more expedient to set  $\eta_{ij}$  equal to zero, especially if only a limited amount of data is available. If  $\eta_{ij}$  is set equal to zero, the mixing rule for  $b_{\text{mix}}$  reduces to a single summation in mole fraction,  $b_i^*$  becomes equal to  $b_i$ , and the equation for the fugacity coefficient of component  $i$  reduces to the original expression given by Peng and Robinson (1976). But Deiters and Schneider (1976) recommend using both parameters when calculating high-pressure phase behavior with the Redlich-Kwong equation. They calculate  $P$ - $x$  isotherms and critical mixture curves for systems that have critical mixture pressures as high as 3,000 bar. They argue that the two adjustable mixture parameters  $k_{ij}$  and  $\eta_{ij}$  are needed because the mixture components differ considerably in molecular structure, size, and intermolecular strength. The results from their studies indicate that a cubic equation of state with two fitted parameters per binary pair in the mixture can successfully model high-pressure fluid phase equilibrium data in the mixture critical region. Similar results are expected with the PR equation since it too is a cubic EOS.

**LIQUID–LIQUID–VAPOR CALCULATIONS**

When there are three equilibrium phases, two sets of relationships must be satisfied for each component in each of the phases.

$$f_i^V(T, P, y_i) = f_i^{L_1}(T, P, x_i^{L_1}), \quad i = 1, 2, 3 \dots m, \quad (5.30)$$

$$f_i^V(T, P, y_i) = f_i^{L_2}(T, P, x_i^{L_2}), \quad i = 1, 2, 3 \dots m, \quad (5.31)$$

where superscript  $L_1$  is for one liquid phase and superscript  $L_2$  is for the other liquid phase. In other words, the fugacity of a component in one phase must be equal to that component's fugacity in each of the other two phases. The expressions for the component fugacities now become

$$f_i^{L_1} = x_i^{L_1} \phi_i^{L_1} P, \quad (5.32)$$

$$f_i^{L_2} = x_i^{L_2} \phi_i^{L_2} P, \quad (5.33)$$

$$f_i^V = y_i \phi_i^V P. \quad (5.34)$$

As with vapor–liquid equilibrium calculations, the fugacity coefficients in equations 5.32 through 5.34 are calculated with equations 5.27 and 5.29. The mixing rules are given in equations 5.23 through 5.26. No ternary parameters are used to calculate the phase behavior of ternary mixtures. Calculating LLV phase behavior with ternary mixtures is numerically very challenging because the thermodynamic expression for the fugacity coefficient is highly nonlinear. A robust algorithm is needed to avoid spurious results when doing these calculations. The computer programs listed in appendix B provide examples of slow but sure techniques for calculating LV and LLV equilibria.

Let us consider a straightforward example of using an EOS to model the phase behavior for a ternary mixture consisting of methane–ethane–octane (Igel, 1985). In particular, we are interested in predicting the occurrence of an experimentally observed LLV region at  $-67^\circ\text{C}$  and 54.7 bar using only pure component data and values for the three sets of binary mixture parameters  $k_{ij}$  and  $\eta_{ij}$  determined by fitting binary  $P$ – $x$  data. In this example, it is reasonable to use only one of the adjustable binary parameters  $k_{ij}$  for each binary pair comprising the ternary mixture—for methane–ethane, methane–octane, and ethane–octane—since the components in the mixture are fairly similar in size, shape, and intermolecular strengths. The physical properties for these three components are given in table 5.3. Our computational problem reduces to the following steps:

1. Determine a value for each binary  $k_{ij}$  by fitting available  $P$ – $x$  isotherms to the EOS.
2. Calculate the ternary phase diagram for the ternary mixture using the best-fit values of  $k_{ij}$  with no more adjustable parameters.
3. Compare the calculated phase diagram with the experimentally obtained diagram and adjust the  $k_{ij}$  values for each binary pair to obtain a better fit of the experimental data if so desired.

**Table 5.3** Physical Properties of Methane, Ethane, and *n*-Octane. Source: Reid, Prausnitz, and Poling (1987)

	Methane	Ethane	<i>n</i> -Octane
Molecular weight	16.4	30.1	114.2
Critical temperature (°C)	-82.6	32.3	295.7
Critical pressure (bar)	46.0	48.8	24.8
Acentric factor ( <i>w</i> )	0.007	0.091	0.394

The first binary system fitted to the EOS is the methane-ethane system. Figure 5.1 shows the comparison of calculated and experimental  $P$ - $x$  isotherms for this system. It is not too surprising that a good fit of the experimental data is obtained with a constant value of 0.02 for  $k_{ij}$  since the temperature range is only 20°C. It is also not surprising that  $k_{ij}$  is a small positive number that is much less than one, since these components are very similar in size and intermolecular strength. In practice,  $k_{ij}$  can vary with temperature, especially if the range in temperature is quite large. Our chances of successfully matching the experimental data for the ternary methane-ethane-octane system would be much higher if we had experimental data at temperatures closer to -67°C. Unfortunately, no such binary data are available for the methane-ethane system, so we will use  $k_{ij} = 0.02$  as a fixed constant for the ternary calculations.

Figure 5.2 shows a comparison of calculated and experimental  $P$ - $x$  isotherms for the ethane-octane system. In this instance a good fit of the experimental data is obtained with  $k_{ij}$  equal to zero. However, the temperature

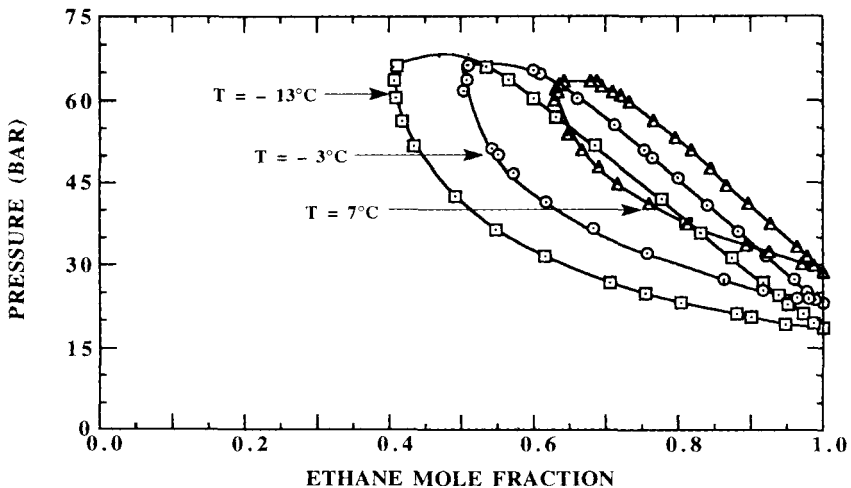


**Figure 5.1** A comparison of calculated (lines) and experimental (symbols) data for the methane-ethane binary system. For these calculations  $k_{ij}$  is 0.02 (Igel, 1985). (14.504 psi = 1 bar)

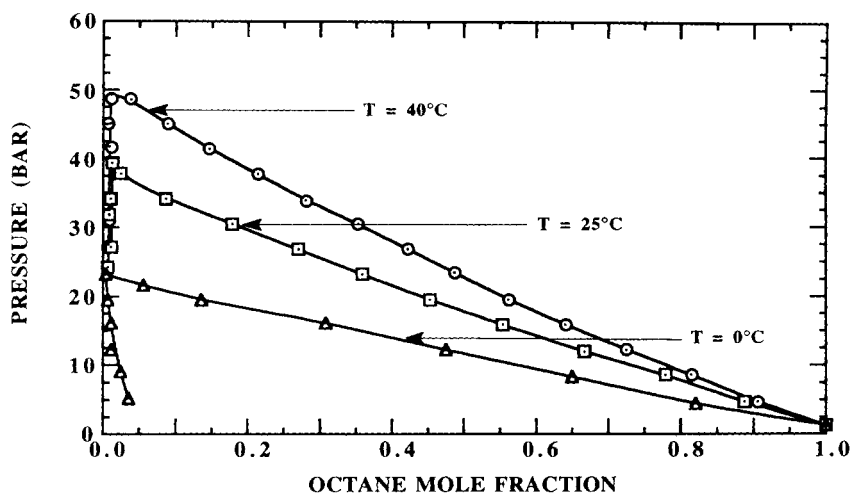


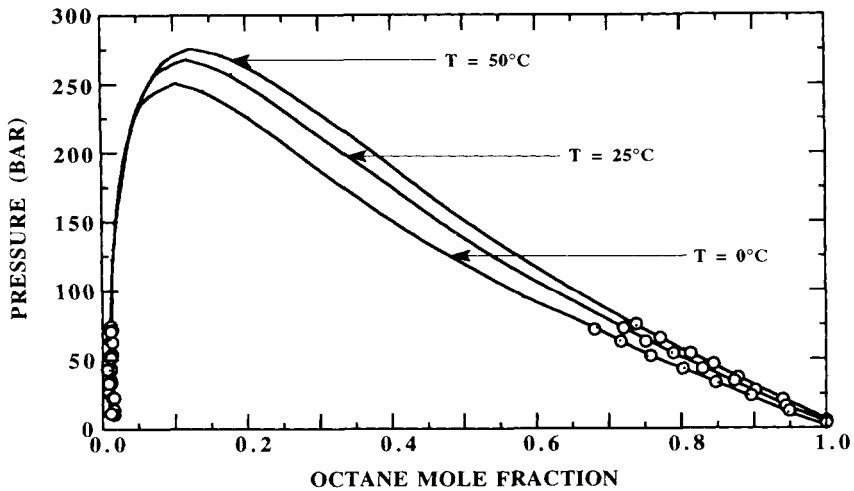
**Figure 5.2** A comparison of calculated (lines) and experimental (symbols) data for the ethane–*n*-octane binary system. For these calculations  $k_{ij}$  is 0.017 (Igel, 1985). (14.504 psi = 1 bar)

range for the data of this binary system is as much as 140°C higher than the temperature range of the ternary data. There are no data available at lower temperatures, so the estimate of  $k_{ij}$  obtained with this higher-temperature data will have to suffice.

The fit of the last binary pair, the methane–octane system, is shown in figure 5.3. This fit was obtained with a value of  $k_{ij}$  equal to 0.01. A few words of caution are warranted in this case. As noted in chapter 3, methane–hydrocarbon mixtures are expected to deviate from type-I behavior if the methane–solute carbon ratio is greater than 5. The  $P$ – $x$  data shown in figure 5.3 are far above the temperatures where a three-phase LLV line is expected for this binary system. However, a three-phase LLV line is predicted near the critical point of methane using  $k_{ij}$  equal to 0.01.

Figure 5.4 shows the calculated ternary phase diagram for the methane–ethane–octane system at  $-67.0^{\circ}\text{C}$  and 54.7 bar. An LLV region is, in fact, predicted for this system but the calculated concentrations of the three equilibrium phases are not in quantitative agreement with the experimental values. Nevertheless, even when no experiments on the ternary system are performed, the approach described here can be used to pinpoint regions in  $P$ – $T$  space where multiple phases could possibly exist. Once these regions of multiple phases are identified, further experimentation can be performed to verify their existence. If the three sets of binary mixture parameters are adjusted slightly, better agreement between calculated and experimental data can usually be obtained.

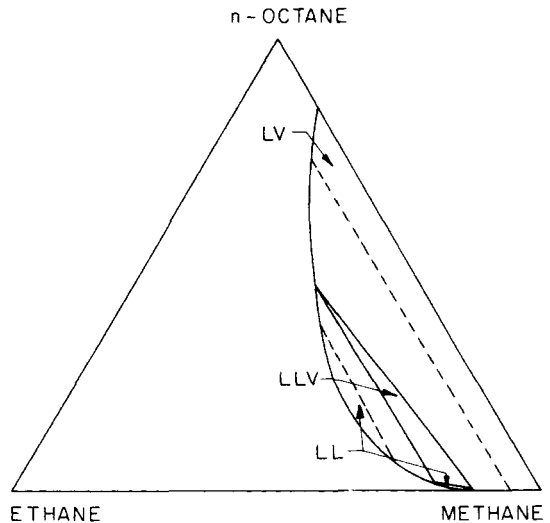
To demonstrate the performance of the Peng–Robinson EOS with nonzero values of  $k_{ij}$  and  $\eta_{ij}$ , we calculate the phase behavior for the isopropyl



**Figure 5.3** A comparison of calculated (lines) and experimental (circles) data for the methane-*n*-octane binary system. For these calculations  $k_{ij}$  is 0.01 (Igel, 1985). (14.504 psi = 1 bar)

benzene- $\text{CO}_2$  system (Occhiogrosso, 1985; Occhiogrosso, Igel, and McHugh, 1986). Figure 5.5 shows a comparison of experimental and calculated  $P$ - $x$  isotherm for the isopropyl benzene (also known as cumene) - $\text{CO}_2$  system over a temperature range 26–110°C. This system exhibits type-I phase behavior, described in chapter 3. With constant values of  $k_{ij}$  and  $\eta_{ij}$ , 0.066 and -0.040, a good fit of the experimental data is obtained over a wide range of temperature.

**Figure 5.4** Calculated ternary phase diagram for the methane-ethane-*n*-octane system at -67°C and 54.7 bar using mixture parameters obtained from a best fit of binary data. The dashed lines are tie lines (Igel, 1985).



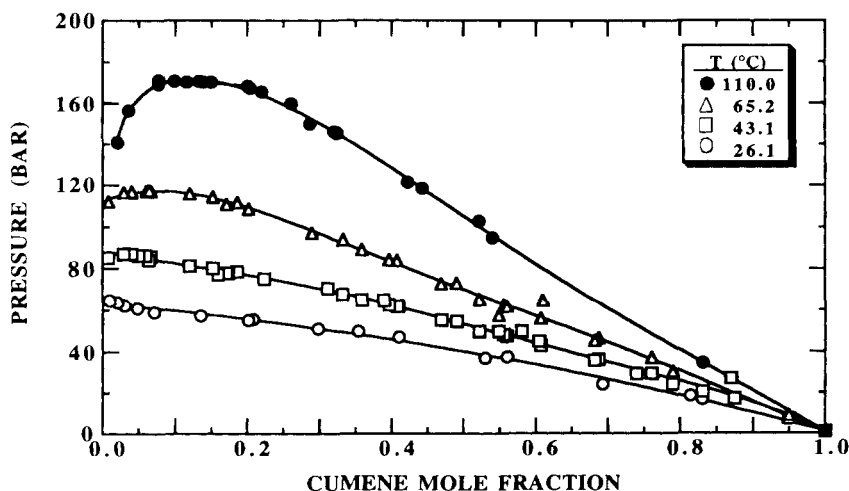


**Figure 5.5** A comparison of calculated (lines) and experimental (symbols)  $P$ - $x$  data for the cumene- $\text{CO}_2$  binary system (Occhiogrosso, 1985; Occhiogrosso, Igel, and McHugh, 1986). For these calculations  $k_{ij}$  is 0.066 and  $\eta_{ij}$  is  $-0.044$ .

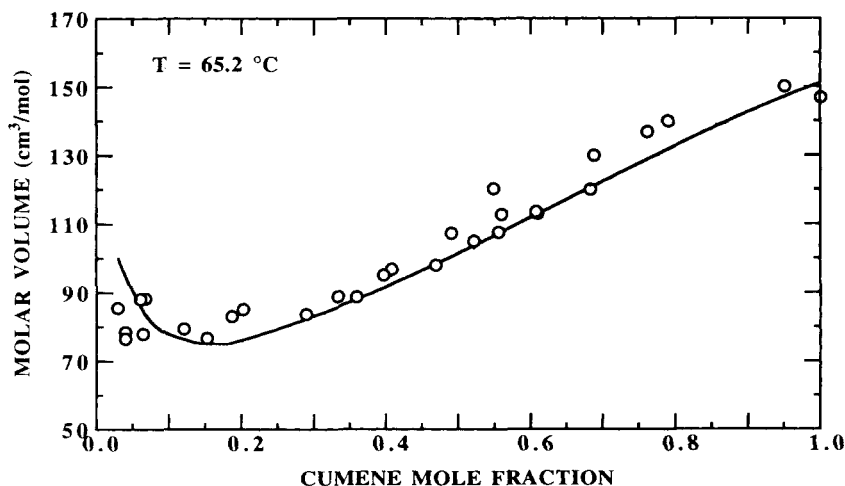


**Figure 5.6** A comparison of calculated (lines) and experimental (symbols) volumetric data for the cumene- $\text{CO}_2$  binary system (Occhiogrosso, 1985). For these calculations  $k_{ij}$  is 0.066 and  $\eta_{ij}$  is  $-0.044$ .

If  $\eta_{ij}$  is set equal to zero, a temperature-dependent  $k_{ij}$  is needed to obtain a good fit of the  $P$ - $x$  data over the entire temperature range. Although not explicitly mentioned earlier, the Peng–Robinson equation of state does predict the mixture molar volume of the equilibrium vapor and liquid phases. Figure



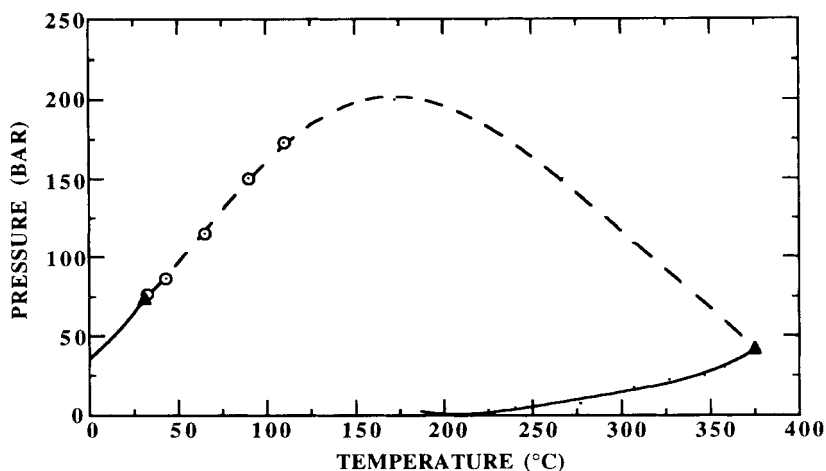


**Figure 5.7** A comparison of the calculated (lines) and experimental (symbols)  $P$ - $T$  trace of the critical mixture curve for the cumene- $\text{CO}_2$  binary system (Occhiogrosso, 1985; Occhiogrosso, Igel, and McHugh, 1986). For these calculations  $k_{ij}$  is 0.066 and  $\eta_{ij}$  is  $-0.044$ .

5.6 shows an example of how well the equation of state models volume-composition data for the cumene- $\text{CO}_2$  system using mixture parameters fitted to  $P$ - $x$  data. Finally, using the values  $k_{ij}$  and  $\eta_{ij}$  found from regressing  $P$ - $x$  data, we can calculate the critical mixture curve for this system. The results of this calculation are shown in figure 5.7.

From this example, it is evident that the Peng-Robinson EOS with two fitted parameters can be used along with a few good data points to generate a reasonable representation of the phase behavior over wide ranges of temperature and pressure. It is not hard to imagine how a combined calculational-experimental approach can save a fair amount of time and experimental anguish.

As demonstrated in the preceding paragraphs, a certain amount of data is needed to obtain a good estimate for  $k_{ij}$  and  $\eta_{ij}$  for a given solute-SCF mixture. But when no binary data are available for the system of interest, it is sometimes possible to use the mixture parameters obtained from a fit of data of a binary system consisting of a chemically similar solute and the same SCF solvent. To illustrate this point, let us use the values of  $k_{ij}$  and  $\eta_{ij}$  obtained for the isopropyl benzene- $\text{CO}_2$  system to calculate  $P$ - $x$  isotherms for the toluene- $\text{CO}_2$  and the *m*-xylene- $\text{CO}_2$  systems. Figure 5.8 shows that a very good fit of the experimental data is obtained with this approach. Hence, with a judicious guess for  $k_{ij}$  and  $\eta_{ij}$  it is reasonable to expect that a good representation of other aromatic- $\text{CO}_2$  systems, such as styrene- $\text{CO}_2$ , can be obtained from calculations alone. Compilations of  $k_{ij}$  and  $\eta_{ij}$  values can be found in the literature for other solute-SCF systems (Sandler, 1989).

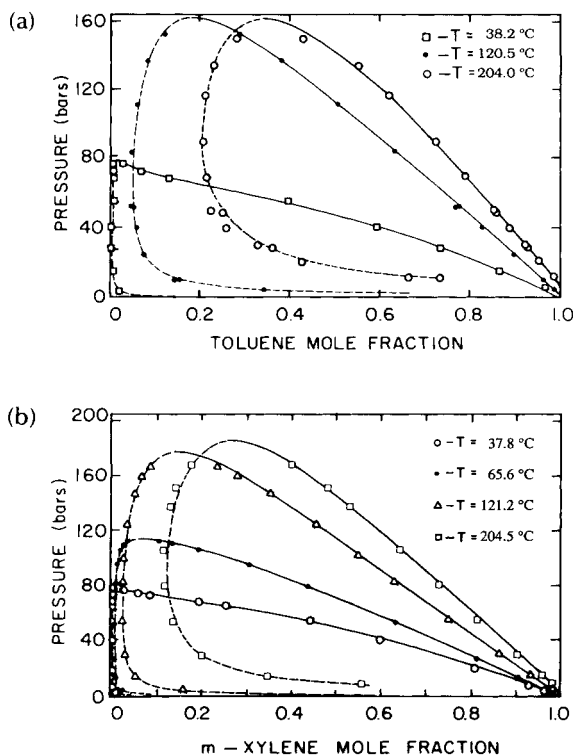


**Figure 5.8** A comparison of calculated (lines) and experimental (symbols) data for (a) the toluene-CO<sub>2</sub> system and (b) the *m*-xylene-CO<sub>2</sub> system. For these calculations  $k_{ij}$  is 0.066 and  $\eta_{ij}$  is  $-0.044$  (Occhiogrosso, 1985).

## POLYMER–SUPERCRITICAL FLUID CALCULATIONS

As will be described in later chapters, perhaps the largest potential application of supercritical fluid technology is in the area of polymer processing. Polymer–SCF phase equilibrium calculations confront us with the situation where the solute molecule can have a molecular weight in the hundreds of thousands. How does our calculation scheme change if the solute is a high molecular weight polymer? Fortunately, all of the fundamental equations and many of the algorithms remain the same as those for small molecule systems. What does change is the equation of state that is used. We must now deal with mixtures of components that differ substantially in molecular size. The techniques used for modeling polymer–SCF phase behavior will be demonstrated using the Sanchez–Lacombe EOS (Sanchez and Lacombe, 1977, 1978; Sanchez, 1980; Sanchez and Balazs, 1989). The Sanchez–Lacombe EOS is known as a lattice–gas model since the  $P$ – $V$ – $T$  properties of a pure component are calculated assuming that the component is broken into parts or “mers” that are placed into a lattice and are allowed to interact with a mean-field-type intermolecular potential. To obtain the correct system density, an appropriate

number of holes are also put into specific lattice sites, hence the name lattice-gas model. Although other equations could be used for these calculations, we choose the Sanchez-Lacombe equation since, in our opinion, this equation works as well as any other lattice-gas model, we have a fair amount of experience working with it, and it is very tractable. Let us first describe the equation of state and then describe its application to modeling vapor-liquid and liquid<sub>1</sub>-liquid<sub>2</sub>-vapor phase behavior.

The Sanchez-Lacombe (SL) EOS is

$$\tilde{\rho}^2 + \tilde{P} + \tilde{T} \left[ \ln(1 - \tilde{\rho}) + \left( 1 - \frac{1}{r} \right) \tilde{\rho} \right] = 0, \quad (5.35)$$

where  $\tilde{T}$ ,  $\tilde{P}$ ,  $\tilde{v}$ , and  $\tilde{\rho}$  are the reduced temperature, pressure, volume, and density, respectively, that are defined as

$$\tilde{T} = T/T^*, \quad T^* = \varepsilon^*/R, \quad (5.36)$$

$$\tilde{P} = P/P^*, \quad P^* = \varepsilon^*/v^*, \quad (5.37)$$

$$\tilde{\rho} = \rho/\rho^* = 1/\tilde{v} = V^*/V, \quad V^* = N(rv^*), \quad (5.38)$$

$$\rho^* = M/(rv^*), \quad (5.39)$$

where  $\varepsilon^*$  is the mer-mer interaction energy,  $v^*$  is the close-packed molar volume of a mer,  $M$  is the molecular weight,  $N$  is the number of molecules,  $r$  is the number of sites (mers) a molecule occupies in the lattice, and  $R$  is the universal gas constant. The parameter  $\varepsilon^*$ ,  $v^*$ , and  $r$  are used to define  $T^*$ ,  $P^*$ , and  $\rho^*$ , which are the characteristic temperature, pressure, and close-packed mass density. Since high molecular weight polymers have no detectable vapor pressure and since they thermally degrade before exhibiting a critical point, it is necessary to fit pure liquid molar volume data to determine either  $T^*$ ,  $P^*$ , and  $\rho^*$  or  $\varepsilon^*$ ,  $v^*$ , and  $r$ . Pottinger and Laurence (1984) present a thorough discussion on the techniques used to fit polymer  $P$ - $V$ - $T$  data with the Sanchez-Lacombe EOS. Sanchez and Lacombe (1978) describe a procedure for determining the characteristic parameters for low molecular weight substances using the vapor pressure curve of the substance and its molar volume at the normal boiling point. The Sanchez and Lacombe (1978) theory is not expected to predict the critical point of a pure component very accurately since it is a mean-field equation. Compilations of characteristic parameters for polymers and low molecular weight substances can be found in the literature (Sanchez and Lacombe, 1976, 1978).

When dealing with mixtures it is necessary to define combining rules for  $\varepsilon_{\text{mix}}^*$ ,  $v_{\text{mix}}^*$ , and  $r_{\text{mix}}$  to use the equation of state to calculate properties of a mixture. In this development we again use the so-called van der Waals-1 rules. These assume random mixing of the components, as they did for small

molecule systems. The mixing rule for the characteristic close-packed molar volume of a mer of the mixture  $v_{\text{mix}}^*$  is

$$v_{\text{mix}}^* = \sum_{i=1} \sum_{j=1} \Phi_i \Phi_j v_{ij}^*, \quad (5.40)$$

with

$$v_{ij}^* = \frac{v_{ii}^* + v_{jj}^*}{2} (1 - \eta_{ij}), \quad (5.41)$$

where  $\eta_{ij}$  corrects for deviations from the arithmetic mean and where subscripts  $i$  and  $j$  are the components in the solution. The volume fraction  $\Phi_i$  is defined as

$$\Phi_i = \frac{m_i}{\rho_i^* v_i^*} \bigg/ \sum_{j=1} \left( \frac{m_j}{\rho_j^* v_j^*} \right), \quad (5.42)$$

where  $m_i$  is the mass fraction of component  $i$  in the mixture, and  $\rho_i^*$  and  $v_i^*$  are the characteristic mass density and close-packed molar volume of component  $i$ , respectively. The mixing rule for the characteristic interaction energy for the mixture  $\varepsilon_{\text{mix}}^*$  is

$$\varepsilon_{\text{mix}}^* = \frac{1}{v_{\text{mix}}^*} \sum_{i=1} \sum_{j=1} \Phi_i \Phi_j \varepsilon_{ij}^* v_{ij}^*, \quad (5.43)$$

with

$$\varepsilon_{ij}^* = (\varepsilon_{ii}^* \varepsilon_{jj}^*)^{0.5} (1 - k_{ij}), \quad (5.44)$$

where  $\varepsilon_{ii}^*$  and  $\varepsilon_{jj}^*$  are the characteristic mer–mer interaction energies for components  $i$  and  $j$ , and  $k_{ij}$  is a mixture parameter that accounts for specific binary interactions between components  $i$  and  $j$  similar to its role in the Peng–Robinson equation. The mixing rule for the number of sites occupied by a molecule of the mixture,  $r_{\text{mix}}$ , is given by

$$\frac{1}{r_{\text{mix}}} = \sum_{j=1} \frac{\Phi_j}{r_j}, \quad (5.45)$$

where  $r_j$  is the number of sites molecule  $j$  occupies in the lattice. For polymer–solvent calculations it is mathematically easier to derive a chemical potential than a fugacity coefficient so that the equilibrium statement in equation 5.4 now becomes

$$\mu_i^{\text{L}} = \mu_i^{\text{V}}, \quad i = 1, 2, 3 \dots m, \quad (5.46)$$

where  $\mu$  is the chemical potential. With appropriate manipulation, the chemical potential of a component in a mixture  $\mu_i$  is derived as

$$\begin{aligned} \mu_i = RT & \left[ \ln \Phi_i + \left( 1 - \frac{r_i}{r} \right) \right] \\ & + r_i \left\{ -\bar{\rho} \left[ \frac{2}{v^*} \left( \sum_{j=1}^c \Phi_j v_{ij}^* \varepsilon_{ij}^* - \varepsilon^* \sum_{j=1}^c \Phi_j v_{ij}^* \right) + \varepsilon^* \right] \right. \\ & \left. + RT\bar{v} \left[ (1 - \bar{\rho}) \ln(1 - \bar{\rho}) + \frac{\bar{\rho}}{r_i} \ln \bar{\rho} \right] + P\bar{v} \left( 2 \sum_{j=1}^c \Phi_j v_{ij}^* - v^* \right) \right\}. \quad (5.47) \end{aligned}$$

In the following example we will model the  $P$ - $T$  trace of the cloud point curve that was obtained at an overall polymer concentration of 5 wt%. The calculational problem is posed as a binary mixture consisting of a single solvent and a single polymer of a fixed molecular weight. In fact, virtually all polymers exhibit a molecular weight distribution. There are calculational techniques available to handle the molecular weight distribution of the polymer. If the polymer was truly monodisperse, the cloud point pressure would be the intersection of the  $P$ - $x$  isotherm at an overall concentration of 5 wt% polymer solution (Koningsveld and Staverman, 1968a, b, c). For the example given here, we will use the cloud points calculated at 5 wt% polymer in solution, ignoring the polydispersity of the polymer. The  $P$ - $T$  trace of the cloud point curve will be obtained by calculating  $P$ - $x$  isotherms at a number of temperatures.

To calculate phase equilibrium data for ternary polymer systems, we first obtain the binary mixture parameters  $k_{ij}$  and  $\eta_{ij}$  by fitting  $P$ - $x$  isotherms for each binary pair of the ternary system. In this example we will model the ternary behavior of a nonpolar/polar copolymer, poly(ethylene-*co*-methyl acrylate) (69 mol%/31 mol%) (EMA<sub>69/31</sub>) with a nonpolar solvent, propane, and a polar cosolvent, acetone. We need to be careful performing this calculation. The first stumbling block confronted when modeling the phase behavior of this copolymer is that  $P$ - $V$ - $T$  data do not exist for pure EMA<sub>69/31</sub>, so we cannot regress pure component characteristic parameters. Instead we estimate them using a prescription of Panayiotou (1987). This averages the properties of the two homopolymers that comprise the copolymer, assuming that the copolymer is statistically random and  $v_{\text{copolymer}}^*$ ,  $\varepsilon_{\text{copolymer}}^*$ , and  $r_{\text{copolymer}}$  can be estimated with slightly modified forms of equations 5.40 through 5.45. Each of the summations in these equations is now taken over the two homopolymers that comprise the copolymer using the characteristic parameters of the homopolymers. Also, the mixture parameters  $k_{ij}$  and  $\eta_{ij}$  are now homopolymer-homopolymer interaction parameters rather than polymer-solvent interaction parameters. Although it is possible to include these two interaction parameters in the calculations to account for specific interactions between the two repeat units in the copolymer, we find they have little effect on the calculated cloud point curves, therefore, they are set equal to zero.

The fit of  $P$ - $x$  data for the acetone-propane binary system (Gomez-Nieto and Thodos, 1978) is shown in figure 5.9. The best fit of the Sanchez-Lacombe

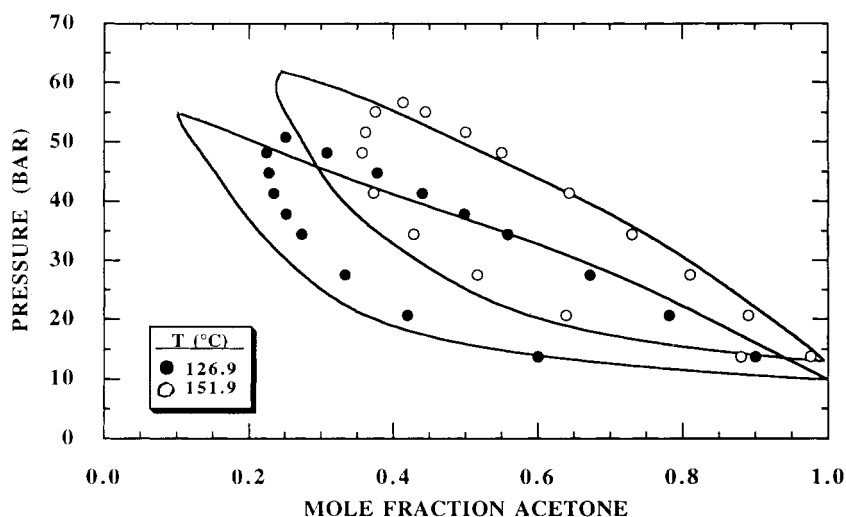


**Figure 5.9** Phase behavior of the acetone–propane system. The symbols represent experimental data (Gómez-Nieto and Thodos, 1978). The solid lines represent calculations with the Sanchez–Lacombe EOS with  $k_{ij} = 0.030$  and  $\eta_{ij} = 0.000$ .

equation for this binary system was obtained with  $k_{ij} = 0.030$  and  $\eta_{ij}$  equal to zero. Similar results in bubble and dew point calculations are obtained at both higher and lower temperatures. The results in figure 5.9 show that the Sanchez–Lacombe equation does only a fair job representing the phase behavior of this system, even with two mixture parameters. The calculated critical mixture pressures are about 6% higher than the experimental values, and the predicted and experimental critical mixture compositions differ by approximately 20%. The equation of state does a reasonable job matching the bubble point line. But the dew point line is overestimated particularly in the region close to the mixture critical point. If  $k_{ij}$  is decreased from 0.030 to zero, the two-phase region is shifted to higher propane concentrations and it is decreased by lowering the bubble point pressures slightly. Increasing the value of  $\eta_{ij}$  from zero to 0.030 has the same effect on the calculated curves as decreasing  $k_{ij}$ .

The calculated cloud point curve for the EMA<sub>69/31</sub>–propane system is shown in figure 5.10. The best fit of the experimental data was obtained with  $k_{ij} = 0.023$  and  $\eta_{ij} = -0.002$ . If  $k_{ij}$  becomes more positive, the curve shifts to higher pressures; if  $\eta_{ij}$  becomes more positive, the curve shifts to lower pressures. But the shift in the curve and its slope are more sensitive to changes in  $\eta_{ij}$  than  $k_{ij}$ .

It is not possible to determine values for the two mixture parameters for the EMA<sub>69/31</sub>–acetone mixture because there are no binary data available in the literature for these mixtures. To minimize the number of adjustable parameters,  $\eta_{ij}$  is set equal to zero. Since EMA<sub>69/31</sub> is slightly soluble in

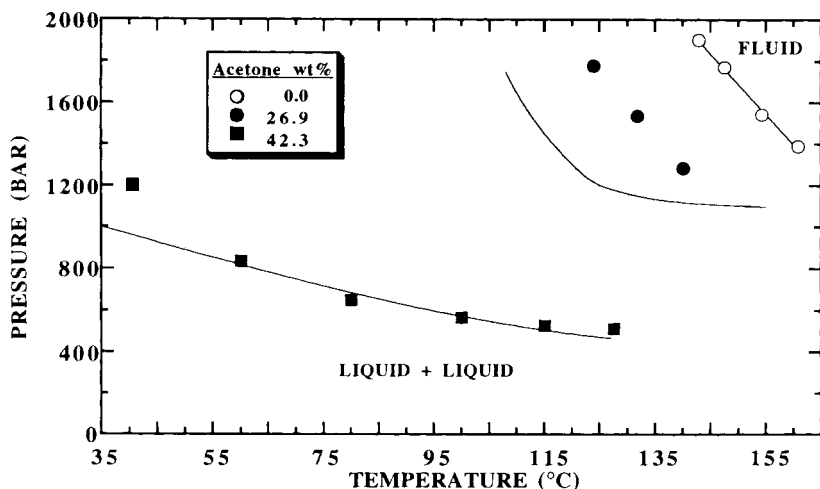


**Figure 5.10** Comparison of calculated (lines) and experimental cloud point data (symbols) of the poly(ethylene-co-methyl acrylate) (69 mol%/31 mol%)-acetone-propane system (Hasch et al., 1993). The polymer concentration is fixed at 5 wt%. The calculations are performed with the Sanchez-Lacombe EOS with  $k_{ij}$  and  $\eta_{ij}$  set equal to zero for the EMA<sub>69/31</sub>-acetone pair,  $k_{ij} = 0.030$  and  $\eta_{ij} = 0.000$  for the propane-acetone pair, and  $k_{ij} = 0.023$  and  $\eta_{ij} = -0.002$  for the EMA<sub>69/31</sub>-propane pair. The weight average and number average molecular weights of EMA<sub>69/31</sub> are 58,900 and 31,000, respectively.

acetone at atmospheric pressure and elevated temperatures,  $k_{ij}$  is also set equal to zero. With these parameter values, the model predicts that EMA<sub>69/31</sub>-acetone will be miscible at elevated pressures in the temperature range where the ternary cloud point data are available.

Figure 5.11 shows the results for the ternary EMA<sub>69/31</sub>-propane-acetone phase equilibrium calculations at a fixed temperature, 145°C, and four pressures. These calculations were performed with only pure component and binary mixture parameters. A single phase exists outside each dome in the diagram, and a two-phase region exists within the domes. The end points of the tie lines indicate the composition of the polymer-rich and solvent-rich phases. For many of the tie lines, the polymer concentration in the light phase is very low; on the scale of this diagram, it is essentially zero. As the pressure isothermally increases from 400 to 1,300 bar, the two-phase region shrinks. Another way of interpreting these results is that at 800 bar approximately 15 wt% acetone is needed to obtain a single phase for a mixture consisting of 5 wt% copolymer. At lower pressures, i.e., 400 bar, more cosolvent is needed to dissolve the polymer. For example, point A in figure 5.11 corresponds to a polymer solution with a composition of 5 wt% polymer, 40 wt% acetone, and 55 wt% propane at 145°C and 400 bar. If the pressure were increased, a solution consisting of this composition would be in a single phase. Reducing

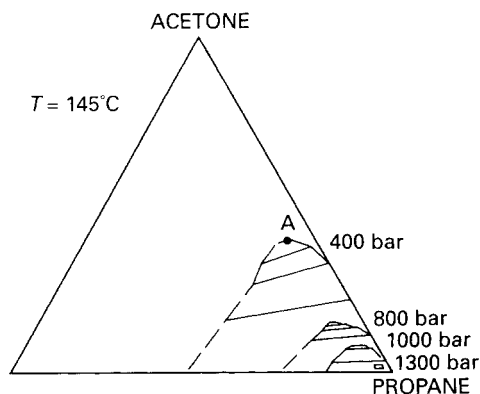


**Figure 5.11** Ternary phase diagram for the poly(ethylene-co-methyl acrylate) (69 mol%/31 mol%)–propane–acetone system at 145°C (Meilchen, 1991). The symbols are experimental data. The dashed and solid lines are phase boundaries and tie lines respectively, using the Sanchez-Lacombe EOS with  $k_{ij}$  and  $\eta_{ij}$  set equal to zero for the EMA<sub>69/31</sub>–acetone pair,  $k_{ij} = 0.030$  and  $\eta_{ij} = 0.000$  for the propane–acetone pair, and  $k_{ij} = 0.023$  and  $\eta_{ij} = -0.002$  for the EMA<sub>69/31</sub>–propane pair. The weight average and number average molecular weights of EMA<sub>69/31</sub> are 58,900 and 31,000, respectively.

the pressure would result in a two-phase system. Point A in figure 5.11 corresponds to a point on a 5 wt% polymer cloud point curve at 145°C and 400 bar. To model an entire fixed-composition, cloud point curve on a  $P$ – $T$  diagram, a new temperature is chosen and the pressure in the ternary calculation is varied until the two-phase boundary intersects the concentration of the ternary mixture. The calculations are then repeated at different temperatures, until the entire cloud point curve is traced.

Figure 5.10 shows the comparison of the calculated and experimental phase behavior of the EMA<sub>69/31</sub>–acetone–propane system for different loadings of acetone. A number of conclusions can be drawn from figure 5.10. The qualitative trends of adding cosolvent to the solution are readily predicted using mixture parameters based solely on binary data. As more acetone is added to the system, the cloud point pressure is reduced and the single-phase region is increased. Quantitatively, the equation of state matches the experimental data for both the cosolvent-free system and the 25 wt% acetone system. The cloud point curve for the low-concentration cosolvent system is not predicted very well. Nevertheless, the agreement is quite satisfactory considering that the characteristic parameters of the copolymer are estimated rather than regressed from experimental data and the equation of state does not directly account for polar interactions. This example shows the utility of



using an equation of state to predict the trends that can be expected when using cosolvents with polymer solutions.

The Sanchez-Lacombe EOS is a mean-field equation that does not directly account for hydrogen bonding and polar interactions. But Sanchez and Balazs (1989) show that it is possible to mimic the trends in the experimental data if the mixture parameters are allowed to vary with temperature. Therefore, when dealing with polar polymers or polar solvents, it may be necessary to force the mixture parameters to vary with temperature to obtain a representative fit of experimental data. In some cases, improved fits of the Sanchez-Lacombe equation to experimental data can also be obtained if the characteristic parameters of the solvent and the solute are obtained by fitting  $P$ - $V$ - $T$  data in the region where the mixture data were obtained. The improved fit of mixture data with characteristic parameters of the light component obtained in this manner is usually at the expense of a poor fit of the vapor pressure curve.

## SOLID-SUPERCritical FLUID CALCULATIONS

For solid-SCF solvent equilibria, the fugacity of component  $i$  in the SCF solvent phase can be calculated in the previously described manner, that is

$$f_i^{\text{SCF}}(T, P, y_i) = y_i \phi_i^{\text{SCF}} P. \quad (5.14)$$

A different expression is used to determine the solid phase fugacity, since a cubic equation of state does not predict the occurrence of a solid phase. Typically the solid is modeled as a pure phase, especially if the solid is crystalline. In this instance, the fugacity of component  $i$  as a pure solid phase (denoted by the superscript *os*) is

$$f_i^{\text{OS}}(T, P) = P_i^{\text{sat}}(T) \phi_i^{\text{sat}}(T) \exp\left(\frac{1}{RT} \int_{P_i^{\text{sat}}}^P v_i^{\text{OS}} dP\right), \quad (5.48)$$

where  $P_i^{\text{sat}}(T)$  is the sublimation pressure of the pure solid at the system temperature,  $v_i^{\text{OS}}$  is the molar volume of the pure solid,  $\phi_i^{\text{sat}}(T)$  is the fugacity coefficient at  $T$  and  $P_i^{\text{sat}}$ , and the exponential term is the Poynting correction for the fugacity of the pure solid. The molar volume of the crystalline solid usually remains constant up to kilobar pressures, so the exponential term in equation 5.47 simplifies to  $\exp[(P - P_i^{\text{sat}})v_i^{\text{OS}}/RT]$ . The fugacity coefficient  $\phi_i^{\text{sat}}$  is a correction term for high saturation pressures; it can be set equal to 1 since the saturation pressure of a crystalline solid is normally much less than 1 bar. The expression for the solubility of a heavy nonvolatile solid in the supercritical fluid solvent phase is obtained by setting equations 5.14 and 5.48 equal and using the above two simplifications.

$$y_i = \frac{P_i^{\text{sat}}(T) \exp\left[\frac{(P - P_i^{\text{sat}})v_i^{\text{OS}}}{RT}\right]}{\phi_i^{\text{SCF}} P}. \quad (5.49)$$

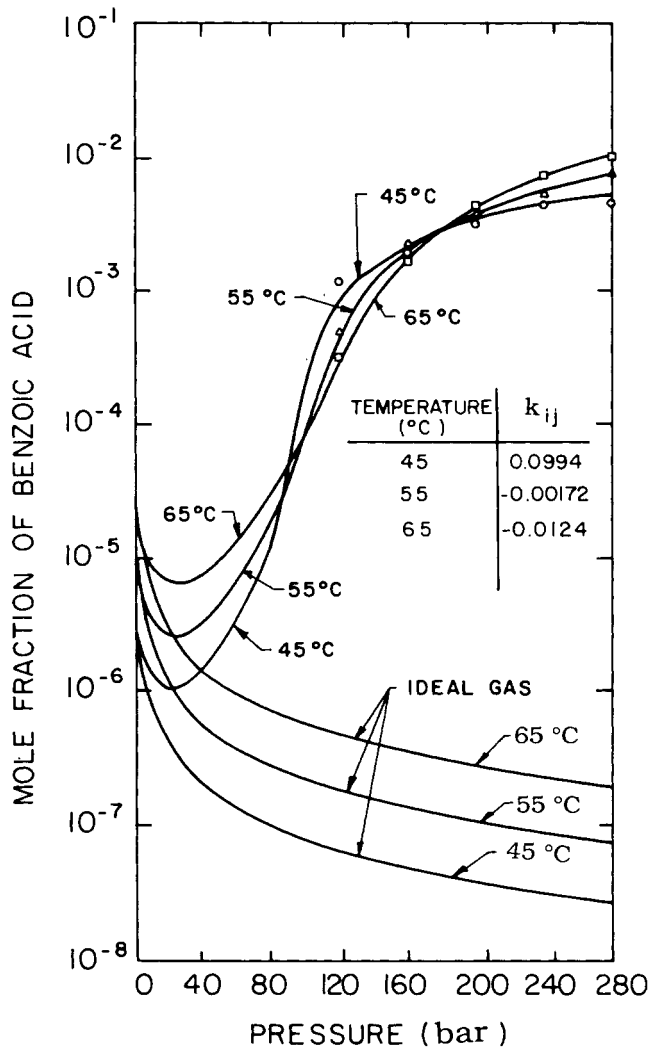
The fugacity coefficient of the heavy solid in the SCF phase is the key variable that drives the large increase in solid solubility when the gas is compressed into the critical region. This fugacity coefficient accounts for the nonidealities that arise as the gas phase density increases from ideal gas densities at very low pressures to liquid-like densities at very high pressures. Using equation 5.49 it is possible to show there are two competing effects that fix the solubility of a heavy solid in an SCF solvent (Lira, 1988). At a fixed temperature, the solubility increases in the SCF solvent as the pressure is increased. This is because  $\phi_i^{\text{SCF}}$  decreases much more rapidly than the pressure increases or than the exponential term in the numerator increases, especially near the critical point of the SCF. The fugacity coefficient is a measure of the difference between ideal gas behavior, where molecules do not interact, and real gas behavior, where they do interact. It decreases as the solvent molecules are pushed into close proximity to the solute molecules. But at very high pressures, where repulsive forces overwhelm attractive forces,  $\phi_i^{\text{SCF}}$  increases, thus lowering solubility.

Figure 5.12 shows a comparison of experimental and calculated solid solubilities using the Peng–Robinson EOS and the ideal gas law, which forces  $\phi_i^{\text{SCF}}$  to be equal to 1 (Kurnik, Holla, and Reid, 1981). Obviously the ideal gas law does a very poor job modeling the data. A single adjustable binary mixture parameter  $k_{ij}$  is used for the calculations with the Peng–Robinson EOS. Although an adequate representation of the experimental data can be obtained with a single adjustable mixture parameter, it must be made a weak function of temperature; this is a bit surprising since the temperature range is only 20°C. The Peng–Robinson EOS does a rather poor job in this case, due to the highly polar interactions expected between benzoic acid and CO<sub>2</sub> and their very nonideal acid–base interactions in solution.

A second adjustable mixture parameter  $\eta_{ij}$  can be used to account for the large size disparity between a heavy nonvolatile solid and a light SCF solvent (Deiters and Schneider, 1976; Chai, 1981; Paulaitis, McHugh, and Chai, 1983; McHugh et al., 1988). Johnston and Eckert (1981) and Johnston, Ziger, and Eckert (1982) forego the Peng–Robinson EOS entirely and use an augmented van der Waals EOS to predict solid solubilities in SCF solvents. They combine the Carnahan–Starling equation for the repulsive contribution to the pressure with the attractive term of the van der Waals equation. Their approach is reasonably successful, especially for extremely nonvolatile solids for which sublimation pressures or critical property information has not been reported.

Kurnik and Reid (1982) also use the Peng–Robinson EOS to correlate their data on the solubility of two pure solids in an SCF solvent. Their results are very sensitive to the value of the binary solid<sub>1</sub>–solid<sub>2</sub> interaction parameter they use. Gopal et al. (1983) found similar results. They show that calculated solid solubilities are dependent on whether the mixture consists of two pure solids or whether the solids have melted and formed a single mixed-solid phase.

As described in some detail in chapter 3, it is extremely important to



**Figure 5.12** A comparison of calculated (lines) and experimental (symbols) data for the benzoic acid- $\text{CO}_2$  system at three different temperatures (Kurnik, 1981).

determine the location of the SLV border curves for solid-SCF systems. One branch of the SLV line is normally very close to the vapor pressure curve of the pure light component. The other branch of the SLV curve originates at the melting temperature of the heavy solid. McHugh and coworkers have shown that reasonable estimates of solid solubilities can be obtained if the  $P$ - $T$  trace of the SLV line is modeled with the Peng-Robinson EOS to fix the values of the two mixture parameters (McHugh et al., 1988). The advantage in this instance is that a fair amount of experimental effort can be avoided by first determining the  $P$ - $T$  trace of the SLV curve then calculating the rest of the phase diagram and solubility isotherms. We demonstrate this technique for the xenon-naphthalene system.

The parameters needed in the Peng–Robinson EOS to model the SLV line are determined by solving equations 5.40 through 5.42.

$$f_2^V(T, P, y_2) = f_2^L(T, P, x_2), \quad (5.50)$$

$$f_2^{OS}(T, P) = f_2^V(T, P, y_2), \quad (5.51)$$

$$f_1^V(T, P, y_1) = f_1^L(T, P, x_1), \quad (5.52)$$

where subscript 2 denotes naphthalene and subscript 1 denotes xenon. Equations 5.50 and 5.52 reduce to

$$x_2 \phi_2^L = y_2 \phi_2^V, \quad (5.53)$$

$$x_1 \phi_1^L = y_1 \phi_1^V. \quad (5.54)$$

Since solid naphthalene is virtually incompressible up to 1,000 bar (Vaidya and Kennedy, 1971), equation 5.51 becomes

$$P_i^{\text{sat}}(T) \phi_i^{\text{sat}}(T) \exp \left[ \frac{(P - P_i^{\text{sat}}) v_i^{\text{OS}}}{RT} \right] = y_2 \phi_2^V P \quad (5.55)$$

The fit of the SLV line is obtained in the following manner. The computer program used to fit the SLV line with the Peng–Robinson equation is given in appendix B. First an estimate of  $k_{ij}$  and  $\eta_{ij}$  is made. At a fixed pressure and temperature, equation 5.55 is solved to determine the composition of naphthalene in the gas phase. Next, equations 5.53 and 5.54 are solved by guessing a liquid phase composition and iterating until the equations are satisfied. The sum of the calculated liquid phase mole fractions is then checked. If this sum is greater than 1.0, the temperature is lowered slightly and the calculational procedure is restarted at equation 5.55 using the same pressure as before. If the sum of the liquid phase mole fractions is less than 1.0, the temperature is raised slightly and the calculational procedure is restarted at equation 5.55 using the same pressure as before. If the sum is equal to 1.0, the result is recorded as a point on the calculated SLV line, the pressure is increased, and the calculations are restarted at equation 5.55. The calculations are stopped at the UCEP where a vapor–liquid critical point is found. The entire procedure is repeated several times with different mixture parameters until a good representation of the SLV line is obtained. Changing  $k_{ij}$  has a large effect on the UCEP temperature and a smaller effect on the UCEP pressure; changing  $\eta_{ij}$  has a large effect on the UCEP pressure and a smaller effect on the UCEP temperature. Increasingly, it is not possible to fit the normal melting point of naphthalene to within 2°C using the pure component parameters for naphthalene found in the literature. But if the value for  $b_{22}$  is multiplied by 0.9944, the melting point can be determined within 0.1°C. This correction factor is used throughout the following calculations.

Figure 5.13 shows the best fit of the naphthalene–xenon SLV line obtained with a value of 0.020 for  $k_{ij}$  and  $-0.025$  for  $\eta_{ij}$ . The calculated UCEP was 46.5°C and 136.8 bar, in good agreement with the experimental value of 46.4°C

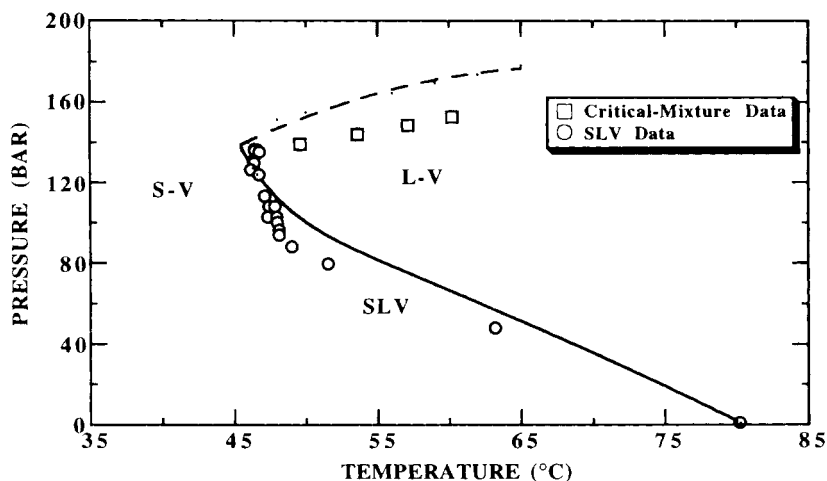


**Figure 5.13** A comparison of the calculated (solid and dashed lines) and experimental (symbols) SLV line and the critical mixture curve for the naphthalene-xenon system using the Peng-Robinson equation with two mixture parameters fitted to the SLV line (McHugh et al., 1988).

and 136.8 bar. Using the best-fit values for  $k_{ij}$  and  $\eta_{ij}$ , the critical mixture curve was calculated. Figure 5.13 also shows the fit of the critical mixture curve. Although the calculated and experimental UCEP are in good agreement, the fit of the SLV line is only in fair agreement with experimental data. A better fit of the low-pressure range of the SLV line could be obtained with different values of  $k_{ij}$  and  $\eta_{ij}$  but it was not possible to simultaneously fit the entire curve and the UCEP. Nor was it possible to obtain as good a fit of the UCEP with  $\eta_{ij}$  set equal to zero. The calculated  $P$ - $T$  projection of the critical mixture curve is consistently higher than the experimentally observed pressure. This is not surprising; most cubic equations do only a fair job of modeling critical points and these data were not fitted directly.

For each vapor-liquid calculation along the SLV line, the equation of state provides an estimate of the density of each phase. Figure 5.14 shows the calculated liquid and gas phase densities along the SLV line. At pressures greater than 130 bar, the Peng-Robinson equation predicts that the gas phase becomes more dense than the liquid phase, in reasonable agreement with the experimental observation that the liquid-gas inversion occurs at about 112 bar. Also, the calculated solid-gas inversion, 100 bar, is reasonably close to the experimentally observed value of 80 bar. Even though the calculated results differ somewhat from the experimentally observed values, it is significant that a phase inversion is predicted at all.

A comparison of calculated and experimental solid solubility isotherms is shown in figure 5.15. These calculations are performed using the values of the mixture parameters fitted to the SLV line. In general, the Peng-Robinson EOS

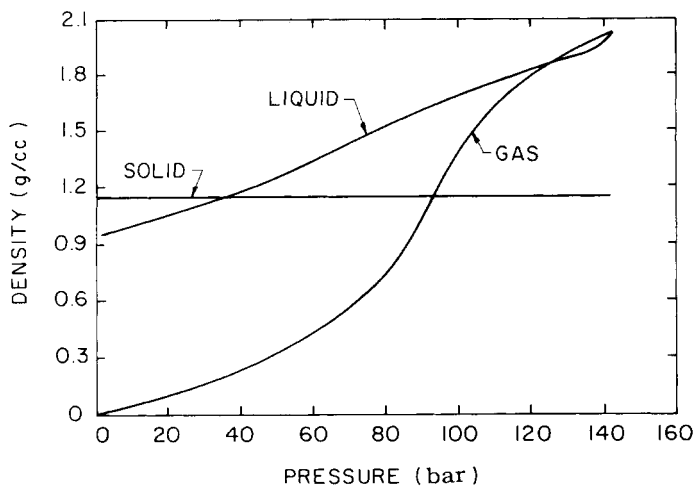


**Figure 5.14** Calculated densities of the gas and liquid phases at  $P$ - $T$  conditions along the SLV line for the naphthalene-xenon system using the Peng-Robinson equation with two mixture parameters fitted to the SLV line (McHugh et al., 1988).

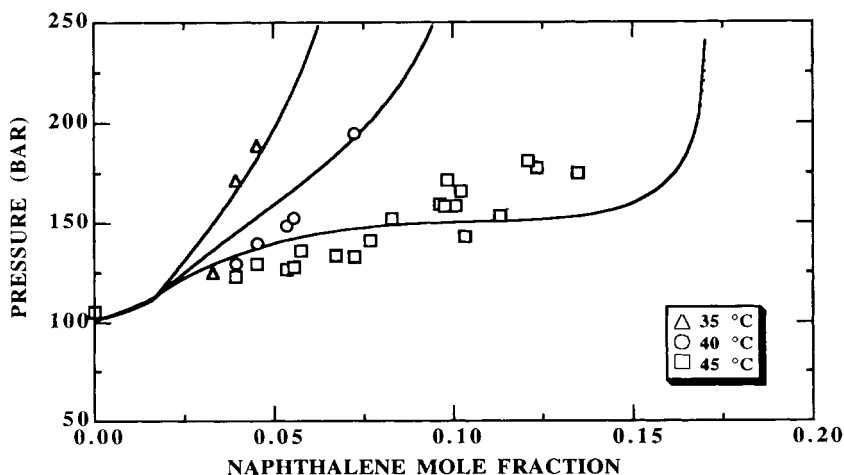


**Figure 5.15** A comparison of the calculated (lines) and experimental (symbols) pressure-composition data for the naphthalene-xenon system using the Peng-Robinson equation with two mixture parameters fitted to the SLV line (McHugh et al., 1988).

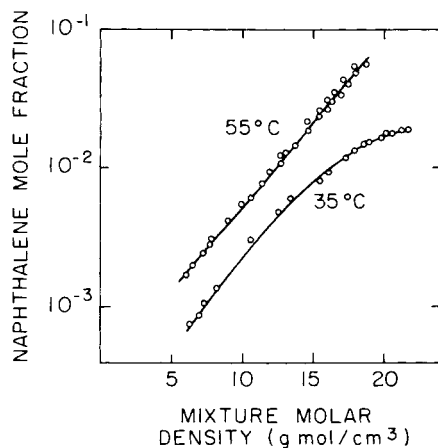


**Figure 5.16** Solid naphthalene- $\text{CO}_2$  solubility data plotted as a function of mixture density (Paulaitis et al., 1984).

overestimates the solubility of naphthalene in supercritical xenon by about 10% at 35°C and by 14 to 16% at 45°C and at pressures close to the UCEP pressure. The predictions are expected to differ from experimental values near the UCEP since these operating conditions are very close to the vapor-liquid critical point, which occurs at the UCEP. If  $k_{ij}$  and  $\eta_{ij}$  are allowed to vary slightly, a much better fit of the solubility isotherms could be obtained at the cost of a poorer fit of the SLV line and the UCEP. Nevertheless, using mixture parameters fitted to the  $P$ - $T$  trace of the SLV line, a reasonable estimate can be made of the solubility of the solid in the supercritical fluid. McHugh et al (1988) obtain slightly better results for these calculations using the Sanchez-Lacombe EOS.

At the high pressures and liquid-like densities encountered in an SCF solvent extraction process, the distinction between gas and liquid phases becomes less clear. Therefore, it is also possible to model the SCF solvent phase as an expanded liquid rather than as a compressed gas (Balder and Prausnitz, 1966). According to Mackay and Paulaitis (1979), this approach may be used to calculate solid solubilities; activity coefficient and EOS parameters are needed but it may be possible to estimate the solubility of a solid in an SCF solvent phase from the solid solubility in the corresponding liquid solvent.

For solid-SCF systems it is also possible to correlate experimental data using plots of concentration of the solid in the SCF phase versus density of the pure SCF or the density of the SCF-solute mixture (Wong, Pearlman, and Johnston, 1985). As described earlier, the solubility of a heavy solute in an SCF solvent is related to the density of the pure SCF solvent. An example of a composition-density plot is shown in figure 5.16 for the naphthalene- $\text{CO}_2$  system. The curves in this plot are linear and parallel to each other. These types of plots can also be used for interpolating experimental data. But there are limitations to using composition-density plots; they are good only for solid-SCF systems. The resultant linear curves on these plots are a consequence of the high degree of correlation between the compressibility of the

SCF and the solubility of the solid in the SCF. Therefore, the isothermal solubility curves deviate from linearity as the SCF approaches a highly compressed constant density, at which point the solid solubility reaches a limiting value. The solubility curves also deviate from linearity as the UCEP for the solid–SCF mixture is approached. This deviation from linearity near the system UCEP is clearly shown in the work of Schmitt and Reid (1984) for the naphthalene–ethylene system. Finally, the solubility curves will deviate from linearity if there are specific solute–solvent interactions, such as acid–base interactions or hydrogen bonding (Schmitt, 1984).

This chapter demonstrates how to calculate phase diagrams and solubility isotherms for binary and ternary supercritical mixtures. As Johnston has pointed out (Wong, Pearlman, and Johnston, 1985; Johnston, Peck, and Kim, 1989), no single model will work for all situations. As the equations describing molecular interactions in dense fluids become more accurate, we can expect our abilities to model complex phase behavior to improve. At present, using a cubic equation of state or a lattice–gas equation appears to offer the best compromise between accuracy and ease of application.



---

## Process Operations

---

As is by now evident to the reader, the phenomenon of solubility in supercritical fluids is not new. Since 1879 (or 1861, if we include the high-pressure, near-critical liquid carbon dioxide studies of Gore), solubility, phase, and spectroscopic studies have been performed on a large number of solute–SCF mixtures. They were made for their inherent scientific and technical interest and value. And they received a resurgence of interest with the work of Diepen, Scheffer, and coworkers in the late 1940s and early 1950s.

In 1955 Todd and Elgin reported on the phase behavior of a number of liquid and solid solutes in supercritical ethylene. Aromatics, substituted aromatics, aldehydes, short- and long-chain alcohols, acids, and paraffins were studied. Examples of the various types of high-pressure phase equilibria described in chapter 3 were found in this work. Todd and Elgin extrapolated their high-pressure phase equilibrium data to the design of a new process for separating mixtures. It is perhaps appropriate that a description of the concept of supercritical fluid extraction appeared in the first issue of the *AIChE Journal*. To wit Todd and Elgin (1955)

Besides the theoretical interest in the unusual phase behavior encountered in these systems, the principles involved can be applied in operations wherein the nonideality is intentionally created. The magnitude of solubility of a compound of low volatility in a gas above its critical temperature . . . is sufficient to consider the gas as an extracting medium, that is fluid–liquid or fluid–solid extraction analogous to liquid–liquid extraction and leaching. In this case the solute is removed and the solvent recovered by partial decompression . . . . Thus compression of a gas over a mixture of compounds could selectively dissolve one compound, permitting it to be removed from the mixture. Partial decompression of the fluid elsewhere would drop out the dissolved compound, and the gas could be reused for further extraction.

To show the potential of SCF processing, we apply the ideas of Todd and Elgin in a hypothetical process. Figure 6.1 shows a schematic diagram of the supercritical fluid extraction process described by Todd and Elgin. Four major pieces of equipment are shown: an extraction vessel, a pressure reduction valve, a separator, and a compressor. For simplicity and ease of discussion,

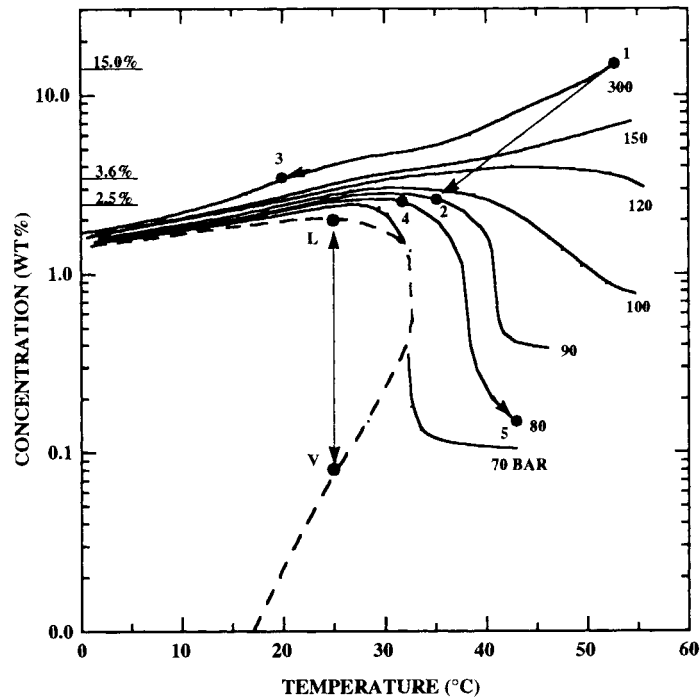
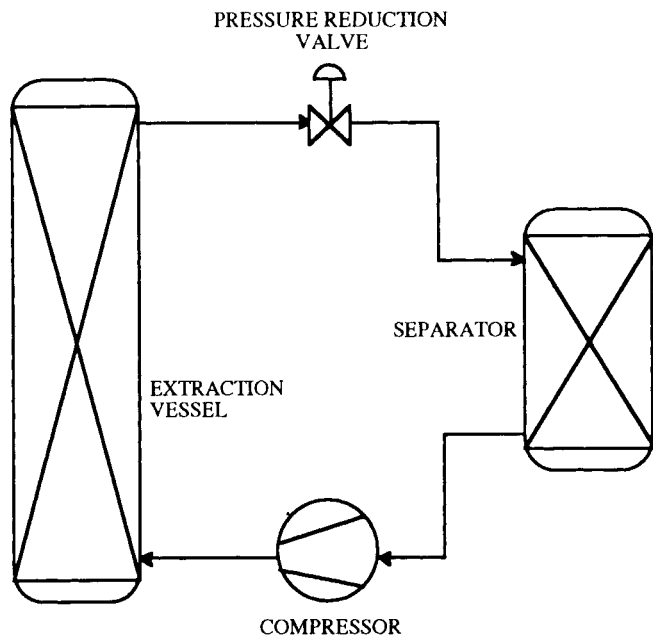


**Figure 6.1** Schematic diagram of a simplified supercritical fluid extraction process; solubility data for naphthalene in CO<sub>2</sub> is illustrated.

ancillary equipment, such as gages, controls, facilities for storing gas, etc., is not shown in the figure. For our hypothetical process we will separate naphthalene from powdered chalk using supercritical  $\text{CO}_2$ . We choose naphthalene because there are extensive data on the solubility of this solid in supercritical  $\text{CO}_2$  over wide ranges of pressures and temperatures, therefore we can demonstrate alternate processing conditions graphically. Powdered chalk, while a highly unlikely contaminant in naphthalene, is chosen since it does not dissolve in carbon dioxide. This hypothetical process is similar to the separation of a high added-value product from an insoluble contaminant. Alternatively, it represents the removal of a soluble contaminant from an insoluble high-value product.

To illustrate the operation of this hypothetical process, let us assume that the extractor has been filled with a 50/50 mixture of naphthalene and powdered chalk. Incidentally, the filling of the vessel with the solid mixture, although "an engineering detail" for this discussion, is not necessarily an easy task and is, furthermore, not without substantial capital and operating costs in the overall separation process. The solid mixture is probably not continuously "pumpable" into the extraction vessel during high-pressure operation; it instead will probably be charged in a batch mode through quick-acting gate valves or through some other motor-activated opening. Because the filling and extraction operations are done in a batch mode, it might be desirable to have two or three extraction vessels in parallel. The extension of the concepts discussed in this section is easily extrapolated to a multivessel system with different solid substances and SCF solvents.

Once the naphthalene-chalk dust mixture is charged to the vessel, carbon dioxide is compressed and heated to the desired operating conditions. When the pressure reaches the desired operating level, the pressure reduction valve is actuated and  $\text{CO}_2$  flow commences. We assume the extraction conditions are 300 bar and  $55^\circ\text{C}$ . As  $\text{CO}_2$  flows through the vessel, naphthalene dissolves in the stream of  $\text{CO}_2$  to a concentration level of 15 wt% (see point 1 in figure 6.1). The loaded  $\text{CO}_2$  phase leaving the extractor is expanded to 90 bar through the pressure reduction valve. When the pressure is lowered, naphthalene precipitates from solution (see point 2 in figure 6.1). If we assume an isenthalpic (i.e., constant enthalpy) expansion of the  $\text{CO}_2$ -rich stream, a concomitant  $19^\circ\text{C}$  drop in temperature occurs, calculated from thermodynamic data for pure  $\text{CO}_2$ . The expansion path on the naphthalene solubility diagram, arrow 1  $\rightarrow$  2, is therefore an oblique line.

At 90 bar and  $36^\circ\text{C}$  the equilibrium solubility of naphthalene in  $\text{CO}_2$  is only 2.5 wt%, therefore naphthalene falls out of solution. The precipitated naphthalene is collected in the separator and the  $\text{CO}_2$  stream is recompressed to the initial extraction conditions of  $55^\circ\text{C}$  and 300 bar and is recycled to the extractor.

It is informative to follow the process cycle on a Mollier diagram for  $\text{CO}_2$  to determine the energy requirements of this SCF process relative to some other process, such as the vaporization of the naphthalene at its boiling point

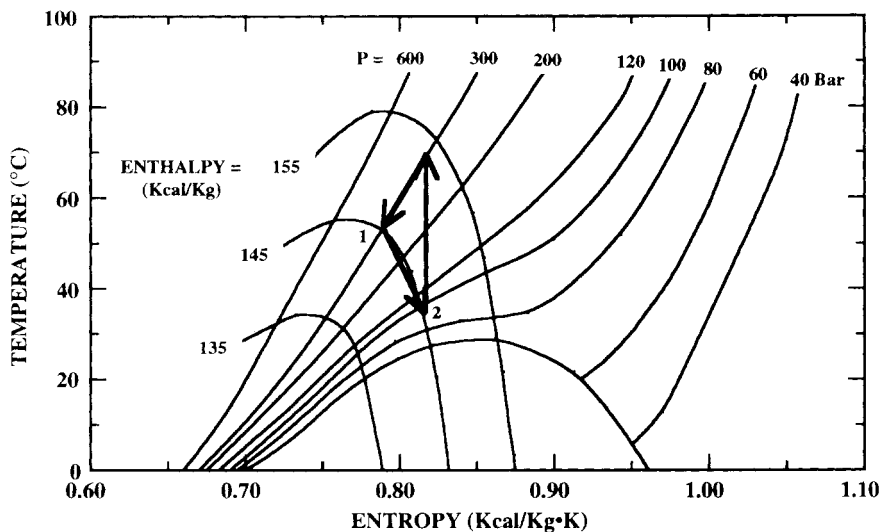


**Figure 6.2** Temperature–entropy diagram for pure CO<sub>2</sub>. Enthalpy  $H$  is measured in kcal/kg.

(218°C). An enlarged view of the pertinent section of the temperature–entropy diagram of CO<sub>2</sub> is given in figure 6.2. The arrows on this figure trace the path of CO<sub>2</sub> in the process cycle. As previously described, the extraction step occurs at 55°C and 300 bar. The CO<sub>2</sub>–naphthalene solution leaving the extractor is isenthalpically expanded across the pressure reduction valve to 90 bar. During the expansion step, the temperature of the CO<sub>2</sub> solution falls about 19°C, ignoring the heat effects associated with the formation of solid naphthalene. The stream of CO<sub>2</sub> leaving the separator is at 36°C and 90 bar. It flows into the compressor and is isentropically compressed to 300 bar. Compressing the CO<sub>2</sub> causes its temperature to rise to 72°C. The energy required to compress CO<sub>2</sub> to 300 bar, 7 kcal/kg (12.6 Btu/lb) of CO<sub>2</sub>, can be read directly from the Mollier diagram. Although it's not shown in figure 6.1, the carbon dioxide is isobarically cooled to 55°C, the initial extraction temperature, before entering the extraction vessel. No attempt is made to integrate the heat exchange steps in the analysis of our hypothetical process. The expansion of CO<sub>2</sub> results in a solubility decrease from 15 wt% to 2.5 wt%, so about 6.6 lb of CO<sub>2</sub> needs to be recycled to extract 1 lb of naphthalene.

Now we compare the energy required to extract naphthalene in our supercritical process to the energy needed to vaporize naphthalene from the chalk dust mixture. The electrical energy required to compress 6.6 lb of CO<sub>2</sub> in the recycle stream (at 12.6 Btu/lb CO<sub>2</sub>) is 83.2 Btu, i.e., the electrical energy input to the process to extract one pound of naphthalene. If we assume that the supercritical process has a Carnot efficiency of 38%, the equivalent thermal energy becomes 219 Btu. The vaporization process requires energy input for latent heat of fusion to melt the naphthalene, sensible heat to increase the

temperature of the liquid naphthalene to its boiling point, and more latent heat to vaporize the naphthalene. The heat of vaporization is 84 Btu/lb naphthalene and a sensible heat input of 350 Btu/lb naphthalene is required to raise the bed temperature from ambient to 218°C (the boiling point of naphthalene). Thus the total thermal energy requirement is 434 Btu/lb naphthalene. With this separation problem, extraction using supercritical CO<sub>2</sub> requires only about one half the energy of the vaporization process.

Figure 6.1 shows we could have chosen more than one process path using supercritical CO<sub>2</sub>. Chapter 3 shows that solubility in supercritical fluids is also influenced by temperature. Changing the temperature of a system can have a dramatic or moderate effect on the solubility behavior, depending on the  $P$ - $T$ - $x$  region of the solubility diagram in which the change occurs. Instead of extraction and separation using pressure reduction, the process can be operated isobarically with changes in temperature. For example, starting at point 1 of figure 6.1, the stream leaving the extractor can flow through a heat exchanger (not shown), instead of a pressure reduction valve, and be cooled to 20°C, indicated by the 1→3 arrow on the 300 bar isobar. As the CO<sub>2</sub>-rich stream is cooled, the concentration of naphthalene decreases from 15 wt% to 3.6 wt%, shown by point 3. The CO<sub>2</sub> leaving the separator can then be heated back to 55°C and recycled to the extractor. This isobaric mode of operation employs a blower, compared with the compressor required for pressure reduction. In isobaric operation, where the naphthalene collects is an important design consideration. For example, problems may ensue if it coats the heat exchanger tubes. Chapter 8 addresses some of these engineering details. Using the solubility data in figure 6.1, this isobaric mode of operation recycles slightly more CO<sub>2</sub> per pound of naphthalene: 7.2 lb versus 6.6 lb.

Temperature variations can be used advantageously in another region of the solubility diagram, the “low-pressure” region or retrograde condensation region, very close to the critical point of pure CO<sub>2</sub>, where increasing temperature causes a decrease in solubility. For the naphthalene–chalk dust separation, the process can operate isobarically between points 4 and 5 in figure 6.1. Extraction occurs at 80 bar and 32°C. Raising the temperature of the loaded CO<sub>2</sub> stream by only 8°C causes the solubility to drop by more than one order of magnitude. The CO<sub>2</sub> leaving the separator is cooled back to 32°C and recycled to the extractor.

A fourth alternative for carrying out the naphthalene extraction utilizes the dissolving capacity of near-critical liquid CO<sub>2</sub>. This operating mode is illustrated in figure 6.1 by the LV tie line. Liquid CO<sub>2</sub> is employed to dissolve and extract the naphthalene from the mixture, and the liquid solution leaving the extractor is heated to vaporize the CO<sub>2</sub> and recover the naphthalene. The CO<sub>2</sub> is then condensed and recycled to the extractor.

In summary, there exist four modes of operating the supercritical extraction of solid substances. The specific mode employed in any instance is a function of many factors, for example, the sensitivity of the material(s) to temperature and the ease of condensation or nucleation. Many facets and

parameters must be considered and evaluated before selecting process and operating conditions for any conventional process. Supercritical fluid extraction is no exception to this rule.

Enough groundwork on the generic nature of solubility behavior in SCF solvents has been developed in the previous chapters of this book for the reader to extrapolate from the idealized situation of separating a mixture of naphthalene and chalk dust to other, more practical systems. Other systems may include the extraction of oleoresins from spices where the desired product is the extract, or the extraction of monomers and oligomers from polymers where the desired product is the purified polymer, or the separation of a mixture of chemicals where both streams are valuable products. Many of these examples are enumerated in the following chapters.

Besides extracting one material from another, there exists an alternative operating scheme for utilizing the properties of supercritical fluids in the separation of liquid mixtures. It is possible to use a supercritical fluid to separate certain pairs of miscible liquids without extracting them. Elgin and Weinstock (1959) discuss the separation of binary water-organic mixtures where supercritical ethylene is used to "salt out" the water. The ternary phase behavior exhibited by certain water-organic-supercritical fluid mixtures was discussed in detail in chapter 3. But the "SCF salting out" concept is not applicable only for water-organic solutions. If the supercritical fluid is highly soluble in, or miscible with, one of the liquids and is insoluble or scarcely soluble in the other, a liquid-liquid phase split can occur when the liquid solution is contacted with the supercritical fluid. The next section of this chapter describes the features of phase-splitting phenomena for polymer-organic solvent-supercritical fluid solvent mixtures. Although the phase behavior of polymer mixtures is explicitly described here, information in chapter 3 suggests that the same phase behavior principles apply to oligomer species having molecular weights well below 1,000.

Polymer-solvent mixtures can be separated and the polymer recovered from solution at the lower critical solution temperature (LCST). This is the temperature at which the miscible polymer-solvent mixture separates into a polymer-rich phase and a solvent-rich phase. LCST phenomena are related to the chemical nature of the mixture components, the molecular weight of the mixture components, especially the polymer, and the critical temperature and critical pressure of the solvent (Allen and Baker, 1965). As the single-phase polymer solution is isobarically heated to conditions near the critical point of the solvent, the polymer and solvent thermally expand at different rates. This means their free volumes change at different rates (Patterson, 1969). The thermal expansion of the solvent is much greater than that of the polymer. Near its critical point, the solvent has expanded so much that it is no longer able to solubilize the polymer. Hence, the polymer falls out of solution. If the molecular weight of the polymer is on the order of  $10^4$  a polymer-solvent LCST can occur within about 20–30°C of the solvent's critical temperature. If the molecular weight of the polymer is closer to  $10^6$ , the LCST phase

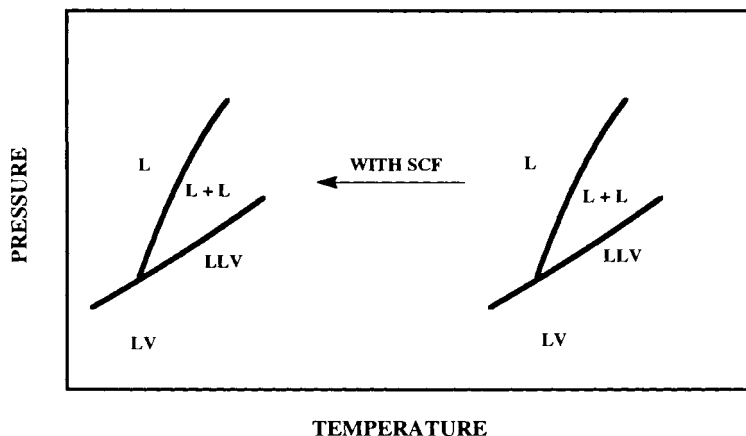


**Figure 6.3** Schematic representation of the effect of an SCF solvent on the phase behavior of polymer-organic solvent mixtures.

separation can occur at a temperature as low as 120°C below the critical temperature of the solvent.

In general, saturated cyclic hydrocarbons, such as cyclohexane or methyl cyclopentane, tend to be good polymer solvents since they have very high cohesive energy densities. These types of solvents have very high critical temperatures, therefore it is often necessary to raise the temperature of the system to well over 200°C to obtain an LCST phase split. At these high temperatures the polymer may thermally degrade. Polymer degradation can be avoided at high LCSTs by adding stabilizers to the polymer solution (Anolick and Slocum, 1973; Anolick and Goffinet, 1971; Caywood, 1970). But there is a way to lower the LCST.

Irani, Cosewith, and Kasegrande (1982), and more recently Guckes et al. (1990), have described processes for lowering the LCST of a polymer-solvent mixture by adding an SCF solvent to the mixture. The effect of an SCF additive on the polymer-solution phase behavior is shown schematically in figure 6.3. Note that the UCST line has been omitted from figure 6.3. Addition of between 5 and 15 wt% supercritical propylene to a poly(ethylene-co-propylene)-hexane mixture shifts the phase border curves for this system to lower temperatures. The polymer-rich phase that is recovered is highly concentrated in polymer, approximately 40 wt%. Conventional solvent-stripping techniques, such as steam stripping, can then be used to recover the polymer from this polymer-rich phase. In this process the amount of residual polymer remaining in the solvent-rich phase at the LCST is reduced by a factor of about three (in some instances from about 0.22 wt% polymer to about 0.08 wt%).

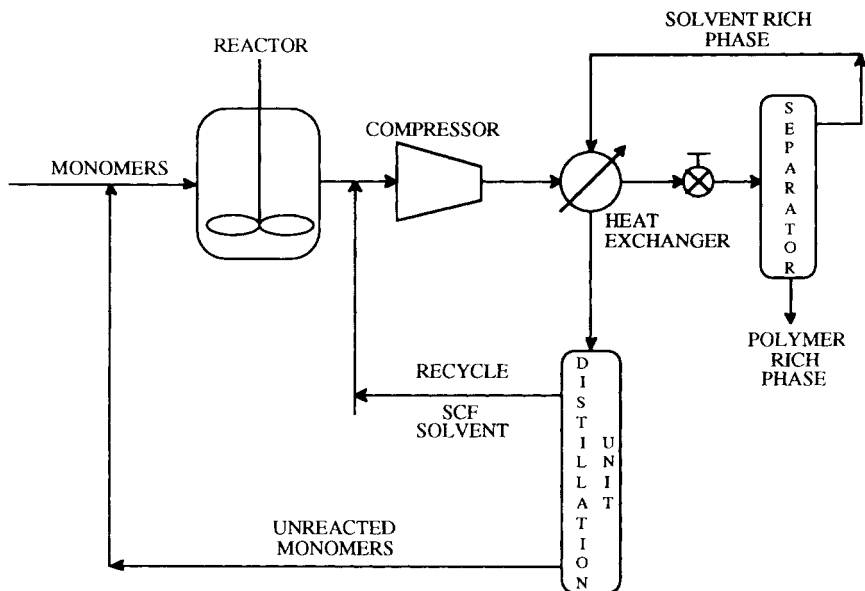


**Figure 6.4** Diagram of proposed process for recovering polymer from solution by adding an SCF solvent to the mixture (McHugh, 1986).

A diagram for a proposed process for a polymer-solvent-SCF additive process is shown in figure 6.4 (Irani, Cosewith, and Kasegrande, 1982). Subcritical propylene ( $T_c = 91.9^\circ\text{C}$ ,  $P_c = 46.2$  bar) is added to the reactor product stream before the compressor. Although other SCF additives will also shift the LCST to lower temperatures (McHugh and Guckes, 1985), propylene is already present in the product stream and therefore does not represent an added component to the system. The entire mixture is compressed to the desired operating pressure then heated to much higher temperatures. The mixture, now a single liquid phase, is throttled to lower pressures. As the pressure is reduced, the LCST curve is intersected and a polymer-rich liquid phase and a solvent-rich liquid phase are formed. If the pressure is further reduced, three phases (LLV) will form in the separator.

Irani, Cosewith, and Kasegrande suggest that a better solvent-polymer split is obtained when the system is operated in the LLV region of the phase diagram, compared with the LL region. A lower operating pressure can be used and the small amount of vapor formed in the LLV region can be vented to maintain a constant operating pressure. The denser polymer-rich phase is recovered as a bottom stream from the separator for further processing. The less dense solvent-rich phase is recovered as an overhead stream, integrated with the heat exchanger to recover its heat content, purified, and recycled back to the front end of the process. Compared with recovering the polymer and solvent by stream stripping the entire reactor product stream, this SCF-solvent



additive process should prove less energy intensive. There should also be less thermal degradation of the polymer at the more moderate process operating temperature. Therefore, control over product quality (i.e., distribution of the molecular weight of the polymer) should be easier, and fewer polymer degradation inhibitors would be needed.

Chapter 9 describes the technique of separating polymer-solvent mixtures by adding an SCF additive to the mixture. Chapter 7 notes that the fundamentals of polymer-solution phase-splitting are identical to the fundamentals of propane deasphalting, a process developed more than fifty years ago.

---

## Early Industrial Applications

---

Before progressing to a discussion of recent supercritical fluid process and applications development, we first describe three processes that were developed more than fifty years ago employing SCF solvents. Our objective in this chapter is to analyze how early supercritical fluid processes were developed. The benefit of this approach is twofold. First, each of the three examples presented here elucidates the steps that comprise the creative engineering employed to develop commercial processes. Second, these examples, along with those reported in chapter 1, should help put to rest the myth that supercritical fluid technology is new and novel. Once engineers and scientists recognize that their predecessors were able to harness this interesting technology perhaps they will become more willing to investigate the potential of SCF technology for their own unique applications.

### PROPANE DEASPHALTING

Half a century ago Wilson, Keith, and Haylett (1936) devised a process for phase equilibrium separations that became the basis of the propane deasphalting process still in use today for refining lube oils. The entire process is not, strictly speaking, a supercritical fluid extraction process because the initial extraction step is carried out at near-critical conditions. But propane deasphalting does make use of the substantial change in the solvent power of a liquid in the vicinity of its critical point. Propane deasphalting is also an example of a process using near-critical property changes to improve energy and phase separation efficiency. Since the solvent characteristics of propane can be changed dramatically in various regimes of  $P$ - $T$  phase space, this single solvent can be used selectively to separate a lube oil feedstock into paraffin wax, asphalt, heavy ends, naphthenes, color bodies, and the desired product, a purified light oil.

Let us briefly consider the propane lube oil refining process shown in figure 7.1. First the compressed liquid propane at 50°C is mixed with the residuum feed in the asphalt settler. Compressed liquid propane dissolves all the constituents of a lube oil feedstock except for the asphalt. Because the

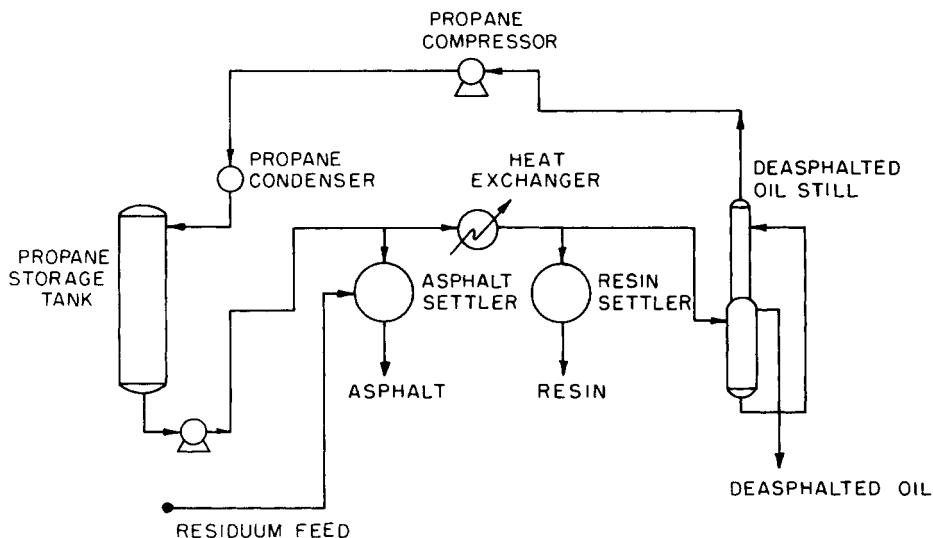


**Figure 7.1** Schematic diagram of the propane-lube oil process (Wilson, Keith, and Haylett, 1936).

propane-lube oil mixture possesses a low viscosity, the asphalt fraction is readily separated from the mixture, hence it is easily recovered. Next the propane-lube oil mixture is cooled to precipitate the waxes from solution. The mixture is cooled to approximately  $4^{\circ}\text{C}$  by evaporating a small portion of the solution, thus taking advantage of the refrigerant properties of propane. (The dewaxing section of the process is not shown in the figure.) Heating the remaining propane-oil mixture to temperatures near  $100^{\circ}\text{C}$  decreases the solvent power of liquid propane; this results in the sequential precipitation of the resins, the heavy ends, and the naphthenic constituents and leaves only the lightest paraffins in solution. Figure 7.1 shows only the asphalt and resin-removing sections of the process.

Before explaining the thermodynamic framework of the propane deasphalting process, we present several paragraphs from the 1936 paper by Wilson, Keith, and Haylett to highlight what was known fifty years ago about near-critical and supercritical fluid processing.

Although there are numerous ways of removing these impurities, the oil industry within the past few years has focused its attention upon the use of selective solvents. Selective solvents quickly made progress in the fields of separating the naphthenic from the paraffinic constituents of lubricating oils which otherwise required the use of large quantities of sulfuric acid with the attendant acid sludge nuisance. Some solvents were found which were able to remove both naphthenic and asphaltic constituents, but, since the resulting extract was a mixture of asphalt

and naphthenic hydrocarbons, it required further refining and separation to make marketable by-products and hence was not very promising. After the oil refiner had learned of the efficiency and cheapness of selective solvents, he was anxious to find solvents (or antisolvents) which would remove not only one or two impurities, but all of the undesirable constituents of lubricating oils, preferably one at a time in order that the by-products might be recovered in useful form. In an effort to discover such a universal solvent, chemists have searched Bielstein and other sources without finding any single chemical whose solvent properties are such that it will selectively remove all these impurities, although several of the improved solvents for the removal of naphthenic compounds have been studied as a result of this search.

Unfortunately, during most of this search for solvents, the refiner neglected to look at his own raw materials. In every refinery and in every crude field, millions of tons of propane gas are available, which, by simple compression and liquefaction, can be converted into a solvent with the unique property (under proper conditions of temperature and pressure) of tending to separate every one of the undesirable constituents. Further, assuming recovery facilities are available, propane is the cheapest liquid per gallon available in the refinery with the exception of water; it is nontoxic, noncorrosive, and extremely stable.

If we consider the diverse chemical and physical characteristics of the five undesirable constituents listed, it would seem almost inconceivable to anyone familiar with the theory of fractional solution that any one solvent could possibly throw all of these different compounds out of solution. As a matter of fact, propane cannot be expected to, and does not, separate them all at the same temperature and pressure. It owes its versatility as a precipitant to the fact that its properties change rapidly over the particular temperature range between  $-44^{\circ}\text{F}$  [ $-42^{\circ}\text{C}$ ] and  $+215^{\circ}\text{F}$  [ $100^{\circ}\text{C}$ ]. Over this range it possesses the properties of a series of solvents, any one of which can be obtained by raising or lowering the temperature or changing the pressure or combining those two operations.

Incidentally, its viscosity and surface tension decrease to nearly negligible values as the critical temperature is approached. Over this range propane changes from a typical liquid to a fluid possessing substantially the properties of gas. As the  $220^{\circ}\text{F}$  [ $100^{\circ}\text{C}$ ] isotherm indicates, gaseous propane at a pressure of 1000 pounds per square inch [69 bar] is much more dense than liquid propane at  $212^{\circ}\text{F}$  [ $100^{\circ}\text{C}$ ] and its saturation pressure. Also, as the liquid approaches its critical temperature, it becomes highly compressible.

At temperatures near the critical, increasing the pressure (which increases density) increases the solubility of oil in propane. The dissolving power of propane appears to be roughly proportional to the density of the propane, and even compressed propane gas at  $220^{\circ}\text{F}$  [ $100^{\circ}\text{C}$ ] and 1000 pounds per square inch [69 bar] pressure dissolves substantially more oil than does liquid propane at 600 pounds [41 bar] and  $204^{\circ}\text{C}$  [ $96^{\circ}\text{C}$ ]. Thus the solvent properties of propane can be strikingly changed by changes in either temperature or pressure or both; and in the magnitude of the resulting change it is probably unique among liquids.

As a result of these unique properties propane is today being commercially employed in numerous large installations for the separation of all five of the undesirable constituents of lubricating oils. That this development should have taken place in the short period of three years is a remarkable tribute both to the versatility of propane and the progressiveness of the petroleum refiner.

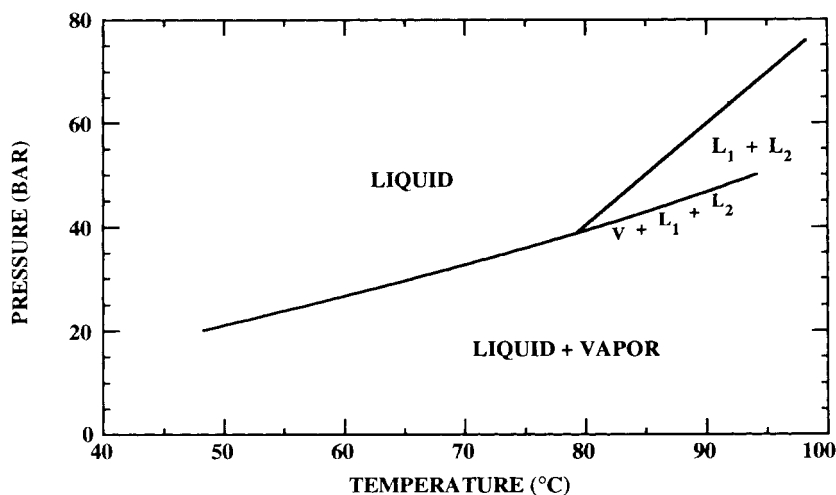


**Figure 7.2**  $P$ - $T$  representation of the phase behavior of the propane-lube oil mixture (Wilson, Keith, and Haylett, 1936).

As is evident in these paragraphs, the authors clearly are excited about the possibilities of processing with a single solvent that has the properties of many solvents. To explain the events that are occurring at various points in the propane-lube oil refining process, we first examine schematic  $P$ - $T$  and ternary phase diagrams similar to the ones found in the original paper of Wilson and coworkers.

Figure 7.2 shows a  $P$ - $T$  representation of the phase behavior of a propane-distillate oil mixture (Wilson, Keith, and Haylett, 1936). This phase diagram is similar to the polymer-solvent diagram described in chapters 3 and 6. The single-phase propane-oil mixture splits into two liquid phases when the LL curve is crossed. This is the type of phase separation that occurs when the resins, heavy ends, and naphthenic constituents are separated from the lube oil mixture with increasing temperature. At the intersection of the LL curve with the LLV curve, two liquid phases become critically identical in the presence of the vapor phase. Technically, this intersection is called the lower critical solution temperature but using polymer separation terminology it is renamed the lower critical end point (LCEP) and the LL curve is called the LCST or cloud point curve. The  $P$ - $T$  conditions at the LCEP in figure 7.2,  $\sim 77^{\circ}\text{C}$  and  $\sim 525$  psia (36.2 bar), are close to the critical point of pure propane,  $96.7^{\circ}\text{C}$  and 616 psia (42.5 bar). The pressure at the LCEP is slightly greater than the vapor pressure of pure propane at  $77^{\circ}\text{C}$ , 423 psia (29 bar).

Although it is not shown on this diagram, the single-phase lube oil mixture also splits into two phases when the temperature is decreased and the UCST curve is crossed at very cold temperatures. This phenomenon is used to separate the wax from the oil where the flashing of a portion of the propane from solution provides the cooling needed to reduce the solution temperature.

For the oil-propane mixture the LCEP occurs within about 22°C of the critical temperature of propane ( $T_c = 96.7^\circ\text{C}$ ) and within about 70 psia ( $\sim 5$  bar) of propane's critical pressure. Because the oil distillate consists of high molecular weight components, the reason for the occurrence of the LCEP is analogous to the reason the LCEP for polymer-solvent systems occurs near the critical point of the solvent. As the single-phase mixture is heated to conditions near the critical point of propane, the mixture components thermally expand at different rates (Patterson, 1968). The thermal expansion of the propane is much greater than that of the heavy components in the oil distillate. Near its critical point, propane has expanded to the point where it is no longer able to solubilize the highest molecular weight fraction in the oil distillate (i.e., the heavy ends). Hence, the heavy ends of the oil precipitate from solution. The degree of separation of the heavy ends can be illustrated by a ternary diagram for an asphalt-oil-propane mixture. Of course, the asphalt and the oil are not single components and, as such, the ternary diagrams are only a qualitative representation of the actual phase behavior.

Shown in figure 7.3 are three schematic ternary diagrams representing the phase behavior of asphalt-oil-propane mixtures at three temperatures (Wilson, Keith, and Haylett, 1936). The principles governing the phase behavior shown in these diagrams are exactly the same as those described for the ternary systems presented in chapter 3. At 37.8°C propane is entirely miscible with the oil, the oil is entirely miscible with the asphalt, but the propane is only partially miscible with the asphalt, therefore the asphalt falls out of solution. This represents the first step of the lube oil refining process. The phase behavior depicted in this diagram indicates that only oil distillates with high concentrations of asphalt are separated by propane at this temperature.

If the temperature is increased to 60°C the two-phase region of the diagram expands considerably. This temperature is much closer to the critical temperature of propane, so liquid propane is in a much more expanded state than at 38°C. Notice that the critical point on this diagram has moved toward greater propane-oil concentrations. If enough propane is added to a 75% asphalt and 25% oil mixture such that the two-phase region of the diagram is entered, a further increase in the amount of propane has two effects. It increases the amount of the light propane-rich phase and improves the degree of separation of the original asphalt-oil mixture. In this case, increased amounts of propane added to the asphalt-oil mixture decrease the solvent power of the oil for the asphalt.

If the temperature is now increased to 82.2°C, the oil-propane binary mixture develops an LV region on the oil-propane axis of the ternary phase diagram and an LLV region appears in the interior of the ternary phase diagram. The three-phase behavior in this ternary diagram is similar to type-II ternary phase behavior described in chapter 3. The LLV behavior occurs because we are in close proximity to the critical point of propane. The degree of separation appears to have improved at this temperature for asphalt-oil feed mixtures which are at least about 60% asphalt.

Wilson, Keith, and Haylett conclude that: (1) higher operating tempera-

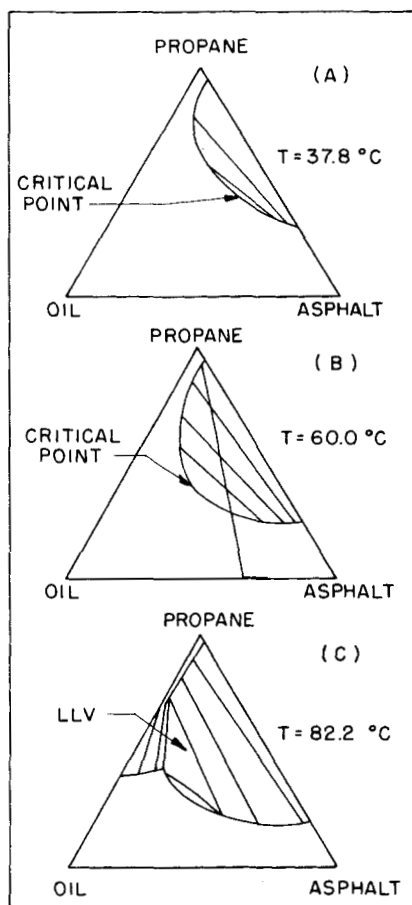


**Figure 7.3** Ternary phase behavior of the asphalt-oil-propane mixture at three different temperatures (Wilson, Keith, and Haylett, 1936).

tures reduce the solubility of the asphalt in the propane-rich phase; (2) increased amounts of propane also reduce the amount of asphalt in the propane-rich phase; (3) increasing pressure in the LL region of the  $P$ - $T$  diagram increases the solubility of asphalt in the propane-rich phase (see figure 7.2); and (4) compressed propane gas dissolves more oil than does liquid propane at slightly lower temperatures and pressures. Their work certainly promotes the use of near-critical and supercritical fluids. It is quite impressive that this fundamental work was done and the process commercialized some fifty years before the current awareness of the unique properties of SCFs.

## SOLEXOL PROCESS

The Sorexol process is similar to propane deasphalting. It was developed a few years later for the purification and separation of vegetable and fish oils

(Dickinson and Meyers, 1952). It too uses propane as a selective solvent and its purpose is to concentrate the polyunsaturated triglycerides (the so-called drying oils) in vegetable oils and to extract the vitamin-A values from fish oils. The Solexol process is described in two publications (Dickinson and Meyers, 1952; Passino, 1949). Compare some descriptive phrases from an early paper with contemporary SCF developments for the case of propane-lube oil refining.

In November, 1946, M. W. Kellogg Company, engineers and contractors of petroleum and chemical plants, announced to industry a solvent process for treating glyceride oils. Given the name "Solexol," it was a development of a process used extensively throughout the world to fractionate lubricating oils from crude petroleum residues. The solvent used in the process is ordinary propane, familiar as liquefied petroleum gas or "bottled gas."

The separations performed in Solexol pilot plants, some of which were described in an article by H. J. Passino, are in many instances, little short of amazing, not only of themselves but in the infinite variety of things which have been done with a single solvent and in a single tower. However, in the almost five years since the announcement there has been a scarcity of information on the extent to which sound commercial operations have borne out the promise for plant explorations.

At this writing there are five commercial Solexol plants in regular service, and a sixth is under construction. Furthermore two of the Solexol units are supplemented by a continuous fractional crystallization (or winterizing) process, not heretofore announced, which goes by the name of "Propane Destearnizing." As the name suggests, it also employs versatile propane as solvent. (Dickinson and Meyers, 1952.)

Dickinson and Meyers go on to describe triglyceride refining plants, some of which operate at throughputs as high as 200,000 lb/day. In the same vein of excitement as exhibited by the authors who wrote about propane deasphalting, the authors of the Solexol paper describe the properties of near-critical and supercritical propane and the ability to extend these properties to the development and, more importantly, to the commercialization of a propane refining process.

A schematic diagram of the Solexol processing of fish oils is shown in figure 7.4. The fish oils are fed to a train of countercurrent extractors where column-to-column variations in temperature as well as temperature variations within each specific column can affect the solvent power of propane in a manner similar to that seen with propane deasphalting.

Fish oil triglycerides are complex compounds consisting of various saturated and unsaturated fatty acids on a glycerol backbone. Staging the temperature within an extraction column and supplying a recycle stream allows the separation of the fish oil triglycerides by virtue of the variable dissolving power of near-critical propane and by virtue of the lower propane solubility of unsaturated triglycerides relative to the propane solubility of saturated



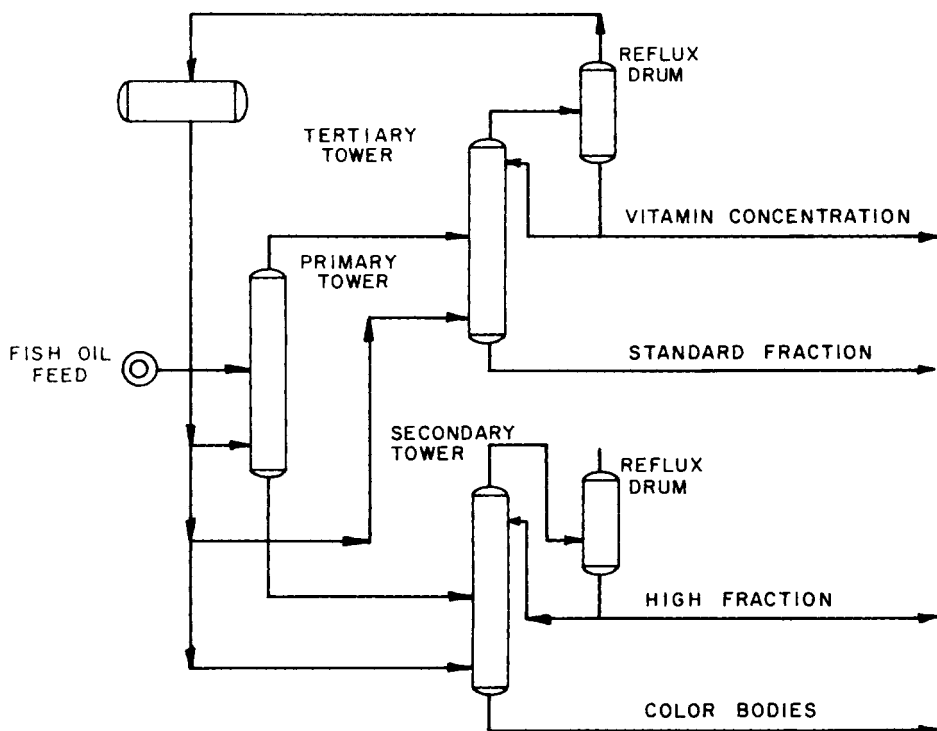


**Figure 7.4** A schematic diagram of the Soxhlet process for separating fish oils (Dickinson and Meyers, 1952).

triglycerides. At room temperature, propane dissolves all the triglycerides. Heating liquid propane decreases its solvent power, as seen for the propane deasphalting process. Within what is termed the paracritical region (the region where the dissolving power can be influenced strongly by pressure and temperature) it is possible to choose operating conditions such that progressive temperature changes near the critical temperature of propane can result in the successive precipitation of various fish oil fractions. With multiple extraction towers it is possible to separate color bodies, “insolubles,” oil fractions with low and high unsaturation levels, and a vitamin-A concentrate with a ten- to twentyfold increase in vitamin potency relative to the crude fish oil feed. It is possible to tailor operating conditions to concentrate the unsaturated triglycerides from seed and fish oils for use as drying oils in the paint and varnish industry.

The underlying thermodynamic principles for this process are identical to those exhibited for the propane deasphalting process. This process is yet another example of the use of the unique solvent characteristics of near-critical and supercritical fluids developed some forty years ago.

## ROSE PROCESS

Following a chronological order and progressing to developments in the 1970s, we come to Kerr McGee's Residuum Oil Supercritical Extraction (ROSE) process (Gearhart and Garwin, 1976). We will compare it with the previous two processes. The ROSE process is also not, strictly speaking, entirely a supercritical fluid extraction process. Its primary extraction step is carried at compressed liquid conditions, not at supercritical conditions. Nevertheless, the process does take clever advantage of the variable solvent power of a near-critical liquid at various stages of the extraction/separation process. It derives its supercriticality from its final stage. The thermodynamics and phase equilibrium principles used in the ROSE process are analogous to those of the propane deasphalting process, so we do not repeat them.

A schematic diagram of the ROSE process is shown in figure 7.5. Residuum is first mixed with compressed liquid butane or pentane and the undesired asphaltene fraction is precipitated. This step is similar in sequencing to propane deasphalting. Butane is used because it has a higher solvent power for the heavy hydrocarbons. This fact is explicitly stated by Wilson, Keith, and Haylett (1936). For the higher molecular weight resid, butane is an effective solvent in dissolving the desired high molecular weight components and precipitating the asphaltenes. It is too effective in the lube oil refining process because the molecular weights of all the components, desired and undesired, are much lower, so that the components cannot be differentiated finely enough by butane.

If an intermediate resin fraction is desired, another separator and stripper system would be installed right after the asphaltene separator in figure 7.5. To recover a resin fraction, the overhead solution from the asphaltene separator, which now consists of butane, resins, and light oils, is heated to near the critical temperature of butane. At this elevated, near-critical temperature the solvent power of compressed liquid butane decreases and the resins precipitate from solution. The overhead stream from this separator consists of light oils dissolved in near-critical liquid butane.

The butane-oil solution from the resin separator (or from the AR separator shown in figure 7.5) is heated to a temperature slightly above the critical temperature of pure butane. At this condition the solvent power of the now supercritical butane decreases and the light oils are precipitated from solution. This final separation step is best explained with reference to the naphthalene-carbon dioxide diagram in figure 6.1, reproduced here as figure 7.6. The light oil precipitation step of the ROSE process is designated schematically as the path  $D \rightarrow P$  in figure 7.6. The idealized path from D (a near-critical liquid) to P (a low-density supercritical fluid) results in a tenfold decrease in dissolving power of supercritical carbon dioxide. In an analogous decrease in the solvent power of supercritical butane, the separation of the desired oil from solution occurs with just a small input of heat in the last step of the ROSE process.



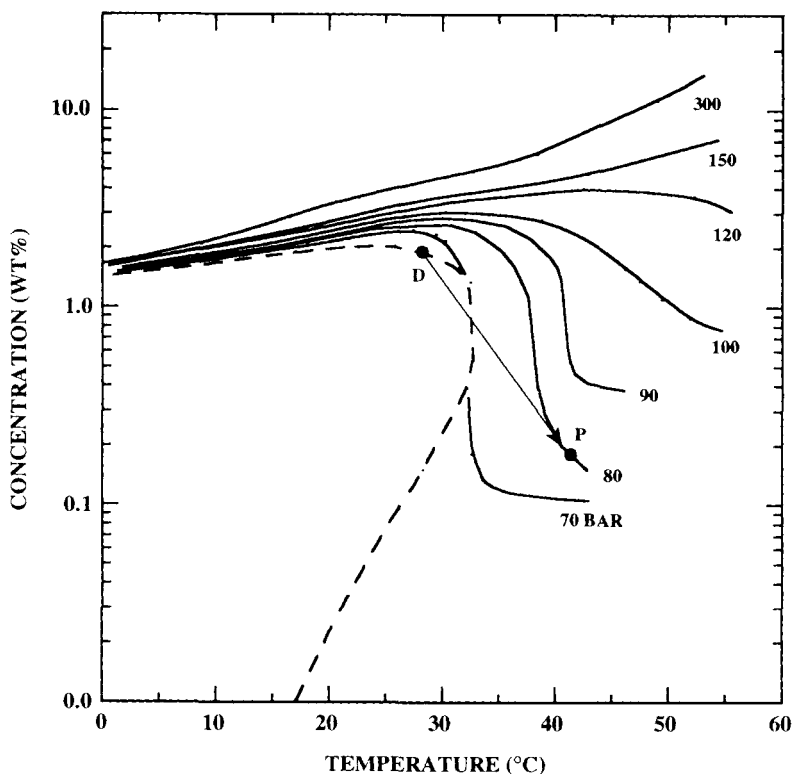


**Figure 7.6** Solubility behavior of naphthalene in supercritical  $\text{CO}_2$ . Line D to P is a path to separate dissolved oils in the ROSE process.

The ROSE process is an optimally engineered process that operates in the vicinity of the critical point of the solvent. The propane deasphalting process, the Solexol process, and the ROSE process all apply thermodynamic fundamentals and high-pressure phase equilibria principles to the design of energy-efficient processes. Binary and ternary equilibrium data along with the properties of near-critical and supercritical fluids first obtained in the laboratory were extended to the development of a separation process. In the case of propane deasphalting, this separation has yet to be superseded. Put lube oil feedstock into a vessel and mix it with a high-pressure gas; one often hears that today for “quick and dirty” supercritical fluid extraction tests. Had early workers done merely that, it is no exaggeration to suggest the separation processes described in this chapter would not have been developed. Suffice it to say that the work reported by the original investigators of these three separation processes indicates they are cognizant of the high-pressure phase

equilibrium principles in operation in their respective processes. Using sound engineering principles, they were able to develop unique separation processes.

Numerous other SCF applications are currently being pursued in industrial research and development laboratories in the United States. In chapters 8 through 10 we describe the state of the art in supercritical fluids research.

---

## Supercritical Fluid Process Development Studies

---

The factors that motivated the use of supercritical fluid solvents in developing separation processes were: the quite rapid increase in the cost of energy during the 1970s; the increased scrutiny of industrial solvents by the government; the public's increased awareness of pollution control; and the increased performance demands made on specialized materials.

The energy shortage in the early and late 1970s was largely responsible for the resurgent interest in supercritical fluid extraction in the United States and was the motivation for a great effort in research and development (R&D), initiated both in industry and in academia. A large number of researchers investigated SCF extraction for separating organics from water to see whether it could displace the more traditional method of distillation. In many instances it is theoretically possible that separation of organic mixtures by supercritical fluid processing will require less energy than is required by distillation or evaporation. For these two processes, compression energy for the recycled solvent and the heat of vaporization for the organics must be compared.

Reducing energy costs became a national obsession in the 1970s. For example, membrane separation processes, such as ultrafiltration and reverse osmosis, have proliferated because of energy considerations. Concentration or separation of a liquid stream requires less energy in membrane technologies because the compression energy necessary to overcome osmotic forces is much less than the evaporation energy needed to separate a liquid from its dissolved salts. Similarly, supercritical fluid extraction can be less energy-intensive than evaporation (chapter 6) but it must be evaluated on a case-by-case basis.

By the late 1970s evidence had accumulated on the potential hazards of certain extraction solvents, especially chlorinated hydrocarbons. Increased scrutiny of traditional industrial solvents is responsible for spawning another large body of R&D programs on SCF processes. Increased consumer awareness of potential chemical hazards coupled with the uncertainty of future governmental regulatory action motivated an examination of supercritical fluids as extraction solvents for foods, beverages, and spices.

During the 1970s the public became aware of the concept of zero discharge. The challenge of zero waste discharge, although not strictly legislated, has resulted in an examination of a variety of cleanup and destruction processes for treating liquid and solid waste materials. Also, increased attention has been given to improving traditional pollution control processes, such as incineration and adsorption. SCF technology found favor among those concerned with the waste problem, and several new SCF processes for accomplishing a variety of cleanup tasks were developed. These SCF processes are described in subsequent sections of this and the following chapters.

In the 1970s manufacturers found increased performance demands being placed on various materials, such as chemicals, polymers, and pharmaceuticals. They found that many of the conventional processing technologies could not satisfy the new requirements. SCF processing is being evaluated in an attempt to find the solution to these problems. It is being tested for the removal of residual solvents and monomers from high molecular weight polymers; for the purification of heat-labile intermediate chemicals and monomers, such as soft lens and dental monomers; for the fractionation of sensitive specialty polymers; and for many other purposes.

In this chapter we analyze a number of process development studies to demonstrate the engineering and scientific principles that must be addressed when evaluating potential applications of SCF technology. Many readers will recognize the tools that we use for these analyses; they are not new nor are they particularly novel. These tools have been used in the evaluation of many industrial unit operations in the past eighty years or so. Many of the less than illustrious applications of SCF technology could have been avoided, or at least should have been less hyped, had the applications been evaluated using well-worn chemical engineering principles before time and money were further invested in ill-fated applications.

## **ACTIVATED CARBON REGENERATION**

The forerunner of all the recent applications of SCF technology reported in the United States is the SCF regeneration of activated carbon first described at an American Chemical Society meeting in 1978 (Modell, de Filippi, and Krukoni, 1978). The phenomena in operation during adsorption of organics from wastewater and the desorption of organics from the activated carbon using supercritical carbon dioxide are similar to those active in other supercritical fluid extraction processes. Therefore, we examine the technical details here.

The potential advantages of SCF regeneration are reduced energy requirements and lower carbon loss compared with the thermal regeneration process currently in operation. It is suggested that, because many organic compounds can be dissolved by supercritical fluid solvents, the organic materials adsorbed onto activated carbon during the cleanup of a wastewater

stream can be desorbed by supercritical carbon dioxide at conditions less severe than the 1,000°C temperature level of an industrial regeneration furnace.

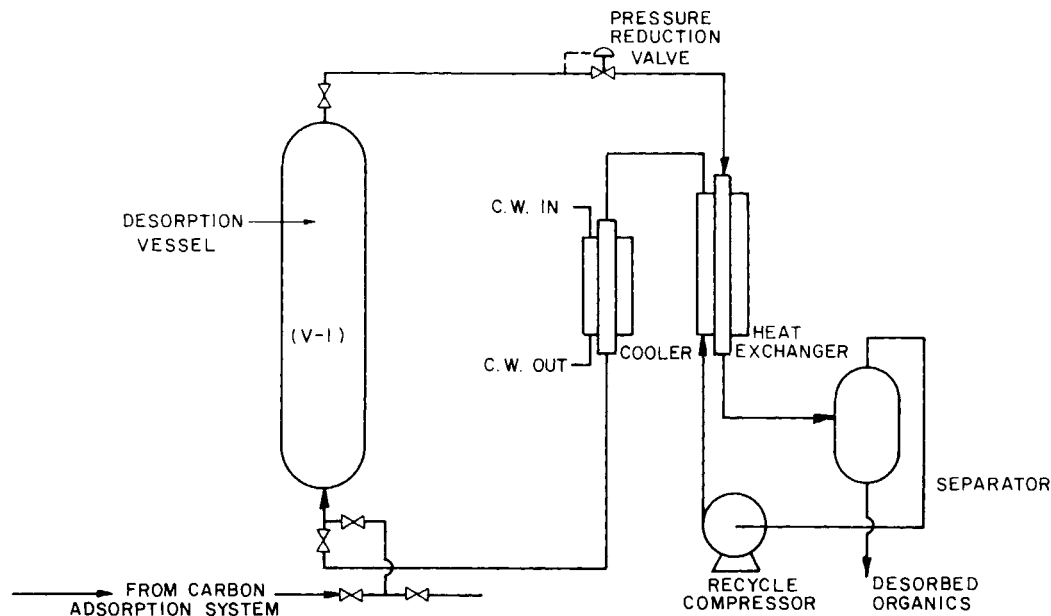
For small-scale processes, which use activated carbon at a rate of a few thousand pounds per day, the desorbers can also serve as fixed-bed adsorption vessels. Hence, in situ carbon regeneration can be carried out when the carbon bed is spent, that is, fully loaded with adsorbed organics. Processes that use much more activated carbon and systems that require many large adsorption vessels, such as those at municipal waste treatment facilities, the spent carbon can be removed from the adsorbers and transferred to the desorbers for regeneration. The transfer of the spent activated carbon from adsorbers to the thermal regeneration furnace is currently standard industrial practice. The spent carbon is transferred by water slurry pumps, sequenced valves, and motor-activated closures. In the following paragraphs we focus on processes that use large amounts of activated carbon.

Figure 8.1 is a schematic diagram of a system for regenerating activated carbon using supercritical CO<sub>2</sub>. Initially, the desorption vessel shown in figure 8.1 is filled with spent carbon. Since current activated carbon regeneration technology uses slurry pumping to transfer spent carbon to the thermal regeneration furnace, the slurry method is utilized in the schematic design of the SCF regeneration system. After the desorber vessel is filled with spent activated carbon, the water is allowed to drain from the vessel and the vessel is pressurized with CO<sub>2</sub> to the desired operating conditions. Flow of supercritical CO<sub>2</sub> through the vessel commences when the pressure reduction valve is actuated. The adsorbed organics are dissolved by the CO<sub>2</sub> flowing through the carbon bed. The organic-laden stream of CO<sub>2</sub> leaving the vessel is then expanded to a lower pressure in order to precipitate the organics and collect them in the separator vessel shown in the figure. The solute-free CO<sub>2</sub> leaving the separator is recompressed and recycled to the desorber vessel, and the process is continued until the activated carbon has been stripped of its adsorbed organics.

At the end of the regeneration step, the CO<sub>2</sub> flow is stopped, the vessel is opened to allow the CO<sub>2</sub> to depressurize, and the activated carbon is removed via slurry pumps. The vessel is then refilled with spent activated carbon, the water drained, and the desorption process repeated. Incidentally, the CO<sub>2</sub> left in the vessel at the end of the regeneration cycle is lost in this procedure. Although the cost of CO<sub>2</sub> is rather low, about 5–10 cents per pound depending upon the volume used, its consumption should be considered in evaluating the viability of a process, especially if the cost of the material being extracted is low. The CO<sub>2</sub> that is lost represents an economic penalty for this process, but part or all of it can be recovered with the installation of an additional CO<sub>2</sub> surge tank system.

The economic viability of any process, not just a supercritical fluid extraction process, requires that equipment utilization be efficient because off-line time is a capital investment penalty. In the present activated carbon





**Figure 8.1** Schematic diagram of an apparatus used for regenerating activated carbon with a supercritical fluid solvent.

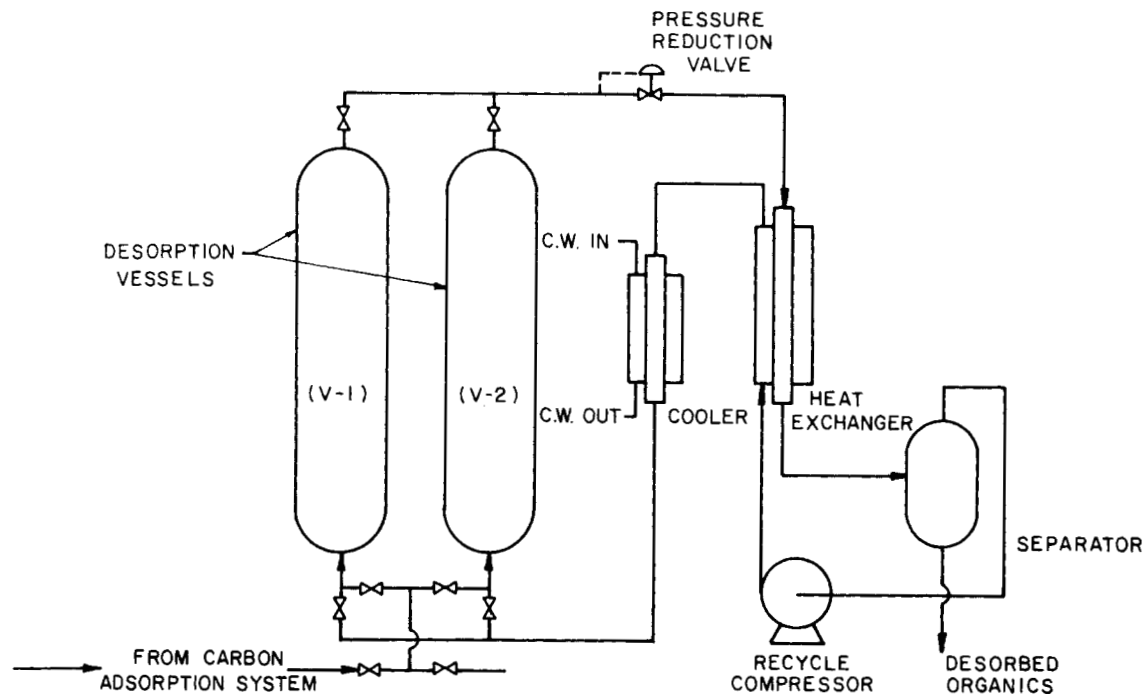
regeneration case, the batch-mode filling and emptying portions of the process require finite amounts of time that may be a significant fraction of the total processing sequence.

Let us now consider the operation of the regeneration process using a second desorber vessel, which can increase equipment utilization. The added vessel provides the capability of minimizing or eliminating the filling and emptying downtime. In the two-vessel operation shown schematically in figure 8.2, while the regeneration process is being carried out in the first vessel, the second vessel is filled with spent activated carbon and the water is drained from the vessel. At the end of the regeneration step (in vessel 1), the  $\text{CO}_2$  flow is stopped, the vessels are allowed to communicate so that one half the  $\text{CO}_2$  is transferred to the second vessel. The  $\text{CO}_2$  remaining in the first vessel is allowed to vent to the atmosphere and, in this two-vessel operation, part of the  $\text{CO}_2$  is saved. The regeneration is started when  $\text{CO}_2$  flow to the second vessel is commenced; the first vessel is emptied and filled while the regeneration of activated carbon in the second vessel is occurring. Thus, part of the  $\text{CO}_2$  is recovered and about one half the downtime is eliminated by the addition of the second vessel to the process layout.

Whether the previously described process is economically optimized depends, of course, on many factors. Whether to recover the  $\text{CO}_2$ , how much to recover, how much downtime can be endured, and similar considerations are a strong function of the amount of activated carbon to be processed, the operating conditions, the cost of the activated carbon, the cost of the equipment, and similar items. For the case of activated carbon regeneration, recovery of  $\text{CO}_2$  should probably be considered, and the additional capital expense of the second vessel may be justified.

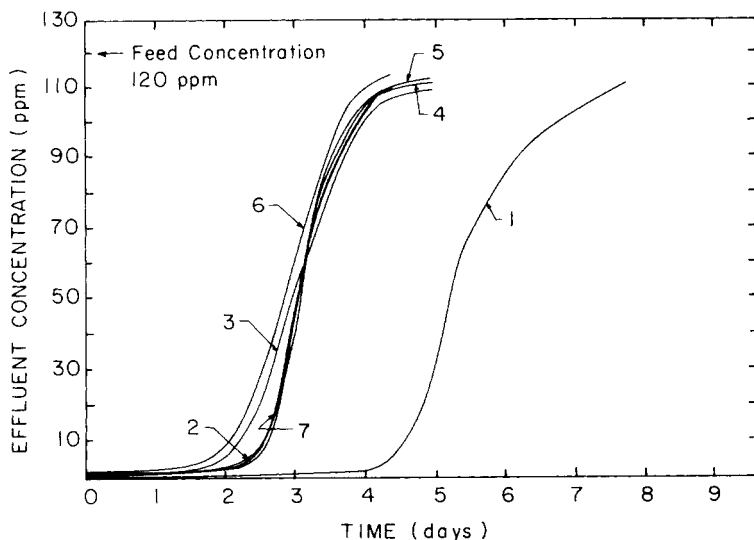
This activated carbon regeneration study (de Filippi et al., 1980) was directed to an evaluation of the regeneration of activated carbon used in the cleaning of wastewaters that emanate from pesticide manufacturing plants. A wide range of pesticides as well as various types of activated carbon were investigated. A large matrix of temperatures and pressures was first examined in order to determine the solubility characteristics of the pesticides before carrying out the more involved adsorption/desorption tests. Illustrative results of this study, described in detail in a report prepared by Arthur D. Little, Inc., for the United States Environmental Protection Agency (de Filippi et al., 1980), are given in the following paragraphs.

Figure 8.3 shows the molecular structure of six pesticides that were tested and their solubility levels in supercritical  $\text{CO}_2$  at one set of test conditions, 275 bar (4,000 psia) and  $100^\circ\text{C}$ . Also included in this figure is the solubility of phenol, which was studied because it is a raw material in the production of some of the pesticides and thus might be found in pesticide plant wastewaters. The solubility of these compounds varies over a one hundredfold concentration range, but the regenerability of activated carbon is not necessarily related solely to the solubility level. Specifically, a high solubility in supercritical  $\text{CO}_2$



**Figure 8.2** Schematic diagram of a variation of the apparatus shown in figure 8.1 used for regenerating activated carbon with a supercritical fluid solvent.





**Figure 8.4** Adsorption breakthrough curves of alachlor on activated carbon; numbers on the curves indicate the number of the cycle.

effluent water from the carbon adsorption column is analyzed on-line using UV-spectrophotometry. With this technique, a breakthrough curve is determined. When the pesticide in the column effluent stream reaches the feed concentration, the water flow is stopped, the water is drained from the column, and supercritical  $\text{CO}_2$ , typically at 275 bar (4,000 psia) and  $100^\circ\text{C}$ , is passed through the carbon bed.

Synthetic alachlor solutions were studied most thoroughly since alachlor exhibited the best regeneration behavior. A series of alachlor adsorption curves is shown in figure 8.4. The area above the adsorption curve is a measure of the capacity of the activated carbon for the pesticide. Curve 1 represents the adsorption breakthrough measured on fresh activated carbon, curve 2 is the adsorption breakthrough, measured after the activated carbon is regenerated with supercritical  $\text{CO}_2$ , and so on. The first cycle capacity of activated carbon for alachlor is greater than subsequent cycle capacities, but curves 2 through 7 essentially superpose, which indicates that a steady state adsorption capacity is achieved with supercritical  $\text{CO}_2$  regeneration. Incidentally, the reasons for the decrease in capacity after the first cycle are not discussed in detail here, but probably are the same as those reported by workers who have examined liquid organic solvent regeneration of spent carbon.

It is well known that the heat of adsorption of a compound varies with the loading of that compound on the activated carbon. At low loadings the heat of adsorption is very high (approaching chemisorption strength) while at higher loadings the heat of adsorption decreases in strength. The heat of adsorption is equated to the high sorption forces between the very active carbon sites and

the organic compound. The most active sites are used first and, as they become titrated, the adsorption forces decrease to levels that are typical of physical adsorption strengths. Thus, we might conclude that some sites of activated carbon are easier to regenerate than others. The ability to achieve a constant but lower adsorption capacity, shown in curves 2 through 7, probably is a manifestation of such relative forces representing the ability of supercritical  $\text{CO}_2$  to remove the less strongly held molecules. The first regeneration cycle probably removes only the molecules held by weaker physical adsorption. Thus, there is a drop in the capacity of the carbon bed and subsequent adsorptions and regenerations probably operate only on the available low-energy sites.

Alachlor is one pesticide that is easily removed from the activated carbon. Some of the other pesticides are not as readily removed by treatment with supercritical  $\text{CO}_2$ . The compounds diazinon, pentachlorophenol, and carbaryl exhibit extremely strong adsorption strengths, which render the activated carbon unregenerable. Hence, the adsorptive capacity of the carbon falls to almost zero after two or three cycles. Although the specific interactions between the activated carbon and the pesticide that lead to the decline in carbon capacity are not reported, the differences in the solubility level of the neat pesticides in  $\text{CO}_2$  are not the only explanation. Figure 8.3 shows that the solubility of diazinon is five times that of alachlor, yet diazinon-spent carbon cannot be regenerated. For example, figure 8.5 shows three adsorption curves with diazinon, and a comparison of the area above the curves shows that the capacity of the activated carbon has fallen to 10% after two adsorption-desorption cycles. Although the primary function of this study was to screen a number of pesticides and not to investigate sorption phenomena, it is probably accurate to assign the inability of supercritical  $\text{CO}_2$  to remove these compounds from activated carbon to strong sorption forces or possibly to surface chemical reactions.

Some desorption tests will next be described in some detail because they have relevance to other solid and liquid SCF extraction studies currently in progress at other industrial and academic laboratories. The results of the desorption tests explain some of the phenomena that are reported in other process studies, and the results also point out some limitations of those processes. Figure 8.6 shows a typical desorption profile; in this case the alachlor concentration in the  $\text{CO}_2$  leaving the activated carbon column is illustrated. The concentration scale represents the average concentration of alachlor in the  $\text{CO}_2$  and the length of the line segment marks the volume of  $\text{CO}_2$  passed through the bed in a given interval over which the concentration is measured gravimetrically. Recall that neat alachlor solubility at these conditions is 10 wt%, shown in figure 8.3, but the concentrations in figure 8.6 are much lower. Mass transfer limitations, either from the surface of the activated carbon or through the pellet pores, are one explanation for the decrease in alachlor concentration measured during desorption. A test of this hypothesis is to carry out the carbon regeneration at different volumetric flow rates, linear

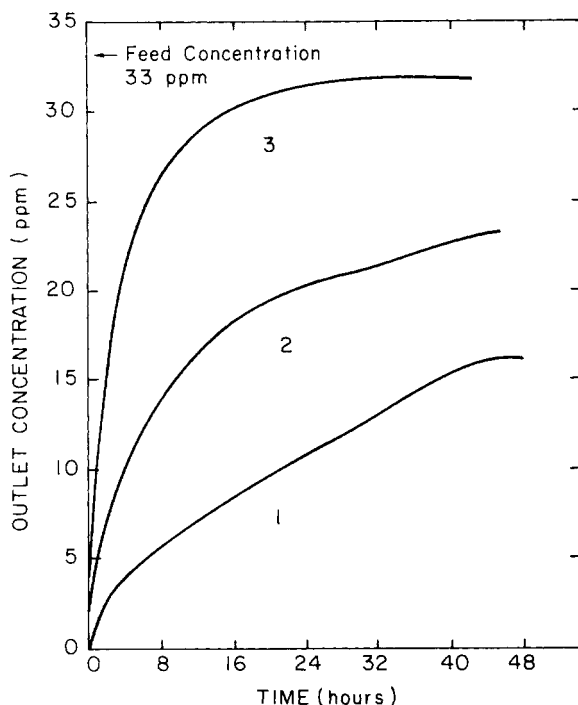


**Figure 8.5** Adsorption breakthrough curves of diazinon on activated carbon; numbers on the curves indicate the number of the cycle.

velocities, carbon particle sizes, and so on. The results of such studies are shown in figure 8.7. The regeneration curves from these tests superpose indicating that SCF regeneration is essentially independent of the parameters tested. The conclusion from these tests is that simple mass transfer limitations are not the controlling factors in the SCF regeneration process.

Another explanation for the shape of the regeneration curves is found in the existence of an adsorption equilibrium in the supercritical  $\text{CO}_2$ -alachlor-activated carbon system, similar to the adsorption equilibria measured for water-organic-activated carbon systems. It is found that the analogue of the adsorption isotherm in water systems represents the controlling mechanism for the desorption process. Adsorption equilibria for the more common water-organic-activated carbon systems are usually given as Langmuir and/or Freundlich isotherms, which correlate the loading of the organic on the activated carbon with the concentration of the organic in the water phase. The shape and slope of these isotherms are found to be related to the adsorptive strength of the organic on the carbon. When the isotherms are fitted to a Langmuir or Freundlich model, the parameters of the model can be determined. These same models should be applicable for the case of  $\text{CO}_2$ , and from the values of the fitted parameters, the data given in figure 8.7 can be explained.

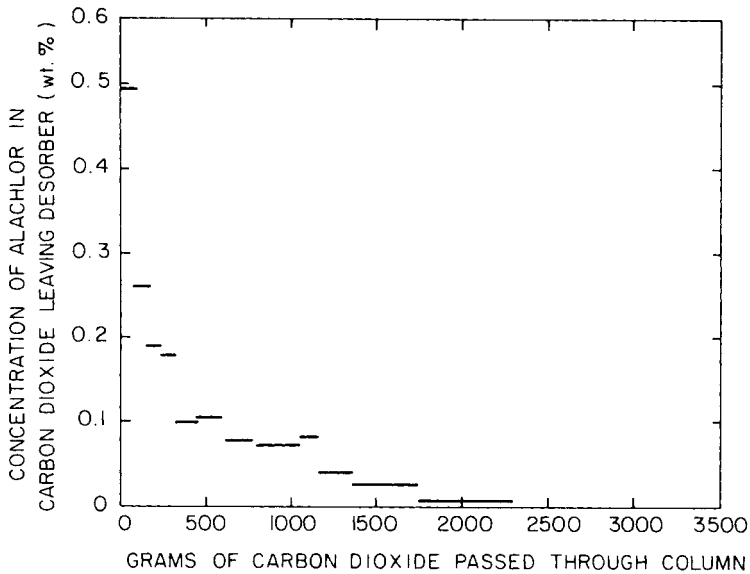


**Figure 8.6** Desorption profile of alachlor on activated carbon using supercritical carbon dioxide.

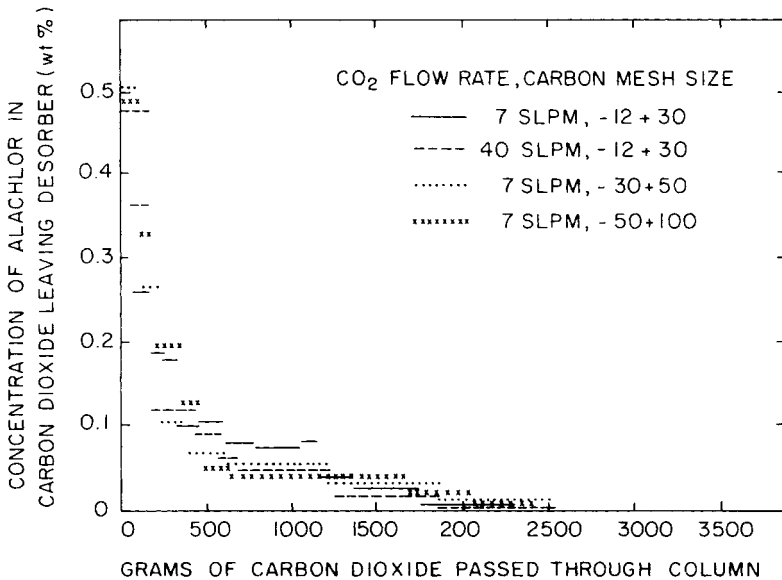


**Figure 8.7** Comparison of effects of mass transfer limitations in the desorption of alachlor from activated carbon using supercritical carbon dioxide; tests with several flow rates and carbon mesh size. SLPM = Standard liters per minute.



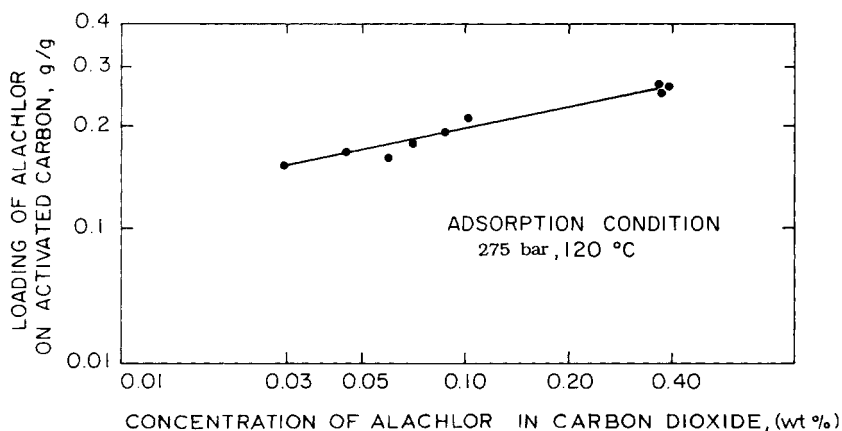


**Figure 8.8** Data for the supercritical carbon dioxide–alachlor–activated carbon system fitted to a Freundlich isotherm.

An equilibrium between the pesticide in the supercritical CO<sub>2</sub> phase and the pesticide in the solid phase has been measured. Data for the supercritical CO<sub>2</sub>–alachlor–activated carbon system are correlated as a Freundlich isotherm, shown in figure 8.8 (Krukoniš, 1977). It is surprising that even at very low concentrations of alachlor, two orders of magnitude below the solubility level shown in figure 8.3, the equilibrium loading on activated carbon is as high as 0.2 g/g. The magnitude of the loading lends credence to the assumption that adsorption–equilibrium limitations are responsible for the shape of the desorption curve and that the solubility in supercritical CO<sub>2</sub> does not represent the limiting step of the regeneration process.

The model and mathematics for the case of adsorbent regeneration, governed by equilibrium effects, is covered in many texts. The discussion by Sherwood, Pigford, and Wilke (1975) is especially thorough. The material balance between the concentration of dissolved material in the CO<sub>2</sub> and the concentration in the solid activated carbon during the course of the desorption is given by the relation

$$\varepsilon \left( \frac{\partial c}{\partial t} \right) + p \left( \frac{\partial q}{\partial t} \right) + \varepsilon v \left( \frac{\partial c}{\partial x} \right) = 0, \quad (8.1)$$

where  $\varepsilon$  is the bed void volume,  $c$  is the concentration of species in the carbon dioxide,  $p$  is the bulk density of activated carbon (approximately 0.8),  $q$  is the concentration of species in the activated carbon, and  $v$  is the linear velocity of carbon dioxide through the bed. If the relation between  $c$  and  $q$  is known either analytically, for example as a Langmuir isotherm  $q = f(c)$ , or graphically as in figure 8.8, equation 8.1 can be solved to give concentration profiles in

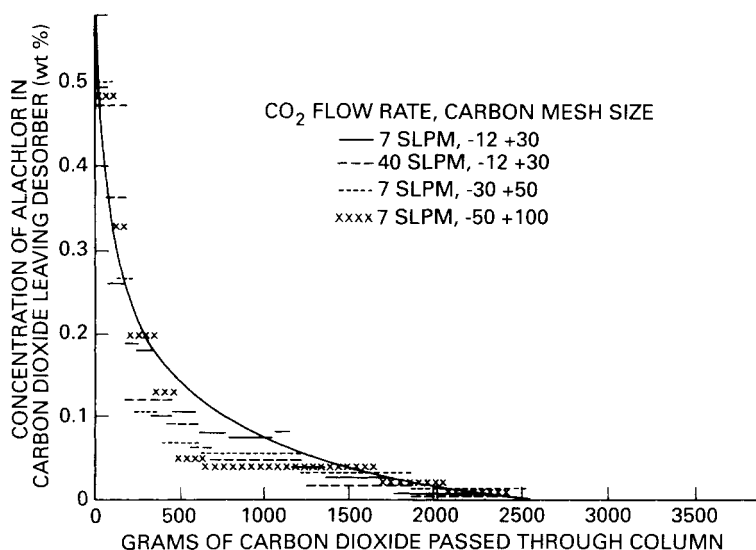


**Figure 8.9** Comparison of calculated and experimental desorption data.

the  $\text{CO}_2$  and in the bed as a function of time. This relation is referred to as the local equilibrium theory model.

With the data in figure 8.8 and the assumption of local equilibrium, we can calculate as a function of time the concentration profile of alachlor in the effluent  $\text{CO}_2$  and the concentration profile of alachlor in the bed of activated carbon. Figure 8.9 shows the calculated profile superposed on the measured regeneration curves given in figure 8.7. The agreement of the measured and calculated profiles is quite good in both shape and magnitude; this strongly suggests that the local equilibrium theory correctly explains the measured desorption profile (Modell et al., 1979).

The existence of the adsorption equilibrium in the  $\text{CO}_2$ -alachlor-activated carbon system is a fundamental limitation of the supercritical carbon dioxide regeneration process. For example, one of the ramifications of local equilibrium is the requirement that one or two orders of magnitude more  $\text{CO}_2$  be passed through the bed to regenerate the activated carbon than is predicted from neat alachlor- $\text{CO}_2$  solubility data. The findings of this study transcend the topic of activated carbon regeneration and have implications in other seemingly unrelated SCF extractions. In particular, SCF coffee decaffeination is an example of another system that exhibits an equilibrium isotherm remarkably similar in appearance to the alachlor-SCF isotherm shown in figure 8.8. Therefore, understanding the SCF-activated carbon regeneration process provides a basis for interpreting other SCF processes. We discuss the decaffeination of coffee in chapter 10.

## SEPARATION OF ORGANIC–WATER SOLUTIONS

### Ethanol–Water

The energy shortages of the 1970s were an impetus for evaluating the use of supercritical fluids for separating organics from water. A process that received substantial governmental and industrial funding is the supercritical CO<sub>2</sub> separation of ethanol from water (Paulaitis, Gilbert, and Nash, 1981; Moses, Goklen, and de Filippi, 1982; Jonas, 1981; Kuk and Montagna, 1983). A primary goal of the work is to break the ethanol–water azeotrope of 95.5 wt% ethanol. But if the azeotrope cannot be broken, a parallel goal is the demonstration of a less energy-intensive process using supercritical fluid extraction in tandem with normal azeotropic distillation. The goal was that it might be possible to combine supercritical fluid extraction and distillation to reduce processing costs in much the same manner that combines reverse osmosis and evaporation, for example.

Conceptually, the ethanol–water separation process using supercritical CO<sub>2</sub> is a chemical engineer's dream. It is not necessary to feed solids through slurry pumps and sequenced solenoid valves; countercurrent operation is now the normal mode of operation. A simplified schematic diagram of the continuous and countercurrent process of ethanol–water separation is shown in figure 8.10. The ethanol–water feed stream and the supercritical CO<sub>2</sub> recycle stream can be pumped continuously to a column, the produce stream can be drawn off from a separator, and the raffinate (depleted in ethanol) can be discharged from the column through a valve shown in the figure. The internals of the extractor may be sieve trays or various packing arrangements. The feed flows down the column from plate to plate through downcomers against the upward flow of CO<sub>2</sub>. There is an upper limit on the operating pressure if the process is to be operated as described since at high pressures the density of the CO<sub>2</sub>-rich phase can approach or exceed that of the water-rich phase. This results in no phase separation and an inability to operate the column, although if CO<sub>2</sub> were the heavy phase, it could be introduced at the top of the column.

During the plate-to-plate contact of the supercritical CO<sub>2</sub>-rich phase with the ethanol–water solution, the ethanol is preferentially extracted. The extract consists of mostly CO<sub>2</sub>, some ethanol, and a little water; it leaves at the top of the column. Figure 8.10 shows the CO<sub>2</sub>-rich solution is expanded across a pressure reduction valve; this reduces the solvent power of the CO<sub>2</sub> and causes the ethanol to precipitate in the separator. The CO<sub>2</sub> is then recompressed and recycled to the extractor.

Let us consider the equations that describe the equilibrium extraction of a material from one phase to another. In practice, equilibrium concentrations in two-phase systems are described in terms of a distribution coefficient (sometimes called a partition coefficient), which relates the equilibrium concentrations of a species in each of the two phases. Physical chemistry texts usually

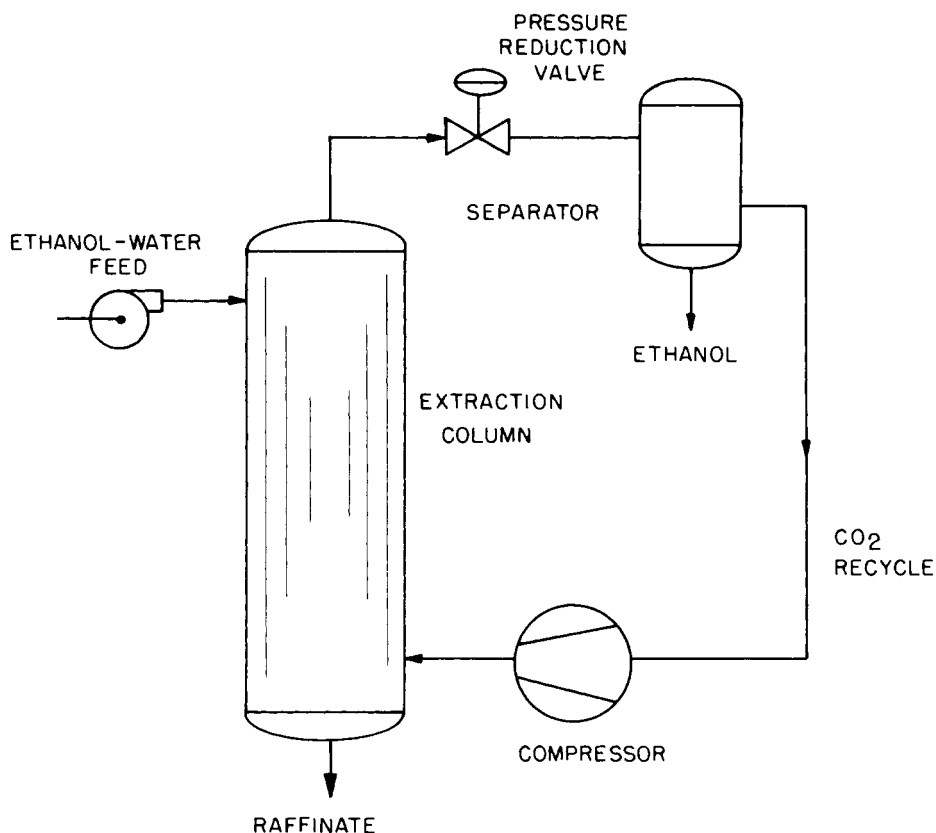


**Figure 8.10** Schematic diagram of a supercritical fluid solvent process for extracting ethanol from water.

define the distribution coefficient for a ternary system in terms of a ratio of ratios; for example, the ethanol distribution coefficient in the CO<sub>2</sub>-ethanol-water system is given as

$$DC = \frac{\left( \frac{y_e}{1 - y_e} \right)}{\left( \frac{x_e}{1 - x_e} \right)}, \quad (8.2)$$

where DC is the distribution coefficient,  $y_e$  is the concentration of ethanol dissolved in the carbon dioxide phase, and  $x_e$  is the concentration of ethanol in the water phase at equilibrium. Although  $x_e$  and  $y_e$  may be given in any consistent units, such as mole fraction, weight percent, or g/l, the units must be

specified so that distribution coefficients can be compared on a dimensionally consistent basis. All DC values in this chapter are given in weight units. For concentrations of ethanol less than ~10 wt% in either phase, the distribution coefficient relation simplifies to

$$DC = \frac{y_e}{x_e} \quad (8.3)$$

This simplified equation is more generally employed by the groups discussing ethanol–water separation studies and we use it in the subsequent discussion.

A number of research and development groups have published data on the CO<sub>2</sub>–ethanol–water system over a range of ethanol concentrations, temperatures, and pressures (Paulaitis, Gilbert, and Nash, 1981; Moses, Goklen, and de Filippi, 1982; Kuk and Montagna, 1983). The data, plotted in figure 8.11, show that the conditions of extraction, i.e., whether the CO<sub>2</sub> is a near-critical liquid or a high-pressure supercritical fluid, do not materially influence the extractability, i.e., the distribution coefficient is not affected to a significant degree. A straight line fits the entire collection of data in figure 8.11 to within about  $\pm 30\%$ . The distribution coefficient is the slope of the line; it is about 0.09 (weight basis). The selectivity of CO<sub>2</sub> for ethanol from an ethanol–water mixture is quite high. At an ethanol-in-water concentration of 10 wt%, the concentration of ethanol in the CO<sub>2</sub>-rich phase is 0.9 wt%. Other measurements show the accompanying water concentration is about 0.1 wt% at 25°C. From these values the selectivity is calculated as 81.

For the case of a constant distribution coefficient, Treybal (1968) shows that the theoretical minimum solvent-to-feed ratio necessary to extract all of a component from a feed stream is equal to the inverse of the distribution coefficient. Recall, however, that the theoretical minimum value of the solvent-to-feed ratio requires an infinitely tall column. In actual practice a greater solvent-to-feed ratio, typically 1.3 to 1.5 times minimum, is employed. We present some elementary but informative graphical design procedures to illustrate the relationship between the distribution coefficient and the operation of the supercritical fluid extraction process for separating ethanol–water.

Let us assume that the concentration of the feed ethanol is 10 wt%, a level readily produced by fermentation processes. For simplicity, let us assume furthermore that the recycled CO<sub>2</sub> contains no ethanol and that the desired recovery of alcohol is 95% of the amount in the feed. Figure 8.12 reproduces the equilibrium line shown previously in figure 8.11. In this case, the minimum solvent-to-feed (S/F) ratio is shown in figure 8.12 by the so-called operating line, the dashed line drawn between the abscissa at 0.5 wt% ethanol in water (we specified that the recovery of ethanol from the feed is 95%) and the equilibrium line at 10 wt% ethanol (the feed concentration). The minimum S/F ratio is 10.5 for this case. This S/F ratio is the equivalent of 105 lb CO<sub>2</sub>/lb ethanol in the feed stream; this is a rather high solvent requirement. Since the operating line touches the equilibrium line, an infinitely tall column is required.

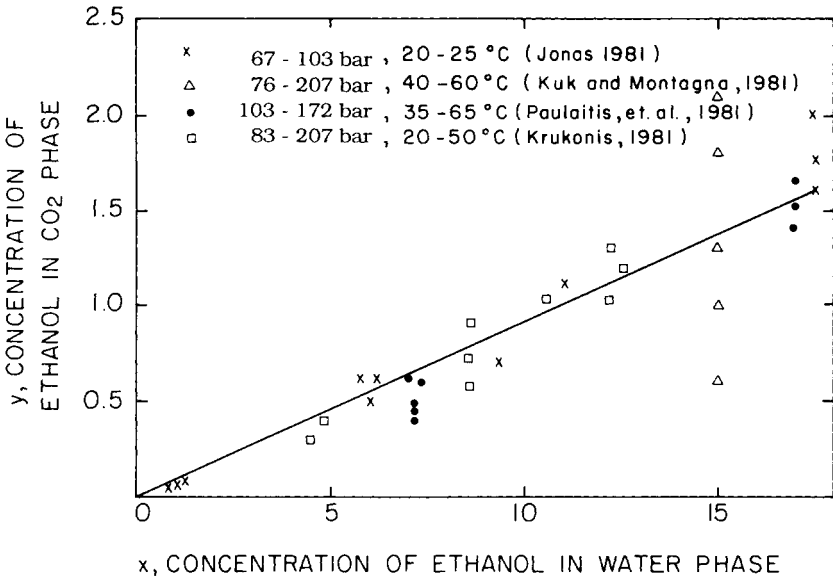


**Figure 8.11** Experimental results for several studies of the ethanol-water-carbon dioxide system.

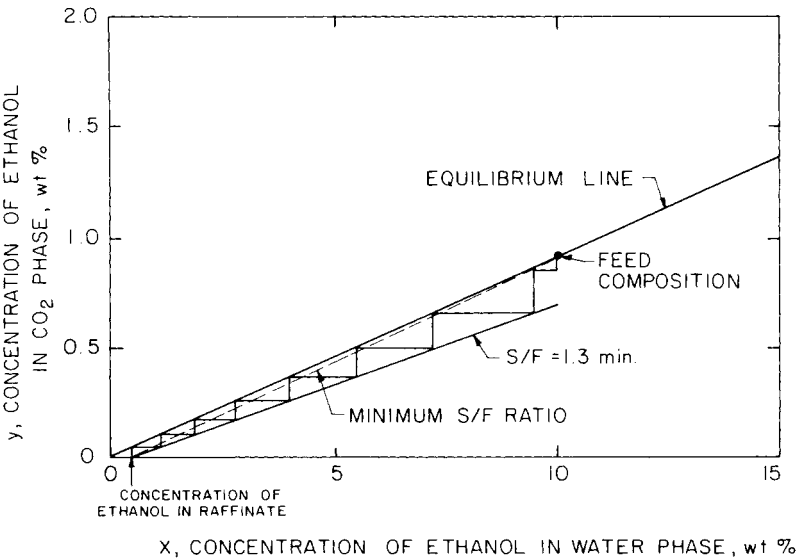


**Figure 8.12** Equilibrium and operating lines for the ethanol-water-carbon dioxide system; in this instance there is no ethanol in the recycled carbon dioxide.

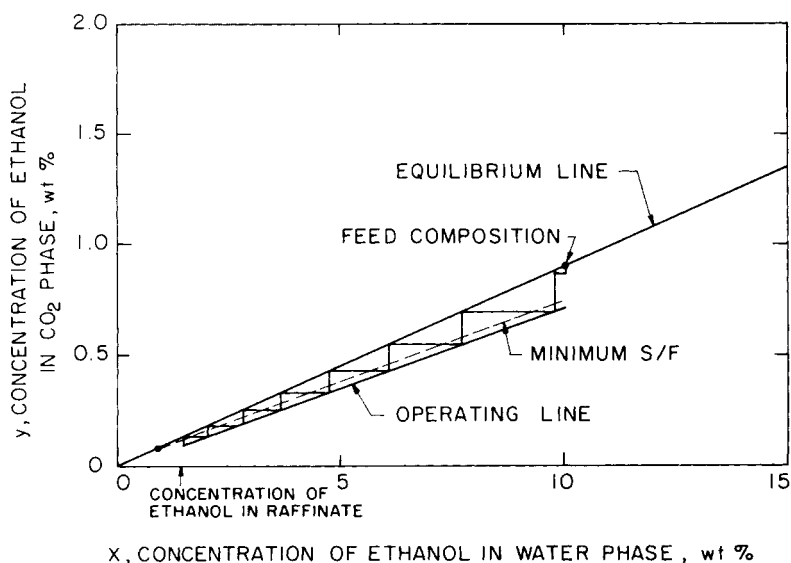


**Figure 8.13** Equilibrium and operating lines for the ethanol–water–carbon dioxide system; in this instance there is 0.1 wt% ethanol in the recycled carbon dioxide.

We shall use an operating line with a solvent-to-feed ratio 1.3 times the minimum (see figure 8.12).

A mathematical solution of the number of extraction stages required to recover 95% of the ethanol via supercritical  $\text{CO}_2$  is obtained by a graphical procedure called stepping off plates. Slightly more than seven (7.3) equilibrium trays are needed for this separation using the graphical construction shown in figure 8.12. In the placement of the operating line and determination of the number of equilibrium stages in figure 8.12, we assume that the entering (recycled)  $\text{CO}_2$  contains no ethanol; in reality the entering  $\text{CO}_2$  will contain some ethanol. Sometimes the presence of a small amount of recycled product has a great impact on the operation, cost, and efficiency of the process. If the distribution coefficient is very low, such as for the ethanol–water separation, the presence of recycled product increases the difficulty of obtaining a high recovery of ethanol.

For the ethanol–water separation, the requirement of thorough removal of ethanol from the recycled  $\text{CO}_2$  represents a technical challenge that increases the complexity and cost of the process relative to the simplified diagram shown in figure 8.10. The reasons for the increased complexity are explained below. Figure 8.13 illustrates the ethanol extraction process in the instance where the recycled  $\text{CO}_2$  has an ethanol concentration of 0.1 wt%. At the raffinate section of the extractor the ethanol concentration in the water-rich phase is now dictated by considerations of equilibrium and by the value of the distribution coefficient. The limitation attributed to equilibrium is indicated by the

operating line in figure 8.13, which has an inverse slope of 13.7 (the same slope as the operating line in figure 8.12) and intersects the equilibrium line at coordinates  $x = 1.1$ ,  $y = 0.1$ . The simple construction in figure 8.13 shows that the presence of a small amount of ethanol in the recycled  $\text{CO}_2$  stream places an upper limit on the amount of ethanol that can be recovered from the feed stream. The ethanol concentration in the raffinate cannot be lowered to below 1.1 wt%; for 0.1 wt% ethanol in the recycle stream, the maximum recovery of ethanol from the feed stream, even with an infinitely tall column, is only 89%.

There are trade-offs to be considered in optimizing recovery costs. When designing a process, the design engineer must make some concessions on the percent recovery of ethanol versus the capital and operating costs of the proposed process. One real operating line is drawn on figure 8.13 (for this example the minimum operating line is shifted so that the number of equilibrium trays is again 7.3). The raffinate stream in this case leaves the column with 1.4 wt% ethanol, achieving a total ethanol recovery of 86%. An economically optimum design depends on many factors, such as the cost of making ethanol by fermentation; the local pollution control legislation, which may place limits on ethanol discharge; and the cost of competing separation technologies. We use the process described in figure 8.13 to explain the extraction column operation that needs to be investigated when considering whether SCF technology offers a viable option to other technologies.

We have not yet described recycle cleanup and product recovery but we have assumed that the concentration of ethanol in the recycle is 0.1 wt%. How did we get it there? Some researchers who present data for ternary phase equilibria for the  $\text{CO}_2$ –ethanol–water system suggest that decreasing the operating pressure, raising the temperature, or both, can result in the precipitation of ethanol from the supercritical  $\text{CO}_2$  phase and that with recompression the  $\text{CO}_2$  can then be recycled. These statements are incorrect because they are based on an extrapolation of data from the two-phase liquid–vapor region of the ternary phase diagram without regard to the type of phase behavior that exists for a pseudobinary mixture consisting of  $\text{CO}_2$  and ethanol (with a small amount of water).

From figure 8.11, at an ethanol concentration of 15 wt%, the solubility of ethanol in  $\text{CO}_2$  at 75.8 bar (1,100 psia) and 40°C is approximately 0.5 wt% (the lowest triangle). At 207 bar (3,000 psia) the solubility is 2.1 wt% (the highest triangle). It has been proposed that a recycle process can operate between these two pressure levels; extraction of ethanol from water at 207 bar (3,000 psia) and recovery of ethanol from the  $\text{CO}_2$ -rich phase at 75.8 bar (1,100 psia). But all the ethanol cannot be recovered from the  $\text{CO}_2$ -rich stream and in fact a large percentage will remain in solution, since we are operating very close to the (pseudo) binary mixture critical point of the  $\text{CO}_2$ –ethanol system. The dew point curve for the  $\text{CO}_2$ –ethanol binary system at 40°C is approximately vertical over a wide pressure range, so reducing the system pressure by a large amount will only knock a very small amount of ethanol out of solution. Thus, the process depicted in figure 8.10 cannot work unless the



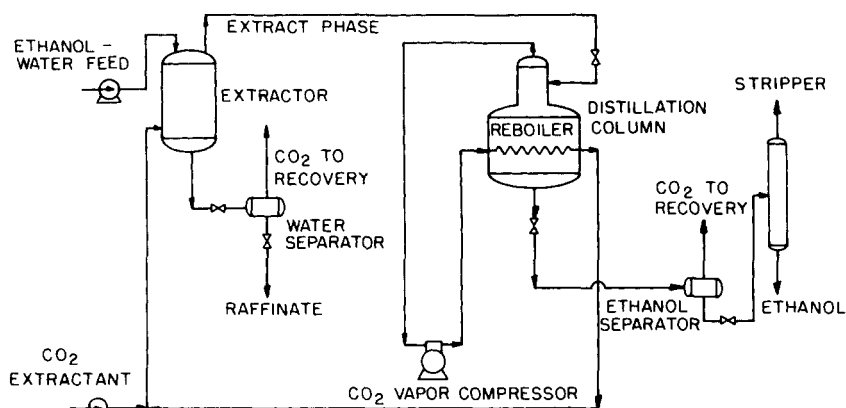


**Figure 8.14** Schematic diagram of a process using supercritical carbon dioxide for extracting ethanol from water combined with distillation for carbon dioxide cleanup.

pressure is reduced to much lower levels, which may not be economically viable.

How, then, is the ethanol to be separated from the CO<sub>2</sub> if pressure reduction cannot accomplish the task? There is a more general question. How can a recycle stream be cleaned up for the case of extraction from very low-concentration streams or from systems with a low distribution coefficient? In principle, reduction to a very low pressure would work, but such a scheme would probably be prohibitively expensive because of gas compression costs. An alternative scheme for recovering the extracted ethanol and cleaning up the recycle stream is described in U.S. Patent 4,349,415 (de Filippi and Vivian, 1982). In this method, a high-pressure distillation column is utilized to distill the CO<sub>2</sub> from the condensed CO<sub>2</sub>-ethanol mixture. A schematic diagram of the full extraction and CO<sub>2</sub> cleanup process is shown in figure 8.14. Ethanol is extracted at about 20°C, and 55.2 bar (800 psia) with liquid CO<sub>2</sub>, and the CO<sub>2</sub>-ethanol extract stream leaving the top of the extractor is expanded slightly to about 48.3 (700 psia) to form a liquid phase and a vapor phase. The two-phase stream is fed to a short distillation tower in which CO<sub>2</sub> vapor essentially free of ethanol is separated from the CO<sub>2</sub>-ethanol phase. The CO<sub>2</sub> vapor leaving the tower overhead is compressed to about 62.1 bar (900 psia). The CO<sub>2</sub> stream becomes heated slightly because of the compression work that has been added by the vapor recompressor. It is discharged from the compressor to the tube side of the heat exchanger of the distillation reboiler. Transfer of sensible and latent heat occurs from the condensing CO<sub>2</sub> inside the reboiler tubes to the boiling ethanol-CO<sub>2</sub> solution. The cooled liquid CO<sub>2</sub> is

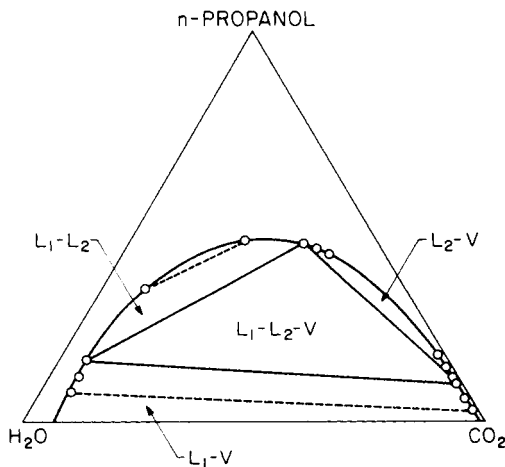
then pumped to the bottom of the extractor to complete the cycle and to continue the extraction process.

The low distribution coefficients, the attendant requirement of recycling  $\text{CO}_2$  containing very little ethanol in order to achieve a high recovery of ethanol from the feed stream, and the inability to achieve the separation of ethanol from the extract stream by pressure letdown required the development of this SCF extraction–distillation process. The diagram shown in figure 8.14 pictorially summarizes that an old distillation technique can be combined with new supercritical  $\text{CO}_2$  extraction to solve the separation problem; supercritical  $\text{CO}_2$  can extract the ethanol from the feed stream, distillation can separate and regenerate the solvent for recycle, and vapor compression can achieve energy efficiency.

## Other Alcohol–Water Systems

The phase-splitting techniques first described by Elgin and Weinstock (1959) for recovering methyl ethyl ketone from water using supercritical ethylene can also be used to separate alcohol–water mixtures. Let us consider recovering *n*-propanol from water using supercritical  $\text{CO}_2$  (Kuk and Montagna, 1983). Supercritical  $\text{CO}_2$  can be used in two different ways to split *n*-propanol–water mixtures in the range approximately 20 wt% to 75 wt% *n*-propanol. The recovery of *n*-propanol from water can be accomplished operating either in the two-phase liquid–liquid (LL) region or in the three-phase liquid–liquid–vapor (LLV) region of the ternary *n*-propanol–water– $\text{CO}_2$  phase diagram shown in figure 8.15. If it is assumed that the process operates in the LLV region of the diagram, then there are no degrees of freedom for this system (see table 3.1), because the temperature is fixed at  $40^\circ\text{C}$  and the pressure is fixed at 104 bar

**Figure 8.15** Ternary phase diagram for the *n*-propanol–water–carbon dioxide system at  $40^\circ\text{C}$  and 104 bar (1,514 psia) (Kuk and Montagna, 1983).



(1,500 psia). Therefore, the composition of the three equilibrium phases is defined by the corners of the triangular LLV region within the ternary phase diagram. Although the relative amounts of the three equilibrium phases will depend on the overall mixture composition within this region, the compositions of the three phases always remain fixed at approximately 18 wt% *n*-propanol–72 wt% water–10 wt% CO<sub>2</sub>, 45 wt% *n*-propanol–20 wt% water–35 wt% CO<sub>2</sub>, and 12 wt% *n*-propanol–1 wt% water–87 wt% CO<sub>2</sub>. Thus, in a single-stage extractor, the *n*-propanol can be recovered by removing either the CO<sub>2</sub>-rich phase, which has a ratio of *n*-propanol to water of 12 to 1, or by removing the middle *n*-propanol-rich phase, which has a ratio of *n*-propanol to water of 2.25 to 1. The costs of the particular process will dictate whether it is more economical to recover *n*-propanol from the middle liquid phase, which has a high loading of *n*-propanol but a low selectivity of *n*-propanol to water, or the CO<sub>2</sub>-rich phase, which has less alcohol but a much higher alcohol-to-water ratio.

The *n*-propanol–water–CO<sub>2</sub> system is another example of a system that exhibits LLV equilibria at conditions near the critical temperature and pressure of CO<sub>2</sub>. This type of phase behavior is described in detail in chapter 3. Many other organic solvent–water–SCF systems can be found in the work of Elgin and coworkers.

The extraction of alcohol from water using supercritical fluids has also been described in some detail by Paulaitis and coworkers (Kander and Paulaitis, 1984; Diandreth and Paulaitis, 1984; Paulaitis, Kander, and Diandreth, 1984; Paulaitis, Gilbert, and Nash, 1981). These researchers show that when a separation process operates in the vicinity of the mixture critical point (i.e., the plait point for a ternary system), large changes in alcohol selectivity and loading in the supercritical fluid phase can occur for relatively small changes in temperature or pressure. Such changes are apparent in the two sets of isopropanol–water–CO<sub>2</sub> diagrams shown in figures 8.16 and 8.17. It has been suggested in the works cited that the two factors controlling the selectivity and loading for alcohol–water mixtures are the compressibility of the SCF solvent and the differences in the liquid phase nonidealities exhibited by the binary alcohol–SCF and alcohol–water mixtures (e.g., the degree of hydrogen bonding present in these mixtures). These two factors, SCF compressibility and mixture nonidealities, determine whether the alcohol–water–SCF mixture will split into an LLV mixture. Full advantage should be taken in alcohol–water–SCF separation processes of the multiphase behavior that occurs for these systems and that greatly affects the selectivity and loading of the SCF solvent.

## Acetic Acid–Water

The potential for achieving a lower-energy process also motivated a substantial effort to examine supercritical fluid extraction for separating acetic acid from water. The work falls into two subcategories: separation of fermentation-

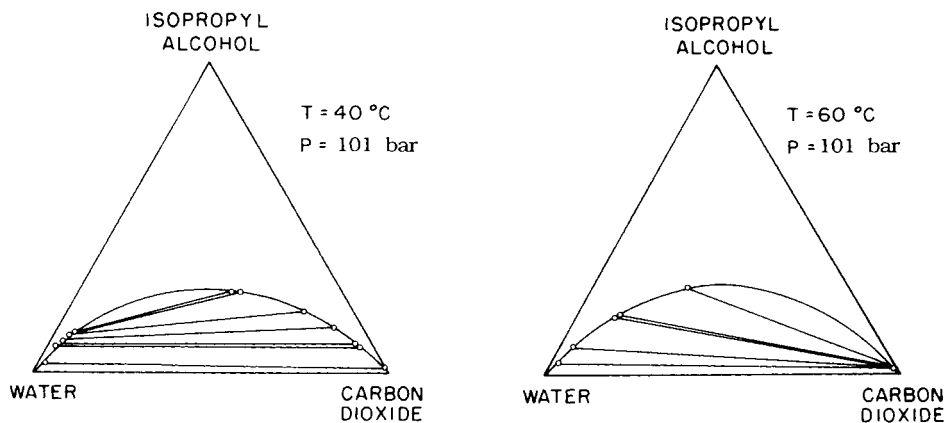


**Figure 8.16** Effect of temperature on the selectivity and loading of isopropanol in supercritical carbon dioxide (Paulaitis, Kander, and Diandreth, 1984).

derived acetic acid and separation of acetic acid–water solutions that are formed during production of cellulose acetate. The recovery of acetic acid from fermentation broths is similar to the recovery of ethanol from fermentation broths. In the cellulose acetate production process, cellulose reacts with glacial acetic acid and acetic anhydride to form cellulose triacetate. Water is then added to the cellulose triacetate–glacial acetic acid solution, which results in the removal of a fraction of the acetate moieties from the cellulose backbone. Water also causes the precipitation of cellulose acetate and, of course, dilutes the acetic acid. The cellulose acetate is filtered, the acetic acid–water solution is separated by distillation, and the glacial acetic acid is recycled to the cellulose acetate reactor. The distillation step is a huge energy consumer, thus

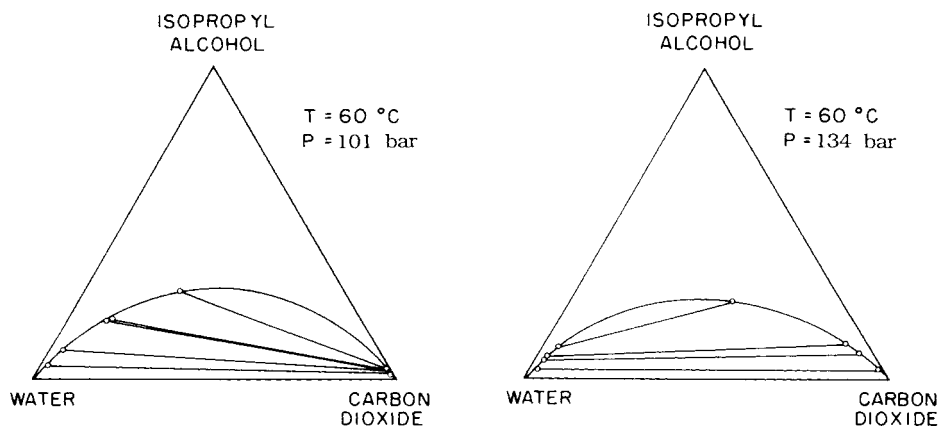


**Figure 8.17** Effect of pressure on the selectivity and loading of isopropanol in supercritical carbon dioxide (Paulaitis, Kander, and Diandreth, 1984).

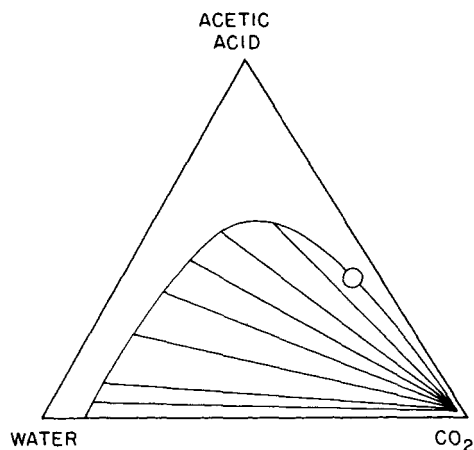


**Figure 8.18** Ternary phase diagram for the acetic acid–water–carbon dioxide system at 25°C and ~64 bar (933 psia) (Francis, 1954).

alternate technologies are continually being evaluated for separating the two compounds.

Acetic acid is quite difficult to extract with  $\text{CO}_2$ ; this was known thirty years ago when Francis studied the  $\text{CO}_2$ –water–acetic acid system (Francis, 1954). A ternary equilibrium diagram of this system is shown in figure 8.18 and the tie line data from the ternary diagram are replotted in  $x$ – $y$  form in figure 8.19. Figure 8.19 shows the equilibrium data do not form a straight line, as was the case with the ethanol system, indicating that the distribution coefficient is not constant. But this fact in itself is not important. What is important is the slope of the equilibrium curve at the dilute acetic acid concentration range; the slope of the tangent in this region determines the solvent-to-feed ratio. Over an acetic acid concentration range 0 wt% to about 5 wt%, the distribution coefficient is about 0.03 (weight basis), seen in figure 8.19. Thus, the minimum  $\text{CO}_2$ -to-feed ratio required to extract all the acetic acid is 33 lb  $\text{CO}_2$  per 1 lb feed solution. For comparison, this value is more than three times the amount of  $\text{CO}_2$  required to extract ethanol from an ethanol–water feed stream. In the real operating case, the solvent-to-feed ratio of 1.3 times the minimum is almost 40 lb  $\text{CO}_2$  per 1 lb feed solution, considered to be prohibitively high.

As if the low distribution coefficient does not present enough of an obstacle, extraction of acetic acid from fermentation broths is made still more unattractive by the high pH of the solutions. For the bioprocesses being evaluated, acetic acid will be produced in a solution with a pH of about 6.0. The  $\text{pK}$  of acetic acid is 4.8 and thus, at a pH of 6.0, virtually all the acetic acid produced in solution exists as an acetate ion. Current extraction/recovery schemes entail acidification (with HCl, for example) to convert the acetate ion to free acetic acid. Then the free acid can be extracted with an organic solvent. If  $\text{CO}_2$  is used as the extractant, HCl is not required. Carbonic acid from the  $\text{CO}_2$ –water equilibrium will neutralize part, but not all, of the acetate ion; this can be determined from a material and charge balance of species in solution.

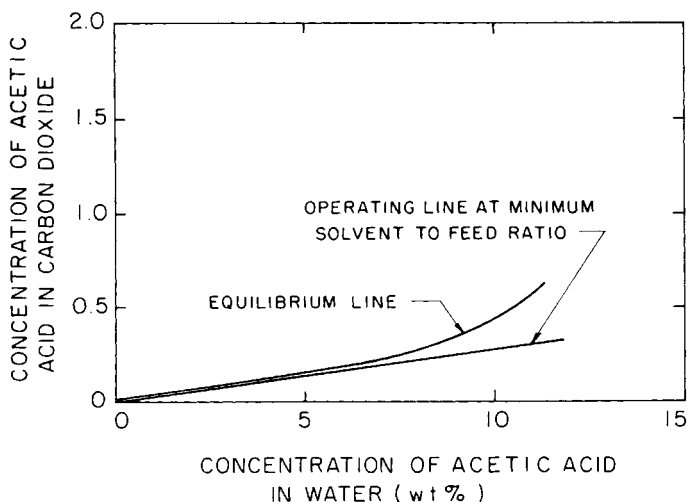


**Figure 8.19** Plot of the equilibrium and operating lines for the acetic acid–water–carbon dioxide system at 25°C and ~57 bar.

A patent covering the concept of extraction of organic acids from high-pH solutions provides data from which the extraction efficiency of this concept can be analyzed (Shimshick, 1981). Example 6 from the patent is reproduced.

Carbon dioxide at  $2400 \pm 200$  psig . . . and  $50^\circ \pm 2^\circ\text{C}$  was used to extract acetic acid from an aqueous *Clostridium thermoaceticum* fermentation broth containing about 0.23 M sodium acetate and 0.03 M acetic acid, pH 5.7. About 1% of the acetic acid/sodium acetate in the fermentation broth was recovered as acetic acid in bomb 32, trap 33 and trap 34.

From the data and from the experimental procedure described in the patent the overall distribution coefficient based on total acetate is calculated as 0.004. This is an extremely small number, which, of course, is a consequence of the small amount of free acid available in solution at the high pH of the solution. Other authors (Yates, 1981; Busche, Shimshick, and Yates, 1982) address the problem of incomplete extraction of organic acids from high-pH solutions using  $\text{CO}_2$ . The authors suggest that the raffinate from the extractor can be recycled to the fermentor.

In the past few years, many other organic–water separations have been screened in feasibility tests. Some have received substantial research and development effort because they require large consumptions of energy for separation by distillation. A partial list of the organics includes dioxane, acetone, formamide, *N,N*-dimethyl formamide, and ethylene glycol. Most of these compounds hydrogen bond to water and to themselves, which inhibits

facile extraction with CO<sub>2</sub>. Formamide and ethylene glycol are two compounds that readily hydrogen bond to themselves and to water. Therefore, it is especially difficult to extract these compounds from water with CO<sub>2</sub>. For instance, formamide exhibits an extremely poor distribution coefficient of 0.001. A distribution coefficient that low suggests it is virtually impossible to extract formamide from water. As a matter of interest, the selectivity of CO<sub>2</sub> for formamide is less than 1.0, that is, CO<sub>2</sub> extracts water preferentially from formamide–water solutions (Krukonis, 1981b).

## BREAKING AN AZEOTROPE

### The Trimethyl Borate–Methanol System

As described in the preceding pages, the selectivity values for a variety of SCF solvents for ethanol can be as high as 50–80 at ethanol concentrations of ~10 wt% but the distribution coefficient of ethanol,  $(y/x)_{\text{alcohol}}$ , is only on the order of 0.1 (weight basis) in this region. With such a low distribution coefficient, supercritical solvent-to-feed ratios of 10 or more are needed to extract ethanol from water. Furthermore, in none of these studies was it possible to surpass the alcohol–water azeotropic concentration. In this section we describe a study by Unterreiner, McHugh, and Krukonis (1991) on the ability of supercritical methane to extract trimethyl borate (TMB) from methanol and to break the TMB–methanol azeotrope (70 wt% TMB). TMB–methanol azeotropic solutions result from the synthesis process for producing TMB. The resultant TMB–methanol solution must be processed in a three-column distillation sequence or by some combination of extraction and distillation. The TMB–methanol system forms a weak, Lewis acid–base complex, which occurs when the oxygen on the methanol donates a pair of electrons to the unfilled orbital of boron (Kreevoy and Kantner, 1977).

To extract TMB from TMB–methanol mixtures it is necessary to find a solvent that is relatively immiscible in methanol yet is miscible with TMB at the same conditions. TMB is very soluble in benzene, hexane, heptane, nonane, and carbon tetrachloride indicating that it exhibits very lipophilic characteristics (Plank and Christopher, 1976; Niswonger, Plank, and Laukhuf, 1985; Schmidt, Plank, and Laukhuf, 1985; Munster et al., 1984). Hence, TMB should be soluble in the more common supercritical fluid solvents such as ethane and carbon dioxide. Methanol is moderately miscible with xenon, ethane, ethylene, and carbon dioxide since a single phase is obtained at pressures of less than ~200 bar at temperatures between the respective critical temperatures of the binary components (Brunner, 1985). To obtain quickly an estimate of the distribution coefficient for TMB in carbon dioxide, ethane, and ethylene, rapid screening experiments were performed with a dynamic flow apparatus at temperatures ranging from 0 to 55°C at a number of pressures. From this preliminary study it was found that carbon dioxide does not

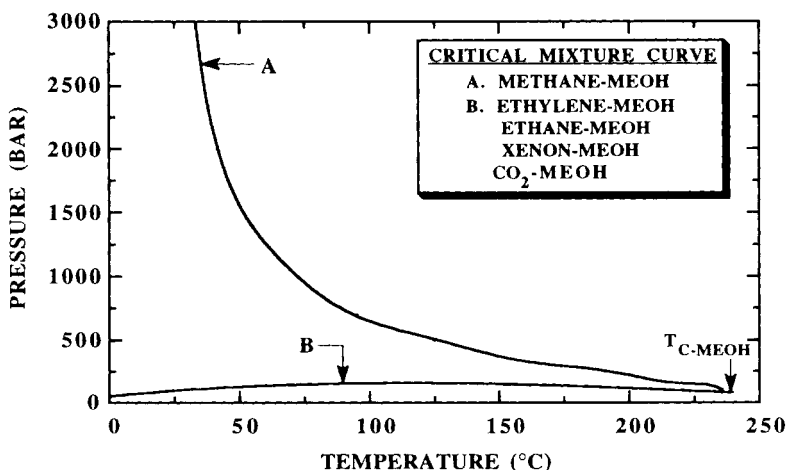


**Figure 8.20** Critical mixture curves for methanol with methane, ethane, ethylene, xenon, and carbon dioxide (Robinson, Peng, and Chung, 1985; Brunner, 1985; Francesconi, Lentz, and Franck, 1981). The  $P$ - $T$  traces for the ethane, ethylene, xenon, and carbon dioxide systems are virtually indistinguishable in the region shown in the graph. But near  $-50^{\circ}\text{C}$  the ethane-methanol critical mixture curve turns up abruptly. Not shown in this figure are the three phase lines exhibited by the ethylene-methanol and the ethane-methanol systems at conditions close to their respective critical points.

discriminate between TMB and methanol even at moderate pressures, since it dissolves them both to very high levels. Ethane and ethylene also fail to separate TMB from methanol.

Further screening experiments were performed using methane at  $0^{\circ}\text{C}$  and 150 bar with the expectation that methane would not be as strong a supercritical solvent as ethane, ethylene, or carbon dioxide, since methane has a low polarizability and density. In these preliminary tests methane exhibited a high selectivity for TMB relative to methanol. This result should not be too surprising since literature data show that methane and methanol are not very miscible (Francesconi, Lentz, and Franck, 1981; Brunner, 1985). Figure 8.20 shows a portion of the  $P$ - $T$  trace of the critical mixture curves for the methane-methanol, ethane-methanol, ethylene-methanol, and carbon dioxide-methanol systems. Pressures in excess of  $\sim 2,500$  bar are needed at room temperature to obtain a single phase with the methane-methanol system, while only  $\sim 150$  bar is needed to obtain a single phase with ethane, ethylene, xenon, or carbon dioxide (Robinson, Peng, and Chung, 1985; Brunner, 1985). The  $P$ - $T$  data shown in figure 8.20 suggest that the solvent power of methane, the weakest of the supercritical solvents shown in this figure, can be fine-tuned using pressure, while the other solvents are already too strong even at relatively low pressures.



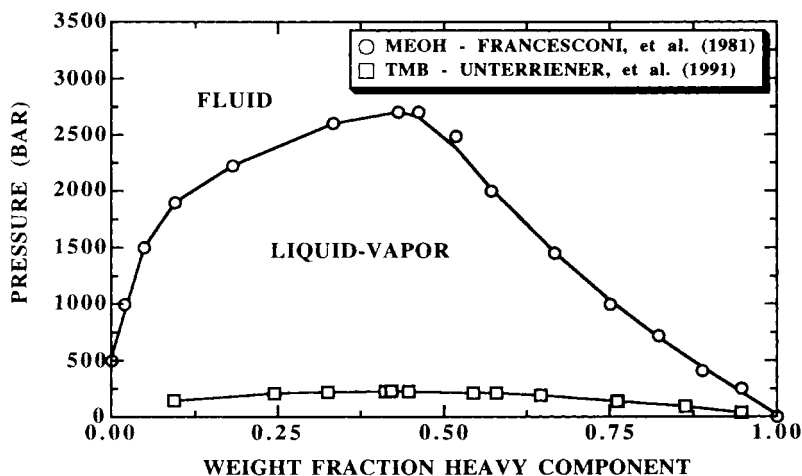
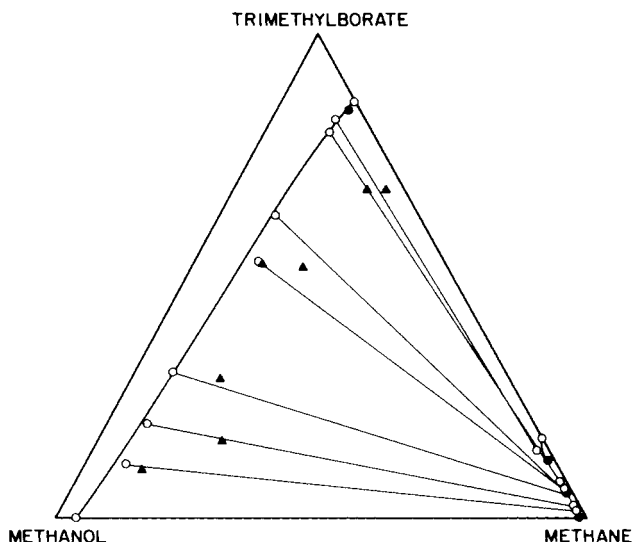


**Figure 8.21**  $P$ - $x$  behavior of the methanol-methane (Francesconi, Lentz, and Franck, 1981) and the TMB-methanol systems at 35°C (Unterreiner, McHugh, and Krukons, 1991).

Further evidence of the preference of methane for TMB relative to methanol is given in figure 8.21. Modest pressures of ~225 bar are needed to obtain a single phase with the TMB-methane system at any concentration. But, at the same temperature and concentration, up to ~2,500 bar can be needed with the methanol-methane system. The extremely high pressure needed to dissolve methanol in methane is probably a result of the strong hydrogen bonding between methanol molecules in the liquid phase (Prausnitz, 1969; Franck and Deul, 1978). The density of methane at 35°C and ~2,500 bar comes to within a factor of about two of the density of liquid methanol before complete miscibility is obtained (Diguët, Deul, and Franck, 1987). This suggests that methane and methanol must be packed closely together to allow the weak forces of attraction between methane and methanol to have an effect. Only modest pressures are needed to solubilize TMB in methane, since TMB primarily interacts through dispersion forces. Dispersion forces are much less than the specific chemical interactions found with methanol, thus they are more compatible with nonpolar methane. The differences in binary phase behavior of methane with TMB and with methanol suggest that it may be feasible to extract readily TMB from methanol. But it is necessary to determine ternary phase behavior information, since it is known that TMB and methanol form a weak acceptor-donor complex which may preclude the efficient extraction of TMB from these mixtures (Kreevoy and Kantner, 1977).

Figure 8.22 shows ternary TMB-methanol-methane data at 35°C and 152 bar, conditions very similar to those used in the screening study. Several features of this diagram indicate that methane is the supercritical fluid solvent of choice for the separation of TMB from methanol. The shape of the two-phase region and the slopes of the tie lines reveal that greater than 70 wt%

**Figure 8.22** Ternary tri-methyl borate–methanol–methane weight percent data at 35°C and 152 bar (Unterreiner, McHugh, and Krukoni, 1991). The open symbols are analyzed samples, the triangles are loadings, and the closed circles are visually determined phase boundaries.



TMB (solvent-free basis) can be obtained in the methane-rich extract phase if the TMB–methanol azeotropic mixture is extracted with methane. Not only is the loading of TMB in the methane-rich phase quite high, ~12 wt%, it remains essentially constant as the concentration of TMB decreases in the liquid phase. The methanol that is complexed to TMB also hydrogen bonds to other methanol molecules. Intermolecular interactions between methane and methanol are not strong enough to compete with the hydrogen bonding that occurs between methanol molecules, so the methanol remains essentially insoluble at this low pressure. Even large amounts of methane dissolved in methanol scarcely disrupt the hydrogen bonding (Diguët, Deul, and Franck, 1987). It is interesting that the presence of relatively large amounts of TMB in the methane-rich gas phase has little effect on the solubility of methanol in this phase, even though TMB and methanol form a weak complex. This lack of entrainer effect is surprising.

Since the binodal curves intersect the TMB–methane axis, it is possible to obtain pure TMB using a countercurrent extraction process with reflux. If the system pressure were increased above the TMB–methane critical pressure at 35°C, a closed-dome, two-phase region would exist and it would not be possible to obtain pure TMB with a countercurrent process.

Figure 8.23 shows the results obtained when a TMB–methanol azeotropic mixture is extracted. Notice that the concentration of TMB in the extract phase remains essentially constant as the extraction proceeds, consistent with the trends in the equilibrium data shown in figure 8.22. The slight difference in operating conditions shown in figures 8.22 and 8.23 is not expected to have a significant effect on the data (Francesconi, Lentz, and Franck, 1981). The data presented in this figure are not strictly equilibrium data at the flow rates used

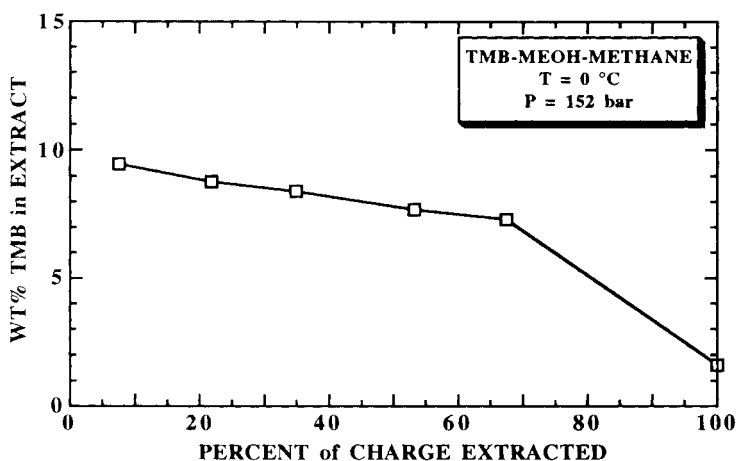


**Figure 8.23** Performance of the dynamic extraction of the trimethyl borate-methanol azeotrope mixture using supercritical methane (Unterreiner, McHugh, and Krukonis, 1991).

for the extraction, although it is estimated that the solution exiting the column comes to within  $\sim 80\%$  of its equilibrium value. The concentration curve exhibits the characteristics found when extracting a single component (i.e., in the dynamic measurement of solubility of a pure liquid or solid at a fixed temperature and pressure, the concentration in the extract phase initially remains constant then drops off rapidly once the material in the column becomes depleted). The distribution data for TMB in table 8.1 show that the distribution coefficient increases as the extraction proceeds. The distribution coefficient for TMB is also about an order of magnitude higher than that found with ethanol extracted from water using a supercritical fluid solvent.

The geometry of ternary phase diagrams allows us to show that any liquid mixture azeotrope can be broken if the system has binodal curves similar to those exhibited by the TMB-methanol-methane system in figure 8.22. For example, it would be possible to break the ethanol-water azeotrope with a supercritical fluid if the system is processed at a low pressure such that the ethanol-SCF axis is intersected by the binodal curves. Since the mutual miscibility of water and hydrocarbons or carbon dioxide is relatively insensitive to pressure at around room temperature, the operating pressure for a supercritical extraction process must be lower than the pressure needed to obtain a single phase with the ethanol-SCF binary system. Only modest pressures are needed at around room temperature to obtain a single phase for ethanol with ethylene (Paulaitis, Gilbert, and Nash, 1981; Ohgaki et al., 1983), ethane (McHugh, Mallett, and Kohn, 1983), and carbon dioxide (Francis, 1954; Paulaitis, Gilbert, and Nash, 1981), therefore the extraction pressure used with the ethanol-water-SCF system must be very low to avoid a closed, two-phase dome. Obviously a low operating pressure limits the practical

**Table 8.1** Sequential Extraction Data for the Trimethylborate (TMB)–Methanol System with Methane at 0°C and 152 bar Using a Dynamic Flow Technique (Unterreiner, McHugh, and Krukoni, 1991). The weight percent of TMB in the extract is measured and the weight percent of TMB in the extraction column is calculated to within  $\pm 5\%$  from a mass balance

<i>Fraction</i>	<i>Liquid Extract Collected (g)</i>	<i>Methane From Degassed Extract (g)</i>	<i>TMB in Extract<sup>a</sup> (wt%)</i>	<i>TMB in Column<sup>a</sup> (wt%)</i>	$\left( \frac{y_{TMB}}{1 - y_{TMB}} \right)^c$ $\left( \frac{x_{TMB}}{1 - x_{TMB}} \right)$
Loading	20.71	—	—	70.0	—
1	1.56	14.28	96.2	67.9	1.4
2	2.95	28.56	93.7	63.2	1.5
3	2.72	28.57	96.5	56.5	1.7
4	3.79	42.85	94.5	41.7	2.1
5	2.95	35.71	95.7	18.1	3.6
6 <sup>b</sup>	6.74	55.40	14.8	~0	—

<sup>a</sup>Methane-free basis.

<sup>b</sup>For this fraction, CO<sub>2</sub> was used and the column was completely depleted of liquid solution.

<sup>c</sup>Weight fraction basis.

application of using a supercritical fluid solvent to break the ethanol–water azeotrope, since the amount of ethanol in the SCF-rich phase would be prohibitively low. This solubility behavior is in marked contrast with the TMB–methanol–methane system, which has a high solubility of TMB at pressures below 175 bar while maintaining a very low solubility of methanol at this modest pressure. Even the presence of large amounts of TMB in the methane-rich gas phase has little effect on the solubility of methanol in this phase.

The TMB–methanol azeotrope can be broken at its azeotropic concentration using supercritical methane at very mild temperatures and pressures. Operating countercurrently with reflux it is possible to obtain essentially pure TMB, since the binodal curve intersects the TMB–methane axis. The relative strength in the intermolecular forces in operation in the binary systems, TMB–methanol, TMB–methane, and methanol–methane, and in the ternary TMB–methanol–methane system can be interpreted with information on the types of phase behavior exhibited by each of these binary mixtures and the physicochemical properties of each component. TMB, a lipophilic substance, dissolves quite readily in nonpolar methane at moderate pressures. But intermolecular interactions between methane and methanol are not strong enough to compete with the hydrogen bonding found with liquid methanol at 35°C until high methane densities are obtained at very high operating pressures.

Radically different binary phase behavior is found for the methane–TMB and the methane–methanol systems. This suggests that TMB can be extracted from methanol. To verify this conjecture experimental information was obtained on the TMB–methanol–methane system to ascertain whether the weak TMB–methanol complex can be broken by nonpolar methane. Interestingly, carbon dioxide, ethane, and ethylene, all much better supercritical solvents than methane, dissolve both methanol and TMB to such a large extent that they are not selective for either component. But with methane, the interactions between methane and TMB are strong enough to maintain a constant concentration of TMB in the extract phase as TMB is removed from the methanol-rich liquid phase. This means that the distribution coefficient for TMB increases as the concentration in the liquid phase decreases. We know of no other system that exhibits this type of distribution coefficient behavior.

The examples in this chapter highlight many facets of the development of SCF processes and applications that need to be addressed, understood, and solved before scaleup is considered. The same procedure is necessary for any kind of separation process. Supercritical fluid extraction has the potential to reduce energy costs but that does not necessarily mean it will be less expensive overall. Frequently, capital and other operating costs can more than offset decreased energy costs. Subsequent chapters discuss developments in the application of supercritical fluid solvents to the solution of technically and economically difficult separation problems in which the improved performance of the processed materials can support the processing cost.

---

## Polymers and Monomers Processing

---

Prior to about 1985, very little had been reported in the literature regarding the use of supercritical fluids (SCF) to process polymers or monomers. Since 1985 many reports have emerged describing the potential of SCF solvents to fractionate polymers with respect to molecular weight, chemical composition, and backbone structure and to purify specialty monomers that cannot be processed by other separation techniques. The SCF-polymer studies described in this chapter are categorized first in six general areas: high-pressure polyethylene polymerization/fractionation; fractionation of other polymers; extraction of low molecular weight oligomers from polymers; supercritical fluid chromatography analysis of polystyrene; polymer-organic solvent phase separation; and polymer fiber spinning.

We begin with a description of the high-pressure polymerization process since it is an authentic example of how the principles of thermodynamics and kinetics can be combined with creative engineering to develop an economically viable high-pressure process. These principles can be generalized and extended to other high-pressure processes. After describing the polyethylene process, we move on to more recent work on polyethylene and ethylene copolymers, followed by a discussion of other recent SCF studies with a variety of other polymers and monomers.

### HIGH-PRESSURE POLYETHYLENE POLYMERIZATION

The high-pressure polyethylene process described in the literature (Shreve and Brink, 1977; Anon., 1981b), represents, in our opinion, the ultimate supercritical fluid process. Figure 9.1 is a diagram of the now forty-year-old process redrawn from *The Kirk-Othmer Encyclopedia of Science and Technology*. This process was under development at the Imperial Chemical Industries laboratories in the late 1930s. A rapid scan of the operating conditions in the reactor section, figure 9.1, shows pressure levels of 2,700 bar! Either a well-stirred autoclave or a tubular reactor can be used to carry out the polymerization.

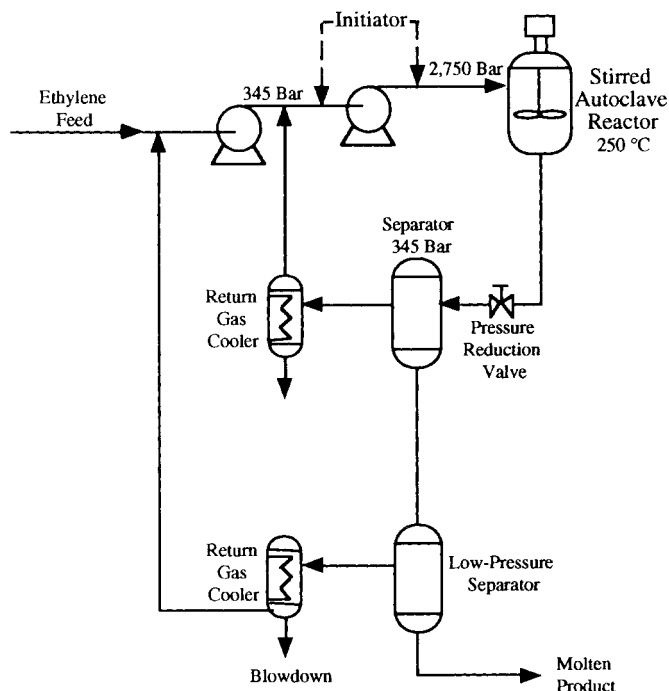


**Figure 9.1** Schematic diagram of the high-pressure polyethylene process that uses a stirred autoclave.

Ethylene is compressed to 2,700 bar and a free-radical initiator, e.g., trace amounts of oxygen or a peroxide, is injected into the feed stream to promote the free-radical polymerization. The polyethylene polymer that is formed remains dissolved in the supercritical ethylene phase at the operating temperature, which ranges from  $\sim 140$  to  $250^\circ\text{C}$ . The heat of reaction is removed by through-wall heat transfer when the tubular reactor is used and by regulating the rate of addition of initiator when the autoclave reactor is used.

Downstream of the reactor section the polyethylene–ethylene solution is expanded to a lower pressure, typically to about 350 bar. Because the solvent power of supercritical ethylene is lowered during the pressure reduction, the polyethylene formed in the reactor nucleates, precipitates from solution, and is collected in the separator. Note that this separation step is exactly analogous to the separation of naphthalene in the model extraction/separation process described in chapter 6. The low-pressure ethylene from the polyethylene separator is recompressed and recycled to the reactor. Interestingly, high-pressure ethylene is both the reactant and the solvent for the product in this process.

There are some other facets to the operation of this process that are worth noting since they illustrate the SCF phenomena that are in operation; the

phenomena can be understood with the aid of the naphthalene solubility diagram. Recall that it was stated a number of times in chapter 6 that many SCF-solute systems exhibit generic solubility behavior (see figure 6.1). The same generic solubility isobars (but not the absolute solubility values) describe the solubility behavior of polyethylene in supercritical ethylene in some regimes of  $P$ - $T$  space at conditions above the melting point of the polymer. Although the concentration profiles for the polyethylene-ethylene system are not presented here, the slope of the 2,700 bar solubility isobar is positive with temperature; that is, concentration increases with increasing temperature.

In the preceding discussion of the operation of the tubular reactor polymerization scheme, we stated that the heat of reaction is removed by through-wall heat transfer. What exactly occurs in the vicinity of the wall? If the characteristic of the high-pressure (300 bar) naphthalene isobar is interpreted as a schematic representation of the solubility of polyethylene in ethylene at a pressure of 2,700 bar, we can use it to predict that polyethylene will precipitate in the boundary layer near any relatively cold surfaces in the reactor or downstream lines. If the precipitation of polyethylene does occur on these internal surfaces and if it is not appropriately removed, the buildup of the polymer on the wall can result in decreased heat transfer from the hot gas-polymer solution, and the attendant decrease in heat transfer can lead to the runaway reaction that is occasionally encountered in high-pressure polyethylene plants.

The removal of precipitated polyethylene from the wall is an interesting operation. About once every 2-3 sec the expansion valve is opened more fully than required for the expansion/precipitation function; this results in a rapid decrease in pressure in the reactor of as much as 300-600 bar. The concomitant rapid increase in the velocity of the gas phase in the tubular reactor shears the walls and strips off any deposited polyethylene so that a reasonably steady state heat transfer situation exists. This description of the operation of the polymerization process, the polyethylene precipitation step, and the accentuated expansion, which maintains a clean wall and a high heat transfer coefficient, help to illustrate the interesting SCF solubility behavior and they also supply some information on the commercial reality of high-pressure processing in what we consider to be an extreme case.

Quite often the sentiment is expressed that high-pressure phase equilibria studies are interesting academically and that the SCF applications development effort might work at the laboratory level, but any extension to industrial levels is usually considered skeptically. Response to the skepticism is best provided by summarizing the previous discussion: high-pressure, low-density polyethylene has been produced in plants operating at 300 to 500 million lb/yr at pressure levels of 2,700 bar and temperature levels of 150-300°C with pressure expansion ratios of 10 across small orifices and, moreover, with valves cycling every few seconds. These plants operate continuously for months at a time and, furthermore, have been in operation since the early 1950s. Based on the operating experiences with the high-pressure polymerization process, we



certainly do not envision any new design and operating problems that would hinder the development of SCF extraction applications that operate at the much more modest conditions of 300 or 400 bar; furthermore, the plants described in chapter 1 attest to this fact.

Many polymer fractionation patents of the 1940s derive directly from the high-pressure polymerization process. For example, the fractionation of polyethylene during a multiple pressure letdown of the polymerization process is described in United States Patents 2,388,160 (Krase, 1945) and 2,396,791 (Krase and Lawrence, 1946), both assigned to E. I. du Pont (which also started research and development in polyethylene formation in the late 1930s); 2,457,238 (Hunter and Richards, 1945), to Imperial Chemical Industries; and 3,294,772 (Cottle, 1966), to Phillips Petroleum. The ability to achieve separation by molecular weight was reported and the following excerpt from the ICI patent presents in descriptive terms the results from a particular high-pressure polyethylene fractionation process:

The process involves the lowering of the reaction pressure under constant temperature by a series of stages and collecting the products which precipitate at each stage. It is possible to obtain high molecular weight products from ethylene that vary in physical characteristics from hard horny solids to waxy semisolids with a large group of intermediate products.

The ICI patent also discusses processing of polystyrene and polyisobutylene, but it explains that these polymers were extracted of their low molecular weight oligomers rather than fractionated. These early patents provide a wealth of information on the technical aspects of processing polymers at high pressures. Their very existence, along with the industrial facilities that are currently in operation producing these polymers, should mollify those individuals who frequently question or comment upon whether operating at high pressures is technically feasible or, perhaps more importantly, profitable.

## **POLYMER FRACTIONATION PROCESSES**

### **Isothermal Decreasing Pressure Profiling**

Before presenting the results of specific polymer fractionation processing, we give an overview of the equipment and procedures that are used for such a process. Supercritical fluid fractionation of a synthetic oil or polymer is typically carried out in a multiple, sequential pressure reduction system, which is an extension of the operation philosophy described in chapter 6. A schematic diagram of a continuous fractionation system employing a supercritical fluid to separate the homologous series members of a synthetic polymer is shown in figure 9.2 (Krukoniš, 1983a). Four extraction/separation vessels (arbitrarily) shown in this figure. During operation of the fractionation process a

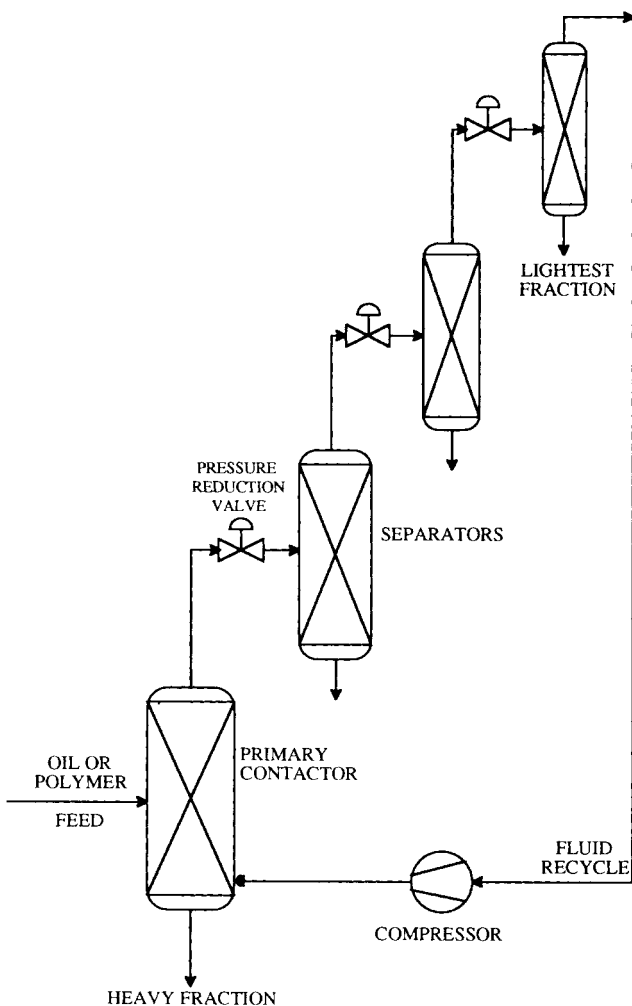


**Figure 9.2** Schematic diagram of an apparatus using a supercritical fluid solvent to fractionate a polymer.

synthetic oil, such as a polydimethylsiloxane with a broad molecular weight distribution, is pumped into the primary contactor/extractor at the top, and the supercritical fluid enters at the bottom. The extract phase leaving the vessel contains dissolved polymer, and the solubility level is consistent with the solubility characteristics and operating parameters in the primary extraction vessel.

In the figure, a “heavy” fraction leaving the primary contactor vessel is indicated; this is the highest molecular weight fraction that has not been dissolved based upon the extraction pressure and temperature. If the extraction pressure or temperature or both are changed such that the dissolving power is greater, the entire feed could just as easily be dissolved, but to isolate the

heavy fraction in this latter case would require another pressure letdown stage; in the case shown in figure 9.2 the heavy fraction is obtained for “free.”

The solution of polymer and SCF that leaves the primary vessel is expanded to some lower pressure, which causes the next highest molecular weight oligomers in the solution to precipitate. The remaining stream is further stagewise reduced in pressure through the subsequent expansion valves, which results in further fractionation by molecular weight. The molecular weight distribution (polydispersity) of the polymer in each fraction can be reduced to a very low value if very small pressure decrements are taken between each pressure level; the trade-off is that smaller pressure decrements result in reduced amounts of each fraction albeit with low polydispersity index. After expansion to the lowest pressure, the almost polymer-free gas is recompressed and recycled. The number of fractions that are obtained is consistent with the number of pressure reduction stages, and the molecular weight range of each fraction is related to the ratio of pressure reduction per stage.

Although the density of the supercritical extractant is typically lower than that of the polymer, the column could as easily operate upside down, that is, if the density of the supercritical extractant was higher than that of the feed oil, the inlet positions of the respective streams shown in figure 9.2 would be reversed. Later in this chapter some phase and fractionation studies on an acrylate-ethylene copolymer with supercritical chlorodifluoromethane are presented. Over much of its active  $P$ - $T$  range, supercritical chlorodifluoromethane is more dense than some of the polymers. Therefore, if that system were to be scaled to continuous operation at the commercial level, the liquid or melted polymer would be fed to the bottom of the extractor and chlorodifluoromethane to the top; the subsequent fractions would be removed from the top of each separation vessel instead of from the bottom, as shown in the figure. In the polymers patent section of this book, we describe a process for polymer fractionation via stepwise pressure reduction exactly analogous to the process shown schematically in figure 9.2—the Hunter and Richards 1945 patent.

## **Isothermal Increasing Pressure Profiling**

Although the decreasing pressure profiling fractionation is easily practiced on an industrial scale, fractionation of any new polymer at the laboratory scale is most easily carried out using an increasing pressure profile. Operation of increasing pressure fractionation is best explained with reference to figure 9.3, a schematic diagram of a laboratory extraction system. An amount of polymer (either liquid or solid) is charged to a small vessel and connected to the laboratory system shown in figure 9.3 (a variant of the system shown in figure 4.5). The charge is extracted sequentially at increasing pressure levels.

In a simplistic description of the laboratory process, a low pressure is first used and the extraction continued until no more polymer is collected in the

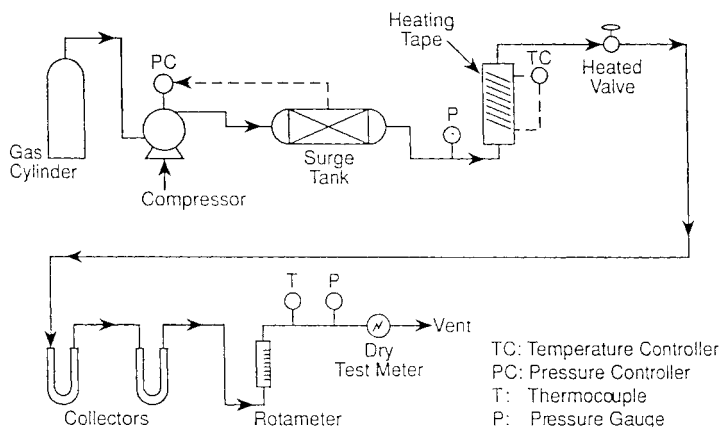


**Figure 9.3** Schematic diagram of a laboratory apparatus using a supercritical fluid solvent to fractionate a polymer.

U-tube shown in the figure. The term “no more” is a relative one since the rate of extraction will slow down markedly, but not necessarily to zero, after the polymer fraction that is most soluble, or more precisely, after the fraction that exhibits the highest distribution coefficient in the gas, is dissolved and removed from the column. When the extraction rate drops markedly, indicating that the oligomers of extractable molecular weight have been removed at the specific pressure level, the pressure level is raised, the collection vessel changed, and a new polymer fraction is collected in the U-tube. The sequential pressure increase/collection sequence is continued until all the polymer is dissolved, or until some maximum pressure dictated by the system design is reached.

Increasing pressure fractionation can be practiced on laboratory scale equipment with as little as 2–5 g of polymer. However, 2–5 g of polymer would get lost in the lines and vessel walls if the polymer were fractionated using a continuous, decreasing pressure profiling fractionation. Since the life cycle for most new polymers begins with a laboratory-scale synthesis at the 2–5 g level, these polymers can be fractionated readily using the equipment in figure 9.3. While fractionation of small amounts of polymer is most advantageously carried out by the increasing pressure profiling procedure, by no means is this process limited only to small quantities; the equipment and technique can be readily scaled to accommodate several kilograms of polymer quite easily.

## SCF Solvent Selection

In addition to fixing the operating mode of the fractionation, an appropriate supercritical fluid solvent must be chosen to dissolve or fractionate the

polymer. Usually only very straightforward chemistry principles need to be considered in the selection of the SCF solvent. For example, consider the fractionation of an amino-terminated polysiloxane, described later in some detail. Carbon dioxide would not at all be considered as a suitable solvent because of the well-known reaction between primary aliphatic amines and carbon dioxide to form carbamic acids. SCF solvents such as ethylene, ethane, or propane are more advantageous for purifying, extracting, or fractionating the amino-terminated polysiloxanes. The specific SCF solvent selected depends upon the molecular weight of the polymer. Ethane and ethylene are excellent solvents for amino-terminated polysiloxanes of up to about 500,000 molecular weight, while propane is a better solvent for polysiloxanes above about 500,000 (Krukoniš, 1985a; Gallagher and Krukoniš, 1993). One very interesting use of carbon dioxide in a reaction/separation scheme is discussed later in this chapter for the fractionation of poly(dimethylsiloxane-*co*-diphenylsiloxane).

Chapter 5 shows that a solvent will not dissolve a polymer unless it can interact favorably with the polymer through intermolecular forces, such as hydrogen bonding and dipole-dipole interactions (Krukoniš, 1985b; DeSimone et al., 1988a; McHugh and Krukoniš, 1989; Meilchen, Hasch, and McHugh, 1991; Watkins and Krukoniš, 1991; Watkins et al., 1992; Gallagher and Krukoniš, 1993). Therefore, the specific choice of SCF solvent for a given polymer fractionation is highly dependent on the intermolecular forces in operation between solvent-solvent, solvent-polymer, and polymer-polymer pairs in solution. This principle of favorable interactions is also true when choosing a liquid solvent. There is one more degree of freedom with an SCF solvent that is not available with a liquid solvent, density, or free volume manipulation. The solvent quality of a liquid solvent is typically moderated by changing the temperature or by adding a liquid nonsolvent. In contrast, the quality of an SCF solvent can be regulated by varying the operating pressure and/or temperature which affect the free volume of the solvent.

The interplay between polymer-solvent interactions is readily demonstrated by considering the solvent selection for fractionating polymethyl methacrylate (PMMA). Because PMMA is a very polar polymer, it does not dissolve in nonpolar solvents, such as hexane, or in moderately polar solvents, such as toluene. PMMA does dissolve in chloroform or methylene chloride even at room temperature because both of them have large dipole moments and both of them are capable of donating a hydrogen to the basic acrylate group on the polymer. Even low molecular weight PMMA of 50,000 does not dissolve in ethane or propane at pressures up to 700 bar and temperatures up to 150°C, since these solvents are strictly nonpolar. Neither will this molecular weight PMMA dissolve in carbon dioxide or ethylene at 700 bar and 150°C even though both of these solvents have quadrupole moments and carbon dioxide has some acid-base character. Increasingly, PMMA, in the hundreds of thousands molecular weight range will readily dissolve to 20 wt% in chlorodifluoromethane at a modest temperature of 120°C and pressures of 200–300 bar. Chlorodifluoromethane is a very polar hydrogen-donor solvent that is capable of hydrogen bonding to the basic acrylate group in the backbone of

PMMA. If the lone hydrogen on chlorodifluoromethane is replaced with a chlorine atom to make dichlorodifluoromethane, even low molecular weight PMMA will not dissolve at pressures as high as 700 bar and temperatures up to 150°C (Krukoniš, 1985b). The hydrogen replacement with a chlorine eliminates the very strong hydrogen bonding interactions that make chlorodifluoromethane such a formidable solvent for basic, polar polymers.

It should be stressed that lack of polymer solubility in a given solvent is not necessarily a negative finding. For example, the gas can be used efficiently for extraction of residual reactants or liquid solvents while leaving 100% of the polymer intact. Watkins and Krukoniš (1991) show that a glycidyl azide polymer (whose structure is given later) can be fractionated over the entire molecular weight distribution range using chlorodifluoromethane because of the favorable hydrogen bonding between the polymer and the solvent. Using carbon dioxide it is only possible to dissolve the residual cyclic reactants and low molecular weight oligomers in the parent polymer material. Thus, the moderate solvent power of carbon dioxide is used to effectively purify this polymer.

The principles of polymer fractionation using supercritical and near-critical solvents are the same as those for liquid solvent fractionation except with the addition degree of freedom that the solvent power of gases can be more finely tuned using pressure. Differences in solubility behavior that arise from subtle differences in molecular weight or architecture can be exploited for separation of discreet fractions with respect to these properties. Because of their variable solvent strengths, SCF solvents are ideal candidates for carrying out fractionation of polymers. From a process standpoint the decrease in solubility associated with a decrease in pressure makes a supercritical solvent convenient for process recycle and the rapid dissipation of the gaseous solvent at low pressure promotes facile recovery of a solvent-free polymer.

The efficacy of dissolving or fractionating polymers with gaseous solvents does not reside solely in the solvent strength of the gas since polymer-polymer interactions have a large influence on polymer solubility. The physical state of the polymer, i.e., whether it is in its liquid or solid state at the conditions of interest, has a major impact on the ability of the SCF solvent to dissolve or fractionate it, as is brought out in many subsequent examples. Polymer-polymer interactions are greatly influenced by the backbone structure of the polymer and the functionality of the repeat units. Differences in backbone structure, e.g., linearity, branching, and tacticity, often give rise to differences in physical properties of polymers, such as melting point and dissolution temperature in organic solvents, that allows these polymers to be fractionated using temperature profiling with a single organic solvent. In this instance it is the polymer-polymer interactions that are advantageously manipulated. Fractional crystallization and temperature rising elution fractionation, TREF (Wild et al., 1982) are examples of these thermal separation techniques using liquid solvents. TREF is discussed in more detail later when its supercritical counterpart is described.

In the remainder of this chapter, we present a large number of examples

of polymer and monomer separations to point out the potential of supercritical fractionation for fundamental studies and industrial applications. In addition to enhancing the performance characteristics of many polymers that are discussed in the chapter, supercritical fluids are advantageously applied to fundamental investigations such as phase equilibria, polymers and synthesis kinetics elucidation, and other fundamental areas. A breadth of industrial applications is presented with insight provided by phase equilibrium and chemistry principles used to interpret the data.

Many of the examples highlight specialty materials usually requiring high purity and narrow molecular weight ranges for use as lubricants, hydraulic fluids, and surfactants. In some cases these materials are currently processed only by molecular distillation to achieve the requisite qualities; however, molecular distillation is limited in its separation capabilities when, for example, the vapor pressure of the oil is less than about  $10^{-3}$  mm, or if the oil is heat-sensitive, or if the impurities present in the feed material exhibit the same vapor pressure as the desired fractions. Most of the materials that are discussed subsequently are refractory in their inability to be handled by conventional processing to achieve the specific product performance desired, and the results that are described point out that supercritical fluid processing of oils and polymers is a viable concept in treating such materials.

## POLYETHYLENE FRACTIONATION

Polyethylene is commercially produced either by a high-pressure free-radical polymerization or by a Ziegler–Natta or Unipol catalytic process. The polyethylene produced in these processes typically has not only a distribution of molecular weights, but also a distribution in backbone structure or branch content. Therefore, it should be possible to fractionate the parent material with respect to either molecular weight or backbone structure although, as subsequently described, the experimental techniques used to carry out these two types of fractionations are quite different. Let us first consider the properties of polyethylene that fix the operating philosophy used to fractionate with respect to backbone structure.

The primary structural feature that determines crystallinity is the concentration of short chain branches along the polymer backbone. These short chain branches disrupt the local ordering of the chains and, thus, reduce the degree of crystallinity in the material. The melting point ( $T_{\text{melt}}$ ) of the polymer is directly related to the amount of short chain branches in the material. Regardless of the supercritical fluid used, exceptionally low solubilities are found at temperatures below  $T_{\text{melt}}$ . At temperatures above  $T_{\text{melt}}$  the strong crystalline forces are disrupted and polyethylene can be dissolved to a very high degree in a suitable SCF solvent. Since polyethylene consists of a distribution of polymer chains with varying backbone structure and crystallin-

ity, the operating philosophy to fractionate with respect to backbone structure is to use an increasing temperature profile at a pressure that is sufficiently high to dissolve the crystalline fraction that melts.

Fractionation with respect to molecular weight is readily accomplished by operating at temperatures above  $T_{\text{melt}}$  using an isothermally increasing pressure profile. It is in the liquid-gas region of the phase diagram where polyethylene exhibits reasonable solubility levels in the SCF solvent. The mechanism and driving forces for each fractionation are described in the following sections by examining the characteristics of polyethylene-solvent phase behavior at high pressures.

## Phase Behavior Considerations

Figure 9.4 shows a schematic diagram of the phase behavior of a semicrystalline polymer having a narrow molecular weight distribution. The two-phase envelopes located beneath the liquid-gas, critical mixture curve represent equilibrium between a molten, polymer-rich phase and a compressed, solvent-rich phase. If the pressure is isothermally increased to a point above the two-phase envelope, the liquid and gas phases merge to form a single homogeneous phase. As described in some detail in chapter 3, the border

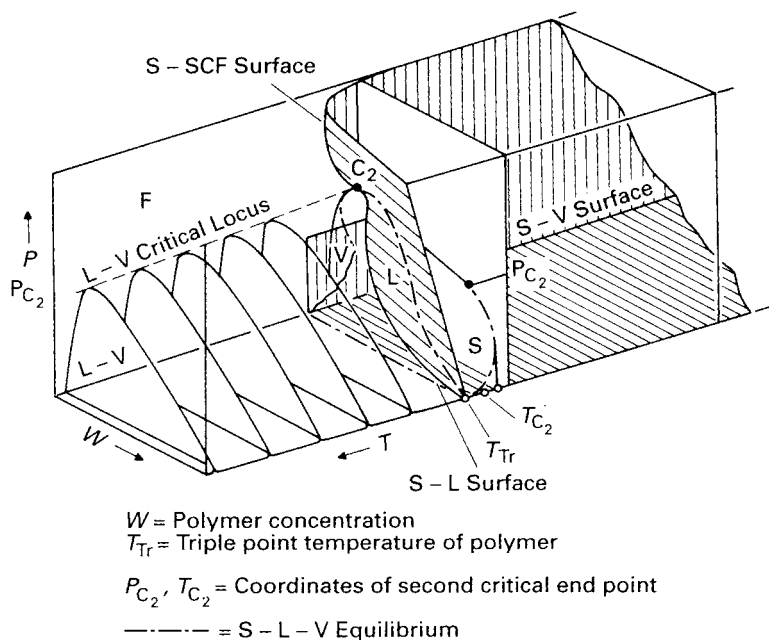


**Figure 9.4** Phase diagram for a narrow molecular weight distribution, semicrystalline polymer with a light gas.



between the liquid–gas, two-phase region and the single-phase, fluid region is typically referred to as a cloud point curve.

The phase diagram shows that a crystallization surface exists at temperatures in the neighborhood of the upper critical end point (UCEP) temperature. The shape of the crystallization surface indicates that there is negligible solubility of the solid polymer in the gas phase regardless of the pressure. Coleman et al. (1990), working with the high-density polyethylene–propane system, show that increasing the temperature and crossing the crystallization surface results in a rapid increase in polymer solubility. If the crystallization surface is crossed at a pressure level above the cloud point curve, the polymer and solvent form a single phase. Controlling solubility by the sharp delineation between virtual insolubility and total miscibility as a consequence of physical state of the polymer is a convenient means for fractionating polymer with differing crystallization temperatures. The location of the crystallization surface with respect to temperature is largely dependent on backbone structure of the chains provided that the molecular weight of the chains is sufficiently high so that the chain ends of the polymers do not contribute significantly to the disruption of local order. For polyethylene, the effect of molecular weight on crystallinity typically becomes insignificant at degrees of polymerization above 100.

Flory (1953) has shown that the weight average molecular weight of the polymer largely determines the location of the cloud point curves with respect to pressure. Ehrlich and Kurpen (1963) measured cloud point pressures for four fractions of high-density polyethylene of various molecular weights in propane at 110°C. The samples had similar backbone structure with each exhibiting a methyl branch content of approximately 1.3%. Figure 9.5 is a pressure–composition plot of Ehrlich's data; it demonstrates the sensitivity of cloud point pressure to molecular weight. The data suggest that fractionation of polyethylene with respect to molecular weight can be accomplished with an isothermal increasing pressure profile in the liquid–gas region of the phase diagram.

The data in tables 9.1 and 9.2 were taken from Watkins et al. (1991) who demonstrate the impact of the crystallization boundary on the fractionation behavior of high-density polyethylene (HDPE). The second critical end point temperature for this sample of HDPE in propane is approximately 125°C. The data in table 9.3 show that HDPE can be selectively fractionated with respect to molecular weight across its entire molecular weight distribution using an isothermally increasing pressure profile in the liquid–gas region of the phase diagram.

The data in table 9.2 show that HDPE *cannot* be efficiently fractionated when the HDPE is a solid at extraction conditions. Less than 5 wt% of the HDPE charged to the column could be dissolved at pressure levels as high as 663 bar (9,615 psia) at a temperature below the second critical end point of the polymer. The material that was extracted in this fractionation was likely amorphous low molecular weight polymer present at or near the surface of the

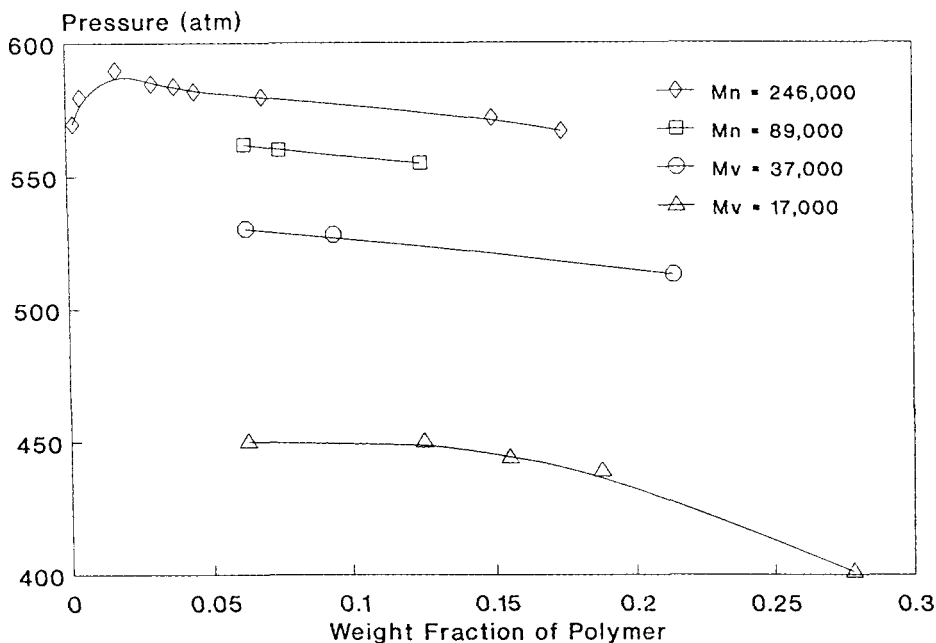


**Figure 9.5** Effect of molecular weight on the pressure–composition behavior for the high-density polyethylene (1.3% methyl content)–propane system at 110°C.

crystalline solid. Table 9.2 shows that a fraction with a weight average molecular weight of only 1,400 was dissolved at 663 bar (9,615 psia) at 105°C, whereas table 9.1 shows that a fraction with a weight average molecular weight of 151,000 was dissolved at 639 bar (9,270 psia) and 130°C. This is clearly a dramatic indication of the impact of crystalline forces in operation in the solid HDPE.

## LLDPE Fractionation with Respect to Molecular Weight and Backbone Structure

Watkins et al. (1992) demonstrate how semicrystalline LLDPE can be fractionated both by molecular weight and backbone structure. The first step of this double fractionation is to fractionate with respect to molecular weight. In this step the fractionation is carried out as an isothermally increasing pressure profile. The second step is to fractionate with respect to backbone structure using an isobarically increasing temperature profile. They termed the second step of the double fractionation CITREF, which is an acronym for critical isobaric temperature rising elution fractionation, a supercritical fluid variation of TREF, a liquid phase fractionation called temperature rising elution

**Table 9.1** Properties of Fractions of HDPE Obtained by an Isothermally Increasing Pressure Profile with Propane at 130°C, a Temperature Above the Melting Point of the Parent Material

<i>Fraction</i>	<i>Pressure (bar)</i>	$\Sigma$ wt% <sup>a</sup>	$M_w$	$M_w/M_n$
1	84	1.0		
2	194	4.0	2,700	1.59
3	322	8.0	5,100	1.76
4	373	15.0	7,300	1.83
5	408	24.0	9,300	2.11
6	432	31.0		
7	446	39.0	14,800	2.11
8	477	46.0	19,800	2.13
9	494	64.0	25,100	2.07
10	518	72.0	34,200	1.30
11	542	80.0	45,000	1.30
12	570	87.0	56,500	1.32
13	570	94.0	64,600	1.31
14	639	100.0	151,000	1.62
		Parent	43,000	5.89

<sup>a</sup>Cumulative amount of polymer removed from the columns.**Table 9.2** Properties of Fractions of HDPE Obtained by an Isothermally Increasing Pressure Profile with Propane at 105°C, a Temperature Below the Melting Point of the Parent Material

<i>Fraction</i>	<i>Pressure (bar)</i>	$M_w$	$M_w/M_n$
1	122	1,000	
2	294	2,000	5.00
3	415	1,100	1.83
4	553	1,000	2.00
5	663	1,400	1.27
	Parent	43,000	5.89

fractionation. TREF was developed by Wild and coworkers (Wild et al., 1982) to separate low-density polyethylene resins on the basis of short chain branching and, therefore, crystallinity. The TREF process utilizes a fractional recrystallization followed by a separation based on dissolution temperature in a liquid organic solvent. In the TREF process, a polymer is first precipitated onto an inert support in a packed column by slow cooling from hot organic

**Table 9.3** Properties of Fractions of LLDPE Obtained by an Isothermally Increasing Pressure Profile with Propane at 130°C

Fraction	Pressure (bar)	Parent (wt%)	$M_w$	$M_w/M_n$	$\Delta H^{fusion}$ (J/g)	$T_{melt}$ (°C)
1	248	2.3				
2	296	3.7	10,700	1.2	104	115
3	379	6.3	16,200	1.3	108	116
4	421	8.8	29,100	1.2	114	121
5	455	11.2	32,300	1.5	106	123
6	483	12.4	50,100	1.3	107	123
7	507	11.5	61,800	1.3	110	123
8	527	11.0	79,600	1.3	114	123
9	545	11.2	108,000	1.4	124	121
10	558	10.1	155,700	1.4	115	121
11	600	8.6	177,300	1.3	132	123
12	655	2.9	273,000	1.6	146	126
		Parent	160,000	5.0	113	123

solution. The precipitation serves as a fractional crystallization in which the most crystalline material deposits first and material of decreased crystallinity deposits in sequential layers as the solution is cooled. Separation of the polymer by crystallinity is then carried out by continuously eluting the column with a solvent such as xylene at a controlled flow rate and with an increasing temperature profile. Separation is based on the temperature at which the polymer melts and dissolves into the solvent. The TREF process is a valuable analytical tool for determining short chain branching distribution. However, like any liquid solvent-crystalline polymer technique, the quantity of material that may be fractionated is limited by the labor-intensive recovery of each fraction of polymer from the dilute, liquid solution.

With CITREF the operating pressure must be chosen sufficiently high to insure solubility of the entire polymer sample when it melts. If the pressure is too low, it will not be possible to dissolve the chains of high molecular weight, therefore a molecular weight fractionation will be superimposed onto the CITREF process.

Table 9.3 shows step one of the double fractionation of LLDPE carried out with propane at 130°C. The increasing pressure profile began at ~250 bar (3,600 psia) and increased to 675 bar (9,800 psia) in increments of ~25 bar. The parent LLDPE with a polydispersity of 5.0 has been separated into fractions with a molecular weight range from about 10,000 to 200,000 and polydispersities of 1.2 to 1.6. There is only a weak dependence of enthalpy of fusion ( $\Delta H^{fusion}$ ) and peak melting temperature on molecular weight. The results are consistent with the notion that molecular weight is the dominant factor in liquid-gas equilibrium. The  $\Delta H^{fusion}$  values, which reflect the crystallinity of

**Table 9.4** Properties of the Fractions of LLDPE Obtained by Isobaric, Increasing Temperature Profiling at a Fixed Pressure of 656 Bar

Fraction	Temperature	Parent (wt%)	Peak $T_{melt}$ (°C)	$\Delta H^{fusion}$ (J/g)	$M_w$	$M_w/M_n$
	Range (°C)					
1	50–60	3.9	71.2	9.1	43,900	5.3
2	60–72	4.5	84.8	48.0	25,100	1.9
3	72–77	3.9	91.6	53.9	33,300	2.0
4	77–82	5.8	96.0	59.7	30,300	2.2
5	82–86	6.1	103.2	71.4	41,100	2.5
6	86–90	6.5	104.6	65.4	57,900	1.8
7	90–93	9.4	107.4	86.8	69,900	1.7
8	93–97	7.1	107.4	76.2	73,100	1.9
9	97–100	8.7	113.9	106.9	80,200	1.9
10	100–102	7.4	112.3	87.5	86,300	1.9
11	102–105	8.7	117.4	108.6	75,400	2.1
12	105–108	9.4	120.3	117.4	101,100	1.5
13	108–110	7.8	122.0	106.5	114,100	2.2
14	110+	10.7	125.6	115.9	221,600	3.0
		Parent	123.1	113.3	106,000	5.0

each fraction, indicate that the fractionation was not selective with respect to structure, which also suggests that structure is of secondary importance in determining liquid–gas behavior (Hasch et al., 1992).

Table 9.4 shows the CITREF step of the double fractionation. The data in this table clearly demonstrate a strong dependence of peak melting temperature of a fraction on the extraction temperature and a strong trend of increasing heat of fusion with increasing extraction temperature. In contrast, the molecular weight is weakly dependent on extraction temperature. Exceptions are found for the low molecular weight material, which dissolves at low temperatures due to the high concentration of chain ends. The results are consistent with the prediction that a fractionation based on structure may be accomplished by taking advantage of the differences in the location of the crystallization surface for fractions exhibiting different crystallizability. Watkins et al. note that the fluctuations in the  $\Delta H^{fusion}$  values in fractions 9 through 14 are indicative of mass transfer difficulties that can occur when fractionating solid material.

When LLDPE solidifies, chains of lower crystallizability can become trapped in the solid formed of chains of higher crystallinity. Therefore, these lower crystalline chains become inaccessible until the more crystalline material surrounding them melts. Watkins et al. (1991) speculate that mass transfer limitations can be eliminated if the entire LLDPE charge is solubilized in the solvent and a descending temperature profile is used to achieve the fractiona-

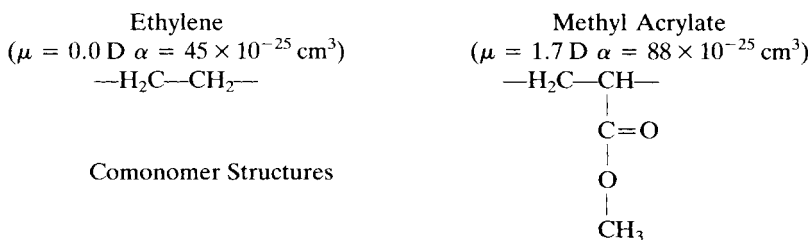
tion. But the anomalies in the data in table 9.4 do not detract from the demonstration of the utility of CITREF in fractionating LLDPE, especially when it is considered that tens of hundreds of grams (rather than milligrams) of polymer can be fractionated by crystallinity.

## FRACTIONATION OF ETHYLENE-BASED COPOLYMERS

McHugh and coworkers describe the fractionation of various poly(ethylene-*co*-methyl acrylate) copolymers using supercritical propane, propylene, 1-butene, and chlorodifluoromethane (Meilchen, Hasch, and McHugh, 1991; Pratt, Lee, and McHugh, 1993). The objective of their work was to extend the work of Krukoniš and coworkers (Scholsky et al., 1987; Watkins and Krukoniš, 1991) who demonstrated the ability of fractionating by chemical composition of the polymer as well as molecular weight. This concept is also described with other polymer-SCF solvent systems in the next few sections of this chapter.

Table 9.5 lists the properties of the four poly(ethylene-*co*-methyl acrylate) copolymers (30, 40, 60, 70 wt% methyl acrylate, EMA<sub>30/70</sub>, EMA<sub>40/60</sub>, EMA<sub>60/40</sub>, EMA<sub>70/30</sub>, respectively). As ethylene repeat units are replaced with methyl acrylate units the copolymer becomes very polar. The size and polarizability of a

**Table 9.5** Structure and Physical Property Information for the Poly(ethylene-*co*-methyl acrylate) Copolymer Fractionated by McHugh and Coworkers (Meilchen, Hasch, and McHugh, 1991; Pratt, Lee, and McHugh, 1993). The Copolymers are Designated EMA<sub>*a/b*</sub> where *a/b* Represent the Weight Percent of Ethylene and Methyl Acrylate in the Backbone, Respectively. The Polarizability is  $\alpha$  and the Dipole Moment,  $\mu$ , is in Units of Debye (D)



Copolymer	Methyl Acrylate (wt%)	$M_w$	$M_n$	$M_w/M_n$	Crystallinity (%)
EMA <sub>70/30</sub>	29.9	123,800	36,400	3.4	12
EMA <sub>60/40</sub>	39.3	140,300	40,500	3.5	4
EMA <sub>40/60</sub>	63.2	108,900	33,000	3.3	0
EMA <sub>30/70</sub>	73.3	110,400	42,000	2.6	0

**Table 9.6** Physical Properties (Reid, Prausnitz, and Poling, 1987) of the Five Solvents Used to Fractionate Poly(ethylene-co-methyl acrylate) copolymers. The Polarizability is  $\alpha$  (Miller and Savchik, 1979), and the Dipole Moment is  $\mu$ 

<i>Solvent</i>	$T_C$ (°C)	$P_C$ (bar)	$\rho_C$ (g/ml)	$\alpha \cdot 10^{25}$ (cm <sup>3</sup> )	$\mu$ (debye)
Propane	96.7	42.5	0.217	62.9	0
Propylene	91.9	46.2	0.236	62.6	0.4
F-22 <sup>a</sup>	96.2	49.7	0.522	61.5	1.5
<i>n</i> -Butane	152.1	38.0	0.228	81.4	0
1-Butene	146.5	39.7	0.236	79.1	0.3

<sup>a</sup>Chlorodifluoromethane.

methyl acrylate repeat unit are much greater than that of an ethylene repeat unit. As methyl acrylate is added to the backbone of polyethylene the percent crystallinity also decreases. All four copolymers have about the same molecular weight and polydispersity.

Table 9.6 lists the physical properties of the candidate SCF solvents used in this study. Propane, propylene, and chlorodifluoromethane (F-22) have similar critical temperatures and pressures but very different densities and polarities. Nonpolar propane will be a good solvent for the high ethylene-content copolymers while propylene will be a moderately good solvent for the acrylate-rich copolymers due to the favorable interaction of the quadrupole moment of propylene with the dipole moment of the acrylate group in the copolymer (Hasch et al., 1992, 1993). F-22 is expected to be an excellent solvent for the high acrylate-content copolymers since F-22 hydrogen bonds to methyl acrylate, but it does not hydrogen bond to itself (Izatt et al., 1983; Uematsu and Franck, 1989; Meilchen, Hasch, and McHugh, 1991; Hasch et al., 1992). Butane and butene, which have higher polarizabilities than the C<sub>3</sub> hydrocarbons, are used in this study since lower pressures should be needed to solubilize the high acrylate-content copolymers than those needed with the C<sub>3</sub> hydrocarbons. Therefore, it will be possible to perform the fractionation without modifying the existing experimental equipment to operate to higher pressures. The difference in the copolymer solubility behavior in butane and butene is expected to be similar to that found with propane and propylene. Cloud point data are presented with the fractionation data to demonstrate how a quick screening study can be used to facilitate the choice of fractionation solvent.

The fractionation and phase behavior data are presented in order of increasing polarity of the copolymer starting with EMA<sub>70/30</sub>. The phase behavior of EMA<sub>70/30</sub> in propane and propylene is shown in figure 9.6. The cloud point curves in butane and butene are not shown since they are at such low pressures that it is not possible to effectively fine-tune these solvents during

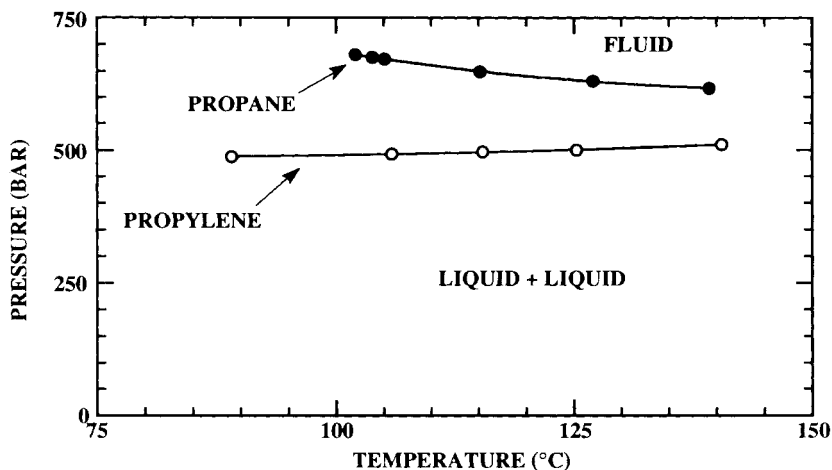


**Figure 9.6** Cloud point curves for EMA<sub>70/30</sub> at 5 wt% in propane and propylene (Hasch et al., 1992).

a fractionation. The cloud point curve in chlorodifluoromethane is also not shown since the parent copolymer is not completely soluble in chlorodifluoromethane. But this is not a negative finding; it suggests that chlorodifluoromethane should be used as the first solvent to remove only the acrylate-rich oligomers from the parent material. If either propane or propylene is used first, the entire parent copolymer could be fractionated since the cloud points are at pressures lower than the highest operating pressure of the equipment (~650 bar).

Fractionation data are shown in table 9.7 for EMA<sub>70/30</sub> fractionated with chlorodifluoromethane followed by propane, both at 151°C. Chlorodifluoromethane is only able to extract ~68% of the copolymer charge to the fractionation columns. The polydispersities of the first seven fractions are about one half that of the parent material even though sample sizes of 1–2 g are obtained at each pressure level. The concentration of methyl acrylate in the backbone of the copolymer is about 4 wt% greater than that in the parent material confirming that chlorodifluoromethane preferentially solubilizes the more polar oligomers.

Fractions 8 through 13 in table 9.7 were obtained with propane. Again the polydispersities of the fractions are less than that of the parent material. The concentration of methyl acrylate in the backbone of the fractions is now about 4 wt% less than that of the parent. Also, notice that molecular weights of the first few fractions obtained with propane are lower than those of the final fractions obtained with chlorodifluoromethane; this indicates that chlorodifluoromethane can remove only fractions rich in acrylate even if the molecular weight is greater than available oligomers that have a higher ethylene content.



**Table 9.7** Fractionation of EMA<sub>70/30</sub> with Chlorodifluoromethane and Propylene at 151°C (Pratt, Lee, and McHugh, 1993)

#	P (bar)	$\Sigma$ wt% <sup>a</sup>	Sample Weight (g)	$M_w$	$M_w/M_n$	MA <sup>b</sup> (wt%)
<i>Chlorodifluoromethane</i>						
1	308	4	0.58	10,500	1.5	32.5
2	375	12	1.09	18,300	1.3	33.5
3	449	28	2.11			33.1
4	482	36	1.09	44,000	1.3	33.6
5	514	47	1.40	50,800	1.3	32.9
6	551	60	1.79	80,400	1.5	31.1
7	588	68	1.02			30.9
<i>Propane</i>						
8	484	70	0.27			26.1
9	507	74	0.57			25.5
10	528	83	1.12	30,700	2.1	26.3
11	558	93	1.32	43,400	2.4	25.2
12	591	99	0.87	43,800	2.2	26.1
13	624	100	0.12	62,100	2.6	25.1
		Parent	13.35	123,800	3.4	29.9

<sup>a</sup>Cumulative amount of copolymer removed from the columns.<sup>b</sup>Methyl acrylate content determined by FTIR.

The phase behavior of EMA<sub>60/40</sub> in propane, propylene, chlorodifluoromethane (F-22) is shown in figure 9.7. In this instance, F-22 completely solubilizes the parent copolymer at very low pressures since this copolymer has a higher acrylate content and is more polar than EMA<sub>70/30</sub>. As a consequence, chlorodifluoromethane should not be used first in the fractionation since it is too good a solvent. The phase behavior data suggest that propane should be used first to remove the ethylene-rich oligomers and that either propylene or F-22 could then be used to remove the rest of the parent material. Propane is not expected to fractionate the entire parent copolymer at temperatures below about 135°C since the pressures needed to obtain a single phase exceed the upper limit of the apparatus. Notice that the solvents become less discriminatory as the temperature increases above about 135°C, where polar interactions between two acrylate segments in the copolymer and between a polar solvent molecule and an acrylate segment are expected to decrease, as described in chapter 5. Hence, the cloud point curves should come closer together in pressure at high temperatures, despite the large differences in solvent polarity noted in table 9.6. It is interesting that the cloud point curves in propane and propylene are significantly different from one another, especially at low

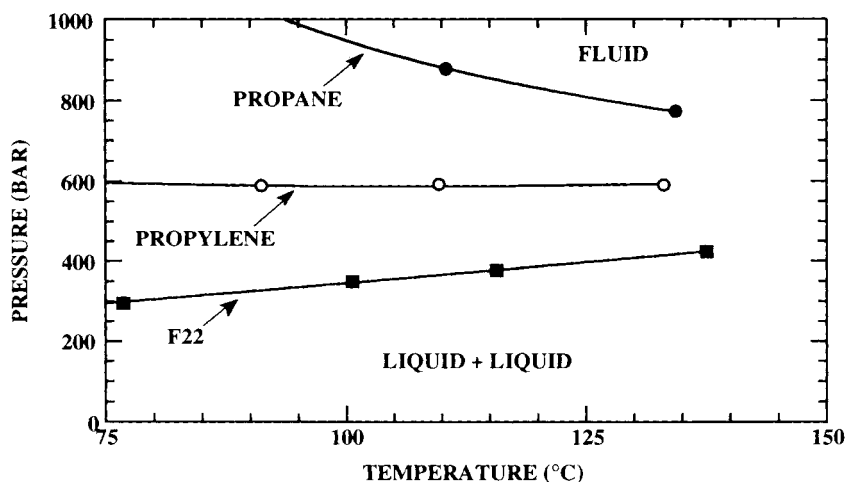


**Figure 9.7** Cloud point curves for EMA<sub>60/40</sub> at 5 wt% in propane, propylene (Hasch et al., 1992), and chlorodifluoromethane (F-22) (Pratt, Lee, and McHugh, 1993).

temperatures where polar forces are expected to be strongest. This difference is attributed to the slight dipole moment in propylene and to the quadrupole moment in propylene that is a result of the unsaturated double bond. Both of these polar moments enhance the interchange energy between a propylene segment and a segment of EMA<sub>60/40</sub> as described in chapter 5.

Fractionation data are shown in table 9.8 for EMA<sub>60/40</sub> fractionated with propane first and then with propylene at 130°C. Propane is only able to extract ~31% of the copolymer charged to the fractionation columns. The polydispersities of the first six fractions are less than that of the parent material and the concentration of methyl acrylate in the backbone of the fractions is only about 0.5 wt% less than that of the parent material.

Fractions 7 through 13 in table 9.8 were obtained with propylene. Again the polydispersities of the fractions are much less than that of the parent material. The concentration of methyl acrylate in the backbone of the fractions is about 3.7 wt% greater than that of the parent. And the molecular weight of the first fraction obtained with propylene is lower than that of the final fraction obtained with propane, indicating that propane can only remove fractions that are lean in acrylate even if the molecular weight is greater than available oligomers that have a higher acrylate content.

EMA<sub>60/40</sub> was also fractionated with F-22 to confirm that chlorodifluoromethane is too good a solvent for this copolymer; the results are given in table 9.9. Using very small pressure increments, fourteen fractions were obtained with modest polydispersities. No discernible trend was detected with the backbone composition of the fractions indicating that F-22 was only able to discriminate on the basis of molecular weight and not on the basis of

**Table 9.8** Fractionation of EMA<sub>60/40</sub> with Propane and Propylene at 130°C (Pratt, Lee, and McHugh, 1993)

#	P (bar)	Σ wt% <sup>b</sup>	Sample Weight (g)	M <sub>w</sub>	M <sub>w</sub> /M <sub>n</sub>	MA <sup>b</sup> (wt%)
<i>Propane</i>						
1	449	1	0.26	14,400	2.6	38.7
2	488	5	0.57	20,400	2.3	38.2
3	524	9	0.87	27,800	2.1	38.7
4	552	14	0.90	31,200	2.0	38.5
5	587	21	1.22	41,100	1.7	
6	624	31	1.86	52,800	1.5	39.7
<i>Propylene</i>						
7	449	33	0.29	46,400	1.7	41.6
8	484	36	0.61	73,500	1.5	45.0
9	507	47	2.00	88,500	1.4	
10	528	60	2.23	127,800	1.7	42.9
11	558	80	3.70	202,900	1.8	42.7
12	591	91	1.89	334,300	2.1	
13	624	94	0.67			42.9
		Parent	18.11	140,300	3.5	39.3

<sup>a</sup>Methyl acrylate content determined by NMR.<sup>b</sup>Cumulative amount of copolymer removed from the columns.

composition. The fractionation and cloud point data both highlight the impact of hydrogen bonding on the fractionation behavior. The solubility of the high-acrylate oligomers in propane was reduced by decreasing the operating temperature. Consequently it was possible to fractionate by both chemical composition and molecular weight with propane. With F-22 this was not possible, presumably because hydrogen bonding between the solvent and the acrylate groups was too strong even at 150°C. F-22 is indeed a high-quality solvent for this copolymer even at modest pressures of less than 500 bar. This is in contrast to the previous case, where F-22 was not capable of dissolving the parent material that had only 10 wt% less acrylate groups.

The phase behavior of EMA<sub>40/60</sub> in propane, butane, propylene, 1-butene, and chlorodifluoromethane (F-22) is shown in figure 9.8. The pressure and temperature axes are expanded in this instance to include cloud point data for EMA<sub>40/60</sub> in butane and 1-butene. The propane cloud point curve is shifted to slightly higher temperatures than the butane curve because of the meager solvent power of propane. The cloud point curves in both of the saturated hydrocarbons rise very steeply in pressure for small change in temperature in the range 130–175°C. Evidently, the polar polymer–polymer interactions are highly favored as the temperature decreases and polar interactions increase.

**Table 9.9** Fractionation of EMA<sub>60/40</sub> with Chlorodifluoromethane at 150°C (Pratt, Lee, and McHugh, 1993)

#	<i>P</i> (bar)	Σ wt% <sup>b</sup>	Sample Weight (g)	<i>M<sub>w</sub></i>	<i>M<sub>w</sub>/M<sub>n</sub></i>	MA <sup>a</sup> (wt%)
1	137	1	0.15	1,100	1.4	
2	171	2	0.15	3,300	1.7	
3	205	4	0.28	5,900	1.5	
4	241	7	0.34	7,800	1.5	
5	274	10	0.50	10,000	1.7	
6	309	17	0.90	26,500	1.5	45.3
7	330	28	1.48	32,400	1.5	40.4
8	343	36	1.11	47,100	1.5	40.4
9	364	46	1.33	58,200	1.4	42.7
10	385	58	1.55	78,100	1.5	44.1
11	406	75	2.31	105,600	1.5	40.8
12	424	83	1.11	162,500	2.5	41.1
13	446	94	1.45	239,100	1.7	42.3
14	470	100	0.87	513,700	1.5	43.4
		Parent	13.53	140,300	3.5	39.3

<sup>a</sup>Methyl acrylate content determined by FTIR.

<sup>b</sup>Cumulative amount of copolymer removed from the columns.

Samples 6 through 13 and the parent material had an average crystallinity of 3.6%.

The cloud point curves in the unsaturated hydrocarbons increase in pressure with decreasing temperature much less radically. And the impact of hydrogen bonding is evident with the F-22 cloud point curve, which is situated at very low pressures.

It is impractical to use propane to fractionate EMA<sub>40/60</sub> since the pressures needed to obtain a single phase are more than 1,000 bar greater than the highest operating pressure obtainable with the fractionation equipment. The two solvents chosen for fractionating EMA<sub>40/60</sub> are butane at 139°C and 1-butene at 118°C. Although both operating temperatures are below the critical temperature of the respective solvents, a good fractionation can be obtained since these two near-critical solvents are still highly compressible. Also, in the temperature range 115–140°C the respective cloud point curves are at very different pressures, suggesting that it may be possible to remove the ethylene-rich oligomers with butane and the acrylate-rich oligomers with butene.

Fractionation data are shown in table 9.10 for EMA<sub>40/60</sub> fractionated with butane first and then with 1-butene. Butane extracts ~21% of the copolymer charged to the columns. The polydispersities of the first six fractions are less than one half that of the parent material, although the concentration of methyl acrylate in the backbone of the copolymer for these fractions is essentially the same as that of the parent material.

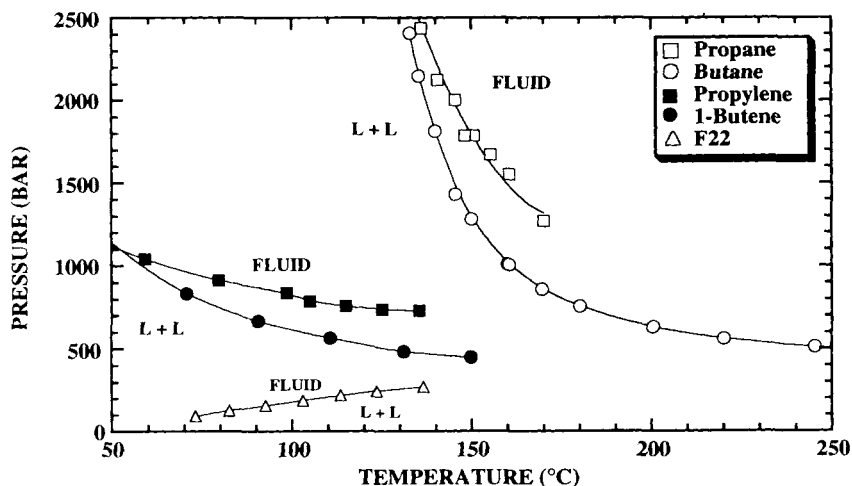


**Figure 9.8** Cloud point curves for EMA<sub>40/60</sub> at 5 wt% in propane, butane, propylene, 1-butene, and chlorodifluoromethane (F-22) (Hasch et al., 1992; Pratt, Lee, and McHugh, 1993).

Fractions 7 through 14 in table 9.10 were obtained with 1-butene at 118°C, a subcritical temperature. Again, the polydispersities of the fractions are much less than that of the parent material and the concentration of methyl acrylate in the backbone of the copolymer is essentially the same as that of the parent material. And the molecular weight of fraction 7 obtained with 1-butene is slightly greater than the final fraction obtained with butane, indicating that butane does not discriminate by chemical composition. This lack of chemical discrimination was somewhat surprising since the shape and location of the butane cloud point curve in  $P$ - $T$  space suggests that highly polar EMA oligomers should not be readily dissolved at 139°C.

The phase behavior of EMA<sub>30/70</sub> in propylene, 1-butene, butane, and chlorodifluoromethane (F-22) is shown in figure 9.9. At low temperatures the cloud point curve for butene is at higher pressures than that for propylene, while at higher temperatures the opposite behavior is observed. This shift in the two cloud point curves is probably a consequence of the smaller quadrupole per unit volume in butene, making it a less effective solvent at low temperatures even though it has a higher polarizability than propylene. At higher temperatures, where polar interactions are expected to be diminished, the butene curve is now at pressures below that of the propylene curve. The cloud point curve for F-22, an excellent solvent for EMA<sub>30/70</sub>, is at very low pressures, making it an unattractive fractionation solvent in this instance. The enhanced solvent power of F-22 relative to butene, the physically larger solvent, is attributed to the hydrogen bonding between F-22 and EMA<sub>30/70</sub>. For this fractionation propylene will be used first followed by butene.

**Table 9.10** Fractionation of EMA<sub>40/60</sub> with Butane and 1-Butene at Subcritical Temperatures (Pratt, Lee, and McHugh, 1993)

#	P (bar)	$\Sigma$ wt% <sup>b</sup>	Sample Weight (g)	$M_w$	$M_w/M_n$	MA <sup>a</sup> (wt%)
<i>Butane at 139°C</i>						
1	382	4	0.79	19,600	1.4	61.7
2	414	6	0.52	22,600	1.3	63.4
3	448	9	0.56	28,600	1.4	62.4
4	500	13	0.87	35,500	1.3	61.9
5	561	16	0.43	54,500	1.6	61.4
6	637	21	1.07	51,000	1.3	62.5
<i>1-Butene at 118°C</i>						
7	276	24	0.74	53,000	1.2	62.0
8	310	31	1.38	68,900	1.4	61.9
9	337	40	1.86	68,800	1.2	62.0
10	368	50	2.09	87,300	1.2	61.8
11	396	66	3.16	112,100	1.2	61.9
12	430	81	3.07	152,700	1.2	61.7
13	465	91	1.97	178,200	1.2	
14	521	100	1.92	277,900	1.3	
		Parent	20.44	108,900	3.3	63.2

<sup>a</sup>Methyl acrylate content determined by NMR.

<sup>b</sup>Cumulative amount of copolymer removed from the columns.

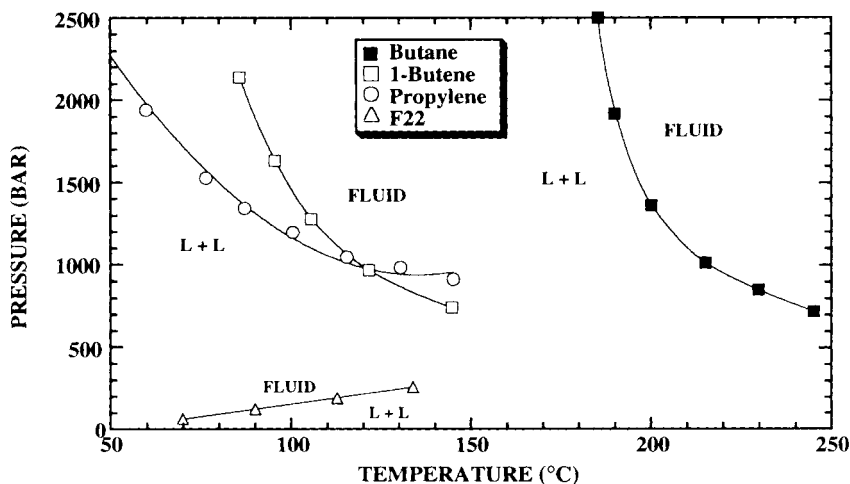


**Figure 9.9** Cloud point curves for EMA<sub>30/70</sub> at 6wt% in propylene, 1-butene, butane, and chlorodifluoromethane (F-22) (Hasch et al., 1992; Pratt, Lee, and McHugh, 1993).

**Table 9.11** Fractionation of EMA<sub>30/70</sub> with Propylene at 137°C and with 1-Butene at 157°C (Pratt, Lee, and McHugh, 1993)

#	<i>P</i> (bar)	Σ wt% <sup>b</sup>	Sample Weight (g)	<i>M<sub>w</sub></i>	<i>M<sub>w</sub>/M<sub>n</sub></i>	MA <sup>a</sup> (wt%)
<i>Propylene at 137°C</i>						
1	482	2	0.34	9,600	2.3	
2	518	3	0.37	11,600	1.7	71.7
3	553	5	0.36	15,300	1.7	71.8
4	588	7	0.42	18,500	1.5	
5	622	9	0.40	21,900	1.4	
6	656	11	0.60	26,200	1.3	
<i>1-Butene at 157°C</i>						
7	244	15	0.84			
8	277	16	0.14			
9	344	18	0.46	38,900	1.5	
10	415	26	1.84	46,300	1.4	73.9
11	450	34	1.60	55,300	1.3	
12	485	48	3.16	68,100	1.3	73.3
13	506	59	2.36	82,900	1.3	
14	527	66	1.60	102,500	1.3	72.3
15	548	73	1.63	114,100	1.3	
16	579	84	2.36	142,400	1.3	72.0
17	621	96	2.54	173,900	1.3	
18	653	100	0.96	247,400	1.3	
		Parent	21.92	110,400	2.6	73.3

<sup>a</sup>Methyl acrylate content determined by NMR.<sup>b</sup>Cumulative amount of copolymer removed from the columns.

Table 9.11 shows the results for EMA<sub>30/70</sub> fractionated with propylene at 137°C then with 1-butene at 157°C. Propylene, to a pressure of 650 bar, is only able to extract ~11% of the copolymer charged to the columns. The polydispersities of the first six fractions are quite modest, although the concentration of methyl acrylate in the backbone of the copolymer for these fractions is essentially the same as that of the parent material. Evidently, the high acrylate content of this copolymer makes the high molecular weight oligomers essentially insoluble in propylene at pressures to ~650 bar. This solubility behavior is not entirely unexpected since the cloud point pressure of EMA<sub>30/70</sub> in propylene at this temperature is greater than the operating pressure of the fractionation apparatus.

Table 9.11 shows that fractions 7 through 18, obtained with 1-butene, have small polydispersities and essentially the same concentration of methyl acrylate in the backbone of the copolymer as that of the parent material. One plausible

**Table 9.12** Proportions of the Four Copolymers Used to Make EMA<sub>44/56</sub> (Pratt, Lee, and McHugh, 1993)

Parent Polymer	Weight (g)
EMA <sub>70/30</sub>	1.03
EMA <sub>60/40</sub>	9.06
EMA <sub>40/60</sub>	6.92
EMA <sub>30/70</sub>	6.87

explanation for the poor fractionation with respect to chemical composition in this case is that the parent EMA<sub>30/70</sub> has a narrow chemical composition distribution and it is not possible to fractionate it any further. Based on the results reported in table 9.9 for EMA<sub>60/40</sub>, the chemical composition distribution for EMA<sub>30/70</sub> need only be less than about  $\pm 2$  wt%.

To test the efficacy of fractionating with respect to chemical composition, all four copolymers were thoroughly mixed together to produce an artificial mixture of 44 wt% ethylene and 56 wt% methyl acrylate (EMA<sub>44/56</sub>, see table 9.12) and fractionated, in order, with propane at 132°C, butane at 147°C, propylene at 147°C, and 1-butene at 157°C. The results of this fractionation are shown in table 9.13. The values for the glass transition temperature ( $T_g$ ) and the percent crystallinity of each fraction shown in table 9.13 correlate quite well with the Fourier transform infrared (FT-IR) determination of the acrylate content in the copolymer. As the acrylate content increases  $T_g$  increases as expected since the  $T_g$  of poly(methyl acrylate) is  $\sim 0^\circ\text{C}$ . The percent crystallinity decreases rapidly with increasing acrylate content in the backbone as the acrylate groups disrupt the regular ethylene structure that would facilitate crystallization. Based on mass balance considerations and on the chemical composition analyses, propane has extracted all of EMA<sub>70/30</sub> and about half of the available EMA<sub>60/40</sub>. With butane, fractions 6 through 9 are much larger than fractions 10 through 13, even though the pressure is continuously increasing and the solvent power of butane is also increasing. Based on the previously described cloud point data and on the amount of material in fractions 6 through 13, butane has removed the rest of EMA<sub>60/40</sub> and about 2 g of EMA<sub>40/60</sub>.

Propylene is able to extract another 2.28 g of oligomers rich in EMA<sub>40/60</sub>, but low in molecular weight. Based on the composition of the starting material there should be approximately 2.4 g of EMA<sub>40/60</sub> left in the columns. The molecular weights of the fractions obtained with butene increase up to fraction 18, decrease for fraction 19, then increase again with increasing pressure. The gel permeation chromatogram (GPC) of fraction 18 reveals a small shoulder on the low molecular weight side of the GPC trace. The concentration of acrylate



**Table 9.13** Fractionation of EMA<sub>44/56</sub> (Pratt, Lee, and McHugh, 1993)

#	<i>P</i> (bar)	$\Sigma$ wt% <sup>b</sup>	Sample Weight (g)	$M_w$	$M_w/M_n$	MA <sup>a</sup> (wt%)	$T_g$ (°C)	Crystallinity (%)
<i>Propane at 132°C</i>								
1	408	2	0.44	12,200	1.7	40.7		
2	475	5	0.73	17,800	1.7	41.9	−38.8	8.8
3	548	9	1.09	20,600	2.2	42.5	−36.6	11.2
4	606	15	1.27	37,600	2.2		−34.5	11.8
5	659	22	1.71	50,100	2.9	40.6	−33.9	11.2
<i>Butane at 147°C</i>								
6	323	25	0.77	60,500	2.5	44.7	−34.1	8.7
7	379	32	1.72	113,300	3.3	42.1	−32.6	9.2
8	416	39	1.70	172,000	4.1	43.4	−32.4	8.2
9	452	44	1.09	76,700 <sup>d</sup>	4.9	44.4	−31.0	6.7
10	481	46	0.56	53,500 <sup>d</sup>	4.9	49.8	−30.9	5.9
11	535	48	0.43	47,100 <sup>d</sup>	6.7	53.1	−27.3	5.2
12	591	49	0.34	37,800	3.8		−27.6	2.9
13	660	51	0.44	42,012	2.2		−27.4	1.7
<i>Propylene at 147°C</i>								
14	652	61	2.28	39,900	2.0	68.9	−26.8	0.6
<i>1-Butene at 157°C</i>								
15	346	63	0.51	66,400	1.6		−31.1	0.1
16	396	69	1.50	83,200	1.8	66.3	−27.5	0.5
17	438	79	2.39	103,000	2.7	65.2	−27.1	0.0
18	465	83	0.92	116,500 <sup>d</sup>	2.8		−25.3	0.0
19	523	87	0.93	93,900	1.6	72.3	−19.7	0.0
20	589	93	1.39	127,800	1.5	71.8	−18.1	0.0
21	652	100	1.69	201,200	1.8	69.5	−16.6	0.5
		Parent	23.96	58,200	4.0	57.6 <sup>c,e</sup>		

<sup>a</sup>Methyl acrylate content determined by FTIR.<sup>b</sup>Cumulative amount of copolymer removed from the columns.<sup>c</sup>Calculated from a material balance of starting polymers.<sup>d</sup>Binodal chromatogram.<sup>e</sup>Three values of  $T_{gm}$  were found: −33.8°C, −26.8°C, and −18.1°C.

in the backbone of the oligomers increases steadily in butene. The behavior of the molecular weight and the chemical composition of the fractions in butene shows conclusively that butene first dissolves the oligomers with the lower acrylate content even if the molecular weights of these oligomers are higher than those with the higher acrylate content.

## **POLYSILOXANE AND POLYSILOXANE/PMMA COPOLYMER FRACTIONATION**

Starting in 1986 Phasex Corporation and Virginia Polytechnic Institute and State University (Virginia Tech) collaborated on a three-year National Science Foundation-funded program to investigate the application of supercritical fluids to purify and fractionate a wide variety of polymers synthesized and studied by researchers at Virginia Tech (Gallagher and Krukons, 1993). The NSF program with Virginia Tech was a multifaceted project that involved several areas of polymer synthesis, separation, and analysis of star and graft copolymers, linear and cyclic siloxane macromonomers, and  $\alpha,\omega$ -aminopropyl-terminated polysiloxanes. The collaborative effort involved synthesis of polymers at Virginia Tech by Professor J. E. McGrath and his students and extraction/fractionation with supercritical fluids at Phasex. Detailed characterization of these novel polymers was possible since reasonably large discrete fractions of varied molecular weight and/or chemical composition were obtained (Smith et al., 1987; Elsbernd et al., 1987, 1990a, 1990b, 1991; DeSimone et al., 1988a, 1988b, 1989, 1990). In this section only two types of polymers are described from this extensive study: graft copolymers of polymethylmethacrylate (PMMA) and polysiloxanes and  $\alpha,\omega$ -aminopropyl-terminated polysiloxanes.

### **Poly(methylmethacrylate)-g-Poly(dimethylsiloxane) (PMMA-g-PDMS) Fractionation**

Supercritical fluids were used to fractionate the graft copolymers synthesized at Virginia Tech. The goal was to obtain fractions that could be analyzed for their chemical composition distribution (CCD)—the weight ratio of PDMS grafts to PMMA backbone. The ultimate objective of the research was to evaluate and compare the CCD of the copolymers made by free-radical, anionic, and group transfer polymerization (GTP) techniques. Although classical liquid antisolvent fractionation can be used to determine the CCD, it is extremely time-consuming and laborious, and it produces only very small amounts of material. SCF fractionation was found to be a relatively simple and versatile method for fractionating the graft copolymers and ten to hundred gram quantities of material could be processed. Supercritical chlorodifluoromethane was used to fractionate the PMMA-g-PDMS copolymers produced in the NSF study (DeSimone et al., 1988a, 1988b). Before describing the fractionation, we provide some background on the synthesis of the PMMA-g-PDMS copolymers.

The anionic and group transfer polymerizations used for this study are “living” polymerization techniques that typically produce copolymers having very narrow molecular weight distributions, whereas copolymers produced by a

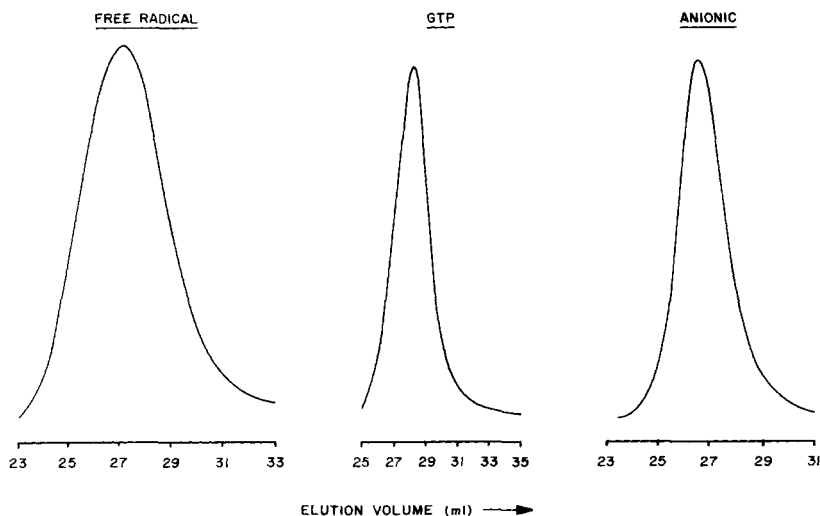
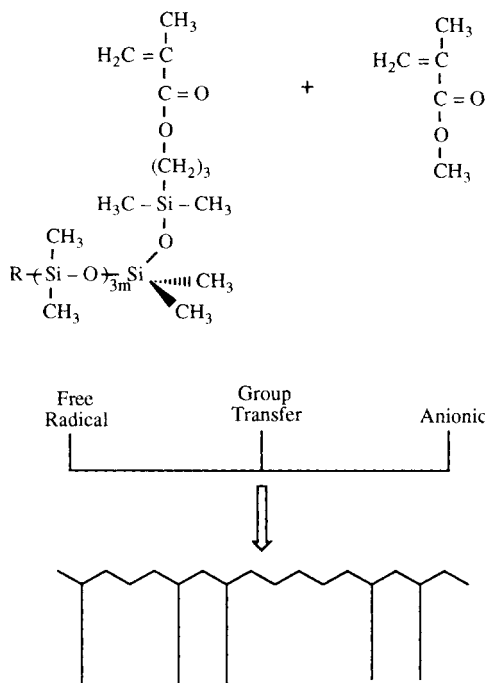


**Figure 9.10** Comparison of typical gel permeation chromatograms of PMMA-g-PDMS copolymers produced by various methods (DeSimone et al., 1988b).

free-radical mechanism tend to have a much broader distribution. Figure 9.10 (DeSimone et al., 1988b) compares the gel permeation chromatograms of the PMMA-g-PDMS produced by the three respective methods. Each copolymerization was carried out using the Macromer<sup>®</sup> (Milkovich, 1981) technique. A polymer with a functional (polymerizable) end, called the macromonomer, is reacted in the mixture. In the PMMA-g-PDMS case, a PDMS polymer tail with a methacryloxy head is incorporated as branches along the PMMA backbone by reacting the methyl methacrylate monomer and the methacryloxy-terminated PDMS macromonomer.

A simplified scheme outlining the Macromer<sup>®</sup> method is given in scheme 9.1. The molecular weight and polydispersity of the PDMS macromonomers can be closely controlled for subsequent production of well-defined graft copolymers of PMMA-g-PDMS. The choice of a methacryloxy end group, rather than a styrenic or other functionality for terminating the PDMS macromonomers is not an arbitrary one. For living polymerization techniques, the most useful way of obtaining a statistical copolymerization is to use a macromonomer whose end group closely emulates the low molar mass monomer, thereby eliminating any conversional heterogeneities that can arise due to differences in reactivity between the functional end group and the monomer.

The distribution in chemical composition (CCD) of the copolymers can be expressed as the distribution of the amounts of respective monomeric units (Elias, 1984). In simple terms, the CCD of a graft copolymer describes the relation between the number of grafts per backbone, the molecular weight of

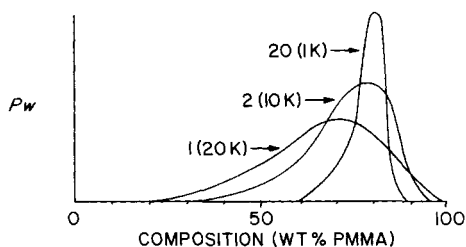


**Scheme 9.1** General schematic of the synthesis of PMMA-g-PDMS copolymers using the Macromer® technique (DeSimone et al., 1990).

the grafts, and the overall copolymer molecular weight. A CCD arises due to chemical heterogeneities; two types are found for statistical copolymers (Glockner et al., 1984): conversional heterogeneity (Meyer and Lowry, 1965) and statistical heterogeneity (Stockmayer, 1945). Stejskal and Kratochvil (1989) have shown that the CCD developed as a result of conversional heterogeneity is not affected by the molar mass and molar mass distribution of the macromonomer. But in this case, the CCD is dependent on the relative reactivities of the monomer and the functional end group of the macromonomer. By choosing a reactive end group that is chemically similar to the monomer, the influence of conversional heterogeneity on the CCD can be minimized or eliminated.

Statistical heterogeneity, which can also give rise to a CCD in the copolymer, originates from the statistics of copolymerization (Stockmayer, 1945). The statistical heterogeneity quickly approaches zero with increasing degree of polymerization for copolymerization of monomers with roughly the same molar mass (Stockmayer, 1945). However, synthesis of copolymers using the macromonomer technique results in a significantly broader CCD compared to that observed for the copolymerization of conventional low molar mass monomers (Stejskal and Kratochvil, 1987). For example, there is statistical heterogeneity even for the case of a methyl methacrylate monomer and a PMMA macromonomer.

**Figure 9.11** Theoretical chemical composition distribution (CCD) profiles for PMMA-g-PDMS copolymers with various graft molecular weights at constant composition (Podesva et al., 1987).



While the chemical heterogeneity of copolymers containing monomers having equivalent molecular weights can be evaluated by the Stockmayer equations (Stockmayer, 1945), they do not apply for copolymers in which the components of the copolymerization have widely different molecular weights. Stejskal and Kratochvil (1982, 1987) have modified Stockmayer's equations to account for situations that arise for PMMA-g-PDMS prepared using the macromonomer technique. Their model predicts that the CCD narrows as the number of grafts is increased at a constant weight percent macromonomer in the reaction mixture and with random incorporation of the macromonomer along the backbone. Figure 9.11 depicts the theoretical prediction (Podesva et al., 1987) and the sample calculation beneath the figure clarifies the origin of each curve. Additionally, copolymers prepared by the macromonomer technique are expected to display a CCD that is a function of the molecular weight of the macromonomer as well as the number of grafts per backbone (Stejskal et al., 1987).

#### *Sample Calculation*

$$M_w = 100,000 \text{ g/mol}$$

$$20 \text{ wt\% PDMS-80\% PMMA}$$

If macromonomer  $M_w = 1,000 \text{ g/mol}$

$$\frac{20,000}{1,000} = 20 \text{ grafts/backbone}$$

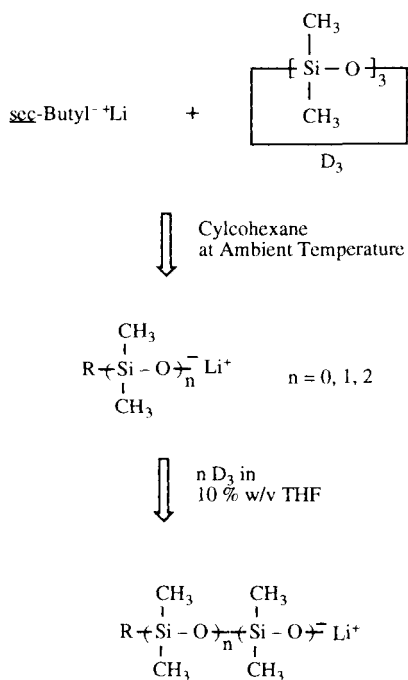
If macromonomer  $M_w = 10,000 \text{ g/mol}$

$$\frac{20,000}{10,000} = 2 \text{ grafts/backbone}$$

If macromonomer  $M_w = 20,000 \text{ g/mol}$

$$\frac{20,000}{20,000} = 1 \text{ graft/backbone}$$

The polydispersity of the PDMS macromonomer is dependent upon the reactants and the polymerization process employed. The macromonomers of



**Scheme 9.2** General schematic of the anionic ring-opening polymerization of  $\text{D}_3$  (Hellstern, 1989).

methacryloxy-terminated PDMS for the Virginia Tech studies were produced using living anionic ring-opening polymerization of hexamethylcyclotrisiloxane ( $\text{D}_3$ ), shown in scheme 9.2. Polymerization of  $\text{D}_3$  yielded monofunctional macromonomers of controlled molecular weight and very narrow molecular weight distributions (Hellstern, 1989) depicted in figure 9.12. In contrast, preparation of PDMS macromonomers using octamethylcyclotetrasiloxane ( $\text{D}_4$ ) with a potassium siloxanolate catalyst results in the formation of an equilibrium mixture of cyclic species and  $\alpha, \omega$  difunctionally terminated macromonomer. Use of the strained cyclic monomer, hexamethylcyclotrisiloxane, with *sec*-butyllithium in cyclohexanone as the initiator for the ring opening polymerization of  $\text{D}_3$ , produces extremely well-defined macromonomers with respect to molecular weight and functionality since the initiation occurs very rapidly relative to propagation. Interestingly, use of  $\text{D}_4$  with the same initiator can produce monofunctionally terminated macromonomer but the molecular weight distribution is quite broad and cyclic species will also form. This is because the ring is not very strained, therefore initiation does not occur essentially all at once.

After synthesis, the methacryloxy-terminated PDMS macromonomers were purified, and the macromonomers were copolymerized with methyl methacrylate using free-radical, anionic, and group transfer polymerization. Detailed descriptions of the polymerization are provided by DeSimone (1990) and Hellstern (1989). In addition to well-defined graft copolymers, there is

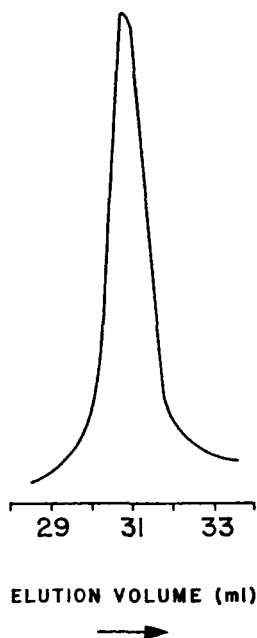


**Figure 9.12** Gel permeation chromatogram of polydimethylsiloxane macromonomer prepared by anionic ring opening polymerization of  $D_3$  (Hellstern, 1989).

always some unincorporated PDMS macromonomer in the product mixture. These unreacted PDMS grafts can be removed from the mixture by simple solvent extraction. This extraction step is necessary prior to characterizing the copolymer. Figure 9.13 (Hellstern, 1989) shows two gel permeation chromatograms of the PMMA-g-PDMS copolymer prepared anionically using the macromonomer technique. Figure 9.13a is a chromatogram of the parent copolymer and figure 9.13b is a chromatogram of a sample of copolymer after Soxhlet extraction with hexane. For comparison with the Soxhlet extraction technique of purifying the copolymer, a sample of copolymer was stripped of its residual PDMS macromonomer using supercritical carbon dioxide at 60°C and 340 bar. The chromatograms of the parent and stripped copolymers are shown in figure 9.14 (Hellstern, 1989). The effectiveness of the supercritical extraction is evident since unincorporated PDMS macromonomer is not present in the extracted sample. There was still a small amount of unincorporated PDMS remaining after hexane extraction but not enough to show up as a peak on the chromatogram. This residual PDMS macromonomer can be extracted with supercritical carbon dioxide (see later).

To confirm Stejskal and Kratochvil's theories of chemical composition distribution, graft copolymers of methyl methacrylate (MMA) and MMA-terminated PDMS were first synthesized by free-radical procedures by the Virginia Tech researchers. Any unincorporated PDMS macromonomer was then stripped with supercritical carbon dioxide and finally the polymer was

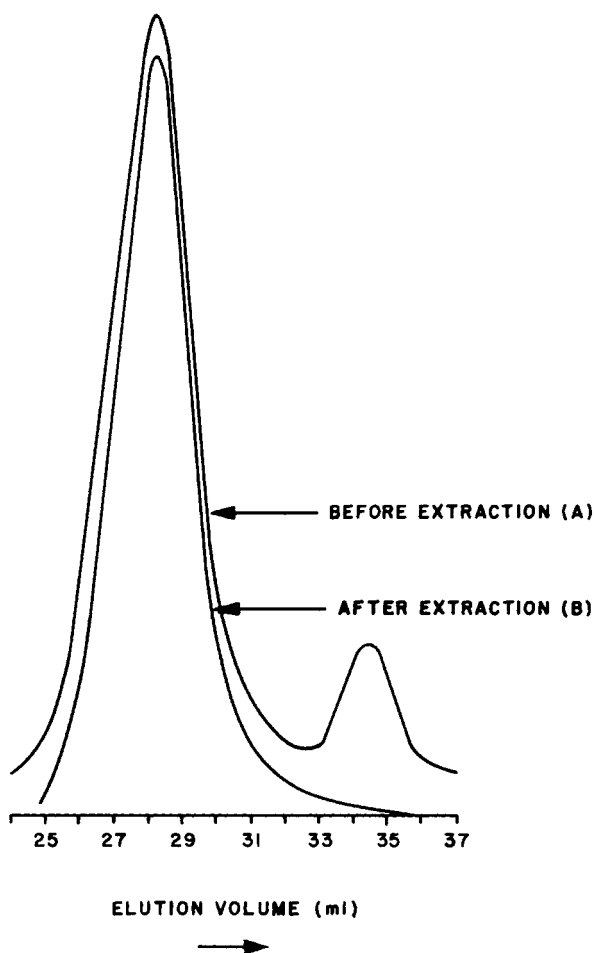


**Figure 9.13** Gel permeation chromatogram of anionically prepared PMMA-g-PDMS copolymer: (A) parent copolymer as prepared and (B) parent copolymer after Soxhlet extraction with hexane (Hellstern, 1989).

fractionated with chlorodifluoromethane at 120°C using an isothermal increasing pressure profile up to a maximum pressure of 400 bar. For each graft copolymer in the comparative series, the average molecular weight of the graft was 10,000, but the ratio of MMA monomer to PDMS macromonomer was varied to obtain different numbers of grafts per backbone over a range of 13 wt% to 45 wt% PDMS. Isorefractive light scattering techniques were used to determine the weight average molecular weight of the backbone prior to fractionation, and the individual fractions were characterized using  $^1\text{H-NMR}$  to determine the backbone/graft composition.

The results of a set of three graft copolymers produced by free radical polymerization are shown in figure 9.15 (DeSimone et al., 1988b). The points on the curves represent the composition of the fractions obtained by supercritical chlorodifluoromethane fractionation of the parent copolymer. The



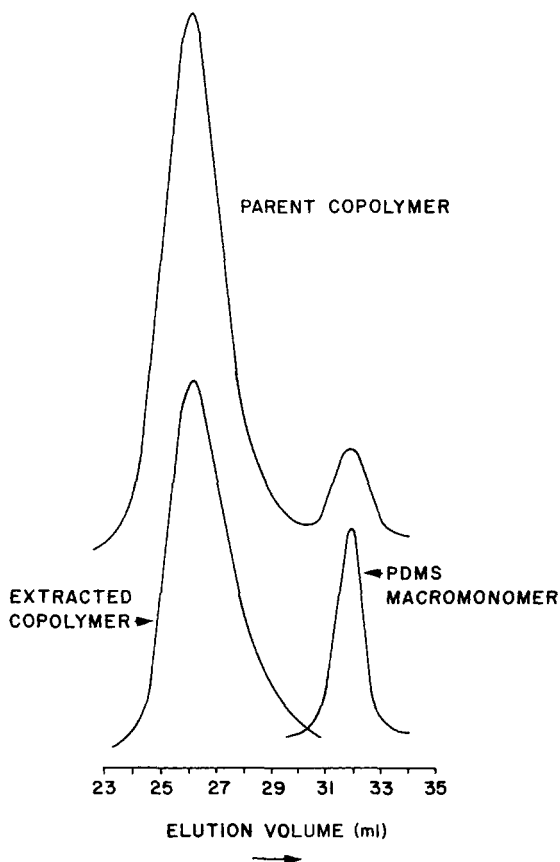
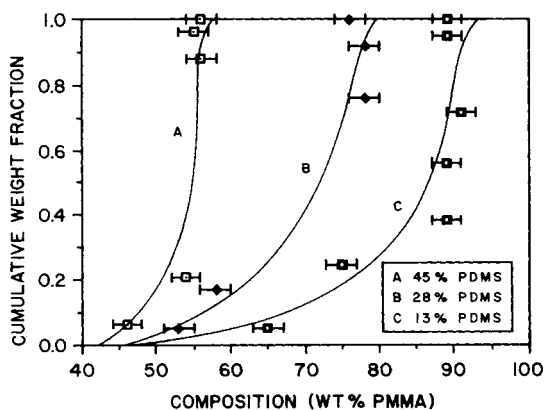


**Figure 9.14** Gel permeation chromatograms of PMMA-g-PDMS copolymer before and after extraction with supercritical carbon dioxide. GPC trace of extract (PDMS macromonomer) is shown, too (Hellstern, 1989).

overall profiles show the progression of composition for the cumulative weight fractions. The CCD profiles correlate well with the predicted theory; as the number of PDMS grafts per backbone of the parent polymer increases, the breadth of the chemical composition distribution becomes much narrower. For example, with 10,000 molecular weight grafts, there are more grafts per backbone for the 45% PDMS copolymer than for 28% or 13% PDMS composition.

Two PMMA-g-PDMS copolymers were also prepared with roughly similar composition (20 wt% and 26 wt% PDMS) and with the same molecular weight PDMS grafts ( $M_n = 10,000$ ) by free radical polymerization and by anionic polymerization. The copolymers were first extracted of any unincorporated methacryloxy-terminated PDMS using supercritical carbon dioxide then they were fractionated with supercritical chlorodifluoromethane. Each fraction was characterized in the same manner as described for the three polymers depicted in figure 9.15; and the results are shown in figure 9.16 (DeSimone et al., 1990). The differences in chemical composition distribution profiles of the copolymers

**Figure 9.15** Experimentally determined CCD profiles for PMMA-g-PDMS copolymers prepared free radically using 10,000 molecular weight PDMS grafts (DeSimone et al., 1988b).



produced by free-radical and by anionic polymerization routes are striking. The free-radical polymerization produces a graft copolymer whose PMMA content varies from 48% to 87% as the molecular weight of the fractions of each polymer increases, whereas the copolymer produced by anionic polymerization has a PDMS content that is essentially constant as a function of molecular weight.

The synthesis of PMMA-g-PDMS using group transfer polymerization (GTP) was conducted at Virginia Tech with the primary goal of establishing GTP as a synthetic route for preparing graft and block copolymers (Hellstern, 1989). The elucidation of the CCD profiles was a small but significant part of that research. While direct comparison of those profiles determined by fractionation of graft copolymers synthesized by GTP versus free-radical and anionic polymerization cannot readily be made because the systems differed widely in PDMS composition and graft length, some general conclusions can be drawn from the work. Based on the trend exhibited in figure 9.11, that anionic and GTP methods produce copolymers having quite narrow molecular weight distributions, and based on the nature of "living" polymerizations, it was anticipated that the anionic and GTP methods would produce graft copolymers having similar chemical composition distribution profiles. But analysis of the fractions obtained with supercritical chlorodifluoromethane showed that the CCD of the copolymer produced by GTP, shown in figure 9.17, was more nearly like that of the free-radically produced copolymer. This was a quite interesting and unexpected result that merited further investigation. The CCD profiles in figure 9.17 do support the model of Stejskal and Kratochvil in that the breadth of the distribution decreases as the percent PDMS increases for copolymers containing grafts of the same molecular weight.

One explanation for the unexpected difference in the CCD profiles of the GTP and anionically produced copolymers is that a small amount of unincorporated PDMS macromonomer is still present in the GTP product mixture even

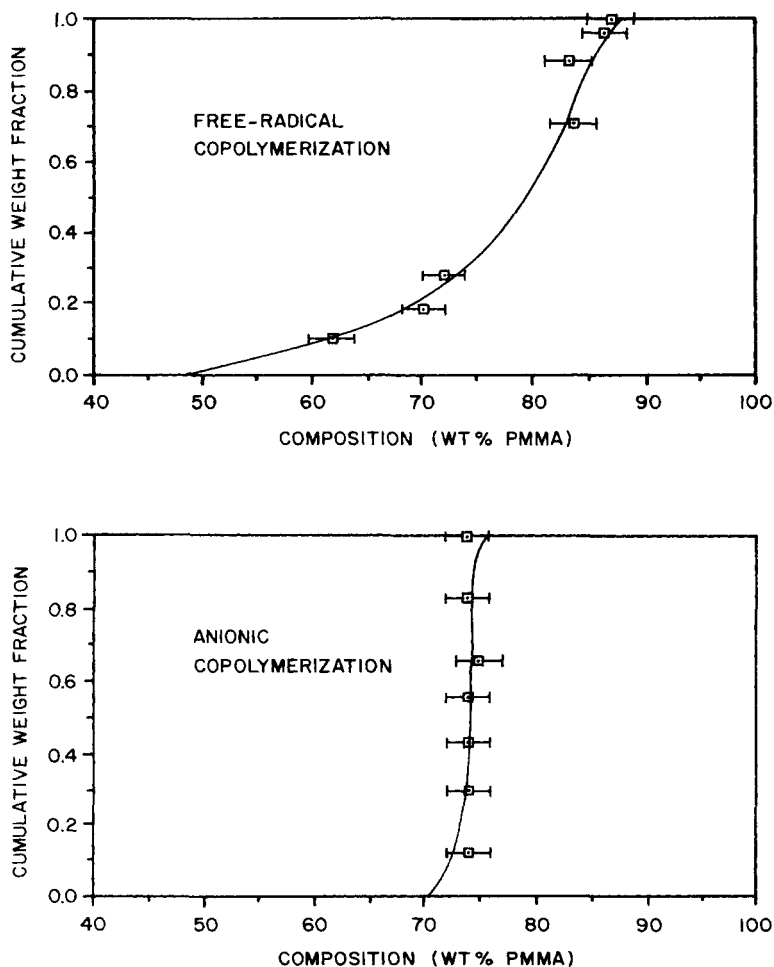
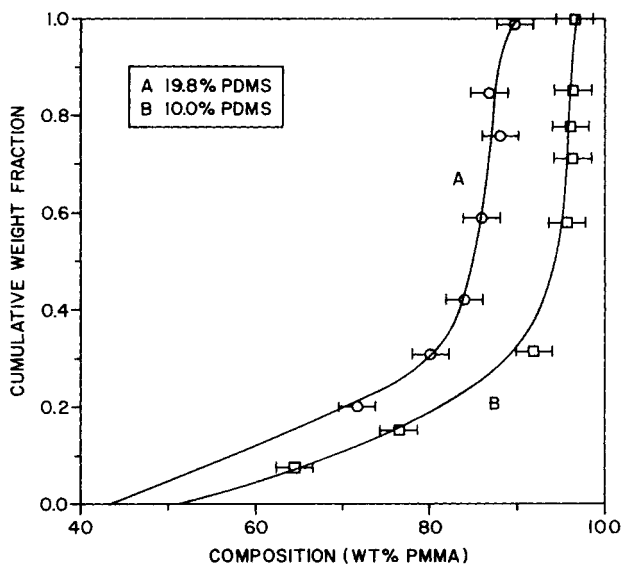


**Figure 9.16** Experimentally determined CCD profiles for PMMA-g-PDMS copolymers prepared free radically and anionically using 10,000 molecular weight PDMS grafts (DeSimone et al., 1988b).

after vigorous Soxhlet extraction with hexane. Careful GPC analyses of the parent copolymers were carried out, and although no residual macromonomer was found, a tiny peak was seen at an elution volume that does not correspond with that of the PDMS macromonomer. The presence of the peak suggests that during the synthesis reaction a small fraction of material is produced with a PMMA backbone that contains a very high weight percent of PDMS. After further analysis it was discovered that even after rigorous hexane extraction some unincorporated methacryloxy-terminated PDMS macromonomer remains in the reaction mixture even though the GPC chromatogram of the parent

**Figure 9.17** Experimentally determined CCD profiles for PMMA-g-PDMS copolymers prepared by group transfer polymerization using 20,000 molecular weight grafts: (A) Hexane extracted before fractionation and (B) Hexane extracted and CO<sub>2</sub> extracted before fractionation (tabulated data in Hellstern, 1989).



copolymer indicated that it had all been removed. We consider the experimental evidence to support the conclusion that short PMMA backbones containing large amounts of PDMS were formed during GTP. The graft copolymers prepared by GTP were both stripped of unincorporated PDMS macromonomer using Soxhlet extraction prior to fractionation. The copolymer whose CCD is depicted by curve B of figure 9.17 was further extracted with supercritical carbon dioxide at 340 bar before fractionation, removing about 1.3 wt% of the sample. This extract and the first three fractions obtained subsequently with chlorodifluoromethane were analyzed by GPC. The chromatograms shown in figure 9.18 indicate that fractions 1 (i.e., the carbon dioxide extract) and 2 exhibited bimodal molecular weights. Furthermore, fraction 1 contains material that has a higher molecular weight than material in fraction 2. The bimodal nature of the curves implies that something else, in addition to PDMS macromonomers, was extracted by the carbon dioxide (as well as by chlorodifluoromethane).

The peak eluting at ~32 ml in fraction 1 corresponds to PDMS macromonomer, showing that it was indeed present and could be concentrated with carbon dioxide. The peak eluting at ~29 min corresponds to the tiny peak observed on the GPC of the parent material after hexane extraction. To explain the presence of this unknown material, Gallagher and Krukoni (1993) postulated that the copolymers with very short PMMA backbones have enough PDMS to make them soluble in supercritical carbon dioxide at 340 bar, the same conditions needed to dissolve the PDMS macromonomer. If so, then, relative to fraction 2, fraction 1 contains both free PDMS macromonomer and copolymer of extremely high PDMS content and of a higher molecular weight.

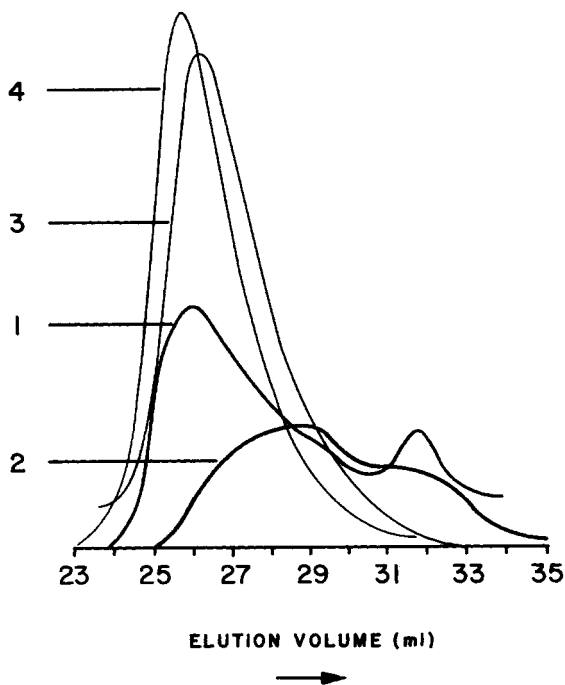


**Figure 9.18** Gel permeation chromatograms of fractions of PMMA-g-PDMS copolymer: fraction 1 obtained with supercritical carbon dioxide and fractions 2, 3, 4 obtained with supercritical chlorodifluoromethane (Hellstern, 1989).

Additionally, the same phenomena could be occurring in the early stages of a fractionation of the parent copolymer where no previous carbon dioxide stripping of the PDMS macromonomer was employed, since chlorodifluoromethane is a very good solvent for polysiloxanes (Gallagher, 1988). This is evidenced by the bimodal GPC trace for fraction 2. GPC analysis of several other reaction mixtures fractionated only with chlorodifluoromethane after hexane extraction also resulted in bimodal traces for the early fractions. These data support the hypothesis that the graft copolymers prepared by GTP do indeed form some very short PMMA backbones with high PDMS content and that free PDMS macromonomer remains in trace amounts even after hexane extraction. To summarize the GTP portion of the NSF program, supercritical fluid fractionation was able to provide fractions of materials that could be used to elucidate the CCD and the anomalous behavior during GTP kinetics of the MMA and MMA-terminated PDMS system.

The anomalies observed in the GPC traces of the early fractions implicate GTP mechanisms rather than SCF extraction efficiencies. Unlike anionic and free-radical polymerization mechanisms, GTP is catalyzed, and a silicon atom is central to the catalysis mechanism. It is plausible that the presence of nonfunctional PDMS may interfere with the normal rate of propagation (Hellstern, 1989) since silicon atoms in the PDMS chain may act as alternative catalyst sites. Hellstern (1989) compared the extent of MMA polymerization in the presence of nonfunctional PDMS with the extent of MMA-PDMS

copolymerization, and found that competitive inhibition may indeed be occurring. Although extensive kinetic studies would be necessary to confirm this hypothesis, further characterization of the graft copolymers by thermal gravimetric analysis, dynamic mechanical thermal analysis, and X-ray photo-spectroscopy, support it (Hellstern, 1989).

The efficiency of SCF fractionation of the PMMA-g-PDMS copolymers was also compared to the traditional fractionation method of solvent demixing (or liquid antisolvent precipitation). For this comparative study, two copolymers were prepared anionically using PDMS macromonomer of 20,000 number average molecular weight. The composition of one copolymer was 17 wt% PDMS and the other 34 wt% PDMS. One half of the starting material for each copolymer was fractionated with supercritical chlorodifluoromethane as previously described, and the other half was fractionated by liquid antisolvent precipitation by dissolving the copolymer in trichloroethylene and precipitating it with dimethyl sulfoxide (DMSO). The resultant CCD profiles from both techniques are depicted in figures 9.19 and 9.20 (DeSimone et al. 1988b).

These figures show that the CCD profiles of anionically polymerized PMMA-g-PDMS copolymers are narrow, regardless of the fractionation technique employed, i.e., 98% of the copolymer exhibits a CCD that is predicted from the initial PDMS composition. In addition, both methods are comparable in efficiency for the graft copolymers of low and high PDMS content. But with liquid antisolvent precipitation, a shoulder is observed to extend to the low PMMA content region of the CCD for very low cumulative weight fractions. This shoulder is unpronounced in the SCF fractionated material but indicates that, even in anionically produced copolymers, some very short PMMA chains having high PDMS content are formed. The SCF fractionation technique could also resolve this shoulder if the initial fractions were made extremely small, e.g., less than 1 wt% of the parent. However, the overall conclusion is that, based on the fractionation time, sample size, and ease of operation, SCF fractionation is the more suitable and versatile tool for elucidation of CCD profiles in graft copolymers.

Although the primary focus of the graft copolymer fractionation research at Phasex focused on PMMA-g-PDMS polymers, several other graft and block copolymers were also investigated, e.g., poly(*t*-butyl)-g-PDMS, polystyrene-g-PDMS, poly(*t*-butylstyrene)-g-PDMS and polystyrene-*b*-PDMS. All of these copolymers can be fractionated using chlorodifluoromethane using an isothermal increasing pressure profile (Gallagher and Krukons, 1993). In certain instances the fractionation was preceded by an extraction step where supercritical carbon dioxide was used to remove any unincorporated PDMS grafts.

### **$\alpha,\omega$ -Aminopropyl-Terminated Polysiloxane Fractionation**

Another major portion of the research effort undertaken with Virginia Tech focused on synthesis of  $\alpha,\omega$ -aminopropyl terminated PDMS and the subse-

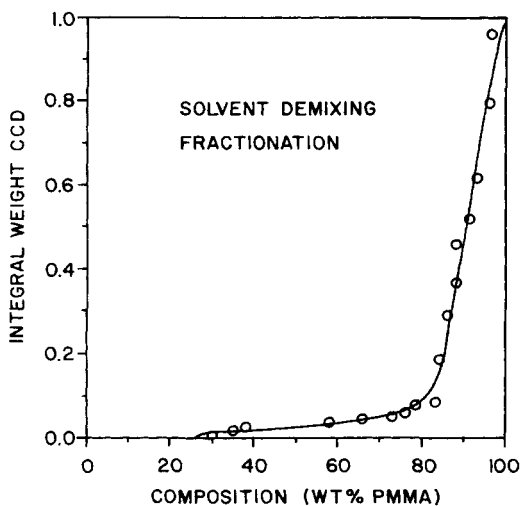
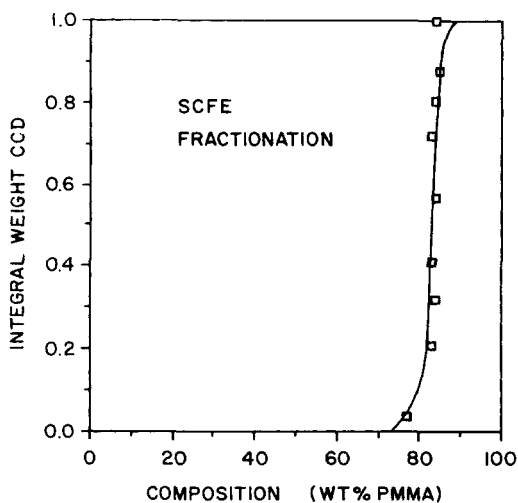


**Figure 9.19** CCD profiles for PMMA-g-PDMS copolymers of low PDMS content (17 wt% PDMS) prepared anionically using 20,000 molecular weight PDMS grafts: (top) supercritical chlorodifluoromethane fractionation; (bottom) solvent demixing fractionation (DeSimone et al., 1988b).

quent purification, fractionation, and evaluation of the polymers using supercritical fluids. The principal thrust of the program was to investigate the effect of the concentration and type of various siloxanolate catalysts on the reaction kinetics in the presence of a functional endblocker (Elsbernd, 1988). Fractionation of the polymers allowed the researchers to more fully characterize the polymers and also provided material of narrow molecular weight distribution for preparing siloxane-containing block copolymers.

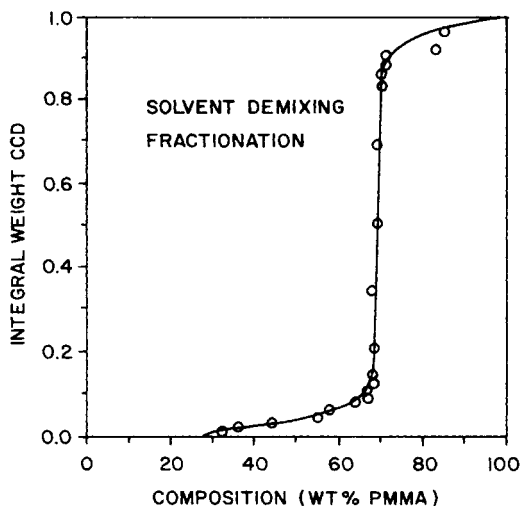
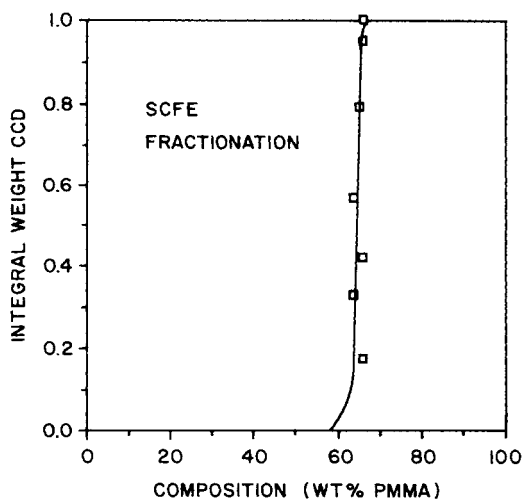


**Figure 9.20** CCD profiles for PMMA-g-PDMS copolymers of high PDMS content (34 wt% PDMS) prepared anionically using 20,000 molecular weight PDMS grafts: (top) supercritical chlorodifluoromethane fractionation; (bottom) solvent demixing fractionation (DeSimone et al., 1988b).

### Polydimethylsiloxanes

Anionic or cationic ring-opening polymerization of cyclic siloxanes in the presence of a functional disiloxane or endblocker is generally used to prepare linear, functionally terminated polysiloxane oligomers for subsequent use in organosiloxane block copolymers. Although either acid- or base-catalyzed ring-opening polymerization of octamethylcyclotetrasiloxane ( $D_4$ ) can be used



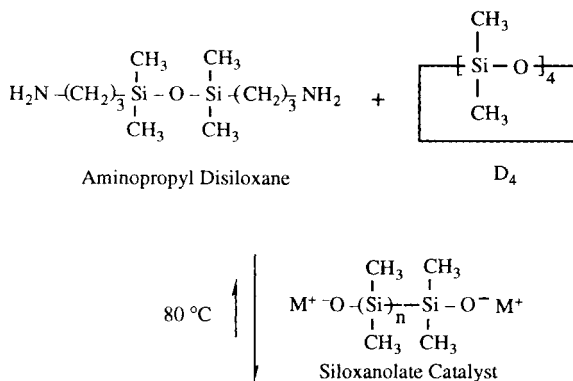
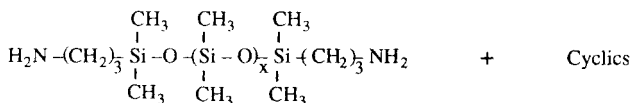


**Figure 9.3** General schematic of the synthesis of amino-propyl-terminated poly(dimethylsiloxane) (Elsbernd et al., 1987).



to readily prepare difunctionally terminated polysiloxanes, the work at Virginia Tech focused on the base-catalyzed (anionic) route. This equilibration reaction is not living and, therefore, results in the formation of both linear and cyclic species since it proceeds by a series of redistribution processes. The anionic ring-opening polymerization of  $\text{D}_3$  is a living polymerization; its advantage is that monofunctionally terminated polysiloxanes having very narrow molecular weight distributions can be produced without forming cyclic species. However, the functionality and applicability of oligomers formed from  $\text{D}_3$  is limited since they are monofunctionally terminated macromonomers. As a result, the much preferred starting material is  $\text{D}_4$  since the cyclic species produced during the ring-opening polymerization can be selectively stripped from the product using supercritical fluids.

Many previous papers describing supercritical fluid fractionation of polysiloxanes have discussed cyclics extraction (Krukoni, 1983c; Krukoni, 1985a; McHugh and Krukoni, 1989). We describe the equilibration reaction. The ring-opening catalyzed polymerization of  $\text{D}_4$  was conducted in a bulk reaction with the functional endblocker, 1,3-bis-(3-aminopropyl) tetramethyldisiloxane or simply aminopropyl disiloxane. Scheme 9.3 shows the general reaction scheme for synthesizing the aminopropyl-terminated polydimethylsiloxane (Elsbernd et al., 1987).

During the reaction  $\text{D}_4$ ,  $\text{D}_5$  (five  $(\text{CH}_3)_2\text{SiO}$  moieties in a ring),  $\text{D}_6$ , etc., form in various amounts due to the redistribution of the  $\text{D}_4$  reactant. Although vacuum stripping of the product to remove unreacted disiloxane and the low molecular weight cyclics can be performed, some cyclics remained in the polymer even with high vacuum stripping (Elsbernd, 1988). The vacuum step

can be efficiently replaced with supercritical fluid extraction as the first step of the fractionation to remove the low molecular weight cyclic material.

The properties of siloxane-containing block copolymers prepared from the functionally terminated siloxanes are influenced by the molecular weight distribution of the material which is typically Gaussian. The range of potential applications of the block copolymers can be extended if the molecular weight distributions of the siloxane blocks can be minimized. Thus, the impetus for evaluating supercritical fluid fractionation, aside from its utility as a characterization tool, as a means of improving end product performance is established.

It is well known that primary, aliphatic amines react with  $\text{CO}_2$  to form carbamic acids; this eliminates  $\text{CO}_2$  as a candidate fractionation solvent. Supercritical ethane was used instead to process the amine-terminated polysiloxanes. Many parent polymers were synthesized ranging in average molecular weight from 2,000 to 10,000 with polydispersities of 2 to 3; they were all first stripped of cyclics using ethane at  $80^\circ\text{C}$  then fractionated with ethane at  $80^\circ\text{C}$  with increasing pressure profiling from 55 bar to 275 bar.

Many of the  $\alpha,\omega$ -aminopropyl-terminated polymers synthesized by Elsbernd were fractionated between fifteen and twenty-five separate fractions that were characterized by molecular weight, molecular weight distribution, structure, and functionality. GPC of the amino-terminated parent polymer or the corresponding fractions was not possible because of the propensity of primary amino-functional oligomers to adsorb on the GPC column stationary phases (Elsbernd, 1988). To carry out the complete characterization, each fraction was first subjected to titration of the amine end groups with alcoholic HCl to determine the number average molecular weight and to confirm the presence of functionality (or the absence of it, in the case of the cyclics). Then, following a procedure developed by researchers at Virginia Tech (Elsbernd et al., 1987), each fraction was derivitized with benzophenone to convert the primary amine to an imine functionality. The titration of end groups was also necessary so that the correct amount of benzophenone needed to derivitize each fraction could be determined.

Because the interfering amine functionality was replaced with an imine, it was possible to analyze each fraction for molecular weight distribution by GPC using either polystyrene or specially synthesized polydimethylsiloxane calibration standards. The low molecular weight cyclic content of the early fractions was determined by HPLC and the higher cyclics ( $\text{D}_6$ ,  $\text{D}_7$ ,  $\text{D}_8$ ) were identified by GC-MS. The absence of amine functionality in the early fractions, which is indicative of the presence of cyclics, was also confirmed by FT-IR. It is apparent, then, that complete characterization of the fractionated polymer was no small task, especially in light of the fact that even though supercritical fluid fractionation can process initial sample sizes of 20–25 g, some of the fractions were only 0.5–1.0 g in size, and therefore the workup required substantial effort and care.

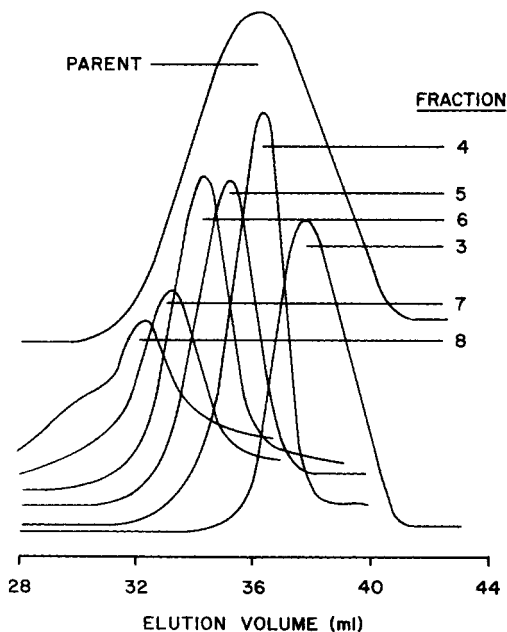
Table 9.14 and figure 9.21 show the results of the ethane fractionation of an aminopropyl-terminated PDMS having a number average molecular weight

**Table 9.14** Fractionation of Aminopropyl-Terminated Polydimethylsiloxane with Ethane at 80°C

<i>Fraction</i>	$\Sigma \text{ wt}\%$ <sup>a</sup>	<i>Titred <math>M_n</math></i>	$D_4$ (wt%)	$D_5$ (wt%)	$M_w/M_n$
Parent		4,200	4.5	4.2	2.14
1	3.1	<sup>b</sup>	41	45	
2	3.9	<sup>b</sup>	0	5	
3	15.7	1,460	0	0	1.30
4	27.2	2,820	0	0	1.25
5	55.4	4,920	0	0	1.26
6	72.4	6,600	0	0	1.33
7	94.1	9,550	0	0	1.36
8	100.0	15,550	0	0	1.71

<sup>a</sup>Cumulative amount of polymer removed from the columns.<sup>b</sup>Contains only nonfunctional cyclic species.

The molecular weight data were obtained using polystyrene standards.

**Figure 9.21** Gel permeation chromatograms of aminopropyl-terminated polydimethylsiloxane: number average molecular weight of parent polymer is 4,200; fractions obtained using supercritical ethane at 80°C (Elksbernd et al., 1987).

of 4,200 and a molecular weight distribution of 2.14. Early in the studies GPC analysis of the samples from supercritical fluid fractionation was conducted using polystyrene standards because polysiloxane standards were not available. But the use of polystyrene standards is not a true indication of the molecular weight distributions, since the hydrodynamic volume of polystyrene of a given molecular weight is different than that of polysiloxane of the same molecular weight. Therefore, Elsbernd prepared polydimethylsiloxane standards by anionic ring-opening polymerization of  $D_3$  terminated with a UV active moiety, phenyldimethylchlorosilane, for more complete GPC characterization of the amine-terminated (but benzophenone derivitized) PDMS polymers and fractions.

Whereas most of the work with the PMMA-g-PDMS copolymers previously discussed involved PDMS grafts of 10,000 to 20,000 molecular weight, the aminopropyl terminated PDMS studies were concerned with much lower average molecular weight polymers, e.g., ~1,500 to 8,000, and the efficacy of supercritical fluid fractionation to obtain low polydispersity fractions of these materials was investigated. The polymers synthesized by Elsbernd were in most cases one of a kind for the purpose of comparing different catalysts, concentrations, conditions, and the like. Many of the subsequent fractionations carried out on the polymers were by no means optimized, very often progressing from initial observations of the events during isothermal increasing pressure profiling. The most difficult separation of the cyclic species ( $D_4$ ,  $D_5$ ,  $D_6$ , etc.) is experienced when the average molecular weight of the polymer sample is less than 3,000 or 2,000.

Table 9.15 presents the molecular weight data of fractions obtained from a 1,900 molecular weight  $\alpha,\omega$ -aminopropyl PDMS that had been vacuum stripped of cyclics prior to ethane fractionation. As previously mentioned, even with vacuum stripping, some cyclics remain in the sample, and this was an unanticipated finding which surfaced after analysis of the first three fractions indicated an unusually high molecular weight. The presence of cyclic material in a polymer of such low molecular weight (1,900) would influence to calculated  $M_n$  of these early fractions. Fractions 4 through 18 display a monotonic increase in molecular weight and quite narrow molecular weight distributions. The characterization of molecular weight by GPC gave results that were in good agreement with the titrated values. To further emphasize the importance of using the polysiloxane standards, polydispersities of several of the fractions of amine-terminated polydimethylsiloxane were determined and it was found that based on polystyrene standards a molecular weight polydispersity of 1.20 translates to a value of 1.12 when calculated based on polysiloxane standards. Figure 9.22 shows the GPC chromatograms of the parent polymer and several selected fractions that demonstrate the efficacy of the ethane fractionation in providing narrow fractions of low polydispersity.

In order to confirm the difunctional nature of the fractions, number average molecular weight of several of the fractions was determined by vapor

**Table 9.15** Fractionation of Aminopropyl-Terminated Polydimethylsiloxane with Ethane at 80°C

<i>Fraction</i>	$\Sigma$ wt% <sup>a</sup>	<i>Titrated M<sub>n</sub></i>	<i>M<sub>n</sub></i>	<i>M<sub>w</sub>/M<sub>n</sub></i>
Control		1,900	1,400	1.58
1	1.8	1,700		
2	7.6	1,300		
3	12.3	1,000	500	1.33
4	17.8	850	700	1.13
5	23.4	1,050	600	1.22
6	28.9	1,300	1,000	1.14
7	35.0	1,550	1,300	1.12
8	43.5	1,800	1,700	1.12
9	49.9	1,900	1,800	1.13
10	56.6	2,300	2,100	1.06
11	63.1	2,550	2,600	1.12
12	69.4	2,900	2,900	1.12
13	76.2	3,250	3,500	1.15
14	83.0	3,900	4,000	1.12
15	89.1	4,450	4,600	1.10
16	95.4	5,100	5,300	1.09
17	98.8	5,900	6,700	1.18
18	100.0			

<sup>a</sup>Cumulative amount of polymer removed from the columns.  
 The molecular weight data were obtained using polysiloxane standards.

phase osmometry (VPO) and the VPO data compared to the number average molecular weight determined by titration of the amine end groups. As reflected by the results presented in table 9.16, there is excellent agreement of the molecular weight data thereby confirming the difunctionality of the samples before and after ethane fractionation.

The molecular weight data for the fractionation of ~5,000 molecular weight aminopropyl PDMS are given in table 9.17, and the GPC traces for the parent polymer and select fractions are shown in figure 9.23. In this case, this sample had not been vacuum stripped of cyclics; table 9.17 shows that these species were extracted from the parent polymer in the first two fractions. As mentioned previously, the absence of amine functionality in the early fractions was confirmed by FT-IR and the cyclic content was determined by HPLC for D<sub>4</sub> and D<sub>5</sub>. GC-MS was used to identify the higher cyclics (D<sub>6</sub>, D<sub>7</sub>, D<sub>8</sub>) in the early fractions. Although there are a few anomalies in the titrated *M<sub>n</sub>* values, the overall results and GPC traces show a monotonic progression of molecular weights and reasonably narrow molecular weight distributions.

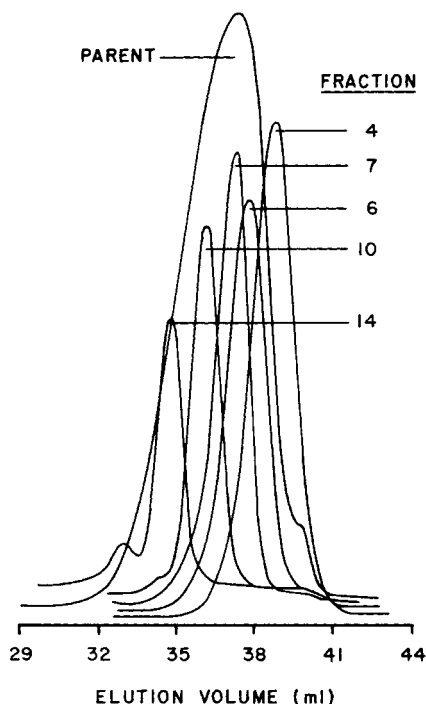


**Figure 9.22** Gel permeation chromatograms of aminopropyl-terminated polydimethylsiloxane: number average molecular weight of parent polymer is 1,900; fractions obtained using supercritical ethane at 80°C (Elsbernd et al., 1987).

**Table 9.16** Molecular Weight Characterization of Fractionated Aminopropyl-Terminated Polydimethylsiloxane

Fraction	Titrated $M_n$	$M_n$
Control	1,900	1,710
4	850	760
6	1,300	1,330
7	1,550	1,520
10	2,300	2,420
14	3,900	3,970

The molecular weight data were obtained by vapor phase osmometry in toluene at 63°C.

### *Poly(dimethyl)-co-(diphenyl) Siloxanes*

It is common practice to incorporate phenylmethyl or diphenyl substituents along the siloxane chain for improving thermal and oxidative stability of the polymer relative to polydimethylsiloxane. The presence of the phenyl group brings about a strengthening of the siloxane bond and can also improve

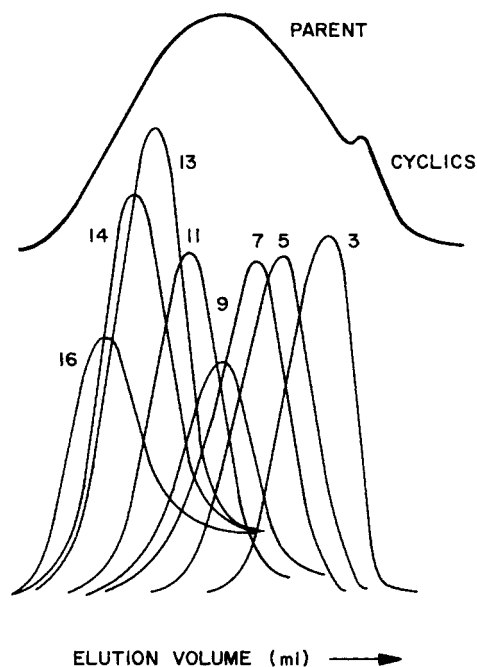


**Figure 9.23** Gel permeation chromatograms of aminopropyl-terminated polydimethylsiloxane: number average molecular weight of parent polymer is 4,700; fractions obtained using supercritical ethane at 80°C (Elsbernd et al., 1987).

low-temperature flexibility by disrupting the symmetry and crystallization of the methyl sequences. But too many phenyl groups can result in crystallization of long phenyl sequences. Incorporation of phenyl groups increases the glass transition temperature and the viscosity, and, due to enhanced intermolecular interactions, increases the solubility parameter of the substituted siloxane. Poly-(dimethyl)-*co*-(diphenyl) siloxanes are particularly useful precursors for siloxane-containing copolymer systems since they exhibit enhanced miscibility with many organic polymers (Elsbernd, 1988). Furthermore, utilization of the copolymers as blocks or grafts in other systems may impart beneficial properties to the materials.

The synthesis route for preparation of poly(dimethyl)-*co*-(diphenyl) siloxane is shown in scheme 9.4 (Elsbernd, 1988). A mixture of octamethylcyclotetrasiloxane ( $D_4$ ) and octaphenylcyclotetrasiloxane ( $D_4'$ ) are reacted simultaneously, using the base-catalyzed ring-opening polymerization technique described earlier for  $D_4$ . The resulting polymer is  $\alpha,\omega$ -terminated with an aminopropyl moiety, which derives from the aminopropyl disiloxane reactant. The cyclic products formed from this equilibration reaction contain mixed amounts of dimethyl silicon and diphenyl silicon moieties in the ring, and trace amounts of  $D_4$  and  $D_4'$  are present as well. The high boiling points of  $D_4'$  and the mixed cyclics make them difficult to remove from the functional copolymers by conventional separation techniques, e.g., thin film distillation, therefore

**Table 9.17** Fractionation of Aminopropyl-Terminated Polydimethylsiloxane with Ethane at 80°C

Fraction	$\Sigma$ wt% <sup>a</sup>	Titrated $M_n$	$D_4$ (wt%)	$D_5$ (wt%)	$M_w/M_n$
Control		4,700	7.3	4.7	2.7
1	4.9	<sup>b</sup>	65.0	35.0	<sup>b</sup>
2	8.7	<sup>b</sup>	31.0	43.0	<sup>b</sup>
3	15.4	2,260	0	2.5	2.12
4	19.4	3,300	0	0	2.23
5	26.8	3,900	0	0	2.00
6	32.0	3,320	0	0	1.70
7	38.6	3,650	0	0	1.45
8	45.7	3,930	0	0	1.48
9	49.8	2,900	0	0	1.24
10	57.1	4,220	0	0	1.29
11	63.3	4,700	0	0	1.19
12	72.3	6,300	0	0	1.18
13	80.1	8,040	0	0	1.18
14	86.2	8,500	0	0	1.18
15	92.8	11,300	0	0	1.14
16	99.3	14,800	0	0	1.17
17	100.0		0	0	

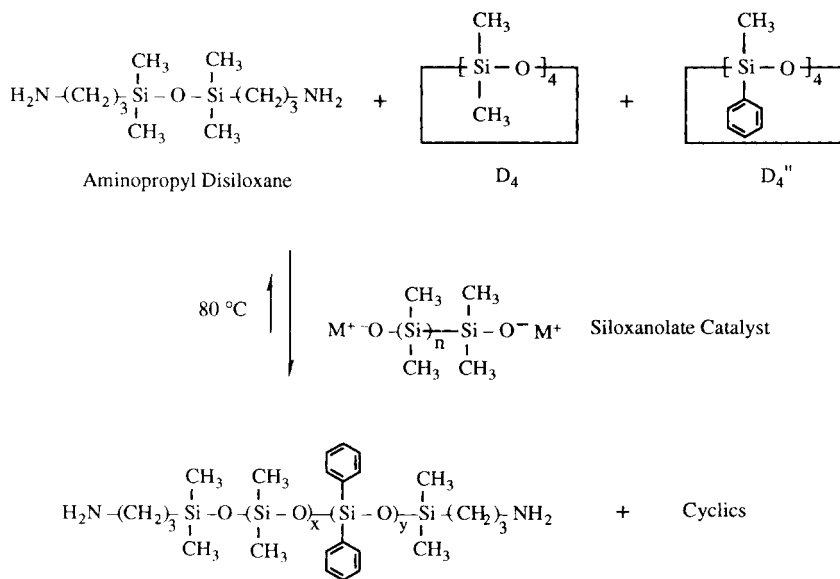
<sup>a</sup>Cumulative amount of polymer removed from the columns.<sup>b</sup>Contains nonfunctional cyclics.

The molecular weight data were obtained using polysiloxane standards.

supercritical fluids were investigated for their ability to separate the complex mixture of cyclics from the linear species and to subsequently fractionate the copolymers.

The initial approach to removing the cyclics was the same straightforward one used for stripping cyclics from the all dimethyl polysiloxanes. That is, if the cyclics were higher in solubility at low pressures than the bulk of the polymer, they could be completely removed from the sample in the early fractions by following the isothermally increasing pressure profiling procedure. The efficacy of the fractionation increases as the molecular weight of the parent material increases to the 100,000 to 500,000 range. (Some previous work by Phasex on  $D_4'$  extraction followed by fractionation of a poly(dimethyl)-*co*-(diphenyl) siloxane showed that  $D_4'$  and mixed  $D_4$ - $D_4'$  cyclics could be separated cleanly from a parent copolymer that had an  $M_n$  of 78,000 (McHugh and Krukons, 1989).) The polymers synthesized by Elsbernd were of relatively low molecular weights in the 5,000 to 10,000 range, therefore there was some uncertainty as to whether or not the cyclic diphenyl tetramer could be selectively extracted. Measurement of  $D_4'$  solubility in ethane at pressures of  $\sim 140$  bar was carried





**Scheme 9.4** General schematic of the synthesis of aminopropyl-terminated poly(dimethyl)-*co*-(diphenyl)siloxane (Elsbernd, 1988).

out and a value on the order of  $\sim 0.1$  wt% was obtained. ( $\text{D}_4$  has a solubility of  $\sim 0.8$ – $1.0$  wt% in ethane at 55 bar and  $80^\circ\text{C}$  (Gallagher, 1987).)

Figure 9.24 shows the GPC chromatogram for a 5,000 molecular weight amino-terminated poly(dimethyl)-*co*-(diphenyl) siloxane composed of 50% dimethyl and 50% diphenyl substituents. The silicon polymer community use the convention that all percent values are weight percent. There is a significant amount of free cyclics present, and the peak for the cyclics is in close proximity to the peak for the parent. If this were a 500,000 molecular weight polymer the two curves would be separated by a relatively large distance. Twelve fractions were obtained using an isothermally increasing pressure profile from 55 bar to 450 bar at  $80^\circ\text{C}$ . Every one of the fractions contained some cyclic diphenyl tetramer, although it tended to concentrate primarily in the first six fractions. Figure 9.25 shows the GPC chromatograms for fractions 5 and 9. There was so much overlap of the curves that the molecular weight distributions for fractions 1 through 7 were not calculated. The molecular weight distributions for fractions 8 through 12 were computed ignoring the  $\text{D}_4''$  peak; the polydispersities ranged from 1.44 to 1.60 with titrated number average molecular weights of 4,650 to 12,400. The experiments achieved fractionation but not complete separation of  $\text{D}_4''$  and mixed cyclics from the polymer.

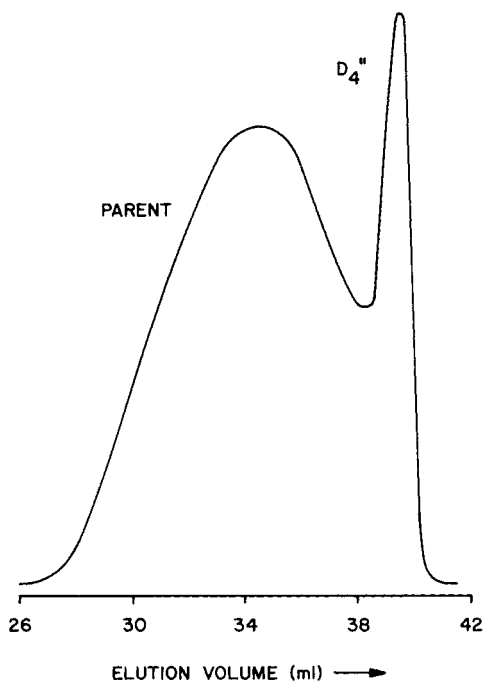


**Figure 9.24** Gel permeation chromatograms of aminopropyl-terminated poly(dimethyl)-*co*-(diphenyl)siloxane composed of 50 wt% dimethyl and 50 wt% diphenyl substituents: number average molecular weight is 5,000 (Elsbernd et al., 1990b).

Following this unsuccessful attempt to isolate the diphenyl tetramer from the low molecular weight copolymer, a unique approach to the problem was tested. The concept takes advantage of the chemical interaction between carbon dioxide and primary amines and involves the following steps:

1. React the  $\alpha,\omega$ -aminopropyl terminated copolymer with  $\text{CO}_2$  to form a dicarbamic acid; because the carbamic acid moiety is so polar it was reasoned that the reaction product would be insoluble or of very low solubility in  $\text{CO}_2$ . The cyclic products would not react with  $\text{CO}_2$  since they have no amine functionality, and thus they would be extractable.
2. Extract the cyclic compounds with  $\text{CO}_2$ . The solubility of  $\text{D}_4''$  in  $\text{CO}_2$  at 300 bar and  $80^\circ\text{C}$  is  $\sim 0.18$  wt% (Gallagher, 1987).
3. Convert the dicarbamic acid back to the diamine, carefully flushing the system with low-pressure ethane to remove generated  $\text{CO}_2$ .
4. Carry out the fractionation with ethane.

The procedure is somewhat oversimplified, but utilization of the concept resulted in some very interesting and previously unreported findings.

A model system was chosen for a careful investigation of the ability to convert the carbamic acid back to amine. Using aminopropyl disiloxane (for endcapping the polymer) as the model compound, a series of tests were

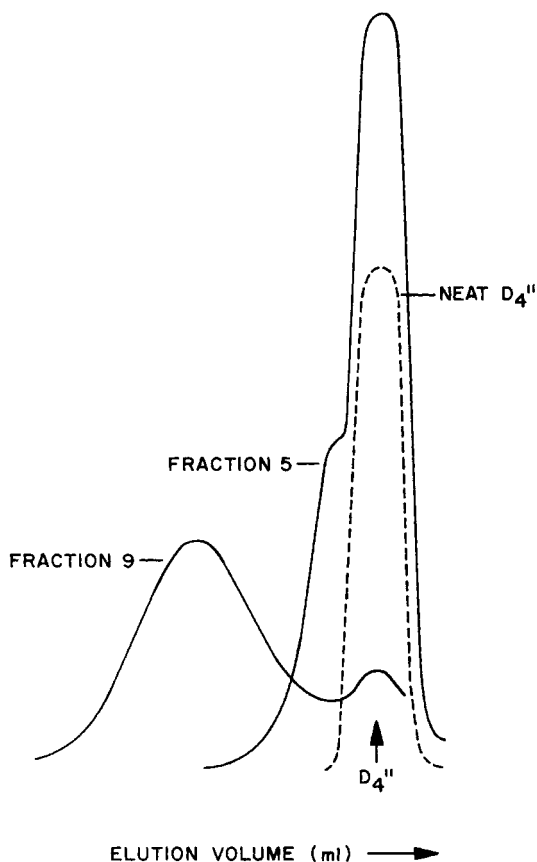
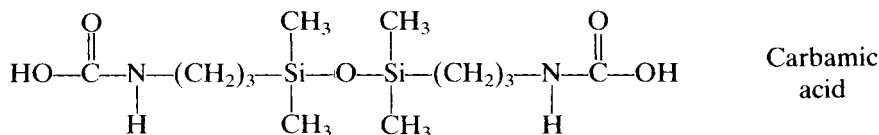
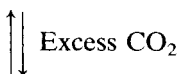
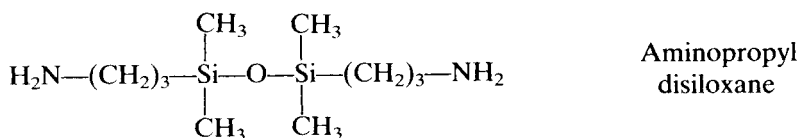


**Figure 9.25** Gel permeation chromatograms of two fractions obtained from the parent copolymer shown in figure 9.24 using supercritical chlorodifluoromethane; dashed line indicates peak for neat D<sub>4</sub> (Elsbernd et al., 1990b).

conducted using an excess of CO<sub>2</sub> at high pressures followed by various ethane treatments. A very rapid screening with the disiloxane had been done previously to show that reversion occurs.

Carbon dioxide reacts with primary amines to form a carbamic acid (Pine et al., 1980). Carbamic acids are unstable; the very act of dissolving the carbamic acid in a solvent for titration or for conducting NMR studies, for example, converts the acid back to amine plus CO<sub>2</sub> (Elsbernd, 1988). Heating the acid to about 50–100°C can force the reaction in the reverse direction, and if the CO<sub>2</sub> that is generated is removed, the amine can be recovered. Although the conversion of carbamic acid back to amine plus CO<sub>2</sub> occurs quite readily (Pine et al., 1980) the reversion is not instantaneous (Gallagher and Krukoni, 1987). What can also occur during the reverse reaction is reaction between any unconverted carbamic acid and the amine that has just reformed to form a urea.



Titration of the urea compound (for analytical purposes) would not result in a reversion back to amine plus  $\text{CO}_2$ , and molecular weight analysis would clearly indicate that this reaction had occurred. Since the reversion of the carbamic acid is not instantaneous, the necessary ingredients for urea formation would be present, viz., some carbamic-acid-terminated PDMS and some amine-terminated PDMS, both of which are soluble in ethane. A definitive study of reaction kinetics would be necessary to establish the extent to which the respective reactions occur. While that clearly was not the intent of this investigation, some insight into this chemistry was gained during the course of the experimental study; the findings are another interesting facet of supercritical fluid behavior.

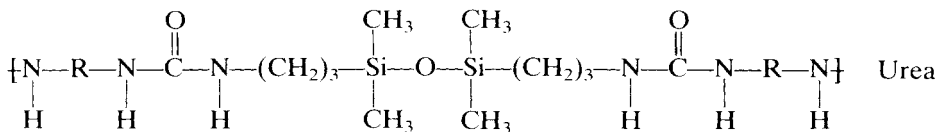
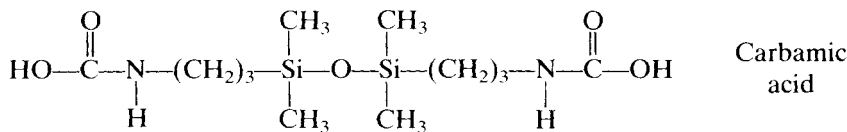


**Table 9.18** Reaction/Extraction Results with Aminopropyl Disiloxane at 60°C

<i>Fraction</i>	<i>Pressure/Solvent (bar)</i>	<i>Weight Collected (g)</i>	<i>Gas Used (g)</i>	<i>Appearance</i>
1	300/CO <sub>2</sub>	~0.03	180	A scant white solid film
2	92/C <sub>2</sub> H <sub>6</sub>	0.14	120	A white semisolid
3	112/C <sub>2</sub> H <sub>6</sub>	0.51	98	A water-white liquid and a white solid
4	143/C <sub>2</sub> H <sub>6</sub>	1.06	300	A water-white liquid and a white solid

Aminopropyl disiloxane was first studied as the model system; its solubility in ethane at ~100 bar and 80°C was measured to be ~1.2 wt%. This value would be of importance when trying to qualitatively determine if, after reacting with CO<sub>2</sub> then flushing with ethane, the reaction product itself or the reverted amine was being dissolved with ethane.

The aminopropyl disiloxane, a low-viscosity, water-white liquid, was first reacted with excess CO<sub>2</sub> at 300 bar and 60°C flowing through the extractor/reactor; the heat of reaction was manifested as a temperature rise. Such an excess of CO<sub>2</sub> was used that complete reaction with the amine was assumed. But to be quantitative in the evaluation, a sample of the white solid that was formed was collected for subsequent analysis. Virtually nothing was dissolved by supercritical CO<sub>2</sub> as it flowed through the extractor. Ethane was introduced, and the pressure was sequentially increased to determine what was extractable. Sequential extracts were collected, and depending upon the conditions and the length of time from the initial introduction of ethane, the extract was at first a semisolid, then a mixture of solid and liquid, and finally almost completely liquid, indicating that, even at the relatively high temperature of 60°C, substantial time is required to revert the carbamic acid. A summary of the test conditions and observations is given in table 9.18.

A qualitative conclusion could be drawn from this experiment: reaction had occurred with the CO<sub>2</sub> and from the first entry in table 9.18 it can be concluded that the carbamic-acid-terminated PDMS reaction product is essentially insoluble in CO<sub>2</sub> at conditions of 300 bar and 60°C. This is not an unexpected finding if the polarity of the material is considered. Based on this reasoning, the reaction product would be expected to be insoluble in ethane as well. Furthermore, the material which dissolved in ethane could not be solely disiloxane (a water-white liquid) based on the appearance of the extract and on the measured solubility. Since some water-white liquid was collected using ethane, some reversion may have occurred, but white solid continued to appear in the extract after about 1 h, showing clearly that the reversion was

neither instantaneous nor complete. Two important questions remained to be answered:

1. Is the amine-CO<sub>2</sub> reaction completely reversible in ethane? If so, under what conditions?
2. Is there any formation of a urea compound by reaction of the carbamic acid and the amine?

The first question was answered by carrying out tests in ethane at a higher temperature of 100°C and at a lower pressure. The second question was answered quite readily with infrared (IR) analysis. IR spectra for the aminopropyl disiloxane and for fraction 4 are reproduced in figures 9.26 and 9.27, respectively. The noticeable difference between the two spectra indicates a structural difference. The primary amine doublet (figure 9.26) becomes a secondary amine singlet (figure 9.27) indicating reaction of one hydrogen. While both figures have peaks indicative of primary amine N—H bend, indicating that there is some aminopropyl disiloxane in fraction 4, a new peak appears in figure 9.27 at 1,637 cm<sup>-1</sup>. Considering the reactants involved, this

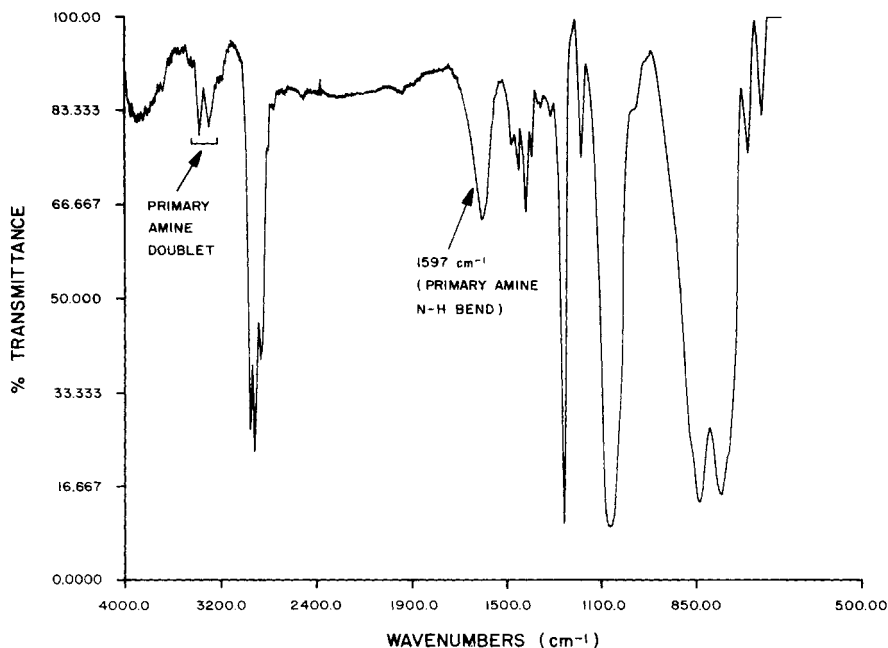


**Figure 9.26** Infrared spectrum of aminopropyl disiloxane (significant peaks are indicated) (Elsbernd, 1988).

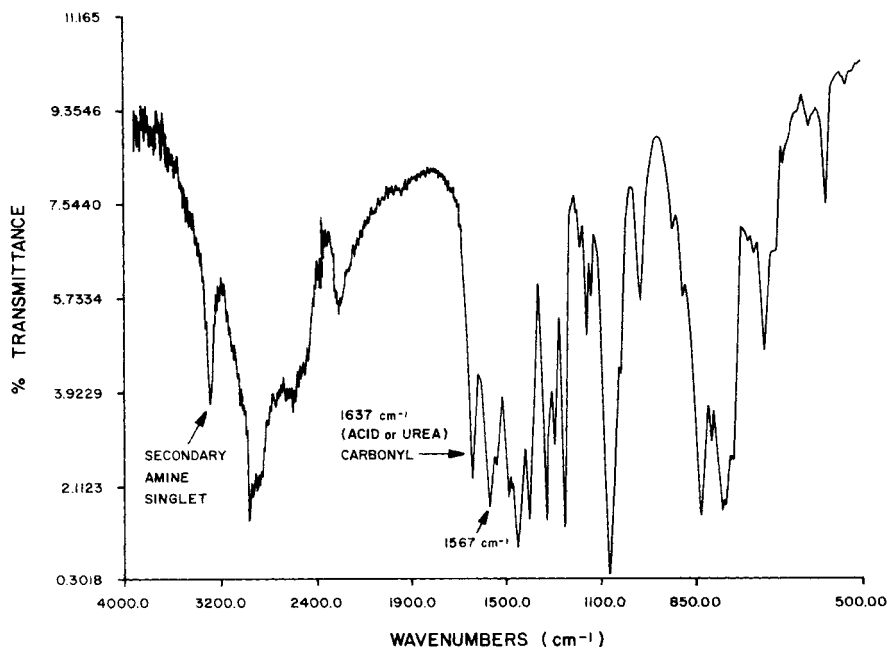


**Figure 9.27** Infrared spectrum of a fraction of aminopropyl disiloxane obtained with ethane at 60°C and 143 bar after reaction with carbon dioxide at 60°C and 300 bar (significant peaks are indicated) (Elsbernd, 1988).

new peak is suggestive of a carbamic acid carbonyl but it could also represent a urea carbonyl. The broad peak between  $2,500\text{ cm}^{-1}$  and  $3,300\text{ cm}^{-1}$  could be indicative of the O—H stretch of the carbamic acid.

To clarify that the acid rather than the urea had formed, number average molecular weights of fractions 3 and 4 were determined by titration; they were found to be 273 and 257 g/mol, respectively, very close to the theoretical value of 248.5 g/mol for the aminopropyl disiloxane. The carbamic acid reverts back to the amine during titration, the urea does not; therefore, the conclusion from this series is that only the carbamic acid had formed. It was possible to isolate the carbamic acid in the presence of some reformed amine, even though the acid is generally unstable and there is rapid equilibration between the amine and the carbamic acid, which usually makes isolation difficult (Pine et al., 1980). It is speculated that the high pressure is retarding the back reaction (Gallagher and Krukoni, 1987). Furthermore, the highly polar reaction product is virtually insoluble in supercritical  $\text{CO}_2$  yet is reasonably soluble in supercritical ethane (Gallagher and Krukoni, 1993).

Several subsequent tests were conducted using aminopropyl disiloxane to determine qualitatively the extent to which the amine- $\text{CO}_2$  reaction can be reversed and under what conditions. After reacting the disiloxane with  $\text{CO}_2$ ,

ethane at 15 bar was flowed through the system at a rate of ~5 standard liters/min for 1 h. Samples of the material in the extractor were removed periodically and analyzed. The variable in this series of tests was the temperature which ranged from 70 to 130°C, and the following results were obtained:

1. At 70°C, the carbamic acid is only partially converted back to amine in a period of a few hours.
2. At 100 to 130°C, complete conversion of carbamic acid back to amine occurs within ~20 min.
3. No urea is formed under any test conditions with ethane at 15 bar.

Although not tested further, complete reversal at 70°C may indeed be possible if left for a longer period of time, and even though no urea formation was indicated at 70°C, it would be preferable to carry out the reverse reaction quickly to reduce the likelihood of urea formation.

From discussions with Dr Judy Riffle at Virginia Tech (Riffle, 1988) it was learned that the reaction of amine and carbamic acid to form a urea can readily occur in the gas phase if there is an excess of amine present. It had been shown earlier that aminopropyl disiloxane is soluble in ethane (~1.2 wt% at 100 bar and 80°C and ~3.8 wt% at 170 bar and 130°C) and that the carbamic acid also has some solubility in ethane (on the order of 0.2–0.5 wt% at 70°C and pressures ranging from ~82 to 130 bar; see table 9.18). The extent of reaction would depend on the rate of dissolution into the gas phase versus the reaction kinetics of reversion of the carbamic acid to amine. Although the kinetic parameters were not quantitatively determined, a series of experiments established that the formation of urea indeed occurred in the presence of excess amine.

A sample of the amine–CO<sub>2</sub> reaction product (a carbamic acid) was placed in an extractor and an equal mass of aminopropyl disiloxane was placed in an upstream extractor. The temperature of each vessel was maintained at 70°C, so the carbamic acid would not convert back to amine very rapidly. Ethane at 15 bar was briefly flushed through the system to remove some of the CO<sub>2</sub> generated during the reverse reaction; the system was then pressurized to 275 bar and allowed to sit for 1 h. At conditions of 70°C and 275 bar, the carbamic acid is soluble to about 0.5 wt% in ethane. The disiloxane is much more soluble, so that in the gas phase there is an excess of disiloxane relative to the carbamic acid.

Flow of ethane at 275 bar was commenced and almost immediately, water-white liquid began to collect in the U-tube. It is presumed that this was excess aminopropyl disiloxane that was originally in the vessel and that had dissolved in the ethane, not the product of the reverse reaction. After collecting ~90% of the disiloxane that was charged, an opaque semisolid began to collect and finally a white powder. IR analysis and titration of the semisolid indicated that this sample was a mixture of disiloxane (whether it is strictly the



original disiloxane or that produced from the reverse reaction of the acid is unknown) and the carbamic acid. FT-IR analysis of the white solid that was dissolved later in the test showed evidence of a primary amine and "some kind of" carbonyl; analysis by  $^1\text{H}$ -NMR and  $^{13}\text{C}$ -NMR indicated that there were no acid groups present and the conclusion was that a urea had indeed been produced by gas phase reaction of excess aminopropyl disiloxane with the carbamic acid.

All of these studies with the model system were important for evaluating what might occur when the concept was tested with the actual polymer. What could not be predicted was the influence the molecular weight or molecular weight distribution of the  $\alpha,\omega$ -aminopropyl poly(dimethyl)-*co*-(diphenyl) siloxane upon the relative rate of dissolution versus the reaction rates for reversion and urea formation.

Several samples of poly(dimethyl)-*co*-(diphenyl) siloxane of molecular weights between 5,000 and 10,000 and containing either 25% or 50% diphenyl substituents were tested for removal of  $\text{D}_4$  and other cyclics using the reaction/extraction concept. Before attempting to fractionate the polymer, it was of interest to first establish that the reacted polymer, like the disiloxane, could indeed be reversed back to the amine functionality. The results of two tests using a 5,000 molecular weight polymer having 25% diphenyl substituents and containing ~13–14 wt% free cyclic species are discussed here. The results for a 10,000 molecular weight polymer were essentially the same.

In both tests the polymer sample was reacted with  $\text{CO}_2$  at low pressure (~100 bar) and  $80^\circ\text{C}$ , followed by flow-through of  $\text{CO}_2$  at 300 bar and  $80^\circ\text{C}$ . A hazy liquid was collected, and HPLC analysis indicated that essentially all of the cyclics were removed in the first fraction. Ethane was then introduced and the system was heated to  $150^\circ\text{C}$ , well above the reversion temperature of  $100^\circ\text{C}$  found with the model compound. Ethane at 15 bar was slowly flushed through the system for ~1 h to promote the reversal of the carbamic acid to amine. The pressure was then raised to 300 bar and a sample was collected. The remainder of the polymer was extracted with ethane at a higher pressure of 400 bar. Table 9.19 gives the results of the first test, and table 9.20 gives the results of the second test.

Note that although the parent molecular weight is 5,600 the second fraction already exhibits an  $M_n$  of 11,000 and the last fraction an  $M_n$  of 27,000, much higher than the normal progression of molecular weights in a fractionation, especially in one with only two or three fractions. The unusual molecular weight behavior is seen in the data for the second test as well (see table 9.20).

Figure 9.28 shows GPC chromatograms for the parent polymer and for fraction 2 (i.e., the first sample collected using ethane) from the first test. The elution volume data show the average molecular weight of the fraction is significantly higher than that of the parent. From the GPC chromatogram and from the titrated  $M_n$  values in tables 9.19 and 9.20, it appears that something unusual was happening with these polymers. Had the amine end groups merely reacted with  $\text{CO}_2$  to form the carbamic acid, dissolving the samples in a solvent

**Table 9.19** Reaction/Extraction Results with Poly(dimethyl)-*co*-(diphenyl)siloxane

Fraction	Gas Used	Temperature (°C)	Pressure (bar)	Σ wt% <sup>a</sup>	Titrated $M_n$
Parent					5,600
1	CO <sub>2</sub>	80	300	12.9	Cyclics <sup>b</sup>
2	C <sub>2</sub> H <sub>6</sub>	150	300	41.2	11,200
3	C <sub>2</sub> H <sub>6</sub>	150	400	100.0	26,800

<sup>a</sup>Cumulative amount of polymer removed from the columns.

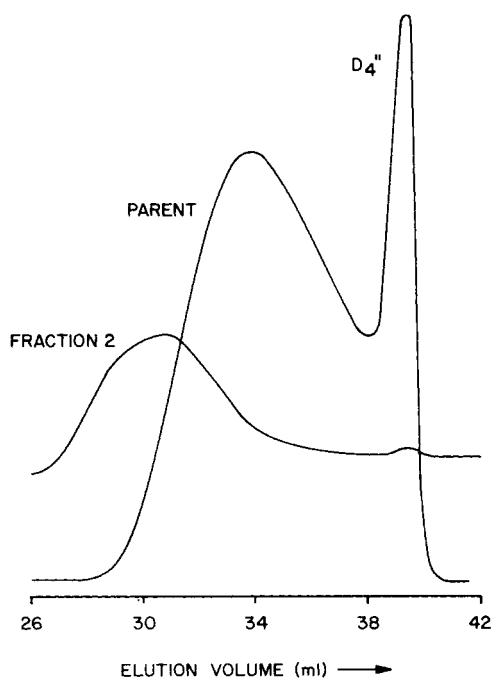
<sup>b</sup>8% D<sub>4</sub>.

**Table 9.20** Reaction/Extraction Results with Poly(dimethyl)-*co*-(diphenyl)siloxane

Fraction	Gas Used	Temperature (°C)	Pressure (bar)	Σ wt% <sup>a</sup>	Titrated $M_n$
Parent					5,600
1	CO <sub>2</sub>	80	300	14.1	Cyclics
2	C <sub>2</sub> H <sub>6</sub>	150	300	40.5	12,270
3	C <sub>2</sub> H <sub>6</sub>	150	400	100.0	44,300

<sup>a</sup>Cumulative amount of polymer removed from the columns.

**Figure 9.28** Gel permeation chromatograms of a 5,000 molecular weight aminopropyl-terminated poly-(dimethyl)-*co*-(diphenyl)siloxane parent copolymer containing 25 wt% diphenyl substituents and of fraction 2 obtained with supercritical ethane at 150°C and 300 bar after reaction with supercritical carbon dioxide at 80°C and 100 bar (refer to data in table 9.17) (Elsbernd et al., 1990b).



for titration would have reversed the reaction (even if heating to 150°C and flushing with ethane had not) and the titrated  $M_n$  would have been much closer to that of the parent. However, the results showed that a urea compound formed, and this was later confirmed with FT-IR.

Despite the unexpected results of these tests, two interesting and important aspects emerge:

1. All of the cyclic siloxane species could be stripped from the carbamic acid reaction product using CO<sub>2</sub>.
2. A fairly high molecular weight siloxane-urea compound was soluble in ethane at pressures of 200–300 bar and 150°C.

What can also be concluded is that the kinetics of forming the urea compound by further reaction of the carbamic acid are very different for this polymer relative to the model system of aminopropyl disiloxane. There is continued interest in the reaction/extraction concept and research is ongoing to more conclusively establish the true nature of the reactions.

The use of the reaction concept is a positive approach to removing the D<sub>4</sub> (and mixed cyclics) from the amino-terminated polymers and may provide a simpler alternative to conventional stripping techniques utilizing, for example, thin film evaporation or selective fractionation with liquid solvents. Riffle (1988) has suggested that after stripping the cyclics, the reaction could be reversed in other ways; fractionation of the poly(dimethyl)-*co*-(diphenyl) siloxanes using ethane could then be carried out.

## **FRACTIONATION OF POLYMER BINDERS FOR SOLID PROPELLANTS**

Supercritical fractionation was investigated for the special-purpose polymers of both the diol and triol of a glycidyl azide polymer and a hydroxy-terminated polybutadiene. Hydroxy polybutadiene is used on a large scale as an ingredient in plastic bonded explosive (PBX) propellant formulations; the hydroxy functionality of the polybutadiene reacts with an isocyanate functionality of another prepolymer to form a urethane. In the polysiloxanes section we referred to functionally terminated polymers as macromonomers; in the terminology of the urethane industry, however, isocyanate-terminated polyester polymers are normally referred to as prepolymers in their reaction to form the urethane, even though the prepolymers are typically between 1,000 and 10,000 molecular weight.

The heterogeneous nature of polymeric propellant binders has long been suspected of contributing to the significant variability encountered in the cure and combustion properties of solid propellants. The feasibility of purifying and fractionating propellant binders with supercritical fluids to remove those

species which detract from propellant performance was the subject of a 1990 Air Force program (Watkins and Krukonis, 1990). Hydroxy-terminated polybutadiene (HTPB), a widely used inert binder, and glycidyl azide polymer (GAP), an energetic propellant binder that has been under development for several years, were examined for their potential improvement using supercritical fluid fractionation. These polymers were fractionated across their entire molecular weight distribution using propane and chlorodifluoromethane, respectively. Many of the physical properties of the binders that ultimately dictate performance are molecular weight dependent, so fractionation can be used to obtain fractions of material with optimum properties for a given application. This is in addition to removing objectionable species.

## Hydroxy-Terminated Polybutadiene (HTPB)

A commercially available HTPB (R-45M), was studied for the experiments described in this section. The manufacturer (Atochem North America) lists the number average molecular weight for R45-M as 2,800 and gives a hydroxyl value of 0.70  $m_{eq}/g$  although the  $m_{eq}/g$  value can vary from 0.68 to 0.80. Both carbon dioxide and propane were tested with HTPB. Carbon dioxide dissolved only about 12% of the parent HTPB at pressure levels up to 587 bar. Propane dissolves virtually all of the parent material at moderate pressure, therefore, propane was used for the fractionation experiments.

The polymer was fractionated by the conventional means using an isothermal increasing pressure profile. In one test HTPB was separated into ten fractions in propane at 130°C. The first nine fractions were obtained at sequential pressure levels between 34 and 338 bar. The final fraction was dissolved at ~538 bar. A summary of the fractionation conditions, fraction weights, and weight fraction  $w_i$  of each cut is given in table 9.21.

The fractions and a sample of the parent polymer were analyzed for molecular weight by GPC and the hydroxyl equivalent weight was obtained by FTIR. The results of the GPC and FTIR analysis are presented in table 9.22, and the last two columns give calculated functionality relations based upon number average and weight average molecular weight and the hydroxyl equivalent weight.

The parent polymer had an  $M_n$  of 2,956, an  $M_w$  of 6,253 ( $M_w/M_n = 2.12$ ), and a hydroxyl equivalent weight of 1,256 (0.796  $m_{eq}/g$ ) in good agreement with the advertised values. The fractions exhibited number average molecular weights ranging from 781 to 11,757 and weight average molecular weights from 969 to 21,539. The polydispersities of most of the fractions are of the order of 1.2. Interestingly, the hydroxyl equivalent weight was nonlinear with molecular weight, especially in the latter fractions. As a result, both number average functionality,  $F_n$ , and weight average functionality,  $F_w$ , increase markedly in the last two or three fractions. The  $F_n$  ranged from 1.98 and 4.85 and the  $F_w$  from 2.44 to 8.88. The dependence of the calculated functionalities on

**Table 9.21** Fractionation of Hydroxy-Terminated Polybutadiene with Supercritical Propane at 130°C

<i>Fraction</i>	<i>Pressure Range (bar)</i>	<i>Propane Used (g)</i>	<i>Mass Collected<sup>a</sup> (g)</i>
1	34–55	810	0.05
2	124–165	1,150	1.30
3	152–207	1,750	1.67
4	193–207	1,320	1.37
5	207–234	1,460	1.15
6	234–262	1,130	1.08
7	248–276	1,120	1.20
8	276–317	1,150	1.24
9	303–338	1,800	1.28
10	517–552	990	3.31

<sup>a</sup>The material balance in all cases was of the order of 93–95%.

**Table 9.22** Analysis of Hydroxy-Terminated Polybutadiene Fractions

<i>Fraction</i>	$M_n$	$M_w$	$M_w/M_n$	<i>OH Eq. wt.</i>	$F_n$	$F_w$
1	780	970	1.24	354	2.21	2.73
2	1,410	1,690	1.20	650	2.17	2.59
3	2,060	2,540	1.23	1,041	1.98	2.44
4	2,830	3,300	1.17	1,268	2.23	2.60
5	3,450	4,110	1.19	1,481	2.33	2.78
6	4,300	5,010	1.16	1,705	2.52	2.94
7	4,690	6,010	1.28	1,902	2.47	3.16
8	5,860	7,420	1.27	2,073	2.83	3.58
9	6,940	9,050	1.30	2,200	3.15	4.11
10	11,760	21,540	1.83	2,426	4.85	8.88
Parent	2,960	6,250	2.12	1,256	2.35	4.98

molecular weight is plotted in figure 9.29, a plot of  $F_n$  versus  $M_n$ , and in figure 9.30, a plot of  $F_w$  versus  $M_w$ .

The increased functionality in the last three fractions is indicative of branching in the high molecular weight material. It is believed that the mechanical properties of the final cured resin are determined almost exclusively by the high molecular weight, highly functional portion of the polymer (Stephens et al., 1978).

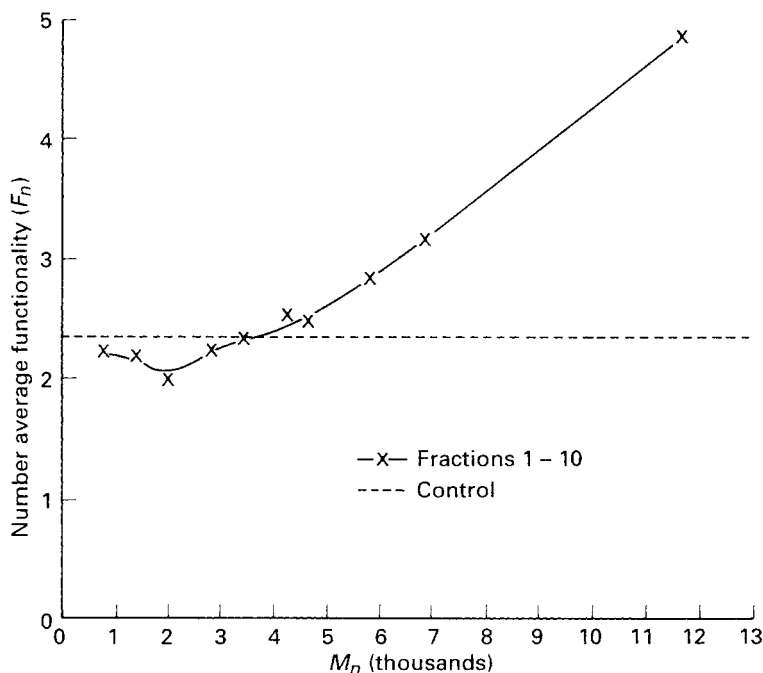


**Figure 9.29** Number average functionality versus number average molecular weight for HTPB fractions.

## Fractionation of Glycidyl Azide Polymer

Glycidyl azide polymer (GAP) is a promising solid rocket propellant binder currently in development. GAP exhibits several desirable performance properties including its energetic and smokeless characteristics. But its widespread use has been slowed by performance problems which could be related to low molecular weight species contained in the parent material (Watkins and Krukonis, 1990). Removal of oligomeric material from the polymer is a natural fit for supercritical fluid processing. Additionally, the ability to fractionate the polymer across its entire molecular weight distribution would make it possible to provide samples so that the mechanical properties of PBXs formulated with GAP could be evaluated as a function of molecular weight.

Two forms of GAP, the diol and triol, have been under evaluation. The experiments described in this section were performed on the diol having a molecular weight in the neighborhood of 2,350. The sample of GAP used in these experiments was designated L-11391 (3M Company) and contained approximately 2.5% of nonfunctional cyclic and oligomeric material. The structure of GAP diol is given in figure 9.31.

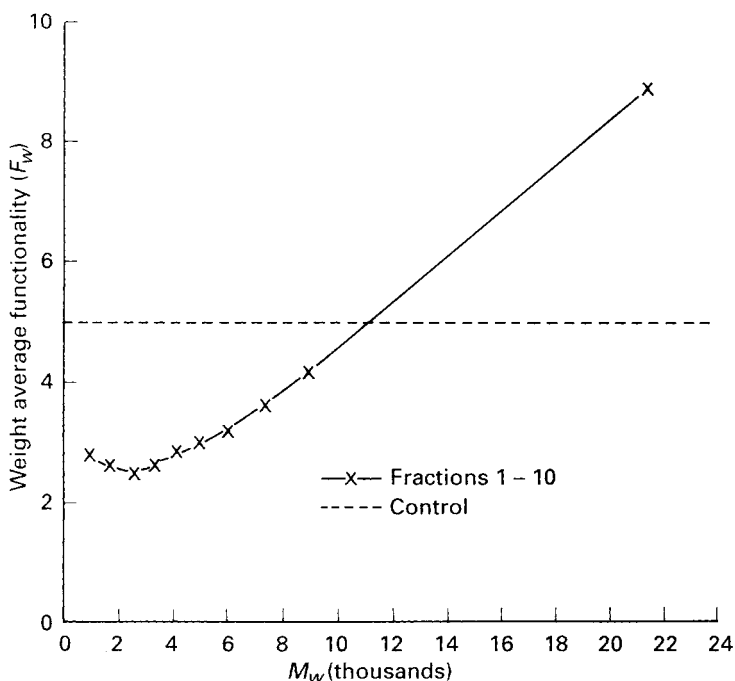
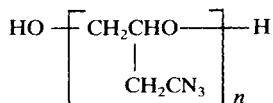


**Figure 9.30** Weight average functionality versus weight average molecular weight for HTPB fractions.

**Figure 9.31** Structure of GAP diol.



Approximately 11% by weight of the parent material could be extracted using carbon dioxide at 60°C up to a pressure of 648 bar. A summary of a carbon dioxide extraction of GAP L-11391 is given in table 9.23. Reverse phase HPLC chromatograms which demonstrate the removal of the low molecular weight species from the parent material are given in figure 9.32.

It is also desirable to fractionate GAP across its entire molecular weight distribution. It was found that GAP L-11391 is completely soluble in chlorodifluoromethane (F-22) at modest temperatures and pressures, therefore it could be used to fractionate the polymer. Prior to fractionation with F-22, the oligomeric material was once again removed with carbon dioxide. A summary of the conditions used in the experiment is given in table 9.24. The chromatograms of the parent material and each of the fractions are given in figure 9.33, and the progression of molecular weight is obvious.

**Table 9.23** Extraction of Glycidyl Azide Polymer (L-11391) with Supercritical CO<sub>2</sub> at 60°C. The Amount of Polymer Charged to the Column was 15.3 g

<i>Fraction</i>	<i>Maximum Pressure (psig)</i>	<i>CO<sub>2</sub> Used (g)</i>	<i>Mass Collected (g)</i>
1	2,500	1,150	0.19
2	4,200	1,120	0.75
3	7,200	970	0.38
4	9,400	1,080	0.43

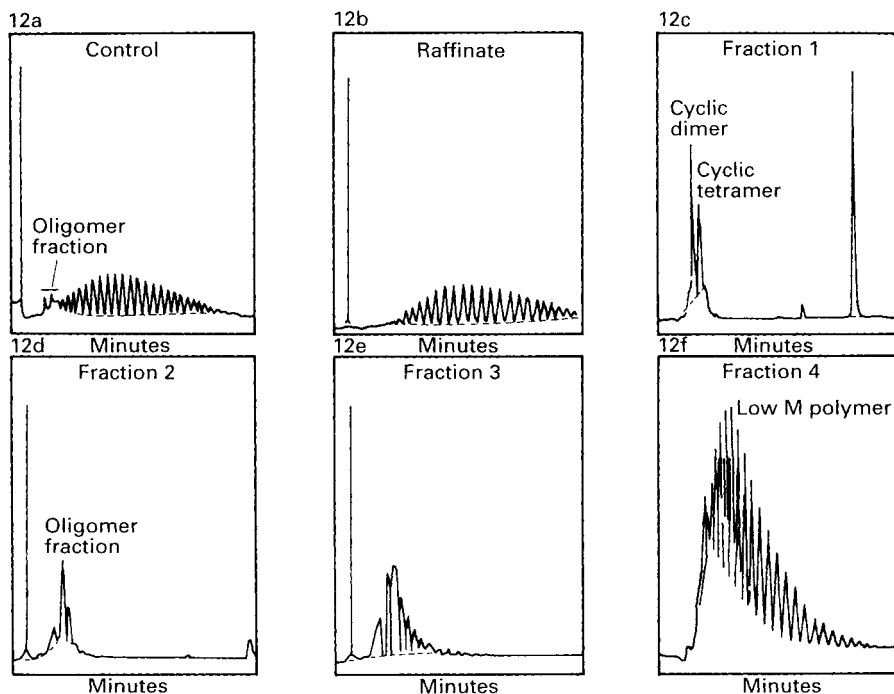


**Figure 9.32** HPLC chromatograms of L-11391 fractions from carbon dioxide extraction.

At the conditions used for the fractionation, chlorodifluoromethane is a liquid and is somewhat compressible. Because of the limited solubility of GAP in liquid chlorodifluoromethane (1–2% from the data in table 9.24) fractionation occurs by preferential dissolution of the lower molecular weight material, not by a dramatic increase in solvent strength with pressure. But there is some increase in solvent strength of liquids with pressure; Lemert and DeSimone



**Table 9.24** Fractionation of Glycidyl Azide Polymer (L-11391) with CO<sub>2</sub> and Liquid Chlorodifluoromethane (F-22) at 45°C. The Amount of Polymer Charged to the Column was 101.7 g

<i>Fraction</i>	<i>Solvent</i>	<i>Maximum Pressure (bar)</i>	<i>CO<sub>2</sub> Used (g)</i>	<i>Mass Collected (g)</i>	<i>Σ wt%<sup>a</sup></i>
1	CO <sub>2</sub>	345	3,890	4.66	0.044
2	CO <sub>2</sub>	655	5,220	7.16	0.112
3	F-22	179	775	15.97	0.263
4	F-22	221	830	21.39	0.466
5	F-22	221	1,080	20.63	0.661
6	F-22	255	1,300	16.21	0.815
7	F-22	359	2,430	17.50	0.980
8	F-22	483	1,170	2.07	1.000

<sup>a</sup>Cumulative amount of polymer removed from the columns.

(1991) have shown that the spectral polarity indices of gases, such as ethane, propane, and methyl ether, are a function of pressure at temperature levels significantly below their critical point. For example, the polarity index for propane increases from 0.82 at 50 bar to 1.37 at 300 bar at 37°C, conditions that are approximately 60°C below propane's critical temperature. Lemert points out that in liquid alkanes, an increase of approximately the same magnitude is seen when the solvent is changed from *n*-hexane to *n*-decane. The change in polarity indices with pressure for propane above its critical point is, as expected, much more dramatic. It is likely to be a combination of both factors, preferential dissolution and a slight change in solvent strength with pressure, which permits selective fractionation of GAP to occur using the conditions summarized in table 9.24.

The remainder of this chapter covers the material given in the first edition but with some modification and more explanation where necessary. Although much of the information on polymers/monomers given in the first edition is now ten years old, some of the work is serving as a motivation for the reexamination of supercritical fluids in several current applications. For example, the 1976 Georgia Institute of Technology work on spinning fibers from supercritical fluid solution is being reconsidered as a potentially attractive research area. This is because some solvents used in fiber spinning are experiencing increased scrutiny due to adverse environmental effects. Spinning fibers from "gas solvents" may provide attractive environmental and technical benefits. Some of the work that we described in the first edition was carried out in the 1980s for exploratory reasons. However, current regulatory pressures on polymers used in a variety of applications including food packaging and medical tubing and structures, is motivating an examination of SCF processing to reduce the amount of residual solvents and monomers that can migrate to

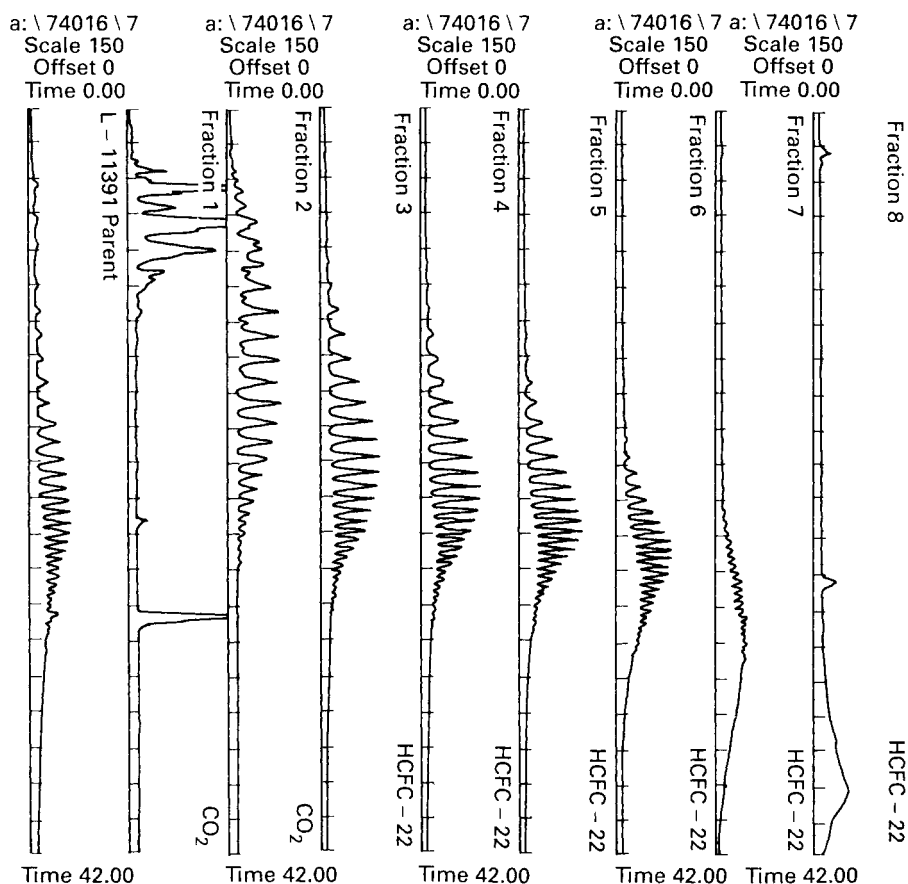


Figure 9.33 HPLC chromatograms of L-11391 fractions.

the surface of the polymer. High-vacuum and wiped-film evaporation is often unable to achieve the low levels sought, and supercritical fluid extraction can be a viable alternative technology for selected applications.

## OLIGOMER EXTRACTION FROM POLYMERS

There are a number of studies in the literature that describe the use of supercritical fluids to extract cyclic and low molecular weight oligomers from polymers. U.S. Patent 4,306,058 (Copelin, 1981), assigned to E. I. du Pont, describes the removal of cyclic oligomers from polyoxyalkylene. For instance, bubbling supercritical propylene at conditions of 100°C and 80 bar through the

polymer was effective in reducing the cyclic content in the polymer from 8 wt% to 2 wt%. These cyclic oligomers, which are saturated entities, are considered impurities since they are not incorporated in the polyurethane that is formed when the polyoxyalkylene is subsequently reacted. The results described in the patent represent the extraction of low molecular weight oligomers from polymers in a wider range of molecular weights. The examples given in this patent point out the ability of supercritical fluids to purify a polymer, which would be quite difficult to purify by distillation or by liquid organic solvent extraction because the vapor pressure of the interfering species is too low or the liquid organic solvent cannot be made sufficiently selective.

Another reference on the supercritical extraction of low molecular weight oligomers from polymers describes the upgrading of a silicone polymer, designated OV-17, used as a gas chromatography stationary phase (Barry, Ferioli, and Hubball, 1983). The material tested, a polyphenylmethylsiloxane, is a very viscous polymer containing macrocyclic and low molecular weight linear oligomers that interfere with the performance of the material when it is used as a chromatographic substrate in a wide temperature scan, temperature-programmed analysis. The low molecular weight oligomers can bleed from the chromatographic column during a temperature-programmed ramping. It is reported that supercritical carbon dioxide at conditions of about 140 bar and 35°C is found to extract 30% of the original polymer, and the residual heavier molecular weight portion yielded much improved characteristics in the chromatography application.

The specific extraction test described in the paper is not strictly a fractionation into a number of narrow cuts, as suggested by the title of the paper. But the results given in the paper show that polyphenylmethylsiloxane polymers can be dissolved by supercritical carbon dioxide at quite modest pressures. Other work has been carried out on both extraction and fractionation of OV-17, and quite different results have been obtained (Krukoniš, 1982b). The fractionation results are given later in this chapter (in the section on silicone oils and polymers). To summarize, the results show that carbon dioxide at 40–100°C and at pressure levels as high as 448 bar (6,500 psia) cannot dissolve the phenylmethylsiloxane polymer and that less than 5% of the material can be extracted at this pressure level.

## **SUPERCritical FLUID CHROMATOGRAPHY ANALYSIS OF POLYSTYRENE**

The third category of supercritical fluid–polymer activity reported in the literature describes the use of SCF chromatography to separate oligomers. The classic paper in this field is by Jentoft and Gouw (1969), who reported their work on the supercritical fluid chromatographic separation of a “monodisperse” polystyrene. Jentoft and Gouw use the quotation marks because, as they report later in the article, the polystyrene sample that they tested

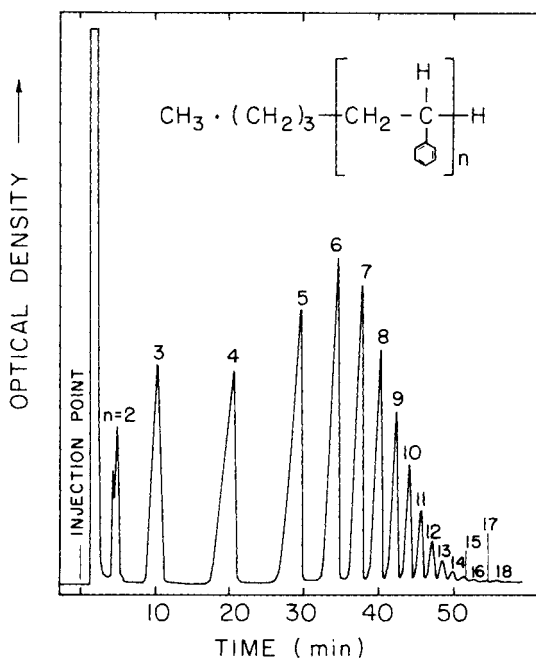


**Figure 9.34** Chromatogram of a polystyrene sample fractionated in a process using a supercritical fluid chromatograph (redrawn from Jentoft and Gouw, 1969). The sample has a nominal molecular weight of 600.

contained a large number of oligomers. The particular material that was tested is a highly purified calibration standard used for determining gel permeation chromatography elution profiles. The authors show that the "monodisperse" standard can be separated into at least seventeen separate oligomers. In this instance the SCF mobile phase of the chromatograph was *n*-pentane containing 5 wt% methanol. Figure 9.34 shows the resolution achieved with the SCF chromatograph. In a later paper, Jentoft and Gouw (1970) present the data verifying the molecular weight fractionation that they achieved.

The resolution of the polystyrene oligomers shown in figure 9.34 is influenced more by the interactions of the small amount of methanol in the mobile phase with the stationary phase of the chromatographic column than by the pressure-dependent dissolving capabilities of a supercritical fluid. Supercritical pentane was such a good solvent for polystyrene that without 5 wt% methanol the polystyrene would quickly elute from the column unfractionated. After the Jentoft and Gouw paper appeared, many other authors published on the use of supercritical fluid chromatography to fractionate low molecular weight oligomers of polystyrene (Klesper and Hartmann, 1977) and polyethylene glycol and polyvinyl chloride (Giddings, Myers, and King, 1969).

Fractionation of a polymer into its separate oligomers, as reported by Jentoft and Gouw, is an impressive achievement for supercritical fluid solvents. However, in general it is achieved only in conjunction with chromatography with materials processed at microgram to milligram levels. Supercritical fluid

chromatography is not covered in this book in any detail but polymer resolution studies are given where relevant. Enough literature exists on supercritical fluid chromatography, dating from the first paper by Klesper and coworkers in 1964 to the present, to fill a comprehensive volume on that subject alone. As was related in the first edition, in March 1985 fifteen papers on emerging supercritical fluid chromatography were presented at the Pittsburgh Conference in New Orleans. Since that time there have been literally a score of sessions at various conferences and several books and symposium proceedings have been published.

## POLYMER FIBER SPINNING

A 1977 report for the National Science Foundation describes an interesting program, performed at Georgia Institute of Technology, for spinning polymer fibers from a supercritical fluid solution (Bangert et al., 1977). This novel process entails dissolving a polymer in a high-pressure fluid and "extruding" the gaseous solution through a die. Polymers studied in the program include polypropylene, polybutene-1, and nylon-6. The solubilities of these materials in carbon dioxide and in *n*-butane, given in the report, are reproduced in table 9.25.

The Georgia Tech workers show that the polymers dissolve in carbon dioxide to high solubility levels at modest pressures. As noted in this chapter and in chapter 3, the pressure levels needed to dissolve a polymer are directly related to the molecular weight of the polymer, its backbone structure (i.e., crystallinity), and its chemical composition. No information on the comparative molecular weight of the polymers is given in the report, but, from the data on melting (softening) points provided it is inferred that the molecular weight is typical of commercial material. Polymer solubility in supercritical fluids is also directly related to polymer tacticity (Krukoniš, 1981e). The polypropylene used in the Georgia Tech solubility studies is isotactic, inferred from the melting range listed in table 9.25; a melting range around 170°C is typical of isotactic

**Table 9.25** Solubility of a Variety of Polymers in Different Supercritical Fluids (Bangert et al., 1977)

<i>Polymer</i>	<i>Gas</i>	<i>Pressure (bar)</i>	<i>Temperature (°C)</i>	<i>Solubility (wt%)</i>	<i>Polymer Melting Range (°C)</i>
Polypropylene	CO <sub>2</sub>	456–861	163–208	6–38	162–176
Nylon-6	CO <sub>2</sub>	405–517	233–241	13–16	212–225
Polybutene-1	CO <sub>2</sub>	304–912	131–150	6–38	~126
Polybutene-1	<i>n</i> -Butane	122–172	167–190	5–21	~126
Polypropylene	<i>n</i> -Butane	132–193	166–186	5–20	162–176

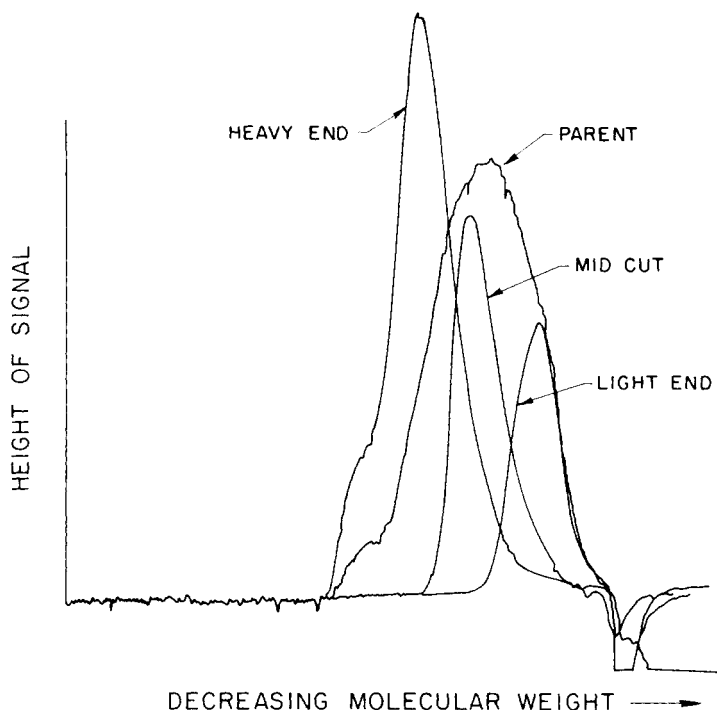


**Figure 9.35** GPC chromatogram of a polycarbosilane fractionated with supercritical ethylene.

polypropylene. In comparison, atactic (amorphous) polypropylene melts at temperatures as low as 80°C and it is quite soluble in carbon dioxide at low pressure and temperature levels. Solubility at 100°C and 250 bar is 10–20 wt%, depending upon the grade of atactic polypropylene; for comparison, the solubility of isotactic polypropylene in carbon dioxide at these conditions is virtually nil (Krukoniš, 1981e).

An interesting statement is made in the NSF report about the relative solubilities of the three polymers in carbon dioxide (Bangert et al., 1977). For example, it is found at 400 bar pressure that the solubility of nylon-6 is about twice that of the other two polymers. Table 9.25 shows that the temperature tested to dissolve nylon-6 is 50 to 100°C higher than that for polypropylene and polybutene-1. The substantially higher temperature of 240°C might be expected to lower the solvent power of carbon dioxide relative to that at the 130–150°C level tested for polybutene-1. But in spite of the higher temperature, nylon dissolves to a higher concentration. From this finding the researchers suggest that “carbon dioxide with no dipoles but with strong quadrupoles . . . may be a good solvent for relatively polar hydrogen bonded and, perhaps, other dipole bonded polymers.” Although a higher temperature is needed to dissolve

nylon-6, the density of carbon dioxide is still at density levels of 0.44–0.52 g/cc at 400 to 500 bar so that carbon dioxide can realistically be considered a dense gas. The higher temperature is needed to soften the polymer and to impart enough thermal motion to the molecules to weaken the nylon–nylon interactions, which allows easier solvation by carbon dioxide. The report goes on to describe the spinning studies that are the major thrust of the program, and it is reported that fibers with diameters ranging up to 25  $\mu\text{m}$  can be spun from polypropylene dissolved in supercritical propylene.

## FRACTIONATION OF VARIOUS POLYMERS

### Polycarbosilane

Polycarbosilane polymers are being examined for use in producing silicon carbide shapes used in high-temperature applications, such as turbine blades or vanes for advanced aircraft engines. Traditionally, ceramics, such as silicon carbide and silicone nitride, have been used as materials for extending combustion temperatures in engines to higher levels, thus achieving higher energy conversion efficiency. Most ceramic parts are currently produced by hot-pressing or sintering powders at a very high temperature, typically 2,500°C. The production process is quite expensive and the sintering process requires the use of SiC or Si<sub>3</sub>N<sub>4</sub> powder of high purity, which is also quite expensive. In contrast, liquefied polycarbosilane polymers have the advantage that they can be poured into a specific mold and converted to a silicon carbide shape at about 1,200°C, thus they potentially lower the cost of producing ceramic parts, especially when complex shapes are needed.

Polycarbosilane is used to spin fibers that can be converted into silicon carbide reinforcements. To optimize spinning or part formation, a polycarbosilane polymer that has a narrow molecular weight distribution is required. Figure 9.35 gives a pictorial comparison of the gel permeation chromatograms (GPCs) of a polycarbosilane with a nominal molecular weight of 7,000 and the three fractions obtained using supercritical ethylene as the fractionating solvent. The operating conditions are at 100°C and over a pressure range of 190 to 517 bar. An inspection of the peak widths of the respective fractions in figure 9.35 shows that a substantial narrowing of the molecular weight range in each fraction has been achieved and that high and low molecular weight oligomers can be excluded from the desired fraction.

### Silicone Polymers

Other studies reported in the literature involve the fractionation of a high molecular weight silicone oil, a poly(dimethyl)siloxane (Krukoniš, 1983c). In the early 1980s, the material was being tested for an electronics application,

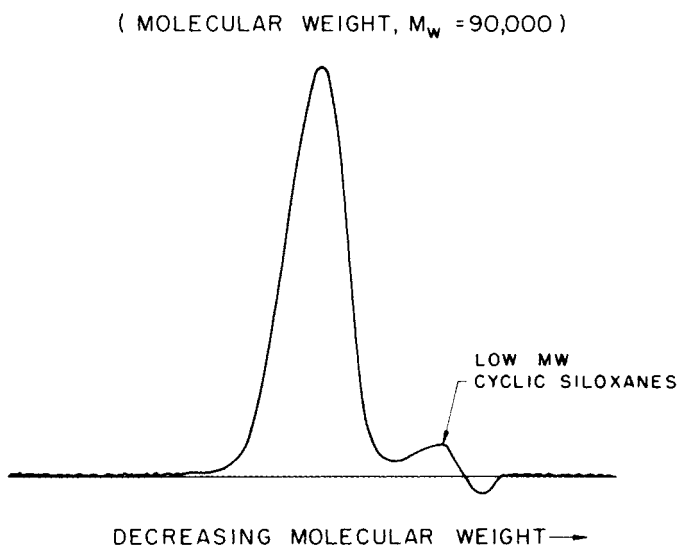


**Figure 9.36** GPC chromatogram of a polydimethylsiloxane polymer.

but migration of low molecular weight species hindered the performance of the polymer. Figure 9.36 is a GPC chromatogram of the parent oil from which it can be seen that the oil contains low molecular weight cyclic reactant and equilibration products discussed earlier. The polymer was extracted with supercritical carbon dioxide at 80°C over an ascending pressure range from 124–448 bar (1,800–6,500 psia). Six arbitrary fractions were obtained from the parent charge. The molecular weight analysis of the parent and of the fractions is given in table 9.26. The fractions are not of equal size and the percent contributions of each fraction are listed in the third column of the table.

As a pictorial comparison of the peak widths of these fractions, figure 9.37 superposes the chromatograms of fraction 1 and fraction 6 onto the chromato-

**Table 9.26** Molecular Weight Distribution in Parent Polydimethylsiloxane and in Fractions Separated by Supercritical CO<sub>2</sub>

<i>Fraction</i>	<i>Number Average Molecular Weight</i>	<i>Weight Average Molecular Weight</i>	<i>Parent (wt%)</i>
Parent	42,500	90,000	100.0
1	428	789	4.0
2	3,310	11,500	5.1
3	27,100	53,200	27.7
4	43,000	57,500	27.9
5	58,900	91,500	28.3
6	112,600	149,900	7.0



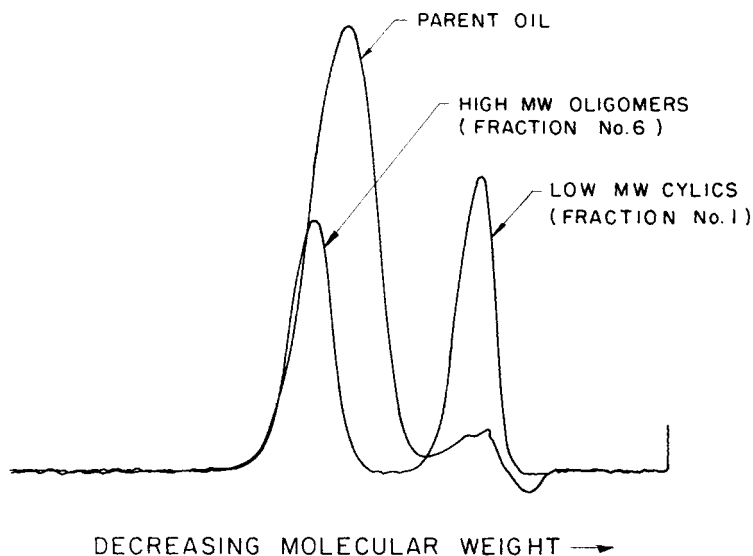


**Figure 9.37** Gel permeation chromatogram of the parent polydimethylsiloxane polymer with fractions 1 and 6 obtained by fractionating with a supercritical fluid solvent.

gram of the parent. Figure 9.37 shows that fraction 1 contains only the low molecular weight cyclics and linears. The degree of fractionation depicted in this figure is an excellent example of the adjustable dissolving and extracting power of a supercritical fluid. The GPC chromatogram of the high molecular weight fraction shown in figure 9.37 and the corresponding data in table 9.26 show that a silicone polymer with a molecular weight of 100,000 can be dissolved by supercritical carbon dioxide at 448 bar (6,500 psia).

The behavior of poly(phenylmethyl)siloxane is quite different from poly(dimethyl)siloxane. The replacement of one of the methyl groups on the silicon with a phenyl group lowers the solubility dramatically. The molecular weight of the parent polymer is given in table 9.27. The average molecular weight of the parent is about 2,100, and the polymer of this molecular weight does not dissolve to any reasonable extent in carbon dioxide. For example, in stripping tests at the extraction pressures as high as 448 bar (6,500 psia) and over a temperature range of 40–100°C, only 4 wt% of the polymer is found to be extracted (Krukons, 1982c). These results are not in agreement with the results described by Barry, Ferioli, and Hubball (1983), who reported that 30% could be extracted with carbon dioxide at 40°C and at the low pressure of 103 bar (1,500 psia).

Supercritical ethylene is a better solvent and propane and propylene still

**Table 9.27** Molecular Weight Distribution in Parent Poly(phenylmethyl)siloxane and in Fractions Separated by Supercritical Fluid Ethylene

<i>Fraction</i>	<i>Number Average Molecular Weight</i>	<i>Weight Average Molecular Weight</i>	<i>Parent (wt%)</i>
Parent	2,130 <sup>a</sup>	2,610	100.0
1	1,510	1,587	4.5
2	1,530	1,628	3.1
3	1,514	1,637	12.3
4	1,730	1,839	17.7
5	1,810	2,134	25.8
6	2,660	2,825	9.3
7	3,420	3,780	25.0
8	5,300	6,500	2.3

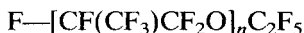
<sup>a</sup>The poly(phenylmethyl)siloxane used for gas chromatography substrates derives from a molecular distillation of commercial poly(phenylmethyl)siloxane and hence contains little low-molecular-weight material. The typical commercial material has a distribution of number average molecular weight 1,380–weight average molecular weight 2,260.

better for poly(phenylmethyl)siloxane. In fact, the latter two gases exhibit such a high dissolving power that narrow-cut fractionation is much more difficult to achieve. Recall that for deasphalting (chapter 7) Wilson, Keith, and Haylett related that butane was “too good” a solvent for the petroleum fractions and separation could not be achieved. Similarly propylene is such a good solvent that it cannot easily fractionate the poly(phenylmethyl)siloxane unless the pressure is kept very low. The results of supercritical ethylene fractionation are given in table 9.27. An ethylene pressure of 586 bar (8,500 psia) at 80°C is required to dissolve a poly(phenylmethyl)siloxane of molecular weight 5,000. For comparison, carbon dioxide at 448 bar (6,500 psia) can dissolve poly-(dimethyl)siloxane polymers with molecular weight as high as 100,000.

Why would the solubility levels of poly(phenylmethyl)siloxane and poly-(dimethyl)siloxane differ so considerably in carbon dioxide, ethylene, propane, and propylene? The answer has to do with the physical properties of the side groups on the backbone of the polymer. Replacing a nonpolar methyl group with a quadrupolar phenyl group greatly increases the polarity of the polymer. And the side groups are constrained to interact with one another since they are fixed to the backbone of the polymer. The results from the siloxane fractionations are similar to those described earlier for the ethylene–methyl acrylate copolymer fractionation in propane and F-22. Hasch et al. (1991) have also shown that replacing a nonpolar group with a polar group in the backbone of a copolymer can significantly reduce the solubility of the copolymer in ethane and propane but can increase the solubility in ethylene and propylene.

## Perfluoroalkylpolyether

Krukonis (1983c) reports on the fractionation of a perfluoroalkylpolyether, which is an example of a polymer with a chemical makeup very different in structure from that of the siloxanes and carbosilanes. The perfluoroalkylpolyether has the structure



This oil exhibits an extremely low vapor pressure and is resistant to attack by corrosive or oxidizing materials. Thus, it is used as a diaphragm fluid in severe-service pumping such as compressing fluorine, oxygen, uranium hexafluoride, and similar refractory gases. Its viscosity and lubrication properties coupled with its very low vapor pressure have also motivated its use as a computer disc lubricant and also as a seal fluid for computer disc drives. Its low vapor pressure precludes bleeding into the disc cavity in the computer disc drive applications. In its applications as a computer disc lubricant it provides a long-lasting barrier between the magnetic head and the magnetic memory particles on the surface of the computer disc.

The fluoroether dissolves in a number of gases, e.g., carbon dioxide, ethylene, and ethane. Carbon dioxide was selected for the tests that are described subsequently. The fluoroether was fractionated with supercritical carbon dioxide at 80°C over a pressure range from 82 bar (1,200 psia) to 275 bar (4,000 psia). Five approximately equal fractions were obtained, and they were analyzed for their viscosity characteristics. The results of the viscosity analysis are shown in figure 9.38. Published data on the fluoroether oil, Krytox® 143AD gives the molecular weight of the commercial oil as about 7,000 (Anon., duPont Tech. Bull., G-6). The viscosity of the parent oil at room temperature is about 2,000 cps, whereas the viscosities of the five fractions at room temperature are in the range 800–9,000 cps. If an eight-tenths-power relationship between viscosity and molecular weight is assumed, the average molecular weights of the fractions range from about 3,400 to 23,000.

According to the duPont brochure, fluoroether oil is not soluble in hexane. The solvent properties of carbon dioxide are often compared to those of hexane (Hyatt, 1984). Hyatt examines supercritical carbon dioxide from the perspective of an organic chemist, and his conclusions are a good summary of his findings. He states that

Carbon dioxide exhibits properties typical of hydrocarbon solvents, such as toluene; however, for basic molecules, such as pyrrole, CO<sub>2</sub> provides more hydrogen bonding basicity than do hydrocarbon solvents. No significant difference in polarity can be detected between the liquid and supercritical phases. It is hoped that this view of CO<sub>2</sub> as a “hydrocarbon” solvent with unusual properties (infinite compressibility in the supercritical state, low surface tension and viscosity, low

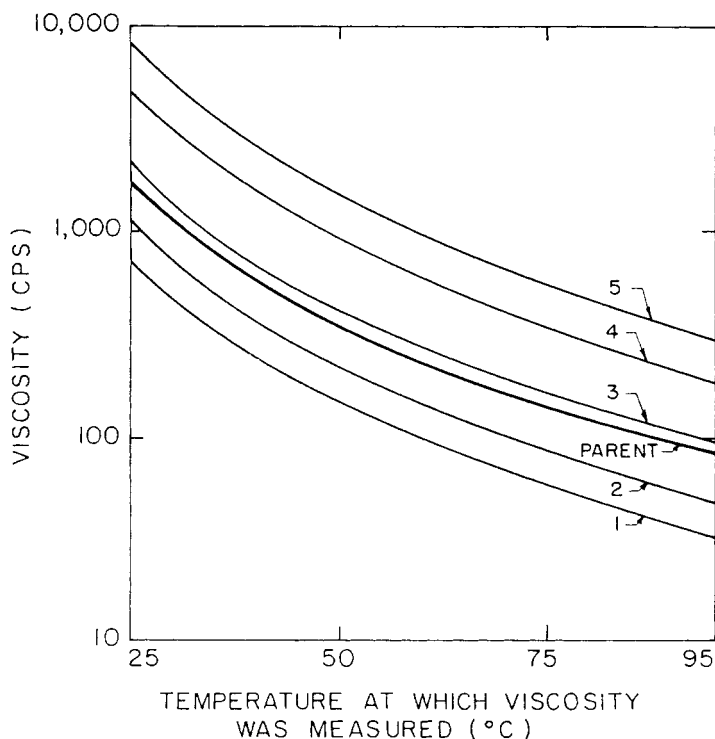


**Figure 9.38** Viscosity behavior of a perfluoroether fractionated with supercritical carbon dioxide.

polarizability, and ease of recovery) will lead to additional exploration of its utility in chemistry.

We would argue that toluene should be replaced with hexane, because hexane exhibits purely dispersion forces that more accurately describe carbon dioxide's solvent characteristics, in spite of the fact that carbon dioxide can also exhibit Lewis acid-base behavior, hydrogen bonding, and polar behavior. Carbon dioxide is not, strictly speaking, a nonpolar molecule, since it has a very strong quadrupole that can interact with dipoles of other molecules. To a good first approximation, it is often possible to generally assess the ability of supercritical carbon dioxide to dissolve a compound by examining the solubility of the compound in hexane. A high percentage of compounds that exhibit hexane solubility dissolve in carbon dioxide, too. In this very interesting case of the fluoroether, the behavior of hexane and carbon dioxide is completely different. The fluoroether is not hexane-soluble but it is carbon dioxide-soluble, and the reasons for this discrepancy are not understood at present.

## Polystyrene

Earlier in this section, several references are discussed on the supercritical fluid chromatography fractionation of a polystyrene standard of molecular weight 600. The same polystyrene standard is used by Krukoni (1983b) to investigate the ability of supercritical fluids to fractionate polystyrene without the use of a chromatographic stationary phase. Sequential stripping of the polystyrene is carried out with carbon dioxide at a temperature of 100°C and at seven pressure levels ranging from 103 bar (1,500 psia) to 524 bar (7,600 psia). In this case, all of the polymer is dissolved by carbon dioxide at 524 bar (7,600 psia). The resulting fractions are analyzed by gel permeation chromatography. The degree of polymerization (DP) of the oligomers comprising the original polystyrene standard ranges from about 2 to 9. The results from the supercritical carbon dioxide fractionation are given in table 9.28, which lists the DP of the oligomers and the concentrations of each oligomer in the respective fraction. Table 9.29 gives the molecular weight data for the respective fractions calculated from the compositions (degree of polymerization) given in table 9.28. Polydispersity values are given in the right-hand column; polydispersity is the ratio of weight average molecular weight to number average molecular weight.

The narrowing of the molecular weight range, i.e., the decrease in polydispersity, of the respective fractions is quite dramatic. The polystyrene standard, itself an already low-polydispersity polymer, has been separated into seven fractions of narrow molecular weight and still lower polydispersity. Recall that supercritical pentane tested by Jentoft and Gouw is “too good” a solvent for polystyrene: it achieved no fractionation. But the addition of 5 wt% methanol to the pentane increased the interaction of the dissolved polymer with the chromatographic stationary phase, which resulted in a relative elution of oligomers.

**Table 9.28** Analysis of Polystyrene of Molecular Weight 600 and Fractions Obtained with Supercritical CO<sub>2</sub>

<i>Fraction</i>	<i>Composition (%) of Degrees of Polymerization</i>								
	<i>1</i>	<i>2</i>	<i>3</i>	<i>4</i>	<i>5</i>	<i>6</i>	<i>7</i>	<i>8</i>	<i>9</i>
Parent	0.7	5.4	12.3	15.8	16.6	15.7	12.7	20.7	—
1	0.7	45.0	33.4	11.4	3.6	—	—	—	—
2	5.7	21.5	35.6	23.5	11.2	5.7	—	—	—
3	2.6	6.0	18.3	26.7	23.8	15.7	9.5	—	—
4	—	3.3	8.7	14.1	18.9	19.7	35.2	—	—
5	—	1.3	2.7	5.3	10.1	13.8	18.0	48.8	—
6	—	—	—	—	10.2	13.0	17.7	19.1	40.0
7	—	—	—	—	—	19.3	17.0	20.4	41.8

**Table 9.29** Molecular Weights of Polystyrene Standard and Fractions

<i>Fraction</i>	<i>Number Average Molecular Weight</i>	<i>Weight Average Molecular Weight</i>	<i>Polydispersity</i>
Parent	552	634	1.15
1	305	330	1.08
2	370	408	1.10
3	489	530	1.08
4	590	647	1.10
5	736	792	1.08
6	827	854	1.03
7	857	875	1.02

Jentoft and Gouw (1969, 1970) worked on supercritical fluid chromatography at the microgram level. The results given in tables 9.28 and 9.29 come from work at the multigram level. And it is easy to extrapolate to the level of hundreds or thousands of kilos. Although the requirement for thousands of kilos of narrow molecular weight polystyrene has not been reported, other polymers can reach or surpass that level if they are successfully developed.

## Chlorotrifluoroethylene

Chlorotrifluoroethylene (CTFE) and bromotrifluoroethylene (BTFE) polymer oils are used as flotation fluids for some inertial guidance devices in missile and space applications. These fluids operate in extremely high-*g* rotational environments, where polymers containing a range of oligomers can actually be fractionated by sedimentation brought about by the high centrifugal forces; the sedimentation interferes with the operation and performance of the guidance system. Substantial effort is being directed to the synthesis of oils and polymers of appropriate density and composition and to the fractionation of the CTFE oil into narrow-polydispersity fractions (or into actual monodisperse oligomers) using molecular distillation or prep-scale liquid chromatography. In general, molecular distillation and prep-scale liquid chromatography are expensive separations processes, and supercritical fluid extraction or fractionation can be viable as an alternative, especially if a superior product can be obtained by the process.

Figure 9.39 is a gas chromatography-mass spectroscopy (GC-MS) analysis of the CTFE parent. It contains four primary peaks corresponding to degrees of polymerization of 6, 7, 8, and 9, respectively. The relative amounts of each of the oligomers in the parent oil are given in table 9.30. As figure 9.39 and the data in table 9.30 show, the oil is composed of primarily 7-mer and 8-mer oligomers.

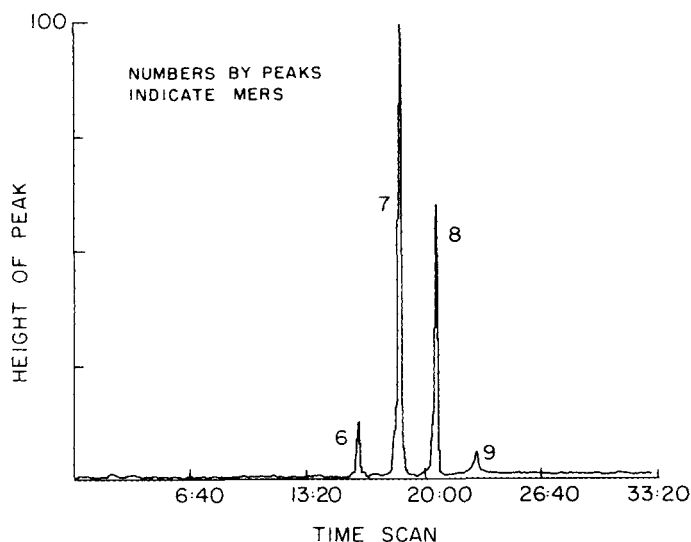


**Figure 9.39** GC-MS chromatogram of a chlorotrifluoroethylene polymer.

CTFE dissolves in a number of gases, e.g., carbon dioxide, ethylene, and the chlorofluorocarbons. In this instance, ethylene is arbitrarily chosen. The polymer is easily fractionated by supercritical ethylene at a temperature level of 90°C and a pressure range from 124 to 330 bar. Although eight fractions are obtained (see table 9.30), these fractions do not represent the results of an

**Table 9.30** Composition of Fractions of Chlorotrifluoroethylene Polymer Obtained by Supercritical Ethylene Processing

Fraction	Oligomer Composition (wt%)				Parent (wt%)
	6-mer	7-mer	8-mer	9-mer	
Parent	4.5	49.5	39.5	6.5	100.0
1	51.1	37.6	12.3		5.8
2	24.4	73.5	2.0		8.6
3	7.6	86.4	6.0		20.2
4	1.8	75.3	22.9		15.2
5	0.7	38.7	58.1	2.5	22.8
6		5.7	94.2	0.1	15.6
7		0.6	66.4	33.0	10.5
8		3.0	55.5	41.5	1.3

optimized SCF fractionation study. Instead, the results are presented for the purpose of indicating the breadth of application of supercritical fluid fractionation.

The composition data in table 9.30 show that substantial changes in the ratios of mers is achieved in any one fraction relative to the parent. For example, in fractions 3 and 6 the predominant oligomer represents about 90% of the fraction. To give a pictorial comparison of the composition of those two fractions relative to that of the parent material, the GC-MS traces of the two fractions, fractions 3 and 6, are shown in figures 9.40 and 9.41, respectively. A comparison of the figures and the data in table 9.30 shows that supercritical ethylene is a reasonably effective fractionation solvent. Again, no effort is made to optimize this SCF fractionation.

Krukonis (1982a) also found that in some cases supercritical fluid fractionation can concentrate polymer species that escape detection during conventional analysis of the parent polymer. Consider, for example, figure 9.42, which is the GC-MS trace of fraction 8, whose composition was given in table 9.30. Although the integrator calculated the 7-, 8-, and 9-mer concentrations of this fraction to total to 100%, a trace of a higher mer (identified by mass spectroscopy to be a 10-mer) is now evident and is identified in figure 9.42. The presence of the additional peak in figure 9.42 is indicative of the ability of supercritical fluid solvents to concentrate and allow easy identification of minute quantities of compounds that are present in a mixture.

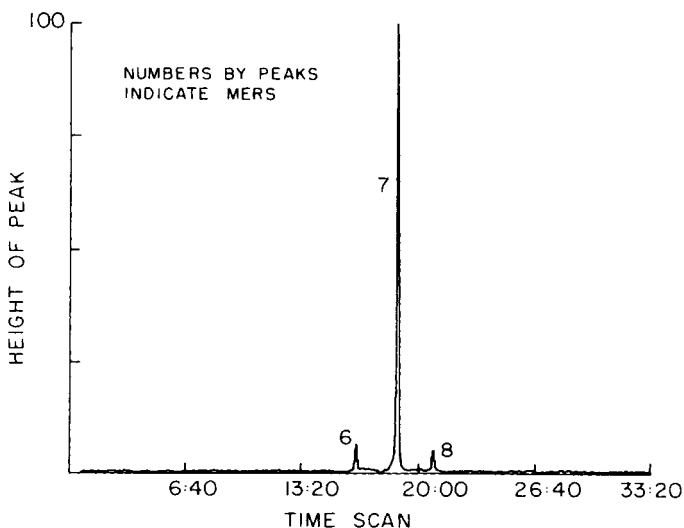


**Figure 9.40** GC-MS chromatogram of fraction 3 of the chlorotrifluoroethylene polymer fractionated with supercritical ethylene.



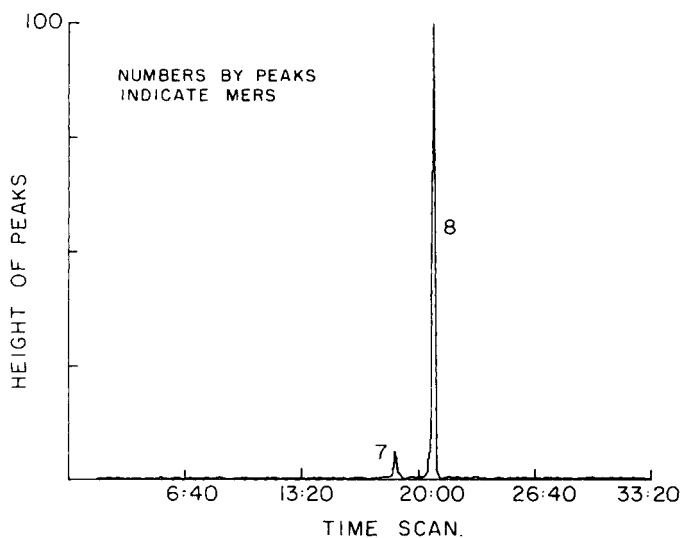


**Figure 9.41** GC-MS chromatogram of fraction 6 of the chlorotrifluoroethylene polymer fractionated with supercritical ethylene.

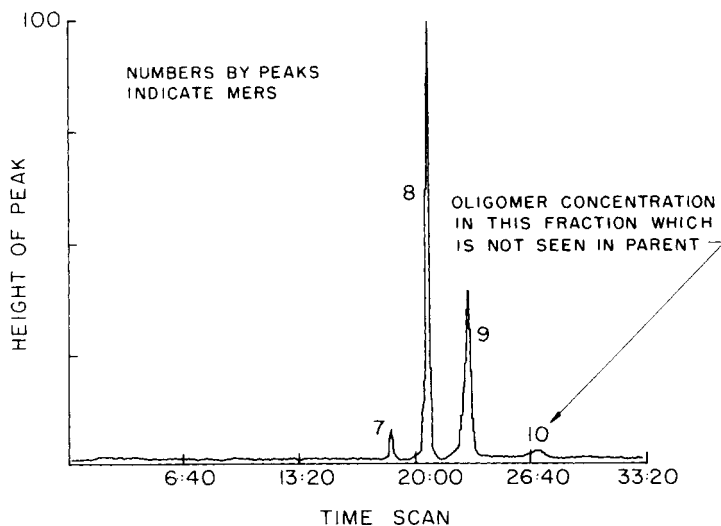


**Figure 9.42** GC-MS chromatogram of fraction 8 of the chlorotrifluoroethylene polymer fractionated with supercritical ethylene.

**Table 9.31** Polymers Tested for Fractionation

Type of Polymer	Name	Structure
Liquid crystal	Functionally terminated poly(dimethyl)siloxanes	$\text{H}_2\text{N}-(\text{CH}_2)_3-\left[\text{Si}(\text{CH}_3)_2\text{O}\right]_x-\left[\text{Si}(\text{C}_6\text{H}_5)_2\text{O}\right]_y-\text{Si}(\text{CH}_3)_2-(\text{CH}_2)_3-\text{NH}_2$
Photoresist	Polysilastyrene	$(\text{CH}_3)_3\text{Si}-\left[\text{Si}(\text{CH}_3)_2\right]_x-\left[\text{Si}(\text{C}_6\text{H}_5)_2\right]_y-\text{Si}(\text{CH}_3)_3$
Polymeric surfactant	Carboxylic acid-terminated perfluoroalkyl-polyether	$\text{HOOC}-[\text{CF}(\text{CF}_2)\text{CF}_2\text{O}]_n\text{C}_2\text{F}_5$

## Functionally Terminated Liquid Crystal and Photoresist Polymers

In the first edition of this book a report of the results completed under the National Science Foundation funding was given of the supercritical fluid fractionation of a number of liquid crystal and photoresist polymers (Krukoniš, 1984b). Table 9.31 gives the structures of several polymers that were tested on the program. Results with three of these polymers are presented in order to illustrate the extent of separation that can be achieved by supercritical fluid fractionation.

The functionally terminated polysiloxanes were under evaluation as precursors of block copolymers. Fundamental studies on the effects of molecular structure, molecular weight, and polydispersity on polymer characteristics and performance are being carried out at a number of laboratories, e.g., by McGrath and Wilkes and coworkers at Virginia Polytechnic Institute and State University (McGrath et al., 1982).

Like many poly(dimethyl)siloxanes the functionally terminated (carboxypropyl) polymer dissolves in a number of gases such as carbon dioxide, ethylene, and ethane. Table 9.32 gives the average molecular weight of the parent carboxypropyl-terminated poly(dimethyl)siloxane and the seven fractions derived from the parent by fractionation using supercritical carbon dioxide. The molecular weight analysis was carried out by end-group titration. As

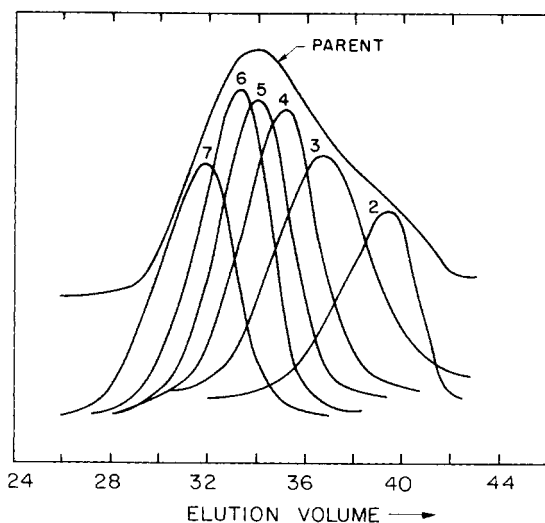
**Table 9.32** Fractionation of Carboxypropyl-Terminated Polydimethylsiloxane of Nominal Molecular Weight 6,000 with Supercritical CO<sub>2</sub>

<i>Fraction</i>	<i>Parent (wt%)</i>	<i>Number Average Molecular Weight</i>	<i>Weight Average Molecular Weight</i>	<i>Polydispersity</i>
Parent	100.0	6,400	13,310	2.08
1	4.5		Cyclics	
2	5.0	1,580	2,000	1.27
3	20.7	3,300	4,690	1.42
4	22.2	5,700	7,350	1.29
5	11.6	7,350	9,480	1.28
6	24.2	10,300	13,080	1.27
7	9.0	12,850	16,320	1.27

expected from consideration of solute-solvent interaction and as shown in the table, fraction 1 contains no titratable functionality, and it is designated "cyclics" (octamethyl cyclotetrasiloxane and other equilibration products). The other data in the table show that the nominal 6,000 number average molecular weight polymer has been fractionated into low polydispersity cuts with molecular weight as high as 13,000.

A pictorial presentation of the fractionation is given in figure 9.43, which compares the GPC chromatograms of each supercritical-fluid-separated fraction with that of the parent polymer. The narrowing of the molecular weight range in the fraction and the progression of average molecular weights is ascertained from the GPC chromatograms assembled below the chromatogram of the parent polymer.

**Figure 9.43** GPC chromatogram of the parent carboxypropyl-terminated polydimethylsiloxane and the fractions obtained by fractionation with supercritical carbon dioxide.



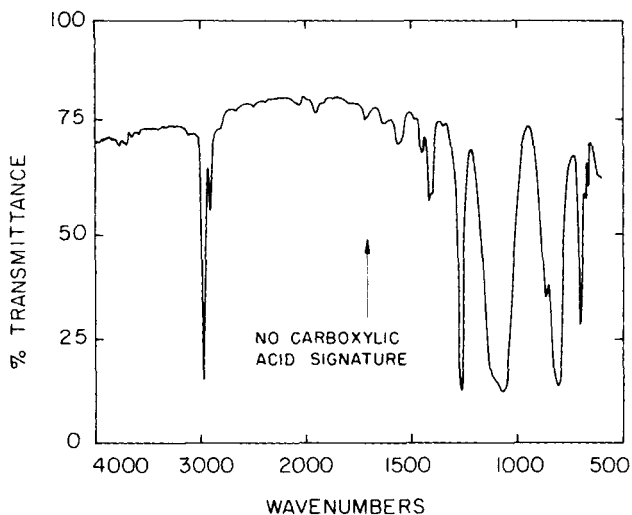


**Figure 9.44** FT-IR spectra of fraction 1 of the carboxypropyl-terminated polydimethylsiloxane.

Some additional chemical and instrumental analyses were carried out on some of the fractions. Fraction 1 was shown by end-group titration to contain no carboxylic groups, and was concluded to be composed of only cyclic siloxanes. Additional corroboration of the conclusion is found in the FT-IR spectrum of this fraction in figure 9.44. Very little carboxylic signature at a wavelength of about  $1,740\text{ cm}^{-1}$  is evident in figure 9.44, verifying the titration result that showed no carboxylic functionality present in the fraction. A sample of another fraction, fraction 7, was also analyzed by FT-IR, and its spectrum is reproduced in figure 9.45. The carboxylic acid signature at a wavelength of  $1,740\text{ cm}^{-1}$  is accented with an arrow.

Another example of the ability to fractionate a wide molecular weight range into narrower cuts is found in the results obtained with supercritical ethylene and an amine-terminated poly(dimethyl)siloxane. As was brought out earlier, supercritical ethylene is used in this case because carbon dioxide reacts with primary and secondary aliphatic amines to form carbamic acids. Depending upon their molecular weight, the carbamic acids may or may not dissolve in carbon dioxide. A temperature of  $70^{\circ}\text{C}$  and a pressure range of 97 bar (1,400 psia) to 275 bar (4,000 psia) was effective in achieving an acceptable fractionation, the result of which is shown in table 9.33. As the results again show, the cyclic species are concentrated with the first fraction, and the number average molecular weight progresses monotonically from about 3,000 to 13,000 as the pressure is increased. The GPC chromatograms of the parent polymer and the SCF fractions are similar in appearance to those shown in figure 9.42 and are not reproduced here.

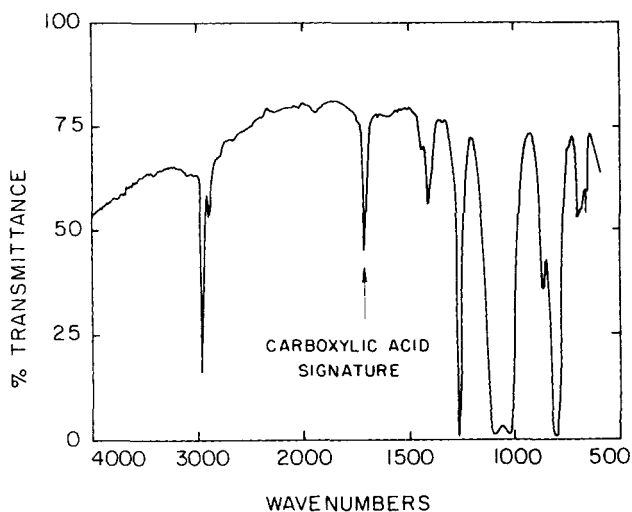


**Figure 9.45** FT-IR spectra of fraction 7 of the carboxypropyl-terminated polydimethylsiloxane.

As the next step in the evaluation of supercritical fluid fractionation of the polysiloxane polymers, fractions are being converted into block copolymers for the purpose of determining the properties that derive from the narrow molecular weight fractions.

Another class of polymers receiving increasing attention is the polysilanes, i.e., polymers with an Si—Si backbone. Because Si—Si bonds are sensitive to incident photons and because the sensitivity to a particular wavelength can be altered and controlled by the nature of the pendant group on the Si and by the

**Table 9.33** Molecular Weight Analysis of Aminopropyl-Terminated Polydimethylsiloxane of Molecular Weight 6,000 Fractionated with Supercritical Ethylene

<i>Fraction</i>	<i>Number Average Molecular Weight<sup>a</sup></i>	<i>Parent (wt%)</i>
Parent	5,910	100.0
1	Cyclics	4.4
2	2,820	7.7
3	5,030	15.8
4	8,250	29.6
5	11,530	16.3
6	13,000 <sup>b</sup>	26.2

<sup>a</sup>Values were obtained by titration; weight average molecular weights were not ascertainable.

<sup>b</sup>Fraction 6 was insoluble in isopropanol and could not be titrated; value is estimated.

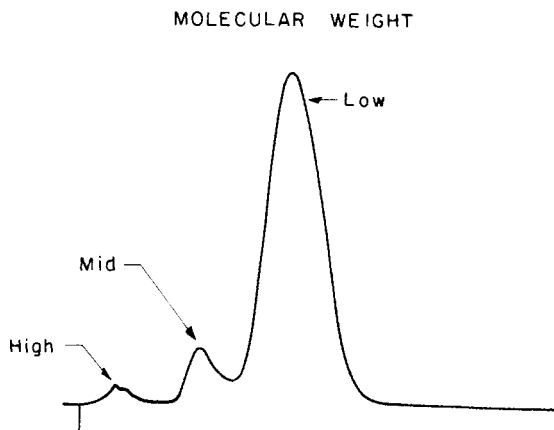


**Figure 9.46** GPC chromatogram of the synthesized cyclohexyl-substituted polysilane polymer.

molecular weight, these polymers are being examined as photoresists in the processing of semiconductor wafers. The synthesis reactions forming polysilanes produce a wide range of molecular weights, as was the case with polysiloxanes. This wide molecular weight range reduces the effectiveness of the polymer because of the variable sensitivity to light energy brought about by the molecular weight spread.

The structure of one of the polysilane polymers reported in the NSF study (Krukonis, 1984b) is shown in table 9.31. Figure 9.46 is a GPC of the material as synthesized. Three primary molecular weight groupings of about 500,000, 50,000, and 10,000 molecular weight comprise the polymer and are designated in the figure. The desired material is the fraction of 500,000 molecular weight. The nominal 10,000-molecular-weight peak shown in figure 9.46 is more than 50% of the total polymer.

This silane polymer was found to be virtually insoluble in carbon dioxide at pressure and temperature levels up to 552 bar (8,000 psia) and 120°C, respectively. Additionally, it was difficult to solubilize in supercritical ethylene and ethane at the same conditions. Supercritical propane proved to be a better solvent, and the extraction of the low molecular weight oligomers was accomplished at conditions of 483 bar (7,000 psia) and 120°C.

A GPC of the extracted material is shown in figure 9.47. Three GPCs are reproduced in the figure because the extract was sequentially collected in three fractions; a slight progression to higher molecular weights is seen. Figure 9.48 is the GPC of the desired polymer. The low molecular weight material is completely extracted. At the operating conditions of 483 bar (7,000 psia) the fraction whose molecular weight is 50,000 did not dissolve; compare this with the results given in table 9.26, which show that poly(dimethyl)siloxane of 100,000 molecular weight can be dissolved in carbon dioxide. It is no surprise

**Figure 9.47** GPC chromatograms of the fractions of the low-molecular-weight cyclohexyl-substituted polysilane polymer fractionated with supercritical propane. (A, B, and C are sequential fractions.)

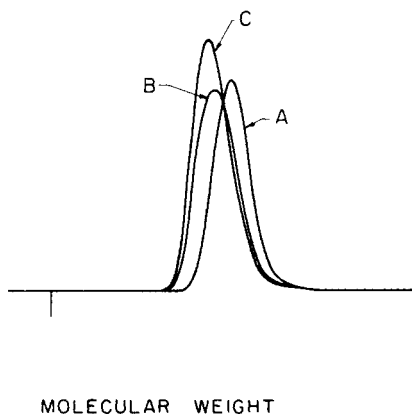


**Figure 9.48** GPC chromatograms of the fractions of the mid- and high-molecular-weight cyclohexyl-substituted polysilane polymer remaining after fractionation with supercritical propane.



that polysiloxane and polysilane polymers exhibit differences in solubility behavior in supercritical fluids; they behave differently with normal liquid solvents.

Krukonis (1982b) has found that supercritical fluid processing is also effective for fractionating a variety of other silicone oils and gums, such as diphenylsiloxanes and fluorosubstituted oils, and reactive silicones with hydroxy, alkoxy, amine, carboxylic, and methacryloxy functionalities. These oils are used for chromatographic stationary phases, lubricants, and other specialty purposes. The high temperature associated with conventional molecular distillation can result in some degradation polymerization when the polymers are processed. The ability to use an SCF to process materials at near room temperatures is an attractive option for fractionating heat-labile materials especially for methacryloxy functionalities.

## Polyisobutylene Surfactant

One final example of SCF fractionation of polymers is given in this section to show the breadth of this technology. The polymer tested in a study by Krukonis (1983c) is a polyisobutylene-succinic anhydride copolymer surfactant used in engine lubricants. The surface-active ends of the polymer complex to

**Table 9.34** Molecular Weight Analysis of Polyisobutylene–Succinic Anhydride Copolymer Fractions

<i>Fraction</i>	<i>Number Average Molecular Weight</i>	<i>Parent (wt%)</i>
Parent	4,000	100.0
1	480	15.9
2	480	9.7
3	530	2.9
4	1,500	7.6
5	2,000	7.6
6	3,000	11.3
7	5,500	26.4
8	7,100	5.3
9	8,000	5.1
10	9,000	5.1
11	9,000	3.3

inorganic and carbon particles, preventing their interference with the lubrication of sliding metal parts. This polymer is also an excellent surfactant for stabilizing suspensions containing high levels of 100 Å particles of magnetite in a hydrocarbon carrier used for seals in computer disc drives. The polymer exhibits a wide molecular weight range and the wide range of chain length introduces adverse effects on the viscosity of the suspension. Because of the presence of long chains in the polymer, the hydrodynamic radius of the suspended particles (and surfactant) is quite large, causing interaction among the suspended particles at relatively low concentrations of solids. The interaction results in a viscosity higher than desired. The polymeric surfactant has not been successfully fractionated by solvent–antisolvent methods. Supercritical fluid fractionation is successfully applied to obtain a mid-cut of molecular weight of this polyisobutylene polymer.

The polymer surfactant was fractionated with supercritical ethylene at 120°C and an increasing pressure range of 62 bar (900 psia) to 317 bar (4,600 psia). For the purpose of determining the degree of fractionation achievable, eleven separate fractions were obtained in the feasibility test. Table 9.34 gives the results of GPC analysis of the molecular weight of the parent polymer and of the fractions. As the table shows, the nominal 4,000-molecular-weight surfactant is separated into fractions whose molecular weights range from 500 to 10,000. In this specific application the removal of the low molecular weight and the high molecular weight species produces a more efficient surfactant (on a weight basis) and concurrently allows a higher solid loading to be achieved without adverse effects on viscosity.



## POLYMER-ORGANIC SOLVENT PHASE SEPARATION

The final type of SCF-polymer separation technique to be discussed in this section is that used to separate polymer solutions by inducing the polymer to fall out of solution. This type of separation can be described using the schematic representation of the phase behavior of a typical polymer-organic solvent mixture depicted in figure 9.49. A single phase solution exists at temperatures and pressures between the UCST and LCST border curves. Therefore, it is possible to split the single-phase mixture into a polymer-rich phase and a solvent-rich phase either by isobarically lowering the temperature until the UCST curve is intersected or by isobarically increasing the temperature until the LCST curve is intersected. For many polymer solutions the UCST curve is not observed, since the polymer solution freezes before the liquid mixture splits into two phases. By contrast, most polymer-solvent mixtures "go the route of an LCST" (Flory, 1984) if they are heated to a high temperature so that it may be viable to recover polymer from solution by inducing an LCST phase split. An LCST phase split to recover polymer from

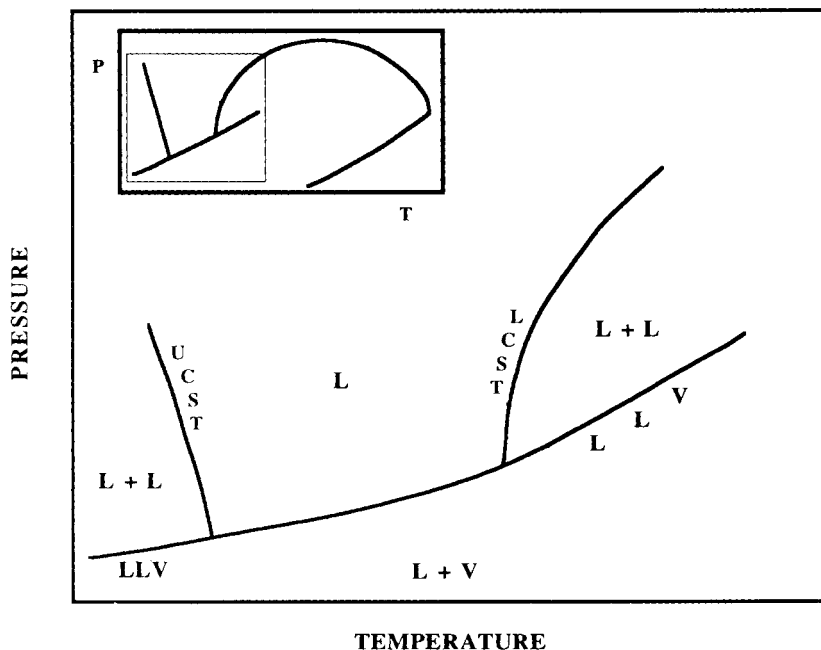


**Figure 9.49** Schematic representation of the  $P$ - $T$  behavior of a polymer-organic solvent mixture. The inset shows the full phase diagram. The hatched area is expanded to show more detail near the critical point of the solvent (McClellan, Bauman, and McHugh, 1985).

solution offers certain advantages over other conventional separation techniques, such as steam stripping. But it is still necessary to heat the polymer solution to temperatures near the solvent's critical temperature; for good polymer solvents, such as cyclohexane ( $T_c = 280.3^\circ\text{C}$ ), these can be high enough to cause thermal degradation of the polymer.

We have a dilemma: we need a high-quality solvent to insure that the polymer remains in solution when it is formed but we need a solvent whose quality can be easily adjusted to induce the polymer to drop out of solution. How can we resolve it? First, we need to know the thermodynamic variables that cause the occurrence of an LCST (chapter 3). The key variable in this instance is the chemical nature of the solvent or, to a first approximation, the critical properties of the solvent. Decreasing the solvent quality shifts the LCST curve to lower temperatures, and it is this variable that we wish to manipulate to force the polymer out of solution. To demonstrate the effect of solvent quality on the location of the LCST curve, consider the difference in LCST behavior for the same polymer, polyisobutylene, in two different solvents, *n*-pentane and cyclooctane. The LCST curve for the polyisobutylene–*n*-pentane system begins at  $\sim 70^\circ\text{C}$ , while for the polyisobutylene–cyclooctane system it begins at  $\sim 300^\circ\text{C}$  (Bardin and Patterson, 1969). Cyclooctane, which has a critical temperature near  $300^\circ\text{C}$ , is a much better solvent than *n*-pentane, which has a critical temperature near  $\sim 200^\circ\text{C}$ , probably because cyclooctane has a greater cohesive energy density that translates into a lower thermal expansion coefficient, or equivalently, a lower free volume. Numerous examples of LCST behavior of polymer–solvent mixtures are available in the literature, demonstrating the effect of solvent quality on the location of the LCST (Freeman and Rowlinson, 1960; Baker et al., 1966; Zeman and Patterson, 1972; Zeman et al., 1972; Allen and Baker, 1965; Saeki et al., 1973, 1974; Cowie and McEwen, 1974).

Irani and coworkers (Irani et al., 1982; Irani and Cozewith, 1986) manipulate the solvent quality by adding a near-critical or supercritical fluid to the polymer solution to demonstrate how the LCST curve can be shifted to lower temperatures. The SCF dilates the solvent without raising its temperature, thus avoiding thermal degradation of the polymer. McHugh and coworkers have extended the SCF-additive work of Irani (McHugh and Guckes, 1985; McClellan and McHugh, 1985; McClellan, Bauman, and McHugh, 1985; Seckner, McClellan, and McHugh, 1988; Guckes et al., 1990). They find that not only does the LCST curve shift to lower temperatures with the addition of a supercritical fluid to the mixture, but that the UCST also shifts to higher temperatures. A schematic representation of polymer–solvent–SCF additive behavior is shown in figure 9.50. Eventually the LCST and the UCST curves merge to form a single curve if enough SCF solvent is added to the solution.

The potential of this separation technique is demonstrated by Seckner, McClellan, and McHugh (1988) with the polystyrene–toluene–ethane system shown in figure 9.51. Without any ethane, the LCEP for the polystyrene–

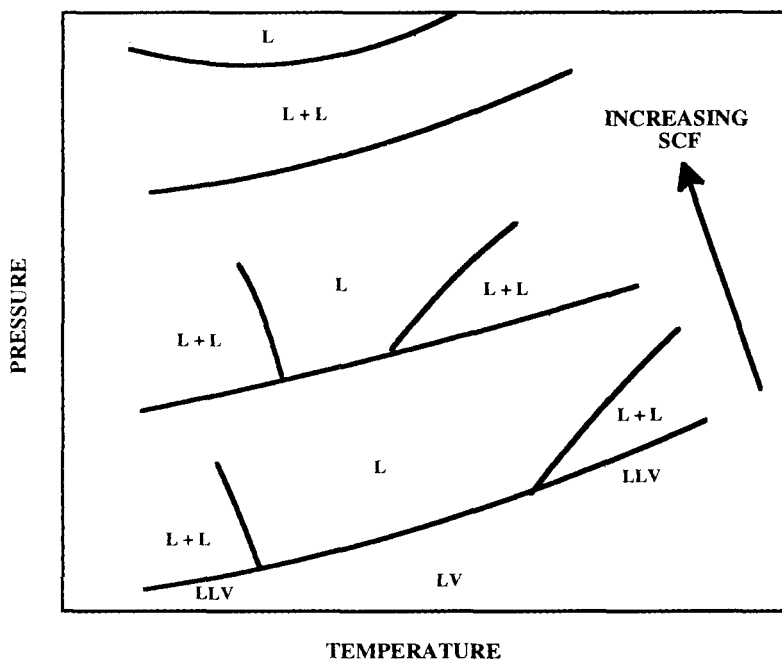


**Figure 9.50** Schematic representation of the effect of an SCF additive on the  $P$ - $T$  behavior of a polymer solution (McClellan, Bauman, and McHugh, 1985).

toluene system occurs at 284°C (Saeki et al., 1974). With the addition of 17.8 wt% ethane the LCEP is lowered to 122°C, a decrease of 162°C. If the ethane concentration is increased to 22.5 wt% the LCEP occurs at 53°C. Finally, if the ethane concentration is increased just slightly, to 24.9 wt%, the LCST and UCST curves merge as shown schematically in figure 9.50. This means that the polystyrene-toluene solution can be separated at temperatures where the polymer is less likely to degrade. Also, recovering the polymer from a dilute solution with this technique should be a less energy-intensive recovery technique as compared to solvent evaporation techniques (Irani and Cozewith, 1986). The amount of polymer recoverable from solution is close to 100%, as shown in the ternary diagrams for the polystyrene-toluene-ethane system in figure 9.52. Solvent-rich and polymer-rich phases are obtained at one specific temperature, 70°C, and two different pressures, 62 and 117 bar. At 117 bar, at least 22.5 wt% ethane is required to phase-split the original 5 wt% polystyrene-toluene solution. For overall ethane loadings between 22.5 and 30 wt% the concentration of polystyrene in the solvent-rich phase is less than 1 wt%, and most often near 0.2 wt%. Figure 9.52b shows the phase behavior for the ternary system at 62 bar and 70°C, which now exhibits a three-phase region at high ethane loadings. The data from figure 9.52 suggest that a separation

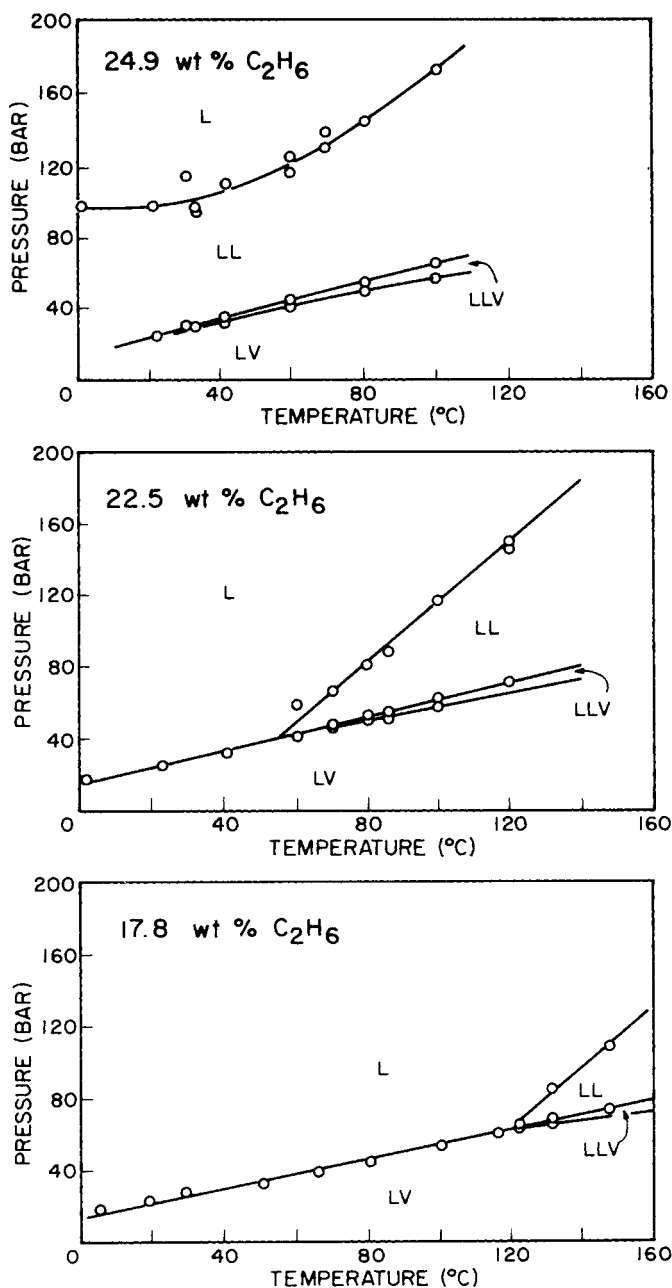


**Figure 9.51** Effect of ethane on the  $P$ - $T$  behavior of the polystyrene-toluene system (Seckner, McClellan, and McHugh, 1988).

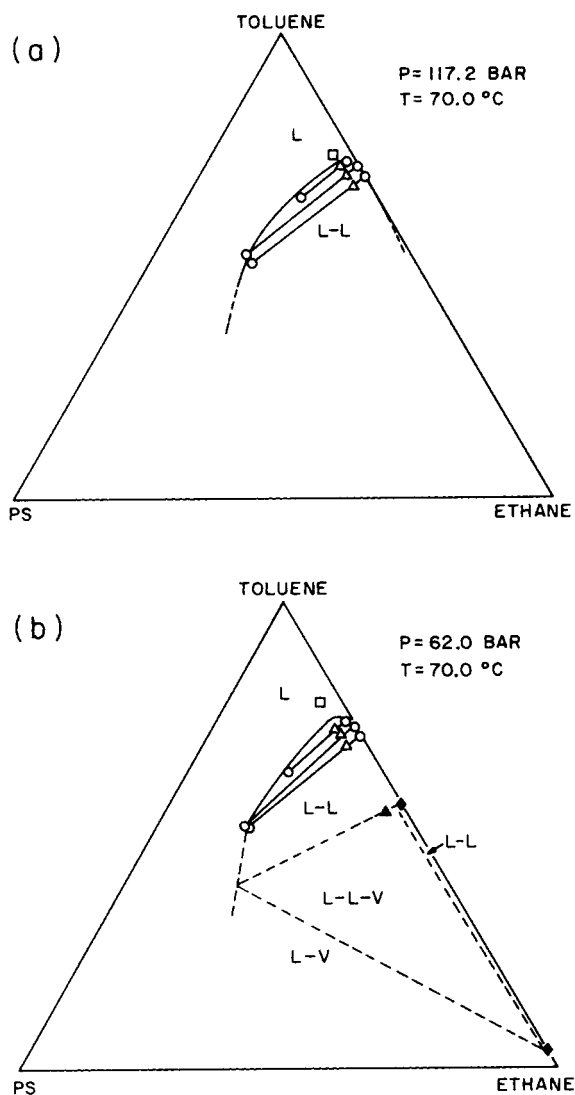


**Figure 9.52** Ternary behavior of the polystyrene-toluene-ethane system (Seckner, McClellan, and McHugh, 1988).

process should operate at the lower pressure of 62 bar since the separation of polystyrene from solution is not improved at the higher pressure.

Before ending this section it is informative to contrast the behavior of a liquid antisolvent and a supercritical fluid antisolvent. Cowie and McEwen (1974) show that a liquid antisolvent could also be added to the polymer solution to shift the LCST to lower temperatures. However, a liquid additive

has a relatively fixed density, unlike an SCF additive, which can be considered as a variable-density additive. Hence, an SCF additive has a much larger effect on the free volume of the liquid organic solvent and it induces the polymer solution to phase-separate at much lower temperatures. Increasing the system pressure increases the density of the SCF additive and decreases the difference in the free volumes of the polymer and the solvent-additive mixture. At a high enough pressure, the two-phase system will coalesce into a single phase. Therefore, pressure can be used at modest temperatures to control the phase separation when using an SCF antisolvent.

## MONOMER PURIFICATION

Reactive monomers for applications that require high purity may be difficult to process by distillation because of their sensitivity to temperature. Instead they can be purified by SCF processing techniques (Krukoni, 1982c). Supercritical fluid purification of three monomers that are converted to diverse products is discussed in this section.

Next-generation soft contact lenses, dental polymers, surface coatings, and similar materials are produced from compounds of varying structure and reactive functionality. For example, currently in development are new soft lenses that will be manufactured from monomers synthesized with dimethylsiloxane backbones. The dimethylsiloxane backbone is terminated with a methacryloxy functionality that supplies the site for polymerization. The siloxane provides lens softness. Occasionally the functionality is formed on both ends of the monomer, resulting in undesired properties. The compound BisGMA is a monomer that is polymerized to form hard dental structures. In the monomer synthesis process impurities are coproduced that interfere with the polymerization. Finally, diacetone acrylamide used in a copolymerization process is another specialty monomer that is occasionally contaminated with difficult-to-remove impurities. These three monomers are quite reactive at modest temperature and cannot be purified by distillation. The three examples that are presented here derive from as yet unpublished research (Krukoni, 1982c).

One soft lens monomer currently in early development is being synthesized in batches of about 1–10 kg. The resulting product is usually found to be contaminated with about 5 wt% difunctional material coproduced in the monomer synthesis scheme. In the subsequent soft lens manufacturing process, the monomer is polymerized across the vinyl groups at a temperature of about 80°C, but cross-linking can occur if two methacryloxy groups are situated on the monomer which obviously is detrimental to softness. The monomer cannot be purified by distillation because at a temperature of 80°C there is very little difference in the vapor pressures of the desired monomer and the impurity, which makes them virtually inseparable even if high-vacuum distillation is used. Additionally, a higher distillation temperature cannot be used because

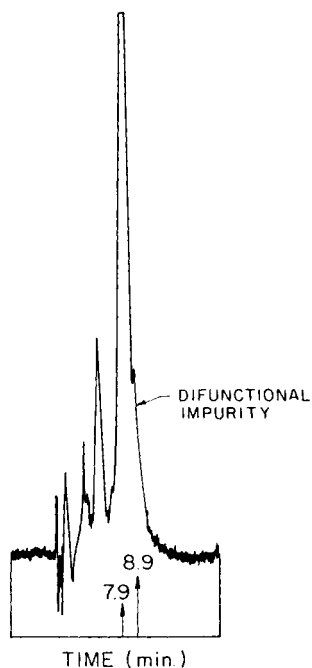


**Figure 9.53** HPLC chromatogram of the silicone lens monomer and difunctional impurity.

the monomer will prematurely polymerize. Separation of a reactive material that cannot be purified by conventional processing, is tailor-made for SCF extraction.

Before describing the SCF extraction tests, let us attempt to determine a priori whether supercritical fluid extraction can be used for this separation problem. Previous sections of this chapter show that siloxanes with molecular weights as high as 100,000 will dissolve in supercritical carbon dioxide. Francis (1954) measured the solubilities of a large number of high molecular weight carboxylic acids and found them quite soluble in near-critical liquid carbon dioxide (chapter 2). Francis also showed that the esterification of an acid, polyacid, or polyhydroxyl compound confers a higher solubility on the compound in carbon dioxide. Thus, the methacrylic ester moiety on the short dimethylsiloxane chain should not adversely affect the dimethylsiloxane solubility in an SCF solvent; it may, in fact, enhance the solubility. Finally, we will assume that incorporating an additional methacryloxy group on a fairly small siloxane oligomer will affect the solubility behavior of the substance. All of these considerations taken collectively lead us to the conclusion that the monofunctional monomer should be separable from the difunctional impurity using supercritical fluid extraction.

Figure 9.53 is a high-performance liquid chromatogram (HPLC) of the solution containing the synthesized monomer, associated raw materials, and the difunctional impurity. HPLC does not completely resolve the monofunc-

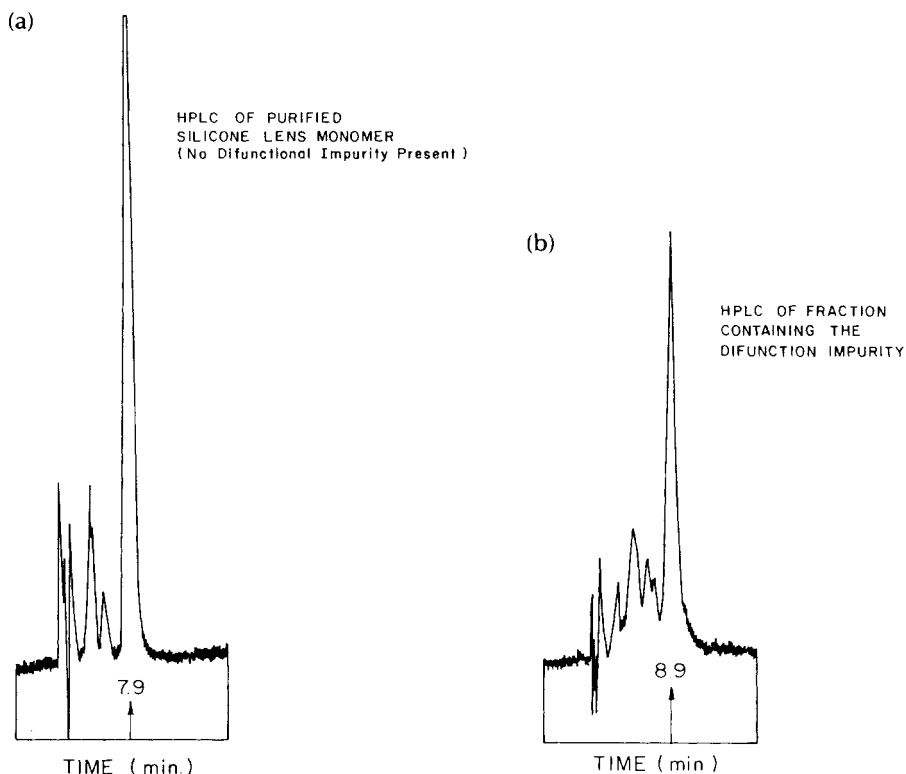


**Figure 9.54** Two HPLC chromatograms of the fractions of the silicone lens monomer; (a) purified monomer (no difunctional impurity present) and (b) concentrated impurity.

tional and difunctional materials in the solution. The signature of the difunctional impurity is visible as the shoulder on the major peak in the solution. Incidentally, the other peaks to the left of the major peak represent unreacted raw materials, which can be resolved from the monofunctional monomer in the HPLC analysis. These unreacted raw materials are also quite readily removed from solution by conventional processing techniques. Thus, the major problem in the development of the new lens monomer is the separation of the difunctional impurity.

The monofunctional and difunctional compounds can be separated with supercritical carbon dioxide at 165 bar (2,400 psia) and 60°C. Although the difference in vapor pressure between the two compounds is not great enough to allow facile separation by distillation, supercritical carbon dioxide is able to separate these compounds, which differ by only one methacryloxy group. Figure 9.54a, b are HPLCs of the two fractions obtained from the extraction. The same scale that is used for the HPLC of the parent solution is drawn on



both fractions. The major peaks in the supercritical fluid-processed fractions have eluted at different times.

Dental materials are increasingly being subjected to the demand of improved performance. Monomers and resins that can be photopolymerized at room temperature to form extremely hard cross-linked structures have been developed, and increasingly sensitive initiators (activated by incident photons) have created the need for purer monomers.

BisGMA resin is an advanced restorative material currently in use but it suffers from certain drawbacks. The chemical name of BisGMA is 2,2-bis(p2'-hydroxy-3'-methacryloxypropoxy)-phenylene-propane. The impurities present in the resin can limit its shelf life and can also interfere with the polymerization reaction to form impervious enamel-like structures. These impurities exhibit very low vapor pressures and cannot readily be removed by conventional distillation techniques. Similar to the soft-lens monomer, heating the mixture of BisGMA results in the premature polymerization of the resin. The ease of polymerization of BisGMA, although advantageous for its end use, can limit its ability to be purified.

BisGMA is synthesized commercially in a two-step process. The first step reacts bisphenol A and epichlorohydrin to form the diglycidyl ether of bisphenol A (DGEBA). The second step reacts DGEBA and methacrylic acid to form BisGMA. Excess epichlorohydrin is used in the first reaction step to ensure the complete solubilization of bisphenol A and to ensure a good yield. But the excess epichlorohydrin is difficult to remove. During the second step of the process the epichlorohydrin causes the conversion of some methacrylic acid to 1-chloro-isopropanol methacrylate, which also is virtually impossible to remove by conventional distillation or vacuum stripping. The chloromethacrylate impurity adversely affects the behavior of BisGMA in the end-use polymerization reaction.

The BisGMA monomer is polymerized by either of two free-radical mechanisms: a thermally induced peroxide initiation or a photoinduced a,b-diketone initiation. Many of the initiator formulations are proprietary to their respective manufacturers, but a typical peroxide initiator is benzoyl peroxide, which forms free radicals when the temperature is raised. The a,b-diketone initiator responds to incident light energy to form free radicals.

In the peroxide formulation initiation, the organochlorine impurities that are present in commercial BisGMA accelerate the decomposition of the peroxides, a process that forms free radicals and reduces the stability and shelf life of the resin. In the a,b-diketone formulation, the organochlorine impurities complex with other additives in the formulation that are present to enhance free-radical formation. The presence of the impurities thus reduces the photoefficiency and negates the advantages of simple photoinitiated diketone curing.

The problems with the chlorinated impurities notwithstanding, BisGMA is the superior dental material available today. If the impurity-induced limitations could be eliminated or reduced, the use of BisGMA could proliferate into

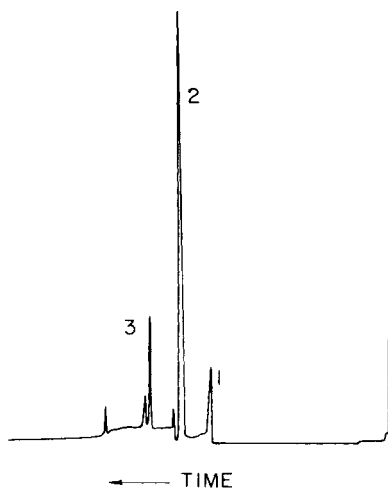


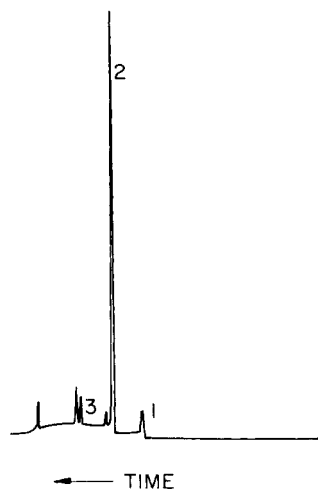
**Figure 9.55** HPLC chromatogram of commercially available BisGMA: (1) 1-chloro-isopropanol methacrylate; (2) BisGMA; and (3) diglycidyl ether of bisphenol-A.

other applications, such as prosthetic bones, in which the advantages of the high tensile and compressive strength of the cross-linked polymer can be coupled to the ease and efficiency of polymerizing the purified monomer into the desired forms.

BisGMA, then, is another material that exhibits the potential for supercritical fluid upgrading. It is quite reactive and, in fact, its reactivity near ambient temperature is one of its attractive properties. BisGMA cannot be purified readily by conventional processing and, as improvements in the initiators continue, it is being faced with a greater performance demand. Figure 9.55 is an HPLC of a commercial BisGMA sample. The major peak in this figure is the product, BisGMA. Two of the other peaks are the 1-chloro-isopropanol methacrylate, which is the predominant impurity, and DGEBA (which, although it is an impurity, does not interfere with either the thermal or photolytic initiation of BisGMA).

An initial test, using carbon dioxide, was made at arbitrarily selected extraction conditions of 124 bar (1,800 psia). The temperature level is kept at 45°C in order to reduce the tendency for the BisGMA to polymerize during extraction. The choice of parameters, although arbitrary for this first BisGMA test, derives from consideration of previous results on the extraction of low molecular weight cyclic siloxanes from a high-viscosity silicone oil. Very frequently, the solubilities of homologous mers decreases with increasing molecular weight; analogously, the relative extraction or selectivity is greatest at the lowest solubility levels. The 1-chloro compound is of lower molecular weight than the BisGMA. It is thus reasoned that the 1-chloro compound might mimic the behavior of a cyclosiloxane present in admixture with higher molecular weight linear siloxanes. Although such simplistic reasoning is usually correct with polymers and oil homologues, it can break down when comparing compounds of very differing functionalities or molecular weights. For example,

**Figure 9.56** HPLC chromatogram of the purified fraction obtained by extracting commercially available BisGMA with supercritical carbon dioxide: (1) 1-chloro-isopropanol methacrylate; (2) BisGMA; and (3) diglycidyl ether of bisphenol-A.



a compound with two ester groups might be more soluble than the same parent compound containing one ester and one hydroxy end. Even though the hydroxy compound has a lower molecular weight, hydrogen bonding can decrease the solubility relative to the diester.

The SCF-extracted residual material is analyzed by HPLC, and the chromatogram of the purified material is shown in figure 9.56. A comparison of figures 9.55 and 9.56 shows that the concentration of the impurities and the concentrations of many of the unidentified components have decreased almost by a factor of five. Hence, SCF extraction works quite well in this instance.

Diacetone acrylamide is a solid monomer. It is also quite heat-labile and is currently used in a specialty copolymerization process. Its HPLC signature, figure 9.57, shows the presence of another peak, designated "impurity," and in the particular sample analyzed it is present at about 100 ppm. The impurity has been identified as a condensation product formed occasionally and unpredictably during the monomer synthesis reaction. When it is found to be present, the impurity-containing batch cannot be used, because the impurity interferes in subsequent polymerization reactions. The monomer cannot be separated from the impurity by conventional processing and the batch is used in applications not requiring the extremely high purity demanded in copolymerization. Both the impurity and the monomer are quite soluble in traditional liquid solvents and neither crystallization nor antisolvent methods are effective in causing a separation of the two. Nor is distillation effective because the monomer tends to degrade (or polymerize) at quite low temperatures. Thus, supercritical fluid extraction is a potential solution for this problem, because, on the basis solely of homologous-series size considerations, the monomer and the much larger condensation product should exhibit different solubilities.

However, supercritical fluid extraction is not a panacea; it must be

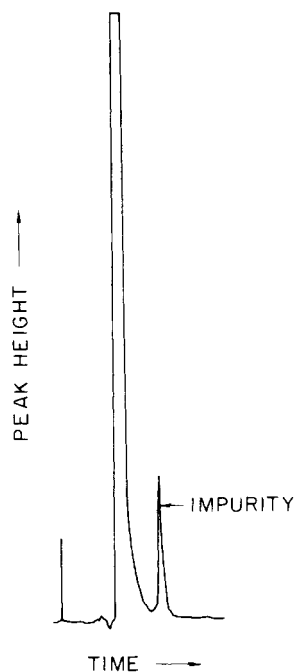


**Figure 9.57** HPLC chromatogram of the monomer diacetone acrylamide.

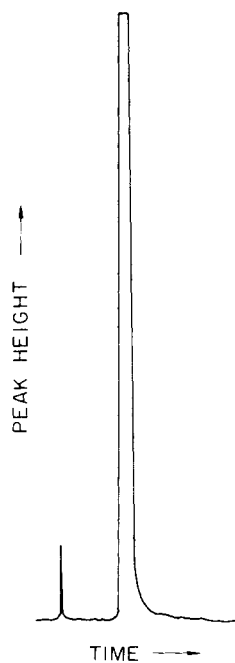


**Figure 9.58** HPLC chromatogram of the purified diacetone acrylamide monomer obtained by treatment with supercritical carbon dioxide.

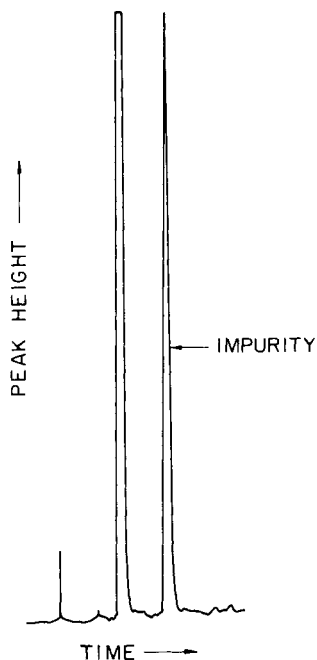


**Figure 9.59** HPLC chromatogram of the impurity-containing fraction removed from the diacetone acrylamide monomer.

evaluated on a case-by-case basis. Supercritical carbon dioxide at 40°C is quite effective in separating the monomer from its condensation impurity (Krukonis, 1981d). A temperature of 40°C was chosen to carry out the extraction because diacetone acrylamide becomes increasingly reactive as the temperature is raised higher. Figure 9.58 shows the HPLC of the purified monomer obtained by supercritical carbon dioxide extraction. The impurity is not present. For completeness, figure 9.59 is included to show the impurity-containing fraction; the impurity has been concentrated considerably. The separation of the impurity from the desired monomer is not perfect; there is a monomer peak in figure 9.59. But isolating the impurity is not important; what matters is the yield of purified monomer, which is quite high at 90%.

---

## Processing Pharmaceuticals, Natural Products, Specialty Chemicals, and Waste Streams

---

A large body of experimental data has been accumulated on the solubility and extractability of natural products, such as steroids, alkaloids, anticancer agents, oils from seeds, and caffeine from coffee beans, in various SCF solvents such as CO<sub>2</sub>, ethane, ethylene, and N<sub>2</sub>O. Carbon dioxide is probably the most widely investigated SCF solvent since its critical temperature ( $T_c = 31.1^\circ\text{C}$ ) makes it an ideal solvent for extracting materials that are thermally labile. Also, CO<sub>2</sub> is nontoxic, nonflammable, environmentally acceptable, and inexpensive.

To determine the solubility characteristics of compounds in SCFs Stahl and coworkers (Stahl and Quirin, 1983; Stahl et al., 1980) have developed a microextraction apparatus that they directly couple with thin-layer chromatography. They find that a number of variables control the solubility of natural products in supercritical CO<sub>2</sub>. They corroborate some of the trends detailed in the preceding pages. For instance, they report that:

1. Fractionation of liquids or solids is possible if the constituents of the mixture exhibit large differences in vapor pressure, mass, and polarity.
2. Low molecular weight hydrocarbons and lipophilic organic compounds, such as esters, ethers, and lactones, are easily extractable.
3. Hydroxyl and carboxyl substituent groups on the mixture constituents reduce the solubility of the substance in the SCF and therefore make the extraction extremely difficult.
4. Sugars and amino acids are not extracted by supercritical CO<sub>2</sub>.

In one study Stahl and Quirin (1983) determined the solubility level of tetracyclic steroids that differed in structure but all of which had virtually the same vapor pressure at the operating temperature of the system using supercritical CO<sub>2</sub>. The carboxyl groups on the steroids, such as bile acids, rendered the steroids virtually insoluble in supercritical CO<sub>2</sub>, whereas carbonyl groups had very little effect on the solubility of similar steroids. The differences

in the molecular weights and melting points of the steroids had no direct influence on the solubility behavior. Numerous other SCF extraction studies have been performed by Stahl and coworkers. Their work, along with the work of Francis and others, forms a large data base that should be referred to when considering whether a compound is soluble in  $\text{CO}_2$ .

In this chapter the SCF processing of two natural products, coffee and edible oils, is described in some detail. The principles involved in the coffee decaffeination process are similar to those described for the regeneration of activated carbon and the extraction of ethanol from water. In the remainder of the chapter a variety of other SCF applications are presented.

## COFFEE DECAFFEINATION

Coffee decaffeination with carbon dioxide has been the object of a large amount of effort in research and development at the Max Planck Institute for Coal Research in Germany and at other academic and industrial laboratories in Europe and the United States. An indication of the intensity of effort applied to this process comes from a review article that lists the United States patents on decaffeination granted up to the end of 1981 (Paulaitis et al., 1983a). Several earlier patents were inadvertently omitted from that list; a corrected version is given in table 10.1. Research activity on supercritical fluid extraction of stimulants from coffee, tea, and cocoa has continued, indicated by the number of United States patents granted since that review article was published; some of them are listed in table 10.2.

Each patent has somewhat different features and claims. We select one patent for more detailed discussion to highlight certain technical facets of the process. First we explain the (often misunderstood) effect of water on the extractability of caffeine by selective supercritical carbon dioxide. A number of references report that dry carbon dioxide cannot extract caffeine from dry coffee, either green or roasted, but moist carbon dioxide can. The inability of dry carbon dioxide to extract caffeine from coffee should not be misconstrued to mean that dry carbon dioxide cannot dissolve neat caffeine. This same moist-versus-dry effect is experienced if, for example, methylene chloride is used to extract caffeine from coffee. Dry methylene chloride cannot decaffeinate dry coffee but moistened coffee can be decaffeinated. It is thought that the caffeine is chemically bound in a chlorogenic acid structure present in the coffee bean. Thus, water somehow acts as a chemical agent; it frees caffeine from its bound form in the coffee matrix in both the carbon dioxide and the methylene chloride processes.

The lack of selectivity of carbon dioxide is further clarified by a comparison of the extraction results with roasted and green coffee. Moist carbon dioxide extracts the caffeine from green coffee beans. Very little else present in green coffee dissolves in carbon dioxide. Coffee aroma oils also dissolve in carbon dioxide but they are not present in green coffee beans; they

**Table 10.1** United States Patents on Coffee Decaffeination (1981 and Earlier)

<i>Date</i>	<i>Patent Number</i>	<i>Title</i>	<i>Assignee</i>
Apr. 23, 1974	3,806,619	Process for recovering caffeine	Studiengesellschaft Kohle, GmbH
Oct. 22, 1974	3,843,824	Method for the production of caffeine-free coffee extract	HAG Aktiengesellschaft
Apr. 22, 1975	3,879,569	Process for the decaffeination of raw coffee	HAG Aktiengesellschaft
Sept. 18, 1979	4,168,324	Process for extracting stimulants from coffee	HAG Aktiengesellschaft
Jan. 20, 1981	4,246,291	Decaffeination of aqueous extracts	General Foods Corporation
Jan. 27, 1981	4,247,570	Process for the decaffeination of coffee	Studiengesellschaft Kohle, GmbH
Feb. 17, 1981	4,251,559	Decaffeination process	Société d'Assistance Technique pour Produits Nestlé SA
Mar. 10, 1981	4,255,461	Preparation of a decaffeinated roasted coffee blend	General Foods Corporation
Mar. 10, 1981	4,255,458	Method for the selective extraction of caffeine from vegetable materials	HAG Aktiengesellschaft
Apr. 7, 1981	4,260,639	Process for the decaffeination of coffee	Studiengesellschaft Kohle, GmbH
Jun. 30, 1981	4,276,315	Method for decaffeinating coffee	General Foods Corporation

are generated during the roasting process. If moist carbon dioxide is used to extract roasted coffee beans, the aroma oils are extracted along with the caffeine. Thus, moist carbon dioxide should not be considered selective for extracting caffeine in green coffee any more than it should be considered selective for extracting naphthalene from (insoluble) chalk dust. The supercritical carbon dioxide extraction of coffee is a sound and clever process. The plant in West Germany operates at a processing level of 60 million lb/yr. Moreover, it is the first example of a supercritical fluid process that has reached the commercial processing level and whose primary step is, indeed, supercritical extraction.



**Table 10.2** United States Patents on Coffee Decaffeination (1982 and Later)

<i>Date</i>	<i>Patent Number</i>	<i>Title</i>	<i>Assignee</i>
Mar. 30, 1982	4,322,445	Process for the decaffeinating of raw coffee	S. Peter and G. Brunner
May 4, 1982	4,328,255	Method for the extraction of coffee containing aroma constituents from roasted coffee	Studiengesellschaft Kohle, GmbH
Jun. 4, 1982	4,341,804	Decaffeination of aqueous roasted coffee extract	General Foods Corporation
Aug. 17, 1982	4,344,974	Process for decaffeinizng raw coffee	Kaffee-Veredelungs-Werk Koffeinfrei Kaffee GmbH & Co
Sept. 7, 1982	4,348,422	Process for the direct decaffeination of aqueous coffee extract solutions	Studiengesellschaft Kohle, GmbH
Dec. 21, 1982	4,364,965	Process for extracting caffeine from solutions thereof in carbon dioxide under high pressure	D. E. J. International Research Company BV
Oct. 25, 1983	4,411,923	Process for the extraction of caffeine supercritical solutions	HAG Aktiengesellschaft
Sept. 18, 1984	4,472,442	Decaffeination process	General Foods Corporation

Let us proceed to some of the technical facets of the decaffeination process. Figure 10.1 is a graph of the solubility of neat caffeine in carbon dioxide (Krukonis, 1981a). The solubility of caffeine is about 0.2 wt% at 60°C and 300 bar. The caffeine content of most coffees is about 1 wt%. If, during the extraction process, the caffeine in coffee dissolves to the solubility limit during extraction at, say, 60°C and 300 bar, the amount of carbon dioxide required to decaffeinate coffee is easily calculated. It is 5.0 pounds per pound of coffee.

We summarize the data from one example of an early coffee decaffeination patent to highlight the specifics of the process (Roselius, Vitzthum and Hubert, 1974). Four hundred grams of rough-ground deoiled roast coffee is wetted with 200 ml of water and is treated with supercritical CO<sub>2</sub> with an

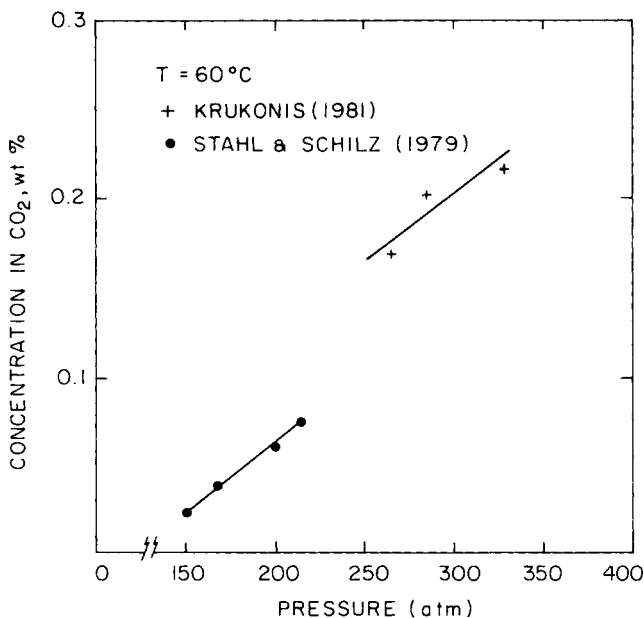


**Figure 10.1** Solubility of neat caffeine in supercritical carbon dioxide (1.01325 bar per atm).

apparatus similar to the one previously described for regenerating activated carbon. Sixty kilograms of carbon dioxide at 300 bar and 45°C are circulated through a bed packed with the coffee for approximately 5 h. Two hundred milliliters of water and 4.2 grams of caffeine contaminated with some residual oil are separated in a collector vessel when the pressure is reduced to 60 bar and the temperature is decreased to 22°C. The percent caffeine in the roast coffee is reduced from an initial value of 1.25 wt% to a final value of 0.06 wt%. Note that 150 lb of carbon dioxide per pound of coffee is passed through the bed to reduce the caffeine content by 95%. In chapter 8 we calculate a solvent requirement of 105 lb of CO<sub>2</sub> per pound of ethanol in the feed stream. Approximately the same solvent requirement is needed for coffee decaffeination. But coffee sells for more than ethanol, so its economics will be different. This large excess of carbon dioxide is not related solely to mass transfer limitations. If, for example, the coffee is ground to a different mesh size or if several flow-rate levels are tested during decaffeination, the total carbon dioxide requirement is not markedly changed. These experimental findings are similar to findings for activated carbon regeneration, discussed in some detail in chapter 8.

A large excess of carbon dioxide is required because caffeine does not dissolve to its (neat) solubility limit during the extraction of coffee beans. Instead, the concentration achieved in the carbon dioxide phase is governed by an equilibrium interaction that is present in the carbon dioxide–caffeine–coffee system (or, more precisely, the carbon dioxide–water–caffeine–coffee system). The measured equilibrium isotherm for the system is given in figure 10.2

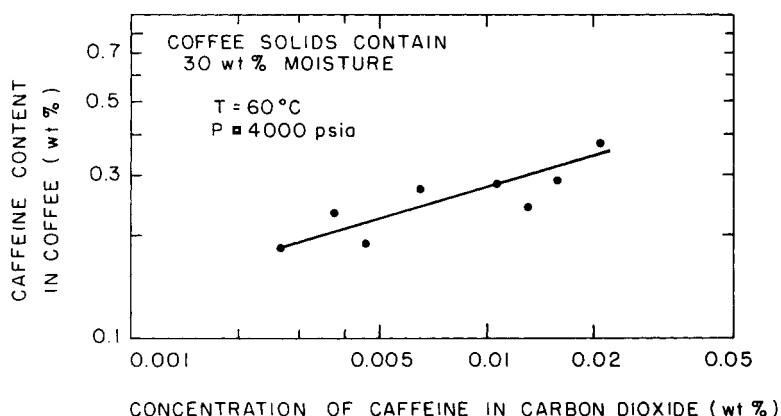


**Figure 10.2** Equilibrium isotherm for the caffeine-coffee-carbon dioxide system (14.504 psia per bar).

(Krukonis, 1981a). It is similar in appearance to the isotherm for activated carbon shown in figure 8.8. Despite the similarity, a different phenomenon is probably active. In the case of activated carbon, high adsorption strength forces lower the activity of an organic on the carbon, thus limiting the concentration of the pesticide in the carbon dioxide phase. For the coffee case it is speculated here that chemical binding between caffeine and the coffee substrate (which again is influenced by moisture) lowers the activity of caffeine so it too does not dissolve to its neat solubility level. In both systems an amount of carbon dioxide in excess of that calculated from solubility considerations is needed to remove the soluble compound as a result of the interactions with the solid phase.

In this instance the separation of caffeine from the carbon dioxide phase leaving the extractor is also more complicated than using a simple pressure reduction. For the recovery of ethanol from the carbon dioxide-rich phase in the ethanol-water extraction process a pressure reduction step does not satisfactorily reduce the ethanol concentration in the recycled carbon dioxide unless a very large pressure reduction is taken. Similarly, in the coffee decaffeination process, because caffeine dissolves to well below its solubility limit, an extremely large pressure reduction is necessary to precipitate the caffeine from the carbon dioxide phase. The ternary equilibrium isotherm for caffeine shown in figure 10.2 indicates that the carbon dioxide recycled to the coffee bed must be essentially free of caffeine. For example, if carbon dioxide is recycled with a caffeine concentration as little as 0.002 wt%, we see from the data in figure 10.2 that the caffeine content of the coffee cannot be reduced to below 0.16 wt%. This equates to a caffeine removal of only 84% for a coffee containing 1.0 wt% caffeine.

How is the carbon dioxide cleaned up for recycle in the decaffeination

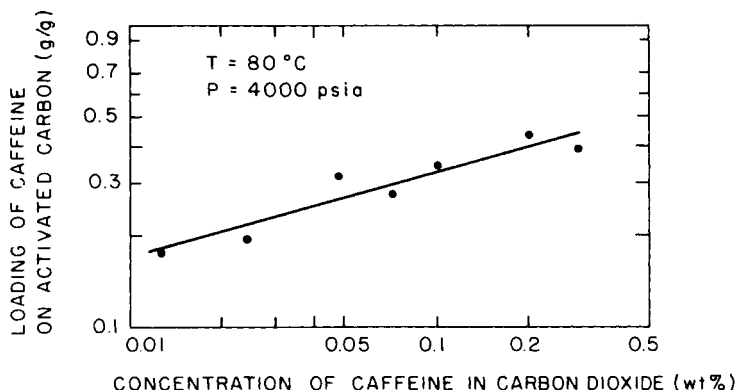


**Figure 10.3** Adsorption isotherm for the caffeine-carbon dioxide-activated carbon system (14.504 psia per bar).

process if pressure reduction cannot accomplish the task? Two options, stripping with water or adsorption onto activated carbon, are described in the patent literature. A brief summary of these processes is presented here.

Distribution coefficients for the ternary system carbon dioxide-caffeine-water have been measured (Krukonsis, 1981c). At conditions of about  $80^{\circ}\text{C}$  and 310 bar (4,500 psia), the distribution coefficient is about 0.03 to 0.04 (weight basis). Although the distribution coefficient is rather small for extracting caffeine from coffee solution with carbon dioxide, it is excellent for the reverse process of removing caffeine from carbon dioxide with a water wash. Two United States patents discuss in more detail the water washing of recycled carbon dioxide (Prasad, Gottesman, and Scarella, 1981; Zosel, 1982).

The other cleanup method utilizes the adsorptive properties of activated carbon to remove caffeine from the carbon dioxide before recycle (Zosel, 1981). An adsorption isotherm of the carbon dioxide-caffeine-activated carbon system, shown in figure 10.3, indicates that it is possible to adsorb the caffeine in the carbon dioxide-rich stream onto activated carbon (Krukonsis, 1983a). In this industrial application an activated carbon bed is used to remove a component from a supercritical carbon dioxide-rich stream rather than having the activated carbon regenerated by the supercritical carbon dioxide. It is perhaps no surprise that spent activated carbon is difficult to regenerate with carbon dioxide, as discussed in chapter 8.

## EDIBLE OILS EXTRACTION

The process development work being carried out at the United States Department of Agriculture's (USDA) Northern Regional Research Center on

the extraction of vegetable oils with supercritical fluid solvents has been reported in the literature (Friedrich, List, and Heaking, 1982). Supercritical carbon dioxide is being considered as a replacement for hexane in soybean oil extraction. As stated earlier, scrutiny by the FDA and awareness of the health and safety hazards associated with the use of hexane have prompted the examination of carbon dioxide as an extracting solvent.

Operation of a supercritical fluid-soybean extraction process is essentially identical to the naphthalene-chalk dust process described earlier; the oil is the SCF-soluble species, and the protein substrate the insoluble species. Flaked soybean (flaked to break the cell membrane walls so the oil will be accessible to the solvent) is first charged to a vessel. Carbon dioxide is passed through the bed, and the carbon dioxide-oil solution leaving the extractor is expanded to a lower pressure to precipitate the oil. The carbon dioxide is then recompressed and recycled to the vessel. As with the naphthalene extraction and the coffee decaffeination processes, multiple vessels can be used to optimize equipment utilization. As an example of some of the factors affecting the economics of the SCF-soybean oil process, the potential of continuous feeding and removal of soybean solids is being explored. One group of investigators considers the development of the continuous feeding of soybean solids as an important factor for demonstrating economic viability for the supercritical carbon dioxide extraction of soybeans. A typical soybean extraction plant using hexane operates at a level of 2,000 tons per day; the operating philosophy and economics will certainly be different from, for example, those of a hops extraction plant operating at 2 tons per day. Also to be considered in the viability analysis is the cost of the products: soybean oil sells for \$.25 per pound while hop extract sells for \$30.00 per pound.

Data on the extraction and oil composition of soybean oil have been described in a number of journals (see, for example, Friedrich and Pryde, 1984), but some not yet widely known information is given here. A number of United States and European researchers have reported triglyceride solubility data (Christianson et al., 1984; List, Friedrich, and Pominski, 1984; Snyder, Friedrich, and Christianson, 1984; Stahl et al., 1980; Stahl et al., 1984). Until a few years ago 621 bar (9,000 psia) was the maximum pressure level tested in soybean extraction or triglyceride solubility determinations. In 1982, Friedrich of the USDA extended the test pressures to 1,000 bar and found some quite interesting results. A copy of the solubility data reproduced from United States patent 4,466,923 (Friedrich, 1984) is given in figure 10.4. At conditions of 70°C and 800 bar, carbon dioxide and soybean triglycerides become miscible, and this finding is the basis of a patented extraction process that operates in a relatively narrow range at high pressure. As the solubility data show, the separation of much of the oil from an 800 bar carbon dioxide-oil stream can be carried out by dropping the pressure by only 150 or 200 bar at 70°C. Incidentally, the triglyceride data shown in figure 10.4 exhibit the same retrograde behavior as the solids solubility data shown in chapter 1. That is, the solubility isotherms cross at low pressure, although "low" in this case is

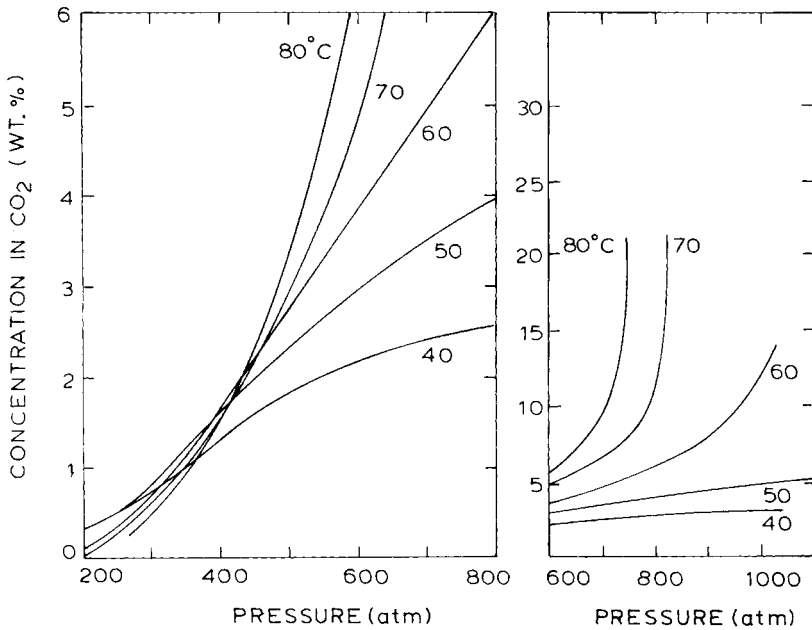


**Figure 10.4** Solubility behavior of soybean triglycerides in supercritical carbon dioxide (Friedrich, 1984) (1.01325 bar per atm).

about 275 bar. The triglyceride data are replotted as solubility isobars in figure 10.5. Interestingly, the curves are quite similar in shape to the naphthalene-carbon dioxide and silica-water data shown in chapter 2.

Carbon dioxide has been tested with other materials, such as corn and wheat germ, sunflower and safflower seeds, and peanuts. To a very good first approximation, the solubility of all vegetable triglycerides is identical, and all these seeds can be extracted completely if the cells are macerated to make the oil accessible.

Some work on the supercritical carbon dioxide concentration of active fatty acid fractions of fish oils has also been reported recently (Krukonis, 1984c). Evidence has accumulated that suggests that certain polyunsaturated fatty acids comprising fish oil triglycerides have a therapeutic effect on the cardiovascular system. Increasing attention is being directed to clinical studies of fish oils in the human diet and the development of new refining methods for purifying and concentrating the active components, such as eicosapentaenoic acid (EPA). The active components possess a high degree of unsaturation and conventional processing by high-vacuum and molecular distillation can cause degradative reactions at the high-temperature levels required to separate the fish oils from free fatty acids, protein residues, and polychlorinated biphenyls.

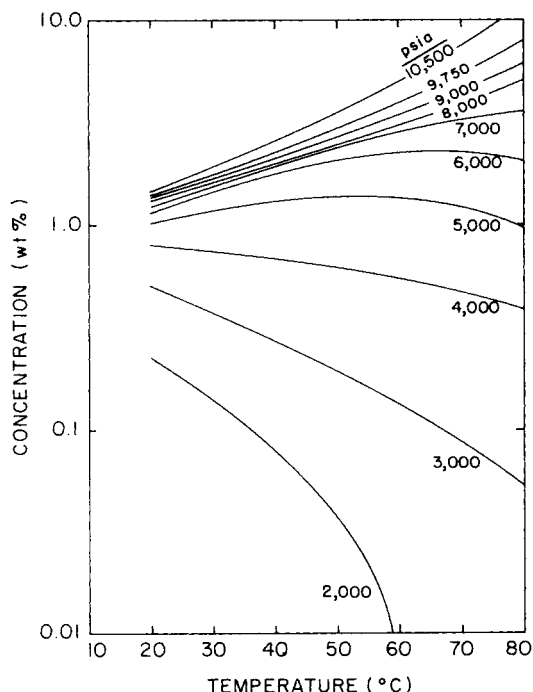


**Figure 10.5** Solubility isobars of soybean triglycerides-carbon dioxide system (14.504 psia per bar).

Because the active fatty acid moieties are in relatively low concentration in fish oils, because they are dispersed on the triglyceride chains with other fatty acids, and because there are many fatty acids with identical carbon number but with varying saturation, it is difficult to concentrate the 20:5 component (a fatty acid having 20 carbons and 5 double bonds) by distillation or by supercritical fluid extraction. But if the triglycerides are first transesterified to methyl (or ethyl) esters, the EPA fraction can be concentrated using supercritical carbon dioxide fractionation. Table 10.3 tabulates the concentrations of the individual fatty acids in four SCF fractions relative to the parent compound. Components having 20 carbons can be increased twofold. A recent paper describes the addition of a reflux stage to the process and reports that in a two-pass processing sequence the 20:5 component fatty acid concentration can be increased to 60 wt% concentration in a selected fraction (Eisenbach, 1984).

Several trade journals describe development work on a supercritical carbon dioxide process for extracting oils from potato chips and other snack foods, an extension of seed- and fish-oils extraction (Hannigan, 1981; Wolkomir, 1984). The motivation for the work lies in increasing consumer awareness of the caloric content of foods and beverages. “Light” beers, wines, and soft drinks are currently very popular, along with “light” peanuts and “light” Pringles® brand potato chips. Figure 10.6 shows a schematic diagram of a

**Table 10.3** Composition of Feed and SCF Fractions (Methyl Esters of Anchovy Oil)

Fraction	Component					Parent (wt%)
	14:0 <sup>a</sup>	16:0	18:1	20:5	22:6	
Parent (100%)	8.8	21.3	13.0	15.4	10.1	100.0
1	21.0	32.8	12.9	5.1	1.7	14.6
2	10.9	29.9	17.4	6.1	1.9	35.8
3	3.5	14.3	14.6	22.4	11.7	30.5
4	2.5	6.1	3.4	29.5	45.8	19.1

<sup>a</sup>14:0 designates the methyl ester composed of a fatty acid having fourteen carbons and no unsaturation, i.e., myristic acid; 18:1 designates a fatty acid having eighteen carbons and one double bond, i.e., oleic acid; and so on.

proposed potato chip deoiling process. It is reported that about one half the oils in potato chips containing about 40–45 wt% oil can be extracted while retaining the original flavor and texture. Furthermore, the oils can be reused in subsequent frying operations.

Recently, a supercritical carbon dioxide process has been proposed to concentrate certain aromatic constituents in lemon oils, specifically the oxygenated components from limonene (Robey and Sunder, 1984). Although the components can be concentrated by either steam distillation or liquid–liquid extraction, these processes suffer from drawbacks, such as product degradation, low yields, or the requirement of subsequent removal of solvent. The supercritical carbon dioxide process being developed operates at 60°C; this precludes degradation of the sensitive essential oils. The extraction and

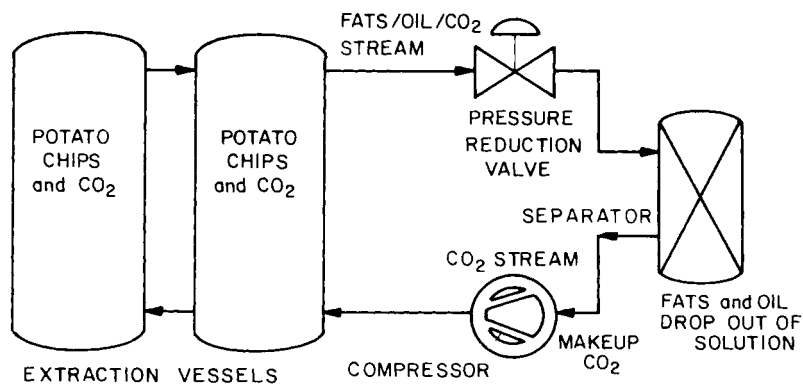


**Figure 10.6** Schematic diagram of the process for deoiling potato chips with supercritical carbon dioxide.



separation steps operate between the pressure levels of 103 bar (1,500 psia) and 55.2 bar (800 psia), respectively. The results to date show that a tenfold concentration of aromatics can be achieved in a single extraction stage, and from the single-stage data the results are extrapolated to a continuous multistage extractor with computer models predicting a twentyfold concentration at 99% yield. At a ten- or twentyfold concentration of aromatics, the supercritical fluid process is competitive with the traditional processes, in fact, the flavor of the essential oil may be superior. This beneficial factor has not yet been included in the economic comparison.

## EXTRACTION OF CHEMOTHERAPEUTIC AGENTS

The properties of carbon dioxide are especially attractive for extracting compounds from biological materials. This section describes some work carried out on the extraction of antineoplastic agents from plant materials (Krukonis, Branfman, and Broome, 1979). The plant materials tested, which are listed in

**Table 10.4** Plant Materials Containing Potential Antineoplastic Agents for Supercritical Carbon Dioxide Extractability

<i>NCI Designation</i>	<i>Plant Material (Specific Name, Variety, Origin)</i>
B628201	<i>Maytenus senegalensis</i> Celastraceae Tanzania
B628259	<i>Maytenus senegalensis</i> Celastraceae Kenya
B628318	<i>Maytenus senegalensis</i> Celastraceae India
B634635	<i>Gypsophila</i> Caryophyllaceae Michigan
B638786	<i>Citharexylum caudatum</i> Verbenaceae Panama
B805592	<i>Maquire calophylla</i> Moraceae Peru
B806512	<i>Rollinia papillionela</i> Annonaceae Peru

**Figure 10.7** Structure of maytansine. Maytansine is found in plant materials.

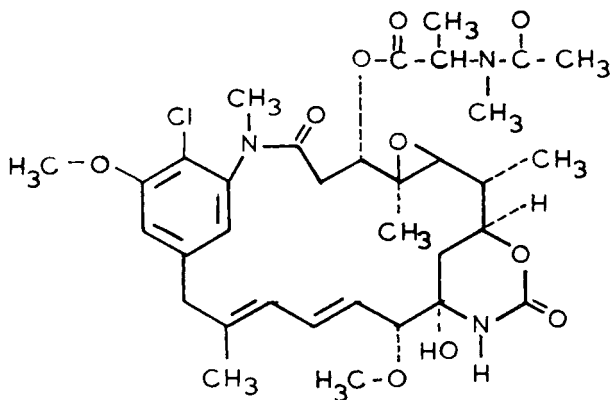


table 10.4, are confirmed by the National Cancer Institute (NCI) to contain active species. As an example of the complexity of the active species, figure 10.7 shows the structure of maytansine, which is present in materials B628318, B628259, and B628201 listed in table 10.4.

The extraction tests were exploratory and arbitrary in nature for two reasons: relatively little plant material was supplied, with the result that no optimization studies could be carried out; and pure material was unavailable for solubility testing. Not only were optimization studies impossible but also the extraction conditions were selected from experience with other complex organic compounds.

Extraction of the plant materials was performed in a flow apparatus similar to that described in chapter 4. The current National Cancer Institute protocol for extracting new plant materials consists of Soxhlet extraction with 95% ethanol. (For comparison purposes a Soxhlet extraction was also done for this study.) Carbon dioxide conditions of 275 bar and 35°C were chosen to achieve a high density at a temperature reasonably close to ambient temperature. About 20 g of plant material were used for each extraction. The material was contacted with 200 standard liters of carbon dioxide in a flow extractor, and the extract that was collected when the carbon dioxide was expanded to ambient pressure was tested in a bioassay test.

For the bioassay or cytotoxicity tests the extract (from both the supercritical extraction and 95% ethanol extraction procedures) is dissolved to various concentration levels in 95% ethanol, and the bioactivity is tested *in vitro* with the 9KB leukemia cell. Samples of cells are treated with various concentration levels of the extract and are then incubated. Cell growth inhibition is determined from protein measurements, which can be correlated to the number of cells. The  $ED_{50}$  value, expressed in mg/l, is defined as the extract concentration at which 50% of the cell growth is inhibited. Obviously, the lower the value, the more cytotoxic the extract.

**Table 10.5** Cytotoxicity of Extracts in 9KB Assay

<i>Plant Material</i>	<i>AD<sub>50</sub> Values (mg extract/l C<sub>2</sub>H<sub>5</sub>OH)</i>		
	<i>Supercritical Carbon Dioxide Extraction</i>	<i>Ambient Temperature Ethanol Extraction</i>	<i>Other Extraction</i>
B638302	11.0	3.7	
B628259	30.0	11.0	
B638318	0.25	0.11	(1) 0.19; (2) 0.03 (sequential collection of extract)
B634635	24.0	43.0	
B638786	4.0	>100.0	
B805592	21.0	126.0	2.3 (ethylene)
B806512	14.0	6.2	0.057 (liquid CO <sub>2</sub> )

The results of the cytotoxicity assay are shown in table 10.5. No optimization of the supercritical fluid extraction was carried out with respect to pressure, temperature, total amount of gas, etc. However, the data in table 10.5 show that all the supercritical fluid extracts yielded positive cytotoxicity results. In fact, for one of the plant materials, B638786, the supercritical fluid extract was substantially more active (i.e., it had a much lower ED<sub>50</sub>) than the standard ethanol extract.

The individual components in the supercritical fluid extracts from the plant materials were not identified, but from visual inspection it was concluded that the extracts probably contained a large percentage of glyceride components in admixture with the active species. It is known that triglycerides and fatty acids exhibit high solubility characteristics relative to more complex species such as alkaloids. For example, many glycerides, fatty acids, and esters exhibit solubility levels in the 1–10 wt% range. Thus, based upon two such different solubility levels, a stripping or fractionation scheme could result in the separation of about 90% or more of the inactive components in the plant materials. During passage of the first 10% of the supercritical fluid through the material, most of the normal vegetable matter present in the plant might be dissolved and be collected separately. The remaining extract would thus be enhanced in the active species. The sequential collection test was carried out on sample B628318, and the results of the 9KB bioassay are given in the right-hand column of table 10.5. The data show that the second fraction (which by visual inspection contained little triglyceride component) exhibited a higher activity than the first fraction. This lends credence to the simple fractionation concept.

Two other extraction tests were carried out, one using supercritical ethylene, the other using liquid carbon dioxide. Plant material B805592 was extracted with 200 standard liters of ethylene at 276 bar (4,000 psia) and 20°C. The bioassay results of the extract show the ethylene extract to be more active than the supercritical carbon dioxide extract. Plant material B806512 was extracted with 200 standard liters of liquid carbon dioxide at 275 bar and 20°C. The cytotoxicity results ( $ED_{50} = 0.057$  mg/l) show that the extract was more active than the extract obtained from supercritical carbon dioxide ( $ED_{50} = 14$  mg/l). It is not known whether the extracting fluids were more specific for the active component or if the differences are related to statistical spread of the combined extraction and bioassay tests. The results show that carbon dioxide and ethylene can dissolve quite complex organic compounds.

## ISOMER SEPARATIONS

A number of aromatic isomers serve as raw materials for a wide variety of chemical, pharmaceutical, and polymer products. Some isomers are difficult to obtain in pure form and frequently the purification of the isomers involves separating an *ortho-para* pair. For the purpose of evaluating the potential of employing supercritical solvents in separating aromatic isomers, the solubilities of one family of isomers, *ortho*-, *meta*-, and *para*-hydroxybenzoic acids, were measured in supercritical CO<sub>2</sub>. This family was chosen as one example for laboratory study because it is representative of a group of isomers that have practical applications. The hydroxybenzoic acids are frequently desired in relatively pure *ortho* and *para* forms for subsequent conversion to other compounds, and they most commonly must be separated from each other in a mixture not usually containing the *meta* isomer. The isomers can be separated by crystallization promoted by lowering the pH of a high-pH solution containing both salts. The pK for the *para* acid is typically higher than that of the *ortho* acid, resulting in a preferential precipitation of the *para* acid form. A relatively pure *para* isomer fraction can usually be prepared by such a process but the remaining salt form of the *ortho* isomer in solution is usually contaminated with some unprecipitated *para* isomer, which is also present as dissolved salt.

The solubility curves of the hydroxybenzoic acid isomers in CO<sub>2</sub> are shown in figure 10.8 (Krukons and Kurnik, 1985). The isomer that melts most readily, *o*-hydroxybenzoic acid, exhibits the highest solubility in CO<sub>2</sub> and its solubility is almost two orders of magnitude higher than the solubilities of the *meta* and *para* isomers.

The relation between solubility and isomer melting point is not surprising nor unexpected. The same type of solid solubility behavior is found with liquid organic solvents. The reasons for the inverse relationship between the solubility of aromatic isomers in liquid organic solvents and their melting points has been discussed by Morrison and Boyd (1983). In families of disubstituted

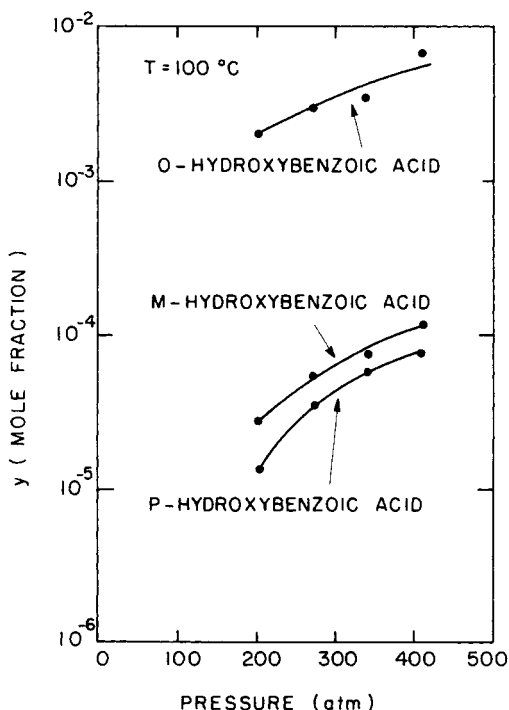


**Figure 10.8** Solubility isotherms for hydroxybenzoic acid isomers in supercritical carbon dioxide (Krukoniš and Kurnik, 1985) (1.01325 bar per atm).

benzenes the *para* isomer usually melts considerably higher than the other two isomers because of its symmetry, thus it is more easily accommodated into a crystal lattice. Since dissolution of a crystal, like melting, involves overcoming strong isomer–isomer intermolecular forces, a lower solubility of the *para* isomer in a given solvent is expected. Supercritical CO<sub>2</sub> acts in a manner quite similar to organic liquid solvents in its dissolving characteristics for *ortho* and *para* isomers. But it also exhibits a pressure-dependent dissolving power at constant temperature, as shown by the data in figure 10.8.

The solubilities of another family of isomers, methyl nitrobenzoate isomers, have also been measured in supercritical CO<sub>2</sub> at 35°C (Chang and Morrell, 1985). The methyl *ortho*-nitrobenzoate isomer is a liquid at ambient conditions, whereas the other two isomers are solids at both ambient and extraction conditions. For the methyl nitrobenzoates, the *ortho* isomer has the highest solubility, followed by the *meta* isomer, and then by the *para* isomers, as seen in figure 10.9. The *ortho* isomer is the most soluble because it is already in liquid form. This means that CO<sub>2</sub> does not have to overcome crystalline intermolecular forces that are very high because of the stereoregularity of the solid matrix.

Solubilities of several other isomers in supercritical CO<sub>2</sub> have been reported by Stahl and coworkers, whose qualitative results are consistent with the observation that the closer the functional groups of an isomer, the higher

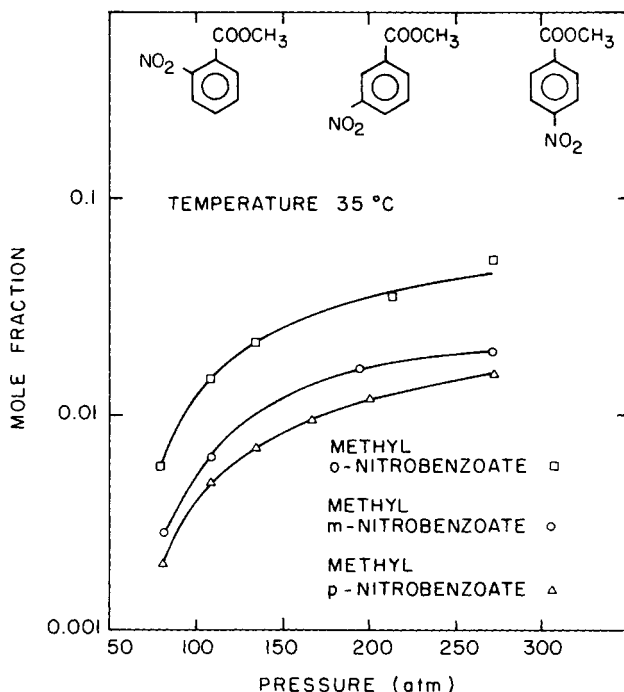


**Figure 10.9** Solubility isotherms for nitrobenzoate isomers in supercritical carbon dioxide (Chang and Morrell, 1985 (1.01325 bar per atm)).

the solubility of the isomer in supercritical CO<sub>2</sub> (Stahl and Schilz, 1979). The positional relation usually determines the stacking pattern in the crystal lattice and thus influences the melting point.

## TREATMENT OF WASTE STREAMS

The industrial research efforts on coffee decaffeination, spice extraction, and flavors concentration are, to a great extent, shrouded by the cloak of proprietary security, but the investigations of the use of supercritical fluids to treat various waste streams is reasonably well publicized. Most familiar, perhaps, is the supercritical waste water detoxification process developed by Modar Inc. This is potentially attractive for detoxifying refractory chemicals such as polychlorinated biphenyls, dioxin, and other toxic materials (Anon., 1982; Modell, 1982). In the Modar process, the toxic chemicals are homogeneously reacted with oxygen in supercritical water, the solvent for the organics and the oxygen. The main feature of the process is a chemical reaction discussed in more detail in chapter 11.

A waste process directed to the cleanup of drilling fluids is being developed by Critical Fluid Systems Inc. (Anon., 1982). Oil-based drilling fluids (commonly termed muds) are used to lubricate and cool drill bits and to

flush drill cuttings to the surface during the drilling of an oil well. The muds and oil-contaminated cuttings represent a disposal problem, especially for offshore platform drilling operations. Because of increasing environmental concerns, nations are instituting increasingly strict pollution control measures which preclude the dumping of hydrocarbon-containing drilling muds and cuttings off shore. A supercritical carbon dioxide extraction process is in development to remove the oil so that the oil-free cuttings can be dumped off shore. The drilling mud, a mixture of solid and oily material, would be processed in a system similar to that described for activated carbon regeneration, i.e., a multiple-vessel, batch-continuous operation. In this case, as in all the other development studies, the economics of the supercritical fluid process depends upon many factors. For example, the drilling mud and cuttings can alternatively be barged to shore for on-land disposal; these costs must be compared with the capital and operating costs of the on-platform supercritical carbon dioxide processing of the cuttings. The economics of the process are being evaluated at present.

The supercritical fluid extraction of oil from mill scale has been described in trade journals and at a national technical society meeting (de Filippi and Chung, 1985). Mill scale, i.e., small particle-size iron and iron oxide, is formed during rolling operations at steel mills, where oil-lubricated rollers shape and form red-hot steel ingots. Concern about oil leaching in landfills is placing severe limitations on dumping of such oil-contaminated material. A supercritical fluid extraction process is being evaluated under Environmental Protection Agency funding (de Filippi and Chung, 1985).

---

## Chemical Reactions in Supercritical Fluids

---

One very interesting and, as yet, not fully investigated area of supercritical fluid extraction technology is the use of a supercritical solvent as a reaction medium in which the solvent either actively participates in the reaction or functions solely as the solvent medium for the reactants, catalysts, and products. With an SCF medium it may be possible to increase the selectivity of a reaction while maintaining high conversions, to dissolve reactants and catalyst in a single fluid phase and carry out the reaction homogeneously, and to capitalize on the solvent characteristics of the supercritical fluid to separate the product species from the reactants, catalyst, and unwanted by-products. Reaction rates may also be enhanced while the process is operating in the mixture critical region as a result of the potentially favorable effect of applied hydrostatic pressure. They also may be enhanced by the highly negative partial molar volumes of the product species, which can occur with dilute reaction mixtures operating near the critical point of the pure SCF solvent.

### ENZYME REACTIONS

Many chemical reactions carried out in supercritical fluid media were discussed in the first edition, and those developments are included in total here after some recent work is described. In the epilogue (chapter 13) of the first edition we made reference to one of the author's work in enzyme catalyzed reactions in supercritical fluids that was (then) soon to appear in the literature. The paper (Hammond et al., 1985) was published while the first edition was in print, and as it turned out, there was a flurry of other activity in SCF-enzyme catalysis; many articles describing work with a variety of enzymes, e.g., alkaline phosphatase, polyphenol oxidase, cholesterolase, lipase, etc., were published starting in mid 1985. Practical motivations were a potentially easier workup and purification of a product if the solvent is a gas (i.e., no liquid solvent residues to contend with), faster reaction rates of compounds because of gas-like transport properties, environmental advantages of carbon dioxide, and the like.



Many enzyme reactions in the pharmaceuticals sector are carried out in an aqueous medium, i.e., the enzyme is dissolved in water, and the reactant is usually a second (water-insoluble) phase. Fundamentally, it would be interesting to learn "what would happen" if the phases were reversed, i.e., if the reactant were dissolved in some solvent and the enzyme the second phase. Klibanov and coworkers had previously reported on enzymatic catalysis reactions in organic liquids with only scant moisture present to render the enzyme active (Zaks and Klibanov, 1984).

It is of pedagogical value to discuss the first two supercritical fluid-enzyme catalysis papers that appeared within two months of each other (Randolph et al., 1985; Hammond et al., 1985). Randolph studied the hydrolysis of the disodium salt of *p*-nitrophenyl phosphoric acid reacting to *p*-nitrophenol. Hammond studied the catalytic oxidation of *p*-substituted phenols to first, orthocatecholic compounds and in series to *o*-quinone compounds, which very quickly polymerize by chemical, not enzymatic, mechanisms to form *o*-quinoid polymers. The product recovered is a poly(*o*-quinone).

Randolph's tests with alkaline phosphatase were carried out in a stirred autoclave. An amount of the disodium salt and some water, which is required for the enzyme catalyzed hydrolysis, were placed in the autoclave along with a sealed glass ampule containing the enzyme. In this case water is necessary not just to render the enzyme active, as Klibanov found, but also to serve as a reactant in the hydrolysis. Carbon dioxide was admitted, the temperature and pressure adjusted to the level desired, and the sealed ampule shattered to expose the enzyme and to mark the zero point of the reaction sequence. In their studies they investigated the effects of changing the relative amount of enzyme on the rate of conversion of the disodium salt of *p*-nitrophenyl phosphoric acid to *p*-nitrophenol. They measured the amount of conversion by UV analysis of the solution removed from the autoclave at the end of a reaction test. The results are shown in Figure 11.1; based upon these results and other experimental results, the authors concluded that the rate-determining step of the enzyme-catalyzed reaction was the dissolution of disodium *p*-nitrophenyl phosphate in supercritical carbon dioxide.

By 1985 the SCF community had developed and accumulated substantial combined knowledge in fundamental behavior, application, and production. But when this paper was published, it resulted in some discussion and confusion within the community. It was our opinion at that time that the sodium salt of *p*-nitrophenyl phosphoric acid could not dissolve in supercritical carbon dioxide, and this opinion was later confirmed in tests on the solubility of the sodium salt of *p*-nitrophenyl phosphoric acid. Krukonis and Hammond carried out tests to measure the solubility of the salt in dry carbon dioxide and to investigate if there could be some cosolvent effect of water in water-saturated carbon dioxide. They found that the solubility was virtually nil, i.e., the salt could not be detected by UV analysis of the extracts in the collection vessel, and there was no visible extract. On the basis of the insolubility of the salt in dry or wet carbon dioxide from the solubility tests, the authors

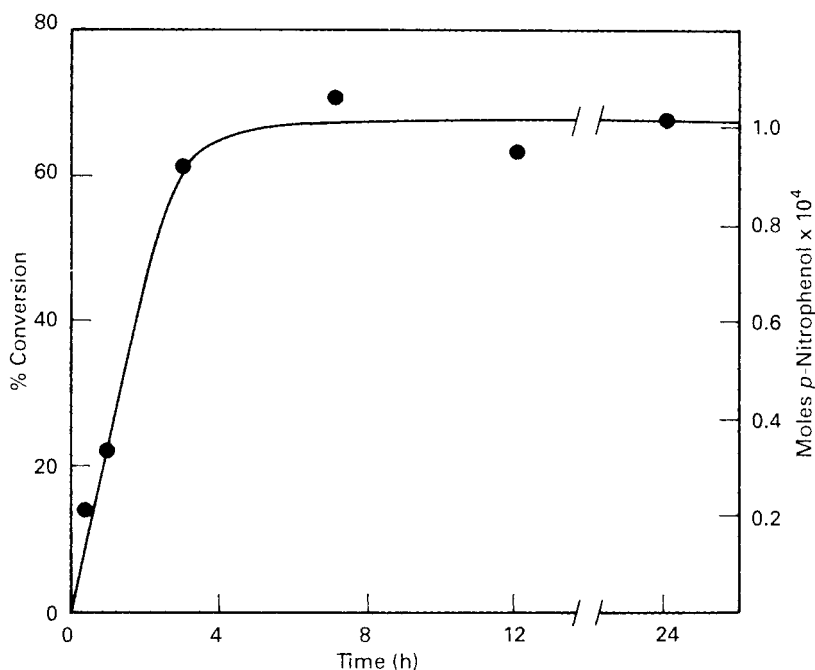


**Figure 11.1** Conversion of disodium *p*-nitrophenyl phosphate to *p*-nitrophenol in supercritical carbon dioxide.

concluded that some mechanisms other than enzyme catalysis of salt dissolved in carbon dioxide must have been responsible for the conversion measured by Randolph et al.

The enzyme-catalyzed oxidation tests of Hammond et al. with polyphenol oxidase and *p*-substituted phenols were carried out in a flow reactor. The physical arrangement of materials in the extractor/reactor is shown in figure 9.3. This laboratory system is shown in figure 11.2 along with an enlarged cross section of the reactor, a 2 cm diameter  $\times$  25 cm long stainless steel vessel. A continuous flow-through extraction/reaction system was employed; the carbon dioxide entered the vessel at the bottom, passed through a section of moistened glass wool so that the carbon dioxide became saturated with water, then passed into the reactant section to pick up the reactant (*p*-cresol, for example). With the dissolved water and *p*-cresol, the carbon dioxide passed into and through the enzyme-containing section where reaction occurred. A glass wool filter between the reactant and the enzyme ensured that no *p*-cresol entered the enzyme section by simple entrainment of particles; any reaction of *p*-cresol to *o*-quinone that was measured must have occurred only via a mechanism involving *p*-cresol dissolved in the carbon dioxide that passed through the enzyme-containing section.

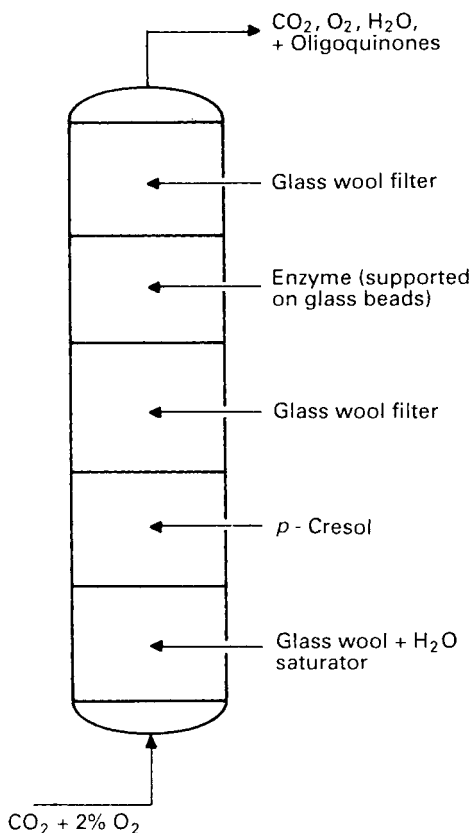
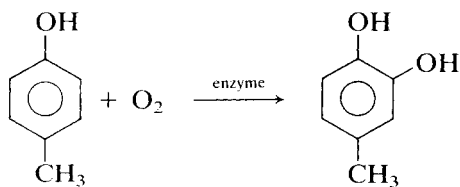
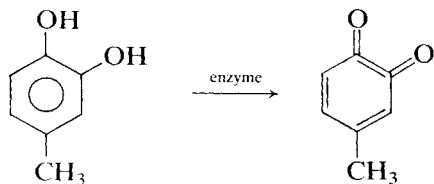


**Figure 11.2** Cross-section of reactor.

The first step is the oxygen insertion reaction.



Further oxidation occurs via



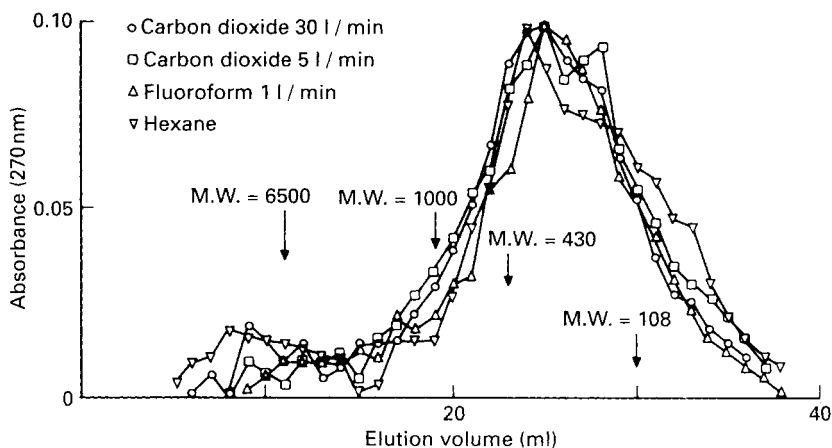


Figure 11.3 Mole weight of products.

Literally within 2 sec of starting the flow of carbon dioxide, a blood-red (*o*-quinone color) extract was collected in the U-tube positioned downstream of the expansion valve. The total residence time of the gas stream in the enzyme section was less than about 5 sec, and within a period of only a few minutes the equivalent of about one half the *p*-cresol that was charged to the extractor was collected in the U-tube. When the extractor was opened, the remaining half was seen to be present on the enzyme and the glass wool at the exit of the reactor. To obtain material for analysis, the enzyme and glass wool were washed with toluene, the solution combined with the extract in the U-tube collector, and the total analyzed by HPLC. Tests with carbon dioxide at different velocity levels and one test with supercritical fluoroform were also carried out. The test with fluoroform was made to determine if there would be a difference in reaction and product distribution when the pH was higher. Carbon dioxide in water at about 50 to 100 bar results in a pH of 3, and it was deemed important to investigate what effects the two gases would have.

The results of all the tests and of one test carried out in hexane (at ambient conditions) are shown in figure 11.3. The molecular weight distributions of the *o*-quinoid polymers formed in all tests are essentially identical. There was no difference in reaction rate seen with carbon dioxide and trifluoromethane but the reaction rate of the oxidation of *p*-cresol in the supercritical solvents was orders of magnitude higher than in hexane, most assuredly because the concentration of oxygen in the gas (2%) was much higher than in the hexane. In fact, where a reaction between a compound and a gas occurs by heterogeneous catalysis, e.g., with enzymes or metal catalysts, supercritical fluids can produce enhanced rates. This is because the concentration of reactant gas can be increased to almost any desired level consistent with keeping the SCF and reactant gas mixture a solvent for the reactants. In perhaps a ridiculous extreme, a concentration of, say, 50% oxygen in carbon

dioxide could not be used because the 50/50 mixture, although a supercritical fluid, would not be a solvent for *p*-cresol, for example.

The remainder of this chapter describes a variety of chemical reaction studies in supercritical fluids. Some are interesting for their fundamental aspects, others are described for their potential practical value. To take full advantage of an SCF reaction medium it is necessary to be cognizant of the phase behavior exhibited by the reaction mixture at high pressures. For instance, it has been shown that some of the kinetic studies reported in the literature on the high-pressure polymerization of ethylene are of little value, since the reaction rate data were analyzed according to the assumption that the reaction was operated homogeneously when, in fact, two phases were present (Ehrlich and Mortimer, 1970). It should be evident after one has read chapter 3 that various types of phase behavior are possible with SCF reaction mixtures. Careful experimentation is therefore necessary when performing high-pressure reaction studies.

An example of investigating the phase behavior of a system before doing reaction studies is given in a patent describing a hydrocarbon isomerization process (Leder, Kramer, and Solomon, 1976). In this instance, the reacting mixture is a multicomponent solution consisting of a hydrocarbon feed, such as *n*-hexane, a metal halide catalyst, a hydrogen-halide solvent, such as HCl, and hydrogen. While it probably is not practical to perform extensive phase behavior experiments on this quaternary system, it is reasonable to assume that the quaternary mixture will exhibit phase behavior that is very similar to the type-I behavior exhibited by the two major components of the mixture, HCl and the hydrocarbon. A schematic *P-T* diagram for this binary mixture is shown in figure 11.4. Kramer and Leder recommend operating the reaction at *P-T* conditions within region II bounded by the critical-mixture curve and the dashed line shown in figure 11.4. Even though this is not strictly a supercritical fluid reaction, since it is run in the near-critical liquid region, it does provide an example of a case in which the researchers first determine the critical mixture behavior of the reactants (see figure 11.5) then proceed with the reaction studies in a well-defined region of the phase diagram. It is probably prudent to perform a few phase behavior experiments to determine the solubility of hydrogen in the solution. Typically hydrogen is sparingly soluble in a liquid but usually the solubility of a sparingly soluble gas is far greater in a supercritical fluid medium.

As a reaction proceeds, the resultant product species, if it contains a different functional group compared with the reactant, may induce the reactant-product-SCF mixture to split into multiple phases near the critical point of the SCF. The work of Francis (1954), Dandge, Heller, and Wilson (1985), and Stahl and coworkers (Stahl and Quirin, 1983; Stahl et al., 1980) should be consulted for information on the types of functional groups that affect the miscibility behavior of solute-SCF mixtures. Chapter 3 shows that binary mixtures tend to exhibit multiphase LLV behavior as the differences in the molecular weights of the mixture components increase (Rowlinson and Swinton, 1982), so it is reasonable to assume that a reacting mixture would also

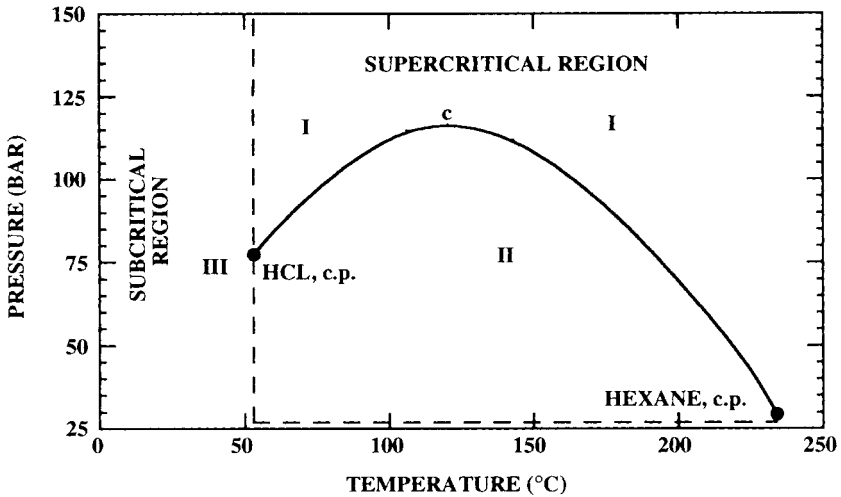


**Figure 11.4** Schematic  $P$ - $T$  diagram of the reacting mixture in the hydrocarbon isomerization process proposed by Leder, Kramer, and Solomon (1976).

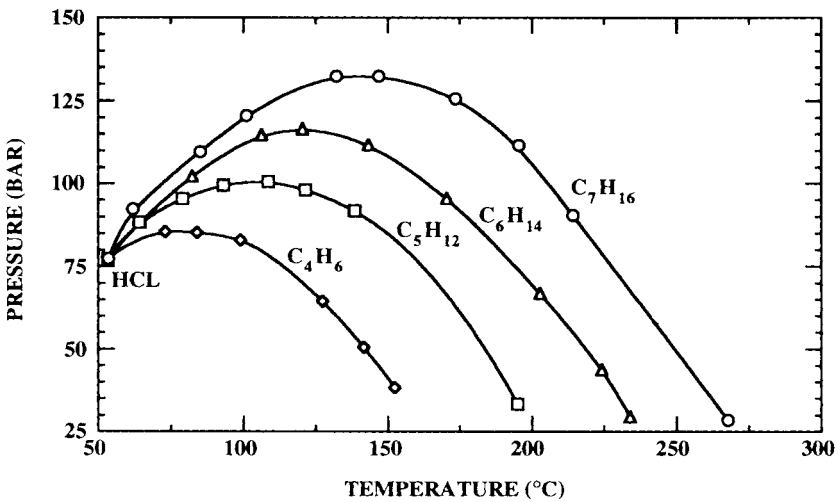
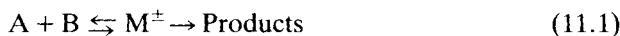


**Figure 11.5** Critical mixture curves for various hydrocarbon-HCl mixtures (Leder, Kramer, and Solomon, 1976).

exhibit multiple phases if the molecular weights of the product species were quite large relative to the SCF solvent. Alexander and Paulaitis (1984) describe a reaction/separation scenario for the Diels–Alder reaction of isoprene with maleic anhydride in supercritical carbon dioxide, where they find that the product precipitates as a solid from the reaction mixture as the reaction proceeds. In this case, the reaction is run at fairly low concentrations in supercritical carbon dioxide near the critical point of pure carbon dioxide.

Reaction rates may be improved if the reaction is run in the mixture critical region. A rate enhancement can potentially occur as a result of applied hydrostatic pressure and as a result of the unusual partial molar volume behavior of a heavy solute solubilized in a supercritical solvent. Numerous authors have used transition state analysis (Laidler, 1965; Eckert, 1972; Ehrlich, 1971) to explain the rate enhancement that can occur at high pressures. For a bimolecular reaction, a chemical equilibrium is assumed to exist between the reactants A and B and the transition state  $M^\pm$ .



The variation of the reaction rate constant  $k$  with pressure is given by

$$\left( \frac{\partial \ln k}{\partial P} \right)_T = \frac{\Delta V^\pm}{RT} \quad (11.2)$$

where  $\Delta V^\pm$ , the volume of activation, is the difference in the partial molar volumes of the activated complex and the reactants and is given by

$$\Delta V^\pm = \bar{V}_M - \bar{V}_A - \bar{V}_B \quad (11.3)$$

Equation 11.2 shows that a reaction with a positive activation volume is hindered by pressure, while a reaction with a negative activation volume is enhanced by pressure. Eckert (1972) noted that equation 11.2 is applicable only if the reaction rate is expressed in terms of mole fractions not concentrations. Otherwise a second term is needed to account for the compressibility of the reaction mixture.

Let us consider the application of transition state analysis to interpret the work of Ehrlich and coworkers on the reaction behavior of ethylene polymerization in supercritical ethylene (Ehrlich, 1971). Ehrlich presents experimental data on the polymerization of ethylene at 130°C and 1,500 bar. At these conditions supercritical ethylene can solubilize ~5 wt% to 10 wt% high molecular weight polyethylene, which is produced during the reaction. Normally, the conversions are kept to ~10% which means that the reacting supercritical ethylene–polyethylene mixture is near a mixture critical point. Ehrlich argues that the partial molar volume of  $M^\pm$ , which has volumetric

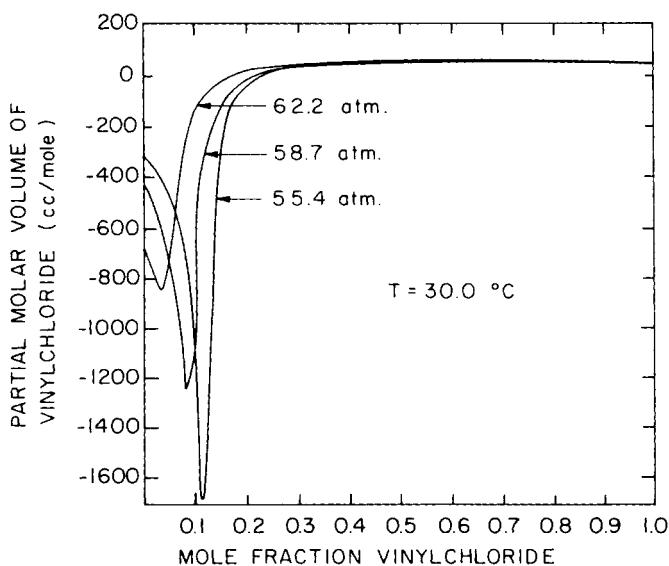


**Figure 11.6** Calculated partial molar volume behavior of vinyl chloride solubilized in supercritical ethylene (Ehrlich and Fariss, 1969) (1.01325 bar per atm).

properties similar to the product polymer, can have a very large negative value in supercritical ethylene. It is well known that very large, negative partial molar volumes can exist for mixtures in which the solute is in dilute concentrations and the solvent is very close to its critical conditions or the mixture is close to the mixture critical point (Eckert et al., 1983; Chappellear and Elgin, 1961; Ehrlich and Wu, 1973). Consider the partial molar volume behavior of vinyl chloride solubilized in supercritical ethylene, shown in figure 11.6 (Ehrlich and Fariss, 1969). Using equation 11.2 and assuming that the absolute value of  $\bar{V}_M$  is much greater than the partial molar volume of ethylene, we would conclude that there should be a large rate enhancement occurring near the mixture critical point of the ethylene-polyethylene system. Ehrlich uses transition state analysis to explain the large pressure effect on the polymerization rate as the pressure is dropped toward the mixture critical value, the small pressure effect on the polymerization rate when crystalline polymer is formed and falls out of solution, and the very high anomalous activation energy for polymerization at a temperature of 100–130°C (the so-called critical polymerization boundary). But in more recent work, Ehrlich and coworkers find that the anomalous activation energy for ethylene polymerization in supercritical ethylene may be attributed to the presence of dissolved oxygen, which can be both a free-radical inhibitor in the subcritical



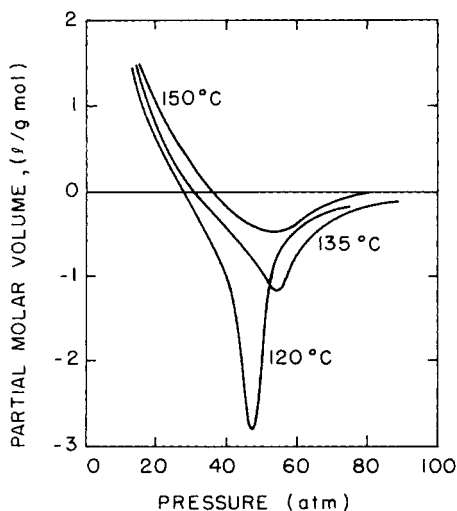


**Figure 11.7** Partial molar volume behavior of the activated complex formed in the dimerization of chlorotrifluoroethylene in its critical region (Simmons and Mason, 1972) (1.01325 bar per atm).

liquid–gas region and a free-radical initiator in the supercritical region (Takahashi and Ehrlich, 1982; Ehrlich and Pittilo, 1960). Without the presence of dissolved oxygen in the system, the polymerization rates are very slow. Hence, the rate enhancements suggested by transition state analysis are quite small in this instance.

Simmons and Mason (1972) employ transition state analysis with an equation of state (EOS) (i.e., Redlich–Kwong and the virial equation) to derive an expression for the pressure dependence of the dimerization rate constant of chlorotrifluoroethylene ( $T_c = 105.7^\circ\text{C}$ ,  $P_c = 40.6$  bar). They predict the volumetric properties of the reactants by fitting experimental rate data. They can obtain the thermodynamic properties, such as the fugacity coefficient and partial molar volume, of the activated complex. The predicted fugacity coefficient of the activated complex exhibits the same trends as those of a normal molecular species. Also, quite interestingly, the partial molar volume of the activated complex,  $\bar{V}_M$ , decreases sharply near the critical point of the dilute reaction mixture (see figure 11.7). On the basis of transition state analysis an enhanced reaction rate might be expected at conditions very near the critical point of the pure chlorotrifluoroethylene. But the observed rate enhancement is only a modest 30% for pressures up to 100 bar. And the Redlich–Kwong EOS only correlates the experimental data to within  $\pm 30\%$ , which hinders the prediction and modeling of reaction rate data in the mixture critical region.

Johnston and Haynes (1987) demonstrate that the rate constant for the unimolecular, thermal decomposition of a chlorobenzyl methyl ether in 1,1-difluoroethane ( $T_c = 113.4^\circ\text{C}$ ,  $P_c = 45.0$  bar) can be increased by an order of magnitude with a small change in pressure if the ether is very dilute and the

operating pressure and temperature are close to the critical point of 1,1-difluoroethane. The increase in rate constant is attributed to the large negative volumes of activation which occur in the vicinity of the critical point of 1,1-difluoroethane where the solution compressibility is very large and where relatively strong solute-solvent interactions are found. However, very slow *rates* of reaction are observed since the reactant is at near-infinite dilution and the rate constant is about an order of magnitude less than the rate constant found for this reaction run in liquid solvents.

For all practical purposes the large rate enhancements that occur as a result of large solute partial molar volumes are limited to the dilute concentration region as shown in figure 11.6 and implied in figure 11.7. Although an enhancement of the reaction rate can occur as a result of hydrostatic pressure alone, excessively high pressures (i.e., greater than 1,000 bar) are needed for pressure to have any appreciable effect (Eckert, 1972).

## HIGH-TEMPERATURE REACTIONS

Pyrolysis reactions are one class of reactions that benefit from the use of an SCF solvent medium since the SCF can solubilize reacted products and remove them from the high-temperature zone, thus avoiding further thermal decomposition. The carbon formation that occurs at the high temperatures normally encountered in pyrolysis reactions can therefore be minimized. Improved yields, selectivities, and product separation have been attained in an SCF reaction medium, compared with conventional pyrolysis methods. There is no doubt that a sufficiently high temperature is needed to provide the thermal energy to break bonds in a pyrolysis reaction. But it is not necessary to operate at excessively high temperatures to increase the vapor pressure of the product materials because the SCF medium has the necessary solvent strength to dissolve the products and remove them from the reaction zone.

Koll and Metzger (1978) report on the use of supercritical acetone as the reaction medium for the thermal degradation of cellulose and chitin. Since the pyrolysis of these polysaccharides occurs at such high temperatures, it is necessary to remove the primary products from the reaction zone as soon as they are formed to avoid degradation of the products into coke. The high operating temperature also adversely affects both yield and product distribution. It is possible to reduce the carbon formation by carrying out the pyrolysis under vacuum but the reaction rate is also reduced because of the poor heat transfer to the reactants.

As an alternative pyrolysis technique, Koll and Metzger react the cellulose in the presence of supercritical acetone ( $T_c = 235.7^\circ\text{C}$ ,  $P_c = 47.6$  bar) using a flow reactor. The reactor, operating isobarically at 255 bar, is temperature programmed from  $150^\circ\text{C}$  to  $290^\circ\text{C}$ . At SCF conditions, 98% extraction of the initial cellulose is achieved. The yield of glucosan is 38.8%; this compares

favorably with the 28.1% yield obtained with vacuum pyrolysis. Interestingly, the cellulose residue has the same crystallinity as the starting cellulose even after 50% degradation. Thus, the use of supercritical acetone as a reaction medium in the thermal degradation of cellulose results in an appreciable amount of extraction, less carbon formation, and better yield at temperatures lower than those used for conventional pyrolysis.

While doing their cellulose and chitin studies Koll and Metzger found condensation products of acetone (such as diacetone alcohol and mesityl oxide) that were apparently formed by a thermally induced aldol condensation (Koll and Metzger, 1978). This is an interesting finding since pyrolysis reactions are expected to dominate at these high temperatures. Metzger et al. (1983) initiated a program to investigate systematically thermal intermolecular reactions at high temperatures ( $\sim 500^{\circ}\text{C}$ ) and high pressures ( $\sim 500$  bar) using a flow reactor with residence times of 1–10 min. They assumed that at such high temperatures and pressures the reacting mixture is a single supercritical fluid. The researchers find that alkanes are added to alkenes (e.g., *n*-alkenes, acrylonitrile, methyl acrylate, methyl vinyl ketone), to 1,3-dienes (e.g., 1,3-cyclohexadiene), and to alkynes (acetylene). Thus, functional groups are added to hydrocarbons at supercritical conditions. The reactant mixture typically consists of an alkane-to-alkene feed in the ratio of 1:5. For example, when cyclohexane ( $T_c = 280.3^{\circ}\text{C}$ ,  $P_c = 40.9$  bar) is the representative alkane and methyl acrylate ( $T_c = 263^{\circ}\text{C}$ ,  $P_c = 42.6$  bar) is the representative alkene, the yield at  $500^{\circ}\text{C}$  (based on methyl acrylate) increases significantly with pressure up to 100 bar and thereafter remains essentially constant. The increase in yield is explained by the increase of density of the reacting mixture with pressure. At higher densities the intermolecular reaction proceeds at a much higher rate.

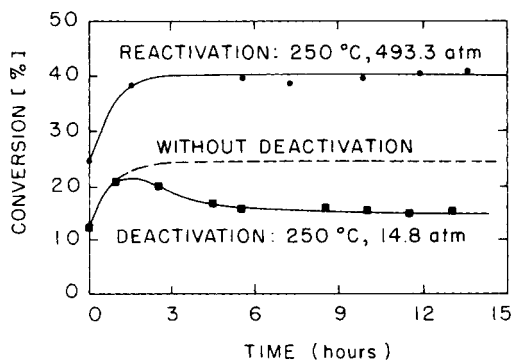
Other reactions studied by these authors include the thermal dimerization of methyl acrylate and the reaction of benzene with certain alkynes in a Diels–Alder reaction. Supercritical extraction in coal processing may also be classified under this scheme. This subject is reviewed by Williams (1981); it is not included in this chapter.

## HETEROGENEOUS CATALYSIS

For certain heterogeneous catalytic reactions the catalyst activity can be renewed by adjusting the pressure and temperature so that the reacting medium is in the supercritical state. The activity of the catalyst can be periodically regenerated by treatment with an SCF solvent or, in fact, the reaction can be run at supercritical conditions, thus maintaining high levels of catalytic activity for longer periods of time. A number of examples of SCF catalytic reactions are given in the following paragraphs.

Tiltscher, Wolf, and Schelchshorn (1984) describe the influence of an SCF reaction medium on the activity of a heterogeneous catalyst used in a

**Figure 11.8** Effect of unwanted oligomeric by-products formed during the catalytic isomerization of 1-hexene (Tilscher, Wolf, and Schelchshorn, 1981) (1.01325 bar per atm).

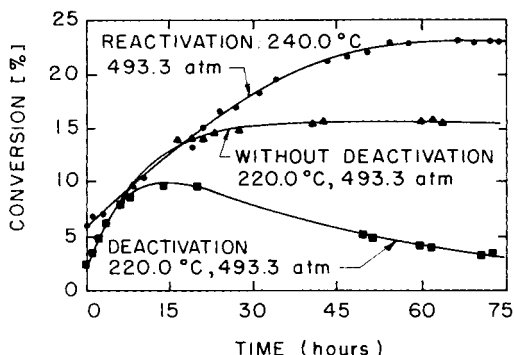


high-pressure differential-recycle reactor to study the catalytic isomerization of 1-hexene ( $T_c = 231^\circ\text{C}$ ,  $P_c = 31.1$  bar) on  $\alpha\text{-Al}_2\text{O}_3$  with 2-chlorohexane as a cocatalyst. In this isomerization reaction they produce 1-hexene, *cis*-2-hexene, *trans*-2-hexene, and *trans*-3-hexene. The authors demonstrate how an SCF reaction medium can be used to reactivate a catalyst that has been poisoned by three different methods.

If the isomerization reaction is carried out in the gaseous phase ( $T = 250^\circ\text{C}$ ,  $P = 15.0$  bar), the resulting conversion-time curve is characteristic of a process where a deactivation process occurs in parallel with the reaction (figure 11.8). The deactivation of the catalyst is a result of unwanted low-volatile oligomeric compounds ( $\text{C}_{12}\text{-C}_{30}$ ) that accumulate on the catalyst surface and eventually cause coking. If the reaction mixture is isothermally compressed to 500 bar, the oligomers are stripped from the catalyst surface. Although the phase behavior of the reactant-product system is not reported by Tilscher and coworkers, it seems safe to assume the following: (1) the isomerization products are so similar to 1-hexene that the critical temperature and critical pressure of the reactant-product(s) mixture is very close to that of pure 1-hexene; and (2) the small amount of chlorohexane present in the system does not significantly affect the pressures and temperatures needed to obtain a single, fluid phase mixture. Therefore, a pressure of 500 bar is more than sufficient to ensure that the reaction mixture plus stripped oligomers is indeed a single fluid phase. If an elevated operating pressure is maintained at this high pressure level, a twofold increase is observed in the overall isomerization rate and about a 30% increase in the *cis/trans*-2-hexene ratio is also observed (Tilscher, Wolf, and Schelchshorn, 1984). At SCF conditions the catalyst activity is maintained at precoking levels even after 12 h of reaction time, as noted from the upper curve of figure 11.8. Not surprisingly, they conclude that higher pressures are needed to enhance reactivation rates as the volatility of the oligomeric coking compounds decrease.

In another test they deactivate the catalyst by introducing a small amount of a finely dispersed catalyst-fouling substance ( $\text{MoS}_2$ ) into the reactor under

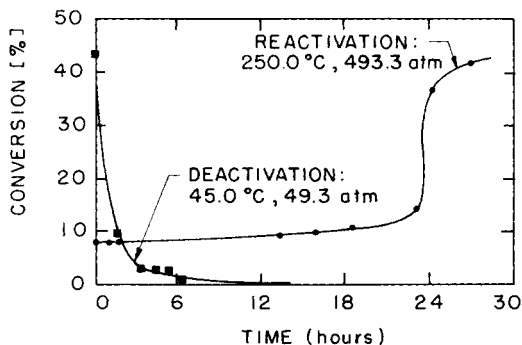
**Figure 11.9** Effect of  $\text{MoS}_2$  formed on the catalyst used for the isomerization of 1-hexene (Tilscher, Wolf, and Schelchshorn, 1981) (1.01325 bar per atm).



liquid phase reaction conditions ( $T = 220^\circ\text{C}$ ,  $P = 500$  bar). In this instance the conversion–time curve is again characteristic of a reaction accompanied by catalyst deactivation (figure 11.6). If the reaction mixture is isobarically heated to  $240^\circ\text{C}$ , it becomes supercritical and eventually the catalyst activity is restored. Although it is not explicitly stated by Tilscher, Wolf, and Schelchshorn, presumably the trace amounts of  $\text{MoS}_2$  are solubilized by the reacting mixture.

In the final deactivation mode reported by the authors, the active acidic sites of the catalyst are poisoned ( $T = 145^\circ\text{C}$ ,  $P = 50$  bar) by continuous addition of a very dilute solution of pyridine to the reacting mixture over a period of 12 h (see figure 11.10). The catalyst can be reactivated by heating and compressing the reaction mixture to conditions well within the mixture critical region ( $T = 250^\circ\text{C}$ ,  $P = 500$  bar). Tilscher and coworkers report that the catalyst poison is precipitated from the product solution as pyridinium chloride. Presumably only a very small amount of pyridinium chloride is needed to deactivate the catalyst since supercritical hexene probably would not be able to solubilize much of this salt. It is surprising, however, that supercritical hexene can overcome the acid–base interactions that are occurring on the catalyst surface and, hence, remove the pyridinium chloride.

**Figure 11.10** Effect of pyridine on the catalyst used for the isomerization of 1-hexene (Tilscher, Wolf, and Schelchshorn, 1981) (1.01325 bar per atm).



## VISCOSITY EFFECTS

It is well known that solvent viscosity can have an effect on the product distribution for certain reactions (Saltiel and Charlton, 1980). The effect of solvent viscosity can be studied with an SCF reaction medium since a wide range of viscosities can be obtained with a single SCF solvent if the system is operated in the vicinity of the critical point of the solvent.

Squires, Venier, and Aida (1983) describe an experimental technique they use to study the effect of solvent viscosity on the *cis/trans* ratio of stilbene irradiated in supercritical CO<sub>2</sub>. They use a dynamic flow technique similar to that described in chapter 4. In their system *trans*-stilbene is coated onto glass beads, which are then packed into a high-pressure column. Supercritical CO<sub>2</sub> flows through the column and solubilizes some of the *trans*-stilbene. The CO<sub>2</sub>-stilbene phase is continuously irradiated with ultraviolet light as it flows through a quartz photoreactor at a fixed temperature and pressure. As the solvent viscosity increases, the photoisomerization of the *cis* isomer is inhibited while that of the *trans* isomer is facilitated. We should expect to see the *cis/trans* ratio of stilbene vary as the density of CO<sub>2</sub> varies. This viscosity effect is clearly shown in figure 11.11. While there is a small effect of pressure on the

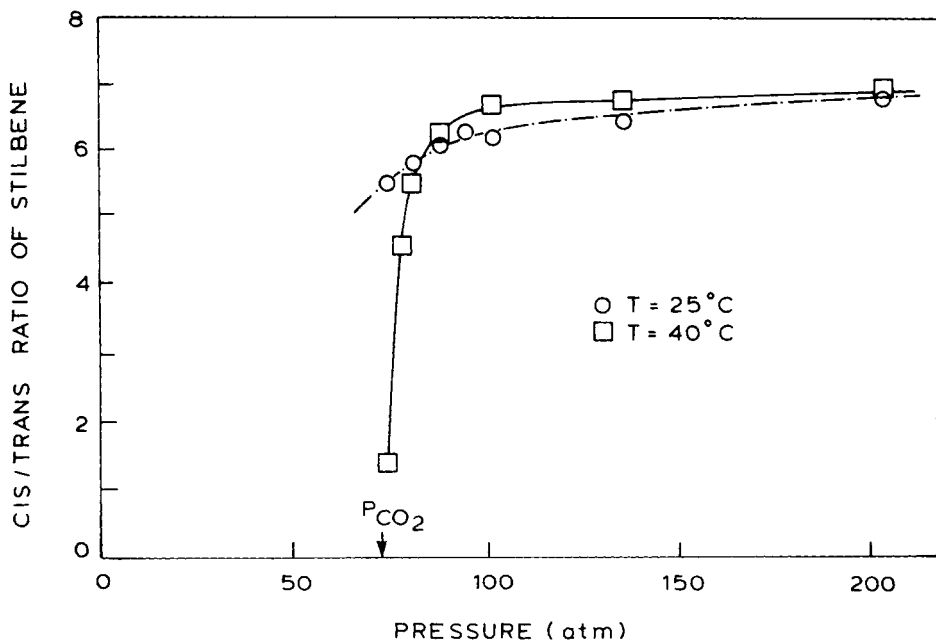


**Figure 11.11** Transient product distribution of the *cis/trans* isomer obtained when stilbene is irradiated in near-critical and supercritical carbon dioxide at 136 atm (1.01325 bar per atm).

*cis/trans* ratio when the photoisomerization is run in near-critical liquid CO<sub>2</sub>, the pressure effect is exacerbated in supercritical CO<sub>2</sub>. This large pressure effect is highly correlated to the changes in CO<sub>2</sub> viscosity at 40°C near the critical pressure of CO<sub>2</sub>. Since the *cis* and *trans* structures exhibit different solubility levels in supercritical CO<sub>2</sub>, it may be possible readily to separate the reaction mixture.

## REACTION/SEPARATION SCHEMES

Supercritical fluid solvents can be employed as solvent media in chemically reacting mixtures, especially where it is difficult or prohibitively expensive to separate the desired species from a reaction-product mixture by conventional techniques such as distillation. It may be fruitful to consider using an SCF reaction medium in which the product can be more easily recovered from solution. For certain reactions, using an SCF reaction medium can also improve the product selectivity without adversely affecting total conversion.

In a recent patent Kramer and Leder (1975) describe an SCF reaction scheme for isomerizing short-chain paraffinic hydrocarbons (4–12 carbon atoms). The reaction medium consists of CO<sub>2</sub>, HBr, or HCl (as a promoter), a paraffinic hydrocarbon, and a Lewis acid catalyst (e.g., AlBr<sub>3</sub>, AlCl<sub>3</sub>, BF<sub>3</sub>).

An SCF reaction scheme offers several advantages compared with a conventional subcritical liquid CO<sub>2</sub> isomerization process. One obvious advantage is that hydrogen can be more easily dissolved in the SCF reaction phase as compared with a liquid reaction phase. The presence of hydrogen facilitates isomerization, as opposed to cracking reactions, and thus improves the selectivity of the reaction while not adversely affecting the conversion level.

SCF processing has been applied to the treatment of wastewater streams. In a recent patent, Modell (1982) describes an efficient processing method for oxidizing the organic materials present in wastewater using supercritical water ( $T_c = 374^\circ\text{C}$ ,  $P_c = 220.5$  bar). The reaction is performed in a single fluid phase at supercritical conditions. For the purpose of minimizing the energy requirements for the process, the heat generated in the reaction is efficiently transferred to the reactor feed stream. An important advantage of the SCF reaction scheme over conventional processing is that virtually total oxidation of the organics can be realized with higher reaction rates. Since the reaction mixture is completely miscible in the mixture critical region, stoichiometric amounts of oxygen are easily added to the system for total oxidation of the organics.

In this process inorganic salts, which are virtually insoluble in supercritical water (1 ppb to 100 ppm in the temperature range 450–500°C), are easily precipitated from solution and readily removed from the system. As a consequence, the outlet water from the reactor is free of inorganic salts, thus eliminating the need for purifying reactor feedwater from sources such as brine and seawater. In addition, the heat liberated during the oxidation of the

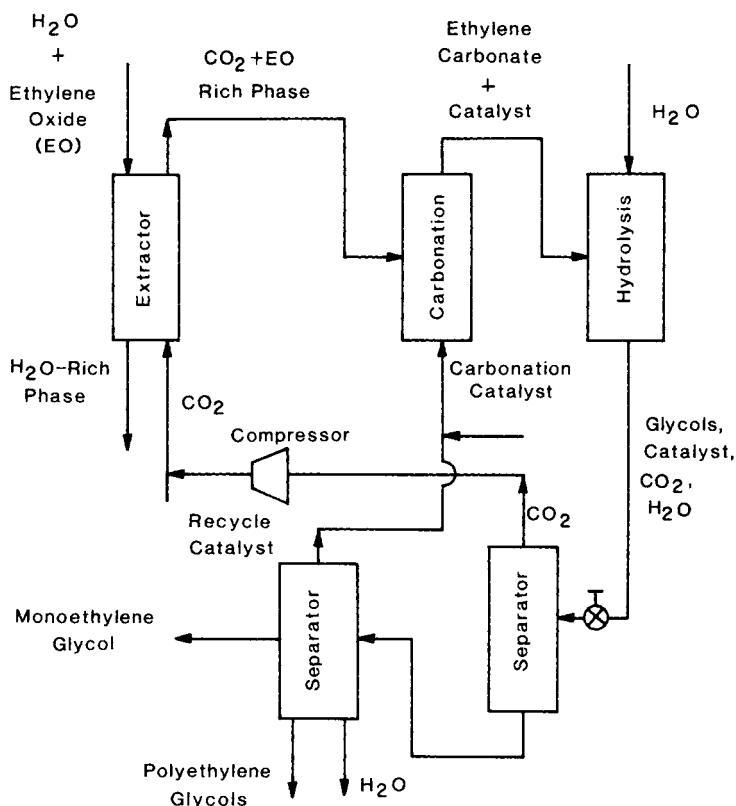


**Figure 11.12** Proposed SCF reaction/separation process for producing ethylene glycol (Bhise, 1983).

organics can be recovered in the form of superheated, supercritical steam without the need for heat transfer equipment.

Another recent patent describes a multistep process for the production of ethylene glycol in near-critical or supercritical  $\text{CO}_2$  (Bhise, 1983). In this instance  $\text{CO}_2$  is first used as a solvent and then used as a reactant. Normally, ethylene oxide is produced by the vapor phase oxidation of ethylene with molecular oxygen over a supported silver catalyst. In conventional ethylene glycol processing, an effluent stream containing the ethylene oxide is scrubbed with water to recover the ethylene oxide. The ethylene oxide is then recovered for hydrolysis to ethylene glycol.

A schematic diagram of the SCF reaction/separation process is shown in figure 11.12 (Bhise, 1983). An ethylene oxide-rich  $\text{CO}_2$  phase is obtained when the aqueous solution is mixed with near-critical or supercritical  $\text{CO}_2$  at temperatures up to  $100^\circ\text{C}$  and pressures ranging to 300 bar. The ethylene



oxide- $\text{CO}_2$  phase, which leaves from the top of the extractor (or from the bottom if the  $\text{CO}_2$  is too dense), is then contacted with a carbonation catalyst (e.g., organic quaternary ammonium halide) and reacted to form a catalyst-ethylene carbonate- $\text{CO}_2$  stream. The catalyst-ethylene carbonate- $\text{CO}_2$  stream is then delivered to another reactor and hydrolyzed to form ethylene glycol and  $\text{CO}_2$ . In this process the carbonation catalyst also catalyzes the hydrolysis reaction. In the final steps of the process the  $\text{CO}_2$  is flashed from the ethylene glycol stream and recycled to the extractor. The ethylene glycol and the catalyst are then recovered. Direct hydrolysis of the ethylene oxide-water stream tends to produce more of the higher glycols, such as diethylene glycol, compared with the SCF reaction/separation scheme.

## ENHANCED REACTION RATES AND SELECTIVITIES

Certain chemical reactions, such as free-radical, vinyl polymerization reactions, can exhibit enhanced reaction rates with different selectivities when the reaction occurs homogeneously in the mixture critical region, compared with heterogeneously in the subcritical gas-liquid region. Hence, it is possible to control the extent of reaction by isothermally adjusting the system pressure such that either the reaction proceeds rapidly when the reaction mixture exists as a single homogeneous supercritical mixture or the reaction slows considerably when the mixture exists as a heterogeneous gas-liquid mixture in the subcritical region.

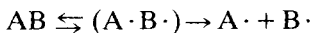
In a very early study Patat (1945) investigated the hydrolysis of aniline to phenol in a water-based acidic solution in near-critical and supercritical water ( $T_c = 374.2^\circ\text{C}$ ,  $P_c = 220.5$  bar). Phosphoric acid and its salts are used as the catalyst for this reaction. The reaction proceeds extremely slowly under normal conditions and reaches equilibrium at low conversion levels. For these reasons, Patat chooses to study the reaction in supercritical water to temperatures of  $450^\circ\text{C}$  and to pressures of 700 bar in a flow reactor. He finds that the reaction follows known, regular kinetics in the entire temperature and pressure space studied and the activation energy of the hydrolysis (approximately 40 kcal/mol) is the same in the supercritical as well as in the subcritical water. He suggests that the reaction is catalyzed by hydrogen ions formed from dissolution of phosphoric acid in supercritical steam. Very small amounts of phosphoric acid and the salts of the phosphoric acid are dissolved in the supercritical steam and are split into ions. Patat lists several dissolution constants for primary ammonium phosphates in supercritical steam. In this instance, the reaction performance is improved when the reaction is operated homogeneously in the mixture critical region and, thus, in intimate contact between the reactants and the catalyst.

Using a batch reactor Blyumberg, Maizus, and Emanuel (1965) studied the oxidation of *n*-butane at conditions near the critical point of butane ( $T_c = 152.1^\circ\text{C}$ ,  $P_c = 38.0$  bar). Both liquid phase and SCF phase oxidations

are studied. In this reaction butane hydroperoxide is first formed via a free-radical chain mechanism and then broken down into products.

The liquid phase oxidation has a long induction period, whereas the SCF phase oxidation has a much shorter induction time. Also, the liquid phase oxidation products are predominantly acetic acid and methyl ethyl ketone, whereas the SCF phase oxidation products are formaldehyde, acetaldehyde, methyl, ethyl, and propyl alcohols, and formic acid. The authors offer no explanation for the differences in product spectrum or induction periods for the reactions.

Subramaniam and McHugh (1986) suggest that the increased reaction rates in the SCF phase may be associated with the more efficient production of free-radical pairs. When initiator molecule AB dissociates to form a geminate radical pair ( $A \cdot B \cdot$ ) it may either diffuse apart to form a free-radical pair or may recombine before it can diffuse apart in the so-called cage effect (Eckert, 1972):



Since the resistance to diffusion will be lower in the mixture critical region than that in the liquid phase it is expected that the ( $A \cdot B \cdot$ ) radical pair should be more readily diffuse apart in the critical region. Although applied hydrostatic pressure favors the recombination of ( $A \cdot B \cdot$ ) to form AB, it seems reasonable to assume that the rate of diffusion dominates the pressure effect as long as the system pressure is maintained below approximately 1,000 bar. Therefore, the formation of free radicals should be facilitated in the SCF phase, as compared with the liquid phase, and shorter reaction times are to be expected.

The difference in product spectrum obtained from a system operating in the SCF phase compared with the liquid phase is probably a function of the types of free radicals that are formed in each phase. In the SCF phase, the butane-derived free radicals have a higher probability of further decomposing into methyl radicals instead of terminating the reaction by recombining. This is because the reaction temperature is greater in the SCF phase than in the liquid phase. If the methyl radicals undergo further oxidation, a broad spectrum of products will be obtained (Winkler and Hearne, 1961).

In a similar process Baumgartner (1983) describes a process for enhancing *t*-butyl-hydroperoxide (TBHP) formation by reacting isobutane ( $T_c = 142^\circ\text{C}$ ,  $P_c = 37.5$  bar) with oxygen in a dense-phase reaction mixture. In previous studies, Winkler and Hearne (1958, 1961) show that the catalytic oxidation of isobutane in the vapor phase produces significant amounts of *t*-butyl alcohol and minor amounts of other oxidation products such as acids, aldehydes, ketones, and other alcohols, in addition to the desired TBHP. They also demonstrate that reacting isobutane with molecular oxygen noncatalytically in the liquid phase of a two-phase liquid-gas mixture at  $100\text{--}150^\circ\text{C}$  and 28.6 bar produces reaction products consisting of TBHP and tertiary alcohol. But this

liquid-gas phase reaction suffers from very low reaction rates and a low selectivity for TBHP. The occurrence of a broader spectrum of products in the gas phase oxidation of isobutane, compared with its liquid phase oxidation, is consistent with the observations of Blyumberg, Maizus, and Emanuel (1965) in the case of the oxidation of *n*-butane.

In the work of Baumgartner, isobutane is oxidized at conditions significantly higher than the  $T_c$  and  $P_c$  of isobutane and also above the critical pressure of the reaction mixture. The reactor operating variables must be carefully optimized and controlled to attain enhanced TBHP selectivities. Also, as with the case of *n*-butane oxidation, enhanced TBHP formation is observed when the reaction is run homogeneously in the dense phase, compared with the corresponding formation obtained when the reaction is run in the liquid phase (Baumgartner, 1983).

Suppes, Occhiogrosso, and McHugh (1989) studied the oxidation of isopropyl benzene (cumene) in supercritical carbon dioxide ( $T_c = 30.1^\circ\text{C}$ ,  $P_c = 73.8$  bar), xenon ( $T_c = 16.5^\circ\text{C}$ ,  $P_c = 58.4$  bar), and krypton ( $T_c = -63.8^\circ\text{C}$ ,  $P_c = 55.0$  bar). Their objective was to perform the oxidation near the mixture critical point of the initial reacting mixture where the concentration of cumene is high ( $\sim 12$  mol%) and the reaction rates are reasonable. The properties of the SCF solvents differed quite substantially in this study. Krypton and xenon are both nonpolar, inert solvents with very different critical temperatures. Carbon dioxide has a critical temperature close to that of xenon but it also has a quadrupole moment which should affect the rate of oxidation since the reaction of cumene with a cumyl peroxy radical forms a dipolar activated complex during the propagation period of the mechanism. Even if the activated complex is only weakly dipolar, it should be more effectively solvated by  $\text{CO}_2$  than by either krypton or xenon. Unfortunately, free radical reactions are also catalytically affected by metals. Hence, the material of construction of the high-pressure reactor can have a significant affect on the rate of reaction.

Over the range investigated, pressure and proximity to the mixture critical point had little or no effect on the overall rate of oxidation of isopropyl benzene at  $110^\circ\text{C}$  in supercritical carbon dioxide, xenon, and krypton. The predominant effect was due to the presence of the catalytic metal surfaces of the reactor. Although increased amounts of oxygen were soluble in the critical region of the mixture as compared to neat cumene, virtually no effect of oxygen concentration was observed for this oxidation reaction. There is, however, one potential advantage of operating in the critical region. Occhiogrosso (1987) has shown that cumene hydroperoxide can be separated from the reacting mixture by isothermally decompressing the mixture to induce the formation of hydroperoxide-rich liquid phase. Removing cumene hydroperoxide from the reaction mixture before it can thermally degrade should help maintain a high selectivity to the hydroperoxide.

During the 1960s and 1970s Ehrlich and coworkers compiled a comprehensive picture of the free-radical polymerization of ethylene in supercritical fluid

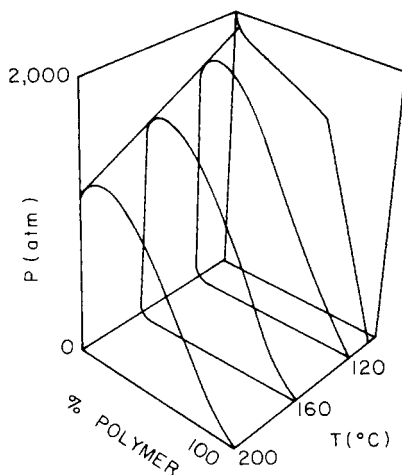


**Figure 11.13** Schematic  $P$ - $T$ - $x$  diagram of the ethylene-polyethylene system (Ehrlich and Mortimer, 1970) (1.01325 bar per atm).

ethylene ( $T_c = 9.3^\circ\text{C}$ ,  $P_c = 50.4$  bar) (Ehrlich and Mortimer, 1970; Takahashi and Ehrlich, 1982; Ehrlich and Pittilo, 1960; Ehrlich and Kurpen, 1963; Ehrlich, 1965; Takahashi, 1980). Ehrlich and Graham (1960) found that polyethylene is soluble in supercritical propane when the pressure is increased above 500 bar. Knowledge of this solubility behavior is extremely important since it has a direct bearing on the interpretation of reaction time data. In an effort to interpret a large body of polymerization rate data, Ehrlich and coworkers augmented the kinetic data with a comprehensive study on the phase behavior of polyethylene-ethylene mixtures at high pressures. The results from his phase behavior studies are shown in figure 11.13 as a schematic  $P$ - $T$ - $x$  diagram for the polyethylene-ethylene system. The two-phase liquid-vapor region for polymer-solvent systems persists to pressures in the neighborhood of 2,000 to 3,000 bar. Ehrlich and Mortimer (1970) conclude that many of the kinetic studies reported in the literature on ethylene polymerization are of little value since the authors of the studies are unaware of the phase behavior involved with SCF systems at moderate or high pressures. Many times polyethylene polymerization studies reported in the literature are performed on systems that are thermodynamically undetermined because of the number of phases present and the number of constituents in the system.

Much of the earliest information on ethylene polymerization can be found in the patent literature. In a 1946 patent Krase and Lawrence (1946) describe an SCF reaction process for making ethylene polymers. Ethylene is reacted in the presence of a catalyst at temperatures between  $40^\circ\text{C}$  and  $400^\circ\text{C}$  and at pressures from 800 to 4,000 bar. The polymer is then recovered using a stepwise reduction in pressure with the objective of reducing compression costs. The authors note in this very early patent that appreciable quantities of the polymer are still solubilized in the supercritical fluid phase at pressures as low as 150 bar. More than likely, the material still soluble at 150 bar consists of

very low molecular weight oligomers, residual monomer, and spent catalyst. The authors suggest that the solubility behavior can be used to produce a product polymer that is essentially free of these lower molecular weight species.

In a patent entitled *Supercritical Polymerization of Olefins*, Cottle (1966) describes a process for reacting and separating polymers made from olefins. In this case propylene is reacted to polypropylene in a process using a catalyst and operating at conditions above the critical temperature and pressure for propylene ( $T_c = 91.9^\circ\text{C}$ ,  $P_c = 46.2$  bar). At the end of the reaction the system pressure is reduced to precipitate the crystalline polypropylene from solution while leaving the noncrystalline fraction solubilized in the propylene-rich phase. This fractionation behavior is another example of the effect of polymer tacticity on solubility level. In this process the supercritical fluid is used as both a reactant and a solvent, as in the ethylene polymerization processes previously described.

It is clear from the several examples cited in this chapter that supercritical fluids can be advantageously used as reaction media but many unanswered questions remain. How do near-critical or supercritical conditions affect the rates and paths of chemical reactions? How is the phase behavior of the initial reactants affected by product formation? Is it possible to exploit the above results to devise efficient reaction/separation schemes? These questions pose considerable experimental and theoretical challenges.

Most of the studies reported in this chapter fail to include the phase behavior of the reacting mixture. Since multiple phases can occur in the mixture critical region, reaction studies need to be complemented with phase behavior studies so that we may gain an understanding of the fundamentals of the thermodynamics and kinetics of chemical reactions in solution. Chapter 5 describes how a simple cubic equation of state can be used to extend and complement the phase behavior studies. An equation of state can be used to determine the location of phase-border curves in  $P$ - $T$  space and, with transition-state theory, to correlate the pressure dependence of the reaction rate constant when the pressure effect is large (i.e., at relatively high pressures).

The advantages of using a supercritical fluid reaction medium are that it may be possible to run the reaction in a single, homogeneous phase, thus eliminating interphase mass transfer limitations. Labile reaction products may be more readily isolated from the reaction mixture by adjusting the pressure or temperature to induce a phase split, thus avoiding unwanted side reactions. To a lesser degree, reaction rates may be advantageously enhanced by running the reaction in the dilute mixture region at conditions close to the critical point of the pure supercritical fluid. However, the rate enhancement does not appear to be extremely large and it is restricted to the dilute mixture region where long periods of time are needed to obtain any measurable product. The reader is directed to a very thorough review by Caralp, Clifford, and Coleby (1993) for more examples of SCF reactions.

---

## Special Applications

---

In the first edition we discussed several examples of employing certain properties of supercritical fluids in ways other than merely extractive; in this edition we add several new examples that exploit transport, surface tension, and other properties of supercritical fluids and their solutions.

Instead of discussing the most recent work then progressing to material from the first edition, we start with the older material then progress to the new. Our first topic is supercritical fluid nucleation.

### **SUPERCritical FLUID NUCLEATION**

The first reports of solubility phenomena in supercritical fluids emphasized the pressure-dependent dissolution characteristics of high-pressure gases and liquids. But the authors of those early papers point out the potential application of using SCF solvents as media from which to nucleate solid materials. For example, Hannay and Hogarth write in the closing statements of their 1879 publication:

We have, then, the phenomenon of a solid with no measurable gaseous pressure, dissolving in a gas. When the solid is precipitated by suddenly reducing the pressure, it is crystalline, and may be brought down as a “snow” in the gas, or on the glass as a “frost,” but it is always easily redissolved by the gas on increasing the pressure.

The “snow” and “frost” described are almost assuredly of different morphology, particle size, and size distribution than the starting material; Hannay and Hogarth studied salts such as cobalt chloride and potassium iodide. Incidentally, the reference to the precipitation of the solid is not an isolated report of nucleation from a supercritical fluid. For example, many other references to “snow,” “fog,” “fumes,” and “crystals” formed during depressurization of a solution of a solute in a supercritical fluid have been made by researchers studying supercritical fluid solubility phenomena.

The particle size and size distribution of solid materials formed in industrial processes is frequently not desired for subsequent reaction or use of

these materials. Crushing, grinding, ball milling, and precipitation from solution are examples of methods for particle size redistribution applied to chemicals, pharmaceuticals, dyes, and polymers. Precipitation from solution is carried out on the basis of the temperature dependence of solubility in a liquid solvent, the reactivity of the desired component to form an insoluble component, or the application of an antisolvent to decrease the solubility of a material that is dissolved in solution. There are generally advantages and disadvantages with any particle size reduction process that must be evaluated for a specific material. Simple grinding is usually quite inexpensive, but it may not be applicable to certain polymers unless the grinding is carried out at cryogenic temperatures.

There are many other solids that are difficult to process by grinding or by solution techniques for one reason or another. For example, a few such difficult-to-comminute materials are certain dyes, explosives, biological compounds, and chemical intermediates that are subsequently used in solid-gas reaction schemes. Nucleation from supercritical fluid solutions containing such materials is an alternative comminution technique that can alter particle size and particle size distribution at very mild temperatures, thus avoiding unwanted degradation of the material and, in some cases, unwanted reaction of the material. We describe SCF nucleation of many materials and we present optical and scanning electron micrographs (SEMs) that show the concept can be applied to a number of refractory materials. There are virtually no references in the literature on SCF comminution, and discussion of the concept derives from the work of Krukoniš, who reported on this technique at the annual AIChE meeting in San Francisco, California, in November 1984 (Krukoniš, 1984d). (For further information, see the discussion of U.S. Patent 2,457,238 in appendix A.)

The compounds are dissolved in a supercritical fluid in a flow apparatus similar to the one described in chapter 4. For the most part, carbon dioxide at conditions of about 345 bar (5,000 psia) and 55°C is used as the solvent in the studies. The precipitated material is collected downstream of the pressure reduction valve and is analyzed for particle size by optical microscopy. The optical microscopy is done at 150 $\times$  and 600 $\times$ , and most of the SEM microscopy is carried out at about 2,000 $\times$ . In some of the photographs that are presented the particles are so small that individual particles are barely discernible at 600 $\times$  magnification. But the smallness of the particles attests to the potential of this technique. Although Krukoniš presented results on numerous solid materials, only five are presented below.

Figure 12.1a,b compare before and after particles of  $\beta$ -estradiol. As figure 12.1a shows, particle sizes range from a few micrometers to hundreds of micrometers in the commercial  $\beta$ -estradiol. The material also appears to be crystalline, as suggested by the faceted particles. Although barely discernible, and almost a blur because the particles are at the limit of resolution at 600 $\times$ , the nucleated particles shown in figure 12.1b are strikingly different in size from the parent particles. The magnification scale provides a measure for

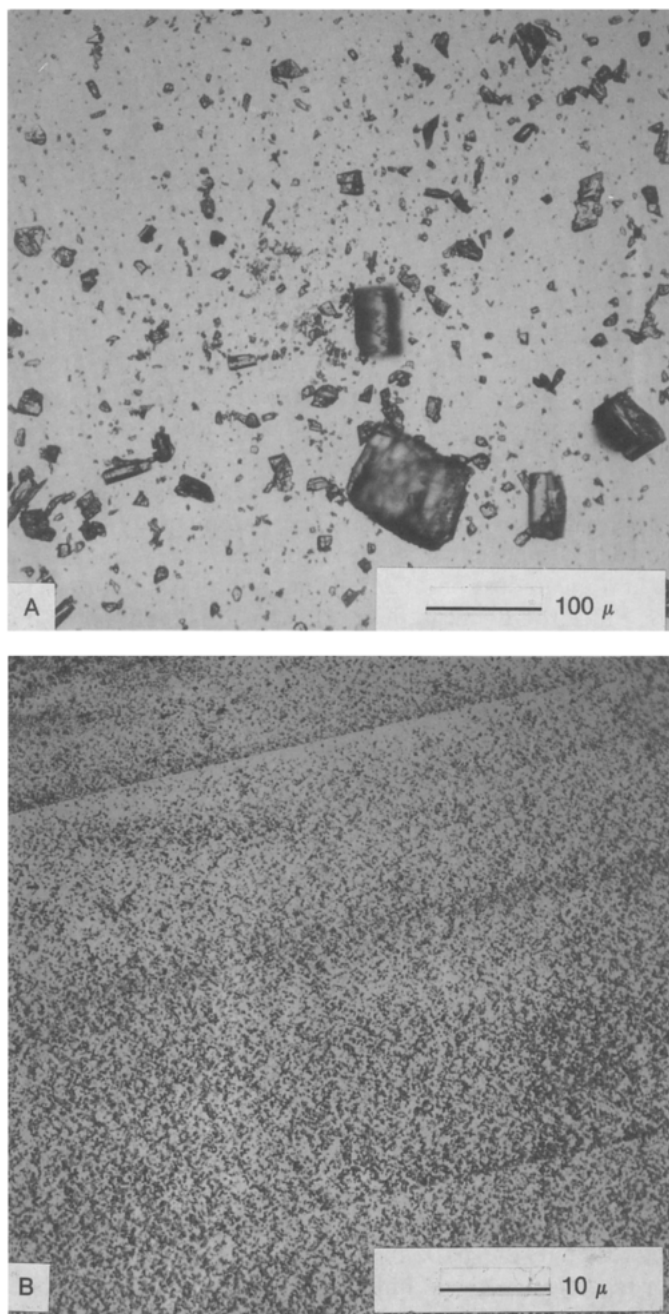


**Figure 12.1** Photomicrographs: (A) virgin particles of  $\beta$ -estradiol; (B) particles of  $\beta$ -estradiol nucleated from an SCF solution.



estimating the diameters of individual particles, which appear to be on the order of less than  $1\text{ }\mu\text{m}$ .

Figure 12.2a,b shows SEMs of ferrocene (dicyclopentadienyl iron), as supplied and after supercritical fluid processing. The scales allow the particle sizes to be readily compared, and again a size reduction is seen. It is quite interesting that ferrocene, a compound whose melting point is  $178^{\circ}\text{C}$ , exhibits a solubility level of the order of about 20 wt% in carbon dioxide at 345 bar (5,000 psia) and  $55^{\circ}\text{C}$ .

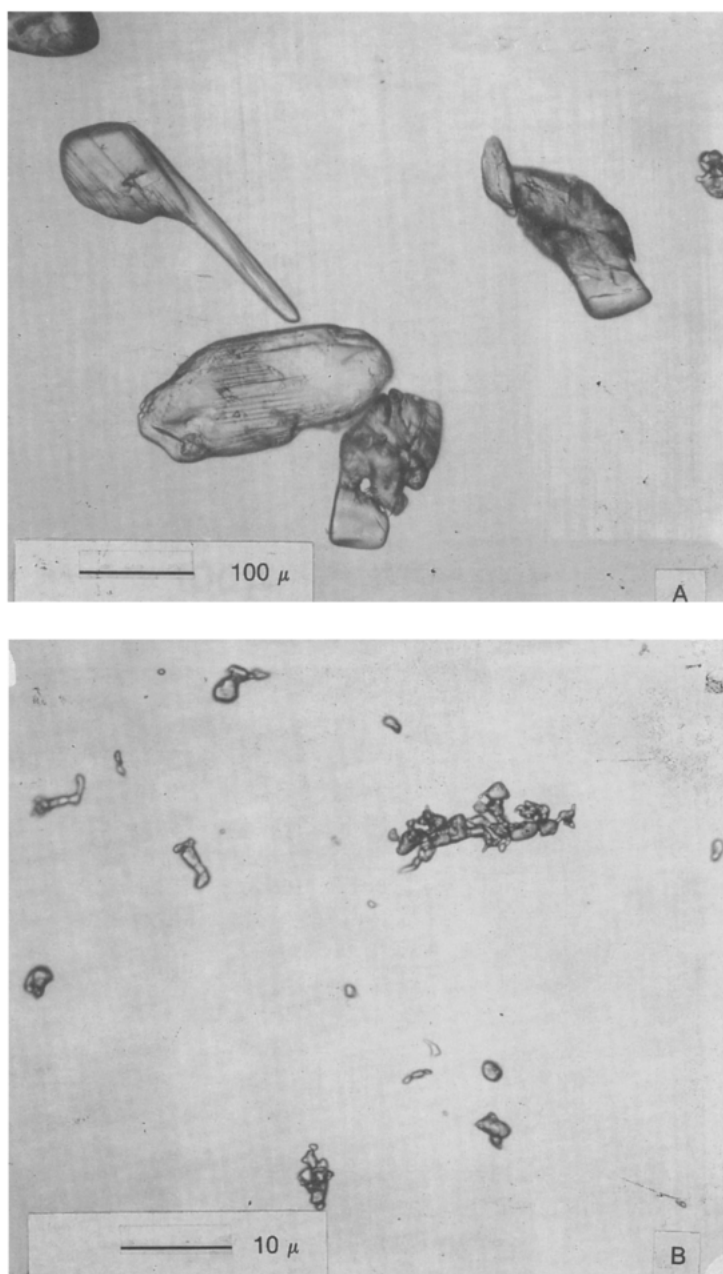
Figure 12.3a,b show the effects on the particle size and morphology of dissolving and subsequently nucleating a navy-blue dye. This dye is soluble in carbon dioxide at 345 bar (5,000 psia) to a level of a few tenths of a weight percent. The particle size of the commercial dye is about  $50\text{--}150\text{ }\mu\text{m}$ , as seen from the low-magnification SEM. The particles formed during expansion of the SCF solution are much smaller in size, and in this case their size can be quantitatively estimated from figure 12.3b.

Figure 12.4a,b,c shows SEMs of dodecanolactam (lauryl lactam), the monomer that polymerizes to nylon-12. The parent material, shown in figure 12.4a, is a powder composed of irregular particles of about  $5\text{--}10\text{ }\mu\text{m}$  in size. Figure 12.4b, at a magnification of  $2\text{ mm}/\mu\text{m}$ , shows what appear to be clumps of short fibers. Since the detail in figure 12.4b is relatively poor, the nucleated dodecanolactam was ultrasonically separated and subsequently inspected at a higher magnification, as shown in figure 12.4c. A quite large aspect (length-to-diameter) ratio is seen in this figure. The primary particles are needle-like in appearance with a length of  $10\text{--}40\text{ }\mu\text{m}$  and with a diameter of less than  $1\text{ }\mu\text{m}$ .

The final example of SCF comminution is a comparison of polypropylene particles "out of the bottle" and after supercritical fluid nucleation. Instead of carbon dioxide, supercritical propylene at 241 bar (3,500 psia) and  $140^{\circ}\text{C}$  is used to dissolve the sample of polypropylene. Figure 12.5a is a high-magnification SEM of a single parent particle. As shown in figure 12.5b, a very different particle size and shape results from the supercritical fluid process.

The optical and scanning electron micrographs presented in this chapter show that the particle size of solid materials, such as polymers, monomers, and intermediate chemicals, can be altered by precipitation from a supercritical fluid solution. The only requirement for carrying out the SCF particle reduction process is that the compound must exhibit some solubility in a supercritical fluid. Because the pressure reduction rates are so rapid during the expansion of the solution, supersaturation ratios can be achieved that are much, much greater than can be achieved by thermal, chemical, or antisolvent precipitation processes. Furthermore, it is conjectured that such rapid nucleation rates can result in the particle formation of some materials with a size distribution or morphology that cannot now be achieved by any other process.

Many other papers on supercritical fluid nucleation later appeared in the literature. Larson and King (1986) studied the nucleation of various pharmaceuticals. Smith and coworkers, e.g., Matson, Peterson, and Smith (1986), reported on metal oxides, polymers, and other materials. Smith and coworkers



**Figure 12.2** Photomicrographs: (A) virgin particles of ferrocene; (B) particles of ferrocene nucleated from an SCF solution.

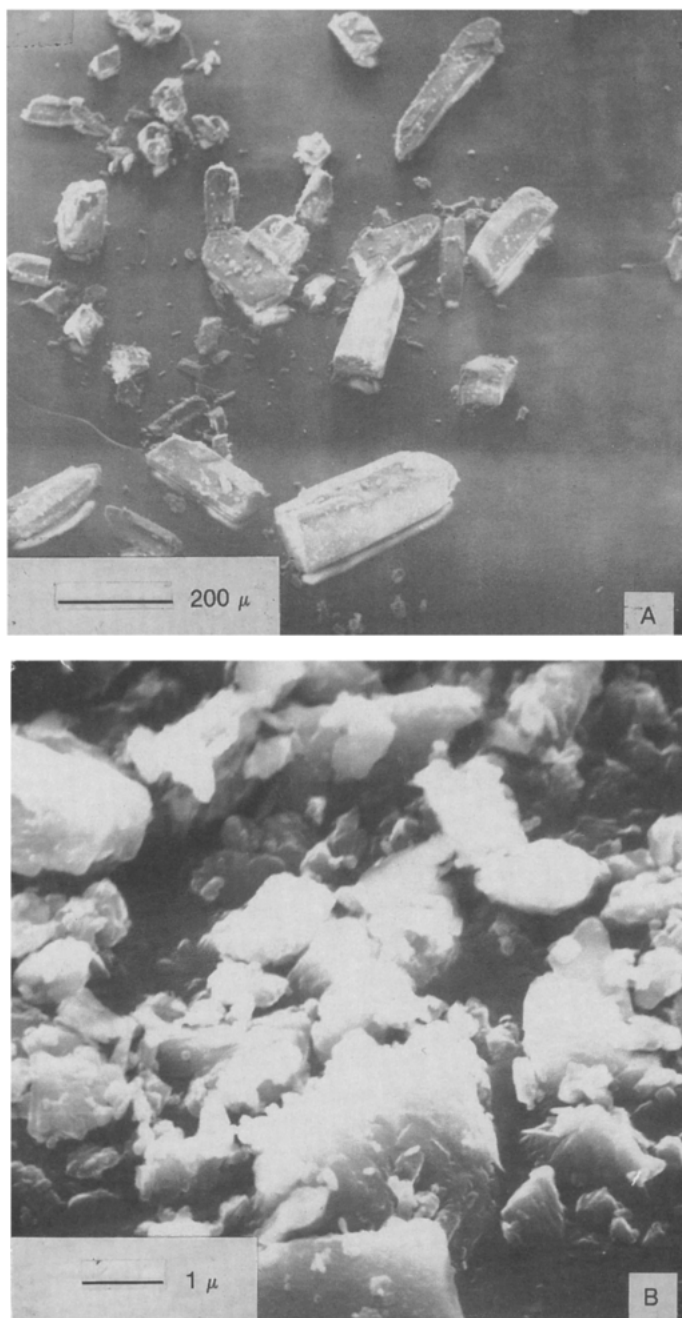


**Figure 12.3** Scanning electron micrographs: (A) virgin particles of navy-blue dye; (B) particles of navy-blue dye nucleated from an SCF solution.

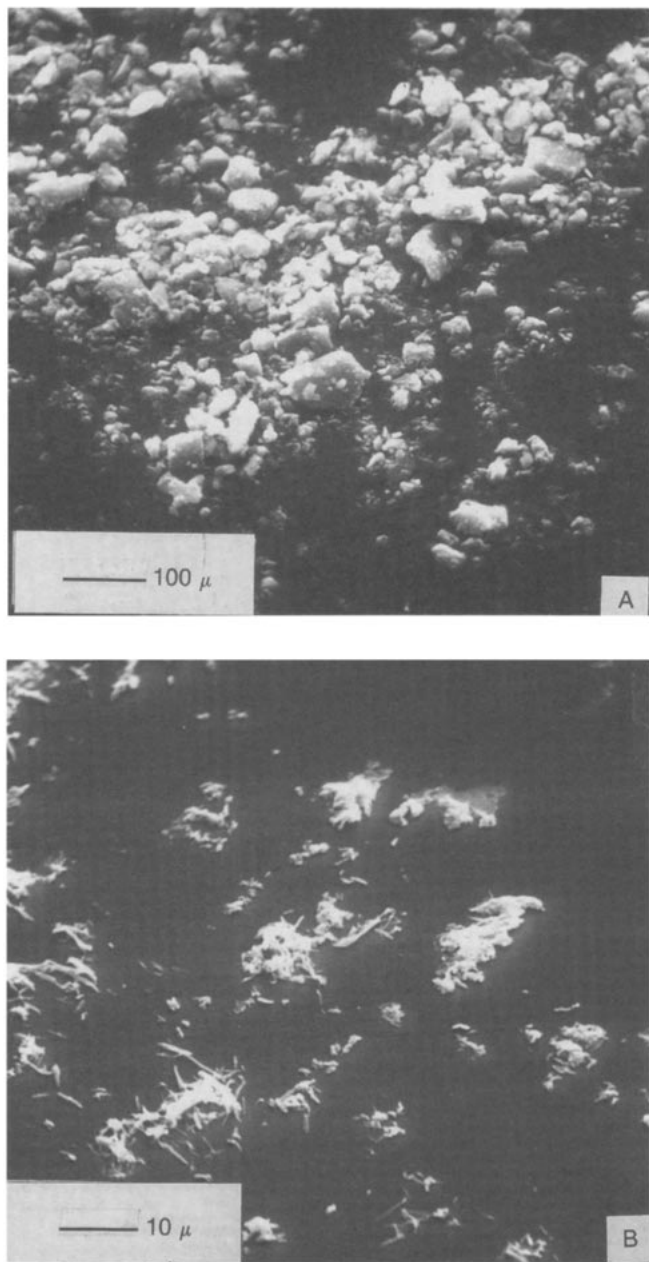


**Figure 12.4** Scanning electron micrographs: (A) virgin particles of dodecanolactam; (B) particles of dodecanolactam nucleated from an SCF solution; (C) same as (B) except that the SCF-treated particles are sonically separated before being analyzed.

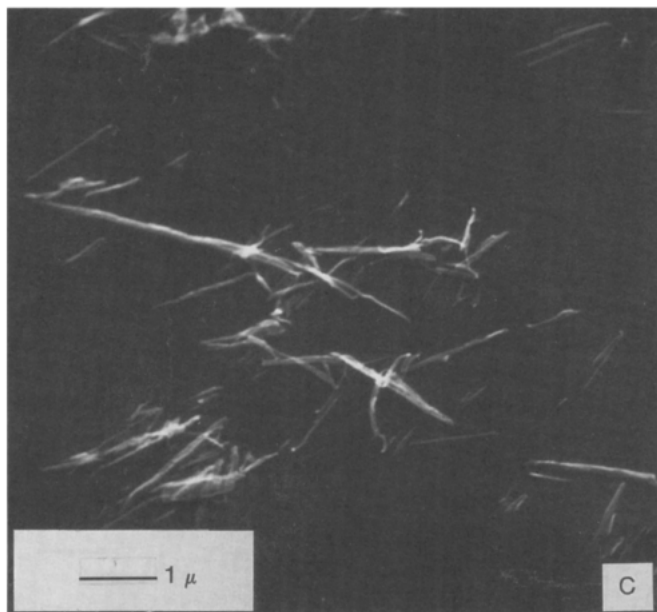


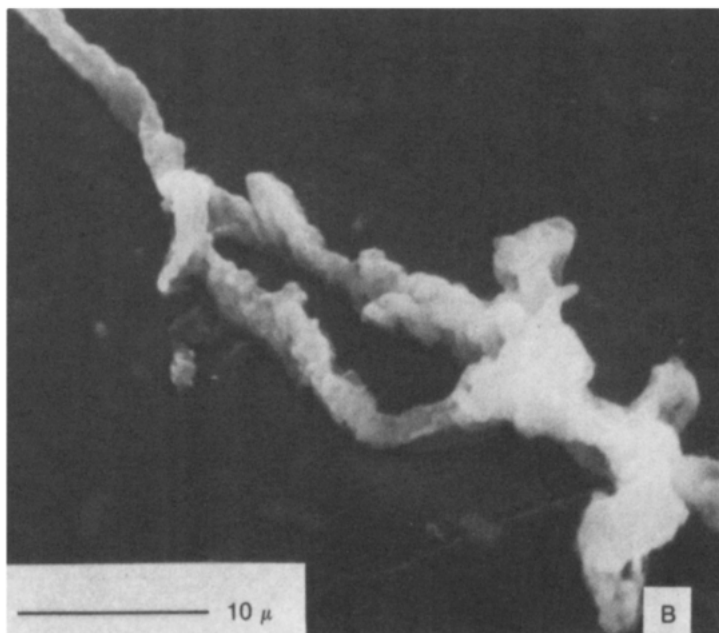
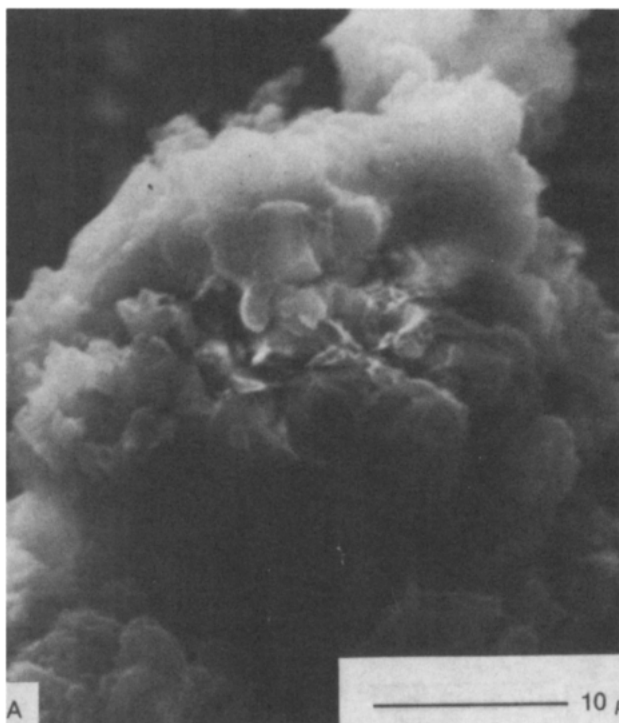
**Figure 12.4—*contd.***

referred to the process of supercritical fluid nucleation as rapid expansion of supercritical solutions, with the acronym RESS. Later Debenedetti et al. (1989) studied supercritical fluid nucleation and reported on nucleation of naphthalene and other materials from carbon dioxide.

In a program for the National Science Foundation (NSF), Coffey and Krukonis (1989) studied two steroids, progesterone and testosterone, as representative of products of the pharmaceuticals industry; progesterone represented the class of very soluble compounds and testosterone represented the class of sparingly soluble compounds in supercritical carbon dioxide. As another representative example of the ability of the process of supercritical fluid nucleation to recrystallize materials figure 12.6a is a photomicrograph of supercritical fluid nucleated progesterone recrystallized from 350 bar and 60°C; it is compared to the as-received progesterone in figure 12.6b. Comparative testosterone photomicrographs are given in figure 12.7a, as-received material, and figure 12.7b, the supercritical fluid nucleated material from 350 bar and 60°C.

An extension of supercritical fluid nucleation to industrial operation is shown schematically in figure 12.8. In the supercritical fluid nucleation report to NSF, Coffey and Krukonis (1989) carried out economic viability analyses of the process. A solid material is charged to an extraction vessel and an appropriate gas, such as carbon dioxide, passed through the charge. The

**Figure 12.5** Scanning electron micrographs of (A) virgin particulate polypropylene; particles of polypropylene nucleated in an SCF solution.



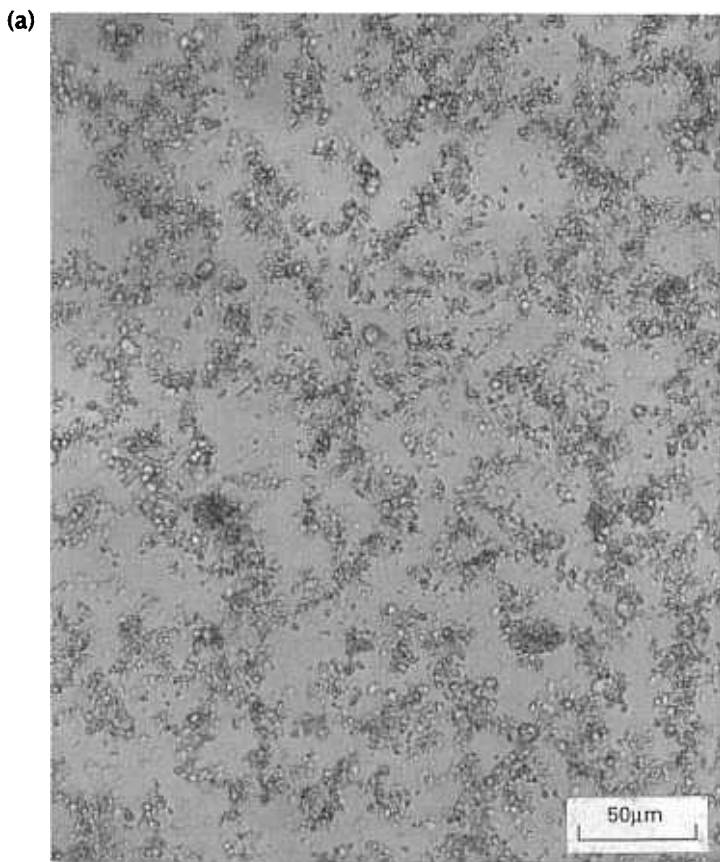


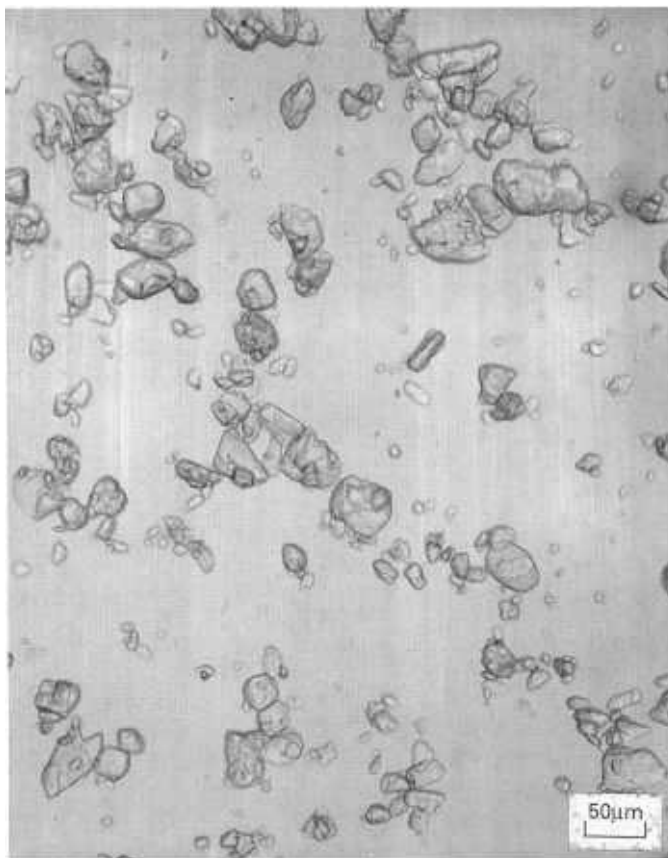
**Figure 12.6** Optical micrographs: (a) nucleated progesterone; (b) virgin progesterone.

solution is expanded to a lower pressure, the particles that are formed separated from the gas in a collector, and the gas recompressed and recycled. The multiple vessels shown in figure 12.8 permit practical economies of operation to be achieved. The processing costs vary with production volume as would be expected, but at two processing levels, 100,000 and 10,000 lb/yr, the costs are \$4 and \$15, respectively.

## GAS ANTISOLVENT RECRYSTALLIZATION

Compounds not soluble in a supercritical fluid can be recrystallized in a process termed gas antisolvent (GAS) recrystallization. The process was first applied to the recrystallization of an explosive, RDX (cyclotrimethylenetrinitramine) into

(b)



void-free particles, and it has been extended to the recrystallization of other explosives and to pharmaceuticals and fine chemicals, both organic and inorganic.

The process acronym, GAS, describes how supercritical fluids are employed in the process; the gas is used as an antisolvent to precipitate a solute from a liquid solution. The process is generally applicable to the recrystallization of materials if two conditions are satisfied; (1) if the compound is insoluble (or only slightly soluble) in the gas, and (2) if the gas is (very) soluble in the liquid. If a liquid solution containing the compound to be recrystallized is contacted with a gas, e.g., carbon dioxide, the gas will dissolve into the solution and, when sufficient gas is absorbed by the solution, the gas will act as an antisolvent and the material will recrystallize.



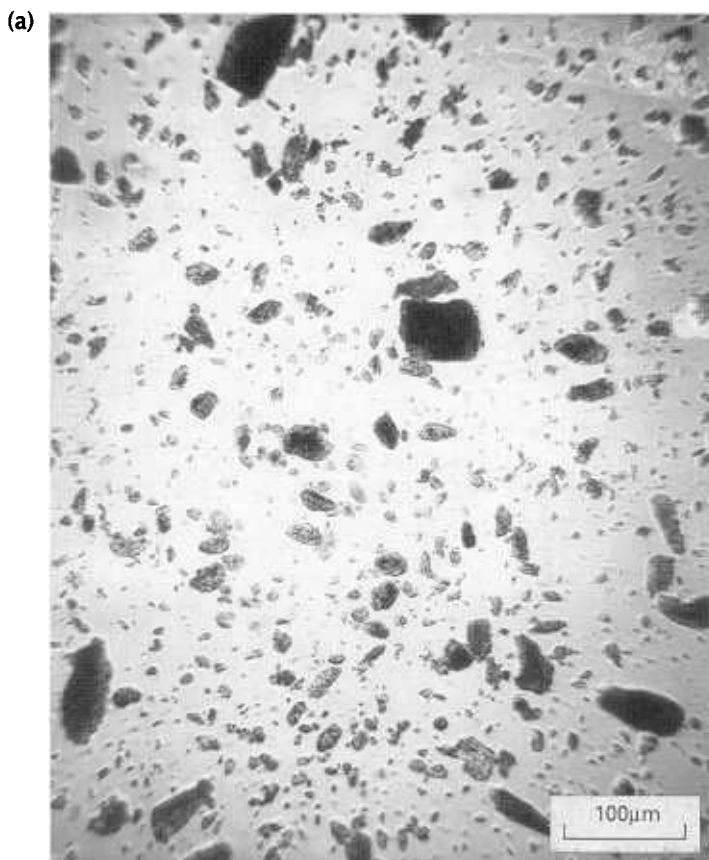
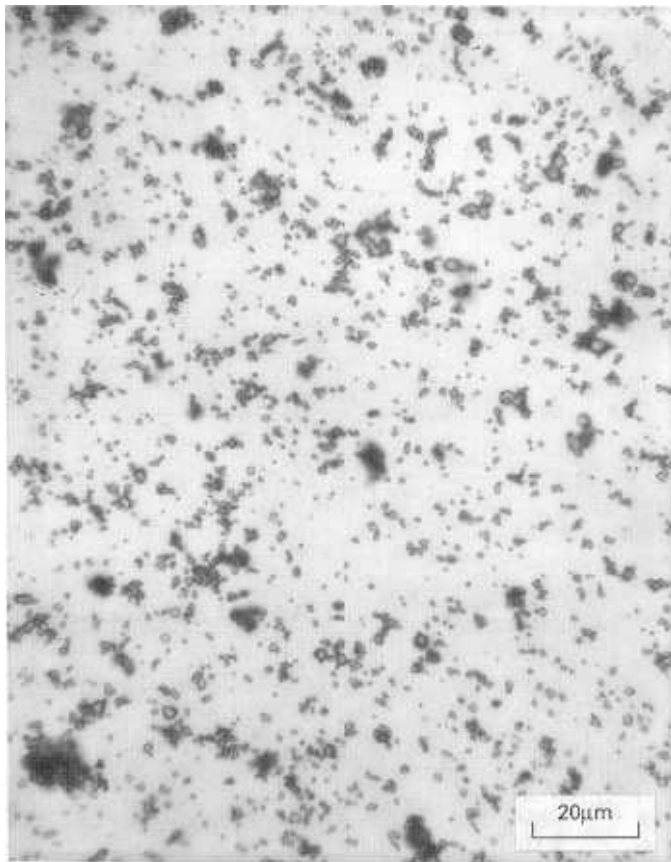


**Figure 12.7** Optical micrographs: (a) virgin testosterone; (b) nucleated testosterone.

Carbon dioxide and other gases dissolve in many, many liquid solvents. Francis (1954) studied the solubility behavior of many classes of liquids, such as hydrocarbons, ketones, and alcohols, with carbon dioxide. He found that at about 25°C and 800 psi, many of the liquids are miscible with CO<sub>2</sub>. In a prelude to the studies of GAS recrystallization, the absorption of CO<sub>2</sub> into several liquids was studied using a sight glass (Jerguson gauge). The work of Francis was extended to higher temperatures than 25°C because of yield, particle size, and economic considerations.

Absorption of CO<sub>2</sub> into a liquid occurs with an expansion of the liquid. An example of the expansion behavior of cyclohexanone is given in figure 12.9, which shows three expansion curves at three temperature levels; cyclohexanone is one of the solvents used in the industrial manufacture of RDX. As expected, higher pressure is required at higher temperature to reach equivalent

(b)



expansion (absorption). It was important to determine the volumetric expansion characteristics as a function of temperature and pressure in a sight glass because of subsequent experimental considerations. For example, vessel dimensions dictate the maximum amount of solution that can be added to a vessel before it is completely filled due to expansion; if too much solution is employed in a test (in a vessel without a sight glass), full recrystallization will not occur or perhaps there will be no recrystallization at all.

The initial recrystallization tests were also carried out in the sight glass; this was to provide a facility for visual determination of recrystallization behavior. Recrystallization of materials is very complex irrespective of the process, be it with liquid antisolvents or with gas antisolvents. For example, the particle size and particle size distribution (PSD) that results during recrystallization is a function of the solute, the solvent, the concentration of solute in

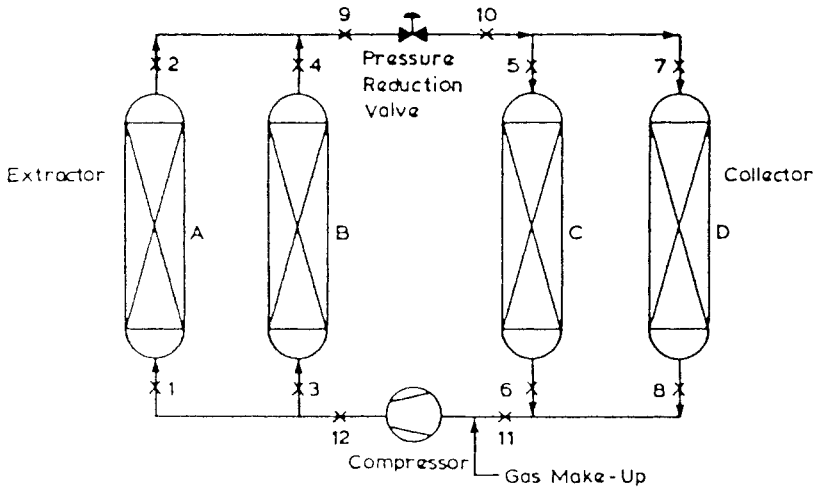


**Figure 12.8** Schematic diagram of supercritical fluid nucleation operated at commercial scale.

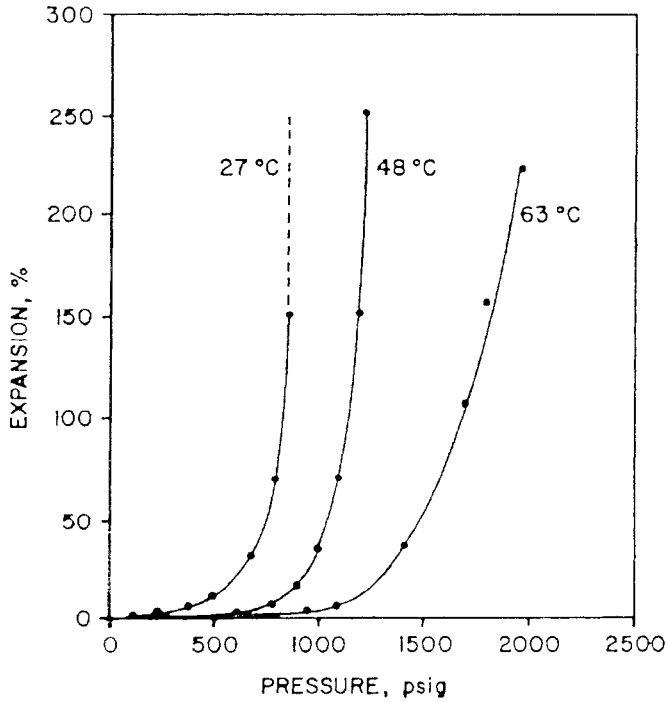


**Figure 12.9** Expansion of cyclohexanone by carbon dioxide.

the solvent, the gas (or in the case of a liquid antisolvent, the liquid), the rate and extent of introduction of the gas (or liquid) into the solution, and still many other factors. The results of testing various combinations of parameters are most easily carried out by observing the events in a sight glass.

Results with explosives, pharmaceuticals, and certain inorganic compounds (see later) show that GAS recrystallization exhibits some interesting technical and economic advantages and attributes. One of the most important features is the ability to intermix the liquid and the gas antisolvent on an almost instantaneous time scale and intimate geometric scale, eliminating inhomogeneities in local concentration and supersaturation. The almost instantaneous intermixing can lead to very small particles with a narrow PSD. A practical feature of GAS recrystallization is the ability to separate solvent and antisolvent without large expenditures of energy. With liquid antisolvents, distillation to separate and recover liquids is much more energy-intensive than the pressure letdown and recompression to recover the gas. On the other hand, the capital costs may be higher for GAS recrystallization. As we have repeatedly said, however, each application must be evaluated case by case. There may not be a motivation for studying the process other than the gathering of fundamental information but, if there are some characteristics of particle size and particle size distribution that cannot be achieved by conventional processing, GAS recrystallization can potentially provide a means of obtaining the desired products, especially if they are ultrafine particles.

In determining the parameters for carrying out GAS recrystallization, the single most important piece of information is the conditions that result in the initial visible formation of nuclei, termed the onset of nucleation. The onset of nucleation is the departure point for a number of alternative paths of particle growth, and we shall discuss reasonably straightforward classical nucleation theory to point out the effects of various parameters on particle size and PSD. At the onset of nucleation the number of nuclei formed is related to the level of supersaturation ( $C_{\text{act}}/C_{\text{sat}}$ ) achieved in solution; the higher the supersaturation ratio the higher the rate of nucleation (Adamson, 1963; Becker and Doring, 1935); catastrophic nucleation is a term that is applied to the transition of the rate from imperceptible to perceptible. Once the initial or catastrophic nucleation has occurred, particles can grow by a diffusional concentration difference driving force of undepleted concentration or by particle collision mechanisms. At any time during the course of the recrystallization process, if the solute concentration in solution is high enough, continued nucleation can also occur concurrent with particle growth. Thus, the ultimate particle size and PSD is a balance of rate of nucleation, number of particles formed, and undepleted solute concentration. If concentration is below the supersaturation that causes catastrophic nucleation, solute concentration will be depleted only by growth mechanisms. The two extreme recrystallization situations can be easily predicted from simple material balance considerations in a fixed amount of solution.

At one extreme, if there is an initial formation of many nuclei, the

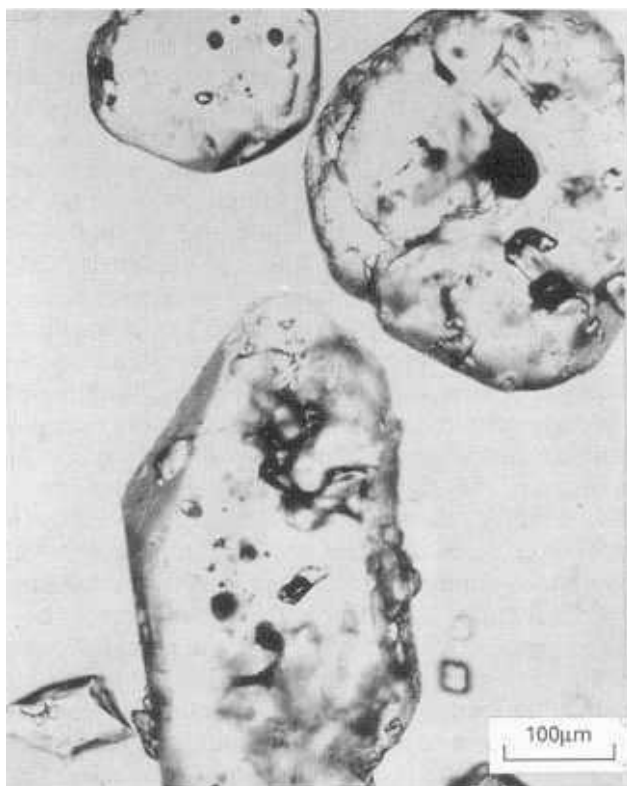


**Figure 12.10** Optical micrograph of as-produced RDX.

resultant final particles will be small because, after the catastrophic nucleation event, there will be little material left in solution for subsequent growth to occur. At the other extreme, in the case of the initial formation of only a few nuclei, there is still much undepleted concentration, substantial growth can occur, so the particles will be large. In somewhat simplistic but accurate terms, control of the final particle size resides in the ability to control the number of nuclei initially formed during the catastrophic nucleation event. Supersaturation ratio, which is such an important influence on nucleation, is controlled by the rate and intimacy of mixing of gas and solution; one of the chief attributes of the GAS recrystallization process is its ability to achieve extremely high levels of supersaturation because of that intimacy and rapidity of mixing. The first application of the process was directed to recrystallizing void-free RDX and one of the goals of the program was the formation of ultrafine particles (also void-free).

Figure 12.10 is a photomicrograph of as-produced RDX (from the Holsten Army Ammunition Plant, Kingsport, TN); the large black spots are

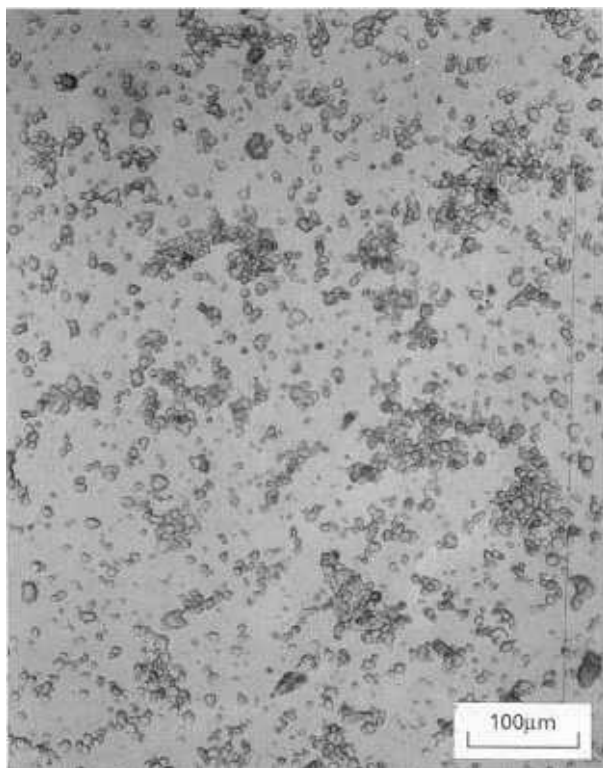


**Figure 12.11** Optical micrograph of small-particle RDX produced by rapid injection of  $\text{CO}_2$  anti-solvent.

intragranular cavities, and the voids can interfere in the performance of the explosive in the propellant formulation. Figure 12.11 is one example of RDX obtained from GAS recrystallization by very rapid intermixing of the carbon dioxide with the RDX-cyclohexanone solution. The particle size ranges from about 5 to 15  $\mu\text{m}$ . Figure 12.12 shows another example of particles that can be produced by controlling the parameters; no intragranular voids are evident in this large-particle RDX, recrystallized by slow intermixing of  $\text{CO}_2$  with the solution. The slow introduction resulted in the formation of only a few nuclei, and growth of the particles occurred (Krukons, Coffey, and Gallagher, 1988).

Several photomicrographs of other recrystallized materials are shown here to provide an indication of the versatility of the process. GAS recrystallization of another explosive, nitroguanidine, was also studied. Figure 12.13 is as-produced nitroguanidine, an insensitive (but high-energy) explosive being evaluated for new and safer propellants and munitions applications. The small-diameter high-aspect-ratio needles of the currently produced material result in a low bulk density. Nitroguanidine in needle form cannot be

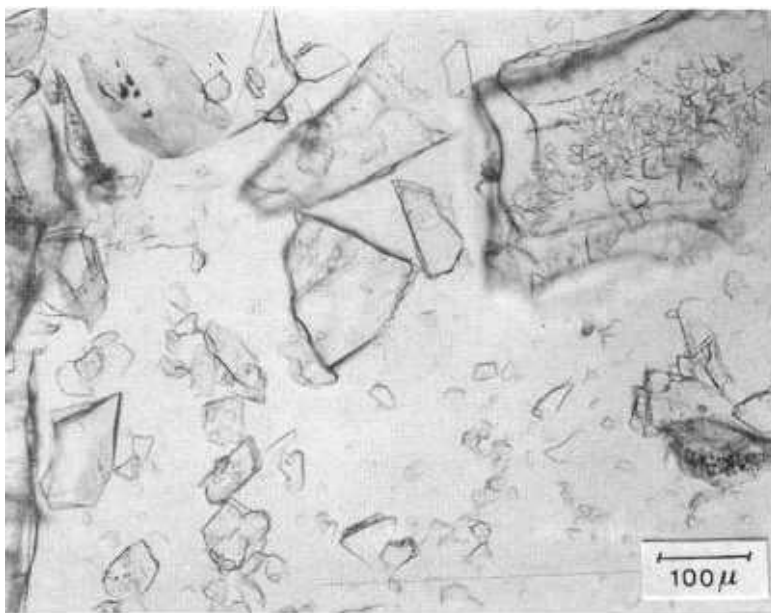


**Figure 12.12** Optical micrograph of large-particle RDX formed by slow injection of CO<sub>2</sub> anti-solvent.

incorporated into explosive formulations to high levels because the viscosity of the mix rises too high for easy loading into casings; high-density spheres of  $\sim 100\ \mu\text{m}$  size were desired for evaluation in propellant formulations.

Figure 12.14 shows an example of GAS recrystallization to form  $100\ \mu\text{m}$  spheres of nitroguanidine in large volume for testing by the armament laboratory, Eglin AFB (Gallagher and Krukonsis, 1991). The material was formed using *N*-methyl pyrrolidone solutions of nitroguanidine and chlorodifluoromethane as the gas antisolvent.

Cobalt chloride is shown here for its historical significance; cobalt chloride was the first compound tested by Hannay and Hogarth (1879) using supercritical ethanol. In 1991, cobalt chloride was GAS recrystallized from liquid ethanol solution with carbon dioxide. As-produced  $\text{CoCl}_2$  is shown in figure 12.15 and the GAS recrystallized material is shown in figure 12.16; the difference in particle size, PSD, and morphology are evident. Thus, GAS recrystallization is not limited to only organic materials.

In the simplest and most general explanation of supercritical fluid infiltration, if a material can be extracted from a microporous substrate by a supercritical fluid, a material (that is dissolved in the supercritical fluid) can be deposited in the pores of that or another substrate by “reversing” the extraction process. In practice, a material is dissolved in a gas, the solution



**Figure 12.13** Optical micrograph of as-produced nitroguanidine.

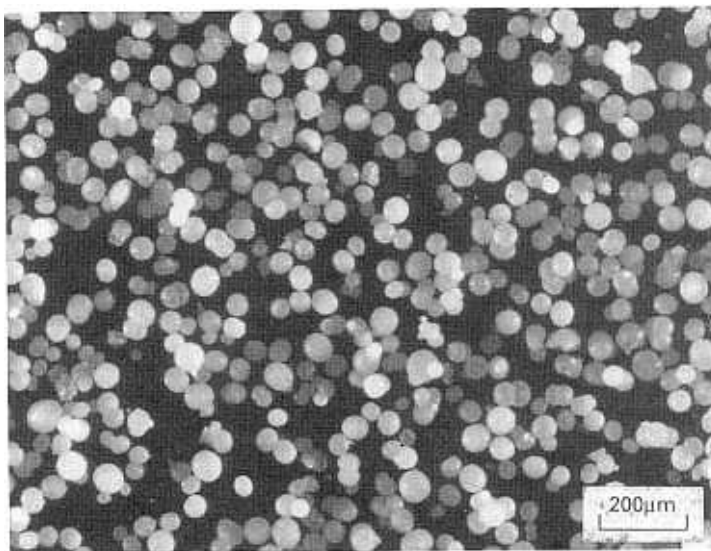


**Figure 12.14** Optical micrograph of nitroguanidine produced by GAS recrystallization.



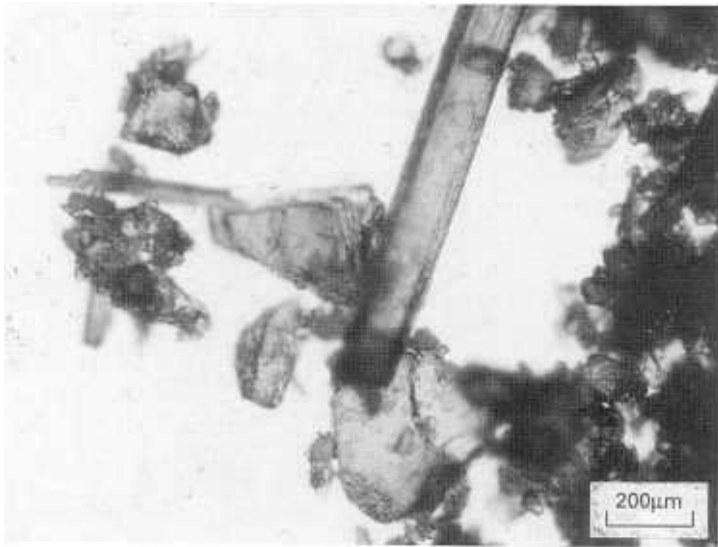


**Figure 12.15** Optical micrograph of cobalt chloride.

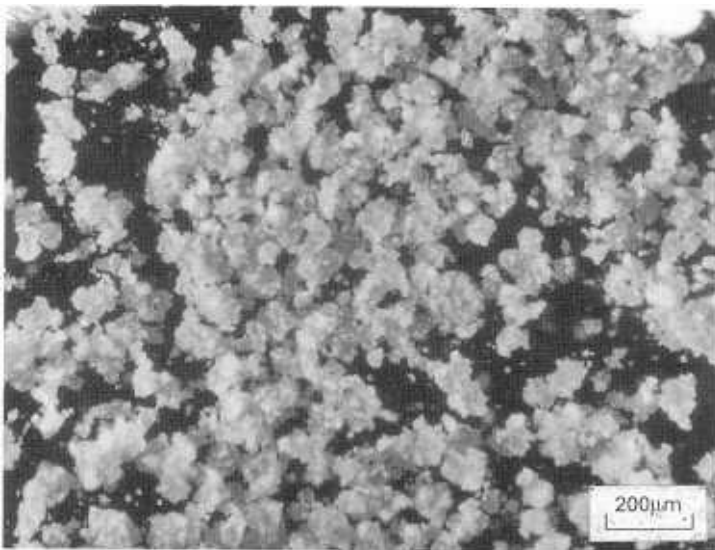


**Figure 12.16** Optical micrograph of cobalt chloride GAS-recrystallized from ethanol solution.

conveyed to a microporous substrate into which the gaseous solution permeates, and by appropriate manipulation of temperature and pressure the solution is caused to give up its dissolved material, which precipitates in the pores of the substrate.

The concept of supercritical fluid infiltration (SFI) was first described in 1981. Subsequently under DOD funding (a joint program from Air Force Office of Scientific Research/Defense Advanced Research Projects Agency, AFOSR/DARPA) SFI was addressed to the problem of improving the oxidation resistance of carbon/carbon composite materials used in rocket engines and missile nose cones (Wagner, Krukonis, and Coffey, 1988).

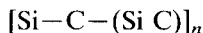
Carbon/carbon (C/C) composites are state-of-the-art materials that exhibit the highest strength/highest stiffness at high temperature. Such classifications as ACC2 or ACC4 designate the material, advanced carbon composite, that is manufactured in a sequence of steps; the manufacturing process is referred to as PIC, for pressure-infiltration-carbonization. Briefly, a preform of carbon fibers, either a woven mat or a knitted three-dimensional structure, is placed in an autoclave, and the autoclave and preform are pumped down to a vacuum. Using hydrostatic pressures of 700–1,400 bar, a carbon precursor, such as hot phenolic resin or petroleum pitch, is pumped into the autoclave. Once infiltrated, the resin-containing preform is removed from the autoclave and placed in an inert atmosphere carbonization furnace. It is then subjected to a temperature ramp reaching 2,000°C; pyrolysis converts the resin to carbon. The product is called ACC-1 (for advanced carbon composite, one PIC cycle completed). ACC-1 is a very porous material, because even though the pressure infiltration step fills the voids in the carbon preform with resin, the carbonization step, with attendant gas formation during pyrolysis, results in the formation of many voids and fissures. A second cycle of pressure, infiltration, and carbonization forms ACC-2 (with fewer voids). Infiltrating and carbonizing the filled C/C composite is successively carried out four times to produce ACC-4, the carbon/carbon material that results from four PIC cycles.

ACC-4 still has about 3–4% voids and fissures, which are detrimental to the performance of the material. In its use as a missile nose cone or rocket nozzle, the extremely hot gas environment can result in rapid degradation of the part because the chemically reactive gases can rapidly permeate the structure via the interconnecting fissures and voids and attack the carbon fibers. Furthermore, in the bow shock wave of a missile nose cone that reenters the ionosphere, the atomic oxygen that is formed can similarly permeate and attack the fibers. Further densification of ACC-4 by another PIC cycle (to reduce the voids to below the 3% level) is virtually impossible because the resin or pitch cannot be forced into the microcracks and pores of the composite even under extremely high hydrostatic pressure of 700–1,500 bar, because of viscosity and surface tension considerations.

A gas has low viscosity, it does not exhibit surface tension limitations, i.e., it can permeate literally nanoscale pores, and it can dissolve many polymers, therefore it seemed possible to realize the concept of utilizing a supercritical

fluid solution of a polymer to convey the polymer to and deposit it in the interstices of the composite. Additionally, if the right polymer was chosen, complete filling of the voids might not be a necessary requirement, e.g., if the walls of the fissures and voids were sufficiently coated with a ceramic polymer precursor that formed, upon pyrolysis, an oxidation-resistant ceramic, such as silicon carbide or silicon nitride, enhanced oxidation resistance could be imparted to the composite structure.

Several silicon carbide precursors were tested on the AFOSR/DARPA study, e.g., polycarbosilanes (PCSs) with backbones



and polyvinylsilanes (PVSs)



Both polymers give off hydrogen when they pyrolyze to form SiC at about 800–900°C in an inert environment. The hydrogens are not indicated in the structures. Carbon dioxide at 675 bar and 140°C dissolves PCS to about 5% and PVS to 7%; propane at only 400 bar and 140°C dissolves both polymers to about 30%. Propane's combination of lower pressure and its ability to infiltrate more polymer per SFI step into the composite led to its choice for the AFOSR/DARPA program.

The extraction system shown schematically in figure 9.3 is quite versatile in its capabilities; it can serve as an extraction system per se, as a GAS recrystallization system, or as an infiltration system. For infiltration, two "extraction" vessels are connected in series, the polymer is placed in the bottom vessel (the first one the gas sees), and the parts to be infiltrated are placed in the top vessel. On the program C/C pieces of about  $0.2 \times 1 \times 20$  cm in size were initially used; later pieces up to 4 cm diameter were tested. In an SFI cycle, propane enters the polymer vessel, dissolves the polymer, and conveys it to the specimens. After about 15–30 min to allow diffusion, bulk flow, and attainment of equilibrium, the specimen-containing vessel is cooled, the pressure is lowered, and the propane (containing only a small amount of dissolved polymer) is removed, leaving the major portion of the preceramic polymer deposited in the pores. The infiltrated specimens are then subjected to polymer pyrolysis at 800°C in an inert atmosphere. The extent of infiltration is determined by cross-sectioning the specimens and analyzing them by scanning electron microscopy (SEM) and energy-dispersive spectroscopy (EDS) to determine the silicon content and location within the composite.

Figure 12.17a is an SEM of a cross-section of an ACC4 specimen that has been subjected to SFI. The carbon fibers, about 7–8  $\mu\text{m}$  in diameter, can be distinguished in the micrograph; note the 10  $\mu\text{m}$  scale marker. The white areas in the figure, some that appear to be microcracks and some that are voids in the carbon matrix adjacent to the fibers, accent the SiC that has been deposited

by supercritical fluid infiltration of a polycarbosilane solution at 400 atm, 140°C. The energy-dispersive spectrogram of the same cross-section is shown in figure 12.17b; the "dots" designate high silicon areas. The visual (SEM) and chemical (EDS) pictures are virtually identical.

As a means of determining the efficacy of the SFI process to enhance the oxidation resistance of C/C composites, specimens that had been infiltrated with polycarbosilane were subjected to a high-temperature oxygen environment; weight loss of the specimens and noninfiltrated (control) specimens was used as an indication of improved oxidation resistance. Figure 12.18 compares the weight loss of the control ACC4 and the weight loss of specimens that had been processed by SFI; the improvement in oxidation resistance of the SFI-processed C/C specimens is pronounced.

There were several interesting findings on the infiltration program; one concerned pyrolysis behavior of the polymer. The entire parent polymer was not used in carrying out the infiltration of the specimens; employed instead was a fractionated sample stripped of about 40% of the low molecular weight tail. The use of only the high molecular weight portion of the polymer was gradually developed over the course of the research program. In the initial infiltration tests, examination of SiC present in the microcracks showed the deposits were porous and "frothy" in appearance; this was considered indicative of excessive gasification of the polymer during the pyrolysis. Some gasification is required by the stoichiometry of the pyrolysis reaction, which results in the formation of hydrogen.

After initially obtaining deposits of very porous SiC thought to result from excessive gasification, a detailed study of the pyrolysis behavior of the precursor polymer was undertaken using narrow fractions of the polymer obtained with supercritical propane in an ascending pressure profile from 60 to 400 bar at 140°C. From the solid polycarbosilane parent, fractions varied in increasing molecular weight and appearance from thick liquid to fluffy powder. From the thick liquid polyvinylsilane parent, fractions varied from very low viscosity liquid to fluffy solid. Samples of the parent polymer and the fractions were subjected to pyrolysis in an inert atmosphere at 800°C and gravimetric analysis of SiC yield was carried out.

Table 12.1 gives the pertinent information on molecular weight and SiC yield for one of the polymers tested on the program, polyvinylsilane, and the fractions derived with supercritical propane. As shown in chapter 9, where other polymer fractionation data are discussed, the molecular weight increases progressively and the polydispersity for the fractions decreases relative to the parent polymer, typical of results obtained with pressure profiling fractionation. But more important for the AFOSR program, the low molecular weight fractions completely vaporized rather than pyrolyzed to SiC.

The observations of the behavior of the polymer fractions during pyrolysis were instrumental in explaining the formation of frothy deposits of the SiC in the microcracks of the C/C, viz., when the entire parent was used, some portion of the precursor polymer was completely gasifying during pyrolysis,

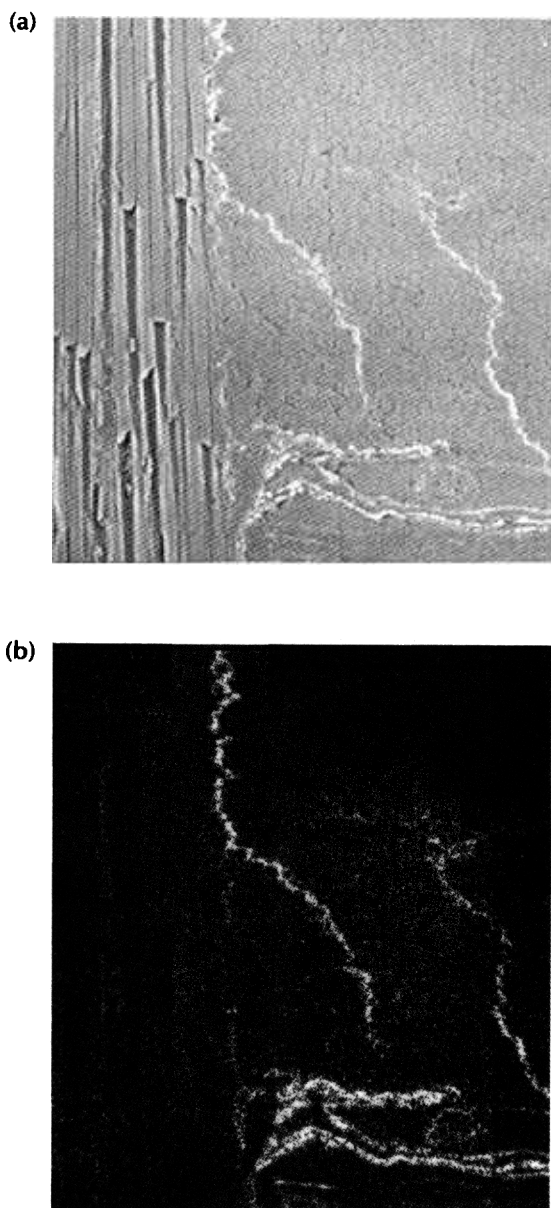


**Figure 12.17** (a) Scanning electron micrograph of a cross-section of a carbon/carbon composite; (b) energy-dispersive spectroscopy analysis showing location of silicon.

**Figure 12.18** Comparison of weight loss of infiltrated and non-infiltrated carbon/carbon specimens.

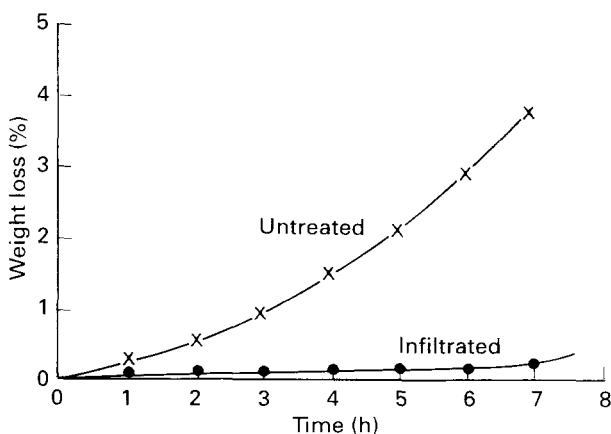


**Table 12.1** Molecular Weight and Yield of Polycarbosilane Fractions

Fraction	$M_n$	$M_w$	Polydispersity $M_n/M_w$	SiC Yield (%)
Parent	831	2,640	3.17	80
1	249	307	1.23	0
2	299	382	1.28	5
3	401	550	1.37	26
4	642	953	1.49	52
5	1,000	1,530	1.52	80
6	1,650	2,570	1.58	82
7	4,500	7,180	1.60	83
8	6,770	9,460	1.40	85

and the extensive gasification was responsible for the low-density “frothy” SiC deposits in the microcracks. In the later work on the program, the polymer was first stripped of about 40% of its low molecular weight component, and monolithic SiC was formed. The stripping conditions using supercritical propane were 140°C and 200 bar.

## SWELLING OF POLYMERS

At sufficiently high pressure, the absorption of certain gases can result in substantial swelling of the polymer; this can be beneficial or deleterious. The solubility of gases in amorphous polymers is important in a variety of membrane and polymer technologies. In membrane technology, it has been shown that membrane performance is dependent on the solubility of the

desired component in the membrane itself. High-pressure gradients across the membrane increase the solubility of the component. But if the pressure gradient is too high, the membrane can swell and the selectivity decreases. Schroeder and Arndt (1976a,b,c) report on the solubility of compressed gases in polymers, and describe the ability of high-pressure carbon dioxide to act as a plasticizer.

Swelling a solid polymer matrix with a high-pressure gas can, however, aid in the deposition of temperature-sensitive materials into the polymer. Sand (1986) has shown that substances such as fragrances, pest control agents, and pharmaceutical drugs can be impregnated in a solid polymer if the polymer is exposed to a supercritical fluid (SCF) during the impregnation process. The SCF swells the polymer and allows the substance to migrate into the polymer matrix. Swelling the polymer effectively increases the diffusion coefficient of the heavy dopant by several orders of magnitude; this allows it to be transported into the polymer within a reasonable time. When the system is depressurized, the supercritical fluid is removed from the polymer; the heavy dopant, which is trapped in the matrix, slowly diffuses out of the solid at a rate now orders of magnitude slower than the rate it was put into the polymer. This technique can be used to form novel controlled-release devices since very large molecules can be impregnated into a swollen polymer matrix at operating temperatures low enough to avoid thermal degradation of material if an SCF solvent is used as the swelling agent.

Polymers can be effectively stripped of low molecular weight impurities, including entrapped solvent, residual catalyst, or low molecular oligomers, by contacting with a high-pressure gas or a supercritical fluid. In this instance, the pure supercritical fluid would swell the polymer, diffuse into the polymer matrix and dissolve the impurity, then diffuse out of the swollen matrix to remove the impurity. This supercritical fluid extraction process is somewhat analogous to those used for the decaffeination of coffee beans and the removal of low molecular weight constituents from solid coal particles (Ozawa, Kusumi, and Ogino, 1974).

There are also practical applications for high-pressure sorption studies. A nontrivial problem is the swelling of O-rings in the presence of solvents at high pressures and when subject to the rapid release of gas pressure. With sorption data, an intelligent selection of O-rings can be made, avoiding the time and expense required when selecting O-rings by trial and error.

An example of SCF-solid, amorphous polymer behavior is described here for the polymethyl methacrylate, PMMA-CO<sub>2</sub> system (Liau and McHugh, 1985; Wissinger and Paulaitis, 1987). The properties of PMMA are listed in table 12.2. Figure 12.19 shows the significant amount of carbon dioxide that is dissolved into PMMA at temperatures ranging from 41°C to 68°C and over a pressure range of 0 to 276 bar. As shown in figure 12.19, the sorption of carbon dioxide in PMMA increases linearly at low pressures for all the isotherms investigated in this study. This behavior is in agreement with the work done by Durrill and Grisley (1966). The solid lines in figure 12.19 represent calcula-

**Table 12.2** Properties of Polymethyl Methacrylate

Weight average molecular weight $M_w$	60,600
Number average molecular weight $M_n$	33,200
Weight/number average ratio $M_w/M_n$	1.82
Glass transition temperature $T_g$	105°C

tions with the Sanchez-Lacombe equation of state with one fitted mixture parameter (Kiszka, Meilchen, and McHugh, 1988; McHugh and Krukoni, 1989). For these calculations the solid amorphous polymer is modeled as a liquid, and it is assumed that PMMA is insoluble in the carbon dioxide-rich phase. (The solubility of PMMA in carbon dioxide under the conditions shown in figure 12.19 is nil.)

The swelling of PMMA over the same temperature and pressure ranges is shown in figure 12.20. Each of the isotherms exhibits very similar behavior.

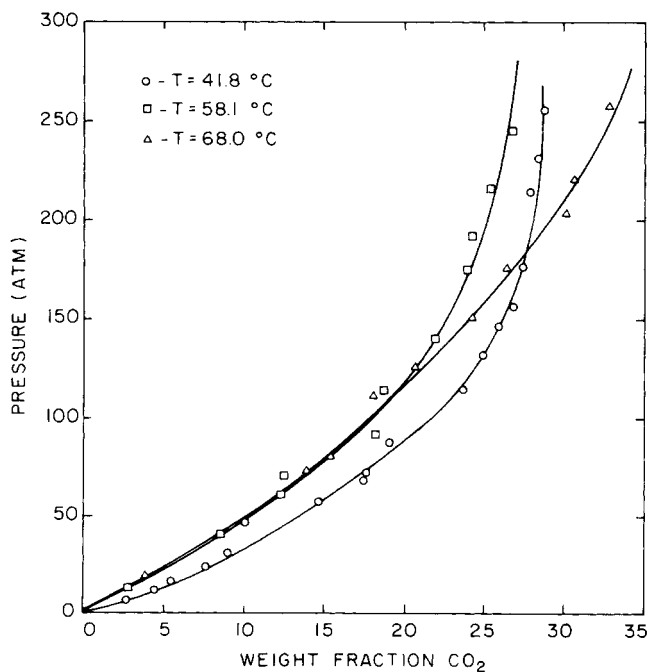


**Figure 12.19** Sorption of carbon dioxide in PMMA at high pressures.



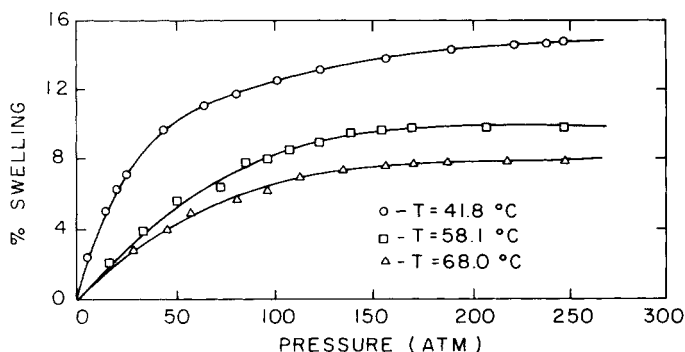


**Figure 12.20** Swelling of PMMA in the presence of high-pressure carbon dioxide.

The swelling increases linearly with pressure for pressures up to about 50 bar. As the pressure increases above 50 bar, the swelling data of Liao and McHugh increase very slowly and reach a limiting value at very high pressures. The swelling data of Wissinger and Paulaitis continue to increase up to the pressure limitation of their apparatus, 100 bar. Had Wissinger and Paulaitis extended their study to higher pressures, the isotherm would be expected to level off, as suggested by the calculated results shown in figure 12.19. More than likely the technique used by Liao and McHugh to obtain swelling data was unreliable for pressures greater than about 50 bar (Kiszka, Meilchen, and McHugh, 1988).

The works of Huvard and Behrens (Behrens, Huvard, and Korsmeyer, 1988) and Wissinger and Paulaitis (1987) give more information on many other polymer-SCF solvent systems including information on the kinetics and equilibria of the supercritical sorption process. Huvard and Behrens report that the sorption of carbon dioxide increases with the number of carbonyl or nitrile groups in the polymer, indicating that specific, polar solvent-solute interactions must be operative. They also report that the diffusivity of carbon dioxide increases over two orders of magnitude as the carbon dioxide sorbs into the polymer. Bonner (1977) also presents information on polymer-gas systems available in the literature up to about 1977.

## FORMATION OF POROUS POLYMERS

Polymers with broad molecular weight distributions or with specially constructed molecular weight distributions can be extracted of low molecular weight oligomers to form a substrate with a different morphology. We illustrate this concept using isotactic polypropylene.

The polymer discussed is composed of an artificially assembled distribution

of oligomers obtained by admixing a certain amount of low molecular weight polypropylene with commercial polypropylene. The low molecular weight fraction is obtained by extracting commercial polypropylene with supercritical carbon dioxide at 448 bar (6,500 psia) and 155°C. At these conditions about 20% of the polypropylene is dissolved in a reasonable extraction time. The extract polypropylene is obtained in a powder or fluff form, quite similar in appearance to the nucleated polypropylene particles whose structure is shown in figure 12.5b. The particles shown in that micrograph were obtained from a process using supercritical propylene as the extractant, but carbon dioxide was specifically used for extracting the low molecular weight fraction. It was reasoned that if the majority of the polymer is not dissolved by carbon dioxide at 448 bar (6,500 psia) and 155°C, then the bulk of the substrate shape formed from a mixture of the original parent polymer and the carbon dioxide extract would not be altered significantly during extraction. This reasoning resulted in a reasonable demonstration of the concept.

The synthetically prepared polypropylene mixture is composed of 50% parent polymer and 50% extract. The substrate "shape" that is tested to examine the feasibility of the concept is a thin sheet. To form the sheet, a few grams of the synthetic mixture is pressed between heated platens maintained at 170°C. The thickness of the pressed preform is 4 mil. Depending upon the amount of polymer used, the sheets obtained were 3–5 in in diameter.

The pieces for extraction were preforms cut into small sections; one was maintained for SEM examination, the others were extracted at a variety of conditions. The extraction system is a variation of the flow-through system shown in figure 4.1.

Figure 12.21 is an SEM of the pressed preform sheet. A barely perceptible scale marker is imprinted on the micrograph and an additional scale marker is added for clarity. The magnification of the preform SEM was made especially high in order to point out that the surface is quite smooth. (The white object at the left edge of the micrograph is a speck of dust used by the microscopist to aid focusing.)

A section of preform was extracted with supercritical carbon dioxide at a slightly lower pressure and temperature, 414 bar (6,000 psia) and 150°C, than was used in obtaining the low end from the parent polymer. Figure 12.22 is an SEM of the extracted sheet. A porous surface is formed and, with the aid of the scale marker, the "pores" can be determined to be a few tenths of a micrometer in size.

The tests on porous polymer formation described in this section are quite rudimentary. Certainly more need to be performed before such factors as pore size and size distribution can be controlled or predicted. Examination of swelling, plasticization, and melting phenomena in a view cell; determination of molecular weight distributions of the extract and substrate (and of the parent polymer); and investigations of other thermoplastic polymers are just a few areas for study. In spite of the rudimentary nature of the experiments, the feasibility tests have established that the concept is reduced to practice, at least

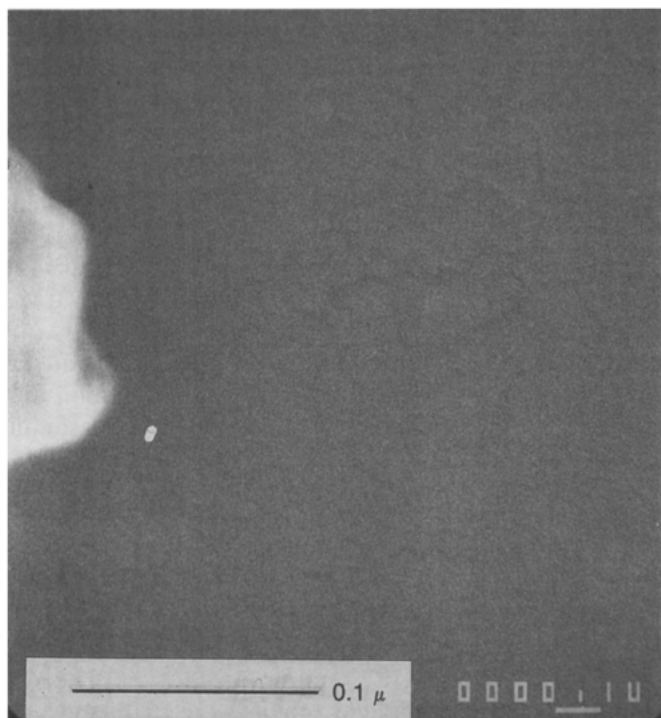


**Figure 12.21** Scanning electron micrograph of pressed polypropylene.

at the laboratory level. The formation of porous polymers by supercritical processing might show advantage in membrane or controlled-release applications.

We have described early investigations of three topics that advantageously combine the properties of supercritical fluids. There are scores of others in still earlier stages or only in the thinking stage. One example is the formation of aerogels, which are now receiving increasing attention. Aerogels are structures of ceramics or polymers with extremely small pores. If the liquid is removed, via evaporation, for example, the surface tension forces active in small-diameter capillaries can collapse the structure. Critical point drying was developed twenty years ago so that botanical and biological specimens for examination by scanning electron microscopy could be dried quickly with preservation of structure. If, for example, the specimen were merely desiccated, surface tension forces at the water vaporization interface can distort or collapse the structure, rendering it unfit for microscopy. In the critical point drying process, the water is exchanged with a miscible organic liquid and the

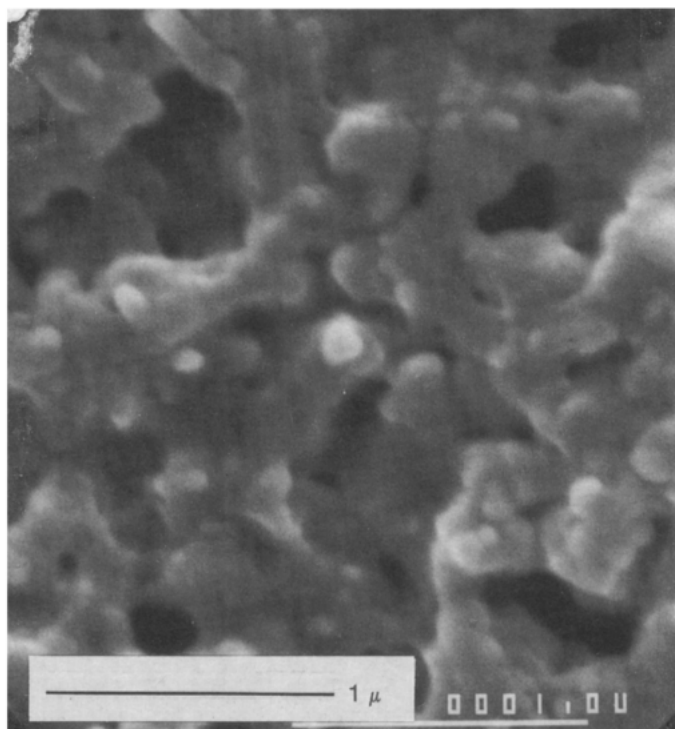


**Figure 12.22** Scanning electron micrograph of pressed polypropylene sheet extracted with supercritical  $\text{CO}_2$  at  $150^\circ\text{C}$  and 414 bar (6,000 psia).

organic is exchanged with liquid carbon dioxide, subsequently raised to above its critical point then removed under conditions in which the temperature never falls below  $31^\circ\text{C}$ . Because the pores are “filled” only with a gas during the pressure decrease, no collapse of the structure occurs.

A similar concept is applied to the removal of liquid from gels. Kistler (1932) studied the formation of transparent silica, alumina, stannic oxide, and other materials. More recently, Schmitt, Grieger-Block, and Chapman (1983) presented a description of a process for forming transparent silica via this concept. They formed gels of silica in water, exchanged the water with methanol, then brought the system to above the critical point of methanol ( $P_c = 81.0$  bar,  $T_c = 239.4^\circ\text{C}$ ) to remove the methanol while maintaining the methanol in the “gaseous” state.

The process is theoretically applicable to polymers but, practically, most of the solvents that can support the formation of polymer gels of, say, polyethylene or polypropylene, have critical temperatures too high to permit polymer aerogels to be formed without melting. But there is a variation of the

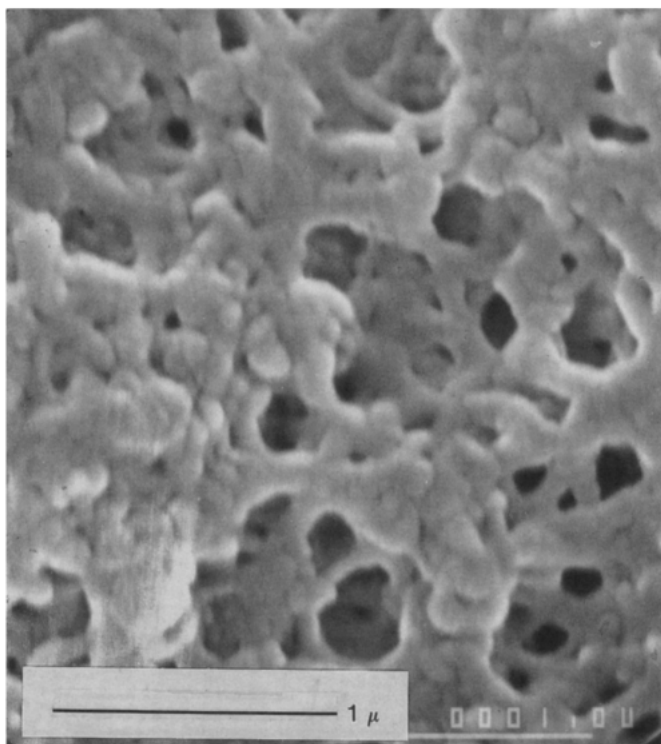


**Figure 12.23** Scanning electron micrograph of pressed polypropylene sheet extracted with supercritical propylene at 135°C and 207 bar (3,000 psia).

critical point drying method: the solvent in which the polymer gel is formed can be exchanged with supercritical carbon dioxide (or some other low critical temperature gas, such as ethylene, fluoroform, or chlorotrifluoromethane); it is removed while the system is maintained above the critical temperature. The carbon dioxide is then removed from the system while it is maintained above the critical temperature of the gas. Figure 12.25 is a micrograph of a polyethylene aerogel produced by this technique (Krukoni, 1984a) from a polyethylene-xylene gel provided by Lawrence Livermore National Laboratories.

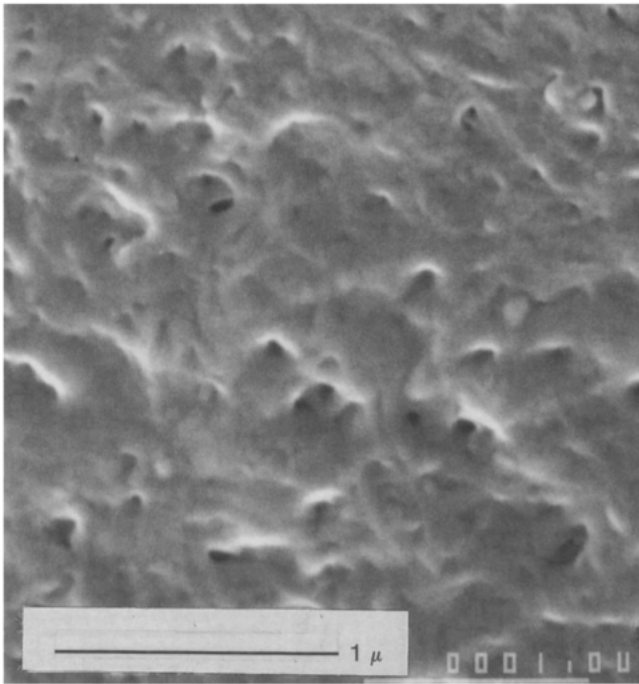


**Figure 12.24** Scanning electron micrograph of pressed polypropylene sheet extracted with supercritical propylene at 150°C and 276 bar (4,000 psia).

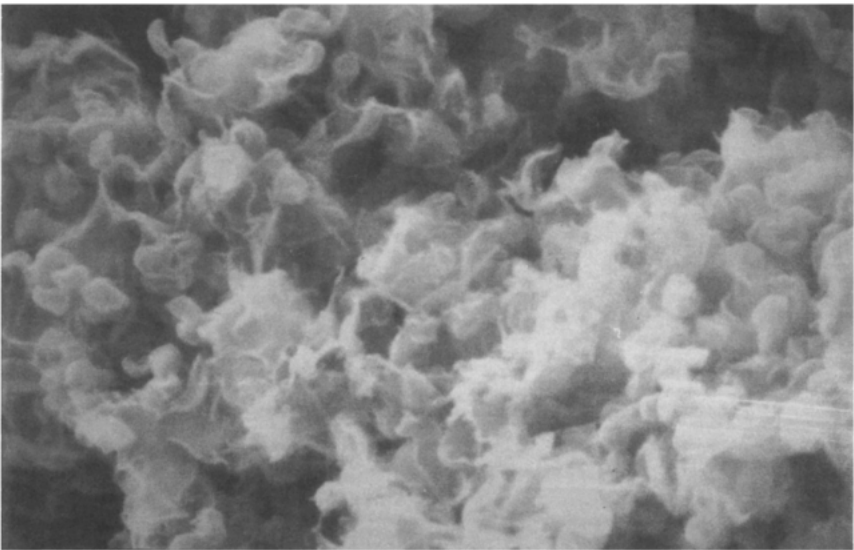


**Figure 12.25** Micrograph of a polyethylene aerogel produced by supercritical extraction.

Having reached this chapter, you may be wondering how to apply SCF technology for your particular application. It is not our desire to espouse any hard and fast rules about SCF technology. In fact, the potential for this technology, in our opinion, is bounded only by the imagination of the researcher who speculates on its potential application. But, as we demonstrated repeatedly throughout the book and in the patent appendix, imagination should not cloud sound engineering judgement. Certainly the literature should be reviewed to see whether SCF processing has either already been applied to the problem or whether the technology will a priori work for the application. When reviewing the literature it is important to remember that there are terminologies associated with any new technology that connote different things to different disciplines. For instance, it is necessary to be cognizant of what some researchers define as “solubility” or “extractibility.” As an example let us consider further the work of Stahl and coworkers, analytical chemists who present much of their data in terms of “threshold pressures,” that is the pressure at which a compound is detected as being soluble in a supercritical fluid.

The detection of a compound solubilized in an SCF is a function of the sensitivity of the detector and the measurement technique. For example, in a flow system such as described in chapter 4, gravimetric analysis is usually used to identify the material collected. For this detection technique, levels of at least a few milligrams of collected material are required to establish the concentration of the compound with some reasonable accuracy. But suitably modified, the same flow-through apparatus can be used quite accurately to determine substantially lower concentrations and absolute amounts of material. The modified collection scheme consists of a chromatographic valve-trap and the collected material is measured by gas chromatography, as shown in chapter 4. As a third detection alternative, Stahl and coworkers (1980) use a flow-through system coupled with a thin-layer chromatograph (TLC). The expansion valve in this system is extremely small; its overall dimensions are a few hundredths of a centimeter and it has a short capillary tube of 0.005 cm inner diameter located downstream of the orifice. The compound that precipitates from the expanding stream impinges directly onto a TLC plate. The effect of system

**Table 13.1** Detection Limits of Common Monitors

<i>Detection Principle</i>	<i>Sensitivity (g)</i>
Gravimetric	$10^{-3}$
Infrared spectroscopy	$10^{-7}$
Ultraviolet spectroscopy	$10^{-9}$
Mass spectrography	$10^{-9}$
Flame ionization	$10^{-10}$
TLC visualization	$10^{-12}$

temperature and pressure on the extraction characteristics of the SCF is evaluated by allowing the stream leaving the expansion valve to impinge on different sections of the TLC plate, which is subsequently developed to determine the amount of material present. TLC analysis is an extremely sensitive analytical technique that will identify much smaller amounts of a compound at a given threshold pressure than will a gravimetric method.

Table 13.1 lists the detection limits (King, 1984) of a number of spectroscopic and chromatographic analytical methods employed in supercritical extraction studies. A gravimetric method requires a few milligrams of material for analysis; TLC analysis can detect materials at solubility levels one billion times lower! If we are measuring the threshold pressure at which the compound dissolves at a detectable level, an analytical method that can identify  $10^{-12}$  g will result in the identification of a lower threshold pressure than can be ascertained in the gravimetric method. The threshold pressure is therefore a function of the sensitivity of the analytical method. By itself, it is certainly not the critical criteria for determining the feasibility of a potential SCF process. Nevertheless, the work of Stahl provides us with a wealth of solubility information that we briefly consider here.

Figure 13.1 is a graph of data from Stahl et al. (1980). It shows the solubility of a number of compounds in  $\text{CO}_2$  at  $40^\circ\text{C}$  and a range of pressures, and it highlights the relative order of progression of solubility of the compounds ranked on the basis of structure and functional groups. Although naphthalene is not shown in this graph, let us consider the solubility of naphthalene in  $\text{CO}_2$ . Naphthalene is of reasonably low molecular weight, so we would expect it to dissolve to some respectable concentration level. Benzoic acid, even though lower in molecular weight than naphthalene, can hydrogen bond to itself, thus increasing the difficulty for  $\text{CO}_2$  to solubilize the compound. The solubility data for a benzoic acid in this figure corroborate this fact. Progressing down the column of molecular structures, we find that increasing numbers of hydroxyl groups lower a compound's solubility quite dramatically. For example, frangulin exhibits a solubility level of only 0.0001 wt%. The last, and least soluble, compound in the figure is glycine, the





referring to the literature for information on the solubility behavior of compounds in SCFs, it is important to evaluate as quantitatively as possible (or as realistically as possible) the rather qualitative question: Is the compound soluble in  $\text{CO}_2$  or any other SCF?

In the same manner in which we discussed solubility let us examine extractability. Quite frequently a compound's extractability by a supercritical fluid has no relation to its solubility in that supercritical fluid. Chapter 8 showed that the pesticide diazinon dissolves to a high level in  $\text{CO}_2$ , but it is not extractable from activated carbon. Chapter 8 also discusses separation of acetic acid from water. Acetic acid is infinitely miscible with  $\text{CO}_2$  but it exhibits a distribution coefficient of only 0.03. Again, strictly speaking, acetic acid is extractable but we feel that extractability should be evaluated in terms of a potential practical process. Supercritical extraction of acetic acid would probably not be an attractive alternative relative to traditional distillation. On the other hand, a distribution coefficient of 0.03 might be satisfactory for the extraction of a heat-labile compound from dilute solution. Therefore, even though we have developed certain useful generalities, it is still important to evaluate each case separately.

How does one evaluate the process viability of an SCF application? We have touched on economics several times in the preceding chapters, but only superficially. As there are no hard and fast answers to questions of viability with traditional processes, so are there none with supercritical fluid extraction. Nevertheless, both of us are asked quite frequently: How much will it cost? To indicate why there is no single answer, we list below just a few of the parameters that influence the cost of a supercritical fluid separation process:

- pressure level;
- pressure reduction ratio;
- distribution coefficient;
- solubility level; and
- amount of material to be extracted.

All these items must be specified and they all affect capital and operating costs. We have mentioned product cost several times in this book, but we do not mean to imply that product cost is the most important factor to be considered. As we related in chapter 7, there are hop extraction plants in operation, and hop extract sells for \$30 per pound; yet there are also many propane deasphalting and residuum extraction plants in operation, and these petroleum products sell for only 10 cents per pound. These two products are on the opposite ends of the commodity spectrum, and their respective processes represent the potential breadth of application of supercritical fluid technology.

We have attempted to give you an inclusive, in-depth analysis of this, no longer, unconventional technology. Our intent has been to teach you the fundamentals of this technology as much as to give you examples of its application. As we described in the preceding chapters, in certain areas the

technology was successful, in others it wasn't. For example, in the first chapter we described SCF processes that operate at the multi-million pounds per year level. In chapter 8, we described some processes that did not reach the industrial level. However, in the analysis of these applications, we have supplied you with guidelines and criteria which you can now apply when considering supercritical fluids for your particular needs. As the myth and mystery of supercritical fluids are removed, practicing scientists and engineers will become more comfortable with applying this technology to as yet undefined separation problems.

---

## References

---

- Adamson, A. W. 1963. *Physical chemistry of surfaces*. Easton, PA: Interscience Publishers.
- Alexander, G., and M. E. Paulaitis. 1984. Solvent effects on reaction kinetics in supercritical fluid solvents. Paper presented at the AIChE Annual Meeting at San Francisco, CA, November.
- Allada, S. R. 1984. Solubility parameters of supercritical fluids. *IEC Proc. Des. Dev.* 23:344.
- Allen, B., and C. H. Baker. 1965. Lower critical solution phenomena in polymer-solvent systems. *Polymer* 6:181.
- Amagat, E. G. 1879. Researches on the compressibility of gases as elevated pressures. *Comptes Rendus des Seances de L'Academie des Sciences* 88(I):336.
- Andrews, T. 1875–76. The Bakerian lecture—On the gaseous state of matter. *Proc. R. Soc. London* 24:455.
- Anolick, C., and E. P. Goffinet. 1971. Separation of ethylene copolymer elastomers from their solvent solutions. U.S. Patent 3,553,156.
- Anolick, C., and E. W. Slocum. 1973. Process for isolating EPDM elastomers from their solvent solutions. U.S. Patent 3,726,843.
- Anon. 1981a. Novel solvent recovery enhances residuum upgrading. *Chem. Eng.*, November 30, 69.
- Anon. 1981b. Olefin polymers. In *Kirk-Othmer encyclopedia of chemical technology*, 3d ed., vol. 16. New York: John Wiley and Sons.
- Anon. 1982. Supercritical CO<sub>2</sub> cleans drill cuttings. *Chem. Eng. News*, February 8, p. 30.
- Anon. Krytox fluorinated lubricants. *duPont Tech. Bull.* G-6.
- Baker, C. H., C. S. Clemson, and G. Allen. 1966. Polymer fractionation at a lower critical solution temperature phase boundary. *Polymer* 1:525.
- Balder, J. R., and J. M. Prausnitz. 1966. Thermodynamics of ternary liquid-supercritical gas systems with applications for high pressure vapor extraction. *Ind. Eng. Chem. Fundam.* 5:449.
- Bangert, L. H., J. L. Lundberg, J. D. Muzzy, G. H. Hoyes, L. H. Olson, and W. D. Freeston, Jr. 1977. Advanced technology applications in garment processing. Report prepared for the National Science Foundation, National Technical Information Service Report PB 284,779, September.
- Bardin, J. M., and D. Patterson. 1969. Lower critical solution temperatures of polyisobutylene plus isomeric alkanes. *Polymer* 10:9.
- Baron, N. 1990. A new polyolefin product family based on Exxpol catalyst technology.

- Paper presented at the 2d International Symposium on High Pressure Chemical Engineering, Erlangen, Germany, September.
- Barry, E. F., P. Ferioli, and J. A. Hubball. 1983. Purification of OV-17 by supercritical fluid fractionation for fused silica capillary gas chromatography. *J. High Resolut. Chromatogr. Chromatogr. Commun.* 6:172.
- Baumgartner, H. J. 1983. Oxidation of isobutane in the dense phase and at low oxygen concentration. U.S. Patent 4,408,082.
- Becker, R., and W. Doring. 1935. *Ann. Physik.* 24:719.
- Behrens, A. R., G. S. Huvard, and R. W. Korsmeyer. 1988. Application of compressed carbon dioxide in the incorporation of additive into polymers. Paper presented at the 1988 AIChE Annual Meeting, Washington, D.C., November.
- Bhise, V. S. 1983. Process for preparing ethylene glycol. U.S. Patent 4,400,559.
- Blyumberg, E. R., Z. K. Maizus, and N. M. Emanuel. 1965. The liquid-phase oxidation of *n*-butane at temperatures and pressures near to the critical. In *The oxidation of hydrocarbons in the liquid phase*, ed. N. M. Emanuel. New York: Macmillan.
- Bolaños, G., T. Hochgeschurtz, and M. C. Thies, 1991. Production of mesophase pitch by supercritical fluid extraction. Paper presented at the 2d International Symposium on Supercritical Fluids. Boston, MA, May.
- Bonner, D. C. 1977. Solubility of supercritical gases in polymer—A review. *Polym. Eng. Sci.* 17:65.
- Booth, H. S., and R. M. Bidwell. 1949. Solubility measurement in the critical region. *Chem. Rev.* 44:477.
- Brennecke, J. F., and C. A. Eckert. 1990. Molecular interactions from fluorescence spectroscopy. Paper presented at the International Symposium on Supercritical Fluids. Nice, France, October.
- Brunner, E. 1985. Fluid mixtures at high pressures II. Phase separation and critical phenomena of (ethane + *n*-alcohol) and of (ethene + methanol) and (propane + methanol). *J. Chem. Thermodynamics* 17:871–885.
- Brunner, G., and S. Peter. 1981. Zum Stand der Extraktion mit komprimierten Gasen. *Chem.-Ing.-Tech.* 53:529.
- Büchner, E. G. 1906. "Die beschränkte Mischbarkeit von Flüssigkeiten das System Diphenylamin und Kohlensäure." *Z. Phys. Chem.* 56:257.
- Busche, R. M., E. J. Shimshick, and R. A. Yates. 1982. Recovery of Acetic Acid from Dilute Acetate Solution. Biotech. Bioeng. Symp. 12:249.
- Cagniard de la Tour, C. 1822. Effect obtained by simultaneous application of heat and pressure on certain liquids. *Ann. Chim.* 22:410.
- Caillietet, L. 1891. Description of a manometer in open air of 300 meters, established at the Eiffel Tower. *Comptes Rendus des Séances de L'Academie des Sciences* 112:764.
- Caralp, M. H. M., A. A. Clifford, and S. E. Coleby, 1983. Ch. 3 in *Extraction of Natural Products Using Near-critical Solvents*, ed. M. B. King and T. R. Bott, Glasgow, U.K., Blackie Academic & Professional.
- Castellan, G. W. 1971. *Physical Chemistry*. Ch. 25. 2d ed. Reading, MA: Addison-Wesley Publishing.
- Caywood, S. W. 1970. Crude EPDM copolymer stabilized with a Lewis base. U.S. Patent 3,496,135.
- Cernia, E. M., and C. Mancini. 1965. A new method for determination of the solubility parameters of the polyethylene–ethylene pair at high temperature and pressure. *Polym. Letters* 3:1093.

- Chai, C. P. 1981. Phase equilibrium behavior for carbon dioxide and heavy hydrocarbons. Ph.D. diss., Univ. of Delaware.
- Chang, H., and D. G. Morrell. 1985. Solubilities of methoxy-1-tetralone and methyl nitrobenzoate isomers and their mixtures in supercritical carbon dioxide. *J. Chem. Eng. Data* 30:74.
- Chappelear, D. C. 1960. Phase equilibria in the critical region: Binary systems with chlorotrifluoromethane. Ph.D. diss., Princeton Univ.
- Chappelear, D. C., and J. C. Elgin. 1961. Phase equilibria in the critical region: Binary systems with chlorotrifluoromethane. *J. Chem. Eng. Data* 6:415.
- Chen, S. J., and M. Radosz. 1991. High-pressure phase equilibria in binary and ternary systems of alternating poly(ethylene-propylene). Paper presented at the 2d International Symposium on Supercritical Fluids. Boston, MA, May.
- Christensen, J. J., and R. M. Izatt. 1984. An isothermal flow calorimeter designed for high temperature, high-pressure operation. *Thermochimica Acta* 73:117-129.
- Christensen, J. J., L. D. Hansen, R. M. Izatt, and D. J. Eatough. 1981. Isothermal, isobaric, elevated temperature, high-pressure, flow calorimeter. *Rev. Sci. Instrum.* 52:1226-1231.
- Christianson, D. D., J. P. Friedrich, G. R. List, K. Warner, E. B. Bagley, A. C. Stringfellow, and G. E. Inglett. 1984. Supercritical fluid extraction of dry-milled corn germ with carbon dioxide. *J. Food Sci.* 49:229.
- Close, R. E. 1951. Vapor-liquid equilibrium in the critical region: Systems of aliphatic alcohols with propane and propylene. Ph.D. diss., Princeton Univ.
- Cochran, H. D., and L. L. Lee. 1989. Solvation structure in supercritical fluid mixtures based on molecular distribution functions. In *Supercritical fluid science and technology*, ed. K. P. Johnston, J. M. L. Penninger, ACS Symposium Series 406:27.
- Coffey, M. P., and V. J. Krukonsis. 1989. Supercritical fluid nucleation: An improved ultra-fine particle formation process. Phasex Corporation Final Report to National Science Foundation, Contract ISI 8660823.
- Coleman, E. J., P. D. Condo, Jr., L. T. Yang, and P. Ehrlich. 1990. Solid-fluid and liquid-gas equilibria of linear polyethylene with supercritical propane. Paper presented at the ACS Meeting, Boston, MA, April.
- Condo, P. D. 1989. Fractionation of polyethylene in *n*-propane: solid-fluid and liquid-gas equilibria at 110°C to 140°C and to 750 bar. M.S. diss., State University of New York at Buffalo.
- Coorens, H. G. A., C. J. Peters, and J. de Swaan Arons. 1988. Phase equilibria in binary mixtures of propane and tripalmitin. *J. Fluid Phase Equil.* 40:135-151.
- Copelin, H. B. 1981. Method for reducing oligomeric cyclic ether content of a polymerizate. U.S. Patent 4,306,058.
- Cottle, J. E. 1966. Supercritical polymerization of olefins. U.S. Patent 3,294,772.
- Cowie, J. M. G., and I. J. McEwen. 1974. Polymer-cosolvent systems. IV: Upper and lower critical solution temperatures in the systems methylcyclohexane-diethyl ether-polystyrene. *Macromolecules* 7:291-296.
- Culberson, O. L., and J. J. McKetta. 1951. Phase equilibria in hydrocarbon-water systems. III. The solubility of methane in water at pressures to 10,000 psia. *Trans AIME, Petrol.* 192:223.
- Czubyrt, J. J., M. N. Meyers, and J. C. Giddings. 1970. Solubility phenomena in dense carbon dioxide in the range 270-1900 atmosphere. *J. Phys. Chem.* 74:4260.
- Dahl, S., Aa. Fredenslund, and P. Rasmussen. 1991. The MHV2 model: prediction of

- phase equilibria at sub- and supercritical conditions. Paper presented at the 2d International Symposium on Supercritical Fluids. Boston, MA, May.
- Dandge, D., J. P. Heller, and K. V. Wilson. 1985. Structure solubility correlations: Organic compounds and dense carbon dioxide binary systems. *Ind. Eng. Chem. Prod. Res. Dev.* 24:162.
- de Filippi, R. P., and M. E. Chung. 1985. Laboratory evaluation of critical fluid extraction for environmental applications. Report EPA-600/2-85-045. April.
- de Filippi, R. P., and J. E. Vivian. 1982. Process for separating liquid solutes from their solvent mixtures. U.S. Patent 4,349,415.
- de Filippi, R. P., V. J. Krukonis, R. J. Robey, and M. Modell. 1980. Supercritical fluid regeneration of activated carbon for adsorption of pesticides. Report EPA-600/2-80054, March.
- de Goede, R., C. J. Peters, H. J. van der Kooi, and R. N. Lichtenthaler. 1989. Phase equilibria in binary mixtures of ethane and hexadecane. *J. Fluid Phase Equil.* 50:305-314.
- de Loos, T. W., W. Poot, and G. A. M. Diepen. 1983. Fluid phase equilibria in the system polyethylene + ethylene. I. Systems of linear polyethylene + ethylene at high pressure. *Macromolecules* 16:111.
- de Swaan Arons, J., and G. A. M. Diepen. 1963. Thermodynamic study of melting equilibria under pressure of a supercritical gas. *Rec. Trav. Chim.* 82:249.
- Debenedetti, P. G. 1987. Clustering in dilute, binary supercritical fluid mixtures based on molecular distribution functions. *Chem. Eng. Sci.* 42:2203.
- Debenedetti, P. G., I. B. Petsche, and R. S. Mohamed. 1989. Clustering in supercritical fluid mixtures: Theory, applications, and simulations. *J. Fluid Phase Equil.* 52:347.
- Deiters, U., and G. M. Schneider. 1976. Fluid mixtures at high pressures: Computer calculations of the phase equilibria and the critical phenomena in fluid binary mixtures from the Redlich-Kwong equation of state. *Ber. Bunsenges. Phys. Chem.* 80:1316.
- DeSimone, J. M. 1990. Synthesis of well-defined single and multiphase polymers using various living polymerization methods. Ph.D. diss., Virginia Polytechnic Institute and State University.
- DeSimone, J. M., A. M. Hellstern, E. J. Siochi, S. D. Smith, T. C. Ward, P. M. Gallagher, V. J. Krukonis, and J. E. McGrath. 1990. Homogeneous and multiphase poly(methyl methacrylate) graft copolymers via the macromonomer method. *Makromol. Chem., Macromol. Symp.* 32:21.
- DeSimone, J. M., S. D. Smith, A. M. Hellstern, T. C. Ward, P. M. Gallagher, V. J. Krukonis, and J. E. McGrath. 1988a. Molecular weight distribution and chemical composition distribution studies of poly(methylmethacrylate)-g-poly(dimethylsiloxane) copolymers. Paper presented at the ACS Meeting, Toronto, Canada, June.
- DeSimone, J. M., A. M. Hellstern, T. C. Ward, J. E. McGrath, S. D. Smith, P. M. Gallagher, V. J. Krukonis, J. Stejskal, D. Strakova, and P. Kratochvil. 1988b. Elucidation of the chemical composition distribution of graft copolymers prepared by the macromonomer technique. Paper presented at the ACS Meeting, Los Angeles, CA, November.
- . 1989. Synthesis, characterization, and chemical composition distribution investigations of graft copolymers prepared by the macromonomer technique. In *Contemporary topics in polymer science*, vol. 6: *Multiphase macromolecular systems*, ed. B. M. Culbertson. New York: Plenum Press.
- Diandreth, J. R., and M. E. Paulaitis. 1984. Three phase liquid-liquid-gas behavior in

- alcohol-water-supercritical fluid systems. Paper presented at the 1984 AIChE Annual Meeting, San Francisco, CA, November.
- Dickinson, N. L., and J. M. Meyers. 1952. Solexol fractionation of menhaden oil. *J. Am. Oil Chem. Soc.*, June, 29:235-239.
- Diepen, G. A. M., and F. E. C. Scheffer. 1948a. On critical phenomena of saturated solutions in binary systems. *J. Am. Chem. Soc.* 70:4081.
- . 1948b. The solubility of naphthalene in supercritical ethylene. *J. Am. Chem. Soc.* 70:4085.
- . 1953. The solubility of naphthalene in supercritical ethylene, II. *J. Phys. Chem.* 57:575.
- Diguet, R., R. Deul, and E. U. Franck. 1987. Static dielectric constant and density of supercritical methane-methanol mixtures to 200 MPa. *Ber. Bunsenges. Phys. Chem.* 91:551-556.
- Donnelly, H. G., and D. L. Katz. 1954. Phase equilibrium in the carbon dioxide-methane system. *Ind. Eng. Chem.* 46:511.
- Durrill, P. L., and R. G. Griskey. 1966. Diffusion and solution of gases in thermally softened or molten polymers: Part I. Development of technique and determination of data. *AIChE J.* 12:1147.
- Eckert, C. A. 1972. High pressure kinetics in solution. *Annu. Rev. Phys. Chem.* 23:239.
- Eckert, C. A., D. H. Ziger, K. P. Johnston, and S. Kim. 1986. Solute partial molal volumes in supercritical fluids. *J. Phys. Chem.* 90:2738-2746.
- Eckert, C. A., D. H. Ziger, K. P. Johnston, and T. K. Ellison. 1983. The use of partial molal volume data to evaluate equations of state for supercritical fluid mixtures. *J. Fluid Phase Equilib.* 14:167.
- Economou, I. G., and M. D. Donohue. 1990. Mean field calculations of thermodynamic properties of supercritical fluids. *AIChE J.* 36:1920-1924.
- Ehrlich, P. 1965. Phase equilibria of polymer-solvent systems at high pressures near their critical loci. II. Polyethylene-ethylene. *J. Polym. Sci., Part A* 3:131.
- . 1971. Partial molal volume anomaly in supercritical mixtures and the free radical polymerization of ethylene. *J. Macromol. Sci. Chem.* A5:1259.
- Ehrlich, P., and E. B. Graham. 1960. Solubility of polymers in compressed gases. *J. Polym. Sci.* 45:246.
- Ehrlich, P., and G. A. Mortimer. 1970. Fundamentals of free-radical polymerization of ethylene. *Adv. Polym. Sci.* 7:386.
- Ehrlich, P., and J. J. Kurpen. 1963. Phase equilibria of polymer-solvent systems at high pressures near their critical loci: Polyethylene with *n*-alkanes. *J. Polym. Sci., Part A* 1:3217.
- Ehrlich, P., and P. C. Wu. 1973. Volumetric properties of supercritical ethane-*n*-heptane mixtures: The isothermal compressibility in the critical region. *AIChE J.* 19:540.
- Ehrlich, P., and R. H. Fariss. 1969. Negative partial molar volumes in the critical region: Mixtures of ethylene and vinyl chloride. *J. Phys. Chem.* 73:1164.
- Ehrlich, P., and R. N. Pittilo. 1960. A kinetic study of the oxygen-initiated polymerization of ethylene. *J. Polym. Sci.* 43:389.
- Eisenbach, W. 1984. Supercritical fluid extraction: A film demonstration. *Ber. Bunsenges. Phys. Chem.* 88:882.
- Elgin, J. C., and J. J. Weinstock. 1959. Phase equilibrium at elevated pressures in ternary systems of ethylene and water with organic liquids: Salting out with a supercritical gas. *J. Chem. Eng. Data* 4:3.



- Elias, H. G. 1984. *Macromolecules: structures and properties*, 2d ed. New York: Plenum.
- Ellis, S. R. M. 1971. Vapor phase extraction process. *Br. Chem. Eng.* 16:358.
- Elsbernd, C. S. 1988. Synthesis, kinetics, and supercritical fluid fractionation studies of functional organosiloxanes and their incorporation into segmented copolymers. Ph.D. diss., Virginia Polytechnic Institute and State University.
- Elsbernd, C. S., J. M. DeSimone, A. M. Hellstern, S. D. Smith, P. M. Gallagher, V. J. Krukoni, and J. E. McGrath. 1990b. The application of supercritical fluids in the fractionation and characterization of siloxane oligomers and graft copolymers. Paper presented at the ACS Meeting, Boston, MA, April.
- Elsbernd, C. S., M. Spinu, V. J. Krukoni, P. M. Gallagher, D. K. Mohanty, and J. E. McGrath. 1990a. Synthesis and fractionation studies of functionalized organosiloxanes. In *Silicon-based polymer science*, ed. J. M. Zeigler and F. W. G. Fearon, 145. Advances in Chemistry Series No. 224. Washington, D.C. American Chemical Society.
- Elsbernd, C. S., D. K. Mohanty, J. E. McGrath, P. M. Gallagher, and V. J. Krukoni. 1987. Synthesis and supercritical fluid extraction studies on aminopropyl-terminated polysiloxanes. Paper presented at the ACS Meeting in New Orleans, LA, August.
- Fall, D. J., and K. D. Luks. 1984. Phase equilibria behavior of the systems carbon dioxide + *n*-dotriacontane and carbon dioxide + *n*-docosane. *J. Chem. Eng. Data* 29:413.
- Fall, D. J., J. L. Fall, and K. D. Luks. 1985. Liquid-liquid-vapor immiscibility limits in carbon dioxide + *n*-paraffin mixtures. *J. Chem. Eng. Data* 30:82.
- Flory, P. J. 1953. *Principles of Polymer Chemistry*. Ithaca, NY: Cornell University Press.
- . 1984. Liquid-liquid phase separations in polymer systems from a molecular point of view. Paper presented at the Symposium on Application of Phase Diagrams in Polymer Science, at the National Bureau of Standards, Gaithersburg, MD, October.
- Francesconi, A. Z., H. Lentz, and E. U. Franck. 1981. Phase equilibria and PVT data for the methane-methanol system to 300 MPa and 240°C. *J. Phys. Chem.* 85:3303–3307.
- Francis, A. W. 1954. Ternary systems of liquid carbon dioxide. *J. Phys. Chem.* 58:1099–1114.
- Franck, E. U., and R. Deul. 1979. Dielectric behavior of methanol and related polar fluids at high temperatures and pressures. *Farad. Discuss. Chem. Soc.* 66:191–198.
- Freeman, P. I., and J. S. Rowlinson. 1960. Lower critical points in polymer solutions. *Polymer* 1:20.
- Friedrich, J. P. 1984. Supercritical CO<sub>2</sub> extraction of lipids from lipid-containing materials. U.S. Patent 4,466,923.
- Friedrich, J. P., and E. H. Pryde. 1984. Supercritical CO<sub>2</sub> extraction of lipid-bearing materials and characterization of the products. *J. Am. Oil Chem. Soc.*, 61:223.
- Friedrich, J. P., G. R. List, and A. J. Heaking. 1982. Petroleum-free extraction of oil from soybeans with supercritical CO<sub>2</sub>. *J. Am. Oil Chem. Soc.* 59:288.
- Gallagher, P. M. 1987. Solubility of octamethylcyclotetrasiloxane (D<sub>4</sub>) in supercritical ethane. Unpublished data.
- . 1988. Fractionation of polysiloxanes with chlorodifluoromethane. Unpublished data.

- Gallagher, P. M., and V. J. Krukoni. 1987. Studies on the reaction of amines and carbon dioxide. Unpublished data.
- . 1993. Supercritical fluid fractionation of polymers: fundamental and practical implications. Report to National Science Foundation, Contract ISI-8509931.
- Gangoli, N., and G. Thodos. 1977. Liquid fuels and chemical feedstocks from coal by supercritical gas extraction. *Ind. Eng. Chem. Process Des. Dev.* 16:208.
- Gearhart, J. A., and L. Garwin. 1976. ROSE process improves resid feed. *Hydrocarbon Process.* May, 55:125–128.
- Giddings, J. C., M. N. Meyers, S. McLaren, and R. A. Keller. 1968. High pressure gas chromatography of non volatile species. *Science* 162:67.
- Giddings, J. C., M. N. Meyers, and J. W. King. 1969. Dense gas chromatography at pressures to 2000 atmospheres. *J. Chromatogr. Sci.* 7:276.
- Gloeckner, G., J. H. M. van den Berg, N. L. T. Meijerink, T. G. Scholte, and R. Koningsveld. 1984. Size exclusion and high-performance precipitation liquid chromatography of styrene-acrylonitrile copolymers. *Macromolecules.* 17:962–967.
- Gómez-Nieto, M., and G. Thodos. 1978. Vapor-liquid equilibrium behavior for the propane-acetone system at elevated pressures *Chem. Eng. Sci.* 33:1589–1595.
- Gopal, J. S., J. D. Holder, I. Wender, and A. A. Bishop. 1983. Supercritical behavior in multicomponent systems. Paper presented at the AIChE Meeting, Houston, TX, March.
- Gore, G. 1861. On the properties of liquid carbonic acid. *Philos. Trans. R. Soc. London, Ser. A* 151:83.
- Guckes, T. L., McHugh, M. A., Cozewith, C., and R. L. Hazelton. 1990. Phase separation processes. U.S. Patent 4,946,940.
- Hammond, D. A., M. Karel, A. M. Klibanov, and V. J. Krukoni. 1985. Enzymatic reactions in supercritical gases. *Appl. Biochem. Biotechnol.* 11:393.
- Hannay, J. B. 1880. On the solubility of solids in gases, II. *Proc. R. Soc. London* 30:484.
- Hannay, J. B., and J. Hogarth. 1879. On the solubility of solids in gases. *Proc. R. Soc. London* 29:324.
- . 1880. On the solubility of solids in gases. *Proc. R. Soc. London* 30:178.
- Hannigan, K. J. 1981. Extraction process creates low fat potato chips. *Chiltons Food Eng.*, July, 53:77.
- Hasch, B. M., M. A. Meilchen, S.-H. Lee, and M. A. McHugh. 1992. High pressure phase behavior of mixtures of poly(ethylene-co-methyl acrylate) with low molecular weight hydrocarbons. *J. Polym. Sci. Polym. Phys. Ed.*, 30:1365–1373.
- . 1993. Cosolvency effects on high pressure copolymer solutions. *J. Polym. Sci. Polym. Phys. Ed.*, 31:429–439.
- Hasch, B. M., S.-H. Lee, M. A. McHugh, J. J. Watkins, and V. J. Krukoni. 1993. Effect of backbone structure on the cloud point behavior of polyethylene-ethane and -propane mixtures. *Polym.*, 34:2554–2558.
- Hellstern, A. M. 1989. Synthesis, characterization, and kinetic investigations of heterophase materials prepared using group transfer polymerization. Ph.D. diss., Virginia Polytechnic Institute and State University.
- Hicks, C. P., and C. L. Young. 1975. The gas-liquid critical properties of binary mixtures. *Chem. Rev.* 75:119.
- Hildebrand, J. H. 1951. The term "Regular Solution". *Nature* 168:868.
- Hildebrand, J. H., and R. L. Scott. 1949. *Solubility of Nonelectrolytes*. New York: Reinhold Publishing.

- Hottovy, J. D., J. P. Kohn, and K. D. Luks. 1981. Partial miscibility behavior of the methane + ethane + *n*-octane system. *J. Chem. Eng. Data* 26:135.
- . 1982. Partial miscibility behavior of the ternary systems methane + propane + *n*-octane, methane + *n*-butane + *n*-octane, and methane + carbon dioxide + *n*-octane. *J. Chem. Eng. Data* 27:298.
- Huie, N. C., K. D. Luks, and J. P. Kohn. 1973. Phase-equilibria behavior of systems carbon dioxide-*n*-eicosane and carbon dioxide-*n*-decane-*n*-eicosane. *J. Chem. Eng. Data* 18:311.
- Hunter, E., and R. B. Richards. 1945. Polymeric fractionation. U.S. Patent 2,457,238.
- Hutchenson, K. W., J. R. Roebers, and M. C. Thies. 1990. Vapor-liquid equilibrium for phenanthrene-toluene mixtures at elevated temperatures and pressures. *J. Fluid Phase Equil.* 60:309–317.
- Hyatt, J. A., 1984. Liquid and supercritical CO<sub>2</sub> as organic solvents, *J. Org. Chem.*, 49:5097.
- Igel, J. T. 1985. Model calculations of the phase behavior of mixtures at high pressures. M.S. thesis, Univ. of Notre Dame.
- Irani, C. A., and C. Cozewith. 1986. Lower critical solution temperature behavior of ethylene propylene copolymers in multicomponent solvents. *J. Appl. Polym. Sci.* 31:1879–1899.
- Irani, C. A., and E. W. Funk. 1977. Separations using supercritical gases. In *CRC handbook: Recent developments in separation science*, vol. 3, Part A, 171. Boca Raton, FL: CRC Press.
- Irani, C. A., C. Cozewith, and S. S. Kasegrande. 1982. New method for high temperature phase separation of solutions containing copolymer elastomers. U.S. Patent 4,319,021.
- Izatt, R. M., R. S. Schofield, P. W. Faux, P. R. Harding, S. P. Christensen, and J. J. Christensen. 1983. The excess enthalpies of liquid freon-22 + 2,3 dimethylbutane mixtures from 363 to 423K at 5.5 MPa. *Thermochimica Acta.* 68:223–232.
- Jacoby, R. H., and M. J. Rzasa. 1952. Equilibrium vaporization ratios for nitrogen, methane, carbon dioxide, ethane and hydrogen sulfide in absorber oil-natural gas and crude oil-natural gas systems. *Trans. AIME, Petrol.* 195:99.
- Jentoft, R. E., and T. H. Gouw. 1969. Supercritical fluid chromatography of a “monodisperse” polystyrene. *J. Polym. Sci., Part B* 1:811.
- . 1970. Pressure-programmed supercritical fluid chromatography of wide molecular weight range mixtures. *J. Chromatogr. Sci.* 8:138.
- Johnston, K. P. 1984. Supercritical fluids. In *Encyclopedia of Chemical Technology*, 3d ed., suppl. vol., p. 872. New York: John Wiley & Sons.
- Johnston, K. P., and C. A. Eckert. 1981. An analytical Carnahan-Starling van der Waals model for solubility of hydrocarbon solids in supercritical fluids. *AIChE J.* 27:773.
- Johnston, K. P., and C. Haynes. 1987. Extreme solvent effects on reaction rate constants at supercritical fluid conditions. *AIChE J.* 33:2017.
- Johnston, K. P., D. G. Peck, and S. Kim. 1989. Modeling supercritical mixtures: How predictive is it? *Ind. Eng. Chem. Res.* 28:1115–1125.
- Johnston, K. P., D. H. Ziger, and C. A. Eckert. 1982. Solubilities of hydrocarbon solids in supercritical fluids: The augmented van der Waals treatment. *Ind. Eng. Chem. Fundam.* 21:191.
- Johnston, K. P., S. Kim, and J. Combes. 1989. Spectroscopic determination of solvent strength and structure in supercritical fluid mixtures: A review. In *Supercritical fluid*

- science and technology, ed. Johnston, K. P., and J. M. L. Penninger. Ch. 5. ACS Symp. Ser. 406:52.
- Jonas, J. 1981. Critical fluid extraction of ethanol from water. Paper presented at the Central and South Jersey Section of the AIChE, September.
- Kander, R. G., and M. E. Paulaitis. 1984. Alcohol-water separations using supercritical fluid solvents. Paper presented at the Annual AIChE Meeting, San Francisco, CA, November.
- Katz, S. N. 1989. Method for decaffeinating coffee with supercritical fluid. U.S. Patent 4,820,537.
- Katz, S. N., J. E. Spence, M. J. O'Brian, R. H. Skiff, G. J. Vogel, and R. Prasad. 1990. Method for decaffeinating coffee with a supercritical fluid. U.S. Patent 4,911,941.
- Kennedy, G. C. 1950. A portion of the system silica-water. *Econ. Geol.* 45:629.
- Kim, S., and K. P. Johnston. 1987a. Clustering in supercritical fluid mixtures. *AIChE J.* 33:1603.
- . 1987b. Molecular interactions in dilute supercritical fluid solutions. *Ind. Eng. Chem. Res.* 26:1206.
- Kim, Y. J., J. A. Carfagno, D. S. McCaffrey, and J. P. Kohn. 1967. Partial miscibility phenomena in the ternary system ethane + *n*-nonadecane + *n*-eicosane. *J. Chem. Eng. Data* 12:289.
- King, A. D., Jr., and W. W. Robertson. 1962. Solubility of naphthalene in compressed gases. *J. Chem. Phys.* 37:1453.
- King, J. W. 1984a. Supercritical fluid chromatography measurements. Implications for critical fluid extraction. Paper presented at the 75th AOCS Meeting, Dallas, TX, April.
- . 1984b. Supercritical fluid extraction of polymers and solvents: utilization of the solubility parameter concept. *Poly. Mat. Sci. Eng. Preprints* 51:707.
- Kiran, E., V. P. Saraf, and Y. L. Sen. 1990. Solubility of polymers in supercritical fluids. *Int. J. Thermo.* 10:437-446.
- Kiran, E., W. Zhuang, and Y. L. Sen. 1991. Solubility and demixing of polyethylene in supercritical binary fluid mixtures: carbon dioxide-cyclohexane, carbon dioxide-toluene, carbon dioxide-pentane. Paper presented at the AIChE meeting. Los Angeles. November.
- Kistler, S. S. 1932. Coherent expanded aerogels. *J. Phys. Chem.* 36:52.
- Kiszka, M. B., M. A. Meilchen, and M. A. McHugh. 1988. Modeling high-pressure gas-polymer mixtures using the Sanchez-Lacombe equation of state. *J. Appl. Polym. Sci.* 36:583.
- Klesper, E., and W. Hartmann. 1977. Supercritical fluid chromatography of styrene oligomers. *Polym. Lett.* 15:9.
- Knutson, B. L., D. L. Tomasko, C. A. Eckert, P. G. Debenedetti, and A. A. Chiavlo. 1992. Local density augmentation in supercritical solutions: A comparison between fluorescence spectroscopy and molecular dynamics results. In *ACS Symp. Ser.*, 488:60-72.
- Kohn, J. P. 1967. Volumetric and phase equilibria of methane-hydrocarbon binary systems at low temperatures and high pressures. *Chem. Eng. Progr. Symp. Ser.* 63:57.
- Kohn, J. P., E. S. Andriele, K. D. Luks, and J. D. Colmenares. 1980. Phase equilibria of ethylene and certain normal paraffins. *J. Chem. Eng. Data* 25:348.
- Kohn, J. P., R. C. Merrill, Jr., and K. D. Luks. 1983. Liquid-liquid-vapor equilibria in

- cryogenic LNG mixtures. Phase III Nitrogen rich systems. Research Report 67, Gas Processors Assoc., May.
- Koll, P., and J. Metzger. 1978. Thermal degradation of cellulose and chitin in supercritical acetone. *Angew. Chem. Int. Ed. Engl.* 17:754.
- Koningsveld, R., and A. J. Staverman. 1968a. Liquid-liquid phase separation in multicomponent polymer solutions. I. Statement of the problem and description of methods of calculation. *J. Polym. Sci.: Part A-2.* 6:305-323.
- . 1968b. Liquid-liquid phase separation in multicomponent polymer solutions. II. The critical state. *J. Polym. Sci.: Part A-2.* 6:325-347.
- . 1968c. Liquid-liquid phase separation in multicomponent polymer solutions. III. Cloud point curves. *J. Polym. Sci.: Part A-2.* 6:349-366.
- Koningsveld, R., and G. A. M. Diepen. 1983. Supercritical phase behavior involving solids. *J. Fluid Phase Equilib.* 10:159.
- Koningsveld, R., G. A. M. Diepen, and H. A. G. Chermin. 1966. Fluid phase equilibria in the system polyethylene-ethylene, II. *Rec. Trav. Chim.* 85:504.
- Koningsveld, R. L. A. Kleintjens, and G. A. M. Diepen. 1984. Solubility of solids in supercritical solvents. I. General principles. *Ber. Bunsenges. Phys. Chem.* 88:848.
- Kramer, G. M., and F. Leder. 1975. Paraffin isomerization in supercritical fluids. U.S. Patent 3,880,945.
- Krase, N. W. 1945. Separating ethylene polymers. U.S. Patent 2,388,160.
- Krase, N. W., and A. E. Lawrence. 1946. Process for the preparation of ethylene polymers. U.S. Patent 2,396,791.
- Kreevoy, M. M., and S. S. Kantner. 1977. The methanol-trimethoxyborane azeotrope as a solvent. *Croatica Chemica Acta* 49:31-39.
- Krukonis, V. J. 1977. A new process for activated carbon regeneration and for recovery of hazardous pesticide wastes. Report to the Environmental Protection Agency, Contract R804-554-010, September.
- Krukonis, V. J. 1981a. Adsorption isotherm for the caffeine-coffee-carbon dioxide system. Unpublished data.
- . 1981b. Carbon dioxide extraction of low concentration formamide-water solutions. Unpublished data.
- . 1981c. Distribution coefficients in the caffeine-water-carbon dioxide system. Unpublished data.
- . 1981d. Purification of an acrylamide monomer. Unpublished data.
- . 1981e. Solubility of atactic and isotactic polypropylene in carbon dioxide. Unpublished data.
- . 1982a. Fractionation of chlorotrifluoroethylene oligomers. Unpublished data.
- . 1982b. Fractionation of polyphenylmethylsiloxanes OV-17 and SC 2250. Unpublished data.
- . 1982c. Supercritical fluid processing of dental monomers, silicone lens monomer, and coating monomer. Unpublished data.
- . 1983a. Adsorption isotherm for the carbon dioxide-caffeine-activated carbon system. Unpublished data.
- . 1983b. Fractionation of polystyrene. Unpublished data.
- . 1983c. Supercritical fluid fractionation An alternative to molecular distillation. Paper presented at AIChE Meeting, Houston, TX, March.
- . 1984a. Polyethylene gel production. Unpublished data.
- . 1984b. Research on a new process to fractionate polymers. Report prepared for the National Science Foundation, contract CPE-8361087, September.

- . 1984c. Supercritical fluid fractionation of fish oils. Concentration of eicosapentaenoic acid. Paper presented at 75th Annual American Oil Chemists Society Meeting, Dallas, April.
- . 1984d. Supercritical fluid nucleation of difficult-to-comminute solids. Paper presented at the AIChE Annual Meeting, San Francisco, CA, November.
- . 1985a. Processing of polymers with supercritical fluids. *Polymer News*. 11:7–16.
- . 1985b. Fractionation of poly(methyl methacrylate) with chlorodifluoromethane. Unpublished data.
- Krukoniš, V. J., A. R. Branfman, and M. G. Broome. 1979. Supercritical fluid extraction of plant materials containing chemotherapeutic drugs. Paper presented at the AIChE Meeting, Boston, MA, August.
- Krukoniš, V. J., and R. T. Kurnik. 1985. Solubility of the solid aromatic isomers in carbon dioxide. *J. Chem. Eng. Data*, 30:247.
- Krukoniš, V. J., M. A. McHugh, and A. J. Seckner. 1984. Xenon as a supercritical solvent. *J. Phys. Chem.* 88:2687.
- Kuenen, J. P., and W. G. Robson. 1899. On the mutual solubility of liquids. Vapour pressure and critical points. *Philos. Mag.* 5th ser. 48:180.
- Kuk, M. S., and J. C. Montagna. 1983. Solubility of oxygenated hydrocarbons in supercritical carbon dioxide. In *Chemical Engineering at supercritical fluid conditions*, ed. M. E. Paulaitis, J. M. L. Penninger, R. D. Gray, and P. Davidson, 101. Ann Arbor, MI: Ann Arbor Science.
- Kurnik, R. T. 1981. Supercritical fluid extraction: A study of binary and multicomponent solid-fluid equilibria. Ph.D. diss., Massachusetts Institute of Technology, Cambridge, MA.
- Kurnik, R. T., and R. C. Reid. 1982. Solubility of solid mixtures in supercritical fluids. *J. Fluid Phase Equilib.* 8:93.
- Kurnik, R. T., S. J. Holla, and R. C. Reid. 1981. Solubility of solids in supercritical carbon dioxide and ethylene. *J. Chem. Eng. Data* 26:47.
- Laidler, K. J. 1965. *Chemical Kinetics*, Ch. 5. New York: McGraw-Hill Book Co.
- Larson, K. A., and M. L. King. 1986. Evaluation of supercritical fluid technology in the pharmaceutical industry. *Biotechnol. Prog.* 2:73.
- Leder, F., G. M. Kramer, and H. J. Solomon. 1976. Hydrocarbon isomerization process. U.S. Patent 3,946,088.
- Lee, L. L. 1988. *Molecular Thermodynamics of Nonideal Fluids*. Boston: Butterworths.
- Lemert, R. M., and K. P. Johnston. 1989. Solid-liquid-gas equilibria in multicomponent supercritical fluid systems. *J. Fluid Phase Equil.* 45:265–286.
- . 1990. Solubilities and selectivities in supercritical fluid mixtures near critical end points. *J. Fluid Phase Equil.* 59:31–55.
- Lemert, R. M., and J. M. DeSimone. 1991. Solvatochromic characterization of near- and supercritical ethane, propane, and dimethyl ether using 9-( $\alpha$ -perfluoroheptyl- $\beta$ , $\beta$ -dicyanovinyl)julolidine. *J. Supercritical Fluids*. 4:186.
- Li, Y.-H., K. H. Dillard, and R. L. Robinson, Jr. 1981. Vapor-liquid phase equilibrium for carbon dioxide-*n*-hexane at 40, 80, and 120°C. *J. Chem. Eng. Data* 26:53.
- Liau, I. S., and M. A. McHugh. 1985. High pressure solid polymer-supercritical fluid phase behavior. In *Supercritical Fluid Technology*, ed. J. M. L. Penninger, M. Radosz, M. A. McHugh, and V. J. Krukoniš, 415. New York: Elsevier.
- Liphard, K. G., and G. M. Schneider. 1975. Phase equilibria and critical phenomena in fluid mixtures of carbon dioxide + 2,6,10,15,19,23-hexamethyltetracosane up to 423 K and 100 MPa. *J. Chem. Thermodyn.* 7:805.

- Lira, C. T. 1988. Physical chemistry of supercritical fluids. A tutorial. In *ACS Symp. Ser.*, 366:1-25.
- List, G. R., J. P. Friedrich, and J. Pominski. 1984. Characterization and processing of cottonseed oil obtained by extraction with supercritical carbon dioxide. *J. Am. Oil Chem. Soc.* 61:1847.
- Luks, K. D., and J. P. Kohn. 1984. The topography of multiphase equilibria behavior: What can it tell the design engineer. *Proc. 63rd Annu. Convention, Gas Processors Assoc.*, 181.
- Mackay, M. E., and M. E. Paulaitis. 1979. Solid solubilities of heavy hydrocarbons in supercritical solvents. *Ind. Eng. Chem. Fundam.* 18:149.
- Mansoori, G. A., J. F. Ely, D. S. Hacker, and J. W. King. 1985. Supercritical fluid extraction/retrograde condensation with applications. AIChE Tutorial Symposium, held at the Gas Research Institute, Chicago, IL, May 25.
- Matson, D. W., R. C. Peterson, and R. D. Smith. 1987. Production of fine powders by the rapid expansion of supercritical fluid solutions. *Adv. in Ceramics* 21:109.
- McClellan, A. K., and M. A. McHugh. 1985. Separating polymer solutions using high pressure LCST phenomena. *J. Polym. Sci. Eng.*, 25:1088.
- McClellan, A. K., E. G. Bauman, and M. A. McHugh. 1985. Polymer solution supercritical fluid phase behavior. In *Symposium Proceedings on Supercritical Fluid Technology*, ed. J. M. L. Penninger, M. Radosz, M. A. McHugh, and V. J. Krukonis, 161. Amsterdam: Elsevier.
- McGrath, J. E., J. S. Riffle, A. K. Banthia, I. Yilgor, and G. L. Wilkes. 1982. An overview of the polymerization of cyclosiloxanes. *Am. Chem. Soc. Symp. Ser.* 212:145.
- McGuigan, D. B., and P. A. Monson. 1990. Analysis of infinite dilution partial molar volumes using a distribution function theory. *J. Fluid Phase Equil.* 57:227-247.
- McHugh, M. A. 1981. An experimental investigation of the high pressure fluid phase equilibrium of highly asymmetric binary mixtures. Ph.D. diss., Univ. of Delaware.
- . 1986. Extraction with supercritical fluids. In *Recent developments in separation science*, vol. IX, ed. N. N. Li and J. M. Calo. Boca Raton, FL: CRC Press, p. 75.
- McHugh, M. A., A. J. Seckner, and T. J. Yogan. 1984. High pressure phase behavior of octacosane and carbon dioxide. *Ind. Eng. Chem. Fundam.* 23:493.
- McHugh, M. A., A. J. Seckner, and V. J. Krukonis. 1984. Supercritical xenon. Paper presented at the Annual AIChE Meeting, San Francisco, CA, November.
- McHugh, M. A., and M. E. Paulaitis. 1980. Solid solubilities of naphthalene and biphenyl in supercritical carbon dioxide. *J. Chem. Eng. Data* 25:326.
- McHugh, M. A., and T. J. Yogan. 1984. A study of three-phase solid-liquid-gas equilibria for three carbon dioxide-solid hydrocarbon systems, two ethane-hydrocarbon solid systems, and two ethylene-hydrogen solid systems. *J. Chem. Eng. Data* 29:112.
- McHugh, M. A., and T. L. Guckes. 1985. Separating polymer solutions with supercritical fluids. *Macromolecules* 18:674.
- McHugh, M. A., and V. J. Krukonis. 1984. Processing with supercritical fluids. Short course held at the AIChE Annual Meeting in San Francisco, CA, November.
- . 1989. Supercritical Fluids. *Encyclopedia of Polym. Sci. & Eng.* 16:368-399.
- McHugh, M. A., B. M. Hasch, and S.-H. Lee. 1991. Effect of methyl acrylate content on the high pressure solution behavior of poly(ethylene-co-methyl acrylate) mixtures. Paper presented at the Annual AIChE meeting, Los Angeles, CA, November.

- McHugh, M. A., J. J. Watkins, B. T. Doyle, and V. J. Krukonis. 1988. High-pressure naphthalene-xenon phase behavior. *Ind. Eng. Chem. Res.* 27:1025–1033.
- McHugh, M. A., M. W. Mallett, and J. P. Kohn. 1983. High pressure fluid phase equilibria of alcohol-water-supercritical solvent mixtures. In *Chemical engineering at supercritical fluid conditions*, ed. M. E. Paulaitis, J. M. L. Penninger, R. D. Gray, and P. Davidson, 113. Ann Arbor, MI: Ann Arbor Science.
- McHugh, M. A., V. J. Krukonis, and P. Davidson. 1985. Extraction with supercritical fluids. Short course held at the University of Notre Dame, April 22–23.
- Meilchen, M. A. 1991. Thermodynamics of copolymer solutions at high pressures. Ph.D. diss., Johns Hopkins Univ.
- Meilchen, M. A., B. M. Hasch, and M. A. McHugh. 1991. Effect of copolymer composition on the phase behavior of mixtures of poly(ethylene-co-methyl acrylate) with propane and chlorodifluoromethane. *Macromolecules* 24:4874–4882.
- Meilchen, M. A., B. M. Hasch, S.-H. Lee, and M. A. McHugh. 1991. Poly(ethylene-co-methyl acrylate)-solvent-cosolvent phase behavior at high pressures. *Polymer*. 33:1922–1925.
- Melhem, G. A., and R. Saini. 1991. On the application of concentration dependent mixing rules to systems containing large numbers of compounds. Paper presented at the 2d International Symposium on Supercritical Fluids. Boston, MA. May.
- Merrill, R. C. 1983. Liquid-liquid-vapor phenomena in cryogenic liquefied natural gas systems. Ph.D. diss., Univ. of Notre Dame.
- Merrill, R. C., K. D. Luks, and J. P. Kohn. 1983. Three phase liquid-liquid-vapor equilibria in the methane + *n*-pentane + *n*-octane, methane + *n*-hexane + *n*-octane, and methane + *n*-hexane + carbon dioxide systems. *J. Chem. Eng. Data* 28:210.
- Metzger, J., J. Hartmans, D. Malwitz, and P. Koll. 1983. Thermal organic reactions in supercritical fluids. In *Chemical engineering at supercritical fluid conditions*, ed. M. E. Paulaitis, J. M. L. Penninger, R. D. Gray, and P. Davidson, 515. Ann Arbor, MI: Ann Arbor Science.
- Meyer, V. E., and G. C. Lowry, 1965. Integral and differential binary copolymerization equations. *J. Polym. Sci., Part A*. 3:2843–2851.
- Milkovich, R. 1981. In *Anionic polymerization: kinetics, mechanisms, and synthesis*, ed. J. E. McGrath, 41. ACS Symposium Series vol. 166. Washington, D.C. American Chemical Society.
- Miller, K. J., and J. A. Savchik. 1979. A new empirical method to calculate average molecular polarizabilities. *J. Am. Chem. Soc.* 101:7206–7213.
- Modell, M. 1982. Processing methods for the oxidation of organics in supercritical water. U.S. Patent 4,338,199.
- Modell, M., R. P. de Filippi, and V. J. Krukonis. 1978. Regeneration of activated carbon with supercritical carbon dioxide. Paper presented at the ACS Annual Meeting, Miami, FL.
- Modell, M., R. J. Robey, V. J. Krukonis, R. P. de Filippi, and D. Oestereich. 1979. Supercritical fluid regeneration of activated carbon. Paper presented at National AIChE Meeting, Boston, MA.
- Morrison, R. T., and R. N. Boyd. 1983. *Organic chemistry*. Boston: Allyn and Bacon.
- Moses, J. M., K. E. Goklen, and R. P. de Filippi. 1982. Pilot plant critical fluid extraction of organics from water. Paper presented at the Annual AIChE Meeting, Los Angeles, November.
- Munk, P. 1989. *Introduction to macromolecular science*. New York: John Wiley & Sons.



- Munster, N., C. A. Plank, W. L. S. Laukhuf, and P. M. Christopher. 1984. Vapor-liquid equilibria of the ternary system methyl borate-methyl alcohol-benzene. *J. Chem. & Eng. Data* 29: 178–181.
- Najour, G. C., and A. D. King, Jr. 1966. Solubility of naphthalene in compressed methane, ethylene, and carbon dioxide: Evidence for a gas-phase complex between naphthalene and carbon dioxide. *J. Chem. Phys.* 45:1915.
- Ng, H.-J., and D. B. Robinson. 1978. Equilibrium phase properties at the toluene-carbon dioxide system. *J. Chem. Eng. Data* 23:325.
- Niswonger, D. C., C. A. Plank, and W. L. S. Laukhuf. 1985. Vapor-liquid equilibria of the system trimethyl borate (1)-*n*-heptane (2). *J. Chem. & Eng. Data* 30:209–211.
- Occhiogrosso, R. N. 1985. Phase behavior studies of organic hydrocarbon-supercritical carbon dioxide mixtures. M.S. thesis, Univ. of Notre Dame.
- . 1987. Critical-mixture oxidation of cumene. Ph.D. thesis, Johns Hopkins University.
- Occhiogrosso, R. N., J. T. Igel, and M. A. McHugh, 1986. The phase behavior of isopropyl benzene-CO<sub>2</sub> mixtures. *J. Fluid Phase Equilib.*, 26:165.
- Ohgaki, K., H. Nishii, T. Saito, and T. Katayama. 1983. High pressure phase equilibria for the methanol-ethylene system at 25°C and 40°C. *J. Chem. Eng. Japan* 16:263–267.
- Ozawa, S., S. Kusumi, and Y. Ogino. 1974. High pressure adsorption of carbon dioxide on several activated carbons with different pore size distribution. *Proc. 4th Int. Conf. High Pressure, Kyoto, Japan*.
- Panayiotou, C. G. 1987. Thermodynamics of random copolymer mixtures. *Makromol. Chem.*, 188:2733–2743.
- Passino, H. J. 1949. The solexol process. *Ind. Eng. Chem.* 41:280.
- Patat, F. 1945. The hydrolysis of analine. *Monatsh. Chem.* 77:352.
- Patterson, D. 1968. Role of free volume changes in polymer solution thermodynamics. *J. Polym. Sci., Part C* 16:3379.
- . 1969. Free volume and polymer solubility. A qualitative view. *Macromolecules* 2:672.
- Paul, P. M. F., and W. S. Wise. 1971. *The principles of gas extraction*. London: Mills and Boon Ltd.
- Paulaitis, M. E., J. M. L. Penninger, R. D. Gray, and P. Davidson, eds. 1983. *Chemical engineering at supercritical fluid conditions*. Ann Arbor, MI: Ann Arbor Science.
- Paulaitis, M. E., M. A. McHugh, and C. P. Chai. 1983. Solid solubilities in supercritical fluids at elevated pressures. In *Chemical engineering at supercritical fluid conditions*, ed. M. E. Paulaitis, J. M. L. Penninger, R. D. Gray, and P. Davidson, 139. Ann Arbor, MI: Ann Arbor Science.
- Paulaitis, M. E., M. L. Gilbert, and C. A. Nash. 1981. Separation of ethanol-water mixtures with supercritical fluids. Paper presented at the 2d World Congress of Chemical Engineers, Montreal, Canada, October.
- Paulaitis, M. E., R. G. Kander, and J. R. Diandreth. 1984. Phase equilibria related to supercritical-fluid solvent extractions. *Ber. Bunsenges. Phys. Chem.* 88:869.
- Paulaitis, M. E., V. J. Krukonis, R. T. Kurnik, and R. C. Reid. 1983a. Supercritical fluid extraction. *Rev. Chem. Eng.* 1:179.
- Peng, D. Y., and D. B. Robinson. 1976. A new two constant equation of state. *Ind. Eng. Chem. Fundam.* 15:59.
- Peters, C. J., H. J. van der Kooi, and J. de Swaan Arons. 1987. Measurements and

- calculations of phase equilibria for (ethane + tetracosane) and ( $p$ ,  $V_m$ ,  $T$ ) of liquid tetracosane. *J. Chem. Thermodyn.* 19:395–405.
- Peters, C. J., J. L. de Roo, and J. de Swaan Arons. 1987. Three-phase equilibria in (ethane + pentacosane). *J. Chem. Thermodyn.* 19:265–272.
- Peters, C. J., J. L. de Roo, and R. N. Lichtenthaler. 1987. Measurements and calculations of phase equilibria of binary mixtures of ethane + eicosane. Part I: Vapour + liquid equilibria. *J. Fluid Phase Equil.* 34:287–308.
- Peters, C. J., J. Spiegelaar, and J. de Swaan Arons. 1988. Phase equilibria in binary mixtures of ethane + docosane and molar volumes of liquid docosane. *J. Fluid Phase Equil.* 41:245–256.
- Peters, C. J., R. N. Lichtenthaler, and J. de Swaan Arons. 1986. Three-phase equilibria in binary mixtures of ethane and higher  $n$ -alkanes. *J. Fluid Phase Equil.* 29:495–504.
- Petsche, I. B., and P. G. Debenedetti. 1990. Influence of solute-solvent asymmetry upon the behavior of dilute supercritical mixtures. *J. Phys. Chem.* 95:386–399.
- Pine, S. H., J. B. Hendrickson, D. J. Cram, and G. S. Hammond. 1980. *Organic chemistry*, 4th ed. New York: McGraw Hill Book Co.
- Plank, C. A., and P. M. Christopher. 1976. Vapor-liquid equilibria of methyl borate-carbon tetrachloride and methyl borate-benzene systems. *J. Chem. & Eng. Data* 21:211–212.
- Podessa, J., J. Stejskal, and P. Kratochvil. 1987. Relationship between the molar mass distribution width of blocks and chemical heterogeneity of a diblock copolymer: comparison between theory and experiment. *Macromolecules*. 20:2195–2201.
- Pottinger, M. T., and R. L. Laurence. 1984. The PVT behavior of polymeric liquids represented by the Sanchez-Lacombe equation of state. *J. Polym. Sci. Polym. Phys. Ed.* 22:903–907.
- Prasad, R., M. Gottesman, and R. A. Scarella. 1981. Decaffeination of aqueous extracts. U.S. Patent 4,246,291.
- Pratt, J. A., S.-H. Lee, and M. A. McHugh. 1993. Supercritical fractionation of copolymers based on chemical composition and molecular weight. *J. Appl. Polym. Sci.* 49:953–966.
- Prausnitz, J. M. 1958. Regular solution theory for gas-liquid solutions. *AIChE J.* 4:269.
- . 1969. *Molecular thermodynamics of fluid-phase equilibria*, Ch. 5. Englewood Cliffs, NJ: Prentice-Hall Inc.
- Prausnitz, J. M., and P. R. Benson. 1959. Solubility of liquids in compressed hydrogen, nitrogen, and carbon dioxide. *AIChE J.* 5:161.
- Prins, A. 1915. On critical end-points and the system ethane-naphthalene. *Proc. Acad. Sci. Amsterdam* 17:1095.
- Ramsay, W. 1880. On the critical state of gases. *Proc. R. Soc. London* 30:323.
- Rance, R. W., and E. L. Cussler. 1974. Fast fluxes with supercritical solvents. *AIChE J.* 20:353.
- Randall, L. G. 1982. The present status of dense (supercritical) gas extraction and dense gas chromatography: Impetus for DGC/MS development. *Sep. Sci. Tech.* 17:1.
- Randolph, T. W., H. W. Blanch, M. J. Prausnitz, and C. R. Wilke. 1985. Enzymatic catalysis in a supercritical fluid. *Biotechnology Letters* 7:325.
- Rätzsch, M. T., P. Wagner, Ch. Wohlfarth, and D. Heise. 1982. Studies on the high-pressure equilibrium in mixtures of ethylene and ethylene-vinyl acetate copolymers. *Acta Polymerica* 33:463–467.
- Rätzsch, M. T., P. Wagner, Ch. Wohlfarth, and S. Gleditsch. 1983. Studies of the phase equilibria of ethylene and (ethylene-vinyl acetate) copolymers at high

- pressures. Part III. Effect of molecular weight distribution. *Acta Polymerica* 34:340–344.
- Rätzsch, M. T., R. Findeisen, and V. S. Sernow. 1980. Investigation of the phase behavior of monomer-polymer systems at high pressures. *Z. Phys. Chem.* 261:995–1000.
- Reid, R. C., J. M. Prausnitz, and B. E. Poling. 1987. *The properties of gases and liquids*, 4th ed., New York: McGraw-Hill Book Co.
- Riffe, J. S. 1988. Discussion of gas phase reactivity of amines with carbamic acids. Private communication, Virginia Polytechnic Institute and State University.
- Robey, R. J., and S. Sunder. 1984. Applications of supercritical fluid processing to the concentration of citrus oil fractions. Paper presented at the Annual AIChE Meeting, San Francisco, CA, November.
- Robinson, D. B., D. Y. Peng, and S. Y.-K. Chung. 1985. The development of the Peng-Robinson equation and its application to phase-equilibrium in a system containing methanol. *J. Fluid Phase Equil.* 24:25–41.
- Rodrigues, A. B. J., D. S. McCaffrey, Jr., and J. P. Kohn. 1968. Heterogeneous phase and volumetric equilibrium in the ethane-*n*-octane system. *J. Chem. Eng. Data* 13:164.
- Rodrigues, A. B., and J. P. Kohn. 1967. Three phase equilibria in the binary systems ethane-*n*-docosane and ethane-*n*-octacosane. *J. Chem. Eng. Data* 12:191.
- Roselius, W., O. Vitzthum, and P. Hubert. 1974. Method for the production of caffeine-free coffee extract. U.S. Patent 3,843,824.
- Rowlinson, J. S., and F. L. Swinton. 1982. *Liquids and liquid mixtures*, 3d ed., Ch. 6. Boston: Butterworth and Co. Ltd.
- Rowlinson, J. S., and M. J. Richardson. 1958. The solubility of solids in compressed gases. *Adv. Chem. Phys.* 2:85.
- Saeki, S., N. Kuwahara, S. Konno, and M. Kaneko. 1973. Upper and lower critical solution temperatures in polystyrene solutions. *Macromolecules* 4:246–250.
- Saeki, S., S. Konno, N. Kuwahara, M. Nakata, and M. Kaneko. 1974. Upper and lower critical solution temperatures in polystyrene solutions III. Temperature dependence of the  $\chi$  parameter. *Macromolecules* 7:521.
- Saini, R., G. A. Melhem, and B. M. Goodwin. 1991. A modified cubic equation of state with binary parameters predicted from a group contribution method. Paper presented at the 2d International Symposium on Supercritical Fluids. Boston, MA, May.
- Saltiel, J., and J. L. Charlton. 1980 *Rearrangements in ground and excited states*, vol. 3, 25–89. New York: Academic Press.
- Sanchez, I. C. 1980. Statistical thermodynamics of bulk and surface properties of polymer mixtures. *Macromol. Sci.-Phys.* B17:565–589.
- Sanchez, I. C., and A. C. Balazs. 1989. Generalization of the lattice-fluid model for specific interactions. *Macromolecules* 22:2325–2331.
- Sanchez, I. C., and R. H. Lacombe. 1976. An elementary molecular theory of classical fluids. Pure fluids. *J. Phys. Chem.* 80:2352–2362.
- . 1977. An elementary equation of state for polymer liquids. *Polym. Lett.* 15:71–75.
- . 1978. Statistical thermodynamics of polymer solutions. *Macromolecules* 11:1145–1156.
- Sand, M. L. 1986. Method for impregnating a thermoplastic polymer. U.S. Patent 4,598,006.

- Sandler, S. I. 1989. *Chemical and Engineering Thermodynamics*. New York: John Wiley & Sons.
- Saraf, V. P., and E. Kiran, 1988a. Solubility of polystyrenes in supercritical fluids. *J. Supercritical Fluids* 1:37–44.
- . 1988b. Supercritical fluid-polymer interactions: phase equilibrium data for solutions of polystyrenes in *n*-butane and *n*-pentane. *Polymer* 29:2061–2065.
- Schmidt, M. B., C. A. Plank, and W. L. S. Laukhuf. 1985. Liquid-liquid equilibria for three methyl alcohol-trimethyl borate-*n*-alkane systems. *J. Chem. & Eng. Data* 30:251–253.
- Schmitt, W. J. 1984. The solubility of monofunctional organic compounds in chemically diverse supercritical fluids. Ph.D. diss., Massachusetts Institute of Technology.
- Schmitt, W. J., and R. C. Reid. 1984. The influence of the solvent gas on solubility and selectivity in supercritical extraction. Paper presented at the Annual AIChE Meeting, San Francisco, CA, November.
- Schmitt, W. J., R. A. Grieger-Block, and T. W. Chapman. 1983. The preparation of acid-catalyzed silica aerogel. In *Chemical engineering at supercritical fluid conditions*, ed. M. E. Paulaitis, J. M. L. Penninger, R. D. Gray, Jr., and P. Davidson. Ann Arbor, MI: Ann Arbor Science.
- Schneider, G. M. 1970. Phase equilibria in fluid mixtures at high pressures. *Adv. Chem. Phys.* 17:1.
- . 1978. Physicochemical principles of extraction with supercritical gases. *Angew. Chem. Int. Ed. Engl.* 17:716.
- Schneider, G. M., E. Stahl, and G. Wilke, eds. 1980. *Extraction with supercritical gases*. Weinheim, W. Germany: Verlag Chemie.
- Schneider, G. M., J. Ellert, U. Hoarhaus, I. F. Hölscher, G. Katzenski-Ohling, A. Kopner, J. Kulka, D. Nickel, J. Rübesamen, and A. Wilsch. 1987. Thermodynamic, spectroscopic and phase equilibrium investigations on polar fluid mixtures at high pressures. *Pure & Appl. Chem.* 59:1115–1126.
- Scholsky, K. M., O'Connor, C. S. Weiss, and V. J. Krukonsis, 1987. Characterization of copolymers fractionated using supercritical fluids, *J. Appl. Polym. Sci.* 33:2925.
- Schroeder, E. and K. F. Arndt. 1976a. Löslich Keitsverhalten von Makromolekülen in Komprimierten gasen. I. Einführung und Meßmethodik. *Faserforschung und Textiltechnik* 27:135–139.
- . 1976b. Löslich Keitsverhalten von Makromolekülen in Komprimierten gasen. II. Experimentelle Ergebnisse über das Druckverhalten von Polyvinylchlorid, Polymethylmethacrylat und Polystyrol in fluidem CO<sub>2</sub>. *Faserforschung und Textiltechnik* 27:141:146.
- . 1976c. Löslich Keitsverhalten von Makromolekülen in Komprimierten gasen. III. Theoretische Betrachtung der Versuchsergebnisse. *Faserforschung und Textiltechnik* 27:159–164.
- Scott, R. L. 1972. Thermodynamics of critical phenomena in fluid mixtures. *Ber. Bunsenges. Phys. Chem.* 76:296.
- Scott, R. L., and P. B. van Konynenburg. 1970. Static properties of solutions: van der Waals and related models for hydrocarbon mixtures. *Discuss. Faraday Soc.* 49:87.
- Seckner, A. J., A. K. McClellan, and M. A. McHugh. 1988. High-pressure solution behavior of the polystyrene-toluene-ethane system. *AIChE J.* 34:9–16.
- Sen, Y. L., and E. Kiran. 1990. A new experimental system to study the temperature and pressure dependence of viscosity, density, and phase behavior of pure fluids and solutions. *J. Supercritical Fluids* 3:91–99.

- . 1991. Viscosity and density of polystyrene solutions in near and supercritical *n*-butane and *n*-pentane. Paper presented at the 2d International Symposium on Supercritical Fluids. Boston, MA, May.
- Shaw, R. W., T. B. Brill, A. A. Clifford, C. A. Eckert, and E. U. Franck. 1991. Supercritical water. A medium for chemistry. *Chem. Eng. News*. 69:26–39.
- Sherwood, R. T., R. L. Pigford, and C. K. Wilke. 1975. *Mass transfer*. New York: McGraw-Hill Book Co.
- Shim, J.-J., and K. P. Johnston. 1991. Phase equilibria, partial molar enthalpies, and partial molar volumes determined by supercritical fluid chromatography. *J. Phys. Chem.* 95:353–360.
- Shimshick, E. J. 1981. Removal of organic acids from dilute aqueous solutions of salts of organic acids by supercritical fluids. U.S. Patent 4,250,331.
- Shreve, R. N., and J. A. Brink, Jr. 1977. Chemical process industries. In *Plastics industries*. New York: McGraw-Hill Book Co.
- Simmons, G. M., and D. M. Mason. 1972. Pressure dependency of gas phase reaction rate coefficients. *Chem. Eng. Sci.* 27:89.
- Simnick, J. J., C. C. Lawson, H., M. Lin, and K. C. Chao. 1977. Vapor-liquid equilibrium of hydrogen/tetralin systems at elevated temperatures and pressures. *AIChE J.* 23:469:479.
- Siow, K. S., G. Delmas, and D. Patterson. 1972. Cloud-point curves in polymer solutions with adjacent upper and lower critical solution temperatures. *Macromolecules*. 5:29–34.
- Smith, S. D., J. M. DeSimone, G. York, D. W. Dwight, G. L. Wilkes, and J. E. McGrath. 1987. Blends of poly(methyl methacrylate)-poly(dimethyl siloxane) graft copolymers with poly(methyl methacrylate) and poly(vinyl chloride). Paper presented at the ACS Meeting, New Orleans, LA, August.
- Smits, A. 1903. *Z. Electrochem.* 33:91.
- Snyder, J. M., J. P. Friedrich, and D. D. Christianson. 1984. Effect of moisture and particle size on the extractability of oil from seeds with supercritical CO<sub>2</sub>. *J. Am. Oil Chem. Soc.* 61:1851.
- Soave, G. 1972. Equilibrium constants from a modified Redlich-Kwong equation of state. *Chem. Eng. Sci.* 27:1197.
- Squires, T. G., C. G. Venier, and T. Aida. 1983. Supercritical fluid solvents in organic chemistry. *J. Fluid Phase Equilib.* 10:261.
- Stahl, E., and K. W. Quirin. 1983. Dense gas extraction on a laboratory scale: A survey of some recent results. *J. Fluid Phase Equilib.* 10:269.
- Stahl, E., and W. Schilz. 1979. Mikroanalytische Untersuchungen zur Löslichkeit von Naturstoffen in überkritischem Kohlendioxid. *Talanta* 26:675.
- Stahl, E., K. W. Quirin, A. Glatz, D. Gerard, and G. Rau. 1984. New developments in the field of high pressure extraction of natural products with dense gases. *Ber. Bunsenges. Phys. Chem.* 9:900.
- Stahl, E., W. Schilz, E. Schutz, and E. Willing. 1980. A quick method for the microanalytical evaluation of the dissolving power of supercritical gases. In *Extraction with supercritical gases*, ed. G. M. Schneider, E. Stahl, and G. Wilke, 93. Deerfield Beach, FL: Verlag Chemie.
- Stejskal, J., and P. Kratochvil. 1982. Distribution of the chemical composition of block and graft copolymers assuming gamma distribution of molecular weights of the precursor blocks. *Polym. J.*, 14(8): 603–627.

- . 1987. Statistical chemical heterogeneity of copolymers: modification of the Stockmayer distribution function of chemical composition. *Macromolecules* 20:2624–2628.
- . 1989. Conversion chemical heterogeneity of graft-copolymers prepared from macromonomers. *Macromolecules*. 22:429.
- Stejskal, J., P. Kratochvil, and A. D. Jenkins. 1987. Graft copolymer statistics. 2. Application to graft copolymers prepared from macromonomers. *Macromolecules* 20:181.
- Stephens, W. D., R. E. Campbell, and G. E. Webb. 1978. *Binder properties optimization*. Technical report AFRPL-TR-77-93, Air Force Rocket Propulsion Laboratory, Edwards AFB, CA, February.
- Stockmayer, W. H. 1945. Distribution of chain lengths and compositions in copolymers. *J. Chem. Phys.* 13:199.
- Streett, W. B. 1976. Phase equilibria in gas mixtures at high pressures. *Icarus* 29:173.
- . 1983. Phase equilibria in fluid and solid mixtures at high pressure. In *Chemical engineering at supercritical fluid conditions*, ed. M. E. Paulaitis, J. M. L. Penninger, R. D. Gray, and P. Davidson. Ann Arbor, MI: Ann Arbor Science.
- Subramaniam, B., and M. A. McHugh. 1986. Reactions in supercritical fluids: A review. *Ind. Eng. Chem. Proc. Des. Dev.*, 25:1.
- Suppes, G. J., and M. A. McHugh. 1989a. A variable-volume infrared cell for high-pressure studies. *Rev. Sci. Instrum.* 60:666–669.
- . 1989b. Solvent and catalytic effects on the decomposition of cumene hydroperoxide. *I & EC Research* 28:1146–1152.
- Swelheim, T., J. de Swaan Arons, and G. A. M. Diepen. 1965. Fluid phase equilibria in the system polyethylene-ethene. *Rec. Trav. Chim.* 84:261.
- Takahashi, T. 1980. Absolute rate constants for the free radical polymerization of ethylene in the supercritical phase. Ph.D. diss., State Univ. of New York at Buffalo.
- Takahashi, T., and P. Ehrlich. 1982. Absolute rate constants for the free radical polymerization of ethylene in the supercritical phase. *Macromolecules* 15:714.
- Tiffin, D. L., A. L. DeVera, K. D. Luks, and J. P. Kohn. 1978a. Phase-equilibria behavior of the binary systems carbon dioxide-*n*-butylbenzene and carbon dioxide-*trans*-decalin. *J. Chem. Eng. Data* 23:45.
- Tiffin, D. L., G. Guzman, K. D. Luks and J. P. Kohn. 1978b. Phase equilibria behavior of the ternary systems carbon dioxide-*trans*-decalin-*n*-eicosane and carbon dioxide-*trans*-decalin-2-methylnaphthalene. *J. Chem. Eng. Data* 23:203.
- Tiltscher, H., H. Wolf, and J. Schelchshorn. 1981. A mild and effective method for the reactivation or maintenance of the activity of heterogeneous catalysts. *Angew. Chem. Int. Ed. Engl.* 20:892.
- . 1984. Utilization of supercritical fluid solvent-effects in heterogeneous catalysis. *Ber. Bunsenges. Phys. Chem.* 88:897.
- Todd, D. B. 1952. Phase equilibria in systems with supercritical ethylene. Ph.D. diss., Princeton Univ.
- Todd, D. B., and J. C. Elgin. 1955. Phase equilibria in systems with ethylene above its critical temperature. *AIChE J.* 1:20.
- Travers, M. W., and F. L. Usher. 1906. On the behavior of certain substances at their critical temperatures. *Proc. Roy. Soc. A.* 78:247–261.
- Treybal, R. E. 1968. *Mass-transfer operations*, 2d ed., Ch. 10. New York: McGraw Hill Co.

- Tsekhanskaya, Yu. V., M. B. Iomtev, and E. V. Mushkina. 1962. Solubility of diphenylamine and naphthalene in carbon dioxide under pressure. *Russ. J. Phys. Chem. (Engl. Transl.)* 36:1177.
- . 1964. Solubility of naphthalene in ethylene and carbon dioxide under pressure. *Russ. J. Phys. Chem. (Engl. Transl.)* 38:1173.
- Uematsu, M., and E. U. Franck. 1989. The dielectric constant of chlorodifluoromethane to 200 MPa. *Ber. Bunsenges. Phys. Chem.* 93:177–180.
- Unterreiner, J. M., M. A. McHugh, and V. J. Krukonis. 1991. Breaking the trimethyl borate-methanol azeotrope with supercritical methane. *Ind. Eng. Chem. Res.* 29:740–745.
- Vaidya, S. N., and G. C. Kennedy. 1971. Compressibility of 18 molecular organic solids to 45 kbar. *J. Chem. Phys.* 55:987.
- Valteris, R. L. 1966. The solubility of materials in compressed hydrocarbon gases. *Birmingham Univ. Chem. Eng.* 17:38.
- Van Alsten, J. G., P. C. Hansen, and C. A. Eckert. 1984. Supercritical enhancement factors for nonpolar and polar systems. Paper presented at the AIChE Meeting, San Francisco, CA.
- Van Leer, R. A., and M. E. Paulaitis. 1980. Solubilities of phenol and chlorinated phenols in supercritical carbon dioxide. *J. Chem. Eng. Data* 25:257.
- van Gunst, C. A. 1950. The solubility of mixtures of solids in supercritical gases. Ph.D. diss., Delft Univ., Netherlands.
- van Gunst, C. A., F. E. C. Scheffer, and G. A. M. Diepen. 1953a. On critical phenomena of saturated solutions in binary systems II. *J. Phys. Chem.* 57:578.
- . 1953b. On critical phenomena of saturated solutions in ternary systems. *J. Phys. Chem.* 57:581.
- van Hest, J. A. M., and G. A. M. Diepen, 1963. Solubility of naphthalene in supercritical methane. *Symp. Soc. Chem. Ind., London* 10.
- van Welie, G. S. A., and G. A. M. Diepen. 1961a. The  $P$ - $T$ - $x$  space model of the system ethylene naphthalene (I). *Rec. Trav. Chim.* 80:659.
- . 1961b. The  $P$ - $T$ - $x$  space model of the system ethylene naphthalene (II). *Rec. Trav. Chim.* 80:666.
- . 1961c. The  $P$ - $T$ - $x$  space model of the system ethylene naphthalene (III). *Rec. Trav. Chim.* 80:673.
- . 1961d. The  $V$ - $T$ - $x$  space model of the system ethylene naphthalene (I). *Rec. Trav. Chim.* 80:683.
- . 1961e. The  $V$ - $T$ - $x$  space model of the system ethylene naphthalene (II). *Rec. Trav. Chim.* 80:693.
- . 1963. The solubility of naphthalene in supercritical ethane. *J. Phys. Chem.* 67:755.
- Villard, P. 1888. On some new gas hydrates. *Comptes Rendus des Seances de L'Academie des Sciences*, 106:1602.
- . 1896. Solubility of liquids and solids in gas. *J. Phys.* 5:455.
- von Tapavicza, S., and J. M. Prausnitz. 1976. Thermodynamics of polymer solutions: An introduction. *Int. Eng. Chem.* 16:329.
- Wagner, J. R., Jr., D. S. McCaffrey, Jr., and J. P. Kohn. 1968. Partial miscibility phenomena in the ternary system ethane- $n$ -hexadecane- $n$ -eicosane. *J. Chem. Eng. Data* 13:22.
- Wagner, R. A., V. J. Krukonis, and M. P. Coffey. 1988. A novel impregnation process: application to carbon/carbon composites. *Ceram. Eng. Sci. Proc.* 9:957.

- Walsh, J. M., and M. D. Donohue. 1989. Hydrogen bonding in entrainer cosolvent mixtures: A parametric analysis. *J. Fluid Phase Equil.* 52:397-404.
- Walsh, J. M., G. D. Ikononov, and M. D. Donohue. 1987. Supercritical phase behavior: The entrainer effect. *J. Fluid Phase Equil.* 33:295-314.
- Walsh, J. M., G. Jin, and M. D. Donohue. 1991. Thermodynamics of short-chain polar compounds. *J. Fluid Phase Equil.* 65:209-237.
- Watkins, J. J., and V. J. Krukonis. 1990. *Supercritical fluid processing of propellants*. Technical Report PL-TR-91-3003, OLAC, Phillips Laboratory (AFSC), Edwards Air Force Base, CA, December.
- . 1991. Fractionation of rocket propellant binders with supercritical and near critical fluids. Paper presented at the 2d International Symposium on Supercritical Fluids. Boston, MA, May.
- Watkins, J. J., V. J. Krukonis, S. D. Smith, M. M. Satkowski, and P. Ehrlich. 1992. Submitted to *Macromolecules*.
- Watkins, J. J., V. J. Krukonis, P. D. Condo, D. Pradhan, and P. Ehrlich. 1991. Fractionation of high density polyethylene in propane by isothermal pressure profiling and isobaric temperature profiling. *J. Supercritical Fluids*. 4:24-31.
- Watkins, J. J., V. J. Krukonis, S. Smith, M. Satkowski, B. M. Hasch, S. H. Lee, and M. A. McHugh. 1991. The effect of crystallinity on the phase behavior of LLDPE in propane; A. fractionation with respect to crystallinity, B. Cloud point determination of fractions exhibiting various crystallizabilities. Paper presented at the Annual AIChE meeting, Los Angeles, CA, November.
- Weinstock, J. J. 1952. Phase equilibrium at elevated pressure in ternary systems of ethylene and water and organic liquids. Ph.D. diss., Princeton Univ.
- White, G. L., and C. T. Lira. 1991a. High pressure multiphase equilibria of CO<sub>2</sub> with polycyclic aromatic hydrocarbons. Paper presented at the 2d International Symposium on Supercritical Fluids. Boston, MA, May.
- . 1992. Multiphase behavior of CO<sub>2</sub> with solid aromatics. *J. Fluid Phase Equil.* 78:269-284.
- Wild, L., T. R. Ryle, D. C. Knobloch, and I. R. Peat. 1982. Determination of branching distributions in polyethylene and ethylene copolymers. *J. Polym. Sci. Polym. Phys. Ed.* 20:441-455.
- Williams, D. F. 1981. Extraction with supercritical gases. *Chem. Eng. Sci.* 36:1769.
- Wilson, G. and R. S. Owens. 1970. High temperature vapor-liquid equilibrium studies on synthetic fuel systems. Paper presented at the AIChE meeting, New York, November.
- Wilson, R. E., P. C. Keith, and R. E. Haylett. 1936. Liquid propane: Use in dewaxing, deasphalting, and refining heavy oils. *Ind. Engl. Chem.* 28:1065.
- Winkler, D. E., and G. W. Hearne. 1958. *Tert*-butyl hydroperoxide. U.S. Patent 2,845,461.
- . 1961. Liquid phase oxidation of isobutane. *Ind. Eng. Chem.* 53:655.
- Wissinger, R. G., and M. E. Paulaitis. 1987. Swelling and sorption in polymer-CO<sub>2</sub> mixtures at elevated pressures. *J. Polym. Sci.: Part B: Polym. Phys.* 25:2497.
- Wohlfarth, Ch., P. Wagner, D. Glindemann, M. Völkner, and M. T. Rätzsch. 1984. The high pressure phase equilibrium in the system ethylene + vinyl acetate + ethylene-vinyl acetate copolymer. *Acta Polymerica*. 35:498-503.
- Wohlfarth, Ch. P. Wagner, M. T. Rätzsch, and S. Westmeier. 1982. Studies of phase equilibria in mixtures of ethylene and (ethylene-vinyl acetate) copolymers at high pressure. Part II. Dependence on temperature. *Acta Polymerica* 33: 468-471.



- Wolkomir, R. 1984. Supercritical potato chips. *Omni*, 28. July.
- Wong, J. M., R. S. Pearlman, and K. P. Johnston. 1985. Supercritical fluid mixtures: Prediction of phase behavior. *J. Phys. Chem.* 89:2671–2675.
- Wu, R.-S., L. L. Lee, and H. D. Cochran. 1990. Structure and dilute supercritical solutions: Clustering of solvent and solute molecules and the thermodynamic effects. *Ind. Eng. Chem. Res.* 29:977–988.
- Yang, H., K. D. Luks, and J. P. Kohn. 1976. Phase-equilibria behavior of the system carbon dioxide-*n*-butylbenzene-2-methylnaphthalene. *J. Chem. Eng. Data* 21:330.
- Yates, R. A. 1981. Removal and concentration of lower molecular weight organic acids from dilute solutions. U.S. Patent 4,282,323.
- Yiling, T., Th. Michelberger, and E. U. Franck. 1991. High-pressure phase equilibria and critical curves of (water + *n*-butane) and (water + *n*-hexane) at temperatures to 700 K and 300 MPa. *J. Chem. Thermodynamics* 23:105–112.
- Yonker, C. R., and R. D. Smith. 1988. Solvatochromic behavior of binary supercritical fluids: The carbon dioxide/2-propanol system. *J. Phys. Chem.* 92:2374–2378.
- Yonker, C. R., S. L. Frye, D. R. Kalkwarf, and R. D. Smith. 1986. Characterization of supercritical fluid solvents using solvatochromic shifts. *J. Phys. Chem.* 90:3022–3026.
- Zaks, A., and A. M. Klibanov. 1984. Enzymatic catalysis in organic media at 100°C. *Science* 224:1249.
- Zarah, B. Y., K. D. Luks, and J. P. Kohn. 1974. Phase equilibria behavior of carbon dioxide in binary and ternary systems with several hydrocarbon components. *AIChE Symp. Ser.* 70, no. 140, 90.
- Zeman, L., and D. Patterson. 1972. Pressure effects in polymer solution phase equilibria. II. Systems showing upper and lower critical solution temperatures. *J. Phys. Chem.* 76:1214.
- Zeman, L., J. Biros, G. Delmas, and D. Patterson. 1972. Pressure effects in polymer solution phase equilibria. I. The lower critical solution of polyisobutylene and polydimethylsiloxane. *J. Phys. Chem.* 76:1206.
- Zosel, K. 1981. Process for the decaffeination of coffee. U.S. Patent 4,260,639.
- Zosel, K. 1982. Process for the direct decaffeination of aqueous coffee extract solutions. U.S. Patent 4,348,422.

### Patent Reviews

Since the time that our book was issued in 1986 until 1991, approximately 85 new "supercritical" patents have issued. This accounting does not consider the scores of patents related to supercritical fluid chromatography. We have chosen to include the reviews of only a dozen of these 85 patents with the reviews from the first edition of our book since there was considerable overlap of ideas and information in the remaining 73 patents. In fact, we found that, in our opinions, many of the 85 patents issued in the past six to seven years do not pass the acid test of being "not obvious to those skilled in the art." Compared to the ninety five patents that were included in the first edition, we found many more of the recent patents being based on "thought" experiments only. And many of these "thought" experiments could only achieve reality in the inventor's mind. While these criticisms may appear quite harsh, the reader is reminded that our conclusions are based on the fundamental principles of organic and physical chemistry and chemical engineering as well as time-proven process design principles. These are principles and teachings to which we have all been exposed. Why is it that no one would ever believe that a metal or a salt would dissolve to tens of weight percent in an organic liquid such as hexane, but, the patent examiners must accept what they are told by the inventors in their applications that these compounds can dissolve into supercritical fluid solvents as feable as carbon dioxide? We decided to keep our review of the patents from the prior 50 years found in the first edition of our book since many of these are classic patents whose process ideas show up over and over again in the contemporary patents.

For a patent to be included in this appendix the process described in the patent must utilize the separations advantage of operating in the critical region. The one hundred and seven patents chosen describe quite diverse processes and represent many sectors of industry. Some of the patents are quite important and they describe processes in use today; other ones have passed their seventeen year life but are still of interest for historical or technical reasons; and certain ones are chosen for their quite unusual application of supercritical fluids.

Patents usually follow a standard format. They contain a Background or Prior Art section that describes "old" processes noting their limitations and problems, an Invention section that describes the "new" process often including examples of reduction-to-practice, and the Claims section that defines quantitatively the conditions and limits of the Invention. The information in a patent is reviewed by patent examiners who frequently require that the limits of the claims be revised before the patent is issued. Even with this review process the limits of the claims are frequently much wider than covered in the Examples section. Not all patents have been reduced to practice, and we have included several of these which we refer to as "thought" patents. Some of the patents can work as described even though no data are presented; some cannot work even though data are presented.

Occasionally the Background section exaggerates the limitations of the old processes, and in certain instances the Invention section makes liberal use of adjectives such as "surprising" and "unexpected" when presenting the results. Quite often the exclamations of surprise derive from an inappropriate comparison of new and old results. We present commentary when the "surprise" of the technical findings is unwarranted because of information that existed in the literature at the time of the filing, or when "surprise"

derives from comparing sets of data that have no relevance to each other. Patents are an excellent source of information, but each one must be read carefully and evaluated critically.

In this edition of the book we have eliminated the front page of the patents to conserve space. In many cases this also eliminates information as many of the patent's front page contain schematic diagrams that are quite useful in understanding our description. The reader is encouraged to obtain a copy of the patent to recover this extra information. The patents are discussed in the following order:

1. The Zosel patent (U.S. 3,969,196). The description of this patent could fill a separate appendix. This patent is 30 pages long and it includes 68 examples that describe all sorts of extractions and separations. The discussion of this patent is terse because of constraints on space; however, the patent is must reading for serious researchers and managers.
2. Patents on petroleum and other fossil fuel separations.
3. Patents on coffee decaffeination.
4. Patents on the extraction of vegetable and animal materials, e.g., spices, oil seeds, tobacco, wood, hops, animal fats, etc.
5. Patents on polymer processing.
6. Patents on the separation of organic-water solutions.
7. Patents on materials processing.
8. Miscellaneous Patents. The commonality in this section is the diversity of the patents. For example, grouped together are patents describing a coal slurry combustion process, the dry cleaning of clothes with carbon dioxide, the separation of inorganic salts from water, and the growth of crystals from supercritical solution.

Within each section the patents are described in chronological order unless the material in a "younger" patent helps to explain more easily the information in an "older" one. In discussing some of the patents we draw upon the literature for additional information. If a reference has been cited previously in this book, it is referenced in the normal manner, i.e., (author, year). If a reference is being cited for the first time in the patent discussion or if data are presented that have not yet been published, the entire reference is given in the text. Finally, it is noted that this Appendix draws on information covered in many of the chapters of this book; therefore, the critique and commentary of the patents will be more meaningful if the material in the book is studied first.

**Zosel, K., Process for the separation of mixtures of substances U.S.  
3,969,196 (July 13, 1976).**

As we related in the introduction to Appendix A, this patent should be read by everyone involved in research and process development using supercritical fluids. In his examples, Zosel describes results on neat solubility, separations of liquids and solids, fractionations, etc. A wealth of information is given on the performance of various gases, e.g., ethylene, ammonia, ethane, carbon dioxide, in dissolving a variety of compounds. Several interesting experiments carried out in a plexiglass autoclave are described, and certain phase separations are noted. Some of the information can be found in other references, of course, but not in such succinct form. It is of pedagogical value to reproduce one of the examples here.

Example 66

"A stream of  $\text{CF}_3\text{Cl}$  is passed at 42 °C and 1000 psi through 20 ml of paraffin oil contained in a 50 ml. pressure vessel of plexiglass. The increase in volume of the paraffin oil occurring thereby is hardly noticeable. The supercritical gas withdrawn discharges paraffin oil, the amount of which is low, however, corresponding to the low degree of solvation. When increasing the pressure to about 1075 psi the density of the supercritical gas phase is higher than that of the paraffin oil. This has the result that the paraffin oil migrates to the top of the pressure vessel while the supercritical gaseous trifluorochloromethane is present below it at the bottom. Thus, continuous treatment of the paraffin oil with the supercritical gas requires reversal of the direction of flow of the supercritical gas stream. This example shows that even reversal of the relative densities between the inert gas phase and the mixture of substances to be separated can be achieved by selecting appropriate process conditions."

Many such observations and a quite detailed Invention section make this patent a valuable source of information. There are, however, a few examples which are not accurate. The following is one such example.

Example 61

"Ethylene is passed through a mixture of 300 ml of water and 300 ml of ethanol contained in the apparatus shown in figure 1, the temperature being 20 °C and the pressure 2,860 psi. The ethylene withdrawn did not take up ethanol which has been retained by the water wherein it is dissolved. The situation is the same if methanol is substituted for ethanol under the same conditions and with the same relative proportions."

"If a mixture comprising water and propanol in the same relative proportions is treated under exactly the same operating conditions, 100 gms of ethylene withdrawn discharge as much as 70 ml of 90% propanol as determined by hydrometer. If a corresponding mixture of water and butanol is treated under the same conditions, 100 gm of ethylene withdrawn discharge

about 106 ml of butanol. The significance of the hydroxyl group in proportion to the hydrocarbon radical of the compound is clearly obvious in this case. If the hydrocarbon radical where solvation with the molecules of the supercritical gas phase is initiated is not very large, the linkage force of the hydroxyl group to adjacent molecules predominates and the compound is not taken up in the supercritical gas phase. However, if the hydrocarbon radical becomes greater, this solvation effect outweighs the additional hindrances derived from the present hydroxyl group and the compounds are taken up in the supercritical gas phase."

"This additional hindrance to being taken up in the supercritical gas phase cannot only be attributed to hydroxyl groups. A corresponding phenomenon is also observed if a 1:1 mixture of acetone and water is treated with supercritical ethylene at 20 C and 2340 psi. Here again, acetone is not discharged by the ethylene."

Zosel's explanation is generally accurate concerning the ratio of the hydrocarbon radical to the hydroxyl group. However, ethanol can be extracted from ethanol-water solutions by supercritical ethylene (Paulaitis, Gilbert, and Nash, 1981) and so can acetone from acetone-water solution (Elgin and Weinstock, 1959); a few such inaccuracies still do not detract from the vast amount of data that Zosel provides.

The first claim of the patent is also reproduced here because of its pedagogical value. What is claimed is:

"1. The process of separating a mixture which is in liquid state or solid state or liquid and solid state composed of a plurality of compounds at least one of which contains an organic group which comprises:

a. contacting said mixture with a gas phase preferentially taking up said compound containing an organic group at the contacting conditions, said gas phase during said contacting being maintained under supercritical conditions of temperature and pressure such that the gas takes up at least a portion of said compound containing an organic group, the temperature being in a range in which the quantity of said compound containing an organic group taken up by said gas phase varies inversely with said temperature, and effecting said contacting in a manner so that this occurs, and so that there is a substantial gas component that is identifiable as a gaseous component, the critical temperature of said gas phase being in the range of 0 – 200 °C, the temperature of said gas phase during said contacting being within about 100 °C above the critical temperature.

b. separating the gas phase in the form of said identifiable gaseous component loaded with said portion of the compound containing an organic group taken up during said contacting from any of the mixture not taken up by the gas phase while still maintaining supercritical conditions as aforesaid, thereafter separating at least part of the compound containing an organic group taken up, from the gas phase."

Note that the claim covers only the retrograde region of solubility behavior.

**SECTION 2**  
**Petroleum and other**  
**Fossil Fuels Separations**

- Auerbach, E. B., Process for treating, separating, and purifying oils, U.S. 1,805,751 (May 19, 1931).
- Sullivan, F. W., Jr., Solvent fractionation, U.S. 2,034,495 (Mar. 17, 1936).
- Lantz, V., Extraction process, U.S. 2,188,051 (Jan. 23, 1940).
- Pilat, S. and M. Godlewicz, Method of separating high molecular weight mixtures, U.S. 2,188,013 (Jan. 23, 1940).
- Lorenz, H. W. F., Apparatus for gaseous extraction, U.S. 2,194,708 (Mar. 26, 1940).
- van Dijk, W. J. D., Process for separating high molecular weight mixtures, U.S. 2,281,865 (May 5, 1942).
- Lewis, W. K., Process for treating hydrocarbons with light hydrocarbons, U.S. 2,284,583 (May 26, 1942).
- Katz, D. L. and T. H. Whaley, High pressure separation, U.S. 2,391,576 (Dec. 25, 1945).
- Leonard, R. E., Energy efficient process for separating hydrocarbonaceous materials into various fractions, U.S. 4,305,814 (Dec. 15, 1981).
- Gearhart, J. A., Solvent deasphalting, U.S. 4,239,616 (Dec. 16, 1980).
- Leonard, R. E., Supercritical process for producing deasphalted demetallized and deresined oils, U.S. 4,290,880 (Sept. 22, 1981).
- Roach, J. W., Fractionating coal liquefaction products with light organic solvents, U.S. 3,607,717 (Sept. 21, 1971).
- Gearhart, J. A., Process for separating bituminous materials with solvent recovery, U.S. 4,278,529 (Jul. 14, 1981).
- Roach, J. W., Process for separating bituminous materials, U.S. 4,279,739 (Jul. 21, 1981).
- Audeh, C. A. and T. Y. Yan, Supercritical selective extraction of hydrocarbons from asphaltic petroleum oils, U.S. 4,354,928 (Oct. 19, 1982).
- Poska, F. L., Supercritical tar sand extraction, U.S. 4,341,619 (Jul. 27, 1982).
- Warzel, F. M., Discharge of solids, U.S. 4,397,731 (Aug. 9, 1983).
- Kramer, G. M. and F. Leder, Paraffin isomerization in supercritical fluids, U.S. 3,880,945 (Apr. 29, 1975).
- Zosel, K., Process for the production of aluminum alkyl compounds, U.S. 3,597,464 (Aug. 3, 1971).
- Diaz, F. and J. H. Miller, Drying substantially supercritical CO<sub>2</sub> with glycerol, U.S. 4,478,612 (Oct. 23, 1984).
- Weeter, R. F., Method for producing carbon dioxide from subterranean formations, U.S. 4,235,289 (Nov. 25, 1980).
- Parrish, D. R., Method for enhanced oil recovery, U.S. 4,344,486 (Aug. 17, 1982).
- Paspek, S. C., Jr., Oligomerization of olefins in supercritical water, U.S. 4,465,888 (Aug. 14, 1984).
- Paspek, S. C., Jr., Upgrading heavy hydrocarbons with supercritical water and light olefins, U.S. 4,483,761 (Nov. 20, 1984).
- Coenan, H., R. Hagen, and E. Kriegel, Supercritical extraction and simultaneous catalytic hydrogenation of coal, U.S. 4,485,003 (Nov. 27, 1984).
- Zarchy, A. S., Process for producing high yield of gas turbine fuel from residual oil, U.S. 4,528,100 (Jul. 9, 1985).
- Stearns, R. S. and E. J. Hollstein, Coal extraction process, U.S. 4,192,731 (Mar. 11, 1980).

- Beggs, J. A., W. H. Corcoran, W. S. Fong, P. Pichaichanarong, P.C.F. Chen, and D.D. Lawson, Supercritical multicomponent solvent coal extraction, U.S. 4,388,171 (Jun. 14, 1983).
- Francis, A. W., Solvent extraction, U.S. 2,698,277 (Dec. 28, 1954).
- Roach, J. W., Recovery of organic solvents from liquid mixtures, U.S. 4,508,597 (Apr. 2, 1985).
- Peter, S., Process for the catalytic gasification of solid fluids with steam, U.S. 4,508,543 (Apr. 2, 1985).
- Zarchy, A. S., Supercritical fluid extraction and enhancement for liquid-liquid extraction process, U. S. 4,547,292 (Oct. 15, 1985).
- Auerbach, E. B., Process for treating, separating, and purifying oils, U.S. 1,805,751 (May 19, 1931).**

This is the oldest patent discussed in this appendix, which was filed in 1927. When we covered the propane deasphalting process in Chapter 7, we selected some paragraphs from a literature reference that accurately described the technical facets of the process as well as the excitement of the researchers who reported the results (Wilson, Keith, and Haylett, 1936). We have selected a few paragraphs from this patent for the same purpose; the patentee writes,

“An object of this invention is to disclose a process by means of which oils may be treated and purified without the use of distillation or chemical decomposition. Another object is to disclose a novel method of separating oils substantially in the order of molecular weights of constituent parts thereof.

“I have discovered that the various constituents of oils show a very definite solubility in liquid carbon dioxide, and consequently I have invented a process of separating oils. I have found that my process enables me to separate different oils from each other not only ... in accordance with chemical composition ... but in proportion to the molecular weight.”

Auerbach investigated fatty oils, terpenes, tar oil, resin oils, ester oils, etc., in an apparatus shown schematically on the patent front page. Oil is pressurized and supplied to an extractor where it is distributed through the header. CO<sub>2</sub> is pumped to the lower section of the extractor. During the counter current extraction sequence, the CO<sub>2</sub> dissolves the soluble constituents of the oil, and the undissolved constituents travel downward and pass through perforated plate and are discharged through the bottom of the extractor via a ball valve. The extract leaves the extractor vessel, is reduced in pressure, and is discharged into the separator where the CO<sub>2</sub> is vaporized and recycled. The separated oil is then recovered from the separator vessel as a “heavies” phase.

Many examples are given in the patent, and one is selected to show the separation of materials by molecular weight. The reader is reminded that in a homologous series of components, increasing viscosity is a measure of increasing molecular weight.

“5 kgs of mineral lubricating oil which had an original viscosity of 5.2 cps was treated with 15 kgs of liquid carbon dioxide. 0.5 kgs of oil with viscosity 2.2 cps was obtained from the carbon dioxide extract and the residual 4.5 kgs had a viscosity of 5.9 cps.”

**Sullivan, F. W., Jr., Solvent fractionation, U.S. 2,034,495 (Mar. 17, 1936).**

This patent describes results of extracting hydrocarbons with a mixture of two solvents, sulfur dioxide and CO<sub>2</sub>. Although the mixture is at conditions well below critical, the patent is included because it points out that liquid CO<sub>2</sub> was quite prevalently studied in the 1930s.

Liquid sulfur dioxide has been used in refinery operations since the 1920s. The patentee describes that in the fractionation of motor fuel stocks only about 25% yield of a high (97) octane fuel can be obtained with sulfur dioxide at an extraction temperature of -65 °C, about the lowest temperature that can be reached with SO<sub>2</sub> alone. However, extraction at a lower temperature with SO<sub>2</sub> alone does not improve the yield or the octane number. The invention is the use of a mixture of CO<sub>2</sub> and SO<sub>2</sub>. With a mixture of CO<sub>2</sub> and SO<sub>2</sub> over a range of 1:12 to 1:5, CO<sub>2</sub>/SO<sub>2</sub>, higher yields and/or higher octane number are achieved than with SO<sub>2</sub> alone.

**Lantz, V., Extraction process, U.S. 2,188,051 (Jan. 23, 1940).**

This patent (like several others on hydrocarbon processing that we discuss) cites the Auerbach process in the prior art. The discussion in the patent relates that the Auerbach process suffers from the requirement of substantial amounts of CO<sub>2</sub> to separate the oil constituents. The new process utilizes a light liquid hydrocarbon plus CO<sub>2</sub> as the "extractant." The oil to be separated is dissolved in the hydrocarbon and the CO<sub>2</sub> is dissolved in the oil-hydrocarbon solution to lower the dissolving power of the hydrocarbon and, thus, to precipitate the oil.

The patent teaches that high-pressure oil is mixed with a liquid hydrocarbon and with liquid CO<sub>2</sub>. The resulting mixture is conveyed to a phase separator where the light and heavy phases separate. The light phase consisting of CO<sub>2</sub>, hydrocarbon, and some light oil is withdrawn and pumped to another mixer where more hydrocarbon and CO<sub>2</sub> are added. The mixture is sent to another phase separator where another light phase and heavy phase form and are separated. The light phase consisting of CO<sub>2</sub>, hydrocarbon solvent, and the lightest components in the oil is sent to a flash pot where CO<sub>2</sub> is separated and returned to the storage vessel and the lightest oil-hydrocarbon stream is sent to a stripper where solvent is removed from the oil. The heavy phases leaving the two phase separators are processed identically to the lightest phase. A number of examples give results, and the patentee shows that with isopentane plus CO<sub>2</sub> a separation into fractions can be made with much less CO<sub>2</sub> than for the pure CO<sub>2</sub> case.

**Pilat, S. and M. Godlewicz, Method of separating high molecular weight mixtures, U.S. 2,188,013 (Jan. 23, 1940).**

On page 3 of the patent, the patentees write,

"We are aware of the U.S. patent to Auerbach, No. 1,805,751 disclosing the extraction of oil with liquefied CO<sub>2</sub>. However, our invention, as described, is directed to the method of fractionating mineral oils under conditions at which the gaseous CO<sub>2</sub> is incapable of being liquefied. When higher pressures are necessary to effect the desired fractionation, our process may be operated at temperatures which are above 31 °C, the



critical temperature of CO<sub>2</sub>." This is the earliest reference in the patent literature that we located on the use of supercritical (i.e., gaseous) CO<sub>2</sub> to separate hydrocarbons.

**Lorenz, H. W. F., Apparatus for gaseous extraction, U.S. 2,194,708 (Mar. 26, 1940).**

This patent is one that we have chosen to include for its historical and pedagogical value. Lorenz uses an extractor which is fed with gaseous solvent from the bottom and with feed at the top. The extract leaves at the top and the raffinate at the bottom. We present several statements that Lorenz writes about the workings of his gaseous solvent since these statements corroborate our statement solubility phenomena in supercritical fluids were not only known, but applied, many years ago.

"Before specifically describing my apparatus for continuous gaseous solvent extraction ... I desire to first elucidate the purposes of its use and to give a clear understanding of the subject and the principles involved ...

"Andrews proposed many years ago the use of the word 'gas' for a fluid at any temperature above its critical point ... For every 'gas' there is a certain temperature above which, no matter how high the pressure, it cannot be liquefied even under the greatest pressure ...

"'Gases' when under pressure, and especially high pressures, can possess a high solvent power ... even for bodies possessing little or no volatility the dissolving power may be considerable ..."

Lorenz goes on to relate the pressure dependent dissolving power, the ability to separate by molecular weight, the separation of phases, etc. He discussed the mixing of gases as a means of varying the solvent properties (in addition to changing temperature and pressure), and he relates "that it must also be kept in mind that the extract dissolved in the gaseous solvent has its effect markedly on the critical point of the gas mixture." He presents as two examples that by adding one drop of ethanol the critical temperature of a certain volume of chloroform is reduced 4 °C whereas its boiling point is reduced only 0.2 °C, and that the addition of the drop of ethanol to a volume of ethyl chloride raises the critical temperature 7 °C whereas the boiling point is raised only 1 °C. Many researchers ignore this effect of dissolving a liquid in a supercritical fluid. Although the solvent may enter an extractor at supercritical conditions, the solvent rich stream leaving the extractor is almost assuredly not supercritical.

**Van Dijk, W. J. D., Process for separating high molecular weight mixtures, U.S. 2,281,865 (May 5, 1942).**

The process described is somewhat similar to the propane deasphalting process. The first claim describes the use of a "low molecular weight treating agent in its paracritical state." Some of the patents have described paracritical to be slightly below the critical temperature; this one defines the state to be at a temperature above the critical temperature. The treating agent is used to dissolve a portion of a high molecular weight mixture and subsequently, in another step, the pressure is reduced to precipitate part of the extracted material.

Examples of separating vegetable oils, stand oil, and lubricating oil residues are given in the patent. In each case the first step in the process uses liquid propane (or some other low molecular weight treating agent) to dissolve part of the oils. The extract stream is raised in conditions to above the critical point before carrying out stage wise pressure reduction.

As we see again, the principles and applications of supercritical fluid solubility phenomena were quite well understood at the time of the filing of this patent, March 1936.

**Lewis, W. K., Process for treating hydrocarbons with light hydrocarbons, U.S. 2,284,583 (May 26, 1942).**

Warren K. Lewis and J. M. Whitely in an earlier patent, U.S. 2,202,389, which is not reviewed in this appendix, described a method for changing the solvent power of a solvent in the near critical liquid region by varying the pressure on the liquid. In this patent, varying the solvent power by varying pressure of a solvent above its critical temperature is the invention, and specifically a process for the separation of hydrocarbon oils using 2 to 6 carbon aliphatic solvents is described.

A figure given in the patent shows the operation of the process using propane as the solvent. Propane and oil are mixed in-line and are allowed to disengage in a vessel held at one specific temperature. The temperature is at or above the critical temperature of propane and the pressure is high enough to cause the desired oils, but not the asphalt, to dissolve. Asphalt is withdrawn from the bottom of the vessel.

The oil-propane solution is withdrawn from the top of the vessel, is expanded in pressure through a valve, and is sent to another vessel. Because of the reduction in pressure, the oil-propane solution loses its ability to dissolve the heavier fractions of the oil and part of the oil precipitates. The bottom layer of precipitated oil is removed from this second vessel, and the top phase is reduced in pressure again across another valve and is sent to a third vessel where another oil-rich phase is removed as a bottoms stream. The top phase from the third vessel is reduced in pressure to about the critical conditions of propane and is sent to a separation where propane and the remaining oil are separated. This process looks much like the ROSE process described in chapter 7.

**Katz, D. L. and T. H. Whaley, High pressure separation, U.S. 2,391,576 (Dec. 25, 1945).**

Many of us have previously seen P-T diagrams like the one supplied with this patent and have studied them in distillation and thermodynamics courses. Retrograde condensation is the phenomenon depicted. We were surprised to find that the information presented in the P-T diagram in this patent was the basis of a patent and thus we selected it for inclusion in this section. It is, again, of historical and pedagogical value to present selected phrases and paragraphs of the invention.

"The present invention accomplishes separation of a complex hydrocarbon mixture into fractions by taking advantage of the remarkable change in some of the physical properties of hydrocarbons when the pressure to which the hydrocarbons are subjected is above 800 lbs. per sq. in."

"The present invention effects a separation of hydrocarbon mixtures into fractions by taking advantage of the effects sometimes referred to as 'retrograde vaporization' and 'retrograde condensation.' These concepts are useful in explaining the theoretical and scientific background upon which the invention is based and will be discussed in detail hereinafter."

Katz goes on to present a detailed account of the phenomenon, and he gives a number of examples of separating oil and gas mixtures by applying the phenomenon. This patent like the Zosel patent is must reading; in this case it is not for the many examples described but for the fundamentals that Katz develops.

**Leonard, R. E., Energy efficient process for separating hydrocarbonaceous materials into various fractions, U.S. 4,305,814 (Dec. 15, 1981).**

Leonard, Garwin, Gearhart, and Roach are names that appear liberally in the next few patents. They invented many variations of the basic ROSE process for Kerr-McGee Corporation. After having discussed the basic ROSE process operation in Chapter 7, we have selected other variations of the process to serve as additional teaching tools.

The patent describes an energy efficient, multistep process for separating heavy hydrocarbons such as crude oil residuum, vacuum bottoms, etc., using separators called separation zones. The operation of the process is explained using as an example vacuum residuum consisting of asphaltenes, resins, and the desired oils. Vacuum resid is pumped to the first separation zone along with a solvent, e.g., pentane. The first zone is maintained at or above critical temperature and pressure of the solvent. A heavy phase is withdrawn and is introduced as feed into the second separation zone which is maintained at a temperature that is higher than in the first zone, and at about the same pressure as the first zone. In the second zone, the heavy feed separates into a light phase and a heavy phase consisting of an asphaltene concentrate. The light phase is withdrawn, recycled, and mixed with the feed to the first separation zone. The heavy asphaltene concentrate phase is withdrawn and is steam stripped.

The light phase from the first separation zone is introduced to a third separation zone that is maintained at a higher temperature than in the first zone. A light phase and a heavy phase consisting of resins and some solvent are formed in the third separation zone. The heavy phase from the third zone is withdrawn and introduced to a fourth separation zone which is maintained at a still higher temperature and at about the same pressure as the third zone. The feed to the fourth zone separates into a heavy phase and a light phase. The light phase from the fourth zone is recycled and mixed with feed. The heavy phase from the fourth zone is steam stripped.

The light phase from the third zone is passed to a fifth separation zone. The temperature level in the fifth zone is higher than in the third zone and the feed separates into a light phase and a heavy phase. The light phase from the fifth zone is recycled and mixed with the feed, and the heavy phase from the fifth zone, which is the desired oil fraction, is steam stripped.

The example described shows that the method of operation of the invention results in an energy savings of 20% relative to the method of flashing the first and third heavy phases to recover the solvent.

**Gearhart, J. A., Solvent deasphalting, U.S. 4,239,616 (Dec. 16, 1980).**

The background of this patent is quite extensive in describing variations of solvents and conditions which have been invented both by the assignee and others to produce separated fractions of a heavy hydrocarbon feed. The use of pentane, for example, results in a higher yield of desirable product than does the use of propane, but with pentane more undesired resinous bodies are present in the product.

One method to reduce the resins in the oil product is to employ some countercurrent extraction during the separations steps and the countercurrent contacting is the invention. In the particular embodiment described in this case, a portion of the asphaltenes from a first separation zone is fed to a second separation zone in countercurrent extraction with the light oils (and resins) phase leaving the first separation zone. The countercurrent contact scrubs more of the resins from the oils in the second separation zone and results in a resin free oils fraction leaving the third separation zone.

**Leonard, R. E., Supercritical process for producing deasphalted demetallized and deresined oils, U.S. 4,290,880 (Sept. 22, 1981).**

This patent is included to point out the similarity and difference of this invention with the invention in the previous patent. The invention is as it was in the previous patent is the reduction of resins in the oils using a countercurrent contact in one of the separation zones. In this invention the reduction is accomplished slightly differently. Resins from a second separation zone are recycled and fed countercurrent to the oils stream. (Recall in the previous patent, the asphaltenes were fed countercurrent to the oils stream). In both cases, the resins in the oils leaving the second separation zone are reduced although the patent doesn't say which of the processes, if any, is the superior one.

**Roach, J. W., Fractionating coal liquefaction products with light organic solvents, U.S. 3,607,717 (Sept. 21, 1971).**

Three major objectives of the new coal liquefaction process are described. They are to provide a novel method of separating coal liquefaction products into a plurality of products wherein the solvent may be recovered directly from the final fractionating stage, to provide a novel process for liquefying coal employing selected light organic solvents, and to provide a novel method of separating finely divided insoluble materials derived from coal during liquefaction.

We have discussed the first two objectives, the separation and fractionation of many chemicals, and, thus, the parts of this patent dealing with the first two objectives will not be elaborated upon here. The third objective, however, employs another of the properties of a near critical or supercritical solvent, viz., its low viscosity, to effect a sedimentation of particulates from what would, in the absence of the supercritical fluid, be a very viscous liquid.

The coal extraction process is described using a liquid solvent at high pressure and subcritical temperature. There is another figure on the second page of that patent that describes a deashing step that includes the separation of material matter in the coal and a subsequent fractionation by successive pressure and temperature change. A heavy phase and a light phase form during the first pressure and temperature adjustment of the solvent

and extract that results in the separation of ash particulates. It is theorized in the description of the invention that some of the coal liquefaction products coat the micron-sized ash particles causing them to agglomerate and settle in the low viscosity heavy phase. The heavy phase viscosity is low because the supercritical fluid has dissolved in it. The light phase leaving the deasher is essentially ash-free and the ash containing heavy phase is removed. The light phase continues through the fractionation train where successive pressure and temperature changes brings about successive fraction recovery.

**Gearhart, J. A., Process for separating bituminous materials with solvent recovery, U.S. 4,278,529 (Jul. 14, 1981).**

The prior art discussion presented in the patent describes a problem that is experienced in the operation of bituminous material extraction when the process is operated "normally," i.e., a supercritical extraction followed by pressure reduction. Pressure reduction through a pressure reduction valve results in the formation of a fine mist that solidifies, emulsifies, and settles out in subsequent parts of the process eventually causing disruption of operation.

In the new process, other separation zones are added after the normal first separation zone. The heavy phase from the first zone is sent to a stripper and the vaporized solvent, steam, and fine mist particles are withdrawn from the top and are conveyed to the second separation zone. In the second separation zone, the stream consisting of solvent, steam, and mist particles flow through a circuitous path where it is contacted countercurrently with a stream of light oil which scrubs the asphaltene and resin mist from the solvent. A portion of the light phase oil containing asphaltenes and resins is recycled to the second separation zone or it can be recycled to the first separation zone. The solvent and steam mixture leaving the second zone is conveyed to a solvent condenser and water separation zone. No emulsification problems are experienced because the mist particles have been removed in the first separation zone.

**Roach, J. W., Process for separating bituminous materials, U.S. 4,279,739 (Jul. 21, 1981).**

The prior art discussion in this patent also refers to the problem of mist formation when the heavy phase leaving the first separation zone is decreased in pressure. In the "normal" operation a portion of the bituminous material introduced into the steam stripper is carried out as a fine mist which solidifies and forms a water emulsion that subsequently settles within the process apparatus resulting in eventual plugging and disruption of the process.

This patent describes another method for removing the mist that is carried into the stripper. A third separation zone is added downstream of the solvent condenser to eliminate the problem. The third separation zone in this process variant is a conical vessel which allows the particulates to settle and be removed from the solvent. This patent does not say which variant, this one or the previous one, is more efficient, but note that this patent and the previous one were both filed on the same day. Incidentally, there exists at least a score of other Kerr-McGee patents that we do not discuss in the appendix.

**Audeh, C. A. and T. Y. Yan, Supercritical selective extraction of hydrocarbons from asphaltic petroleum oils, U.S. 4,354,928 (Oct. 19, 1982).**

The process concept involves the extraction of light hydrocarbon oils from asphaltic petroleum supercritical solvents followed by a subsequent fractionation and separation of the oil from the solvent. It is stated that the metal compounds which are present in the asphaltic petroleum do not dissolve in the solvent under the conditions of operation. The primary difference claimed for this new process relative to the old processes is that the solvent is "at or above" the critical temperature rather than below the critical temperature as is described in prior art. The operation is explained in the patent with the aid of a simple distillation-like extraction vessel. Asphaltic feedstock is heated and introduced into the extraction vessel. The solvent is also heated and introduced into the vessel and the two streams are mixed. The temperature is maintained at or above the critical temperature of the solvent. In the extractor, the non-soluble components of the feed settle and are removed and sent to a stripper to recover and recycle the solvent. Several examples give quantitative information when an asphaltic feedstock containing 28 ppm Ni, 220 ppm V is used. The oil yield and metal content results are given below for two cases where the solvent is catalytic cracker gasoline and propane, respectively.

	<u>Example 1</u>	<u>Example 2</u>
	Cat Cracker Gasoline	Propane
Solvent/Oil Ratio	2:1	6:1
Temperature, °F	725	175
Pressure, psig	650	500
<u>Deasphalted Oil</u>		
Yield, wt%	75	68
Ni/V, (w-ppm)	2/12	3/22
<u>Asphalt</u>		
Yield, wt%	26	31

Based upon the data in the table, the statement is made that the new invention using a solvent "at or above its critical point" provides improved yields and metal reduction relative to liquid propane extraction. It is not surprising that supercritical gasoline (at 725 °F) gives different results than liquid propane (at 175 °F) does; we've already seen the wide difference in results with two closely related solvents, such as liquid propane (for propane deasphalting) and liquid butane (in the Kerr-McGee ROSE process). We expect even wider differences between supercritical gasoline and liquid propane which have huge differences in critical temperatures. A more appropriate comparison to evaluate the advantage of the invention would have been to obtain results with liquid gasoline at the same reduced temperature (0.96) as the liquid propane in Example 2.

**Poska, F. L., Supercritical tar sand extraction, U.S. 4,341,619 (Jul. 27, 1982).**

The invention described in this patent is the combination of using a supercritical fluid to dissolve the desired components from tar sands and to recover regeneratively heat from the tar free sand leaving the extractor. Tar sands are fed to an extractor where they are contacted countercurrently with supercritical aromatic solvents such as benzene, toluene, or other substituted benzenes, or with supercritical cycloaliphatic solvents such

as cyclohexane, decalin or straight chain aliphatics. The extract phase leaving the extractor is reduced in pressure and sent to a flash unit for separation of the bitumin. The light phase leaving the flash unit is condensed and sent to another flash unit for separation of light hydrocarbons from the solvent. Both the solvent and the light oil are recycled to the extractor. The hot tar-free sand is passed through a recuperative heat exchanger where the extractant is heated. The sand is discharged through a valve which as the patent states can be a star valve, a screw conveyer, or a "pressure drop channel." Such a "pressure drop channel" is described in the next patent.

**Warzel, F.M., Discharge of solids, U.S. 4,397,731 (Aug. 9, 1983).**

This patent describes the valve that was used in the previous patent to discharge the dry sand from the tar sands extractor. A mixture of solids (the sand) and solvent (which is used to extract the hydrocarbon values from the tar sands) enters the discharge system at the top. The composition at this point is about 50/50 solids/solvent. For the particular case discussed (and this is a calculated case), the solids flow is 140,000 lb/hr, and the dimensions of the conduit is 13.5 in I.D. and 150 ft long. Pressure at the top is about 1,500 psi. Pressure measurement/transmitter devices send a signal to a controller which regulates the opening and closing of the solids throttle located at the bottom of the valve. The hydraulic system operating from the pressure signals actuates the throttle which can operate at a pressure drop of 1,500 psi.

We wonder if this concept was ever tested experimentally in the laboratory.

**Kramer, G. M. and F. Leder, Paraffin isomerization in supercritical fluids, U.S. 3,880,945 (Apr. 29, 1975).**

The invention of operating in the supercritical region, which is described in some detail in Chapter 11, is best shown by comparing operation at supercritical conditions versus operation at liquid conditions. In one example hexane is reacted at 40 °C and 1 atm for 60 min in the presence of methyl tertiary amylether, which is a promoter, and aluminum bromide, which is a catalyst. In another example the same ratio of hexane to promoter and catalyst is charged to an autoclave and CO<sub>2</sub> is added at a ratio of 500 g of CO<sub>2</sub> to 86 g hexane, to form a homogeneous phase. In both cases about 30-35% of the hexane cracked and isomerized to other products. However, in the case of the reaction with liquid hexane, the ratio of isomerization to cracking was 1:1. In the supercritical reaction isomerization was predominant at 5:1. In another example it was described that hydrogen was added to reduce cracking. Hydrogen was found to be miscible in the supercritical phase whereas it has only limited solubility in liquid hexane so that a higher concentration of hydrogen can be achieved in the supercritical reaction. The cracking reactions were virtually eliminated and conversion to isomerizates was 90% when the reaction was carried out with hydrogen added to the supercritical phase.

**Zosel, K., Process for the production of aluminum alkyl compounds, U.S. 3,597,464 (Aug. 3, 1971).**

This patent predates, both in filing and in issue, the "big" Zosel patent described first in this appendix. There are many anecdotal stories, perhaps some apocryphal, that have circulated about the aluminum alkyl work carried out at the Max Planck Institut für Kohlenforschung in Mulheim (Ruhr), Germany. It was found during the aluminum alkyl synthesis studies that supercritical ethylene could separate aluminum trialkyls and olefins by carbon number.

The disclosure section gives an excellent summary of the invention and of the chemistry of the reactions which produce the alkyl aluminum mixtures. A hydrogen dialkyl aluminum can react with alpha olefins to form long chain hydrocarbons in the range of C<sub>1</sub> to C<sub>3</sub>. (Ziegler catalysis mechanisms are in operation during the growth of the chain, and Ziegler, himself, was actively engaged in catalysis research at the Max Planck Institute during the period of Zosel's work.) The long chain hydrocarbon can subsequently be split from the aluminum alkyl compound to produce long-chain-length, alpha olefins. It is also possible to oxidize the aluminum alkyl compounds to alkoxides and, by hydrolysis, to obtain long chain fatty alcohols. The process that is described in the patent employs supercritical fluids to separate the mixture of many trialkyl aluminum compounds that are formed during the process.

One mode of operation is described here. A batch extractor is charged with the mixture to be separated. Gas is passed through the charge and the extract phase passes overhead to a rectifying. The process operates in the retrograde condensation region. Thus, a "hot finger" causes some of the heavier components to precipitate. Part of the condensate can be withdrawn and the remainder is refluxed back to the extractor. The depleted gas stream is lowered in pressure and temperature to liquid conditions and passed into a separator. The liquefied gas is vaporized and recycled via a compressor and the product is withdrawn.

Operating with supercritical ethane over an increasing pressure range from 75 to 100 atm, 50 °C in the extractor and 98 °C at the hot finger, a mixture consisting of 1.5 liters hexadecene, 1.5 liters octadecene, 5.2 liters eicosene and higher, and 1.55 liters tridodecyl were separated into 1 liter of pure hexadecene, 1 liter of an intermediate fraction, 1 liter of octadecene and 3 liters of a mixture up to C<sub>30</sub>-ene. The olefins contained no aluminum alkyls. About 1 liter of a fraction containing some higher olefins and some tridodecyl aluminum, and 1.2 liters of pure aluminum tridodecyl were also separated.

**Diaz, F. and J. H. Miller, Drying substantially supercritical CO<sub>2</sub> with glycerol, U.S. 4,478,612 (Oct. 23, 1984).**

Supercritical CO<sub>2</sub>, which is being used for enhanced oil recovery, is quite plentifully available in many subterranean formations. However, these formations are usually found far from oil fields, and thus, the CO<sub>2</sub> must be conveyed to the fields by pipeline. CO<sub>2</sub> as it comes from the ground is usually wet, and is thus quite corrosive to transmission lines. An ACS monograph (Quinn, E.L. and C.L. Jones 1936. Carbon Dioxide, Chap. 4. Reinhold Publishing Corp., New York.) gives data on pH in a water solution as a function of pressure which is partially reproduced in the following table.



**CO<sub>2</sub> Pressure - pH Relationship at 20 °C**

Pressure of CO <sub>2</sub>	pH of water in equilibrium
350 ppm (in air)	5.7
1mm	5.4
10 mm	4.8
100 mm	4.3
1 atm	3.8
10 atm	3.3
100 atm	3.0

A pH of 5.7 results from an equilibrium with laboratory air. At high CO<sub>2</sub> pressure, the pH of the water levels out at about 3.0 which is quite corrosive to carbon steel. To reduce the corrosiveness of the supply stream it is desired to dry the CO<sub>2</sub>.

The background section of the patent gives a discussion of various compounds that have been used to dry high pressure CO<sub>2</sub>. Although triethylene glycol (TEG) has primarily been used to dry CO<sub>2</sub>, it exhibits appreciable solubility in CO<sub>2</sub> at pipeline conditions. A high level of solubility can result in substantial loss of the drying agent.

Glycerol has a substantially lower solubility in CO<sub>2</sub> as shown in an accompanying graph of glycerol solubility in the patent. The invention is the use of glycerol for drying wet, supercritical CO<sub>2</sub>.

The examples given in this patent are quite interesting because they are described in "dollars and cents" advantages. For instance, Example 2 states that the cost of TEG lost in drying 400 million cubic feet/day of CO<sub>2</sub> at 1,200 psi and 25 °C is \$40,000,000/yr (!) whereas when glycerol is used, the cost of dessicant lost is only \$300,000.

**Weeter, R. F., Method for producing carbon dioxide from subterranean formations, U.S. 4,235,289 (Nov. 25, 1980).**

The previous patent was concerned with drying CO<sub>2</sub> before transmission to oil fields. This patent describes one method for pumping supercritical CO<sub>2</sub> from subterranean formations to the surface. The background relates that CO<sub>2</sub> from a production well that reaches the surface under its own motive force arrives in a two-phase state. Pumping such a mixture over long distances and varying elevations can create fluid "hammer" effects which can cause serious damage to pipelines and related equipment and can result in considerable power loss.

It is the object of this invention to transport CO<sub>2</sub> to the surface in a single, supercritical phase. This is accomplished by positioning a pump within a producing well to boost the pressure to the critical pressure. The pump must account for the amount of CO<sub>2</sub> pressure lost due to static head and the pressure loss due to friction in flowing the CO<sub>2</sub> to the surface.

The patentee describes a proposed field application and gives the conditions of the CO<sub>2</sub> at various positions in two situations. The first situation is if the CO<sub>2</sub> flows to the surface under its subterranean formation pressure and the second is if the improved process is in operation. In subterranean formation CO<sub>2</sub> is found at conditions of 2,400 psig and 75 °C. If it were to flow to the surface unaided, it would arrive at 835 psig and 20 °C. If a pump is placed downhole at an appropriate distance, the CO<sub>2</sub> can be brought to the surface in a supercritical state. In the specific case discussed, "downhole" is at a depth of

6,000 ft with the CO<sub>2</sub> located at a depth of 6,500 ft. CO<sub>2</sub> reaches the pump at conditions of 1,890 psig and 64 °C, and it is boosted by 739 psig (an amount that may change depending upon the amount of contaminants, such as nitrogen, in the CO<sub>2</sub>) with concomitant temperature increase of 13 °C. In its flow to the surface a static head of 1,254 psig and flow losses of 75 psig are experienced. The CO<sub>2</sub> arrives at the surface at approximately 1,300 psig and 38 °C, i.e., supercritical. The CO<sub>2</sub> is then sent to a central collection station and is pumped to an oil field. The next patent describes what is done with CO<sub>2</sub> containing contaminants.

**Parrish, D. R., Method for enhanced oil recovery, U.S. 4,344,486 (Aug. 17, 1982).**

Although this patent on enhanced oil recovery immediately follows the one describing the production of supercritical CO<sub>2</sub>, the two processes are usually carried out in locations separated by hundreds of miles because the oil fields are usually not located next to CO<sub>2</sub> "wells." This patent relates that subterranean CO<sub>2</sub> is often not pure and is found in conjunction with light hydrocarbons and hydrogen sulfide. In order to take full advantage in enhanced oil recovery operations the CO<sub>2</sub> must be purified. Adsorption and cryogenic and membrane separation have been used to carry out the purification. The new invention is the combustion of the hydrocarbon and hydrogen sulfide-containing CO<sub>2</sub> from an underground formation with oxygen enriched gas to form a concentrated CO<sub>2</sub> stream. This stream is then used for enhanced oil recovery.

**Paspek, S. C., Jr., Oligomerization of olefins in supercritical water, U.S. 4,465,888 (Aug. 14, 1984).**

The patentee finds that short chain olefins dissolved in near critical or supercritical water oligomerize without the need of a catalyst. The patentee proposes an explanation of the findings.

"...it is believed that the water-containing medium functions as a catalyst, a reactant, and as a means to control the rate of reaction and rate of heat transfer from the system. As a catalyst, the water-containing medium moderates both free radical and ionic mechanisms. As a reactant, supercritical water is a donor of hydrogen for saturating double bonds. This is evidenced by the resulting liquid hydrocarbons being largely paraffinic and the existence of carbon monoxide and CO<sub>2</sub> in the gaseous effluent from the reactor. Since water is a donor of hydrogen, no externally supplied hydrogen is required for the instant process."

"It is also theorized that in the instant process, there are two competing reactions, the oligomerization of olefins into liquids and the thermal degradation of paraffinic liquids into saturated gases. The water-containing medium appears to suppress the thermal degradation reaction and there appears to be an upper limit on the extent of oligomerization in the instant process. The normally liquid hydrocarbons produced by the instant process contain 4 to 20 carbon atoms and nearly all the saturated hydrocarbons. These products are also highly branched."

The patentee gives five examples that varied pressure, temperature, olefin, and water to olefin ratio. For example, when a 4:1 ratio of water to ethylene was reacted at 427 °C and 4,960 psig for 1 hr, a 72% yield of light liquids was obtained with no coke or oil formation.

**Paspek, S. C., Jr., Upgrading heavy hydrocarbons with supercritical water and light olefins, U.S. 4,483,761 (Nov. 20, 1984).**

This invention by Paspek is the cracking of heavy hydrocarbons in a mixture of supercritical water and light olefins (up to C<sub>5</sub>), and it follows by a few months the previously discussed patent on the oligomerization of olefins in supercritical water. It is reported that the presence of olefins in the reaction mixture reduces gas formation during cracking because of equilibrium considerations. Additionally, olefins increase the yield of light liquids by reacting and combining with thermally cracked fragments and by oligomerizing to liquid range products. It is found that the cracking reactions occur at highest yield in a solvent which can donate a hydrogen to a double bond. Preferred solvents are water, alcohols, and their mixtures.

Three comparative examples taken from the patent verbatim delineate the yield improvement if the invention is practiced.

Example A

"Water and shale oil (W/O ratio = 2) were reacted in an autoclave at 425 °C and 4,750 psig for 60 min. The product distribution was 75 wt% distillate (the desired product), 5 wt% gas, and 2 wt% coke."

This example did not practice the invention.

Example B

"Shale oil and ethylene (E/O ratio = 0.27) were loaded into the autoclave, and reacted at 425 °C and 990 psig for 60 min. The product distribution was 71 wt% distillate, 10 wt% gas, and 31 wt% ."

This example also does not practice the invention.

Example 1

"Water and oil (W/O ratio = 2) was loaded into an autoclave, and ethylene was added to an E/O ratio = 0.2. Reaction was carried out at 425 °C and 4,901 psig for 60 min. The product distribution was 83 wt% distillate, 0 wt% gas, 2 wt% coke."

This example shows the benefits of cracking heavy hydrocarbons in the supercritical water-ethylene solvent.

Although it is not possible to close the material balance in all examples, the overall results show that the presence of olefins in the supercritical water enhances the yield of distillate.

**Coenan, H., R. Hagen, and E. Kriegel, Supercritical extraction and simultaneous catalytic hydrogenation of coal, U.S. 4,485,003 (Nov. 27, 1984).**

Coal is comminuted, mixed with water, and the slurry mixed with oil which is also supplied with catalyst. The coal-water-oil-catalyst mixture is conveyed to the extractor/reactor where the pressure and temperature are maintained at about 350 bar and 500 °C for a reaction period of 40 min resulting in a supercritical water phase containing organic compounds and a coal residue. The rest of the flow sheet depicts condensation, rectification of oil fractions, separation of gases, gasification of coal residue, and recycle of some oil.

The description relates that it is desirable to use a concentration of 0.001 to 0.5 wt% catalyst dissolved in the supercritical water. The catalysts are listed in the abstract.

**Zarchy, A. S., Process for producing high yield of gas turbine fuel from residual oil, U.S. 4,528,100 (Jul. 9, 1985).**

The process described employs two extraction steps and two solvents to produce a high yield of low metals oil which is then suitable for use as a gas turbine fuel. The patentee relates that about 50% of the vanadium is present in residual fuel oil as a vanadyl porphyrin and the invention makes use of the relative solubilities of hydrocarbons and vanadyl porphyrin.

Residual oil and supercritical CO<sub>2</sub> (the preferred solvent, but hexane, propane, butane, etc., may be employed) are supplied to the first extraction vessel where 80-85 wt% of the oil is extracted and about 20-25% of the vanadium present in the residual oil appears in extract leaving the extractor. The asphaltine phase comprises 15-20 wt% of fuel, and it contains 70-85% of the vanadium. The asphaltine phase and supercritical CO<sub>2</sub> (the preferred solvent) are supplied to the second extractor and a second extract is produced. The patentee relates that the extract from this second extractor contains 99% of the vanadium present in the feed to the extractor, but he doesn't tell us the percentages of the two streams leaving the extractor. He also doesn't tell us the conditions to carry out this separation.

**Beggs, J. A., W. H. Corcoran, W. S. Fong, P. Pichaichanarong, P. C. F. Chen, and D. D. Lawson, Supercritical multicomponent solvent coal extraction, U.S. 4,388,171 (Jun. 14, 1983).**

Described in this patent are the relation of solvent molecule size and the ability to penetrate a coal structure on the yield of extract. A small molecule may not be a good solvent for the coal but it can penetrate the coal structure. By contrast, a large molecule may be a good solvent but it probably would not be able to penetrate into small pores.

The patent presents data on the yield of material derived from coal are presented which demonstrate the use of a binary solvent mixture consisting of a minor amount of a solvent with a molecular diameter small relative to the average pore size of the coal in admixture with a good solvent with large diameter. Furthermore, an optimum ratio of the two solvents is shown. As an example, presented here are the yield data from extracting an Illinois No. 6, high-volatile, bituminous coal with mixtures of methanol and toluene. Extraction conditions were 2,000 psig, 360 °C.

**Yield data for the extraction of coal with methanol/toluene mixtures.**

Volume Ratio, MeOH/Toluene	Weight Loss of Coal (wt%)
0/100	16.4
2/98	17.4
5/95	19.0
10/90	16.6
16/84	14.4
20/80	10.5

**Stearns, R. S. and E. J. Hollstein, Coal extraction process, U.S. 4,192,731 (Mar. 11, 1980).**

The invention in this patent is the use of a supercritical fluid extractant consisting of a mixture of from 50 to 75 wt% tetralin and correspondingly from 50 to 25% xylene. The examples give results of comparative coal extraction tests using xylene, tetralin, and the xylene-tetralin mixture. Extraction conditions in all tests were 425 °C and 1,250 to 1,350 psi. With pure xylene as the extractant, the conversion of coal to useful products was found to be only 24%. With pure tetralin, the conversion was high at 65%, but separation of undissolved particulates which were reduced to the form of powder was difficult. A 50-50 xylene-tetralin mixture gave a high conversion, about 40-60%, and, additionally, the separation of particulates was found to be quite easy.

One other example showed that the tetralin/xylene mixture in the supercritical state was required. A test carried out in the liquid region at 300 °C and 250 psi gave a conversion of only 9%. A temperature of 300 °C is quite low relative to the 425 °C tests described above. It would have been more informative to carry out the test at about 10 °C below  $T_c$  and at least the mixture vapor pressure. At these subcritical conditions it would have been possible to determine if there is any difference between yields with strictly supercritical xylene-tetralin and a "very hot" liquid xylene-tetralin mixture. As with previously described patents, quite specific and irrelevant tests are compared for the purpose of showing that the invention is superior to other methods of operation.

**Francis, A. W., Solvent extraction, U.S. 2,698,277 (Dec. 28, 1954).**

We would be remiss if we did not include at least one of Francis' many patents on the use of liquid CO<sub>2</sub> in separating hydrocarbons. Francis cites, among others, Lantz's patent (U.S. 2,188,051) ... the prior art, and he states that the process described in that patent is not a simple extraction but a precipitation. Francis also makes use of CO<sub>2</sub> in conjunction with another solvent to separate oils, but in a different manner. Whereas in the Lantz process the hydrocarbon solvent is completely miscible with the oil, Francis selects solvents that are not completely miscible with the oil. But in both processes, the solvent is miscible with CO<sub>2</sub>. Francis finds that CO<sub>2</sub> and the solvent in admixture exhibit a greater dissolving power for the oil than the solvent alone.

A ternary diagram given on the front page of the patent is used to describe the results in one of the examples that Francis presents. Excerpting from his discussion,

"Figure 1 reveals that furfural and liquid CO<sub>2</sub> are completely miscible, that furfural has a low solvent power for the oil, and that liquid CO<sub>2</sub> has a low solvent power for the oil. The solubility of oil in furfural is 3% as indicated by point f of Figure 1. The solubility is increased to about 16% at i, by adding about 60% of liquid CO<sub>2</sub> in the solvent mixture. A system s is assembled with about 30% oil, 20% furfural and 50% CO<sub>2</sub>; this separates into two layers, e (upper) an extract layer, and r (lower) a raffinate layer."

"Following separation of layers e and r and release of CO<sub>2</sub> (to E and R, respectively), about 80% of the oil dissolved in the extract layer e is separated (at the top), leaving a dilute furfural solution f which is recycled without distillation. The only furfural which need be recovered by distillation or by other means is the relatively small amount dissolved in the raffinate R, and the small amount dissolved in the second oil layer (the extract-raffinate); about 2% of furfural is present in each of such layers. This represents a saving of about 90% in distillation requirements over conventional furfural extractions."

**Roach, J. W., Recovery of organic solvents from liquid mixtures, U.S. 4,508,597 (Apr. 2, 1985).**

This patent is the most recent one located that is assigned to Kerr-McGee and is another variation of extraction of heavy hydrocarbons and coal liquids. The patent is included for discussion here because it relates some difficulties with the heavy hydrocarbon extraction-solvent separation in other supercritical fluid extraction processes. Those of us who have carried out such extractions are all too familiar with the problem described. For example, when a heavy hydrocarbon is extracted with supercritical pentane, for example, a light phase and a heavy phase are formed. The heavy phase is usually subsequently freed of its solvent by a depressurization and steam stripping step. During the process of steam stripping and as the solvent is increasingly removed, the viscosity of the asphalt-bituminous material (the heavy phase) increases, and the high viscosity renders the mixture difficult to strip of its solvent vestiges.

The invention is a method to facilitate recovery of the solvent from the asphalt or solvent refined coal. The heavy phase from a supercritical extraction is heated to lower the solution viscosity and it is sent to a high shear mixer where it is admixed with steam. The intimately-contacted mixture is then conveyed to a solvent separation vessel. The solvent-steam mixture is withdrawn from the separator and sent to a condenser and solvent-water separator. The heavy liquid phase from the solvent separation vessel is withdrawn and sent to storage.

**Peter, S., Process for the catalytic gasification of solid fluids with steam, U.S. 4,508,543 (Apr. 2, 1985).**

This process employs supercritical water to dissolve a catalyst such as alkali or alkaline earth salts and hydroxides. The water-catalyst mixture is expanded to a lower pressure level to nucleate the catalyst to a fine mist (or, if precipitation does not occur, to form an "oversaturated" solution), and this mist is contacted with a coal or coke bed at a temperature of about 850 °C to convert the coal to gaseous compounds.

The results from one example best describe the invention. As a control, pit coke, formed by heating pit coal to 700 °C, was reacted with steam at 140 bar and 850 °C. The product gas, which was 2.4 standard liters per liter of coke, consisted of 55% H<sub>2</sub>, 11% methane, 4% CO, 30% CO<sub>2</sub>. In a second experiment, pit coke was impregnated with potassium carbonate and reacted at the same conditions as given above. The product yield and analyses were about the same as for the previous test. In a third experiment, steam at 300 bar and 500 °C was mixed with potassium carbonate solution, was reduced in pressure to 140 bar, and this stream was reacted with pit coke at 850 °C. The product was 5.8 liters of gas with composition 56% H<sub>2</sub>, 11.5% methane, 2% CO, 30.5% CO<sub>2</sub>. The results show that dissolving the potassium carbonate and subsequently nucleating it in the gas phase gives a higher yield of gas than either the control or the solution treated coal.

**Zarchy, A. S., Supercritical fluid extraction and enhancement for liquid-liquid extraction process, U. S. 4,547,292 (Oct. 15, 1985).**

The review of the inventor's previous supercritical fluid patent was in the first edition of this book (page 318; U. S. 4,528,100) and is included in this edition also. After reading this patent we conclude that, like the first one, this is a paper construction patent. We point out some flaws in logic in the instant patent, notably that light hydrocarbons can be separated from CO<sub>2</sub> by simple pressure reduction. As in many of the patents we have seen, this one has no quantitative data in the examples, so we shall discuss the flow sheet as quantitatively as possible without data.

In a first step of the process propane, butane, pentane, or hexane is used to extract vanidyl porphyrins from residual oil. The liquid extract of hydrocarbon and porphyrins is next subjected to supercritical CO<sub>2</sub> extraction between 90 and 130 °F and 1,075 to 8,000 psi. At almost all combinations of these pressures and temperatures the C<sub>3</sub> through C<sub>6</sub> paraffins are miscible in CO<sub>2</sub>. With a supercritical extraction column we wonder what ratio of CO<sub>2</sub>-to-extract would result in purified oil and what happens to the vanidyl porphyrins. In the process diagram and description, the supercritical CO<sub>2</sub>-liquid solvent extract is expanded to an unspecified different pressure and temperature. But, it is important to relate that pentane and hexane are miscible with CO<sub>2</sub> at room temperature and 800 psi so that the expansion would have to be to conditions higher in temperature and lower in pressure to separate CO<sub>2</sub> and hexane. For propane the miscibility conditions extend to much lower pressure and so the separation of propane from carbon dioxide becomes problematic.

## SECTION 3

### Coffee Decaffeination

- Zosel, K., Process for recovering caffeine, U.S. 3,806,619 (Apr. 23, 1974).
- Roselius, W., O. Vitzthum, and P. Hubert, Method for the production of caffeine-free coffee extract, U.S. 3,843,824 (Oct. 22, 1974).
- Vitzthum, O. and P. Hubert, Process for the decaffeination of raw coffee, U.S. 3,879,569 (Apr. 22, 1975).
- Vitzthum, O. and P. Hubert, Process for the manufacture of caffeine-free black tea, U.S. 4,167,589 (Sep. 11, 1979).
- Roselius, L., H. A. Kurzhals, K. F. Sylla, and P. Hubert, Process of extracting stimulants from coffee, U.S. 4,168,324 (Sep. 18, 1979).
- Prasad, R., M. Gottesman, and R. A. Scarella, Decaffeination of aqueous extracts, U.S. 4,246,291 (Jan. 20, 1981).
- Zosel, K., Process for the decaffeination of coffee, U.S. 4,247,570 (Jan. 27, 1981).
- Margolis, G. and J. Chiovini, Decaffeination process, U.S. 4,251,559 (Feb. 17, 1981).
- Roselius, L., H. A. Kurzhals, and P. Hubert, Method for the selective extraction of caffeine from vegetable materials, U.S. 4,255,458 (Mar. 10, 1981).
- Jasovsky, G. A. and M. Gottesman, Preparation of a decaffeinated roasted coffee blend, U.S. 4,255,461 (Mar. 10, 1981).
- Zosel, K., Process for the decaffeination of coffee, U.S. 4,260,639 (Apr. 7, 1981).
- Roselius, W., O. Vitzthum, P. Hubert, Method of extracting coffee oil containing aroma constituents from roasted coffee, U.S. 4,328,255 (May 4, 1982).
- Katz, S. N., Method for decaffeinating coffee, U.S. 4,276,315 (Jun. 30, 1981).
- Peter, S. and G. Brunner, Process for decaffeinating coffee, U.S. 4,322,445 (Mar. 30, 1982).
- Zosel, K., Process for the direct decaffeination of aqueous coffee extract solutions, U.S. 4,348,422 (Sept. 7, 1982).

**Zosel, K., Process for recovering caffeine, U.S. 3,806,619 (Apr. 23, 1974).**

This patent is chronologically the first in the quite long list of patents on supercritical fluid processing of coffee. It describes along with supercritical extraction of green coffee a means of obtaining crystallized caffeine from the CO<sub>2</sub> stream. In summary of the operation of the process, CO<sub>2</sub> leaving the compressor is saturated with water and is passed through the bed of moistened, green coffee beans. The CO<sub>2</sub> stream that contains the caffeine extracted from the beans leaves the coffee bean bed and is recirculated to the water pool in a separate vessel. The caffeine is extracted from the CO<sub>2</sub> by the water. (Recall it was stated in Chapter 10 that the distribution coefficient for extracting caffeine from water with CO<sub>2</sub> is quite small (~0.03); thus, the extraction from CO<sub>2</sub> using water is quite favorable.) After about one-half the caffeine has been extracted from the coffee beans, the water solution is drained from the vessel into another vessel, fresh water is added to the extractor, and the decaffeination is continued until the caffeine content of the beans has again dropped by one-half. This procedure is repeated two more times with a total of four charges of water added to the vessel.

To start the separation of caffeine from the aqueous solution, a small portion of the solution from a water vessel is pumped to another vessel where it is heated to about 100



°C. Air (or N<sub>2</sub>) at about 4 atm pressure is then blown through the heated caffeine-water solution. The moisture-laden air leaving the vessel is cooled in a heat exchanger and the air and condensed water leaving the heat exchanger are separated in another vessel. The water is returned to it's holding vessel, and the cooled air is returned to the outside shell of the heat exchanger. It is mixed with cool caffeine-water solution that is pumped from it's holding vessel to the heat exchanger. The air-caffeine-water solution in the shell side is heated by the hot air-water stream flowing through the tube side; heat exchange causes the water to vaporize into the air thus concentrating the caffeine in the water solution. At the end of the stripping process, after all the dilute caffeine-water solution has been pumped through the heat exchanger and is then contained in a holding vessel, the hot concentrated caffeine-containing solution is cooled, most of the caffeine precipitates and is filtered and the mother liquor is returned to the original holding vessel for the next coffee bean decaffeination sequence.

**Roselius, W., O. Vitzthum, and P. Hubert, Method for the production of caffeine-free coffee extract, U.S. 3,843,824 (Oct. 22, 1974).**

One example from this patent was previously reproduced in Chapter 10, and one reason for the large CO<sub>2</sub> volume needed to decaffeinate coffee was developed. A three step process for producing a caffeine-free extract is described and additionally the examples contain information which points out that moist CO<sub>2</sub> is not selective for caffeine. The drawing is not given on the patent face page, but it is quite similar to the naphthalene extraction process depicted in chapter 6. In the first step, dry, coarse ground coffee is contacted with dry CO<sub>2</sub> to extract the aroma oils which, it is to be recalled, are generated only during the roasting process. The aroma oil-CO<sub>2</sub> solution leaving the extractor is lowered in pressure and cooled to below the critical temperature of CO<sub>2</sub> which causes the oils to precipitate in a separator. CO<sub>2</sub> is vaporized, condensed, and pumped to the extractor through a heat exchanger. This raises the CO<sub>2</sub> to above its critical temperature. The recycle process continues until all the aroma oils are extracted and collected in the separator.

The second step is the extraction of caffeine. CO<sub>2</sub> is first humidified before being passed through the charge of ground coffee. As we have discussed, caffeine is extracted by the moist CO<sub>2</sub>. Incidentally, one of the examples states that "residual oil," i.e., oil which has not been extracted by dry CO<sub>2</sub> in the first step, is also extracted by the moist CO<sub>2</sub>, which further corroborates the information given in Chapter 10 on the "selectivity." The caffeine is separated from the CO<sub>2</sub> in another separator vessel. Aroma oil and CO<sub>2</sub> recycle continues until all the caffeine has been extracted.

Coffee extract is prepared by pumping water at 160 °C through the vessel containing the ground coffee and spray drying the solution. The aroma oils that had been extracted from the ground coffee in step 1 are dissolved in a solvent, the solution added to the spray dried solids, and the solvent is evaporated.

**Vitzthum, O. and P. Hubert, Process for the decaffeination of raw coffee, U.S. 3,879,569 (Apr. 22, 1975).**

We stated in the introduction to this appendix that we would accent statements of "surprise" in patents when we felt information existed which would make the surprise statement unwarranted or confusing to a reader attempting to garner knowledge about

supercritical fluid properties. In the prior art discussion the patentees present that previous coffee decaffeination processes including supercritical CO<sub>2</sub> extraction are deficient. We have no problem with that statement; they may very well be deficient. It is also related specifically that the temperature range of 40-80 °C used in the supercritical CO<sub>2</sub> extraction process produces a coffee "not satisfactory as to taste"; although we have no experience in judging coffee flavor, we have no problem with that statement either. The patentees will show in their examples that liquid CO<sub>2</sub> will produce a decaffeinated coffee with improved flavor.

In the invention section, however, they compare results of tests that should not be compared, and based upon the comparisons the patentees relate that they are "surprised" at the findings. For example, we read that liquid CO<sub>2</sub> has been reported to extract aroma oils from roasted coffee. Recall we stated that many aroma compounds are soluble in liquid or supercritical CO<sub>2</sub>, but recall also that we said that there are aroma oils only in roasted coffee because they are generated during the roasting process. Nevertheless, the invention is introduced by stating that "it has now surprisingly been discovered that raw coffee ... can be selectively extracted with liquid CO<sub>2</sub> at a pressure above the critical pressure to remove caffeine in a practically pure state without affecting the aroma content of the coffee."

The examples and claims cover the use of CO<sub>2</sub> with rather restrictive conditions, viz., a pressure above the critical pressure and a temperature below 31 °C. They state that operating with these conditions produces a coffee with more satisfying taste. (Several other patents that we discuss subsequently will also claim the use of liquid CO<sub>2</sub> at pressures above the critical pressure. We shall refer to this state as "high pressure liquid CO<sub>2</sub>" in contradistinction to "liquid CO<sub>2</sub>" which is at or near its vapor pressure.)

**Vitzthum, O. and P. Hubert, Process for the manufacture of caffeine-free black tea, U.S. 4,167,589 (Sep. 11, 1979).**

This patent on a three step tea decaffeination process is included in chronological order with the coffee patents because of its similarity to U.S. 3,843,824 which describes a three-step process for the decaffeination of roasted coffee. In the first step, tea aromas are removed from dry tea using dry supercritical CO<sub>2</sub>. In a next step, the tea is moistened and moist CO<sub>2</sub> is passed through the tea to extract the caffeine. In a third step the aromas are returned to the moist tea in the following manner. The aromas are dissolved into a stream of supercritical CO<sub>2</sub> which is then passed first through a heat exchanger to liquify the CO<sub>2</sub> and then to the vessel containing the tea which is now dried. When the tea vessel is filled with the solution of liquid CO<sub>2</sub> and the aromas vapor CO<sub>2</sub> is withdrawn from the vessel and the aromas precipitate into (and onto) the tea.

We previously reviewed the patent that claimed the use of high pressure liquid CO<sub>2</sub> to decaffeinate coffee. There is no sister patent for using liquid CO<sub>2</sub>, either at high pressure or near its vapor pressure, to decaffeinate tea (at least not known to the authors). The reason for this is that it is quite difficult to decaffeinate tea with liquid CO<sub>2</sub>. Although the Vitzthum and Hubert patent gave only the elapsed time and not the volume of liquid CO<sub>2</sub> required to decaffeinate coffee, the ratio of liquid CO<sub>2</sub> required to decaffeinate coffee is about 150 lb/lb coffee. However, the ratio of liquid CO<sub>2</sub> required to decaffeinate tea is 1200(!) (Krukonis 1981, unpublished data). Part of the reason for the higher ratio resides in the higher caffeine content of tea which is typically three times that of the 1% level in most coffees. The other part of the reason is the quite-adverse caffeine equilibrium similar to that described for coffee in Chapter 10.

**Roselius, L., H. A. Kurzhals, K. F. Sylla, and P. Hubert, Process of extracting stimulants from coffee, U.S. 4,168,324 (Sep. 18, 1979).**

The background section of this patent explains that in addition to caffeine in coffee there are other ingredients that can have harmful physiological effects on the gastrointestinal system. These ingredients are lipophilic and are contained in the so-called coffee wax. The patent relates that removing coffee wax improves the digestibility of coffee. Carboxylic acid-5-hydroxy-tryptamides (C-5-HT) are compounds in the wax that can serve as indicators in the removal of wax. The specific invention is the removal of coffee wax (and the C-5-HT) using a supercritical fluid extractant while maintaining caffeine content at its initial level in the coffee.

The water content of the raw coffee beans is adjusted to 20-35% and is contacted with supercritical CO<sub>2</sub> at 250 atm and 80 °C. At these conditions, supercritical CO<sub>2</sub> will also extract caffeine. How, then, is the process operated so as to maintain the caffeine content of the coffee constant?

The extraction vessel is originally charged with raw, moistened coffee beans. Another vessel contains activated carbon which has been contacted with saturated aqueous caffeine solution. The "first" portion of fresh supercritical CO<sub>2</sub> leaving vessel with the beans contains "some" caffeine that is extracted from the coffee. It also contains C-5-HT and other coffee wax constituents. The CO<sub>2</sub> stream is circulated to the activated carbon vessel which has been loaded with activated carbon presaturated with caffeine. Therefore, as the CO<sub>2</sub> stream that contains dissolved caffeine and C-5-HT is passed through the bed of activated carbon, caffeine is not removed from the CO<sub>2</sub>, but C-5-HT is. In the "next" pass of the CO<sub>2</sub> through the extractor no caffeine will be extracted because the CO<sub>2</sub> and its dissolved caffeine are in equilibrium with the caffeine in the coffee substrate but C-5-HT will continue to be extracted. In theory, it should be possible to adjust the caffeine loading on the activated carbon to match the equilibrium of the CO<sub>2</sub>-caffeine coffee system. In practice, however, this may be difficult to do. The patentees suggest the use of a "dosing" pump to inject a caffeine solution into the recirculated CO<sub>2</sub> to maintain the caffeine content of the coffee constant. The examples show that C-5-HT can be removed while maintaining the caffeine constant.

**Prasad, R., M. Gottesman, and R. A. Scarella, Decaffeination of aqueous extracts, U.S. 4,246,291 (Jan. 20, 1981).**

This is the first of the coffee decaffeination patents that describe a continuous, counter-current liquid-liquid extraction. A brief description of the process is provided here. A water extract of roasted coffee beans, called coffee liquor, which contains aromas and caffeine and other water soluble components such as carbohydrate and protein materials is fed to a vacuum stripper. The extract is concentrated to about 30-50% in an evaporator-condenser and is fed to a sieve tray tower. The liquor passes across the trays in the tower downward through downspouts countercurrent to supercritical CO<sub>2</sub> which enters the tower at the bottom and passes upward through the holes in the sieve trays. CO<sub>2</sub> extracts caffeine from the liquor, and the decaffeinated liquor leaves the near the bottom of tower. The condensate water from the vacuum stripper prior to the tray tower is fed to the sieve trays in the top section of the tower. The water washes the caffeine from the supercritical CO<sub>2</sub> passing upward. The caffeine-free CO<sub>2</sub> is recycled to the bottom of the column.

An example described in the patent relates the extraction conditions and the flow rates employed for a test. The flow rates reported are huge. The patent reports that coffee liquor containing 15% solids is fed at 11,000 lb/hr to the evaporator and concentrated to 30% solids; 4,950 lbs/hr of concentrate is fed to the extraction tower, and 5,500 lbs/hr of condensate is sent to the top of the tower. CO<sub>2</sub> at 40 °C and 300 atm and at a flow rate of 495,000 lbs/hr (!) is pumped to the bottom of the tower to strip caffeine from the coffee liquor passing downward through the tower.

It is informative to make some estimates about the size of the column used in this test. In normal liquid-liquid extraction, Treyball discusses that a typical "hole velocity," i.e., the velocity of the lighter liquid passing upward through the holes, is about 0.3 ft/sec, and that a typical hole area is about 10-20% of the plate area. If we use these values to estimate the diameter of the coffee decaffeination tower, we calculate that the total hole area is about 8 ft. Assuming an average 15% hole area the cross sectional area of the column is 54 ft, or a diameter of 8 ft. Like the 495,000 lb/hr flow rate related earlier, an 8 ft diameter column is quite a large column in which to carry out experimental decaffeination tests. Do the data that are reported in the example originate from the operation of a commercial facility somewhere or are the data made up?

**Zosel, K., Process for the decaffeination of coffee, U.S. 4,247,570 (Jan. 27, 1981).**

A variant of the use of activated carbon to remove caffeine from carbon dioxide is described in this patent. A mixture of activated carbon and coffee beans is placed in a vessel, the vessel is pressurized with CO<sub>2</sub> to some supercritical condition, and the contents held statically at those conditions for a period of time. At the end of this period, the CO<sub>2</sub> is vented and the activated carbon is separated from the coffee bean by sieving.

In one of the examples 22 lb of moistened coffee is admixed with 15 lb activated carbon and is held at 80 °C and 190 atm pressure for 15 hours. During this contacting period the caffeine content of the coffee is reduced from 1% to 0.02%.

Conceptually, the operation of the process in this static mode eliminates the energy requirements of recycling the CO<sub>2</sub>. In this process, caffeine from the coffee bean, dissolves in CO<sub>2</sub>, diffuses through the supercritical phase to the activated carbon. In Chapter 1 we said that the high diffusion coefficients of materials in a supercritical fluid do not necessarily ensure that mass transfer will be rapid relative to mass transfer in a liquid. Rate controlling steps must always be considered. However, this process configuration may well be one where the higher diffusivity of a molecule in the supercritical phase can result in a higher extraction rate.

**Margolis, G. and J. Chiovini, Decaffeination process, U.S. 4,251,559 (Feb. 17, 1981).**

This patent is another one on extraction of caffeine from aqueous solution. The examples cover extraction of caffeine from solutions of tea, coffee, and neat caffeine. Batch autoclave extraction, batch-continuous extraction, and continuous counter current extraction are described. The patent gives a large table of decaffeination results, and some of the results are reproduced below. Distribution coefficients given in the last column are calculated from batch-continuous extraction mathematics using the relation  $DC \cdot R = \ln C_i/C_f$ . The decaffeination values accented with an "a" are achieved with a CO<sub>2</sub> density of

0.85 or greater. The invention is the use of CO<sub>2</sub> of density 0.85 or greater. The table shows that if the density is less, the decaffeination values and distribution coefficients calculated are lower.

Solution	CO <sub>2</sub> Ratio	<u>Decaffeination Results</u>		% Decaf.	D.C.
		T (°C)	P (Bar)		
Green	50	70	250	79	0.031
Coffee,	20	70	250	42	0.026
10% Solids	10	70	250	18	0.017
	50	80	450	98	0.078a
	20	80	450	85	0.095a
Tea,	40	91	450	83	0.044
11.8% solid	30	91	450	72	0.042
	8	91	450	24	0.034
	40	80	450	96	0.080a
	30	70	600	98	0.130a
	8	70	650	97	0.440a
Caffeine,	50	70	175	71	0.024
0.4%	30	70	300	80	0.053
	20	70	300	64	0.051
	50	92	500	96	0.064a
	30	92	500	89	0.070a
	20	70	500	90	0.115a

**Roselius, L., H. A. Kurzhals, and P. Hubert, Method for the selective extraction of caffeine from vegetable materials, U.S. 4,255,458 (Mar. 10, 1981).**

This patent discusses the decaffeination of coffee using a cosolvent, or entrainer, admixed with a supercritical fluid. The wording of the first claim describes the state of the mixture as a two component mixture a) whose first component is inherently gaseous under operating conditions of temperature and pressure and b) whose second component is an organic solvent which, by itself has physical properties such that a mixture of a) and b) is liquid at the operating temperature. Use of this mixture is the invention.

One of the examples discusses results of decaffeinating coffee with a CO<sub>2</sub>-acetone mixture. Raw coffee with a moisture content of 36% is extracted with 92% CO<sub>2</sub>, 8% acetone at 90 atm and 40 °C for 8 hours. The caffeine content of the coffee, originally 1.15%, was reduced to 0.07%.

Incidentally, it is not stated in the discussion of the invention whether the phase behavior of an 8% acetone solution at 90 atm and 40 °C was determined, i.e., is it truly liquid as the claim requires, or is it supercritical.

**Jasovsky, G. A. and M. Gottesman, Preparation of a decaffeinated roasted coffee blend, U.S. 4,255,461 (Mar. 10, 1981).**

This patent teaches that lower grade (i.e., poor flavor) coffee beans can be extracted with CO<sub>2</sub> at specific conditions to yield a preferred characteristic. The background relates that most high grade coffees are best decaffeinated at a moisture content of between 26 and 33% using supercritical CO<sub>2</sub> at a temperature between 60 and 85 °C and a pressure of at least 200 atm. If low grade coffee is decaffeinated at the same temperature conditions, the flavor of the low grade coffee (when blended with high grade coffee) is not satisfactory. However, when the low grade coffee is moistened to higher moisture content between 37 and 50% and is extracted at between 100 to 160 °C, the flavor characteristic of the low grade coffee (when blended with high grade coffee) is better. Example 1 from the patent is reproduced in its entirety to explain the results.

**Example 1**

Two separately decaffeinated roasted and ground coffees were obtained for taste comparison with a water-decaffeinated, roasted and ground coffee product produced in accordance with the aforementioned Berry *et al.*, patent (U.S. 2,309,092). Using comparable equipment and procedures, batches of Colombian, Brazilian and Robusta (the lower grade coffee) green coffee beans were separately decaffeinated by first moisturizing the green coffee beans to 30% weight and then contacting the moisturized coffee with a stream of supercritical CO<sub>2</sub> at conditions of 80 °C and 250 atm until about 97% of the caffeine was removed. The thus decaffeinated coffees were then dried to between 10 and 14% moisture and subsequently were separately roasted with the Colombian coffees being split into two fractions and with each fraction being roasted to comparable but discernibly different roast colors. A portion of the green Robusta coffee beans employed above was separately moisturized to 45% water by weight and then contacted with a stream of supercritical CO<sub>2</sub> at conditions of 100 °C and 250 atm. These decaffeinated Robusta beans were then roasted to color comparable to above roasted Robusta beans. Two separate roasted coffee blends were formulated each consisting on a weight basis of 30% Colombians (15% each roast color), 15% Brazilian, and 55% Robusta with Blend A containing the Robustas decaffeinated at 80 °C and Blend B containing the Robustas decaffeinated at 100 °C. Blends A and B were ground and brewed and the resulting beverage was compared to a control beverage prepared from a decaffeinated roasted and ground coffee decaffeinated in accordance with the aforementioned Berry *et al.* patent and containing 55% Colombian coffees and 45% Robusta coffees. In consumer taste tests Blend A lost to the control (46.5% to 53.5%) while Blend B was preferred to the control (52% to 48%).

**Zosel, K., Process for the decaffeination of coffee, U.S. 4,260,639 (Apr. 7, 1981).**

The difference between this patent for decaffeinating raw coffee and the previous Vitzthum and Hubert patent for decaffeinating raw coffee resides in the moisture content of the coffee. Examples in this patent show that raw coffee need not be pre-treated with water; moist CO<sub>2</sub> by itself is sufficient to extract the caffeine. (One of the authors (VJK) has tested moist CO<sub>2</sub> on dry coffee and tea. It works, but a higher recycle ratio of CO<sub>2</sub> is required if the materials are not also moistened.)

It is of value to discuss some incorrect statements made in this patent. Let us start with the "surprising" results: "...the observation that caffeine could be removed relatively easily from moist raw coffee by subjecting it to a supercritical gas phase, for the following reason." The patentees then go on to relate that "The German Democratic Republic Pat. No. 41,362 and also the corresponding British Pat. No. 1,057,911 are concerned with processes for separating mixtures of substances by means of gases in the supercritical state. It is shown in examples 61 and 62 that substances which are dissolved in water or which are present in an aqueous emulsion can only be taken up, with very great difficulty, in a supercritical gas. However, caffeine, dissolved in water, can be taken up relatively easily in gaseous CO<sub>2</sub> in the supercritical state, whereas dry caffeine is not."

We have already seen in Chapter 10, that dry caffeine does dissolve in dry CO<sub>2</sub>; Stahl (1979) and Krukonis (1981) show this. Therefore, the statement that dry caffeine is not taken up by dry CO<sub>2</sub> is wrong. Now let's see if we can determine what is meant by the statement, "substances dissolved in water can only be taken up with great difficulty in a supercritical gas, but caffeine dissolved in water, is taken up relatively easily." Example 61 from the British patent, (which is not reproduced here because of space considerations) describes the extraction of several alcohols from water solution with supercritical ethylene. The example states that no ethanol is extracted from solution by ethylene. CO<sub>2</sub>, on the other hand, can extract ethanol from solution, and, therefore, it is of no relevance to compare the inability of ethylene to extract ethanol with the ability of CO<sub>2</sub> to extract ethanol (or caffeine).

If the reader checks each example and each reference cited for specifics, he will find these quite frequent inconsistent comparisons. Incidentally, he will also find that ethylene can in fact extract ethanol from water (Paulaitis, Gilbert, and Nash, 1981).

**Roselius, W., O. Vitzthum, P. Hubert, Method of extracting coffee oil containing aroma constituents from roasted coffee, U.S. 4,328,255 (May 4, 1982).**

This invention is concerned with a process to remove the aroma constituents from roasted coffee. The prior art discussion brings out that although liquid CO<sub>2</sub> can also extract the aroma substances, it does not extract the natural antioxidants that are present in roasted coffee. The extracted oils, therefore, are not stable. Supercritical CO<sub>2</sub> can extract the natural antioxidants along with the oils.

As we have seen in other patents discussed, there are some "surprise" statements in this patent. For example, the patentees state "From (the) literature it is known that the ability of gaseous CO<sub>2</sub> to absorb oils increases with rising pressure and attains its maximum in the case of liquid CO<sub>2</sub>. It is also known that supercritical CO<sub>2</sub> has increasing solvent power with rising pressure, and that this is so only up to a maximum value which corresponds to that of liquid CO<sub>2</sub>."

We wonder what literature they have been reading that leads them to conclude that supercritical CO<sub>2</sub> cannot dissolve substances to a greater level than liquid CO<sub>2</sub> can. Based upon this conclusion, they now make their surprise statement, "It is therefore extremely surprising that in the method of the invention the ability of the supercritical CO<sub>2</sub> phase to absorb aroma constituents, coffee oils, and antioxidants is considerably greater than the solvent power of liquid CO<sub>2</sub>." We certainly have no problem with the finding that supercritical CO<sub>2</sub> can "absorb" coffee oils and anti-oxidants to a greater level than liquid CO<sub>2</sub> can, but the finding is not "extremely surprising."

**Katz, S. N., Method for decaffeinating coffee, U.S. 4,276,315 (Jun. 30, 1981).**

The abstract on the patent face page describes the use of liquid propane or butane as a decaffeinating solvent. In the abstract the patentee uses the phrase "selectively remove caffeine from moistened green coffee." To describe how effective liquid propane is as a decaffeinating solvent, it is most informative to reproduce Example 3 from the patent.

### Example 3

As shown in the following table, the use of liquid propane at low pressures is equally effective to decaffeinate green coffee beans. In this set of experiments, two kilograms of green Colombian coffee beans were moisturized, placed in a pressure vessel (10 mm I.D., 91.4 cm high), and decaffeinated by means of recirculating stream of liquid propane flowing at a rate of 60 kg/kg beans/hour and a velocity through the bean vessel of about 1.25 cm/sec. The propane was freed of caffeine by passage through a vessel (10 mm I.D., 45.7 cm high) containing 625 grams of activated charcoal.

#### Results from decaffeinating green coffee beans with propane

P (atm)	T (°C)	Moisture (wt%)	Time (hr)	Decaffeination (wt%)
200	80	50	10	80
200	80	35	14	82
40	80	35	10	80
40	70	35	10	73

The decaffeinated beans from Example 3 were roasted and brewed and the flavor of the beverage was considered to be of good quality and comparable to a control beverage prepared from beans which had been decaffeinated by means of supercritical CO<sub>2</sub> at 80 °C and 200 atm. The recycle ratio is equal to 60 kg/kg beans/hr x 10 hours = 600 kg/kg. As the table shows, that ratio achieves only 80% decaffeination, and we suggest that a ratio of at least 1,200 to 1,500 kgs/kg(!) coffee is required to achieve 97+% decaffeination.

**Peter, S. and G. Brunner, Process for decaffeinating coffee, U.S. 4,322,445 (Mar. 30, 1982).**

Before describing the invention, it is of value to discuss the background section of this patent, since it is noteworthy for its confusing statements. The invention in this patent is the use of compressed gases and cosolvents (entrainers) and operating so that the cosolvent and caffeine are subsequently separated from the gas. One example describes that nitrogen at conditions of 200 atm and 40 °C containing 3% formaldehyde dimethylacetal can decaffeinate raw coffee.

In a discussion of prior art, Peter and Brunner refer to an article (Sivetz, M. 1963. Coffee Processing Technology, Vol. 2, 21, Avi Publishing, Westport, CT) which describes the use of liquid CO<sub>2</sub> to produce aroma oil from coffee; however, they do not explain in the prior art section that the article describes aroma extraction from coffee which has been roasted. They then refer to a second article on the use of liquid CO<sub>2</sub> to produce aroma concentrates, Food Technol, No. 23, 11, 50 (1969) and they write, "Thus,



in the extraction of raw coffee with liquid CO<sub>2</sub> removal of caffeine is accompanied by the simultaneous removal of other substances."

Peter and Brunner then refer to the data of Vitzthum and Hubert in U.S. 3,879,569 on the high pressure liquid CO<sub>2</sub> extraction of raw coffee, and they state "an increase of pressure on the extractor, greatly increases the selectivity of liquid CO<sub>2</sub> for caffeine."

What Peter and Brunner apparently want to leave the reader with here is that near-critical liquid CO<sub>2</sub> (at 850 psi and 25 °C) will extract both aromas and caffeine from raw coffee whereas high pressure liquid CO<sub>2</sub> (at 2,000 psi and 25 °C) will extract only the caffeine. Increasing the pressure certainly will not increase the selectivity of CO<sub>2</sub> for caffeine in raw coffee. However, any conclusion can be drawn in comparisons of raw and roasted coffee extraction results or in comparisons of the extraction of aromas and extraction of caffeine. Incidentally, this background discussion which only serves to confuse the reader has no relevance to the use of a mixture of high pressure nitrogen and formaldehyde dimethylacetal for extracting caffeine from coffee.

**Zosel, K., Process for the direct decaffeination of aqueous coffee extract solutions, U.S. 4,348,422 (Sept. 7, 1982).**

Zosel explains in the prior art section that foam formation during supercritical CO<sub>2</sub> extraction of coffee liquor is a problem; the invention eliminates the foaming problem. The improvement in a countercurrent contacting of coffee liquor is to form a thin film of the liquor in the extractor rather than to contact coffee liquor on a sieve tray. The film can be formed in a number of ways, e.g., on packing or in a thin film evaporator.

Coffee extract solution from reservoir is pumped to a packed column filled with, for example, Rashig rings, stainless steel spirals, etc. The coffee liquor flows downward over the packing and is contacted by upward flowing supercritical CO<sub>2</sub>. Caffeine is extracted from the coffee liquor which exits at the bottom of the column, and the caffeine-laden CO<sub>2</sub> stream leaves the extraction column and enters the water wash tower (which is also a packed column) where the CO<sub>2</sub> is stripped of its caffeine. The caffeine-free CO<sub>2</sub> is recirculated to the coffee liquor extraction tower, and the caffeine-water solution is evaporated and the caffeine recovered.

An example gives quantitative data. Coffee liquor is pumped to the column at 17 g/min, and CO<sub>2</sub> at 200 atm and 50 °C is fed at 800 g/min (a solvent to feed ratio of about 50). More than 98% of the caffeine is extracted.

## SECTION 4

### Extraction of other Vegetable and Animal Materials

- Roselius, W., O. Vitzthum, and P. Hubert, Method of producing cocoa butter, U.S. 3,923,847 Dec. 2, 1975).
- Zosel, K., Process for the simultaneous hydrogenation and deodorization of fats and/or oils, U.S. 3,969,382 (July 13, 1976).
- Zosel, K., Process for deodorizing fats and oils, U.S. 4,156,688 (May 29, 1979).
- Zosel, K., Production of fats and oils from vegetable and animal products, U.S. 4,331,695 (May 25, 1982).
- Schwengers, D., Extraction of fat from starch-containing vegetable matter, U.S. 3,939,281 (Feb. 17, 19676).
- Vitzthum, O. and P. Hubert, Process for the production of spice extracts, U.S. 4,123,599 (Oct. 31, 1978).
- Roselius, W. and O. Hubert, Process for the extraction of nicotine from tobacco, U.S. 4,153,063 (May 8, 1979).
- Schultz, W. G., Process for extraction of flavors, U.S. 3,477,856 (Nov. 11, 1969).
- Schultz, W.G., Process for removing residual solvents, U.S. 3,966,981 (June 29, 1976).
- Laws, D.R.J., N.A. Bath, C.S. Ennis, and A.G. Wheldon, Hop extraction with carbon dioxide, U.S. 4,218,491 (Aug. 19, 1980).
- Sims, M., Liquid carbon dioxide extraction of pyrethrins, U.S. 4,281,171 (Jul. 28, 1981).
- Friedrich, J.P., Supercritical CO<sub>2</sub> extraction of lipids from lipid-containing materials, U.S. 4,466,923 (August 21, 1984).
- Christianson, D.D. and J. P. Friedrich, Production of food-grade germ product by supercritical fluid extraction, U.S. 4,496,207 (Jan. 22, 1985).
- Heigel, W., Process for the production of pure lecithin directly usable for physiological purposes, U.S. 4,367,178 (Jan. 4, 1983).
- Schutz, E., H.R. Vollbrecht, K. Sandner, T. Sand, and P. Muhl nickel, Method of extracting the flavoring substances from the vanilla capsule, U.S. 4,470,927 (Sept. 11, 1984).
- Makin, E. C. Purification of vanillin, U.S. 4,474,994 (Oct. 2, 1984).
- Coenen, H., R. Hagen, and M. Knuth, Method for obtaining aromatics and dyestuffs from bell peppers, U.S. 4,400,398 (Aug. 23, 1983).
- Heine, C. and R. Wust, Method for the production of food additives with improved taste, U.S. 4,427,707 (Jan. 24, 1984).
- Behr, N., H. van der Mei, W. Sirtl, H. Schnegelberger, and O. von Ettingshausen, Process for the preparation of spice extracts, U.S. 4,490,398 (Dec. 25, 1984).
- Biernoth, G. and W. Merk, Fractionation of butterfat using a liquefied gas or a gas in the supercritical state, U.S. 4,504,503 (Mar. 12, 1985).
- Amer, G. I., Separation of neutrals from tall oil soaps, U.S. 4,422,966 (Dec. 27, 1983).
- Lawson, N.E. and G. I. Amer, Acidulation and recovery of crude tall oil from tall oil soaps, U.S. 4,495,095 (Jan. 22, 1985).
- Fremont, H. A., Extraction of Coniferous woods with fluid CO<sub>2</sub> and other supercritical fluids, U.S. 4,308,200 (Dec. 29, 1981).
- Blewett, C. W. and Turner, S. W., Process for separating fatty materials from supported nickel catalysts, U. S. 4,584,140 (Apr. 22, 1986).
- Grubbs, H. J., Prasad, R., Howell, T. M., Process for removal of basic materials, U. S. 5,018,540 (May 29, 1991).

**Roselius, W., O. Vitzhum, and P. Hubert, Method of producing cocoa butter, U.S. 3,923,847 Dec. 2, 1975).**

Cocoa butter is the triglyceride which derives from cocoa beans; it is composed of a large amount of palmitic acid on the glycerol backbone. Because of the high saturation, cocoa butter is a solid and exhibits a rather sharp melting point at about body temperature which incidentally, is partially responsible for the pleasant texture of high quality chocolates.

The invention concerns the use of supercritical solvents to extract the cocoa butter from cocoa nibs (comminuted cocoa beans) and cocoa mass (finely crushed beans). The description of other processes in the prior art section of the patent points out that organic solvent extraction results in the presence of residual solvents. Additionally, some of the newer pressing methods, via expellers, for example, introduce waste bean contaminants into the butter which must be removed with economic and taste penalties.

Examples are presented of the application of supercritical CO<sub>2</sub> at typically, 200 to 400 atm and 40 to 60 °C to extract both finely crushed cocoa mass and cocoa nibs. It is related that cocoa mass can be extracted of 99% of its cocoa butter and that cocoa nibs, whether roasted or not or whether treated with caustic or not, can be extracted of 74% of their cocoa butter. One of the authors (VJK) has verified the results with cocoa mass, but finds that less than 5% of the cocoa butter can be extracted from raw, untreated cocoa nibs, even if the extraction is carried out at 7,000 psi and 40 to 60 °C for a period of 8 hours! On the other hand, theobromine and caffeine can be extracted from the nibs almost quantitatively at much less severe conditions resulting in a cocoa product containing almost all its original cocoa butter and flavor but no adverse stimulants (Krukonis unpublished data, 1982).

**Zosel, K., Process for the simultaneous hydrogenation and deodorization of fats and/or oils, U.S. 3,969,382 (July 13, 1976).**

Seed oils such as soy bean and corn germ consist largely of triglycerides of oleic acids and are liquid at room temperature. Industrially, they are partially hydrogenated to produce higher melting point triglycerides that are used as commercial shortenings. The hydrogenation ("hardening" as it is called in the trade) is normally carried out by suspending a catalyst, typically nickel, in the oil and contacting the oil with 1 to 10 atm H<sub>2</sub> partial pressure. No supercritical processing of any kind is involved in current practice.

In this patent a simultaneous deodorization and hardening are described in which the gas phase consisting of CO<sub>2</sub> containing about 1% hydrogen countercurrently contacts a film of oil in a packed column at conditions of 220 atm and 200 °C. The CO<sub>2</sub> extracts the fatty acids which are largely responsible for the odor and off flavors, and the hydrogen dissolves into the oil and reacts with the unsaturated bonds of the triglycerides.

The patentee packs the column with glass beads. Oil from a reservoir is pumped to the top of the column. Fresh CO<sub>2</sub> is introduced into the bottom of the column along with recycled CO<sub>2</sub>. The extract phase containing the fatty acids and, although not stated in the examples, a small amount of triglyceride, exits at the top of the column and is recycled to the column by a compressor after first having passed through an activated carbon adsorber for removal of fatty acids from the CO<sub>2</sub>. An in-line, valve allows the recycle gas to be sampled so that the hydrogen make up can be determined.

Several examples are given. Free fatty acids present in the feed oil are reduced by 95+%, and the iodine number (a measure of unsaturation) is reduced from 191 to 66. Furthermore the melting point of the triglyceride is increased from -2 °C to 34 °C indicating that substantial hydrogenation occurred.

**Zosel, K., Process for deodorizing fats and oils, U.S. 4,156,688 (May 29, 1979).**

This patent is similar to the previous one except that the simultaneous hydrogenation is not carried out. The examples show that 95+% of the odoriferous material is removed by treating seed oil with CO<sub>2</sub> at 200 atm and 250 to 200 °C. It is noteworthy that the major claim is quite restrictive: "Process of deodorizing fat or oil characterized by the presence of odoriferous material, comprising contacting the fat or oil with CO<sub>2</sub> at a temperature of 150 to 250 °C, and a pressure of 100 to 250 atm..." The reason for using such a high temperature is not given. One of us (VJK) has carried out similar free fatty acid removal from seed oils at a much lower temperature of 80 °C also with 95+% removal (Krukoniš, unpublished research 1981). Other data on deodorizing spent cooking oils with supercritical CO<sub>2</sub> at equivalent low temperature have also been reported. (Caragay, A. B. and V. J. Krukoniš, 1981. "Supercritical Fluid Extraction of Triglycerides" at 72nd AOCS Meeting, New Orleans, May.)

**Zosel, K., Production of fats and oils from vegetable and animal products, U.S. 4,331,695 (May 25, 1982).**

Zosel was a prolific experimenter and inventor, and it is instructive to include many of his patents. Near critical liquids are employed to extract triglycerides from a variety of animal and vegetable materials. Seven examples present data including liquid propane at 42 atm and 80 °C and 20 °C; liquid ethane at 48 atm and 20 °C; liquid CO<sub>2</sub> at 73 atm and 18 °C; liquid N<sub>2</sub>O at 72 atm and 20 °C; and liquid isobutane at 37 atm and 120 °C were tested on a variety of vegetable and animal, fats and oils. Residual fat contents in extracted seeds, flake, germ, and ground bones was of the order of 1% or less.

By now we assume that the general similarities among many of the patents are becoming obvious, but we see also that the inventions are different in some slight way. So, of course, are the specific limits in the claims. For example, a near critical liquid at its vapor pressure is different from a high pressure liquid above the critical pressure, but still below its critical temperature, which in turn is different from a supercritical fluid. We continue to read that the prior art in many of the patents describe the "limitations" of all the other processes and point out the advantages of the instant process.

**Schwengers, D., Extraction of fat from starch-containing vegetable matter, U.S. 3,939,281 (Feb. 17, 1967).**

The abstract gives what appears at first glance to be the range of coverage. It also gives the motivation for extracting fat from the materials, i.e., the residual de-fatted material will be used in other operations.

In the discussion of the invention the patentee states that high pressure liquid (again that combination of temperature less than the critical temperature and pressure much

higher than the critical pressure) is "more advantageous." Although he uses the term "supercritical" in the abstract, the claim is restrictive to high pressure liquid, i.e., "a normally gaseous inert solvent in liquid state at a temperature of about 20 to 100 °C and below the critical temperature and a pressure of about 30 to 1000 atm and above the critical pressure of the inert solvent which solvent has a critical temperature below about 200 °C."

In this patent we see that the term "supercritical" is used a second way. We have used the term "supercritical" to refer to the state where pressure and temperature are both above their critical values. We shall see when we discuss a vanillin purification patent, U.S. 4,474,994, that the patentee defines supercritical to be a temperature higher than critical temperature but a pressure not higher than critical pressure. As we have said a number of times concerning such terms as solubility and extractability, we recommend that the reader examine how supercritical is defined.

**Vitzthum, O. and P. Hubert, Process for the production of spice extracts, U.S. 4,123,599 (Oct. 31, 1978).**

This patent describes a process that is supercritical extraction of roasted coffee beans using dry, then, moist CO<sub>2</sub>. Spices are also extracted in a two step process. In the first step a dry CO<sub>2</sub> extraction is performed to dissolve the essential oils which represent the aroma constituents, and in the second step, a moist CO<sub>2</sub> extraction is performed to obtain the flavor components.

Dry CO<sub>2</sub> is pumped through a heat exchanger and valve into a vessel containing crushed spice mass. The extract solution leaving the vessel is expanded to a lower pressure through a valve, and the temperature is adjusted in a heat exchanger. The components precipitated from the CO<sub>2</sub> are separated in another vessel, and the CO<sub>2</sub> is recycled to the extractor. When the desired level of aroma extraction has been accomplished, the CO<sub>2</sub> is then diverted to a humidifier before being passed through the spice mass. Moist CO<sub>2</sub> extracts the desired flavor component(s). The extract solution is separated into its components either in the same vessel or in another vessel depending upon the intended use of the extract.

A number of examples describe the extraction of crushed black pepper, ground cloves, crushed cinnamon sticks and crushed vanilla pods. For the case of black pepper, part of the flavor component, piperine, can be extracted with dry CO<sub>2</sub> and part is extracted with the moist CO<sub>2</sub>.

**Roselius, W. and O. Hubert, Process for the extraction of nicotine from tobacco, U.S. 4,153,063 (May 8, 1979).**

Extraction of nicotine from tobacco using supercritical fluid is carried out in a manner quite similar to the decaffeination of roasted coffee described in U.S. 3,843,824. Tobacco is first contacted with dry supercritical CO<sub>2</sub> which extracts the aroma constituents. The CO<sub>2</sub>-aroma stream is expanded to subcritical conditions via expansion across a valve the aromas precipitate from solution. The CO<sub>2</sub> vapor is recompressed, is adjusted in temperature to supercritical conditions via heat exchangers, and is recycled to the extractor via a compressor. The aromas extraction step continues until the aroma constituents are removed from the tobacco.

In the second step of the process, the supercritical CO<sub>2</sub> is humidified before being passed through the tobacco. Nicotine is extracted by the wet CO<sub>2</sub>. Nicotine is removed from the CO<sub>2</sub>-rich phase by passing the stream through vessel containing a sulfuric acid solution that reacts with the nicotine to form a salt insoluble in CO<sub>2</sub>. The nicotine-free CO<sub>2</sub> leaving the vessel is adjusted in temperature and moisture and is recycled until a satisfactory level of nicotine removal has been achieved. At the end of the nicotine extraction cycle, the tobacco is dried. The aroma constituents contained are dissolved in a liquid solvent and the solution introduced into the extractor containing the tobacco. The solvent is vaporized resulting in the precipitation of aromas in the tobacco.

As a variation of the three step procedure described above, the patent also relates that if tobacco is first moistened, solely nicotine can be extracted with supercritical CO<sub>2</sub>. For example, CO<sub>2</sub> at 70 °C and 300 atm passed through moistened tobacco reduced the nicotine content from 1.36 to 0.08% (dry basis) while leaving the aromas untouched. One of the authors (VJK) has not been able to reproduce this finding in tests with moistened tobacco from commercial cigarettes. Aromas were found to be extracted along with the nicotine. Another example in the patent contains some other curious information. It is related that 5 wt% ammonia is added to supercritical CO<sub>2</sub> at 70 °C and 250 atm and the mixture used to extract nicotine. One of the authors (VJK) has tested this mixture and finds that CO<sub>2</sub> and ammonia react to form a compound, probably ammonium carbamate, which is insoluble in supercritical CO<sub>2</sub> at 70 °C and 250 atm.

**Schultz, W. G., Process for extraction of flavors, U.S. 3,477,856 (Nov. 11, 1969).**

Although this patent is also not a supercritical one it is included in this section for its historical value and because of the renown of the patentee. William Schultz of the USDA's Western Regional Research Center published extensively during the 1960s. on flavors, aromas, and essences extraction from fruits, and the information he describes for liquid CO<sub>2</sub> is applicable to supercritical CO<sub>2</sub>. He was not referenced previously in this book, but two of his quite well known, often-cited publications on flavors and aromas are listed below. A figure on the cover page of the patent shows a flow sheet for the CO<sub>2</sub> extraction of flavor components from a fruit juice. The fruit juice is conveyed to the top of the extraction column and a spray nozzle in the column disperses the juice which contacts liquid CO<sub>2</sub> which is introduced at the mid section of the column. The liquid CO<sub>2</sub> (with density of about 0.7 g/cc) rises countercurrently extracting the flavor components which are esters, aldehydes, ketones and similar compounds. The extract leaves the column and flows to an evaporator where the liquid CO<sub>2</sub> is vaporized. The gaseous CO<sub>2</sub> is conveyed to a condenser and a concentrated flavors stream leaves the evaporator. Make up CO<sub>2</sub> is added from the CO<sub>2</sub> reservoir when required.

Two of the Schultz papers are:

Schultz, W. G., T. H. Schultz, R. A. Carlson, and J. S. Hudson, 1974. Pilot plant extraction with liquid CO<sub>2</sub>, *Food Technol.*, 28, 32.

Schultz, W. G., J. M. Randall, 1970. Liquid CO<sub>2</sub> for selective aroma extraction, *Food Technol.*, 24, 94.

**Schultz, W.G., Process for removing residual solvents, U.S. 3,966,981 (June 29, 1976).**

This patent on liquid CO<sub>2</sub> is also included in this section because the same technique of solvent removal can be carried out with supercritical CO<sub>2</sub>. This patent addresses another area of application, the removal of residual (organic) solvents from solvent extracted residues such as soy bean flake. The background relates that it is difficult to free the flake of its hexane residuals.

One example gives quantitative data. 450 g of hexane-extracted soy bean flake with a residual hexane content of 228 ppm was contacted with 4,250 ml of liquid CO<sub>2</sub> for 72 hrs at 22 °C and 65 to 75 atm in a batch extractor. The flakes were separated, air dried, and the residual hexane content measured as 44 ppm. (The background section of the patent stated that 60 ppm is the maximum allowed by FDA and, thus, the single extraction was satisfactory to produce material within specifications.) Subsequent extractions lowered the hexane content to 0.7 ppm.

As an aside here, the process could have been carried out in a batch-continuous mode, with CO<sub>2</sub>, either liquid or supercritical flowing through the charge. A thorough extraction could have been achieved in a much shorter time than 72 hours.

**Laws, D.R.J., N.A. Bath, C.S. Ennis, and A.G. Wheldon, Hop extraction with carbon dioxide, U.S. 4,218,491 (Aug. 19, 1980).**

This patent covers a liquid CO<sub>2</sub> extraction process, and it is included here because of the large amount of interesting information about hops. In the background section of this patent current hop extraction procedures are described. Organic solvents such as methylene chloride and methanol are used to extract hops, and the crude extract that is obtained must be purified extensively before it yields the alpha-acid resins suitable for isomerization. The iso-alpha-acids are the main bittering components of beer. In traditional beer making, the hops are added directly. When hops are added directly, only about 25% of the alpha-acids are utilized. With an organic solvent extraction of hops about 60 to 80% of the alpha-acids present in the hops is utilized. However, there are solvent residues present in the purified organic solvent extract, and although the extract meets current public health requirements, it may not in the future because of increasing attention that is being directed to the presence of residual solvents in food and beverage products. CO<sub>2</sub> extraction is proposed as the new method.

In the preferred embodiment, liquid CO<sub>2</sub> at conditions of between -5 °C and 15 °C is used. The temperature range of -5 °C to 15 °C is preferred. At conditions below -5 °C, waxes in the hops dissolve preferentially resulting in an impure alpha-acids product. At conditions above 15 °C the solubility of alpha-acids is low requiring long extraction times. The solution leaving the extractor vessel is conveyed to a separator vessel where the CO<sub>2</sub> is separated from the extract by evaporation. The CO<sub>2</sub> is condensed and is recycled to the extractor.

A later patent assigned to the Brewing Patents Limited, Laws, D. R. J., N. A. Bath, C. S. Ennis, J. A. Pickett, and A. G. Wheldon, Production of an Iso-Alpha-Acid Preparation from Hops, U.S. 4,298,626, Nov. 3, 1981, describes the isomerization of the alpha-acids obtained by CO<sub>2</sub> extraction. It describes the advantages of using a supercritical CO<sub>2</sub> extract in the subsequent isomerization process.

**Sims, M., Liquid carbon dioxide extraction of pyrethrins, U.S. 4,281,171 (Jul. 28, 1981).**

The extraction of pyrethrin from pyrethrum flowers has received a reasonable amount of mention in the technical and trade press during the past few years. One article on the liquid CO<sub>2</sub> extraction of these materials has appeared recently. (Sims, M. 1982. Process uses liquid CO<sub>2</sub> for botanical extractions, Chem. Eng. Jan. 25, 50.) Thus this patent is included for brief discussion.

Pyrethrins are natural insecticides. They have low mammalian toxicity and do not accumulate in the environment. The lack of persistence has prevented insects from adapting a resistance to the pyrethrins and thus they are environmentally attractive insecticides. Pyrethrins are low molecular weight ester compounds with additional ether, aldehyde, and ketone functionality. These compounds are very soluble in liquid CO<sub>2</sub>. Other materials that are present in the pyrethrum flower such as long chain fatty acids, sterols, and higher alkanes are only sparingly soluble in liquid CO<sub>2</sub>. Because of the differential solubilities of the pyrethrins and the other compounds present in the flowers an extract with quite high content of pyrethrin can be obtained using liquid CO<sub>2</sub>. Liquid organic solvents cannot differentiate between the active and inactive compounds as finely.

**Friedrich, J.P., Supercritical CO<sub>2</sub> extraction of lipids from lipid-containing materials, U.S. 4,466,923 (August 21, 1984).**

Some of the solubility data given in this patent have already been discussed in Chapter 10. Friedrich has found that at conditions above 60 °C and 550 atm the solubility of triglycerides in CO<sub>2</sub> rises dramatically. He shows that soy bean triglycerides become infinitely miscible above about 800 atm and 70 °C. Based upon these findings he proposes a process for extracting soy beans, cotton seed, and similar oil seeds, using CO<sub>2</sub> at very high pressure with a minimum recycle. For example, solubility levels of 20 to 40% are reported at conditions of 600 atm and 70 °C.

One might extrapolate that such levels of solubility could lead to a process that might not employ the recycle of gas in its operation (Friedrich, private communication 1983). In the case of soy beans, which have an oil content of about 16%, a solubility level of 40 wt-% oil in CO<sub>2</sub> calculates to a CO<sub>2</sub> requirement only 0.24 lb/lb soy beans. At a CO<sub>2</sub> usage of only 0.24 lb, the capital and operating cost of recycling the gas could well be more than the 1 cent cost of the CO<sub>2</sub>.

**Friedrich, J. P. and A.C. Eldridge, Production of defatted soybean products by supercritical fluid extraction, U.S. 4,493,854 (Jan. 15, 1985).**

The prior art section in the patent explains that conventional hexane extraction of soy beans leaves constituents in the extracted meal that give raw, grassy, and bitter flavors that are detrimental to the meal's organoleptic quality. Emphasis has been directed to replace the hexane used in the traditional process with work focused on the development of a supercritical CO<sub>2</sub> extraction process. Most of the research effort has been directed to achieving a high quality of oil. When soy bean flakes are extracted with CO<sub>2</sub>, the color, quality, metals content etc., of the oil are excellent, but the residual flake still retains some of the grassy and bitter off flavors.



The invention that is described concerns the finding that if the moisture content of flake is first adjusted to about 6.5 to 15% and then extracted with CO<sub>2</sub>, a meal is produced with high organoleptic and protein solubility character. Twenty separate examples are given in the patent which present a panel evaluation of the protein solubles and flavor scores of the CO<sub>2</sub> de-oiled soy bean meal. When the moisture content is maintained in the range of 6.5 to 15% during CO<sub>2</sub> extraction, the quality of the soy bean flour is acceptable. The flavor is not acceptable if the moisture content lies outside that range during extraction.

**Christianson, D.D. and J. P. Friedrich, Production of food-grade germ product by supercritical fluid extraction, U.S. 4,496,207 (Jan. 22, 1985).**

The background and prior art section relates that the corn germ flour produced by hexane extraction of corn germ suffers from long term stability problems. The residual lipids left in the germ during normal hexane extraction auto- or enzymatically oxidize and the oxidized products reduce the organoleptic and nutritional qualities of the flour. Inactivation of the oxidative enzymes by toasting has been found to be unsatisfactory from effectiveness and economic considerations.

The results of tests with corn germ flour which has been extracted with CO<sub>2</sub> show that the product contains one-half the residual oil of hexane-extracted flour. Furthermore, the enzymatic activity of CO<sub>2</sub> extracted corn germ flour is reduced seven fold and results in an extended shelf life product with acceptable

**Heigel, W., Process for the production of pure lecithin directly usable for physiological purposes, U.S. 4,367,178 (Jan. 4, 1983).**

Lecithin, a mixture of phosphatidyl choline, phosphatidyl ethanolamine, and phosphatidyl inositol, is used as a surfactant in many food, pharmaceutical, and cosmetic products. Lecithin is a product of soy bean oil degumming operations. It is obtained from the hexane extract of flaked soy beans which contains the seed oil and a portion of the phosphatides that are initially present in the soy bean membrane. The extract is treated with water at 80 °C, and the phosphatides are hydrated rendering them oil insoluble which makes it easy to filter them from the oil. This oil insoluble fraction is termed crude lecithin and consists of about 70% phosphatides and 30% oil. De-oiled lecithin is obtained by treating the crude lecithin with acetone. Lecithin is insoluble in acetone and the oil is, and a separation into a 90 to 95% phosphatides fraction can be achieved quite readily. The prior art discussion in the patent describes the disadvantages of having residual solvents, high energy requirements to evaporate the solvents, and the like in the hexane extraction process.

The new process involves the production of de-oiled lecithin by subjecting crude lecithin to supercritical CO<sub>2</sub> extraction. The soy bean oil dissolves in CO<sub>2</sub> and lecithin does not. One of the examples relates that 1,000 g of crude lecithin is extracted with CO<sub>2</sub> at 60 °C and 400 atm for 4 hours. The CO<sub>2</sub> extracts 380 g of a yellow, clear oil, 30 g of water, and the residual material, 580 g of a solid, light yellow substance, which is the de-oiled lecithin, is removed from the extraction vessel at the end of the cycle.

**Schutz, E., H.R. Vollbrecht, K. Sandner, T. Sand, and P. Muhlnickel, Method of extracting the flavoring substances from the vanilla capsule, U.S. 4,470,927 (Sept. 11, 1984).**

The patentees describe a process for extracting the aromatic flavoring from vanilla beans. The beans are finely ground at a temperature of  $-40^{\circ}\text{C}$ , and the ground mass subjected to high pressure liquid  $\text{CO}_2$  extraction. The term "high pressure liquid" is used because the invention claims the use of  $\text{CO}_2$  at a pressure substantially above the vapor pressure and a temperature below the critical temperature.

In one example the ground material was extracted with  $\text{CO}_2$  at 160 atm and  $25^{\circ}\text{C}$ ; a 98.5% yield of aromatics was obtained. The  $\text{CO}_2$  extract and an alcohol extract of another sample of ground vanilla beans were used in comparative tests to flavor ice cream mixtures. In an evaluation test by a panel of 14 persons, the ice cream flavored with  $\text{CO}_2$  extract was preferred unanimously. Gas chromatographic analyses of the  $\text{CO}_2$  and alcohol extracted materials showed that the  $\text{CO}_2$  extract contained 20 to 30% more of the components responsible for vanilla flavor, and additionally, the  $\text{CO}_2$  extract was found to contain some high volatile flavor components which were not detected in the alcohol extract.

**Makin, E. C. Purification of vanillin, U.S. 4,474,994 (Oct. 2, 1984).**

The patent describes a new supercritical fluid process for purifying crude vanillin which derives from eugenol, safrole, or preferably from wood products, e.g., lignins, lignosulfonates, or spent sulfite cooking liquor. Currently, crude vanillin is obtained from wood products as a result of some fairly lengthy processing. Waste sulfite liquor is reacted with air and  $\text{NaOH}$  and some of the lignosulfonate in the liquor is oxidized. The reacted mass is extracted with 1-butanol and this extract is reacted with aqueous  $\text{NaHSO}_3$ . The aqueous phase from this extraction is subsequently reacted with  $\text{H}_2\text{SO}_4$  and air to produce  $\text{SO}_2$  and crude vanillin. A vacuum distillation of the organic phase increases the purity of the crude vanillin to 50 to 70%. Purified vanillin can be obtained from the crude material by a multiple crystallization process which is related in the background to be expensive. In the reaction scheme to convert lignin to vanillin co-products such as p-hydroxybenzaldehyde, acetovanillone, 5-formyl vanillin, and others are produced with the vanillin and their presence increases the complexity of the total purification process.

In one of the examples, it is described that "supercritical"  $\text{CO}_2$  at conditions of 53 atm and  $40^{\circ}\text{C}$  in a static reactor increased the purity of vanillin from 82% to 93% in a single stage. Compounds such as guaiacol, "light ends and tar," and acetovanillone were dissolved by the  $\text{CO}_2$  preferentially. For additional experimental results, the patentee related that all the tests described in the examples were repeated with liquid  $\text{CO}_2$  at  $25^{\circ}\text{C}$  (no pressure was stated) and that no purity improvement was seen. At the end of the invention section the patentee states that he considers the term "supercritical" in his claims to consist of a temperature higher than the critical temperature but not necessarily a pressure higher than the critical pressure.

**Coenen, H., R. Hagen, and M. Knuth, Method for obtaining aromatics and dyestuffs from bell peppers, U.S. 4,400,398 (Aug. 23, 1983).**

A process for extracting the aromatics and dyestuffs from sweet and hot red peppers is described. Depending upon the method of operation the aromatics and dyestuffs can be individually concentrated. Hot red peppers contain an aromatic fraction consisting of a variety of organic compounds, the most pungent of which is the alkaloid, capsaicin, and a carotinoid fraction, the largest component of which is capsanthin. It is possible to extract the aromatics "preferentially" (i.e., they are much more soluble than are the carotinoids) by operating at two sequential and increasing pressure levels. First, extraction is carried out at a low pressure to extract the aromatic fraction and when the aromatics are dissolved and separated from the gas, a much higher pressure is used to extract the capsanthin.

One of the examples states that 930 g of dried, ground, very hot red pepper is extracted with 120 kg of CO<sub>2</sub> at 120 atm and 40 °C. The extract is 140 g of extremely pungent, orange-yellow paste. The extraction pressure is increased to 320 atm and 50 kg of CO<sub>2</sub> is passed through the charge to extract 22.7 g of dark red liquid concentrate. The dyestuff (the dark red liquid) is free of flavor and fragrance and can be used as a food dye.

**Heine, C. and R. Wust, Method for the production of food additives with improved taste, U.S. 4,427,707 (Jan. 24, 1984).**

The background section relates that the beans of the locust bean tree yield a gum powder that is a swelling substance and that the pods which house the beans yield a product which, because of its brown color, is suitable for extending or substituting for cocoa powder. Sometimes the locust pod powder has an unpleasant odor and tastes like burned fat so that it cannot be used to produce a high quality substitute for cocoa powder. The locust bean gum powder often has an unpleasant taste and odor. The discussion also relates that other gums such as guar gum powder also have similar sensory problems. The gums, incidentally, are used in the manufacture of such products as ice cream, sauces, and puddings.

Several examples gave results of the extraction of locust bean pod powder (the cocoa substitute) and of locust bean and guar gum powder with CO<sub>2</sub> at 350 atm and 45 °C. The extraction with CO<sub>2</sub> produced powders with pleasant odor and agreeable taste.

**Behr, N., H. van der Mei, W. Sirtl, H. Schnegelberger, and O. von Ettingshausen, Process for the preparation of spice extracts, U.S. 4,490,398 (Dec. 25, 1984).**

We previously reviewed a spice extraction patent, U.S. 4,123,559, that described a two step process. First the use of dry CO<sub>2</sub> to extract aromas and then, moist CO<sub>2</sub> to extract the flavor components. The two step process in this patent is different. Subcritical CO<sub>2</sub> is first used to extract the aroma components, typically ester, aldehyde, and ketone compounds, but it is not of sufficient dissolving power to extract the alkaloid (flavor) components.

The patentees carry out CO<sub>2</sub> extraction of black pepper "Madagascar" operating according to the instant invention and according to the invention of the other spice extraction patent, U.S. 4,123,559. The table below taken from the patent compares the results of extracting pepper using both processes.

Comparison of Extract Yields and Analysis

This patent Step 1	CO <sub>2</sub> Conditions liquid, 300 bar, 29 °C	Yield and Analysis 4.5% (2.1% essential oil, 0.9% piperine )
Step 2	supercritical, 350 bar, 55 °C	6.4% (0.1% essential oil, 6.3% piperine)
U.S. 4,123,559 Step 1	CO <sub>2</sub> Conditions dry supercritical, 350 bar, 57 °C	Yield and Analysis 10.4% (1.1% essential oil, 8.2% piperine )
Step 2	moist supercritical, 350 bar. 58 °C	1% (1% piperine)

The patentees state that the total yields in both cases are about the same but that the new process results in the fractionation of piperine from the oils. However, the patentees of U.S. 4,123,559, Vitzthum and Hubert, stated specifically that for the case of black pepper, dry supercritical CO<sub>2</sub> extracted some of the alkaloid flavor component, whereas for some of the other spices they tested dry CO<sub>2</sub> does not extract the alkaloid flavors. It would have been a better evaluation of the effectiveness of the current patent if Behr et al had performed comparative experiments on a spice that Vitzthum and Hubert found to require water in the second step.

**Biernoth, G. and W. Merk, Fractionation of butterfat using a liquefied gas or a gas in the supercritical state, U.S. 4,504,503 (Mar. 12, 1985).**

Butterfat is a complex mixture of triglycerides composed of fatty acids that range from butyric acid (C4) to stearic acid (C18). The major components (in decreasing order of concentration) are lauric (C12), oleic (C18:1), stearic (C18), myristic (C14), caproic (C6) and caprylic (C8). For comparison, most vegetable oils such as corn, cottonseed, soybean, and sunflower are made up essentially exclusively of C16 and C18 fatty acids of varied unsaturation. Because of the closeness of molecular weight and especially because of varying unsaturation within a carbon number, seed oil triglycerides cannot be readily fractionated by supercritical fluid extraction. However, because butterfat is composed of a much wider range of molecular weights, it can be fractionated.

An example provides quantitative information on the use of supercritical CO<sub>2</sub> to separate a butter oil into two fractions. Conditions of 200 bar and 80 °C were used in the extractor and 30 bar and 30 °C in the separator. With a feed of 700 g an extract of 135 g and a residue of 560 g were obtained. The extract consisted primarily of triglycerides composed of C4 to C12 fatty acids with only a small amount of C18's. The residue consisted of primarily C18 fatty acid triglycerides. The extract was used in formulating a margarine blend, and the residual is useful in fat blends used for making (puff) pastry.

**Amer, G. I., Separation of neutrals from tall oil soaps, U.S. 4,422,966 (Dec. 27, 1983).**

Crude tall oil is a mixture of fatty acids, resin acids, and neutrals (i.e., no carboxylic acid functionality). The background section relates that neutrals interfere with the separation of the fatty acids from the resin acids and in industrial practice the neutrals are removed by molecular distillation. However, it is difficult to separate the neutrals from the other components because of vapor pressure similarity considerations. Tall oil soap, the precursor to crude tall oil, is a pasty emulsion of the neutrals and the sodium salts of the fatty and resin acids. The patent states that it is possible to extract neutrals from the soap with a liquid hydrocarbon solvent, but the prior art discussion relates that subsequent liquid hydrocarbon solvent recovery steps are relatively difficult. The neutrals can be separated from the soaps by a hydrocarbon solvent, incidentally, because the neutrals are lipophiles whereas the soaps are ionic and do not dissolve in the hydrocarbon. Similarly the neutrals will dissolve in a supercritical fluid like ethylene, or propane, or the chlorofluorocarbons, and the use of these gases in the supercritical state is the invention. Like the case of liquid hydrocarbon solvents, the ionic soap compounds will not dissolve in the supercritical gases. CO<sub>2</sub> is specifically not listed among the gases, and we shall discuss the case of CO<sub>2</sub> extraction of the emulsion later which is the subject of the next patent.

The figure shown on the patent face page is a flow chart of the laboratory apparatus which was used to carry out the test. A sample of 15 g tall oil soap was charged to the extractor 22; the charge contained 4.9% neutral oil. The sample was extracted with ethylene at 4000 psi, 70 °C. An extract sample weighing 0.54 g was analyzed and was found to contain 64% neutrals which represented almost one-half the neutrals present in the charge. The identity of the other 36% fraction of the extract was not reported but probably consisted of free resin and fatty acids.

**Lawson, N.E. and G. I. Amer, Acidulation and recovery of crude tall oil from tall oil soaps, U.S. 4,495,095 (Jan. 22, 1985).**

We presented some data on pH of CO<sub>2</sub> solutions when we discussed glycerol drying of CO<sub>2</sub> (U.S. 4,478,612), and we also discussed the (partial) conversion of acetate salts to acetic acid using CO<sub>2</sub> as an extractant of acetate solutions. This patent makes use of the ability of wet CO<sub>2</sub> to convert soaps (sodium salts of fatty acids) to fatty acids which are soluble in CO<sub>2</sub>.

The pK's of long chain fatty acids are about 5. Thus, if a soap is in solution, treating the solution with CO<sub>2</sub> will convert some of the salt to free acid and will result in an extraction of the acid into the CO<sub>2</sub>. Strictly speaking, the salts of C18 acids are not soluble in water. However, all that is required is that the CO<sub>2</sub> be moist since dry salts will be converted to free fatty acid by the action of moist CO<sub>2</sub>. (Krukoniš 1981. Unpublished data, fatty and aromatic acids extraction from salts).

Returning now to the patent, the invention taught is the contacting of crude tall oil soaps (a moist mixture of neutrals and sodium salts of fatty and resin acids) with CO<sub>2</sub>. The CO<sub>2</sub> converts the salts to free fatty and resin acids which then dissolve in the CO<sub>2</sub> (but probably so are some of the neutrals). One example describes a laboratory test that reports that from a charge of 9.65 g tall oil soap five fractions were extracted with supercritical CO<sub>2</sub>. The first fraction contained 88% resin + fatty acids, and the fifth fraction contained 72% resin.

**Fremont, H. A., Extraction of Coniferous woods with fluid CO<sub>2</sub> and other supercritical fluids, U.S. 4,308,200 (Dec. 29, 1981).**

The process to extract chemical components from wood is shown in the figure. Wood chips are charged (batchwise) to the extractor 4. CO<sub>2</sub> at conditions of about 1,175 psi and 40 °C is fed to the extractor via line 6. The extract stream consisting of organics such as tall oil and turpentine which dissolve in CO<sub>2</sub> exits the extractor via line 12, and the stream is reduced stagewise in pressure in vessels 14, 20, and 22. Depending upon the particular conditions of pressure and expansion, it is related that two fractions, tall oil and turpentine, or a plurality of fractions, individual terpenes, individual fatty acids, and individual resin acids, can be separated.

We discussed two tall oil extraction patents earlier, and we related that tall oil is the material that derives from wood pulping and that it consists of a mixture of resin acids, fatty acids, and neutrals. Fatty acids are present in trees in primarily triglyceride form, and the triglycerides are saponified to fatty acids during pulping, so we wonder if the patentee means triglycerides are extracted instead of fatty acids. As we develop later, we wonder about many other things that he relates.

An example describes a specific test. Twenty pounds of pine chips (and we assume they contain their normal moisture of about 50+%) are extracted with 29 pounds of CO<sub>2</sub> at 1,175 psi and 40 °C. At the end of one minute of contact, the CO<sub>2</sub> solution is drawn from the vessel and decreased in pressure stagewise, first to 1,145 psi and 40 °C where 0.24 lb of resin acid precipitates from solution; second to 1,115 psi and 38 °C where 0.11 lb of fatty acids precipitate; and last to a vessel at 1,085 psi and 34 °C where 0.037 lb of turpentine collects.

We are very surprised that a pressure decrease of only 30 psi and a simultaneous temperature decrease of only 2 °C can result in the separation of resin acids from fatty acids. We don't believe there are 0.11 lb fatty acid in 20 lb of moist pine chips (and this has been verified in discussions with technical personnel in the pulp and paper industry). Again, we wonder if the patentee means 0.11 lb triglycerides. From the data given in the above example, we can calculate a minimum solubility of the "fatty acids" in CO<sub>2</sub> at 1,145 psi, 40 °C. It is 0.20 wt%. Even though we wonder if the patentee means triglycerides instead of fatty acids, we now state that the 0.11 lb of "fatty acid" recovered in the second pressure reduction step cannot be triglycerides either since the solubility of triglycerides in CO<sub>2</sub> at 1,145 psi, 40 °C is only 0.02 wt%. We wonder what the patentee has extracted. Additionally, he could not have precipitated turpentine at 34 °C and 1,085 psi because the absolute solubility of turpentine is much higher than the 0.07% we calculate from his data in the patent. (Krukons 1984. Unpublished data).

**Blewett, C. W. and Turner, S. W., Process for separating fatty materials from supported nickel catalysts, U. S. 4,584,140 (Apr. 22, 1986).**

Supported nickel catalysts and catalyst-clay mixtures are commonly used in hydrogenation processes where completely saturated products are desired. In these processes, residual fatty acid can often remain on the catalyst, causing a substantial reduction in both the process yield and catalyst activity. In addition, residual fatty acid content interferes with the recovery of nickel from spent catalyst. As a result, it is highly desirable to remove residual fatty acids from supported nickel catalysts.

Prior procedures for the removal of long-chain fatty acids from earths and clays generally involve treatment with aqueous alkali solutions at high temperatures. Commonly,

the clay is washed repeatedly at a temperature of  $\sim 80^{\circ}\text{C}$  with an alkali solution followed by the addition of an acid. Other procedures involve the repeated rinsing of the clays with aliphatic hydrocarbon solvents.

Previous studies have shown that fatty acids are quite soluble in supercritical carbon dioxide. Solubility levels of 1 to 10% are easily obtained for fatty acids, triglycerides, and esters in  $\text{CO}_2$ . In addition, several previous patents exist for the extraction of fatty materials using supercritical fluids. Therefore, a process which uses supercritical  $\text{CO}_2$  for the extraction of fatty acids from spent nickel catalyst should be successful.

The patentees conduct several experiments to test the feasibility of the process. A continuous process is described in which the catalyst with approximately 40 wt% is placed in a 1" x 12" cylindrical cell and the fatty acid is extracted with supercritical  $\text{CO}_2$ . The extractor is brought to a temperature of 50 to  $65^{\circ}\text{C}$ , and pressurized to between 2,000 and 4,000 psi. The carbon dioxide is allowed to flow through the system at a rate of 8 standard cubic feet per hour until about 60 liters of carbon dioxide passes through the system. At a temperature of  $50^{\circ}\text{C}$  and a pressure of 2,500 psi, approximately 65 % of the fatty acid was removed from the catalyst. When the temperature was increased to  $65^{\circ}\text{C}$  at a pressure of 2,500 psi, about 90% of the acid was removed. The use of pressures greater than 2,500 psi did not cause a significant increase in the total percent acid recovered. A separate experiment was conducted in which the catalyst was pretreated with sulfuric acid and subsequently treated with carbon dioxide at 2,500 psi and  $65^{\circ}\text{C}$ . With this method, about 95 to 97% of the acid could be removed.

**Grubbs, H. J., Prasad, R., Howell, T. M., Process for removal of basic materials, U. S. 5,018,540 (May 29, 1991).**

The primary process for the removal of basic materials that the patentees address is the extraction of nicotine from tobacco without materially affecting the content of the other components in the tobacco. The inventors refer to the multistep process taught by Roselius and Hubert (first edition, page 376; U. S. 4,153,063) as being disadvantageous. Roselius teaches to first extract aromas from dry tobacco with  $\text{CO}_2$ , then extract nicotine from moistened tobacco, and finally dissolve the extracted aromas from the first step and deposit them into the tobacco. Grubbs, et al., argue that disadvantages of the Roselius process include expense, time, and potential degradation of aromas during prolonged processing.

The improved process uses  $\text{CO}_2$  to extract both nicotine and aromas in one step and then the nicotine is removed selectively from the  $\text{CO}_2$  before it is recycled to the vessel holding the tobacco. The selective removal is carried out by passing the nicotine-aroma-laden  $\text{CO}_2$  phase through an acid trap. A variety of acids are suggested such as sulfuric, phosphoric, nitric, malonic, succinic, citric, and tartaric and their alkali metal salts. The acid can be dissolved in water or it can be distributed onto a packing.

Additionally the patent describes pretreating the tobacco to render the nicotine extractable at "milder conditions." Ammonium and sodium bicarbonate, glycosylamines, ammonia, trimethyl amine, etc. are effective in "freeing" the nicotine. There is one interesting result in this patent. The inventors state that solely dry  $\text{CO}_2$  can extract nicotine from dry tobacco in contradistinction to Roselius and Hubert. Dry  $\text{CO}_2$  extracts 94.4 % of the nicotine from the dry tobacco at  $70^{\circ}\text{C}$  and 260 atm and at a ratio of 150 lb  $\text{CO}_2$  per pound of tobacco.

Krase, N. W. and A. E. Lawrence, Process for the preparation of ethylene polymers, U.S. 2,396,791 (Mar. 19, 1946).  
Krase, N. W., Process of separating ethylene polymers, U.S. 2,388,160 (Oct. 30, 1945).  
Hunter, E. and R. B. Richards, Fractionation of polymeric ethylene, U.S. 2,457,238 (Dec. 28, 1948).  
Cottle, J. E., Supercritical polymerization, U.S. 3,294,772 (Dec. 27, 1966).  
Copelin, H. B., Method for reducing oligomeric cyclic ether content of a polymerizate, U.S. 4,306,058 (Dec. 15, 1981).

**Krase, N. W. and A. E. Lawrence, Process for the preparation of ethylene polymers, U.S. 2,396,791 (Mar. 19, 1946).**

This patent is concerned primarily with the polymerization of ethylene at conditions high above its critical temperature and pressure. The Krase and Lawrence patent covers polymerization but it also describes the separation of various oligomers by stagewise pressure reduction. The multistep sequence results in a lower energy recycle/separation process which produces discreet fractions of polyethylene of different molecular weight. A portion of the example and process operation is excerpted from the patent to point out once more that supercritical fluid extraction and separation have been known and understood for 40 to 50 years.

“....the reaction mixture is passed from the reactor (the converter 8 shown in the figure) to a pressure let-down valve 10 wherein the pressure is reduced from 4,000 atm to below 500 atm. The stream passes from this valve to a separator 11 in which the liquid and solid constituents separate from the gas....”

Operation of the total process with the multiple pressure reduction steps results in a lowest energy consumption process.

**Krase, N. W., Process of separating ethylene polymers, U.S. 2,388,160 (Oct. 30, 1945).**

This patent was filed earlier and issued earlier than the previous Krase and Lawrence patent just discussed. The previous one described a two (or more) step pressure reduction as part of the overall polymerization process. This one describes the use of isobaric temperature change in some regions of operating space and simultaneous adjustment of pressure and temperature in others. In a discussion of the invention we learn that Krase used an isobaric, decreasing temperature profile to fractionate the polyethylene

“...it has been found that, in lieu of dropping the pressure in stages, effective fractionation can be realized by dropping the temperature in stages while maintaining the pressure substantially constant, and it has been found



that each one of the individual fractions has physical and chemical properties different from the fractions obtained at higher or lower temperature.”

**Hunter, E. and R. B. Richards, Fractionation of polymeric ethylene, U.S. 2,457,238 (Dec. 28, 1948).**

Reference to parts of this patent was made in Chapter 9. There are actually two processes described that are carried out with supercritical fluids: fractionation of solid polymers and comminution of solid polymers that are normally difficult to obtain in the form of fine granules or powders. In the examples given, a number of polymers, operating conditions, and observations are presented. One of the examples is presented here for its informational value.

**Example 3**

“A stirred vertical cylindrical vessel contains a mixture of 12 parts polyethylene of mean molecular weight 21,500 and 100 parts of ethylene at 1,400 atm and 90 °C. The vessel is then cooled by a blast of cold compressed air to 30 °C, the pressure falling to 450 atm. The vessel is blown down to atmospheric pressure and opened. The upper part of the vessel is found to contain 1.2 parts of powdered polyethylene composed of loose aggregates of approximately spherical particles of average diameter below 0.01 mm. of molecular weight 9,000, while the bottom of the vessel contains a fused mass of 10.8 parts of polyethylene of molecular weight 23,000.”

The information from this example tells us that 21,500 molecular weight polymer does not dissolve completely in ethylene, and a “top” phase and a “bottom” phase are formed. When the vessel is cooled (by the blast of cold air), both the phases are, of course, cooled. The example does not say if during the subsequent ethylene blowdown step any polyethylene escapes. However, at the cooled conditions, polyethylene solubility in ethylene is virtually nil and, therefore, we suggest that the aggregates of polyethylene are formed during the cooling step. The description of the polyethylene at the bottom of the vessel as “a fused mass” indicates that most of the ethylene had left the polyethylene before it solidified.

**Cottle, J. E., Supercritical polymerization, U.S. 3,294,772 (Dec. 27, 1966).**

The prior art discussion in the patent tells us that during the reaction to form polypropylene (and other olefin polymers) both crystalline and non-crystalline polymers are produced in the process. For many purposes only the crystalline form is desired, and the noncrystalline polypropylene must be removed in some additional processing steps which add capital and operating costs to the overall process.

The improved polymerization process described in this patent operates at supercritical propylene conditions. The crystalline polymer that is formed (and that is dissolved in the propylene) is separated from the non-crystalline form by pressure reduction. A separation between the two forms is effected because the crystalline polymer precipitates while the non-crystalline polymer remains dissolved. The noncrystalline polymer is separated from

the propylene solvent in another pressure reduction stage, and the propylene (both as reactant and solvent) is recycled.

The flow chart of the process is presented in the figure. The monomer (propylene) is introduced via line 1 into the reactor 2; a catalyst is introduced via line 3. After the desired conversion is achieved, the reactor effluent is reduced in pressure across valve 19 and is passed to vessel 5. Conditions are adjusted by valves 19 and 10 so that the crystalline polypropylene (which is much less soluble than non-crystalline polypropylene) precipitates as a powder and is removed from the vessel via line 7. The remaining solution of non-crystalline polypropylene catalyst and propylene is conveyed to the fractionator 9 where the solvent/monomer is separated from the remaining polypropylene and recycled. An example gives quantitative information. The reaction is carried out at 750 psig and 210 °F, and after sufficient polymerization the reactor effluent is expanded to 130 psig and 60 °F. The crystalline polypropylene precipitates and the non-crystalline material remains dissolved and can thus be separated.

The molecular weight of the crystalline polypropylene formed is not given in the example, but we find it surprising that crystalline polypropylene of any significant molecular weight can be dissolved in supercritical propylene at conditions just barely above its critical point. Recall that in Chapter 9 we reported that propylene at much higher conditions of 6,500 psi and 155 °C dissolved only about 20% of a commercial isotactic (crystalline) polypropylene. Furthermore, that fraction of dissolved polypropylene probably consisted only of the lower molecular weight oligomers (Krukonis 1981e).

**Copelin, H. B., Method for reducing oligomeric cyclic ether content of a polymerizate, U.S. 4,306,058 (Dec. 15, 1981 ).**

Homo and copolymers of tetrahydrofuran (THF) and alkylene oxides (AO) are used as "soft segment" glycols in the preparation of polyurethanes. In the process of producing the THF-AO homo and copolymers certain oligomeric cyclic ethers are also produced and can comprise 7-15% of the polymer. These cyclic ethers are undesirable because when the polymers are used to prepare polyurethane the cyclic ethers tend to degrade the polyurethane's properties.

The use of supercritical fluids to extract the cyclic ethers from the polymerizate is described. In one example it is related that a charge of THF-ethylene oxide polymerizate containing 8% cyclic ethers is contacted in batch continuous mode with propylene at 100 °C and 83 atm. The residual polymerizate contains 2% cyclic ether content. No gas volume is given in this example or in the three other examples with other polymers and copolymers extracted using supercritical ethylene and propylene. Thus, no distribution coefficients can be calculated to determine the potential industrial value of this patent.

- deFillippi, R. P. and J. E. Vivian, Process for separating organic liquid solutes from their solvent mixtures, U.S. 4,349,415 (Sept. 14, 1982).
- Hagen, R. and J. Hartwig, Method for separating ethanol from an ethanol containing solution, U.S. 4,492,808 (Jan. 8, 1985).
- Victor, J. G., Ethanol extraction process, U.S. 4,508,928 (Apr. 2, 1985).
- Bhise, V. S. and R. Hock, Process for recovering ethylene oxide from aqueous solutions, U.S. 4,437,938 (Mar. 20, 1984).
- Bhise, V. S., Process for preparing ethylene glycol, U.S. 4,400,559 (Aug. 23, 1983).
- Hardman, H. F., Dehydration of water soluble monomers with liquid CO<sub>2</sub>, U.S. 4,253,948 (Mar. 3, 1981).
- Shimshick, E. J., Removal of organic acids from dilute aqueous solutions of salts of organic acids by supercritical fluids, U.S. 4,250,331 (Feb. 10, 1981).
- Peyado, P. R. and Sikonia, J. G., Process for the removal of trace quantities of hydrocarbonaceous compounds from an aqueous stream, U. S. 4,568,447 (Feb. 4, 1986).

**deFillippi, R. P. and J. E. Vivian, Process for separating organic liquid solutes from their solvent mixtures, U.S. 4,349,415 (Sept. 14, 1982).**

The use of this process concept for the separation of ethanol from water was discussed in detail in Chapter 8. The invention is the combination of an extractor using near critical liquid or supercritical fluid, a high pressure distillation column to separate ethanol from the extractant, and a vapor recompressor for raising the temperature of the recycled extractant. This stream provides the energy source to the reboiler to carry out the distillation.

Figure 2 in the patent is worthy of discussion. It is reproduced below and it gives the distribution coefficients for various alcohols and esters in equilibrium with CO<sub>2</sub>-water. Note that the units of the ordinate are not given. Throughout this book distribution coefficients have been given in weight units. Recall from the discussion in Chapter 9 that for ethanol, the value is about 0.09. Figure 2 reports the distribution coefficient for ethanol as about 0.24. Therefore, the distribution coefficient values must have been calculated on a mole basis since the ratio of molecular weights of CO<sub>2</sub> to water is 2.4. This fact by itself is not important, since any consistent units for calculating the distribution coefficient are satisfactory as long as they are specified. An evaluation of the economic viability of the ethanol separation process has recently been carried out. (Fong, W. S., 1982. Process Economics Program Report 149, Ethanol for Gasohol, SRI International, Inc.). Fong used the distribution coefficients given in Figure 2 and fixed the solvent to feed ratio in the economic analysis at 0.24. Fong assumed that Figure 2 gives weight basis coefficients which it does not. With a distribution coefficient that is too high, the extraction is predicted to be too easy, and the economics are projected to be optimistic.

**Hagen, R. and J. Hartwig, Method for separating ethanol from an ethanol containing solution, U.S. 4,492,808 (Jan. 8, 1985).**

In this invention ethanol is extracted from solution with supercritical CO<sub>2</sub>. The CO<sub>2</sub> rich phase leaving the extractor is isobarically passed over activated carbon which adsorbs the ethanol. The ethanol-free CO<sub>2</sub> is then recycled to the extractor. When the activated carbon is loaded with ethanol, it is regenerated using gaseous CO<sub>2</sub>.

A flow chart of the process is shown in the figure. The stream from fermenter 1 containing 5.6 wt % ethanol is heated to 75 °C and pumped via 2 to column 3 where it is contacted with CO<sub>2</sub> at 80 atm and 75 °C. The raffinate leaving the column contains 2.2% ethanol and is returned to the fermenter through valve 4. (Note that with recycle of the raffinate to the fermenter, it is not necessary to achieve a high recovery of ethanol.) The CO<sub>2</sub>-ethanol stream, which also contains some dissolved water, leaving the top of the extractor is conveyed to vessel 5 which is filled with activated carbon. The ethanol is adsorbed by the activated carbon, and the CO<sub>2</sub> is recycled by compressor 6 to the extractor.

When the activated carbon becomes saturated with ethanol, it is regenerated by passing CO<sub>2</sub> at 200 °C and 10 atm through the bed. The hot gas stream is cooled to 75 °C in column 11 which causes the ethanol to condense. Ethanol of 98.5% concentration is recovered from the condenser. The CO<sub>2</sub>/feed ratio in the extractor is 7 lb/lb, and the regeneration of activated carbon requires 7 lb CO<sub>2</sub>/lb activated carbon.

Although it is not given in the example, the ethanol concentration of the extract at the conditions of extraction is about 40-50 wt % (CO<sub>2</sub>-free basis). This concentration can be calculated from the distribution coefficient data given in chapter 8 and from the solubility of water in CO<sub>2</sub> at 75 °C which is about 0.6% at conditions in the example. Thus we learn from the patent that the activated carbon acts as a concentration stage, i.e., the activated carbon apparently adsorbs the alcohol preferentially.

**Victor, J. G., Ethanol extraction process, U.S. 4,508,928 (Apr. 2, 1985).**

In some respects this patent is like the deFillippi and Vivian patent, U.S. 4,349,415 although the deFillippi patent claims all near-critical liquids and supercritical fluids for extracting all organics while this one claims propylene as the extractant for ethanol. Both patents describe that the solvent and the extracted organic are separated by distillation. The major difference is in the supply of energy to the reboiler in the solvent distillation column. U.S. 4,349,415 utilized vapor recompression while this one uses a heat pump.

The figure on the patent face page shows the flow sheet for the process. The left hand side of the flow chart shows the extraction sequence, and the right hand side, specifically, extraction column and associated pumps and heat exchangers, the solvent-organic separation. By now the extraction side should be quite familiar.

The heat pump philosophy is the new twist here. A heat exchanger supplies energy to vaporize propylene from the alcohol. The vaporized propylene exits at the top of the extraction column and is condensed in heat exchanger. A heat pump "works" on the heat of condensation of propylene to supply the energy to the reboiler of the heat exchanger.

It would have been informative if the patentee had compared the heat pump and vapor recompression processes.

**Bhise, V. S. and R. Hock, Process for recovering ethylene oxide from aqueous solutions, U.S. 4,437,938 (Mar. 20, 1984).**

In the current process for producing ethylene oxide from ethylene and oxygen, large amounts of water are used to extract the product from the reacted gas stream containing the ethylene oxide. The quite dilute ethylene oxide-water stream from this gas-liquid absorption process is then subjected to a distillation in a subsequent step which the patent says is costly.

The improved process utilizes  $\text{CO}_2$  to extract ethylene oxide from water in a flow scheme which is similar to the other liquid extractions described previously. A block diagram in the patent depicts operation of the process. Ethylene oxidation and adsorption of the ethylene oxide in an absorber are carried out in the traditional manner, but the water stream from the absorber is then sent to a stripper where  $\text{CO}_2$  strip extracts the ethylene oxide from the water solution. The  $\text{CO}_2$  stream containing the ethylene oxide is lowered in pressure and sent to a high pressure distillation column called the ethylene oxide purifier.  $\text{CO}_2$  is vaporized, and as previously described throughout this book, vapor  $\text{CO}_2$  exhibits little dissolving power. Almost pure  $\text{CO}_2$  vapor is distilled and condensed in the column and a concentrated ethylene oxide stream containing some  $\text{CO}_2$  is obtained.

The example relates that an aqueous solution containing 0.24 wt % ethylene oxide is extracted with  $\text{CO}_2$  at 1,250 psi, 32 °C to remove all the product. (In the example concentrations are given in mol % and they have been converted to wt % for this discussion.) Based upon the  $\text{CO}_2$  and product data given in the example the solvent to feed ratio is 0.084 lb  $\text{CO}_2$  /lb feed which is a very small and very attractive value. From this value of the feed ratio it is possible to determine the value of the distribution coefficient. If we assume that the extraction of ethylene oxide from water by the  $\text{CO}_2$  was at "near equilibrium" conditions, the inverse of the solvent to feed ratio gives the distribution coefficient which is about 12 in this instance.

Other data in this ethylene oxide extraction patent provide an independent method to calculate the distribution coefficient. Examples state that the  $\text{CO}_2$  stream leaving the extractor contains 2.9 wt % ethylene oxide which is in equilibrium with a liquid solution containing 0.24 wt % ethylene oxide. The  $y/x$  ratio is 12, a very good independent corroboration of the value calculated from the inverse of the solvent to feed ratio and the assumption that the extraction was an equilibrium one.

**Bhise, V. S., Process for preparing ethylene glycol, U.S. 4,400,559 (Aug. 23, 1983).**

As an extension of the patent describing the use of supercritical  $\text{CO}_2$  to extract ethylene oxide from water solution, this patent describes a process which employs a subsequent chemical reaction in the  $\text{CO}_2$ -ethylene oxide stream to form ethylene glycol. The extraction/reaction process concept is explained with reference to the block diagram. As was given in the previous patent, an aqueous ethylene oxide solution and a supercritical  $\text{CO}_2$  stream are fed to contactor where  $\text{CO}_2$  extracts the ethylene oxide. The  $\text{CO}_2$ -ethylene oxide stream leaving the extractor enters a carbonation tower. A suitable catalyst such as quaternary ammonium or phosphonium halide is supplied to the carbonation tower. Ethylene oxide and  $\text{CO}_2$  react to form ethylene carbonate. The reacted stream, still containing the catalyst, is conveyed to a reactor to which water is added. Hydrolysis of the ethylene carbonate takes place at about 90-200 °C to form monoethylene glycol and some higher homologues.  $\text{CO}_2$  is separated from the water-ethylene glycol mixture and

is recycled to the ethylene oxide extractor. The ethylene glycol is separated from by-products and catalyst.

**Hardman, H. F., Dehydration of water soluble monomers with liquid CO<sub>2</sub>, U.S. 4,253,948 (Mar. 3, 1981).**

As we related in Chapter 2, Historical Perspective, Villard reported on phase equilibria of gas hydrates in the late 1800s. Relative to this patent, hydrates form in the liquid CO<sub>2</sub>-water system at a temperature of 5 °C. The stoichiometry of the hydrate, which has been determined by a number of workers, has the formula CO<sub>2</sub>•6H<sub>2</sub>O (Milton, D. J., 1974. CO<sub>2</sub> Hydrates and the Floods on Mars, *Science*, 183, 654.)

This patent makes use of the phenomenon of forming CO<sub>2</sub> hydrates to concentrate and separate organics from water or, more accurately stated, to separate water from organics. In the specific way the process is described it is applied to aqueous solutions containing quite high concentrations of acrylic acid.

In one of the examples a 31% solution of acrylic acid in water was contacted in a static vessel with a liquid CO<sub>2</sub> at 25 °C and 850 psi at a ratio of 1.97:1 CO<sub>2</sub>:solution. After equilibration the lower aqueous phase was withdrawn (the concentration of residual acrylic acid in the withdrawn aqueous phase was not stated in the example). The top CO<sub>2</sub>-rich phase which contained a high concentration of acrylic acid and some water was then cooled to 0 °C to form white hydrate crystals. The crystals were separated from the liquid phase and the CO<sub>2</sub> was evaporated. The resultant acrylic acid contained only 0.9% water.

In another example, an aqueous solution of 34 wt % acrylic acid was contacted at 25 °C and 850 psi with CO<sub>2</sub> at a solvent to feed ratio of 3 in a countercurrent column composed of six theoretical stages. Recovery of acrylic acid was 95.3% in the extraction, and the composition of the extract phase on a CO<sub>2</sub>-free basis was 42.5% acrylic acid-7.5% water. To remove the water the extract phase, including the CO<sub>2</sub>, was cooled to 0 °C. Crystals were formed and were filtered. The resultant acrylic acid product contained only 1% water.

**Shimshick, E. J., Removal of organic acids from dilute aqueous solutions of salts of organic acids by supercritical fluids, U.S. 4,250,331 (Feb. 10, 1981).**

A specific example from this patent was discussed in Chapter 8 where it was offered that extraction of carboxylic acids from solutions of pH greater than pK was not a very attractive process because all the anion is not converted to the acid form by action of the carbonic acid equilibrium. The abstract of the patent states that CO<sub>2</sub> will react with the salt to form the (free) carboxylic acid which can dissolve in CO<sub>2</sub>. That is strictly correct, but we always suggest that the absolute values be examined to determine such factors as yield and distribution coefficient.

Table 1 summarizes the results obtained. The last column gives an estimate of the distribution coefficient calculated from the material balance and concentration data given in the patent under the assumption that the extraction occurred via extraction into a fixed volume of CO<sub>2</sub> from a fixed volume of liquid containing the carboxylic acid as the sodium salt.

Distribution Coefficients for Extraction of Carboxylic Acids

<u>Example</u>	<u>Acid</u>	<u>Distribution Coefficient (wt. basis)</u>
1	butyric	0.083
6	acetic	0.004
9	methacrylic	0.083
10	benzoic, terphthalic	0.042, 0.058

As the table shows, the distribution coefficients are higher for the higher carboxylic acids. We chose acetic acid for the discussion in Chapter 8, incidentally, because it is a large volume chemical that was considered to be a potential application for supercritical fluid extraction. We know a number of companies evaluated the CO<sub>2</sub> process for recovering acetic acid from water.

**Peyado, P. R. and Sikonia, J. G., Process for the removal of trace quantities of hydrocarbonaceous compounds from an aqueous stream, U. S. 4,568,447 (Feb. 4, 1986).**

We looked at the title of this patent and wondered what difference there might be between it and one issued earlier to deFillippi on the extraction of organic liquid from aqueous streams (first edition, page 426; U.S. 4,349,415). deFillippi was not cited by the inventors nor, we surmise, by the examiner.

deFillippi teaches extraction of organic solutes from their solvent mixtures and, for the most part, the extraction of organics from water. In contrast, the prior art section of the instant patent cites patents on

1. A method to recover bromine from aromatic bromides by reacting the bromides with hydrogen.
2. A method to convert, in the presence of hydrogen, hydrocarbon chlorides to hydrocarbons and hydrogen chloride.
3. A process to regenerate used oils using supercritical fluids.
4. A process to extract both oil and turpentine from coniferous woods.
5. A process to extract spices.
6. A process to produce deasphalted oil from heavy residual hydrocarbons.

We wonder why all the hydrogenation patents and oils and spice extraction patents are cited and not the deFillippi patent which is extremely relevant to Claim 1 of the instant patent ("Claim 1. Process for removal of trace quantities of hydrocarbonaceous compounds from an aqueous stream .. contacting...to dissolve said hydrocarbonaceous compounds...to dissolve at least a portion...of said compounds...to produce an aqueous stream with reduced compounds...separating said compounds...")

Hydrogenation of the extracted impurities is described in the detailed description of the invention as a means of rendering the extracted materials nontoxic, e.g., the hydrogenation of PCBs to nontoxic hydrocarbons. Increasingly, we find that many of the supercritical fluid patents that are issuing are *not* "not obvious to those skilled in the art."

- Berneburg, P. L. and V. J. Krukonis, Method for densification of ceramic materials, U.S. 4,552,786 (Nov. 12, 1985).
- Tewari, P. H. and A. J. Hunt, Process for forming transparent aerogel insulating arrays, U.S. 4,610,863 (Sep. 9, 1986).
- Sievers, R. E. and B. N. Hansen, Chemical deposition methods using supercritical fluid solutions, U.S. 4,970,093 (Nov. 13, 1990).
- Sunol, A. K., Supercritical fluid-aided treatment of porous materials, U.S. 4,992,308 (Feb. 12, 1991).
- Leibovitz, J., Process using supercritical conditions for producing highly accurate and homogeneous powder mixture useful in fabrication of high quality ceramic superconductors, U.S. 5,011,819 (April 30, 1991).

**Berneburg, P. L. and V. J. Krukonis, Method for densification of ceramic materials, U.S. 4,552,786 (Nov. 12, 1985).**

Ceramics exhibit high strength at high temperatures, but the unavoidable presence of flaws leading to slow crack growth has prevented these materials from reaching their full potential. The patentees describe a process to uniformly fill the pores of a ceramic host material with a polymeric ceramic precursor. In this manner the stress intensity is lowered at a flaw site. The ceramic precursor is then subject to further processing to convert the deposited precursor to its final ceramic form. Dissolving the ceramic precursor, infiltrating it into the ceramic host material, and depositing the ceramic precursor in void spaces of the host is accomplished with a supercritical fluid. The desirable characteristics of the supercritical fluids are their ability to dissolve certain oxide and nonoxide precursor ceramics, the low viscosity of the resulting solution, the high diffusivity of the loaded supercritical phase, the ease of depositing the precursor material by reducing the system pressure, and especially the reduced supercritical fluid-solid surface tension that allows for facile penetration of submicron-sized pores.

Four examples were given in the patent, all using supercritical propane with polysilane and aluminum isopropoxide, so-called "precursor ceramic materials." In one instance scanning electron microscopy was used to demonstrate that polysilane was deposited as a smooth surface film on the alumina fibers and fine silicon nitride whiskers. A silicon carbide material with internal pore openings as small as 10 microns was penetrated by supercritical propane laden with aluminum isopropoxide. Weight gains of up to 43% can be obtained depending on the density of the initial host ceramic.

**Tewari, P. H. and A. J. Hunt, Process for forming transparent aerogel insulating arrays, U.S. 4,610,863 (Sep. 9, 1986).**

Making an aerogel involves base-catalyzed hydrolysis and polycondensation reactions of silicon alkoxides in an alcohol followed by 24 hours of aging in the alcohol solvent to produce an alcogel. Then the alcohol is removed from the pores of the alcogel



to form the aerogel. It is the final "drying" step that is the focus of this invention. In the conventional method the alcogel is placed in a bath of alcohol in an autoclave, residual air is purged from the system, and the temperature is raised to about 270 °C, approximately 30 °C above the critical temperature of the alcohol, while maintaining a pressure of approximately 125 bar. The autoclave is slowly depressurized at this elevated temperature to remove the alcohol from the bath and from the gel to minimize the interfacial forces that would be present if there were a vapor-liquid interface in the pores. Therefore, the stress on the gel is minimized and the pore structure is maintained while the alcohol is eliminated. Although mentioned briefly in this patent, it is worth noting that the first aerogels were produced over sixty years ago (Kistler, 1932).

The patentees modify the prior art in the following manner. The alcogel is once again placed in an alcohol bath in an autoclave, but, now the temperature is reduced to 18 °C, and liquid CO<sub>2</sub> at 55 bar is pumped into the autoclave to displace the alcohol. The underlying principle here is that CO<sub>2</sub> and alcohol are infinitely miscible at 18 °C and 55 bar so that a second phase does not form in the pores. The temperature and pressure are adjusted to 40 °C and 82 bar, conditions that are greater than the critical point of pure CO<sub>2</sub> (31.1 °C and 73.9 bar), and the autoclave is slowly vented again avoiding the formation of a second phase, thus minimizing any pore stresses.

The patentees claim that the modified process has a drying time of 6 to 10 hours compared to 2 to 3 days in the prior art, a yield greater than 95% compared to 20 to 50%, and an operating temperature 230 °C less. And, as with all patents that recommend CO<sub>2</sub>, the patentees point out the reduced toxicity of CO<sub>2</sub> compared with other solvents.

While this patent does report on an improved process for making aerogels, the concept of displacing the reaction solvent with a supercritical fluid has been reported as early as 1983 by Schmitt, Grieger-Block, and Chapman as described in chapter 12. In the Schmitt process, the aqueous solvent used to form aerogels of silica is displaced by methanol, the system is heated and pressurized above the critical point of the methanol, and the methanol is vented from the system. The benefit is that methanol has a critical temperature that is 135 °C less than that of water. It is not possible to use CO<sub>2</sub> to displace the water in the gel without the occurrence of a vapor-liquid interface since water and CO<sub>2</sub> are not miscible unless the temperature is raised to greater than 300 °C.

**Sievers, R. E. and B. N. Hansen, Chemical deposition methods using supercritical fluid solutions, U.S. 4,970,093 (Nov. 13, 1990).**

The current technique for making thin film superconductors by chemical vapor deposition requires three separate source gases of the organometallic compounds. It is difficult to precisely control the delivery rate of each organometallic compound from separate metal sources while also obtaining the correct stoichiometry needed to make a high quality superconductor. The process described in this patent attempts to overcome the delivery problem by dissolving the organometallic compounds in desired proportions in a supercritical fluid. The supercritical solution is rapidly expanded producing a vapor or aerosol which undergoes a chemical reaction at or near a substrate surface to form a solid film. The supercritical chemical deposition method is relatively fast and it allows for improved control of reagent stoichiometry and homogeneity in forming thin films.

The patentees examined the delivery of a variety of reagents used to make thin film superconductors. The reagents, metal complexes of Y(THD)<sub>3</sub>, Ba(THD)<sub>3</sub>, Cu(THD)<sub>3</sub>,

and  $\text{Ba}_5(\text{THD})_9(\text{H}_2\text{O})_3(\text{OH})$  were dissolved in n-pentane ( $T_c = 196^\circ\text{C}$ ,  $P_c = 33.7$  bar) at concentrations of 1 to 3 mmolar. The solution was brought to conditions of 1,400 psi and  $210^\circ\text{C}$  and discharged onto a substrate maintained at a low pressure of approximately 1 mm Hg. The metal chelates decomposed at the substrate surface, which was at  $700^\circ\text{C}$ , to form a metallic film of Y, Ba, and Cu. No visible granularities were seen at an electron microscope magnification of 10,000. As desired, the stoichiometric ratios of Y, Ba, and Cu were nearly equal to the ratio of their initial concentrations. In a further experiment the Y-Ba-Cu film was oxidized by an oxygen plasma.

In another example, a metallic yttrium film was prepared by allowing a solidified melt of  $\text{Y}(\text{THD})_3$  to slowly dissolve in supercritical  $\text{N}_2\text{O}$  ( $T_c = 36.4^\circ\text{C}$ ,  $P_c = 72.5$  bar) to form a solution which was discharged at  $140^\circ\text{C}$ . The induced chemical reaction resulted in the deposition of the yttrium on a silicon substrate heated at  $687^\circ\text{C}$ . Micrographs shows uniform distribution of the yttrium. In a fourth experiment, a solidified melt of  $\text{Y}(\text{THD})_3$ ,  $\text{Ba}_5(\text{THD})_9(\text{H}_2\text{O})_3(\text{OH})$ , and  $\text{Cu}(\text{THD})_2$  was slowly dissolved by supercritical  $\text{N}_2\text{O}$  to form a solution. The solution was discharged into a plasma to form a mixed metal oxide film. Although the characteristics of the resultant films were not reported for this experiment, it is not surprising that dissolving a low molecular weight supercritical fluid into the solution would decrease the solution viscosity sufficiently to result in desirable flow characteristics. However, the experiments with nitrous oxide are a bit surprising to us since we have been informed that  $\text{N}_2\text{O}$  decomposes at modestly elevated temperatures. We wonder if the patentees had any difficulty handling  $\text{N}_2\text{O}$  at the reported operating temperatures.

**Sunol, A. K., Supercritical fluid-aided treatment of porous materials, U.S. 4,992,308 (Feb. 12, 1991).**

Monomers and polymers are impregnated into wood to improve the hardness, bending strength, and compressive strength. Usually the wood is immersed into a solution of monomer and polymer and hydrostatic pressure is applied to force the solution into the wood. This impregnation process is time consuming and results in nonuniform impregnation due to impenetrable pores. This method is also used to make polymer impregnated paper, polymer impregnated laminated wood, and polymer impregnated flakeboard, and styapak. The inventors argue that the limitations of the wood impregnation process can be overcome if the monomer or polymer is dissolved into a supercritical fluid that then contacts the wood and by adjusting pressure precipitates the additive into the wood. Moreover, supercritical solvents can be used to promote the polymerization of the monomer deposited into the wood if a polymerization catalyst is also dissolved into the solvent and precipitated into the wood.

A few short examples are given to illustrate the process.

Case 1: At 1,200 psig, wood initially weighing 87.5 g was impregnated with methyl methacrylate to a final weight of 112.0 g.

Case 2: At 1,200 psig, wood initially weighing 84.6 g was impregnated with styrene to a final weight of 109.2 g.

Case 3: A piece of wood impregnated with methyl methacrylate had an initial weight of 34.0 g. The wood was polymerized using azo catalysts at  $52.0^\circ\text{C}$  and 1,500 psig to a final weight of 31.1 g. Unfortunately, the patentee does not present any characterization information about the wood after polymerization.

**Leibovitz, J., Process using supercritical conditions for producing highly accurate and homogeneous powder mixture useful in fabrication of high quality ceramic superconductors, U.S. 5,011,819 (April 30, 1991).**

This is another "process" thought patent. The "inventor" suggests an interesting solution to a tough problem in manufacturing ceramics. A class of ceramic materials known as triple layer perovskite compounds or 1-2-3 compounds have demonstrated the phenomena of superconductivity at temperatures above the boiling point of nitrogen. The manufacture of these compounds requires a high purity, uniform powder mixture of 1 atom of a first element such as lanthanum or yttrium, 2 atoms of one or more rare earth elements, and 3 atoms of copper which is fired in a high temperature oxygen atmosphere. It is the mixing of this compound that is the focus of this patent. The conventional method for producing this powder mixture involves mixing the oxides or carbonates in a ball mill. The ball mill process requires many hours, introduces impurities into the powder, and is not capable of creating a truly uniform mixture.

The inventor proposes an alternate process in claim 1 in which the oxides are dissolved into an unspecified supercritical fluid at unspecified conditions but at 1 to 25 wt% below the solubility of the least soluble component, rapidly expanding the fluid to precipitate a uniform and stoichiometrically accurate mixture, and thermally treating the powder. We wonder how this patent was allowed since the patent by Sievers and Hansen (U.S. 4,970,093) reviewed in this edition of the book, states explicitly the process and conditions needed to dissolve metal complexes for superconductor fabrication. Sievers and Hansen are not quoted by the inventor nor is their quantitative data quoted. We also wonder if the inventor has ever tried to dissolve some of the materials that are listed in the claims section since the instant patent teaches to operate at 1 to 25 wt% less than the saturation amount of the least soluble component: Can we expect compounds such as yttrium to have solubilities at weight percent levels? We do not believe so.

- Hess, H. V., Recovery of fresh water from brine, U.S. 3,318,805 (May 9, 1967).
- Maffei, R. L., Extraction and cleaning process, U.S. 4,012,194 (Mar. 15, 1977).
- Modell, M., Process using a supercritical fluid for regenerating synthetic organic polymer adsorbents and wastewater treatment embodying the same, U.S. 4,061,566 (Dec. 6, 1977).
- Modell, M., R. C. Reid, and S. I. Amin, Gasification process, U.S. 4,113,446 (Sept. 12, 1978).
- Modell, M., Processing method for the oxidation of organics in supercritical water, U.S. 4,338,199 (Jul. 6, 1982).
- Jennings, W. G., R. H. Wohleb, and N. W. Wohlers, High pressure soxhlet extractor, U.S. 4,265,860 (May 5, 1981).
- Dickenson, N. L., Pollutant-free low temperature slurry combustion process utilizing the super-critical state, U.S. 4,292,953 (Oct. 6, 1981).
- Perrut, M., Fractionation process for mixtures by elution chromatography with liquid in supercritical state and installation for its operation, U.S. 4,478,720 (Oct. 23, 1984).
- Eppig, C. P., B. M. Putnam, and R. P. deFilippi, Apparatus for removing organic contaminants from inorganic-rich mineral solids, U.S. 4,434,028 (Feb. 28, 1984).
- Avedesian, M. M., Apparatus and method involving supercritical fluid extraction, U.S. 4,493,797 (Jan. 15, 1985).
- Sumner, W. C., Jr., G. G. Hoyer, and W. G. Kozak, Method of removing water from alkali metal hydroxide solutions, U.S. 4,505,885 (Mar. 19, 1985).
- Schlichta, P. J., Method for growth of crystals by pressure reduction of supercritical or subcritical solution, U.S. 4,512,846 (Apr. 23, 1985).
- Myerson, A. S., Purification of terephthalic acid by supercritical fluid extraction, U.S. 4,550,198 (Oct. 21, 1985).
- Avedesian, M. M., Apparatus and method involving supercritical fluid extraction, U.S. 4,714,591 (Dec. 22, 1987).
- Barstow, L. E., Ward, G. D. and Bier, M., Organic syntheses employing supercritical carbon dioxide as a reaction solvent, U.S. 5,001,224 (Mar. 19, 1991).

**Hess, H. V., Recovery of fresh water from brine, U.S. 3,318,805 (May 9, 1967).**

This patent describes an invention for separating fresh water from brine. The patentees utilize the very low solubility of inorganic salts in organic hydrocarbons and the high-pressure phase behavior of organic hydrocarbon-water mixtures to develop a novel process for recovering salt-free water and for concentrating water soluble salts. The key to the success of the process is the formation of a miscible water-organic hydrocarbon mixture.

As noted in Chapter 3 of this book, the mutual solubility of water-organic mixtures at ambient temperature is very low regardless of the system pressure. The patentees correctly note that the mutual solubility increases as the temperature of the system is increased to near the critical temperature of water. In fact, there is a range of temperatures

and pressures in which water and an organic hydrocarbon are completely miscible. This type of phase behavior is not surprising since it was reported in 1959 by Rebert and Kay (*AIChE J.*, 5, 285) for the benzene-water system. The phase diagram for this system is shown in Chapter 3 of this book and the principles of the high-pressure phase behavior of water-organic hydrocarbon systems are described in detail as a Type IV system.

The first step of the process for recovering fresh water is the removal of inorganic salt, and it is accomplished by forming a water-hydrocarbon phase and an inorganic salt-water phase. The inorganic salt-water phase is then removed from the system. The next step, the recovery of water from the water-hydrocarbon mixture, is accomplished by isothermally increasing the system pressure until the mixture splits into a water-rich phase and a hydrocarbon-rich phase. The degree of separation of water from the hydrocarbon increases with increasing pressure. As we showed in Chapter 3, it is also possible to form two phases by an isobaric temperature change. The patentees relate that the separation of water from the hydrocarbon is more efficient when using an isothermal pressure increase rather than a large isobaric temperature decrease.

**Maffei, R. L., Extraction and cleaning process, U.S. 4,012,194 (Mar. 15, 1977).**

Another thought patent and probably not thought out very thoroughly.

In the operation of the invention, soiled garments are placed batchwise in an extractor, flushed with liquid CO<sub>2</sub>, and a solution of garment oil and CO<sub>2</sub> is separated in an evaporator. The CO<sub>2</sub> is recycled and the process continued until all the garment oil has been extracted.

The process could work (at least technically) for garments soiled with salad oil or light hydrocarbon lubricants. However, garments soiled with milk, spaghetti sauce, beet juice, various desserts, and the like, exemplifying protein, carbohydrate, and anthocyanin dye stains would not be cleaned by this process.

**Modell, M., Process using a supercritical fluid for regenerating synthetic organic polymer adsorbents and wastewater treatment embodying the same, U.S. 4,061,566 (Dec. 6, 1977).**

Three closely related patents on adsorbent regeneration were published between 1977 and 1979, with Modell as the patentee and Arthur D. Little, as the assignee. One of the activated carbon regeneration patents was discussed in Chapter 8. The first in this series of three patents is the application of supercritical fluids to the regeneration of polymeric resin adsorbents. Four flow diagrams of the operation of the process are shown on the face page of the patent, and they depict various operating modes. A polymeric adsorbent spent with organics (from a wastewater treating process, for example,) is regenerated by a supercritical fluid which dissolves the adsorbed organic. The supercritical fluid solution is freed of its dissolved organics by changing pressure and/or temperature of the solution leaving the desorber. In one operating mode, the supercritical fluid exiting the desorber is passed through a turbo-expander to recover energy. In another mode a reactant is added to the supercritical fluid to bring about a chemical reaction with the adsorbate. The other two regeneration patents by Modell are:

U.S. 4,124,528 Process for regenerating adsorbents with supercritical fluids, Nov. 7, 1978.

U.S. 4,147,624 Wastewater treatment with desorbing of an adsorbate from an adsorbent with a solvent in a near critical state, Apr. 3, 1979.

**Modell, M., R. C. Reid, and S. I. Amin, Gasification process, U.S. 4,113,446 (Sept. 12, 1978).**

The better known process which utilizes oxygen or air dissolved in supercritical water to oxidize wastes has been described in Chapter 11 (and it is the next patent covered in this appendix). The present patent was issued three years earlier, and it discusses the gasification and liquification of liquid and solid organic materials in supercritical water.

Examples relate that the gasification tests carried out at conditions above the critical point of water result in little or no char formation whereas tests with the same materials at conditions below the critical point result in substantial and undesirable char yield. For example, at a reaction conditions of 350 °C and 165 atm, about 10% of the carbon in glucose was found as a solid char. If the reaction is carried out at 374 °C and 218 atm, no char is formed.

**Modell, M., Processing method for the oxidation of organics in supercritical water, U.S. 4,338,199 (Jul. 6, 1982).**

This supercritical water patent has been discussed briefly in Chapters 10 and 11, but it is reviewed here briefly.

A mixture of sewage sludge and water in a feed slurry tank is pumped through a heat exchanger, to an eductor where the sludge is mixed with recycle water in the supercritical state. This hot mixture is mixed with oxygen or air and is passed into the oxidizer where reaction of the organics takes place. The heat of reaction raises the temperature of the stream to well above the supercritical temperature of water (374 °C). At these conditions any inorganic materials present in the sludge or the feed water precipitate from solution because supercritical water is not a good solvent for salts. The precipitated inorganic matter is removed in the ash separator. Part of the supercritical water which contains CO<sub>2</sub> formed from the oxidation reactions is sent to a turbine for power generation, and the other part is recycled to the heat exchanger and eductor as described earlier.

**Jennings, W. G., R. H. Wohleb, and N. W. Wohlers, High pressure soxhlet extractor, U.S. 4,265,860 (May 5, 1981).**

This patent is also, like some others we've discussed, not strictly supercritical extraction. However, it is a very clever invention. The device has been used by many groups in their preliminary research programs evaluating supercritical, or liquid, CO<sub>2</sub> extraction.

The patentees place a Soxhlet extractor inside a pressure vessel, a idea that virtually explains itself. An amount of dry ice is placed in the vessel. Solid material which is to be extracted is placed in the thimble in the extractor and the pressure vessel is assembled. Heat is applied to the bath which vaporizes the CO<sub>2</sub>. Cooling water in a condenser acts as

a "cold finger" condensing the vapor  $\text{CO}_2$  in the pressure vessel which trickles downward through the bed of solid material in the thimble. The extract consisting of liquid  $\text{CO}_2$  and dissolved organics continues downward to collect in an internal flask where the  $\text{CO}_2$  is vaporized by the action of the heating bath placed at the bottom of the pressure vessel. The gaseous  $\text{CO}_2$  rises through the internal annular spaces and is recondensed by the condenser to continue its extraction path. When extraction is complete, the system is depressurized slowly. The extract is collected in the internal flask and the residue is in the thimble.

**Dickenson, N. L., Pollutant-free low temperature slurry combustion process utilizing the super-critical state, U.S. 4,292,953 (Oct. 6, 1981).**

The figure in the patent showing the process invention is quite detailed, and the complete description of the operation is quite lengthy and involved. There are no data given so we conclude that this is a thought patent, but it is presented to show the breadth of supercritical fluid applications.

A combustion process is described using a slurry of pulverized coal in a mixture of water and air. The mixture also contains some alkali which is stated to serve as a combustion catalyst. Combustion of the coal raises the temperature to above the critical temperature of water, and the ash that is present in the coal remains suspended in the supercritical medium. This supercritical fluid combustion stream is used to boil water and superheat steam in a countercurrent superheater-boiler train. The steam that is formed in the boiler is used to generate power.

We wonder what the power generation industry thinks about the potential for the invention.

**Perrut, M., Fractionation process for mixtures by elution chromatography with liquid in supercritical state and installation for its operation, U.S. 4,478,720 (Oct. 23, 1984).**

This is the first reference to supercritical fluid chromatography located in the patent literature. The prior art discussion in the patent describes the use of supercritical fluid chromatography for analytical purposes. As described in the patent and in other supercritical fluid chromatography references, gas chromatography cannot be used for separating compounds with high molecular weight if the vapor pressure of these compounds is very low. The patentee relates that liquid chromatography has been effective, but liquid chromatographic separations quite frequently require a quite lengthy analysis time.

The invention is the extension of supercritical fluid chromatography to a scale suitable for the industrial processing of chemicals. The supercritical fluid flows continuously through a chromatographic column which is typically a cylindrical tube filled with a suitable granular porous adsorbent. Periodically, a sample which is to be separated is injected into a mixing station where it is dissolved by the supercritical fluid which first passes through a heat exchanger before entering the chromatographic column. The components in the mixture are displaced at different rates during travel through the column because of their differential affinities for the adsorbent and thus are separated. The separated components are monitored by a detector which actuates the valves sequentially so that the separate components can be isolated in the traps. Separation of the components

from the supercritical fluid by temperature and pressure change occurs in the traps, and the fluid is recycled to a mixer.

Examples presented describe the separation and purification of naphthalene from its associated impurities, alkylated mono- and dicyclic aromatics. Supercritical pentane at 42 atm and 215 °C and a chromatography adsorbent of baked brick impregnated with polyethylene glycol (6000 molecular weight) are used to separate a 95% naphthalene-5% alkylated aromatics mixture into a 99.5% naphthalene fraction of 70% yield and a concentrated impurities fraction of 10% of the feed. Approximately 20% of the product is recycled.

**Eppig, C. P., B. M. Putnam, and R. P. deFillippi, Apparatus for removing organic contaminants from inorganic-rich mineral solids, U.S. 4,434,028 (Feb. 28, 1984).**

The motivation for applying supercritical fluids to the problem of cleaning contaminated solids deriving from platform drilling operations was described in Chapter 10. The patentees suggest that the system would be located on a drilling platform.

In the patent many examples are given of extracting such materials as drilling mud, cuttings, and sand contaminated with fuel oil. CO<sub>2</sub>, halocarbons, and hydrocarbons were tested as the extraction solvents. For example, 48.6 g of drilling mud and cuttings were extracted with 36.4 g of CO<sub>2</sub> at 30 °C and 1,500 psi to yield 1.56 g of clear oil and a non-oily solids product. In another example 32.3 g of oil and cuttings were extracted with 89 g of propane at 60 °C and 500 to 1200 psi to yield 3.5 g clear oil and a gray, dry, non-oily substrate.

**Avedesian, M. M., Apparatus and method involving supercritical fluid extraction, U.S. 4,493,797 (Jan. 15, 1985).**

Although the patentee describes four "examples," we conclude that the examples are made up and that this is another thought patent.

It is of interest to reproduce the first two paragraphs of the patentee's Prior Art section. He writes,

"An extensive literature search conducted by the inventor has revealed that no one has published any information which may have bearing on applicant's invention:

"The search has revealed that no one has thought of extracting lignin and other components from black liquor using supercritical gases, nor of reacting lignin dissolved in supercritical gaseous product in a fluid bed catalytic reactor."

There is one very important reason why the patentee found no published information which "may have bearing on the invention." Supercritical CO<sub>2</sub> cannot dissolve lignin, let alone extract it from a black liquor solution. The patentee describes his four "examples," and we excerpt from one of them.



"Weak black liquor (14% solids) is fed to the autoclave. CO<sub>2</sub> is heated to 60 °C and compressed to 150 bar. The supercritical CO<sub>2</sub> containing the liquor derived organic compounds leaves the autoclave."

And Claim 1 of the patent states:

"A method to extract lignin from a black liquor containing lignin comprising (a) dissolving a black liquor containing lignin in a supercritical fluid, at about or above critical temperature and pressure, (b) separating the black liquor depleted from said lignin from the supercritical fluid containing lignin."

He describes the many advantages of using CO<sub>2</sub> as the extractant in this application, e.g., low cost, ease of separation from the extract, nonflammability, etc.; these advantageous features, however, aren't going to make the concept of extracting lignin from black liquor using CO<sub>2</sub> work.

**Sumner, W. C., Jr., G. G. Hoyer, and W. G. Kozak, Method of removing water from alkali metal hydroxide solutions, U.S. 4,505,885 (Mar. 19, 1985).**

This patent utilizes the same principles that the Hess patent, U.S. 3,308,063, that we discussed previously, viz., the ability of an organic compound at high pressure and temperature to dissolve water. The objective of the Hess patent is the dissolution of water from sea water for subsequent recovery of salt-free water and the salt water is discarded. The objective of the this patent is the dissolution of water from sodium hydroxide solution for the purpose of concentrating the sodium hydroxide and the extracted water is discarded.

The sodium hydroxide solution to be concentrated and a hydrocarbon (e.g., ethyl benzene or t-butyl benzene) are pumped to a pressure of 2,000 psig and passed to a static mixer kept at 330 °C. From the mixer the stream is conveyed to a phase separator kept at 335 °C, where the heavier sodium hydroxide phase settles to the bottom. The hydrocarbon-water phase is withdrawn from the top of the separator, is cooled in a heat exchanger, and is depressurized to ambient across a valve. The hydrocarbon and liquid water separate and are withdrawn separately. The formation of distinct water and hydrocarbon phases actually occurs during the cooling step in heat exchanger.

A number of examples are given. Example 3 shows that a 10.9 wt% NaOH solution is concentrated to 21.6%. The solution feed rate was 360 g/hr, the hydrocarbon rate (t-butyl/benzene) was 236 g/hr, and the extraction was carried out at a pressure of 2,000 psig and a temperature of 330 °C.

**Schlichta, P. J., Method for growth of crystals by pressure reduction of supercritical or subcritical solution, U.S. 4,512,846 (Apr. 23, 1985).**

This patent describes a different application of the properties of supercritical fluids, i.e., using the supercritical fluid as a medium from which to grow crystals. Whereas the nucleation process discussed in Chapter 12 involved homogeneous nucleation during the pressure reduction, (Krukonis, 1984d) this invention involves heterogeneous deposition from an expanding gas solution.

The prior art discussion relates that current crystal growing techniques suffer from some limitations in their operation. Specifically, the "temperature driven crystallization" method requires precise time-temperature regulation and that the earth's gravity field causes convection currents that can interfere in crystal growth.

The patentee employs a "pressure driven crystallization" to form crystals from material dissolved in a supercritical fluid. A seed crystal acts as the heterogenous nucleation site for the precipitating material when the pressure is reduced. We don't know, however, how the patentee intends to prevent homogeneous nucleation during the "pressure driven crystallization."

**Myerson, A. S., Purification of terephthalic acid by supercritical fluid extraction, U. S. 4,550,198 (Oct. 21, 1985).**

This patent describes the purification of terephthalic acid using supercritical CO<sub>2</sub> or supercritical water. In one instance a reaction mass containing terephthalic acid and other materials is contacted with CO<sub>2</sub> at 150 °C and 300 atm. The terephthalic acid and impurities are dissolved and expanded to an unspecified reduced pressure and the acid is recovered in purified solid form. In Claim 1 nothing is revealed as to the fate of the impurities and we wonder if they are of sufficient solubility so as not to be precipitated during the first, pressure-reduction step. In one of the so-called examples no quantitative information is supplied for such items as solvent-to-feed ratio, expansion pressure level, and purity achieved. These omissions always cause us to wonder if the example is a "thought" example.

In another example, air is added as a source of oxygen to the expansion vessel at 150 °C to oxidize 4-carboxy benzaldehyde (a coproduct of p-xylene oxidation?) to terephthalic acid. Again, no quantitative information is given about rates of reaction, conversion, purity, etc. Still other examples relate that water at 327 °C and 200 atm (subcritical not supercritical) either with or without oxygen results in the extraction and production of purified terephthalic acid.

It is possible to determine a rough idea of the solvent-to-feed ratio needed for the proposed purification of terephthalic acid using solubility data obtained by Krukonis in 1981 (unpublished). He shows that 0.01 wt% terephthalic acid dissolves in CO<sub>2</sub> at 100 °C (not 150 °C) and 300 atm and, therefore, 10,000 lbs of CO<sub>2</sub> are needed for every pound of acid produced. Another problem with this patent is that no information is provided for the oxygen concentrations. It is well known that the solvent power of CO<sub>2</sub> can be drastically reduced if other gases such as nitrogen, oxygen, or helium are added to the CO<sub>2</sub>. Hence, the air concentration is a very important piece of information for process design. For instance, if the residual nitrogen in the CO<sub>2</sub> stream is not purged during recycle, the levels of nitrogen will build very fast at a feed ratio of 10,000 lbs CO<sub>2</sub> per pound of acid.

**Avedesian, M. M., Apparatus and method involving supercritical fluid extraction, U. S. 4,714,591 (Dec. 22, 1987).**

We were very critical of a previous patent on the same subject of extracting "valuable lignin and other extractable components from kraft black liquor" in the first edition of our book (see page 460; U. S. 4,493,797). As in the first patent, the use of fluidized beds and catalytic reaction to convert the lignin dissolved in the supercritical

fluid phase to other products is taught, but no credible examples of either equipment or process are given. In the prior art discussion of the current patent, as in the former patent, we learn that there are many specific advantages of supercritical fluid extraction of lignin. Why, at this stage of development of the technology, does the author of this patent insist on relating the time worn advantages of supercritical extraction such as, "... a supercritical fluid diffuses as a gas yet has solvent carrying capacity of a liquid," "... reaction rate of lignin dissolved in a supercritical fluid...is very high...," "...it has the density of a liquid yet diffusivity characteristics of a gas...," and especially with CO<sub>2</sub>, "... supercritical CO<sub>2</sub> has a high volatility...thus facilitating its separation from extract solutions...," "...CO<sub>2</sub> critical temperature and pressure are readily accessible with well established technology and equipment, and CO<sub>2</sub> is non-toxic, non-flammable, not corrosive, and relatively available at relatively low cost."

And after lauding all these advantageous features of CO<sub>2</sub>, we wonder if the inventor has ever tried to extract lignin from kraft black liquor? And if he has, why did he apply for another patent after the first one that was issued on 15 January 1985 was so critically reviewed? The inventor says in the current patent that other solvents suitable for extraction were used, e.g., acetone, tetrahydrofuran, dioxane, and toluene, but again no data are provided. The inventor relates again the advantages of CO<sub>2</sub> by stating "...these solvents (the organics) are generally less practical and therefore less preferred..." They may be less practical and less preferred than CO<sub>2</sub>, but lignin does not dissolve in CO<sub>2</sub>!

**Barstow, L. E., Ward, G. D. and Bier, M., Organic syntheses employing supercritical carbon dioxide as a reaction solvent, U. S. 5,001,224 (Mar. 19, 1991).**

Presently, long-chain amino acid structures (polypeptides) are produced using a series of reactions known as the Merrifield method, which, while effective, are very solvent-intensive and rather inefficient. Initially an amino acid is coupled to a polystyrene resin support through the carboxyl group of the amino acid. At this stage the amino acid has a t-butoxycarbonyl (BOC) group attached to the amino group to block it from reacting. After attachment to the solid support, the amino acid is reacted with a weak acid to remove the t-butoxy group. Once the unprotected reactant is obtained, it is usually rinsed with triethylamine and dichloromethane to remove the acid. The unprotected resin-amino acid is reacted with another BOC-protected amino acid in the presence of dicyclohexyl carbodiimide (DCC) to produce a two-amino acid peptide chain. Excess reagents and by-products are then removed by washing with dichloromethane and methanol. Up to two hours are needed to add each amino acid to the peptide chain. Other syntheses have been developed using other protecting groups, but all have the disadvantages of low yields and repetitive washings with chlorinated solvents. The low yields are, in many cases, a result of the solvents inability to penetrate the solid support.

An alternative method for the production of polypeptides involves the reaction of an amino acid with a reactive amino acid derivative such as N-carboxyanhydride (NCA) in solution. The resulting product is then capable of further reaction with other NCA molecules. This process is far simpler than the Merrifield synthesis, but is not widely used due to poor yields and product impurities.

The patentees suggest that the CO<sub>2</sub> should be used as a reaction solvent, as the high diffusivity of CO<sub>2</sub> will enable it to penetrate the pores of the solid support, and volatile reagents can be removed from the system by venting the CO<sub>2</sub>. The use of CO<sub>2</sub> would potentially eliminate the need for repetitive washings with chlorinated solvents. The

patentees also claim the supercritical CO<sub>2</sub> can be used as a solvent in the polymerization of NCA, as CO<sub>2</sub> may easily facilitate the removal of reaction products from the system before further reacting. The authors also claim that supercritical CO<sub>2</sub> can be used as a replacement for liquid solvents in the analysis of the sequencing of protein chains.

The patentees present sixteen examples of reactions run in CO<sub>2</sub> at pressures of 2,500 to 3,000 psi and temperatures of 95 and 150 °F. At first glance this seems suprising, as Stahl, et al. (1980) reported that amino acids are not soluble in supercritical CO<sub>2</sub>. In fact, the solubility of glycine, the simplest, albeit the most polar, amino acid is given as  $1.0 \times 10^{-5}$  wt% at a CO<sub>2</sub> density of 1.0 g/ml (about ~7,500 psi). However, because the Merrifield method of producing polypeptides is a heterogeneous reaction, it is not necessary to actually solubilize the amino acids. Since the second reactant in the process is either a protected amino acid or a protected amino acid anhydride, the highly polar NH<sub>2</sub> group is shielded by a t-butoxycarbonyl group which apparently decreases the polarity and intra-hydrogen bonding of the compound sufficiently to make it slightly soluble in supercritical CO<sub>2</sub>. In our laboratories we find that approximately 1 wt% t-boc-glycine is soluble in CO<sub>2</sub> at 95 °F (35 °C) and 1300 psig.

The patentees do not conduct any experiments to test the feasibility of using supercritical CO<sub>2</sub> as a solvent for homogeneous reactions of amino acids, but given the very low solubility of amino acids in CO<sub>2</sub>, it is unlikely that this approach would prove beneficial.

# CALCULATING BINARY, VAPOR-LIQUID EQUILIBRIA USING THE PENG-ROBINSON EQUATION OF STATE

## PROGRAM PR2

The basic scheme for modeling the phase behavior of binary mixtures is first to input the pure component characteristic parameters  $T_c$ ,  $P_c$ , and  $\omega$ , and then determine the binary mixture parameters,  $k_{ij}$  and  $\eta_{ij}$ , by fitting data such as pressure-composition isotherms. Normally  $k_{ij}$  and  $\eta_{ij}$  are expected to lie between  $\pm 0.200$ . If the two species are close in chemical size and intermolecular potential, the binary mixture parameters will have values very close to zero. In certain cases a small value of either of these two parameters can have a large influence on the calculated results.

1. Parameter (N = 2) ! # of components
2. Implicit Real\*8 (A-H, O-Z)
3. Dimension H(N, 1000), Q(N, 1000), FPV(N), FPL(N), TEST(N),
4. PR(N,N), ETA(N,N)
5. Dimension X(N), Y(N), AMW(N), W(N2), TC(N), PC(N), U(N), V(N)
6. Common/PENG/AMW, W, TC, PC, PR, ETA
7. Open(Unit=15, File='PR2.DAT', Status='OLD')
8. Open(Unit=16, File='PR2.OUT', Status='NEW')

Variables subscripted #1 designate the volatile component. Variables subscripted #2 designate the nonvolatile component. The second subscript in double subscripted variables is the iteration number so that  $H(2, 1)$  is the distribution K value ( $K = (y/x)$ ) for component #2 for the 1st iteration. The first part of the program is set up to read from an external data file, here named PR2.DAT, physical constants (molecular weight,  $T_c$ ,  $P_c$ , and acentric factor), mixture parameters ( $k_{ij}$  — designated 'PR' in this program — and  $\eta_{ij}$  — designated 'ETA' in this program), and pressure ranges (PHIGH, PLOW, and PINC for pressure increment) for the calculation.

9. Do 10 I = 1, N ! Input T (°C), P (bar),  $M_w$ ,  $T_c$ ,  $P_c$ ,  $\omega$ ,  $k_{ij}$ , and  $\eta_{ij}$
10. Read(15, \*) AMW(I)
11. 10 Read(15, \*) TC(I), PC(I), W(I)
12. Do 50 I = 1, N-1
13. Do 60, J = 1, N-1
14. Read(15, \*) PR(I,J+1), ETA(I, J+1)
15. PR(J+1, I) = PR(I, J+1)
16. ETA(J+1, I) = ETA(I, J+1)
17. 60 Continue
18. 50 Continue
19. Write(6, \*) 'Kij = ', PR(1,2), 'ETAij = ', ETA(1,2)
20. Read(15, \*) T
21. Write(6, \*) T
22. T = T + 273.15
23. Write(\*, \*) 'T = ', T-273.15
24. Write(\*, 12)

```

25.      Write(*, 13)
26.      Write(16, *) 'T = ', T-273.15
27.      Write(16, 12)
28.      Read(15, *) PLOW, PHIGH, PINC
29. 12    Format(/, 1X, 'X-Heavy', 3X, 'Y-Heavy', 6X, 'Pressure', 6X, 'Den-
30.      Liquid', 5X, 'Den-Vapor', 2X, '# Iterations')
31.      Write(16, 13)
32. 13    Format(24X, '(Bar)', 8X, '(g/cc)', 4X, '(g/cc)')

```

The pressure is initialized for the first iteration and initial estimates of the distribution coefficients are set.

```

33.      H(1, 1) = 20.0
34.      H(2, 1) = 0.05
35.      P = PLOW
36.      DP = PINC

```

Now calculate the P-x isotherm. ICOUNT is used to flag the method for updating the distribution coefficients,  $H(i, j)$ , to avoid a singularity. JFLAG is the number of iterations per tie line. The 'Do 20' loop is used to calculate the entire P-x isotherm. The number of iterations is set very high since the program is expected to reach the mixture-critical pressure or the maximum pressure (PHIGH) before reaching the maximum number of iterations in this loop. The 'Do 30' loop is used to calculate a single tie line. Again, the number of iterations is set high since the tie line is expected to converge or a warning statement will be printed to the screen before 250 iterations can be performed.

```

37.      Do 20 ICOUNT = 1, 3000
38.      Do 30 JFLAG = 1, 250
39.          X(2) = (1. - H(1, JFLAG)) / (H(2, JFLAG) - H(1, JFLAG))
40.          X(1) = 1.0 - X(2)
41.          If ((X(1) .LT. 0.0) .OR. (X(1) .GT. 1.0)) Goto 115
42.          Y(1) = H(1, JFLAG)*X(1)
43.          Y(2) = 1.0 - Y(1)

```

The vapor phase fugacity coefficient is arbitrarily calculated first followed by the liquid phase fugacity coefficient.

```

44.      Call PPR(T, P, Y, FPV, DENV, 0, N)
45.      Call PLPR(T, P, X, FPL, DENL, 1, N)

```

The following lines test to determine if the fugacity of each component is equal in each of the phases.

```

46.      Q(1, JFLAG) = (X(1) * FPL(1)) / (Y(1) * FPV(1))
47.      Q(2, JFLAG) = (X(2) * FPL(2)) / (Y(2) * FPV(2))
48.      TEST(1) = ABS (Q(1, JFLAG) - 1.0)
49.      TEST(2) = ABS (Q(2, JFLAG) - 1.0)

```

If TEST(1) or TEST(2) is not within the (adjustable) tolerance, do another iteration at this temperature and pressure with a new estimate of the distribution coefficients.

```

50.          If (TEST(1) .GE. 0.0001 .or. TEST(2) .GE. 0.0001) Then
51.              H(1, JFLAG+1) = H(1, JFLAG) * Q(1, JFLAG)
52.              H(2, JFLAG+1) = H(2, JFLAG) * Q(2, JFLAG)
53.          Else
54.              Goto 35
55.          Endif
56. 30        Continue
57.          Write (*,*) 'THE TIE LINE DID NOT CONVERGE!'
58.          Goto 115

```

Equilibrium has been reached if TEST(1) and TEST(2) are within the (adjustable) tolerance. Now guess an  $x$  and a  $y$  for each component for the next pressure,  $P + DP$ . Here the pressure increment is decreased if the mixture-critical point is approached as determined by how close  $H(2, JFLAG)$  is to one. The method for calculating the  $H$ 's at  $P+DP$  can cause the program to crash if the pressure increment is adjusted at low pressures far removed from the maximum pressure of the  $P$ - $x$  loop. Here we use an arbitrary value of 50 bar to avoid this problem.

```

59. 35      If (P .LE. 50.0) Then
60.          DP = 10
61.      Else
62.          If (H(2, JFLAG) .GT. 0.40) DP = 5.0
63.          If (H(2, JFLAG) .GT. 0.60) DP = 3.0
64.          If (H(2, JFLAG) .GT. 0.70) DP = 2.0
65.          If (H(2, JFLAG) .GT. 0.80) DP = 1.0
66.          If (H(2, JFLAG) .GT. 0.95) Goto 75

```

This last If statement stops the program very near the mixture critical point. Otherwise the program continues until PHIGH is reached.

```

67.          Endif

```

Now calculate a first guess for the values of  $x$  and  $y$  at this new pressure by fitting a straight line through the calculated data and extrapolating to the new pressure.

```

68.          POLD = P - DP
69.          PNEW = P + DP
70.          SS2 = X(2) + (PNEW-P) * ((X(2)-U(2)) / (P-POLD))
71.          If (ICOUNT .EQ. 1) SS2 = X(2)
72.          SS1 = 1. - SS2
73.          TT2 = Y(2) + (PNEW-P) * ((Y(2)-V(2)) / (P-POLD))
74.          If (ICOUNT .EQ. 1) TT2 = Y(2)
75.          TT1 = 1. - TT2
76.          H(1,1) = TT1/SS1
77.          H(2,1) = TT2/SS2
78.          U(1) = X(1)
79.          U(2) = X(2)
80.          V(1) = Y(1)
81.          V(2) = Y(2)

```

Print the results to the screen and to a data file named SL2.OUT.

```

82.      Write(*, 85) X(2), Y(2), P, DENL, DENV, JFLAG
83.      Write(16, 85) X(2), Y(2), P, DENL, DENV, JFLAG
84. 85    Format(1X, F8.6, 2X, F8.6, 4X, F8.2, 4X, F9.3, 2X, F9.3, 1X, I4, 2X,
          F7.4)

```

The program will continue calculating a P-x isotherm as long as the upper limit in pressure has not been reached and H(2, JFLAG) is less than 0.95.

```

85.      If (P .GE. PHIGH) Then
86.          Write(*, *) ' UPPER PRESSURE BOUND REACHED '
87.          Goto 115
88.      Endif
89.      P = P + DP
90. 20    Continue
91. 75    Write(*, *), 'NEAR THE MIXTURE CRITICAL POINT'
92. 115   Write(16, 116)
93.      Write(*, 116)
94. 116   Format(////, 8X, 'THE PROGRAM IS COMPLETED')
95.      END

```

Subroutine PHIPR calculates the fugacity coefficient using the PR EOS. The line numbers start from 1 in this subroutine.

```

1.      Subroutine PHIPR (T, P, Y, FP, DEN, NNN, N)
2.      Implicit Real*8 (A-H, O-Z)
3.      Dimension Y(2), FP(2), A(2, 2), B(2, 2), AMW(2), W(2), TC(2), PC(2),
4.          PR(2,2), ETA(2,2)
5.      Dimension G(2), TR(2), TERM1(2), TERM2(2), TERM3(2), ROOT(3)
6.      Common/PENG/AMW, W, TC, PC, PR, ETA
7.      GASR = 83.14
8.      BM = 0.0
9.      AM = 0.0
10.     SQ2 = 2.0**0.5
11.     Q1 = 1.0 + SQ2
12.     Q2 = SQ2 - 1.0
13.     Q3 = 2.0 * SQ2

```

Calculate the mixture terms, A and B, for the PR EOS. The SUM term will be used later to calculate the mixture density.

```

14.     SUM = 0.0
15.     Do 10 I = 1, N
16.         SUM = SUM + Y(I)*AMW(I)
17.         B(I, I) = 0.0778*GASR*TC(I)/PC(I)
18.         TERM3(I) = 0.0
19.         TR(I) = T/TC(I)

```



```

20.      G(I) = (1.0+(0.37464+1.54226*W(I)-0.26992*W(I)**2)*(1.0-
      TR(I)**0.5))**2
21. 10    A(I, I) = 0.45724*(GASR**2)*(TC(I)**2)/PC(I)*G(I)

22.      J = N-1
23.      Do 20 I = 1, J
24.          Do 21 K = I, J
25.              L = K+1
26.              A(I, L) = (A(I, I)*A(L, L))**0.5*(1.0-PR(I, L))
27.              A(L, I) = A(I, L)
28.              B(I, L) = (B(I, I)+B(L, L))/2.0*(1.0-ETA(I, L))
29.              B(L, I) = B(I, L)
30. 21      Continue
31. 20      Continue

32.      Do 30 I = 1, N
33.          Do 31 J = 1, N
34.              BM = BM+Y(I)*Y(J)*B(I, J)
35.              AM = AM+Y(I)*Y(J)*A(I, J)
36. 31      Continue
37. 30      Continue
38.      AA = AM*P/GASR**2/T**2
39.      BB = BM*P/GASR/T

```

The PR EOS can be written as a cubic equation in compressibility,  $Z = Pv/RT$ . The equation becomes:  $RA1*Z^3 + RA2*Z^2 + RA3*Z^1 + RA4*Z^0 = 0$ . Only one of the three roots is valid. The following routine calculates the valid root to the PR EOS.

```

40.      RA1 = 1.0
41.      RA2 = BB - 1.0
42.      RA3 = AA - 2.0*BB - 3.0*BB**2
43.      RA4 = BB**3 + BB**2 - AA*BB
44.      A1 = (3.0*RA3-RA2**2)/3.0
45.      B1 = (2.0*RA2**3 - 9.0*RA2*RA3 + 27.0*RA4)/27
46.      TEST1 = DABS((A1**3)/27.0)
47.      TEST2 = (B1**2)/4.0
48.      PIE = 3.141559265
49.      If (A1 .LT. 0.0 .And. TEST1 .GT. TEST2) Then
50.          CO = 2.0*(((A1)/3.0)**0.5)
51.          THETA = (DACOS((3.*B1)/(A1*CO)))/3.0
52.          ROOT(1) = CO*DCOS(THETA) - (RA2/3.0)
53.          ROOT(2) = CO*DCOS(THETA + (2.0*PIE)/3.0)-(RA2/3.0)
54.          ROOT(3) = CO*DCOS(THETA + (4.0*PIE)/3.0)-(RA2/3.0)

55.      Do 300 J = 1, 3
56. 300      If(ROOT(J) .LT. 0.0 .And. NNN .EQ. 1) ROOT(J) = 1.E+10

```

The largest root is the vapor and the smallest is the liquid. Depending upon the value of NNN (zero for the vapor phase and one for the liquid phase) either the smallest or the largest root is used to determine the fugacity coefficients of the two components in a particular phase.

```
57.         If(NNN .EQ. 0) ZM = DMAX1(ROOT(1), ROOT(2), ROOT(3))
58.         If(NNN .EQ. 1) ZM = DMIN1(ROOT(1), ROOT(2), ROOT(3))
```

But, A1 may not be greater than zero or TEST1 may not be greater than TEST2.

```
59.         Else
60.           DD = DSQRT(TEST2 + (A1**3)/27.)
61.           AL = 1.0
62.           ALL = 1.0
63.           TEST3 = (-B1)/2. + DD
64.           If (TEST3 .LT. 0.0) AL = -1.0
65.           TEST3 = DABS(TEST3)
66.           A2 = AL*((TEST3)**0.3333334)
67.           TEST4 = (-B1)/2. - DD
68.           If (TEST4 .LT. 0.0) ALL = -1.0
69.           TEST4 = DABS((-B1)/2. - DD)
70.           B2 = ALL * ((TEST4)**0.3333334)
71.           ZM = A2 + B2 - (RA2/3.0)
72.           If (TEST4 .LT. 1.0E-04) Goto 40
73.           TEST5 = DABS(1.0 - DABS(A2/B2))
74.           If (TEST5 .LT. 5.0E-04) ZM = -1.0*((A2+B2)/2.0) - (RA2/3.0)
75. 40      Endif
76.           VM = ZM*GASR*T/P
77.           DEN = (1/VM) * SUM
```

The fugacity coefficient for each component is now calculated.

```
78.         BPRIME = 0.0
79.         Do 60 I = 1, N
80.           BP2 = 0.0
81.           Do 61 INN = 1, N
82. 61      BP2 = 2.0*Y(INN)*B(I, INN)+BP2
83.           BPRIME = BP2 - BM
84.           TERM1(I) = BPRIME*(ZM-1.0)/BM-DLOG(ZM-BB)
85.           TERM2(I) = BPRIME*AA*
86.             DLOG((ZM+Q1*BB)/(ZM-Q2*BB))/(BM*BB*Q3)
87.           Do 62 J = 1, N
88. 62      TERM3(I) = TERM3(I)+2.0*Y(J)*A(J, I)
89.           TERM3(I) = AA*
90.             DLOG((ZM+Q1*BB)/(ZM-Q2*BB))*TERM3(I)/(BB*AM*Q3)
91.           FP(I) = DEXP(TERM1(I)+TERM2(I)-TERM3(I))
92. 60      Continue
93.         Return
94.         END
```

## PR2.DAT

This is the input data file for PR2.FOR. The example given here is for ethane and n-octane.

```

30.07      !Molecular weight of Ethane
305.4      48.8      0.091      !Tc (K), Pc (bar), acentric factor for Ethane

114.23     !Molecular weight of n-Octane
568.8      24.8      0.394     !Tc (K), Pc (bar), acentric factor for Octane

0.017      0.000      !Kij, ηij
40.0       !Temperature (°C)
25         300        3      !Pressures (bar): Starting, Ending, Increment

```

This is a partial listing of an example printout for PR2.FOR. X-Heavy and Y-Heavy represent the mole fraction of heavy component in the liquid and gas phase. Den-Liquid is the density of the liquid phase and Den-Vapor is the density of the vapor. The number of iterations increases substantially when the mixture-critical point is approached.

```

Kij = 1.700 E-02      ETAij = 0.00 E+00
T = 40.0

```

X-Heavy	Y-Heavy (bar)	Pressure (g/cc)	Den-Liquid (g/cc)	Den-Vapor	# Iterations
0.467603	0.003399	25.00	0.579	0.037	6
0.412496	0.003326	28.00	0.565	0.043	6
0.358738	0.003303	31.00	0.549	0.049	4
0.306197	0.003326	34.00	0.531	0.056	4
0.254694	0.003392	37.00	0.509	0.065	5
0.204037	0.003504	40.00	0.483	0.074	5

THE PROGRAM IS COMPLETED

# CALCULATING TERNARY, VAPOR-LIQUID EQUILIBRIA USING THE PENG-ROBINSON EQUATION OF STATE

## PROGRAM PR3LV

PR3LV uses the same subroutine as PR2 to solve for fugacity coefficients. However, with PR3LV, a mass balance must be solved for each equilibrium calculation. PR3LV also allows the user to read in the name of the three components into the program. PR3LV asks for weight fractions of the components, not mole fractions. But, before calculating phase equilibria the subroutine CONVERT is called to convert weight fractions to mole fractions. The last step before printing the result is to call CONVERT again to switch back to weight fractions.

```

1.      Parameter (N = 3)      ! # of components
2.      Implicit Real*8 (A-H, O-Z)
3.      Dimension Q(N), FPV(N), FPL(N), ETA(N, N), PR(N, N)
4.      Dimension X(N), Y(N), Z(N), AMW(N), W(N), TC(N), PC(N)
5.      Dimension TEST1(N), TEST2(N), NAME(N)
6.      Real*8 K(N), K2(N), LA
7.      Common/PENG/AMW, W, TC, PC, PR, ETA
8.      Integer FLAG, NUMIT
9.      Character*20 NAME
10.     Open(Unit = 15, File = ' PR3.DAT', Status = ' OLD')

11.     Read(15, *) T, P      ! Input T (°C), P (bar), Mw, Tc, Pc, w, kij, and ηij
12.     T = T + 273.15
13.     Do 10 I = 1, N
14.         Read(15, 41) NAME(I)
15.         Read(15, *) AMW(I), TC(I), PC(I), W(I)
16.         PR(I, I) = 0.0
17. 10      ETA(I, I) = 0.0

18.     Do 30 I = 1, N - 1
19.         Do 20 J = I, N - 1
20.             Read(15, *) PR(I, J+1), ETA(I, J+1)
21.             PR(J+1, I) = PR(I, J+1)
22.             ETA(J+1, I) = ETA(I, J+1)
23. 20      Continue
24. 30      Continue

25.     Do 170 JJ = 1, 10      ! This loop allows for 10 tie line calculations
26.         Do 40 I = 1, N - 1
27.             Write(*, *) 'Input feed weight fraction (wt%)', NAME(I)
28.             Read(*, *) Z(I)
29. 40      Z(I) = Z(I)/100
30.         Z(3) = 1.0 - (Z(1) + Z(2))

```

The Do 50 loop gives the user three chances to guess the proper concentrations of the three phases before the program returns a message that the mass-balance calculations did not converge.

```

31.      Do 50 I = 1, 3
32.          Write(*, *) 'Input the guess for the light phase'
33.          Do 60 I = 1, N - 1
34.              Write(*, *) 'weight fraction (wt%)', NAME(I)
35.              Read(*, *) Y(I)
36. 60      Y(I) = Y(I)/100.
37.          Y(3) = 1. - (Y(1) + Y(2))

38.          Write(*, *) 'Input the guess for the heavy phase'
39.          Do 70 I = 1, N - 1
40.              Write(*, *) 'weight fraction (wt%)', NAME(I)
41.              Read(*, *) X(I)
42. 70      X(I) = X(I)/100.
43.          X(3) = 1. - (X(1) + X(2))

```

Here the weight fractions are converted to mole fractions to be used with the Peng-Robinson equation and the algorithm for calculating equilibria.

```

44.      Call CONVERT(1,Z,AMW,N)
45.      Call CONVERT(1,Y,AMW,N)
46.      Call CONVERT(1,X,AMW,N)

```

To insure that the program is robust, but not necessarily fast, the updated values of the distribution coefficients,  $K$ , are equal to 90% of the previous value plus 10% of the currently calculated distribution coefficient. The factor of 90%, fixed in Q in Do Loop 80, is adjusted in a later part of the program to speed convergence. In many cases we set Q equal to zero. The convergence is determined when the value of TEST, initialized in line 75, is within a given tolerance.

```

47.      Do 80 I = 1, N
48.          Q(I) = 0.9
49.          TEST2(I) = 1000.0
50. 80      K(I) = Y(I)/X(I)
51.      FLAG = 0
52.      NUMIT = 0

```

Call subroutine FLASH to calculate phase splits from guesses.

```

53.      Call FLASH(LA, K, Z, X, Y, FLAG)
54.      If(FLAG .GE. 1) Then
55.          Write(*, *) 'Mass balance did not converge, try again'
56.          Write(*, *)
57.      Else
58.          Goto 5
59.      Endif
60. 50      Continue

```

Now that the mass balances have converged, check for phase equilibrium. The Do 100 loop is used to calculate a tie line. The number of iterations is set very high since the

program is expected to either converge or return a message that “the mass balance did not converge” before the maximum number of iterations in this loop can be performed.

```

61. 5      JJ = 1
62.      Do 100 JJ = 1, 2000
63.          NUMIT = NUMIT + 1
64.          Call PHIPR(T, P, Y, FPV, DENV, 0, N)
65.          Call PHIPR(T, P, X, FPL, DENL, 1, N)

66.          KK = NUMIT/25
67.          If(KK .EQ. JJ) Then
68.              Write(*,*) 'ITERATIONS = ', NUMIT
69.              Write(*,*) 'CONVERGENCE TEST = ', TEST
70.              Write(*,*)
71.              JJ = JJ + 1
72.          Endif

73.      Do 110 I = 1, N
74. 110      K2(I) = (1.0 - Q(I)) * FPL(I)/FPV(I) + Q(I) * K(I)
75.      TEST = 0.0

```

Calculate equilibrium criterion TEST and adjust the Q parameters to speed up convergence.

```

76.      Do 120 I = 1, N
77.          TEST1(I) = ABS((K2(I) - K(I))/K2(I))
78.          TEST = TEST1(I) + TEST
79.          If (TEST1(I) .GE. TEST2(I)) Then
80.              Q(I) = 0.5 * Q(I)
81.          Else
82.              TEST2(I) = TEST1(I)
83.          Endif
84. 120      Continue

85.      If (TEST .GE. 1E-3) Then          ! Iterate again
86.          Do 130 I = 1, N
87. 130      K(I) = K2(I)

```

Call subroutine FLASH to make sure that the updated distribution coefficients satisfy the mass balances.

```

88.      Call FLASH(LA, K, Z, X, Y, FLAG)
89.      If(FLAG .GE. 1) Then
90.          Write(*,*) 'Mass balance did not converge'
91.          Write(*,*) 'Try again'
92.          Goto 75
93.      Endif
94.      Else
95.          Goto 75

```

96. Endif  
 97. 100 Continue

The program either converged or the mass balances were not satisfied. Print out weight fractions of each component in each phase.

98. 75 Write(\*, 32) T - 273.15  
 99. Write(\*, 33) P  
 100. Write(\*, 34)

Here the mole fractions are converted back to weight fractions before printing out the results.

101. Call CONVERT(0,Z,AMW,N)  
 102. Call CONVERT(0,Y,AMW,N)  
 103. Call CONVERT(0,X,AMW,N)

104. Do 140 I = 1, N  
 105. 140 Write(\*, 35) NAME(I), Z(I) \* 100.0

106. Write(\*, \*) 'Current results are:'  
 107. Write(\*, 36) DENV  
 108. Do 150 I = 1, N  
 109. 150 Write(\*, 35) NAME(I), Y(I) \* 100.0

110. Write(\*, 37) DENL  
 111. Do 160 I = 1, N  
 112. 160 Write(\*, 35) NAME(I), X(I) \* 100.0

113. Write(\*, 38)  
 114. VAPOR = 1.0 - LA  
 115. Write(\*, 39) VAPOR, LA

116. If(NUMIT .LT. 2000) Write(\*, 43) NUMIT  
 117. If(NUMIT .GE. 2000) Write(\*, 42)  
 118. Write(\*, \*) 'Do you want another calculation (1=yes, 0=no)?'  
 119. Read(\*, \*) KEY  
 120. If (KEY .EQ. 0) Goto 25

121. 170 Continue  
 122. 25 Continue

123. 32 Format(/, 1X, 'TEMPERATURE (°C) = ', F8.3)  
 124. 33 Format(1X, 'PRESSURE (BAR) = ', F8.3)  
 125. 34 Format(1X, 'FEED COMPOSITION (WT%) :')  
 126. 35 Format(18X, A20, 2X, F6.3, ' (WT%)')  
 127. 36 Format(/, 1X, 'LIGHT PHASE : DENSITY =', F6.3, ' (g/cc)')  
 128. 37 Format(/, 1X, 'HEAVY PHASE : DENSITY =', F6.3, ' (g/cc)')  
 129. 38 Format(/, 1X, 'PHASE RATIOS :')  
 130. 39 Format(5X, 'V/F = ', F7.4, ' L/F = ', F7.4)  
 131. 43 Format(1X, 'NUMBER OF ITERATIONS = ', I4)

```

132. 41  Format(A20)
133. 42  Format(1X, '!!! Not an equilibrium solution, numit> 2000 ')
134.      END

```

Subroutine FLASH calculates the composition of the two phases given the distribution coefficients. One equation must be solved:

$$\sum_{i=1}^N \frac{Z_i (K_i - 1)}{(K_i - 1)A + 1} = 0 \quad (1)$$

where  $A = V/F$  where  $V = 1.0 - LA$ . For two phases to exist  $0 < A < 1$ . Initially  $A = 0$  and  $A = 1$  are substituted into equation 1. Assume that equation (1) only crosses through zero once. Calculate  $A_{\text{midpoint}} = (A_0 + A_1)/2$  and substitute this value into equation (1). If equation (1) with  $A_{\text{midpoint}}$  is less than zero, replace  $A_0$  with  $A_{\text{midpoint}}$  and retain  $A_1$ , or if equation (1) is greater than zero with  $A_{\text{midpoint}}$  replace  $A_1$  with  $A_{\text{midpoint}}$  and retain  $A_0$ . This halving procedure is continued until equation (1) equals zero to within  $\pm 1 \cdot 10^{-5}$ . The line numbers in this subroutine begin at 1.

```

1.      Subroutine FLASH(LA, K, Z, X, Y, FLAG)
2.      Implicit Real*8 (A-H, O-Z)
3.      Dimension X(3), Y(3), Z(3)
4.      Real*8 K(3), LA
5.      Integer FLAG
6.      N = 3
7.      AL = 0.0
8.      AH = 1.0
9.      FL = 0.0
10.     FH = 0.0

11.     Do 10 I = 1, N
12.         DENOM = (K(I) - 1.0)
13.         FL = FL + Z(I)*DENOM/(DENOM*AL+1.0)
14. 10    FH = FH + Z(I)*DENOM/(DENOM*AH+1.0)
15.     FLAG = 1
16.     If((FL*FH).LT.0.0) Then
17.         Do 50 IJ = 1, 1001
18.             A = (AL+AH)/2.0
19.             F = 0.0
20.             Do 20 I = 1, N
21.                 DENOM = (K(I) - 1.0)
22. 20    F = F + Z(I)*DENOM/(DENOM*A+1.0)
23.             If(ABS(F).GE.1.E-5) Then
24.                 If(((FL.GT.0.0) .And. (F.GT.0.0)) .or. ((FL.LT.0.0) .And.
25.                     (F.LT.0.0))) Then
26.                     AL = A
27.                 Else
28.                     AH = A
29.             Endif

```



```

30.      Else
31.          SUMX = 0.0
32.          SUMY = 0.0
33.          Do 30 I = 1, N
34.              X(I) = Z(I)/((K(I)-1.0)*A+1.0)
35.              Y(I) = K(I)*X(I)
36.              SUMX = SUMX+X(I)
37. 30      SUMY = SUMY+Y(I)
38.          Do 40 I = 1, N
39.              X(I) = X(I)/SUMX
40. 40      Y(I) = Y(I)/SUMY
41.          LA = 1.0 - A
42.          FLAG = 0
43.          Goto 5
44.      Endif
45. 50      Continue
46.      Else
47.          Goto 5
48.      Endif
49. 5      Continue
50.      Return
51.      END

```

Subroutine PHIPR calculates the fugacity coefficient using the PR EOS. PHIPR is identical to that found in PR2 except that there are now three components and three binary  $k_{ij}$ 's and  $\eta_{ij}$ 's.

**Subroutine PHIPR**(T, P, Y, FP, DEN, NNN, N)  
 Implicit Real\*8 (A-H, O-Z)  
 Dimension Y(3), FP(3), A(3, 3), B(3, 3), AMW(3), W(3), TC(3), PC(3),  
 ETA(3, 3)  
 Dimension G(3), TR(3), TERM1(3), TERM2(3), TERM3(3), ROOT(3),  
 PR(3, 3)  
 Common/PENG/AMW, W, TC, PC, PR, ETA

**Lines 7 - 94 of Subroutine PHIPR in Program PR2 go here.**

Subroutine CONVERT converts weight fractions to mole fractions and vice versa. This subroutine is numbered starting at 1.

```

1.      Subroutine CONVERT(NTYPE, X, AMW, N)
2.      Implicit Real*8 (A-H, O-Z)
3.      Dimension X(3), AMW(3)
4.      Real*8 AMW
5.      SUMX = 0.0

6.      If(NTYPE.EQ.1) Then ! Calculate mole fractions given weight fractions
7.          Do 10 I = 1, N
8. 10      SUMX = X(I)/AMW(I) + SUMX

```

```
9.          Do 20 I = 1,N
10. 20      X(I) = (X(I)/AMW(I))/SUMX
11.          Else ! Calculate weight fractions given mole fractions
12.          Do 30 I = 1,N
13. 30      SUMX = X(I)*AMW(I) + SUMX
14.          Do 40 I = 1,N
15. 40      X(I) = X(I)*AMW(I)/SUMX
16.          Endif
17.          Return
18.          END
```

## PR3.DAT

This is the input data file for PR3LV.FOR & PR3LLV.FOR. The example given here is for methane, ethane, and n-octane.

```

- 67.0    54.1          !System temperature (°C) and pressure (bar)
Methane          !Component
16.04  190.6  45.4  0.007 !Molecular Weight, TC (K), PC (bar), acentric factor for
                        Methane
Ethane           !Component
30.1   305.2  48.2  0.091 !Molecular Weight, TC (K), PC (bar), acentric factor for
                        Ethane
Octane          !Component
114.2  568.8  24.5  0.394 !Molecular Weight, TC (K), PC (bar), acentric factor for
                        n-Octane
0.02         0.0          !Kij, ηij for methane-ethane
0.01         0.0          !Kij, ηij for methane-octane
0.017        0.0          !Kij, ηij for ethane-octane

```

This is an example printout of a tie line for PR3LV.FOR.

```

TEMPERATURE (°C) = - 67.000
PRESSURE (bar)   =  54.100

```

```

FEED COMPOSITION (wt%) :
  Methane  90.000 (wt%)
  Ethane   5.000 (wt%)
  Octane   5.000 (wt%)

```

Current results are:

```

LIGHT PHASE: DENSITY = 0.104 (g/cc)
  Methane  95.126 (wt%)
  Ethane   4.840 (wt%)
  Octane   0.035 (wt%)

```

```

HEAVY PHASE: DENSITY = 0.576 (g/cc)
  Methane  24.004 (wt%)
  Ethane   7.065 (wt%)
  Octane   68.931 (wt%)

```

```

PHASE RATIOS
  V/F = 0.9711   L/F = 0.0289

```

NUMBER OF ITERATIONS = 8

DO YOU WANT ANOTHER CALCULATION (1=YES, 0 = NO)?

# **CALCULATING TERNARY, VAPOR-LIQUID-LIQUID EQUILIBRIA USING THE PENG-ROBINSON EQUATION OF STATE**

## **PROGRAM PR3LLV**

With this program it is necessary to input different guesses for a given feed composition to determine whether the calculated tie line is sensitive to the initial guess. The program returns a three-phase result, a message that there may only be a two-phase region, or it returns concentrations that are essentially the same in each phase — that is, a one-phase result. Just try a few different tie line guesses before you believe the results. PR3LLV asks for weight fractions of the components, not mole fractions. But, before calculating phase behavior the subroutine CONVERT is called to convert weight fractions to mole fractions. The last step before printing the result is to call CONVERT again to switch back to weight fractions. The CONVERT subroutine used in this program is identical to that in PR3LV.

```

1.      Parameter (N = 3)      ! # of components
2.      Implicit Real*8 (A-H, O-Z)
3.      Dimension Q(N),R(N),FPV(N),FPL1(N), FPL2(N), ETA(N, N), PR(N, N)
4.      Dimension XA(N), XB(N), Y(N), Z(N), AMW(N), W(N), TC(N), PC(N)
5.      Dimension TESTA1(N), TESTB1(N), TESTA2(N), TESTB2(N),
           NAME(N)
6.      Real*8 KA(N), KB(N), KA3(N), KB3(N), LA, LB
7.      Common/PENG/AMW, W, TC, PC, PR, ETA

```

### **Put in lines 8 to 37 from PR3LV**

```

38.      Write(*, *) 'Input the guess for the first heavy phase'
39.      Do 70 I = 1, N - 1
40.          Write(*, *) 'weight fraction (wt%)', NAME(I)
41.          Read(*, *) XA(I)
42. 70      XA(I) = XA(I)/100.
43.          XA(3) = 1. - (XA(1) + XA(2))

44.      Write(*, *) 'Input the guess for the second heavy phase'
45.      Do 80 I = 1, N - 1
46.          Write(*, *) 'weight fraction (wt%)', NAME(I)
47.          Read(*, *) XB(I)
48. 80      XB(I) = XB(I)/100.
49.          XB(3) = 1. - (XB(1) + XB(2))

```

Here the weight fractions are converted to mole fractions to be used with the Peng-Robinson equation and the algorithm for calculating equilibria.

```

50.      Call CONVERT(1,Z,AMW,N)
51.      Call CONVERT(1,Y,AMW,N)
52.      Call CONVERT(1,XA,AMW,N)
53.      Call CONVERT(1,XB,AMW,N)

```



```

84.          Do 110 I = 1, N
85.             KA3(I) = (1.0 - Q(I)) * FPL1(I)/FPV(I) + Q(I) * KA(I)
86. 110       KB3(I) = (1.0 - R(I)) * FPL2(I)/FPV(I) + R(I) * KB(I)
87.          TEST = 0.0

```

Calculate equilibrium criterion TEST and adjust Q & R parameters to speed up the convergence.

```

88.          Do 120 I = 1, N
89.             TESTA1(I) = ABS((KA3(I) - KA(I))/KA3(I))
90.             TESTB1(I) = ABS((KB3(I) - KB(I))/KB3(I))
91.             TEST = TESTA1(I) + TESTB1(I) + TEST
92.             If (TESTA1(I) .GE. TESTA2(I)) Then
93.                Q(I) = 0.5 * Q(I)
94.             Else
95.                TESTA2(I) = TESTA1(I)
96.             Endif
97.             If (TESTB1(I) .GE. TESTB2(I)) Then
98.                R(I) = 0.5 * R(I)
99.             Else
100.                TESTB2(I) = TESTB1(I)
101.             Endif
102. 120       Continue

103.          If (TEST .GE. 1E-3) Then          ! Iterate again
104.             Do 130 I = 1, N
105.                KA(I) = KA3(I)
106. 130       KB(I) = KB3(I)

```

Call subroutine FLASH to make sure that the updated distribution coefficients satisfy the mass balances.

```

107.          Call FLASH(LA, LB, KA, KB, Z, XA, XB, Y, FLAG)
108.          If (FLAG .GE. 1) Then
109.             Write(*, *) 'MASS BALANCE DID NOT CONVERGE'
110.             Write(*, *) 'TRY AGAIN'
111.             Goto 75
112.          Endif
113.          Else
114.             Goto 75
115.          Endif
116. 100       Continue

```

Program either converged or the mass balances were not satisfied. Print out weight fractions of each component in each phase.

```

117. 75       Write(*, 32) T - 273.15
118.          Write(*, 33) P
119.          Write(*, 34)

```

Here the mole fractions are converted back to weight fractions before printing out the results.

```

120.      Call CONVERT(0,Z,AMW,N)
121.      Call CONVERT(0,Y,AMW,N)
122.      Call CoNVERT(0,XA,AMW,N)
123.      Call CoNVERT(0,XB,AMW,N)

124.      Do 140 I = 1, N
125. 140    Write(*, 35) NAME(I), Z(I) * 100.0

126.      Write(*, *) 'Current results are:'
127.      Write(*, 36) DENV
128.      Do 150 I = 1, N
129. 150    Write(*, 35) NAME(I), Y(I) * 100.0

130.      Write(*, 37) DENL1
131.      Do 160 I = 1, N
132. 160    Write(*, 35) NAME(I), XA(I) * 100.0

133.      Write(*, 38) DENL2
134.      Do 180 I = 1, N
135. 180    Write(*, 35) NAME(I), XB(I) * 100.0
136.      Write(*, 44)
137.      VAPOR = 1.0 - LA - LB
138.      Write(*, 42) VAPOR, LA, LB

139.      If(NUMIT .LT. 2000) Write(*, 43) NUMIT
140.      If(NUMIT .GE. 2000) Write(*, 46)
141.      Write(*, *) 'Do you want another calculation (1=yes, 0 = no)?'
142.      Read(*, *) KEY
143.      If (KEY .EQ. 0) Goto 25
144. 170    Continue
145. 25     Continue
146. 32     Format(/, 1X, 'TEMPERATURE (C) = ', F8.3)
147. 33     Format(1X, 'PRESSURE (ATM) = ', F8.3)
148. 34     Format(1X, 'FEED COMPOSITION (WT%) :')
149. 35     Format(18X, A20, 2X, F6.3, ' (WT%)')
150. 36     Format(/, 1X, 'LIGHT PHASE : DENSITY =', F6.3, ' (G/CC)')
151. 37     Format(/, 1X, 'HEAVY PHASE -1- : DENSITY =', F6.3, ' (G/CC)')
152. 38     Format(/, 1X, 'HEAVY PHASE -2- : DENSITY =', F6.3, ' (G/CC)')
153. 44     Format(/, 1X, ' PHASE RATIOS ')
154. 42     Format(5X, 'V/F = ', F7.4, ' L1/F = ', F7.4, ' L2/F = ', F7.4)
155. 43     Format(1X, ' NUMBER OF ITERATIONS = ', I4)
156. 41     Format(A20)
157. 46     Format(1X, '!!! Not an equilibrium solution, numitT > 2000 ')
158.      END

```

Subroutine FLASH calculates the composition of the three phases given the distribution coefficients. Two equations must be solved for A and B.

$$\sum_{i=1}^N \frac{Z_i (1 - KA_i)}{B(1-A) + (1-A)(1-B) \left[ \frac{KA_i}{KB_i} \right] + A KA_i} = 0 \quad (1)$$

$$\sum_{i=1}^N \frac{Z_i \left[ 1 - \frac{KA_i}{KB_i} \right]}{B(1-A) + (1-A)(1-B) \left[ \frac{KA_i}{KB_i} \right] + A KA_i} = 0 \quad (2)$$

where  $A = V/F$  and  $B = LA/(LA + LB)$ . For three phases to exist  $0 < A < 1$  and  $0 < B < 1$ . The AFIND subroutine solves for A from equation (1) and the BFIND subroutine solves for B from equation (2). Both AFIND and BFIND use the bisection method to solve the equations. Step one is to set  $A = 0$  and solve equation (2) for B. Then with that value of  $B_1$  solve equation (1) for  $A_1$ . Now go back and solve equation (2) again for  $B_2$  and return to equation (1) and solve for  $A_2$ . Iterations are continued until neither A nor B changes within a given tolerance. The line numbers start from 1 in this subroutine and carry through continuously through the subroutines BFIND and AFIND.

```

1.      Subroutine FLASH(LA, LB, KA, KB, Z, XA, XB, Y, FLAG)
2.      Implicit Real*8 (A-H, O-Z)
3.      Dimension XA(3), XB(3), Y(3), Z(3)
4.      Real*8 KA(3), KB(3), LA, LB
5.      Integer FLAG
6.      N = 3
7.      A = 0.0
8.      Do 10 IJ = 1, 101
9.          Call BFIND(A, B, KA, KB, Z)
10.         If((B .GT. 0.0) .And. (B .LT. 1.0)) Call AFIND(A, B, KA, KB, Z)
11.         If((((A .GT. 0.0) .And. (A .LT. 1.0)) .And. ((B .GT. 0.0) .And. (B .LT.
12.             1.0)))) Then
13.             Goto 5
14.         Endif
15.         A = A+0.05
16.         If(A .GT. 0.96) Then
17.             FLAG = 1
18.             Goto 15
19.         Endif
20. 10      Continue
21. 5       TESTA = 0.0
22.       Do 20 JK = 1, 1001
23.           AO = A
24.           BO = B
25.           TESTAO = TESTA

```



```

26.      Call BFIND(A, B, KA, KB, Z)
27.      Call AFIND(A, B, KA, KB, Z)
28.      If((ABS((AO-A)/AO+(BO-B)/BO) .LE. 2E-4)) Then
29.          SUMXA = 0.0
30.          SUMXB = 0.0
31.          SUMY = 0.0
32.          Do 30 I = 1, N
33.              XA(I) = Z(I)/(B*(1.0-A)+(1.0-A)*(1.0-B)*KA(I)/
                  KB(I)+A*KA(I))
34.              Y(I) = KA(I)*XA(I)
35.              XB(I) = Y(I)/KB(I)
36.              SUMXA = SUMXA+XA(I)
37.              SUMXB = SUMXB+XB(I)
38. 30      SUMY = SUMY+Y(I)
39.          Do 40 I = 1, N
40.              XA(I) = XA(I)/SUMXA
41.              XB(I) = XB(I)/SUMXB
42. 40      Y(I) = Y(I)/SUMY
43.          LA = B*(1.0-A)
44.          LB = (1.0-A)*(1.0-B)
45.          FLAG = 0
46.          Goto 15
47.      Endif
48.      If(((A .LE. 0.0) .or. (A .GE. 1.0)) .or. ((B .LE. 0.0) .or. (B .GE. 1.0)))
49.          Then
50.              FLAG = 1
51.              Goto 15
52.          Endif
53.          TESTA = AO+A
54.          If(ABS(TESTAO-TESTA) .LE. 1E-5) A = (A+AO)/2.0
55. 20      Continue
56. 15      Return
57.      END

58.      Subroutine BFIND(A, B, KA, KB, Z)  ! Solve equation (2) given a
        value for A.
59.      Implicit Real*8 (A-H, O-Z)
60.      Dimension Z(3)
61.      Real*8 KA(3), KB(3)
62.      N = 3
63.      BL = 0.0
64.      BH = 1.0
65.      FL = 0.0
66.      FH = 0.0
67.      Do 10 I = 1, N
68.          DENOM = BL*(1.0-A)+(1.0-A)*(1.0-BL)*KA(I)/KB(I)+A*KA(I)
69.          FL = FL+Z(I)*(1.0-KA(I)/KB(I))/DENOM
70.          DENOM = BH*(1.0-A)+(1.0-A)*(1.0-BH)*KA(I)/KB(I)+A*KA(I)
71. 10      FH = FH+Z(I)*(1.0-KA(I)/KB(I))/DENOM

```

```

72.      If ((FL*FH) .LT. 0.0) Then
73.          Do 20 I = 1, 1001
74.              B = (BL+BH)/2.0
75.              F = 0.0
76.              Do 30 J = 1, N
77.                  DENOM = B*(1.0-A)+(1.0-A)*(1.0-B)*KA(J)/KB(J)+A*KA(J)
78. 30      F = F+Z(J)*(1.0-KA(J)/KB(J))/DENOM
79.          If (ABS(F) .GE. 1E-5) Then
80.              If (((FL.GT.FH).And.(F.GT.0.0)).or.((FL.LT.FH).And
                  (F.LT.0.0))) Then
81.                  BL = B
82.              Else
83.                  BH = B
84.              Endif
85.          Else
86.              Goto 25
87.          Endif
88. 20      Continue
89.      Else
90.          If (FL .GT. 0.0) Then
91.              B = 1.0
92.          Else
93.              B = 0.0
94.          Endif
95.          Goto 25
96.      Endif
97. 25      Return
98.      END

99.      Subroutine AFIND(A, B, KA, KB, Z)  ! Solve equation (1) given a
                                           value for B.
100.      Implicit Real*8 (A-H, O-Z)
101.      Dimension Z(3)
102.      Real*8 KA(3), KB(3)
103.      N = 3
104.      AL = 0.0
105.      AH = 1.0
106.      FL = 0.0
107.      FH = 0.0
108.      Do 10 I = 1, N
109.          DENOM = B*(1.0-AL)+(1.0-AL)*(1.0-B)*KA(I)/KB(I)+AL*KA(I)
110.          FL = FL+Z(I)*(1.0-KA(I))/DENOM
111.          DENOM = B*(1.0-AH)+(1.0-AH)*(1.0-B)*KA(I)/KB(I)+AH*KA(I)
112. 10      FH = FH+Z(I)*(1.0-KA(I))/DENOM
113.      If ((FL*FH) .LT. 0.0) Then
114.          Do 20 I = 1, 1001
115.              A = (AL+AH)/2.0
116.              F = 0.0
117.              Do 30 J = 1, N

```

```

118.          DENOM = B*(1.0-A)+(1.0-A)*(1.0-B)*KA(J)/KB(J)+A*KA(J)
119. 30      F = F+Z(J)*(1.0-KA(J))/DENOM
120.          If(ABS(F) .GE. 1E-5) Then
121.              If(((FL .GT. FH).And.(F .GT. 0.0)) .or. ((FL .LT. FH) .And.
                  (F .LT. 0.0))) Then
122.                  AL = A
123.              Else
124.                  AH = A
125.              Endif
126.          Else
127.              Goto 25
128.          Endif
129. 20      Continue
130.      Else
131.          If(FL .GT. 0.0) Then
132.              A = 0.0
133.          Else
134.              A = 1.0
135.          Endif
136.          Goto 25
137.      Endif
138. 25      Return
139.      END

```

Subroutine PHIPR(T, P, Y, FP, DEN, NNN, N) is identical to that found in PR3LV.  
 Subroutine CONVERT(NTYPE, X, AMW, N) is identical to that found in PR3LV.

This is an example printout of a three-phase tie line for PR3LLV.FOR.

TEMPERATURE (°C) = - 67.000

PRESSURE (bar) = 54.100

FEED COMPOSITION (wt%):

Methane 70.000 (wt%)

Ethane 20.000 (wt%)

Octane 10.000 (wt%)

Current results are:

LIGHT PHASE: DENSITY = 0.137 (G/CC)

Methane 88.174 (wt%)

Ethane 11.747 (wt%)

Octane 0.079 (wt%)

HEAVY PHASE -1- : DENSITY = 0.276 (G/CC)

Methane 74.774 (wt%)

Ethane 21.146 (wt%)

Octane 4.080 (wt%)

HEAVY PHASE -2- : DENSITY = 0.434 (G/CC)

Methane 47.737 (wt%)

Ethane 22.856 (wt%)

Octane 29.408 (wt%)

PHASE RATIOS

V/F = 0.1948

L1/F = 0.6019

L2/F = 0.2033

NUMBER OF ITERATIONS = 44

DO YOU WANT ANOTHER CALCULATION (1=YES, 0 = NO)?

# CALCULATING BINARY, SOLID-SCF OR SOLID-LIQUID-GAS EQUILIBRIA USING THE PENG-ROBINSON EQUATION OF STATE

## PROGRAM PRSLV

This program is very similar to PR2. The user is given the opportunity to calculate solid-SCF isotherms or to calculate the SLV, three-phase line. The program is currently set up for solid naphthalene calculations. For other solids, an expression is needed for the sublimation pressure.

```

1.      Parameter (N = 2)      ! # of components
2.      Implicit Real*8 (A-H, O-Z)
3.      Dimension X(N), Y(N), FPL(N), FPL(N), XC(N)
4.      Dimension AMW(N), W(N), TC(N), PC(N), PR(N,N), ETA(N,N)
5.      Common/PENG/AMW, W, TC, PC, PR, ETA
6.      Real*8 LASDEV
7.      Open(Unit=15, File='SOLID.DAT', Status='OLD')
```

**Put in lines 9 through 28 from PR2. Also, the molar volume of the solid is needed for these calculations.**

```

29.      Read(15, *) VS
30.      Write(6, *) VS
31.      X(1) = 0.005
32.      X(2) = 1.-X(1)
```

Specify type of calculation to be performed.

```

33.      IFIRST = 1
34.      Write(6,*) ' Type of calculations? 1 = SV; 2 = SLV'
35.      Read(5,*) ITYPE
36.      If(ITYPE.EQ. 1) Then
37.          Write(6, 11)
38. 11      Format(/, 3x, 'P (bar)', 5x, 'Y(2)', 6x, 'LIQUID (g/cc)')
39.      Else
40.          Write(6, 12)
41. 12      Format(/, 3x, 'P (Bar)', 5x, 'T (°C)', 8x, 'X2', 8x, 'Y2', 5x, 'GAS', 5x,
          'LIQ',/)
42.      Endif
```

Solid-SCF calculations are performed first. These calculations are common for both solid-SCF and SLV calculations.

```

43.      GASR = 83.14
44.      DT = 1.5
45.      P = PLOW
46.      DP = PINC
47.      Do 5 IJ = 1, 2000
48.          P = P + DP
49.          LASDEV = 0.0
```

The user needs to put in the sublimation pressure equation for the solid. Here the equation for  $P^{\text{sub}}$  for naphthalene is input.

```

50.      Do 20 JIJ = 1, 500
51.      PS = 10.**((10.0896-2926.61)/((T-273.15)+237.332))/783.75
52.      If(IFIRST.EQ. 1) Then
53.          Y(2) = PS
54.          Y(1) = 1.-Y(2)
55.      If(ITYPE.EQ. 2) P = 1.0
56.      Endif
57.      ALPHA = (PS/P)*DEXP(VS*(P-PS)/(GASR*T))

```

This part of the program calculates the mole fraction of heavy component in the SCF phase.

```

58.      Do 30 J = 1, 500
59.      Call PHIPR(T, P, Y, FPV, DENV, 0, N)
60.      YC = ALPHA/FPV(2)
61.      DELY = ABS(YC-Y(2))/Y(2)
62.      Y(2) = YC
63.      Y(1) = 1.-Y(2)
64.      If(DELY.LE. 0.001) Goto 35
65.      If (J .GE. 500) Goto 150
66. 30      Continue
67. 35      If(ITYPE.EQ. 1) Goto 25      ! SV calculations only
68.      XY1 = Y(1)*FPV(1)            ! SLV calculations
69.      XY2 = Y(2)*FPV(2)
70.      Do 40 J = 1, 500
71.      Call PHIPR(T, P, X, FPL, DENL, 1, N)
72.      XC(1) = XY1/FPL(1)
73.      XC(2) = XY2/FPL(2)
74.      DELX = (ABS(XC(1)-X(1)))/X(1)
75.      X(1) = XC(1)
76.      X(2) = 1.-X(1)
77.      If(DELX.LE. 0.001) Goto 45
78.      If(J .GE. 500) Goto 80
79. 40      Continue
80. 45      SUMX = XC(1)+XC(2)
81.      DEV = .0 - SUMX
82.      SLV = ABS(DEV)

```

At constant pressure, an appropriate increment is introduced in temperature such that the program eventually computes the SLV equilibrium point.

```

83.      If(SLV.GT. 0.0001) Then
84.          If((DEV*LASDEV).LT. 0.0) DT = 0.5*DT
85.          T = T + SIGN(DT, DEV)
86.          LASDEV = DEV
87.      Else

```

```

88.          Goto 25
89.          Endif
90. 20       Continue

```

Prints out results at each temperature and pressure.

```

91. 25       If(ITYPE .EQ. 1) Write(6, *) P, Y(2), DENV
92.          If(ITYPE .EQ. 2) Write(6, 118)P, T, X(2), Y(2), DENV, DENL

```

For SV case, calculations are terminated if pressure exceeds specified final pressure.

```

93.          IF((ITYPE .EQ. 1) .And. (P. GE. PHIGH)) Goto 90

```

The following is a method to decrease the increment in pressure as the mixture-critical point is approached during the SLV calculations.

```

94.          If (ITYPE .EQ. 2) Then
95.              RRR = Y(2)/X(2)
96.              If(RRR .GT. 0.050) Then
97.                  DP = 5.00
98.                  DT = 0.75
99.              Else
100.                 DT = 1.5
101.             Endif
102.             If(RRR .GT. 0.100) Then
103.                 DP = 2.50
104.                 DT = 0.375
105.             Endif
106.             If(RRR .GT. 0.200) Then
107.                 DP = 1.250
108.                 DT = 0.175
109.             Endif
110.             If(RRR .GT. 0.300) Then
111.                 DP = 0.500
112.                 DT = 0.080
113.             Endif
114.             If(RRR .GT. 0.400) Then
115.                 DP = 0.250
116.                 DT = 0.045
117.             Endif
118.             If(RRR .GT. 0.500) Then
119.                 DP = 0.075
120.                 DT = 0.0125
121.             Endif

```

The following are tests to terminate the calculations near the mixture-critical point. The pressure is arbitrarily set to 50 bar.

```

122.          If(P .GE. 50) Then
123.              TEST = ABS(X(2)-Y(2))
124.              If(TEST .LT. 1.0D-3) Goto 100
125.          Endif
126.      Endif
127.      IFIRST = 0

```

After solving either case for a certain pressure, iterate again to solve for new pressure.

```

128. 5      Continue
129. 80     Write(6,*) ' Warning: Iterations exceed (VLE Part)'
130.       Write(6,*)P, X(1), XC(1)
131.       Goto 90
132. 150    Write(6,*) ' Warning: Iterations exceed (SVE Part)'
133.       Write(6,*)P, Y(1), YC(1)
134.       Goto 90
135. 100    WRITE(6, 110)
136. 90     STOP
137. 110    Format(5x, 'Near mixture critical point')
138. 118    Format(3x, F10.3, 3x, F6.2, 3x, F6.4, 3x, F7.5, 3x, F5.3, 3x, F5.3, 3x, I4)
139.      END

```

Subroutine PHIPR(T, P, Y, FP, DEN, NNN, N) is identical to that found in PR2.



## SOLID.DAT

This is the input data file for PRSLV.FOR. The example given here is for xenon and naphthalene.

131.30			!Molecular weight of Xenon
289.8	58.8	0.000	!Molecular Weight, T <sub>C</sub> (K), P <sub>C</sub> (bar), acentric factor for Xenon
128.2			!Molecular weight of Naphthalene
748.4	40.5	0.302	!Molecular Weight, T <sub>C</sub> (K), P <sub>C</sub> (bar), acentric factor for Naphthalene
0.020	- 0.025		!K <sub>ij</sub> , $\eta_{ij}$ for Xenon-Naphthalene
45.0			!Temperature (°C)
30	400	20	!Pressures (bar): Starting, Ending, Increment
128.60			!Molar Volume of Naphthalene

This is a partial listing of an example printout for PRSLV.FOR where solid-SCF calculations were performed. The liquid density reported here is actually the density of the SCF phase. The output was modified slightly for inclusion in the book.

P (bar)	Y(2)	LIQUID (g/cc)
50.00	1.75E-04	0.345
70.00	5.35E-04	0.604
90.00	3.22E-03	1.077
110.00	1.56E-02	1.577
130.00	4.14E-02	1.866
150.00	9.83E-02	1.992

FORTTRAN STOP

# **CALCULATING BINARY, VAPOR-LIQUID EQUILIBRIA USING THE SANCHEZ-LACOMBE EQUATION OF STATE**

## **PROGRAM SL2**

The basic scheme for modeling the phase behavior of polymer, binary mixtures is similar to that used with the Peng-Robinson, PR2 program. First input pure component characteristic parameters  $T^*$ ,  $P^*$ , and  $r$ , then binary mixture parameters,  $k_{ij}$  — termed SL — and  $\eta_{ij}$  — termed ETA, are determined by fitting binary data such as pressure-composition isotherms. Rather than use fugacities, SL2 uses chemical potentials calculated in subroutine SLCHEMPOT to determine thermodynamic equilibrium. The program asks for weight fractions, but, the SLCHEMPOT subroutine uses mole fractions so the weight-to-mole fraction conversion subroutine, CONVERT, is used. Much of this program is identical to PR2 and, therefore, the reader is directed to the similar parts in PR2 rather than repeating them here. The front part of this program is virtually identical to PR2. Basically all that is needed is to read a data base for pure component parameters and mixture parameters. Also, some formatting statements are needed. There is one big difference between the programs. With SL2 the concentration of polymer in the gas phase can be so small that it causes the program to crash. To avoid this problem, the concentration of polymer in the gas phase is monitored with POLYFLAG. If POLYFLAG is set equal to one the polymer distribution coefficient is frozen for future calculations.

1.           Parameter (N = 2)           ! # of components
2.           Implicit Real\*8 (A-H, O-Z)
3.           Dimension H(N, 1000), Q(N, 1000), POTV(N), POTL(N), TEST(N),  
                  SL(N, N)
4.           Dimension X(N), Y(N), AMW(N), RO(N), TS(N), PS(N), U(N), V(N),  
                  ETA(N, N)
5.           Common/SANCHEZ/AMW, RO, TS, PS, SL, ETA
6.           Character\*12 Name
7.           Open(Unit=15, File='SL2.DAT', Status='OLD')
8.           Open(Unit=16, File='SL2.OUT', Status='NEW')
9.           GASR = 83.14

Lines 9 to 43 from PR2 go here. However, instead of reading in  $T$  ( $^{\circ}\text{C}$ ),  $P$  (bar),  $M_w$ ,  $T_c$ ,  $P_c$ ,  $\omega$ ,  $k_{ij}$ , and  $\eta_{ij}$ , the data base SL2.DAT should be formatted to read in  $T$  ( $^{\circ}\text{C}$ ),  $P$  (bar),  $T^*$ ,  $P^*$ ,  $r$ ,  $M_w$ , SL (i.e.,  $k_{ij}$ ) and  $\eta_{ij}$ . Also, one line needs to be added to flag the concentration of polymer in the gas phase. Right after line 43 from PR2 add the following line to fl. for very low polymer concentrations in the light phase.

44.           If(Y(2) .LE. 5.E-4) POLYFLAG = 1

Another difference from PR2 is that the subroutine SLCHEMPOT calculates the chemical potentials of both components in both phases rather than the fugacity coefficients. Also, SLCHEMPOT calls CONVERT to change the weight to mole fractions to calculate the chemical potential, and it calls CONVERT again to change the fractions back before returning to the main program.

45.           CALL SLCHEMPOT(T, P, Y, POTV, DENV, 0, N)
46.           CALL SLCHEMPOT(T, P, X, POTL, DENL, 1, N)

Here we test to determine if the fugacity of each component is equal in each of the phases. The chemical potentials are used rather than fugacities.

```

47.      Q(1, JFLAG) = DEXP((POTL(1)-POTV(1))/(RO(1)*GASR*T))
48.      Q(2, JFLAG) = DEXP((POTL(2)-POTV(2))/(RO(2)*GASR*T))
49.      TEST(1) = ABS(Q(1, JFLAG) - 1.0)
50.      TEST(2) = ABS(Q(2, JFLAG) - 1.0)
51.      If(POLYFLAG .EQ. 1) TEST(2) = 0.0

```

If either TEST(1) or TEST(2) is not within the (adjustable) tolerance, do another iteration at this temperature and pressure with a new estimate of the distribution coefficients. Freeze the value of the distribution coefficient of the polymer if the concentration of polymer in the light phase is less than 0.05 wt%.

```

52.      If (TEST(1) .GE. 0.0001 .or. TEST(2) .GE. 0.0001) Then
53.          H(1, JFLAG+1) = H(1, JFLAG) * Q(1, JFLAG)
54.          H(2, JFLAG+1) = H(2, JFLAG) * Q(2, JFLAG)
55.          If(POLYFLAG .EQ. 1) H(2, JFLAG +1) = H(2, JFLAG)
56.      Else
57.          Goto 35
58.      Endif
59. 30      Continue

```

The rest of the main part of this program is identical to PR2. Lines 57 to 95 from PR2 go here.

Subroutine SLCHEMPOT is used to calculate the chemical potentials of the components with the Sanchez-Lacombe EOS. The line numbers start from 1 in this subroutine.

```

1.      Subroutine SLCHEMPOT(T, P, Y, CHEMP, DEN, NNN, N)
2.      Implicit real*8 (A-H, O-Z)
3.      Dimension TS(2), PS(2), AMW(2), RO(2), CHEMP(2), ETA (2, 2), SL(2, 2)
4.      Dimension Y(2), ES(2, 2), VS(2, 2), RHOS(2), WF(2), PHIO(2)
5.      Common/SANCHEZ/AMW, RO, TS, PS, SL, ETA
6.      GASR = 83.14
7.      SUMWM = 0.0
8.      SUMPHI = 0.0
9.      RINV = 0.0
10.     VMIX = 0.0
11.     EMIX = 0.0

12.     Call Convert (1, Y, AMW, N)      ! Convert to mole fractions
13.     Do 10 I = 1, N
14.         ES(I, I) = TS(I)*GASR
15.         VS(I, I) = ES(I, I)/PS(I)
16.         RHOS(I) = AMW(I)/(RO(I)*VS(I, I))
17. 10     SUMWM = Y(I)*AMW(I) + SUMWM

```

```

18.      Do 20 I = 1, N
19.          WF(I) = Y(I)*AMW(I)/SUMWM
20. 20    SUMPHI = WF(I)/(RHOS(I)*VS(I, I)) + SUMPHI

21.      Do 30 I = 1, N
22.          PHIO(I) = (WF(I)/(RHOS(I)*VS(I, I)))/SUMPHI
23. 30    RINV = PHIO(I)/RO(I) + RINV
24.      RMIX = 1.0/RINV

25.      Do 40 I = 1, N-1
26.          Do 50 J = I+1, N
27.              ES(I, J) = SQRT(ES(I, I)*ES(J, J))*(1.- SL(I, J))
28.              ES(J, I) = ES(I, J)
29.              VS(I, J) = (VS(I, I) + VS(J, J))/2.0*(1.- ETA(I, J))
30.              VS(J, I) = VS(I, J)
31. 50      Continue
32. 40      Continue

33.      Do 60 I = 1, N
34.          Do 70 J = 1, N
35.              VMIX = PHIO(I)*PHIO(J)*VS(I, J) + VMIX
36.              EMIX = PHIO(I)*PHIO(J)*VS(I, J)*ES(I, J) + EMIX
37. 70      Continue
38. 60      Continue

39.      EMIX = EMIX/VMIX
40.      TMIX = EMIX/GASR
41.      PMIX = EMIX/VMIX
42.      BVMIX = RMIX*VMIX
43.      TR = T/TMIX
44.      PR = P/PMIX
45.      Call GETRHO(TR, PR, RMIX, RHO, NNN)      ! GETRHO calculates
                                                density

46.      VR = 1.0/RHO
47.      DEN = SUMWM*(1./(VR*BVMIX))

48.      Do 80 I = 1, N
49.          GIBBSC = GASR*T*(LOG(PHIO(I)) + 1.0 - RO(I)/RMIX)
50.          SUM1 = 0.0
51.          SUM2 = 0.0
52.          Do 90 J = 1, N
53.              SUM1 = PHIO(J)*VS(I, J)*ES(I, J) + SUM1
54. 90      SUM2 = PHIO(J)*VS(I, J) + SUM2
55.          T1A = 2.0/VMIX*(SUM1 - EMIX*SUM2)
56.          T1 = - RHO*(T1A + EMIX)
57.          T2 = P*VR*(2.0*SUM2 - VMIX)
58.          T3A = (1.0 - RHO)*LOG(1.0 - RHO)
59.          T3B = RHO/RO(I)*LOG(RHO)
60.          T3 = GASR*T*VR*(T3A + T3B)

```

```

61. 80      CHEMP(I) = GIBBSC + RO(I)*(T1 + T2 + T3)
62.      Call CONVERT (0, Y, AMW, N)      ! Convert back to weight fractions
63.      Return
64.      END

```

Subroutine GETRHO is used to calculate the density of the mixture from the Sanchez-Lacombe EOS by a successive-substitution method. The line numbers start from 1 in this subroutine.

```

1.      Subroutine GETRHO(T, P, R, RHO, NNN)
2.      Implicit Real*8 (A-H, O-Z)
3.      Dimension ROOT(3)
4.      RHO = 0.001
5.      STEP = 0.001
6.      TOL = 0.00001

7.      Do 20 IJ = 1, 3
8.          ROOT(IJ) = 0.0
9.          Do 10 I = 1, 10001
10.             If(RHO .LE. 1.0) Then
11.                 F = RHO**2 + P + T*(LOG(1.0 - RHO)+(1.0-1.0/R)*RHO)
12.                 If(ABS(F) .GE. TOL) Then
13.                     If((((IJ .EQ. 1) .or. (IJ .EQ. 3)) .And. (F .LT. 0.0)) .or.
14.                        ((IJ .EQ. 2) .And. (F .GT. 0.0))) Then
15.                         RHO = RHO - STEP
16.                         STEP = STEP*0.1
17.                         RHO = RHO + STEP
18.                     Else
19.                         RHO = RHO + STEP
20.                     EndIf
21.                 Else
22.                     ROOT(IJ) = RHO
23.                     STEP = 0.001
24.                     RHO = RHO + STEP
25.                     Goto 5
26.                 EndIf
27.             Else
28.                 ROOT(IJ) = RHO
29.                 STEP = 0.001
30.                 RHO = RHO + STEP
31.                 Goto 5
32.             Endif
33. 10      Continue
34. 5       Continue
35. 20      Continue

36.      If(NNN .EQ. 1) Then
37.          Do 30 I = 1, 3
38. 30.      If(ROOT(I) .GT. 1.0) ROOT(I) = -1.0

```

```

39.      RHO = DMAX1(ROOT(1), ROOT(2), ROOT(3))
40.      Else
41.      RHO = DMIN1(ROOT(1), ROOT(2), ROOT(3))
42.      If(RHO .GT. 1.0) RHO = -1.0
43.      Endif
44.      Return
45.      END

```

Subroutine CONVERT(NTYPE, X, AMW, N) is identical to that found in PR3LV.

## SL2.DAT

This is the input data file for SL2.FOR. The example given here is for ethane and low density polyethylene.

```

30.07      !Molecular weight of Ethane
315      3272.8      5.87      !T* (K), P* (bar), Ri of Ethane
110000     !Molecular weight of LDPE
645.6      3978.8      7922.7 !T* (K), P* (bar), Ri of LDPE
0.000      0.000      !Kij, ηij
130.0      !Temperature (°C)
200      7000      100      !PLOW, PHIGH, PINC

```

This is a partial listing of an example printout for SL2.FOR. X-Heavy and Y-Heavy represent the weight fraction of polymer in the liquid and gas phase. Den-Liquid is the density of the liquid phase and Den-Vapor is the density of the vapor. The number of iterations increases substantially when the mixture-critical point is approached.

```

Kij = 0.00E+00 ETAij = 0.00E+00
T = 120.0

```

X-Heavy	Y-Heavy	Pressure (bar)	Den-Liquid (g/cc)	Den-Vapor (g/cc)	Iterations
0.901652	0.000027	200.00	0.916	0.250	9
0.871699	0.000026	300.00	0.893	0.312	8
0.843384	0.000025	400.00	0.874	0.350	5
0.815091	0.000024	500.00	0.855	0.377	4
0.785873	0.000024	600.00	0.837	0.398	6
0.755378	0.000023	700.00	0.819	0.416	8
0.723292	0.000022	800.00	0.801	0.430	8
0.689245	0.000021	900.00	0.783	0.443	9
0.652893	0.000020	1000.00	0.764	0.454	11

THE PROGRAM IS COMPLETED

**CALCULATING POLYMER-SOLVENT-SOLVENT, VAPOR-LIQUID EQUILIBRIA  
USING THE SANCHEZ-LACOMBE EQUATION OF STATE  
PROGRAM SL3LV**

SL3LV is very similar to SL2 and PR3LV. In this program weight fractions are entered and are converted to mole fractions in the subroutines that are used to calculate the chemical potential.

```

1.      Parameter (N = 3)      ! # of components
2.      Implicit Real*8 (A-H, O-Z)
3.      Dimension POTV(N), POTL(N), NAME(N), ETA(N,N), SL(N,N), Q(N)
4.      Dimension X(N), Y(N), Z(N), AMW(N), RO(N), TS(N), PS(N), TEST2(N)
5.      Real*8 K(N), K2(N), LA
6.      Common/SANCHEZ/AMW, RO, TS, PS, SL, ETA
7.      Integer FLAG
8.      Character*20 NAME
9.      Open(Unit = 15, File = ' SL3.DAT', Status = ' OLD')
10.     GASR = 83.14

```

Put in lines 11 through 60 from PR3LV to read in pure component data ( $T$  ( $^{\circ}\text{C}$ ),  $P$  (bar),  $T^*$ ,  $P^*$ ,  $r$ ,  $M_w$ ,  $SL$  (i.e.,  $k_{ij}$ ) and  $\eta_{ij}$ ) and start the calculations, but, skip lines 44 through 46 since weight-to-mole conversions are handled inside of subroutine SLCHEMPOT and skip lines 48 and 49 since SL3LV does not bother with trying to speed the calculations with a  $Q$  factor on the distribution coefficients nor is variable TEST2 used. The distribution coefficients are upgraded by direct substitution in SL3LV.

```

70.  5      POLYFLAG = 0
71.      JIJ = 1
72.      Do 100 IJ = 1, 2000
73.          NUMIT = NUMIT + 1
74.          CALL SLCHEMPOT(T, P, Y, POTV, DENV, 0, N)
75.          CALL SLCHEMPOT(T, P, X, POTL, DENL, 1, N)
76.          If(Y(3) .LT. 5.E-4) POLYFLAG = 1
77.          If(X(3) .LT. 5.E-4) POLYFLAG = 1

78.      KK = NUMIT/25
79.      If(KK .EQ. JIJ) Then
80.          Write(*,*) 'ITERATIONS = ', NUMIT
81.          Write(*,*) 'CONVERGENCE TEST = ', TEST
82.          Write(*,*) 'POLYMER Y = ', Y(3)
83.          Write(*,*) 'POLYMER X = ', X(3)
84.          Write(*,*)
85.          JIJ = JIJ + 1
86.      Endif

87.      TEST = 0.0

```

```

88.          Do 110 I = 1, N
89.              K2(I) = EXP((POTL(I) - POTV(I))/(GASR*T*RO(I)))*K(I)
90.              If(POLYFLAG .EQ. 1) K2(3) = K(3)
91. 110        TEST = ABS((K2(I)-K(I))/K(I)) + TEST

```

**Put in lines 85 to 134 from PR3LV, but skip 101, 102, and 103 since the weight-to-mole fraction conversions are handled inside of SLCHEMPOT.**

Subroutine FLASH(LA, K, Z, X, Y, FLAG) and Subroutine CONVERT(NTYPE, X, AMW, N) are identical to those found in PR3LV. Subroutine SLCHEMPOT(T, P, Y, CHEMP, DEN, NNN, N) and Subroutine GETRHO(T, P, R, RHO, NNN) are identical to those found in SL2 except that now there are three not two components.



## SL3.DAT

This is the input data file for SL3LV.FOR & SL3LLV.FOR. The example given here is for ethane, toluene, and polystyrene.

70.0	60.0			!Operating T(°C) & P(Bar)
ETHANE				!Component 1
30.1	315.0	3227.0	5.87	!Molecular Weight, T* (K), P* (Bar), RI OF 1
TOLUENE				!Component 2
92.0	543.0	3967.0	8.50	!Molecular Weight, T* (K), P* (Bar), RI OF 2
POLYSTYRENE				!Component 3
68000.0	777.0	3625.0	3541.0	!Molecular Weight, T* (K), P* (Bar), RI OF 3
0.02	0.00			!K <sub>ij</sub> , η <sub>ij</sub> for ethane-toluene
0.02	0.00			!K <sub>ij</sub> , η <sub>ij</sub> for ethane-polystyrene
0.00	0.00			!K <sub>ij</sub> , η <sub>ij</sub> for toluene-toluene

This is an example printout of a tie line SL3LV.FOR.

TEMPERATURE (°C) = 70.000

PRESSURE (BAR) = 60.000

FEED COMPOSITION (wt%) :

ETHANE	30.000 (wt%)
TOLUENE	60.000 (wt%)
POLYSTYRENE	10.000 (wt%)

Current results are:

LIGHT PHASE: DENSITY = 0.573 (g/cc)

ETHANE	35.756 (wt%)
TOLUENE	64.195 (wt%)
POLYSTYRENE	0.049 (wt%)

HEAVY PHASE: DENSITY = 0.742 (g/cc)

ETHANE	18.555 (wt%)
TOLUENE	51.659 (wt%)
POLYSTYRENE	29.787 (wt%)

PHASE RATIOS

V/F = 0.6654      L/F = 0.3346

NUMBER OF ITERATIONS = 16

DO YOU WANT ANOTHER CALCULATION (1=YES, 0 = NO)?

# **CALCULATING POLYMER-SOLVENT-SOLVENT, VAPOR-LIQUID-LIQUID EQUILIBRIA USING THE SANCHEZ-LACOMBE EQUATION OF STATE**

## **PROGRAM SL3LLV**

Before using this program the user is expected to first use SL3LV which performs two-phase calculations for various ternary feed compositions. After performing two-phase calculations check to see whether any of the tie lines cross or exhibit other unusual behavior. If so, use SL3LLV to calculate three-phase behavior in the regions where the two-phase calculations gave funny tie line behavior. With SL3LLV it is necessary to input different guesses for a given feed composition to determine whether the calculated tie line is sensitive to the initial guess. If the program returns only one tie line regardless of the guess, then there is probably only a two-phase region. It is also possible that the program will calculate a single phase region for a given loading. Just remember to try a few different tie line guesses before you believe the results. Also, this program requests weight fractions, converts to mole fractions in the chemical potential subroutine, and returns weight fraction answers. Many parts of this program are similar to those in SL2 and PR3. The reader is referred to those parts of the appropriate programs rather than duplicating them here.

1.       Parameter (N = 3)       ! # of components
2.       Implicit Real\*8 (A-H, O-Z)
3.       Dimension POTV(N), POTL1(N), POTL2(N), NAME(N), ETA(N,N),  
          SL(N,N)
4.       Dimension XA(N), XB(N), Y(N), Z(N), AMW(N), RO(N), TS(N), PS(N)
5.       Real\*8 KA(N), KB(N), KA3(N), KB3(N), LA, LB
6.       Common/SANCHEZ/AMW, RO, TS, PS, SL, ETA
7.       Integer FLAG
8.       Character\*20 NAME
9.       Open(Unit = 15, File = ' SL3.DAT', Status = ' OLD')
10.      GASR = 83.14

**Put in lines 11 through 37 from PR3LV to read in pure component data ( $T$  ( $^{\circ}\text{C}$ ),  $P$  (bar),  $T^*$ ,  $P^*$ ,  $r$ ,  $M_w$ ,  $SL$  (i.e.,  $k_{ij}$ ) and  $\eta_{ij}$ ). Then add lines 38 through 70 from PR3LLV, but, skip lines 50 through 53 since in SL3LLV any weight-to-mole conversions are done in the subroutine SLCHEMPOT. Also, skip lines 55 through 58 since SL3LLV does not use  $Q$  and  $R$  factors nor does it use TESTA2 or TESTB2.**

Here we need to flag the program for the very low concentrations of polymer in any of the three phases. Therefore, we introduce the variables POLYFLAGY, POLYFLAGXA, and POLYFLAGXB.

67. 5       IJJ = 1
68.       POLYFLAGY = 0
69.       POLYFLAGXA = 0
70.       POLYFLAGXB = 0
71.       Do 100 IJ = 1, 2000
72.       NUMIT = NUMIT + 1

```

73.      Call SLCHEMPOT(T, P, Y, POTV, DENV, 0, N)
74.      Call SLCHEMPOT(T, P, XA, POTL1, DENL1, 1, N)
75.      Call SLCHEMPOT(T, P, XB, POTL2, DENL2, 1, N)
76.      If(Y(3) .LT. 5.E-4) POLYFLAGY = 1
77.      If(XA(3) .LT. 5.E-4) POLYFLAGXA = 1
78.      If(XB(3) .LT. 5.E-4) POLYFLAGXB = 1

79.      K = NUMIT/25
80.      If(K .EQ. JIJ) Then
81.          Write(*,*) 'ITERATIONS = ', NUMIT
82.          Write(*,*) 'CONVERGENCE TEST = ', TEST
83.          Write(*,*) 'POLYMER Y = ', Y(3)
84.          Write(*,*) 'POLYMER XA = ', XA(3)
85.          Write(*,*) 'POLYMER XB = ', XB(3)
86.          Write(*,*) 'CONVERGENCE TEST = ', TEST
87.          Write(*,*) '_____',
88.          JIJ = JIJ + 1
89.      Endif

90.      TEST = 0.0
91.      Do 110 I = 1, N
92.          KA3(I) = EXP((POTL1(I) - POTV(I))/(GASR*T*RO(I)))*KA(I)
93.          KB3(I) = EXP((POTL2(I) - POTV(I))/(GASR*T*RO(I)))*KB(I)
94.          If(POLYFLAGY .EQ. 1) KA3(3) = KA(3)
95.          If(POLYFLAGY .EQ. 1) KB3(3) = KB(3)
96.          If(POLYFLAGXA .EQ. 1) KA3(3) = KA(3)
97.          If(POLYFLAGXB .EQ. 1) KB3(3) = KB(3)
98. 110      TEST = ABS((KA3(I)-KA(I))/KA(I) + ABS((KB3(I)-KB(I))/KB(I) +
          TEST

```

**Put in lines 103 to 158 from PR3LLV, but skip 120 to 123 since the weight-to-mole fraction conversions are handled inside of SLCHEMPOT.**

Subroutine FLASH(LA, LB, KA, KB, Z, XA, XB, Y, FLAG), Subroutine BFIND(A, B, KA, KB, Z), and Subroutine AFIND(A, B, KA, KB, Z) are identical to those found in PR3LLV. Subroutine CONVERT(NTYPE, X, AMW, N) is identical to that found in PR3LV. Subroutine SLCHEMPOT(T, P, Y, CHEMP, DEN, NNN, N) and Subroutine GETRHO(T, P, R, RHO, NNN) are identical to those found in SL2 except that SL3LLV has three components not two.

This is an example printout for a three-phase tie line for SL3LLV.FOR.

TEMPERATURE (°C) = 70.000

PRESSURE (Bar) = 60.000

FEED COMPOSITION (wt%) :

ETHANE	60.000 (wt%)
TOLUENE	30.000 (wt%)
POLYSTYRENE	10.000 (wt%)

Current results are:

LIGHT PHASE: DENSITY = 0.099 (G/CC)

ETHANE	95.257 (wt%)
TOLUENE	4.711 (wt%)
POLYSTYRENE	0.032 (wt%)

HEAVY PHASE -1- : DENSITY = 0.489 (G/CC)

ETHANE	49.500 (wt%)
TOLUENE	50.412 (wt%)
POLYSTYRENE	0.087 (wt%)

HEAVY PHASE -2- : DENSITY = 0.662 (G/CC)

ETHANE	29.201 (wt%)
TOLUENE	46.231 (wt%)
POLYSTYRENE	24.568 (wt%)

PHASE RATIOS

V/F = 0.4095      L1/F = 0.1846      L2/F = 0.4059

NUMBER OF ITERATIONS = 2

DO YOU WANT ANOTHER CALCULATION (1=YES, 0 = NO)?

- ACC-1, 353  
 ACC-2, 353  
 ACC-4, 353–355  
 Acentric factor, 112  
 Acetic acid, and water separation, 178–182  
 Acetic acid–water–carbon dioxide system, 180–181  
 Acetone, 81, 82, 100, 102, 181, 321  
 Acetone–propane binary system, 123  
 Acid–base complex, 102  
 Acrylate–ethylene copolymer, 194  
 Activated carbon, regeneration, 158–169  
 Adamson, A. W., 347  
 Adsorbent regeneration, 168  
 Adsorption/desorption experiments, 161, 163  
 Adsorption equilibria, 166, 169  
*AIChE Journal*, 135  
 Aida, T., 325  
 Alachlor  
   adsorption breakthrough curves, 164  
   concentration profile, 169  
 Alachlor–CO<sub>2</sub> solubility data, 169  
 Alcohol–SCF mixtures, 37, 61  
 Alcohol–water–SCF mixture, 178  
 Alcohol–water systems, 177–178  
 Alexander, G., 318  
 Allada, S. R., 107  
 Allen, B., 65, 140, 281  
 Allen, G., 65, 281  
 $\alpha,\omega$ -aminopropyl-terminated polysiloxane  
   fractionation, 229–250  
 Amagat, E. G., 19  
 Amine-terminated poly(dimethyl)siloxane, 275  
 Aminopropyl disiloxane, 244, 246  
 Amino-terminated polysiloxane, 196  
 Andrews, T., 19  
 Aniline, 328  
 Anolick, C., 141  
 Argon, 22  
 Arndt, K. F., 358  
 Asphalt–oil–propane mixtures, 149  
 Azeotrope breaking, 182–188  
 Baker, C. H., 65, 140, 281  
 Balazs, A. C., 104, 120, 127  
 Balder, J. R., 133  
 Bangert, L. H., 260, 261  
 Bardin, J. M., 281  
 Baron, N., 62  
 Barry, E. F., 258  
 Bauman, E. G., 65, 84, 280, 281, 282  
 Baumgartner, H. J., 330  
 Becker, R., 347  
 Behrens, A. R., 360  
 Benson, P. R., 85  
 Benzene, 10, 102, 322  
 Benzoic acid, 102, 103  
 Bhise, V. S., 327  
 Bidwell, R. M., 10  
 Binary mixtures, phase diagrams, 31–45, 51  
 Biphenyl–carbon dioxide system, 52–56, 59  
 BisGMA, 285, 288, 289  
 Blyumberg, E. R., 328, 330  
 Bolaños, G., 89, 90  
 Bonner, D. C., 360  
 Booth, H. S., 10  
 Botsaris, 350  
 Boyd, R. N., 307  
 Branfman, A. R., 304  
 Brennecke, J. F., 96, 105  
 Brink, J. A., 189  
 Bromotrifluoroethylene (BTFE), 269  
 Broome, M. G., 304  
 Brunner, E., 110, 182, 183  
 Brunner, G., 10  
 Büchner, E. G., 20  
 Busche, R. M., 181  
 Butane, 210, 212  
 Butane hydroperoxide, 329

- Butene, 216  
 1-Butene, 205, 210, 211, 212, 214  
*t*-Butyl-hydroperoxide (TBHP), 329–330  
  
 Cagniard de la Tour, C., 17  
 Cailletet, L., 19  
 Campbell, R. E., 252  
 Camphor, 20  
 Caralp, M. H. M., 332  
 Carbaryl, 165  
 Carbon/carbon (C/C) composites, 353, 355  
 Carbon dioxide, 18, 22, 102, 103, 293  
   and alachlor solubility data, 169  
   and biphenyl, 52–56, 59  
   critical point, 19  
   critical temperature, 9  
   and cumene, 118  
   and isopropanol–water system, 73, 178  
   and isopropyl benzene system, 117, 119  
   and methane system, 48  
   miscibility of, 109  
   and naphthalene system, 22, 133, 136–137  
   phase behavior, 19  
   quadrupole moment, 101  
   self-diffusivity, 14  
   and styrene system, 119  
   ultrahigh-pressure, 369  
   viscosity behavior, 14  
 Carbon dioxide–alachlor–activated carbon system, 168, 169  
 Carbon dioxide–ethanol–water system, 171, 172, 175  
 Carbon dioxide–methanol system, 183  
 Carbon dioxide–squalane, 43  
 Carbon dioxide–water–acetic acid system, 180  
 Carbon disulfide, 20  
 Carboxypropyl-terminated poly(dimethyl)siloxane, 273  
 Castellan, G. W., 100  
 Catalyst–ethylene carbonate–CO<sub>2</sub> stream, 328  
 Catalysts, 328  
   heterogeneous, 322–324  
 Caywood, S. W., 141  
 Cellulose, 321, 322  
 Cellulose acetate, production process, 179  
 Cernia, E. M., 106  
 Chai, C. P., 10, 52, 128  
 Chang, H., 88, 308  
 Chapman, T. W., 363  
 Chappellear, D. C., 71, 319  
 Charlton, J. L., 325  
 Chemical composition distribution (CCD), 217–220  
 Chemical effect, 108  
 Chemical forces, 102  
 Chemical reactions, 311–332  
 Chemotherapeutic agents, 304–307  
 Chen, S. J., 63  
 Chermin, H. A. G., 21  
 Chitin, 321, 322  
 Chlorinated hydrocarbons, 157  
 Chlorobenzyl methyl ether, 320  
 Chlorodifluoromethane, 194, 197, 205–210, 212  
 Chlorotrifluoroethylene, 320  
   fractionation, 269–271  
 Christensen, J. J., 98  
 Christianson, D. D., 300  
 Christopher, P. M., 182  
 Chung, M. E., 310  
 Chung, S. Y.-K., 183  
 CITREF, 201–205  
 Clemson, C. S., 65, 281  
 Clifford, A. A., 332  
 Close, R. E., 71  
 Cloud point, 21, 65, 66, 68, 69, 80–82, 123, 124, 126, 148, 200, 212, 213  
 Cobalt chloride, 350  
 Cochran, H. D., 105  
 Coffee decaffeination, 4, 294–299  
 Coffey, M. P., 340, 343, 349, 353  
 Coleby, S. E., 332  
 Coleman, E. J., 200  
 Combes, J., 96, 105  
 Comminution techniques, 334–336  
 Condo, P. D., 63  
 Cookson, C. B., 4  
 Coorens, H. G. A., 77  
 Copelin, H. B., 257  
 Copolymer–solvent–cosolvent mixtures, 80  
 Cottle, J. E., 192, 332  
 Cowie, J. M. G., 281, 284  
 Cozewith, C., 63, 65, 84, 141, 142, 281, 282  
 Critical opalescence, 33  
 Critical point, 11, 17, 19, 20, 33, 39, 105, 133, 139, 155  
 Critical polymerization boundary, 319  
 Cubic equation of state, 104, 111, 113, 134  
 Culberson, O. L., 41, 73  
 Cumene–CO<sub>2</sub> system, 118  
 Cussler, E. L., 59  
 Cyclohexane, 10, 102  
 Cyclohexanone, 344  
 Cyclohexyl-substituted polysilane polymer, 277  
 Cytotoxicity tests, 305–306  
  
 Dahl, S., 104

- Dandge, D., 71, 316  
 Davidson, P., 10  
 Debenedetti, P. G., 105, 340  
 Decaffeination  
   coffee, 4, 7, 294–299  
   tea, 7  
 Decaffeination column, 6–7  
 de Filippi, R. P., 14, 158, 161, 170, 172, 176, 310  
 de Goede, R., 77  
 Deiters, U., 113, 128  
 Delmas, G., 63, 65  
 de Loos, T. W., 21  
 Density changes in region of critical point, 11  
 Dental materials, 288  
 de Roo, J. L., 77  
 DeSimone, J. M., 196, 217, 218, 219, 221, 223, 224, 225, 226, 229, 230, 231, 255  
 Desorption tests, 165  
 de Swaan Arons, J., 21, 46, 77  
 Deul, R., 91, 184, 185  
 Diacetone acrylamide, 291  
 Diandreth, J. R., 75, 133, 178, 179  
 Diazinon, 165, 166  
 Dibenzofuran, 102  
 Dickinson, N. L., 151, 152  
 Dicyclopentadienyl iron, 336  
 Diels–Alder reaction, 318, 322  
 Diepen, G. A. M., 10, 12, 13, 20, 21, 45, 46, 49, 51–53, 59, 60, 78–80, 135  
 1,1-Difluoroethane, 320–321  
 Diglycidial ether of Bisphenol A (DGEBA), 288  
 Diguët, R., 91, 184, 185  
 Dillard, K. H., 34, 35, 91  
 Dimethyl formamide (DMF), 109, 110, 181  
 Dimethyl sulfoxide (DMSO), 109, 110, 229  
 Dioxane, 181  
 Dipole–dipole interactions, 100  
 Distribution coefficients, 171–172, 177, 180, 182  
 Dodecanolactam, 336  
 Doring, W., 347  
 Donnelly, H. G., 48  
 Donohue, M. D., 102–105  
 Durrill, P. L., 358  
  
 Eckert, C. A., 25, 85, 96, 103, 105, 128, 318, 319, 321, 329  
 Economou, I. G., 105  
 Edible oils extraction, 299–304  
 Ehrlich, P., 63, 69, 200, 316, 318–320, 330, 331  
*n*-Eicosane, 77  
 Eisenbach, W., 302  
 Electron acceptor–donor complexing, 102  
 Elgin, J. C., 39, 40, 71, 73, 75, 76, 107, 135, 140, 177, 319  
 Elias, H. G., 218  
 Ellis, S. R. M., 10  
 Elsbernd, C. S., 217, 230, 232–234, 237, 238, 240–242, 245, 246, 249  
 EMA<sub>69/31</sub>–propane–acetone system, 124–126  
 Emanuel, N. M., 328, 330  
 Enzyme reactions, 311–321  
 Equations of state, 29, 104, 107, 108, 111, 113, 116, 118–124, 127, 128, 130, 131, 133, 134  
 $\beta$ -Estradiol, 334  
 Ethane, 21, 77, 100, 102, 109, 115, 282  
   critical temperature, 9  
 Ethane–butanol system, 37  
 Ethane–ethanol system, 37  
 Ethane–hydrocarbon mixtures, 36, 37  
 Ethane–methanol system, 183  
 Ethane–octane system, 114, 115  
 Ethanol, 17, 20, 81, 82  
   and water separation, 170  
 Ethanol–water–carbon dioxide system, 73  
 Ethanol–water–ethylene system, 73  
 Ethanol–water–ethane system, 73  
 Ethylene, 11–13, 20, 22, 51, 68, 81, 100, 107, 215, 318  
   critical temperature, 9  
   polymerization, 331  
 Ethylene-based copolymer fractionation, 205–216  
 Ethylene-*o*-dichlorobenzene system, 39  
 Ethylene glycol, 181, 182, 327  
 Ethylene–methanol system, 183  
 Ethylene–naphthalene system, 69  
 Ethylene–polyethylene system, 319  
 Ethylene-*n*-propanol system, 39  
 Ethylene–water–organic solvent phase diagrams, 71  
 Explosives, 347  
 Extractibility, 367  
  
 Fall, D. J., 77  
 Fall, J. L., 77  
 Fariss, R. H., 319  
 Ferioli, P., 258  
 Ferrocene, 336  
 Findeisen, R., 63, 80  
 Flory, P. J., 200  
 Flow calorimeter, 98  
 Flow method, 85–90  
 Fluorene, 102

- Fluorenone, 102  
Formamide, 181, 182  
Francesconi, A. Z., 183–185  
Francis, A. W., 22, 71, 180, 186, 316, 344  
Franck, E. U., 43, 91, 183–185, 206  
Fredenslund, Aa., 104  
Free-volume, 103  
Freeman, P. I., 61, 65, 281  
Freundlich isotherms, 166, 168  
Friedrich, J. P., 300, 301  
Fugacity coefficients, 110–114, 127, 128  
Funk, E. W., 10
- Gallagher, P. M., 196, 217, 227–229, 240–242, 246, 343, 349, 350  
Gangoli, N., 10  
Garwin, L., 153  
Gas antisolvent (GAS) recrystallization, 342–357  
Gas compression, 13, 19  
Gearhart, J. A., 153  
Giddings, J. C., 107, 108, 259, 369  
Gilbert, M. L., 73, 75, 88, 170, 172, 178, 186  
Gloeckner, G., 219  
Glycidyl azide polymer (GAP), 251  
    fractionation, 253–257  
Glycine, 368–369  
Goffinet, E. P., 141  
Goklen, K. E., 170, 172  
Gómez-Nieto, M., 123, 124  
Goodwin, B. M., 104  
Gopal, J. S., 79, 128  
Gore, G., 20, 135  
Gottesman, M., 299  
Gouw, T. H., 258, 259, 269  
Graham, E. B., 63, 331  
Grieger-Block, R. A., 363  
Griskey, R. G., 358  
Group transfer polymerization (GTP), 217, 225–228  
Guckes, T. L., 65, 84, 91, 141, 142, 281
- Hammond, D. A., 311, 312  
Hannay, J. B., 17–20, 108, 333, 350  
Hannigan, K. J., 302  
Hansen, P. C., 103  
Hartmann, W., 259  
Hasch, B. M., 64, 80, 81, 125, 196, 204–207, 209, 212, 213, 265  
Haylett, R. E., 145, 146, 148–150, 153, 265  
Haynes, C., 320  
Heaking, A. J., 300  
Hearne, G. W., 329  
Heats of mixing, 106
- Heller, J. P., 71, 316  
Hellstern, A. M., 221–225, 227–229  
Heterogeneous catalysis, 322–324  
*n*-Hexadecane, 77  
Hexamethylcyclotrisiloxane, 221  
Hexane, 109  
1-Hexene, 324  
Hicks, C. P., 27, 34  
High-density polyethylene (HDPE), 200–201  
High-pressure polyethylene polymerization, 189–192  
High-pressure studies, 85–98  
High-temperature reactions, 321–322  
Hildebrand, J., 106, 107  
Historical perspective, 17–26  
HMWP, 318  
Hochgeschurtz, T., 89, 90  
Hogarth, J., 17–20, 333, 350  
Holla, S. J., 22, 25, 85, 128  
Hottovy, J. D., 77  
Hubball, J. A., 258  
Hubert, P., 296  
Hunter, E., 192, 194  
Hutchenson, K. W., 88, 90  
Huvar, G. S., 360  
Hyatt, J. A., 103, 266  
Hydrocarbons, 9, 10, 20  
    isomerization process, 316  
    and water mixtures, 41  
Hydrogen bonding, 102, 113, 127, 210, 212  
Hydroxy-terminated polybutadiene (HTPB), 251–252
- Ideal gas law, 128  
Igel, J. T., 96, 114, 116–119  
Ikononov, G. D., 102, 103  
Industrial applications, 145–156  
Intermolecular forces, 99–105  
Intermolecular potential energy, 101  
Iomtev, M. B., 10, 12, 22  
Irani, C. A., 10, 63, 65, 84, 141, 142, 281, 282  
Isobaric cooling, 95  
Isomer separations, 307–309  
Isopropanol–water–CO<sub>2</sub>, 73, 178  
Isopropyl benzene–CO<sub>2</sub> system, 117, 119  
Isothermal decreasing pressure profiling, 192–194  
Isothermal increasing pressure profiling, 194–195  
Izatt, R. M., 98, 206
- Jacoby, R. H., 91  
Jenkins, A. D., 220  
Jentoft, R. E., 258, 259, 269



- Jin, G., 104  
 Johnston, K. P., 10, 25, 79, 85, 96, 104, 105, 128, 133, 134, 320  
 Jonas, J., 170  
 Joule–Thomson cooling, 87
- Kander, R. G., 75, 133, 178, 179  
 Kantner, S. S., 182, 184  
 Kasegrande, S. S., 141, 142, 281  
 Katz, D. L., 6, 48  
 Keith, P. C., 145, 146, 148–150, 153, 265  
 Kennedy, G. C., 13, 25, 130  
 Kim, S., 96, 104, 105, 134  
 Kim, Y. J., 76, 77  
 King, J. W., 368  
 King, A. D. Jr., 22, 61  
 King, J. W., 107–109, 259, 369  
 Kiran, E., 63, 64, 93, 94  
 Kistler, S. S., 363  
 Kiszka, M. B., 359, 360  
 Kleintjens, L. A., 21, 80  
 Klesper, E., 259  
 Klibanov, A. M., 312  
 Knutson, B. L., 96, 105  
 Kohn, J. P., 30, 73, 74, 76, 77, 186  
 Koll, P., 321, 322  
 Koningsveld, R., 21, 80, 123  
 Korsmeyer, R. W., 360  
 Kramer, G. M., 316, 317, 326  
 Krase, N. W., 192, 331  
 Kratochvil, P., 219, 220  
 Kreevoy, M. M., 182, 184  
 Krukons, V. J., 10, 14, 22, 51, 52, 61, 63, 64, 86, 158, 168, 182, 184, 185–187, 192, 196, 197, 200, 204, 205, 217, 227, 229, 232, 239, 242, 246, 251, 253, 258, 260–262, 264, 266, 268, 271, 273, 277, 278, 285, 292, 296, 298, 299, 301, 304, 307, 308, 312, 334, 340, 343, 349, 350, 353, 359, 364  
 Kuenen, J. P., 37, 61  
 Kuk, M. S., 73, 75, 170, 172, 177  
 Kurnik, R. T., 14, 22, 25, 78, 79, 85, 86, 128, 129, 307, 308  
 Kurpen, J. J., 63, 69, 200, 331  
 Kusumi, S., 358
- Lacombe, R. H., 120, 121  
 Laidler, K. J., 318  
 Langmuir isotherms, 166, 168  
 Lattice–gas equation of state, 104, 121, 134  
 Laukhuf, W. L. S., 182  
 Laurence, R. L., 121  
 Lauryl lactam, 336
- Lawrence, A. E., 192, 331  
 Leder, F., 316, 317, 326  
 Lee, L. L., 104, 105  
 Lee, S.-H., 64, 205, 208–216  
 Lemert, R. M., 79, 255  
 Lentz, H., 183–185  
 Li, Y.-H., 34, 35, 91  
 Liao, I. S., 14, 358, 360  
 Lichtenthaler, R. N., 77  
 Liphard, K. G., 44  
 Liquid–liquid–vapor (LLV) equilibria, 28, 34, 36, 37, 39–41, 43, 65, 70, 71, 104, 114–119, 121, 142, 149  
 Liquid–SCF equilibria, 61  
 Liquid–solid phase equilibria, 47, 48  
 Liquid–vapor (LV) equilibria, 114  
 Lira, C. T., 80, 102, 128  
 List, G. R., 300  
 Little, A. D., 161  
 LLDPE fractionation with respect to molecular weight and backbone structure, 201–205  
 Lower critical end point (LCEP), 30, 49–51, 95, 148, 149  
 Lower critical solution temperature (LCST), 30, 31, 36, 37, 39, 65, 66, 140–142, 148, 280–282, 284  
 Lowry, G. C., 219  
 Luks, K. D., 30, 76, 77
- McCabe, W. L., 14  
 McCaffrey, D. S. Jr., 76, 77  
 McClellan, A. K., 65, 84, 91, 280–284  
 McEwen, I. J., 281, 284  
 McGrath, J. E., 273  
 McGuigan, D. B., 105  
 McHugh, M. A., 10, 14, 22, 25, 45, 49, 51–54, 56–65, 73, 74, 84, 88, 89, 91, 94, 96, 118, 119, 128, 129, 131, 132, 141, 142, 182, 184–187, 196, 205, 206, 208–216, 232, 239, 280–284, 329, 330, 358–360
- Mackay, M. E., 133  
 McKetta, J. J., 41, 73  
 Maizus, Z. K., 328, 330  
 Mallett, M. W., 73, 74, 186  
 Mancini, C., 106  
 Mansoori, G. A., 10  
 Mason, D. M., 320  
 Mass transfer limitations, 165  
 Mass transfer properties, 14–16  
 Matson, D. W., 336  
 Mean-field equations, 104, 105, 127

- Meilchen, M. A., 64, 69, 81, 87, 126, 196, 205, 206, 359, 360
- Melhem, G. A., 104
- Melting point, 21, 46
- Merrill, R. C., 77
- Methane, 20, 22, 115
- Methane-carbon dioxide system, 48
- Methane-ethane, 114
- Methane-ethane-octane system, 115-117
- Methane-hydrocarbon system, 37
- Methane-methanol system, 183, 188
- Methane-octane system, 114, 116
- Methanol, 102, 109, 110
- Methanol-methane system, 184
- Methyl acrylate, 81, 214, 215, 322
- Methyl ethyl ketone (MEK)-water-ethylene system, 76
- N*-methyl pyrrolidone (NMP), 109
- Methylene chloride, 102
- Metzger, J., 321, 322
- Meyer, V. E., 219
- Meyers, J. M., 151, 152
- Meyers, M. N., 107, 108, 259, 369
- Michelberger, Th., 43
- Milkovich, R., 218
- Miller, K. J., 206
- Mixing rules, 112, 113, 122
- Modell, M., 24, 158, 169, 309, 326
- Mohamed, R. S., 105
- Mollier diagram, 137
- Monomers  
  processing, 189-292  
  purification, 285-292
- Monson, P. A., 105
- Montagna, J. C., 73, 75, 170, 172, 177
- Morrell, D. G., 88, 308
- Morrison, R. T., 307
- Mortimer, G. A., 316, 330, 331
- Moses, J. M., 170, 172
- Munk, P., 61
- Munster, N., 182
- Mushkina, E. V., 10, 12, 22
- Najour, G. C., 22, 61
- Naphthalene, 11-13, 20, 22, 24, 51, 368  
  and chalk dust mixture, 137  
  and CO<sub>2</sub>, 22, 133, 136-137  
  and ethylene, 21, 52-56, 59, 134
- Nash, C. A., 73, 75, 88, 170, 172, 178, 186
- Natural products, 293-294
- Navy-blue dye, 336
- Ng, H.-J., 34, 35
- Niswonger, D. C., 182
- Nitroguanidine, 349-350
- p*-Nitrophenol, 312
- p*-Nitrophenyl phosphoric acid, 312
- Nitrous oxide, 20
- NMP, 110
- n*-Nonadecane, 77
- Nucleation, 333-342
- O'Brian, M. J., 4
- Occhiogrosso, R. N., 92, 96, 118-120, 330
- Octamethyl cyclotetrasiloxane, 231, 274
- n*-Octane, 115
- Ogino, Y., 358
- Ohgaki, K., 186
- Oleoresins, 14
- Oligomer extraction from polymers, 257-258
- Organic solvent-SCF mixtures, 71
- Organic solvent-water-ethylene systems, 73
- Organic-water separations, 170-182
- O-rings, swelling of, 358
- Owens, R. S., 88
- Ozawa, S., 358
- Panayiotou, C. G., 123
- Paraffin wax, 20
- Passino, H. J., 151
- Patat, F., 328
- Patterson, D., 63, 65, 66, 140, 149, 281
- Paul, P. M. F., 10
- Paulaitis, M. E., 10, 14, 22, 25, 52, 53, 73, 75, 85, 86, 88, 128, 133, 170, 172, 178, 179, 186, 294, 318, 358, 360
- Pearlman, R. S., 104, 133, 134
- Peck, D. G., 104, 105, 134
- Peng, D. Y., 111, 113, 183
- Peng-Robinson equation of state, 111, 116, 118-119, 122, 128, 130, 131
- Pentachlorophenol, 165
- Perfluoroalkylpolyether, fractionation, 266-267
- Pesticides, 161, 165
- Peter, S., 10
- Peters, C. J., 77
- Peterson, R. C., 336
- Petsche, I. B., 105
- pH effect, 180-181
- Pharmaceuticals, 304-307, 340, 347
- Phase behavior, 27-45  
  binary mixtures, 31-45  
  classification scheme, 29  
  polymer-supercritical fluid, 61-71  
  semicrystalline polymers, 199-201  
  solid-supercritical fluid, 45-61  
  ternary mixtures, 71-84

- type I, 31–34, 72–74
- type II, 34–35, 74–75
- type III, 36–41, 75–84
- type IV, 41–44, 66
- type V, 45
- Phase border curves, methods for determining, 94–98
- Phase rule, 28
- Phase-splitting phenomena, 140, 177
- Phenanthrene, 102
- Phenols, 161, 328
  - p*-substituted, 313
- Phosphoric acid, 328
- Pigford, R. L., 168
- Pine, S. H., 242, 246
- Pittilo, R. N., 320, 331
- Plank, C. A., 182
- Plant materials, extraction, 305
- PMA-chlorodifluoromethane system, 82–83
- Podesva, J., 220
- Polar interactions, 100, 101, 104, 127
- Poling, B. E., 112, 115, 206
- Polycarbosilanes, 354
  - fractionation, 262
- Poly(dimethyl)-*co*-(diphenyl) siloxanes, 237–250
- Poly(dimethylsiloxane) (PDMS)
  - amine-terminated, 275
  - carboxypropyl-terminated, 273
  - see also* Poly(methylmethacrylate)-*g*-poly(dimethylsiloxane)
- Poly(dimethylsiloxane-*co*-diphenylsiloxane), 196
- Polydimethylsiloxanes, 231–236
- Polyethylene, 62
  - aerogel, 364
  - fractionation, 198–205
  - and low molecular weight hydrocarbon mixtures, 70
  - and solvent mixtures, 63
  - and xylene gel, 364
  - see also* High-pressure polyethylene polymerization
- Poly(ethylene-*co*-methyl acrylate), 68, 123, 205, 206
- Poly(ethylene-*co*-propylene)-hexane mixture, 141
- Poly(ethylene-*co*-vinyl acetate)-ethylene-vinyl acetate system, 80
- Polyisobutylene, 66, 192
  - surfactant, 278–279
- Polyisobutylene-succinic anhydride copolymer fractions, 279
- Polymers
  - binders for solid propellants, fractionation of, 250–257
  - fiber spinning, 260–262
  - fractionation, 192–198, 262–279
  - functionally terminated liquid crystal, 273–278
  - and organic solvent phase separation, 280–285
  - photoresist, 273–278
  - porous, 360–364
  - processing, 189–292
    - and SCF mixtures, 61–71
    - and SCF modeling, 120–127
    - and solvent-cosolvent mixtures, 83
    - and solvent mixtures, 61–140
    - and solvent-SCF additive process, 142
  - swelling, 357–360
- Polymethyl methacrylate (PMMA)
  - fractionation, 196–197
  - swelling, 359
- Poly(methylmethacrylate)-*g*-poly(dimethylsiloxane) (PMMA-*g*-PDMS)
  - fractionation, 217–229
- Polyoxyalkylene, 257–258
- Polyphenol oxidase, 313
- Polypropylene, 336
  - isotactic, 360–364
  - pressed sheet, 360–364
- Polysilane polymers, 278
  - cyclohexyl-substituted, 277
- Polysiloxane polymers, 278
  - fractionation, 217–250
  - functionally terminated, 273
- Polysiloxane/PMMA copolymer fractionation, 217–250
- Polystyrene, 192
  - fractionation, 268
  - supercritical fluid chromatography analysis, 258–260
- Polystyrene-toluene-ethane system, 282
- Polyvinylsilanes, 354
- Pominski, J., 300
- Poot, W., 21
- Pottinger, M. T., 121
- Poynting correction, 127
- Prasad, R., 299
- Pratt, J. A., 205, 208–216
- Prausnitz, J. M., 13, 35, 59, 66, 85, 99, 101, 102, 107, 110, 112, 115, 133, 184, 206
- Pressure-infiltration-carbonization (PIC) process, 353
- Process development studies, 157–188
- Process operations, 135–143
  - schematic diagram, 135

- Process viability, 370  
Progesterone, 340  
Propane, 68, 69, 205–210, 215  
    deasphalting, 145–150  
    and distillate oil mixture, 148  
    and hydrocarbon mixtures, 36, 37  
    and lube oil refining process, 145–150  
*n*-propanol–water–carbon dioxide system, 177–178  
*n*-propanol–water–ethylene system, 75  
Propylene, 69, 205–210, 212, 214, 215  
*P*–*T* diagrams, 9, 28, 32–35, 41, 43, 45, 55, 56, 64, 70, 78, 94, 97, 129, 133  
*P*–*T*–*x* diagrams, 22, 28, 29, 31, 34, 37, 39, 46, 52, 331  
*P*–*x* diagram, 32, 33, 39, 41, 55, 56, 71, 72, 123  
Pyridine, 324  
Pyrolysis reactions, 321–322  
  
Quadrupole moment, 69, 100–101  
Quirin, K. W., 293, 316  
  
Radosz, M., 63, 84  
Ramsay, W., 19  
Rance, R. W., 59  
Randall, L. G., 10  
Randolph, T. W., 312  
Rapid expansion of supercritical solutions (RESS), 340  
Rasmussen, P., 104  
Rätzsch, M. T., 63, 80  
RDX (cyclotrimethylenetrinitramine), 342, 348–349  
Reaction rates, 328–332  
Reaction/separation schemes, 326–328  
Recycle cleanup, 175  
Red peppers, 14  
Redlich–Kwong equation, 113  
Regeneration process, 161  
Reid, R. C., 22, 25, 78, 79, 85, 102, 103, 112, 115, 128, 134, 206  
Research and development (R&D), 157–188  
Reverse osmosis, 6, 157  
Richards, R. B., 192, 194  
Richardson, M. J., 10, 48  
Riffle, J. S., 247, 250  
Robertson, W. W., 22, 61  
Robey, R. J., 303  
Robinson, D. B., 34, 35, 111, 113, 183  
Robinson, R. L. Jr., 34, 35, 91  
Robson, W. G., 37, 61  
Rodrigues, A. B. J., 76  
Roebbers, J. R., 88, 90  
  
ROSE process, 153–156  
    light oil precipitation step, 153  
    schematic diagram, 153  
Roselius, W., 296  
Rowlinson, J. S., 10, 30, 31, 33, 34, 37, 48, 50, 61, 65, 281, 316  
Rzasa, M. J., 91  
  
Saeki, S., 281, 282  
Saini, R., 104  
Saltiel, J., 325  
Sampling technique, 89  
Sanchez, I. C., 104, 120, 121, 127  
Sanchez–Lacombe equation of state, 120, 121, 123–124, 127, 133  
Sand, M. L., 358  
Sandler, S. I., 119  
Saraf, V. P., 63, 64  
Savchik, J. A., 206  
Scarella, R. A., 299  
Scheffer, F. E. C., 10, 12, 13, 21, 45, 49, 51–53, 78, 79, 135  
Schelchshorn, J., 322–324  
Schilz, W., 309  
Schmidt, M. B., 182  
Schmitt, W. J., 22, 79, 102, 103, 134, 363  
Schneider, G. M., 10, 14, 31, 44, 45, 98, 113, 128  
Scholsky, K. M., 205  
Schroeder, E., 358  
Scott, R. L., 27, 28, 41, 104, 106  
Seckner, A. J., 22, 51, 52, 61–63, 91, 281, 283, 284  
Selectivities, 328–332  
Semicrystalline polymers, phase behavior, 199–201  
Sen, Y. L., 63, 64, 93  
Sernow, V. S., 63, 80  
Shaw, R. W., 105  
Sherwood, R. T., 168  
Shim, J.-J., 96, 105  
Shimshick, E. J., 181  
Shreve, R. N., 189  
Silica–water system, 24–25  
Silicon carbide, 354, 355, 357  
Silicone lens monomer, 286, 287  
Silicone polymers, fractionation, 262–265  
Simmons, G. M., 320  
Simnick, J. J., 85, 88  
Siow, K. S., 63, 65  
Slocum, E. W., 141  
Small-scale processes, 159  
Smith, R. D., 336  
Smith, J. C., 14

- Smith, R. D., 96, 105  
 Smith, S. D., 217  
 Smits, A., 78  
 Snyder, J. M., 300  
 Soave, G., 111  
 Soave–Redlich–Kwong equation of state, 111  
 Soft lens monomer, 285  
 Sollexol process, 150–152  
 Solid–gas equilibria, 55, 131  
 Solid–liquid behavior, 106  
 Solid–liquid–vapor (SLV), 28, 46, 49, 52, 55, 57, 104, 129, 130  
 Solid propellants, fractionation of polymer binders for, 250–257  
 Solid–SCF calculations, 127–134  
 Solid–SCF equilibria, 45, 59, 61, 131, 133  
 Solid–solid–SCF systems, 80  
 Solomon, H. J., 316, 317  
 Solubility, 367  
   dynamic methods for measuring, 85–90  
   parameters, 105–110  
   calculations of, 106–107  
   static methods for measuring, 91–94  
 Solute–solute pairs, 99, 101  
 Solute–solvent behavior, 99, 101, 106, 107  
 Solvent–solvent pairs, 99, 101  
 Solvent-to-feed (S/F) ratio, 172, 174  
 Solvents, 326  
   critical temperatures and pressures for, 9  
   selection, 195–198  
 Spices, 14  
 Spiegelaar, J., 77  
 Squires, T. G., 325  
 Stahl, E., 10, 14, 293, 300, 309, 316, 368  
 Stearic acid, 20  
 Stejskal, J., 219, 220  
 Stephens, W. D., 252  
 Steroids, 340  
 Staverman, A. J., 123  
 Stilbene, 325  
 Stockmayer, W. H., 219, 220  
 Streett, W. B., 27–29, 34, 45  
 Styrene–CO<sub>2</sub> system, 119  
 Subramaniam, B., 329  
 Sunder, S., 303  
 Supercritical fluids, 58  
   chromatographic separation, 258  
   extraction concept, 135  
   extraction tests, 155  
   infiltration, 353–355  
   properties and characteristics of, 7–16  
 Suppes, G. J., 96, 330  
 Swelheim, T., 21  
 Swinton, F. L., 30, 31, 33, 34, 37, 50, 316  
 Takahashi, T., 320, 330, 331  
 Tea decaffeination plant, 7  
 Temperature–entropy diagram, 138  
 Temperature rising elution fractionation (TREF), 197, 202–203  
 Ternary mixtures, phase diagrams, 71–84  
 Testosterone, 340  
 Tetracyclic steroids, 293  
 Thermodynamic modeling, 99–134  
 Thies, M. C., 88–90  
 Thin-layer chromatograph (TLC), 367–369  
 Thodos, G., 10, 123, 124  
 Threshold pressures, 367  
 Tiffin, D. L., 77  
 Tiltscher, H., 322–324  
 Todd, D. B., 39, 40, 71, 107, 135  
 Travers, M. W., 33  
 Treybal, R. E., 73, 172  
 Trifluoromethane, 22  
 Trimethyl borate–methanol system, 182–188  
 Tsekhanskaya, Yu. V., 10, 12, 22  
 Uematsu, M., 206  
 Ultrafiltration, 157  
 Unterreiner, J. M., 182, 184–187  
 Upper critical end point (UCEP), 30, 36, 39, 43, 49, 51, 52, 54–59, 95, 96, 130, 131, 133, 134, 200  
 Upper critical solution temperature (UCST), 30, 35, 41, 65–67, 280, 282  
 Usher, F. L., 33  
 UV-spectrophotometry, 164  
 Vaidya, S. N., 13, 130  
 Valteris, R. L., 10  
 Van Alsten, J. G., 103  
 van der Kooi, H. J., 77  
 van der Waals equation of state, 29, 104, 107, 108, 128  
 van Gust, C. A., 21, 51, 53, 78, 79  
 van Hest, J. A. M., 21, 51, 52, 59, 60  
 van Konynenburg, P. B., 27, 28, 41, 104  
 Van Leer, R. A., 25, 85, 86  
 van Welie, G. S. A., 20, 21, 51, 52  
 Vapor–liquid equilibrium, 32–34, 39, 43, 46, 47, 49, 50, 64, 121  
 Vapor–liquid systems, modeling, 110–113  
 Vaporization process, 138–139  
 Variable-volume view cell apparatus, 93  
 Venier, C. G., 325  
 Villard, P., 20  
 Vinyl chloride, 319  
 Viscosity effects, 325–326  
 Vitzthum, O., 296

- Vivian, J. E., 176  
von Tapavicza, S., 59
- Wagner, J. R. Jr., 76, 77, 353  
Walsh, J. M., 102, 103, 104  
Waste streams, treatment of, 309–310  
Water  
    and organic-activated carbon systems, 166  
    and organic mixtures, 140  
Watkins, J. J., 63, 64, 196, 197, 200, 201, 204,  
    205, 251, 253  
Webb, G. E., 252  
Weinstock, J. J., 71, 72, 73, 75, 76, 77, 140,  
    177  
White, G. L., 80  
Wild, L., 197, 202  
Wilke, C. K., 168  
Wilke, G., 10  
Williams, D. F., 10, 14, 322  
Wilson, R. E., 265  
Wilson, G., 88  
Wilson, K. V., 71, 316  
Wilson, R. E., 145, 146, 148–150, 153  
Winkler, D. E., 329  
Wise, W. S., 10
- Wissinger, R. G., 358, 360  
Wohlfarth, Ch., 63, 80  
Wolf, H., 322–324  
Wolkomir, R., 302  
Wong, J. M., 104, 133, 134  
Wu, P. C., 319  
Wu, R.-S., 105
- Xenon, 22, 96, 100  
Xenon–naphthalene system, 129
- Yang, H., 76  
Yates, R. A., 181  
Yiling, T., 43  
Yogan, T. J., 51–54, 59–62, 91, 94  
Yonker, C. R., 96, 105  
Young, C. L., 27, 34
- Zaks, A., 312  
Zarah, B. Y., 76  
Zeman, L., 63, 65–67, 281  
Zhuang, W., 64  
Ziegler–Natta process, 198  
Ziger, D. H., 25, 128  
Zosel, K., 299